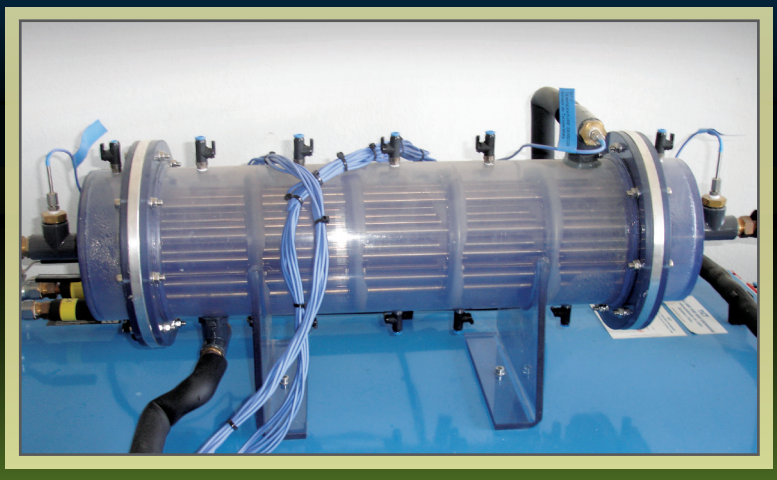
CRC Press
Taylor & Francis Group

Contemporary Food Engineering Series
Da-Wen Sun, Series Editor



FOOD ENGINEERING HANDBOOK

FOOD ENGINEERING FUNDAMENTALS



EDITED BY
Theodoros Varzakas
Constantina Tzia

FOOD ENGINEERING HANDBOOK

Contemporary Food Engineering

Series Editor

Professor Da-Wen Sun, Director
Food Refrigeration & Computerized Food Technology
National University of Ireland, Dublin
(University College Dublin)
Dublin, Ireland
http://www.ucd.ie/sun/

Handbook of Food Processing and Engineering, Volume II: Food Process Engineering, *edited by Theodoros Varzakas and Constantina Tzia* (2014)
Handbook of Food Processing and Engineering, Volume I: Food Engineering Fundamentals, *edited by Theodoros Varzakas and Constantina Tzia* (2014)
Juice Processing: Quality, Safety and Value-Added Opportunities, *edited by Víctor Falguera and Albert Ibarz* (2014)
Engineering Aspects of Food Biotechnology, *edited by José A. Teixeira and António A. Vicente* (2013)
Engineering Aspects of Cereal and Cereal-Based Products, *edited by Raquel de Pinho Ferreira Guiné and Paula Maria dos Reis Correia* (2013)
Fermentation Processes Engineering in the Food Industry, *edited by Carlos Ricardo Soccol, Ashok Pandey, and Christian Larroche* (2013)
Modified Atmosphere and Active Packaging Technologies, *edited by Ioannis Arvanitoyannis* (2012)
Advances in Fruit Processing Technologies, *edited by Sueli Rodrigues and Fabiano Andre Narciso Fernandes* (2012)
Biopolymer Engineering in Food Processing, *edited by Vânia Regina Nicoletti Telis* (2012)
Operations in Food Refrigeration, *edited by Rodolfo H. Mascheroni* (2012)
Thermal Food Processing: New Technologies and Quality Issues, Second Edition, *edited by Da-Wen Sun* (2012)
Physical Properties of Foods: Novel Measurement Techniques and Applications, *edited by Ignacio Arana* (2012)
Handbook of Frozen Food Processing and Packaging, Second Edition, *edited by Da-Wen Sun* (2011)
Advances in Food Extrusion Technology, *edited by Medeni Maskan and Aylin Altan* (2011)
Enhancing Extraction Processes in the Food Industry, *edited by Nikolai Lebovka, Eugene Vorobiev, and Farid Chemat* (2011)
Emerging Technologies for Food Quality and Food Safety Evaluation, *edited by Yong-Jin Cho and Sukwon Kang* (2011)
Food Process Engineering Operations, *edited by George D. Saravacos and Zacharias B. Maroulis* (2011)
Biosensors in Food Processing, Safety, and Quality Control, *edited by Mehmet Mutlu* (2011)

Physicochemical Aspects of Food Engineering and Processing, *edited by Sakamon Devahastin* (2010)

Infrared Heating for Food and Agricultural Processing, *edited by Zhongli Pan and Griffiths Gregory Atungulu* (2010)

Mathematical Modeling of Food Processing, *edited by Mohammed M. Farid* (2009)

Engineering Aspects of Milk and Dairy Products, *edited by Jane Sélia dos Reis Coimbra and José A. Teixeira* (2009)

Innovation in Food Engineering: New Techniques and Products, *edited by Maria Laura Passos and Claudio P. Ribeiro* (2009)

Processing Effects on Safety and Quality of Foods, *edited by Enrique Ortega-Rivas* (2009)

Engineering Aspects of Thermal Food Processing, *edited by Ricardo Simpson* (2009)

Ultraviolet Light in Food Technology: Principles and Applications, *Tatiana N. Koutchma, Larry J. Forney, and Carmen I. Moraru* (2009)

Advances in Deep-Fat Frying of Foods, *edited by Serpil Sahin and Servet Gülüm Sumnu* (2009)

Extracting Bioactive Compounds for Food Products: Theory and Applications, *edited by M. Angela A. Meireles* (2009)

Advances in Food Dehydration, *edited by Cristina Ratti* (2009)

Optimization in Food Engineering, *edited by Ferruh Erdoğdu* (2009)

Optical Monitoring of Fresh and Processed Agricultural Crops, *edited by Manuela Zude* (2009)

Food Engineering Aspects of Baking Sweet Goods, *edited by Servet Gülüm Sumnu and Serpil Sahin* (2008)

Computational Fluid Dynamics in Food Processing, *edited by Da-Wen Sun* (2007)

FOOD ENGINEERING HANDBOOK

FOOD ENGINEERING FUNDAMENTALS

EDITED BY
Theodoros Varzakas
Constantina Tzia

CRC Press
Taylor & Francis Group
Boca Raton London New York

CRC Press is an imprint of the
Taylor & Francis Group, an **informa** business

CRC Press
Taylor & Francis Group
6000 Broken Sound Parkway NW, Suite 300
Boca Raton, FL 33487-2742

© 2015 by Taylor & Francis Group, LLC
CRC Press is an imprint of Taylor & Francis Group, an Informa business

No claim to original U.S. Government works
Version Date: 20140903

International Standard Book Number-13: 978-1-4822-6170-7 (eBook - PDF)

This book contains information obtained from authentic and highly regarded sources. Reasonable efforts have been made to publish reliable data and information, but the author and publisher cannot assume responsibility for the validity of all materials or the consequences of their use. The authors and publishers have attempted to trace the copyright holders of all material reproduced in this publication and apologize to copyright holders if permission to publish in this form has not been obtained. If any copyright material has not been acknowledged please write and let us know so we may rectify in any future reprint.

Except as permitted under U.S. Copyright Law, no part of this book may be reprinted, reproduced, transmitted, or utilized in any form by any electronic, mechanical, or other means, now known or hereafter invented, including photocopying, microfilming, and recording, or in any information storage or retrieval system, without written permission from the publishers.

For permission to photocopy or use material electronically from this work, please access www.copyright.com (http://www.copyright.com/) or contact the Copyright Clearance Center, Inc. (CCC), 222 Rosewood Drive, Danvers, MA 01923, 978-750-8400. CCC is a not-for-profit organization that provides licenses and registration for a variety of users. For organizations that have been granted a photocopy license by the CCC, a separate system of payment has been arranged.

Trademark Notice: Product or corporate names may be trademarks or registered trademarks, and are used only for identification and explanation without intent to infringe.

Visit the Taylor & Francis Web site at
http://www.taylorandfrancis.com

and the CRC Press Web site at
http://www.crcpress.com

Dedicated to my wife Elia and my daughter Fotini
for their endless support and love. To my mother for her love
and understanding and to the memory of my father.

Theodoros Varzakas

Dedicated to the memory of my parents.

Constantina Tzia

Contents

Series Preface xi
Preface xiii
Acknowledgments xv
Series Editor xvii
Editors xix
Contributors xxi

Chapter 1 Introduction 1
Theodoros Varzakas and Constantina Tzia

Chapter 2 Mass and Energy Balances 3
N. Zogzas

Chapter 3 Fundamental Notes on Chemical Thermodynamics 41
Petros Tzias

Chapter 4 Heat Transfer 75
Ioannis K. Kookos and Nikolaos G. Stoforos

Chapter 5 Steam Generation: Distribution 113
Theodoros Varzakas

Chapter 6 Heat Exchangers 141
Theodoros Varzakas

Chapter 7 Rheology in Use: A Practical Guide 179
Niall W.G. Young

Chapter 8 Fluid Mechanics in Food Process Engineering 217
Ricardo D. Andrade P., Carmen E. Pérez C., and German J. Narvaez G.

Chapter 9 Diffusion 263
Theodoros Varzakas

Chapter 10 Absorption 309
Giovanni A. Escamilla García and Eleazar M. Escamilla Silva

Chapter 11 Distillation for the Production of Fortification Spirit 343
Malcolm S. Allen, Andrew C. Clark, Leigh M. Schmidtke, and Peter J. Torley

Chapter 12 Food Products Evaporation 369
Jorge F. Vélez-Ruiz

Chapter 13 Food Irradiation Processing 427
Joong-Ho Kwon, Jae-Jun Ahn, and Hafiz Muhammad Shahbaz

Chapter 14 Food Formulation 491
V. Giannou, Constantina Tzia, and Theodoros Varzakas

Chapter 15 Reaction Kinetics 529
Petros S. Taoukis, Theofania N. Tsironi, and Maria C. Giannakourou

Series Preface

CONTEMPORARY FOOD ENGINEERING

Food engineering is the multidisciplinary field of applied physical sciences combined with the knowledge of product properties. Food engineers provide the technological knowledge transfer essential to the cost-effective production and commercialization of food products and services. In particular, food engineers develop and design processes and equipment to convert raw agricultural materials and ingredients into safe, convenient, and nutritious consumer food products. However, food engineering topics are continuously undergoing changes to meet diverse consumer demands, and the subject is being rapidly developed to reflect market needs.

In the development of food engineering, one of the many challenges is to employ modern tools and knowledge, such as computational materials science and nanotechnology, to develop new products and processes. Simultaneously, improving food quality, safety, and security continues to be a critical issue in food engineering studies. New packaging materials and techniques are being developed to provide more protection to foods, and novel preservation technologies are emerging to enhance food security and defense. Additionally, process control and automation regularly appear among the top priorities identified in food engineering. Advanced monitoring and control systems are developed to facilitate automation and flexible food manufacturing. Furthermore, energy saving and minimization of environmental problems continue to be important food engineering issues, and significant progress is being made in waste management, efficient utilization of energy, and reduction of effluents and emissions in food production.

The Contemporary Food Engineering Series, consisting of edited books, attempts to address some of the recent developments in food engineering. The series covers advances in classical unit operations in engineering applied to food manufacturing as well as topics such as progress in the transport and storage of liquid and solid foods; heating, chilling, and freezing of foods; mass transfer in foods; chemical and biochemical aspects of food engineering and the use of kinetic analysis; dehydration, thermal processing, nonthermal processing, extrusion, liquid food concentration, membrane processes, and applications of membranes in food processing; shelf-life and electronic indicators in inventory management; sustainable technologies in food processing; and packaging, cleaning, and sanitation. These books are aimed at professional food scientists, academics researching food engineering problems, and graduate-level students.

The editors of these books are leading engineers and scientists from different parts of the world. All the editors were asked to present their books to address the market's needs and pinpoint cutting-edge technologies in food engineering.

All contributions are written by internationally renowned experts who have both academic and professional credentials. All authors have attempted to provide critical, comprehensive, and readily accessible information on the art and science of a

relevant topic in each chapter, with reference lists for further information. Therefore, each book can serve as an essential reference source to students and researchers in universities and research institutions.

Da-Wen Sun
Series Editor

Preface

It is an innovative piece of work coming in a two-volume set bringing together aspects of food engineering and food process engineering phenomena and operations. This handbook provides a stimulating and up-to-date review of fundamental food engineering phenomena. An in-depth coverage of the major technologies compared with the broader coverage of others will be the deciding factor for would-be purchasers or academics considering prescribing the book as a food engineering textbook.

It addresses the basic principles of food engineering methods used in food processing operations around the world. While it covers the theory it combines this with a practical hands-on approach. The book is a comprehensive resource that explores the basic and applied aspects of food engineering from mass transfer and heat transfer to steam and boilers, heat exchangers, diffusion, absorption, evaporation, and novel food processes such as irradiation technology.

In each chapter, the addition of case studies and problem calculation is highlighted and this makes the key difference between it and other textbooks on food engineering.

Acknowledgments

The contributions by well-known, reputable, and distinguished researchers from around the world are much appreciated. We would like to acknowledge their valuable support and professionalism.

Series Editor



Born in Southern China, Professor Da-Wen Sun is a world authority in food engineering research and education; he is a member of the Royal Irish Academy (RIA), which is the highest academic honor in Ireland; he is also a member of Academia Europaea (The Academy of Europe) and a fellow of the International Academy of Food Science and Technology. His main research activities include cooling, drying, and refrigeration processes and systems, quality and safety of food products, bioprocess simulation and optimization, and computer vision technology. Especially, his many scholarly works have become standard reference materials for researchers in the areas of computer vision, computational fluid dynamics modeling, vacuum cooling, and so on. Results of his work have been published in over 700 papers including more than 350 peer-reviewed journal papers (Web of Science h-index = 53; Google Scholar h-index = 66). He has also edited 13 authoritative books. According to Thomson Scientific's *Essential Science Indicators*SM, based on data derived over a period of 10 years from the ISI Web of Science, there are about 2500 scientists who are among the top 1% of the most cited scientists in the category of agriculture sciences. For many years, Professor Sun has consistently been ranked among the very top 50 scientists in the world (he was at 31st position in 2010).

He received a first class BSc Honors and MSc in mechanical engineering, and a PhD in chemical engineering in China before working in various universities in Europe. He became the first Chinese national to be permanently employed in an Irish university when he was appointed college lecturer at the National University of Ireland, Dublin (University College Dublin [UCD]), in 1995, and was then continuously promoted in the shortest possible time to senior lecturer, associate professor, and full professor. Dr. Sun is now a professor of Food and Biosystems Engineering and the director of the Food Refrigeration and Computerised Food Technology Research Group at the UCD.

As a leading educator in food engineering, Professor Sun has significantly contributed to the field of food engineering. He has trained many PhD students, who have made their own contributions to the industry and academia. He has also delivered lectures on advances in food engineering on a regular basis in academic institutions internationally and delivered keynote speeches at international conferences. As a recognized authority in food engineering, he has been conferred adjunct/visiting/consulting professorships from 10 top universities in China, including Zhejiang University, Shanghai Jiaotong University, Harbin Institute of Technology, China Agricultural University, South China University of Technology, and Jiangnan University. In recognition of his significant contribution to food engineering worldwide and for his outstanding leadership in the field, the International Commission

of Agricultural and Biosystems Engineering (CIGR) awarded him the "CIGR Merit Award" in 2000, and again in 2006, the Institution of Mechanical Engineers based in the United Kingdom named him "Food Engineer of the Year 2004." In 2008, he was awarded the "CIGR Recognition Award" in honor of his distinguished achievements as the top 1% of agricultural engineering scientists in the world. In 2007, he was presented with the only "AFST(I) Fellow Award" in that year by the Association of Food Scientists and Technologists (India), and in 2010, he was presented with the "CIGR Fellow Award"; the title of Fellow is the highest honor in CIGR and is conferred to individuals who have made sustained, outstanding contributions worldwide. In March 2013, he was presented with the "You Bring Charm to the World" Award by Hong Kong-based Phoenix Satellite Television with other award recipients including Mr Mo Yan—the 2012 Nobel Laureate in Literature and the Chinese Astronaut Team for Shenzhou IX Spaceship. In July 2013, he received the "Frozen Food Foundation Freezing Research Award" from the International Association for Food Protection (IAFP) for his significant contributions to enhancing the field of food freezing technologies. This is the first time that this prestigious award was presented to a scientist outside the United States.

He is a fellow of the Institution of Agricultural Engineers and a fellow of Engineers Ireland (the Institution of Engineers of Ireland). He has also received numerous awards for teaching and research excellence. He is the editor-in-chief of *Food and Bioprocess Technology—An International Journal* (2012 Impact Factor = 4.115), former editor of *Journal of Food Engineering* (Elsevier), and editorial board member for a number of international journals, including *Journal of Food Process Engineering, Journal of Food Measurement and Characterization,* and *Polish Journal of Food and Nutritional Sciences.* He is also a chartered engineer.

On May 28, 2010, he was awarded membership in the RIA, which is the highest honor that can be attained by scholars and scientists working in Ireland; at the 51st CIGR General Assembly held during the CIGR World Congress in Quebec City, Canada, on June 13-17, 2010, he was elected incoming president of CIGR and became CIGR president in 2013-2014—the term of his CIGR presidency is six years, two years each for serving as incoming president, president, and past president. On September 20, 2011, he was elected to Academia Europaea (The Academy of Europe), which is functioning as the European Academy of Humanities, Letters and Sciences, and is one of the most prestigious academies in the world; election to the Academia Europaea represents the highest academic distinction.

Editors

Theodoros Varzakas earned a bachelor's (honors) in microbiology and biochemistry (1992), a PhD in food biotechnology, and an MBA in food from Reading University, United Kingdom (1998). Dr. Varzakas was a postdoctoral research staff member at the same university. He has worked in large pharmaceutical and multinational food companies in Greece for 5 years and has at least 14 years experience in the public sector. Since 2005, he has served as an assistant and associate professor in the Department of Food Technology, Technological Educational Institute of Peloponnese (ex Kalamata), Greece, specializing in issues of food technology, food processing, food quality, and safety. Dr. Varzakas has been a reviewer in many international journals such as the *International Journal of Food Science and Technology*, *Journal of Food Engineering*, *Waste Management*, *Critical Reviews in Food Science and Nutrition*, *Italian Journal of Food Science*, *Journal of Food Processing and Preservation*, *Journal of Culinary Science and Technology*, *Journal of Agricultural and Food Chemistry*, *Journal of Food Quality*, *Food Chemistry*, and *Journal of Food Science*. He has written more than 90 research papers and reviews and has presented more than 90 papers and posters at national and international conferences. He has written two books in Greek, one on genetically modified food and the other on quality control in food. He has edited a book on sweeteners, published in 2012 by CRC Press and another book on biosensors published by CRC Press in 2013.

Dr. Varzakas has participated in many European and national research programs as a coordinator or scientific member.

He is a fellow of the Institute of Food Science & Technology (2007).

Constantina Tzia earned a diploma (1977) and PhD (1987) in chemical engineering from the National Technical University of Athens (NTUA), Greece, and is a professor in the School of Chemical Engineering, NTUA, Greece.

Professor Tzia's main research fields are food science, food engineering, food quality, sensory evaluation of foods, food hygiene, food safety and HACCP (hazard analysis and critical control points), food processing (freezing, edible films/coatings, extraction, encapsulation), food technology (fats and oils, olives and olive oil, bakery products, dairy products), and utilization of food by-products (protein isolates).

Dr. Tzia has more than 70 articles in international scientific (SCI) journals, 2 books in the Greek language, 1 book (editor), and 6 chapters in international scientific books. She has more than 120 presentations at international conferences and more than 100 at Greek conferences. She has participated in European research projects and has coordinated many national research projects and projects in cooperation with Greek food industries. She has been a reviewer in many international journals.

Contributors

Jae-Jun Ahn
School of Food Science and Biotechnology
Kyungpook National University
Daegu, Korea

Malcolm S. Allen
School of Agricultural and Wine Sciences
Charles Sturt University
New South Wales, Australia

Ricardo D. Andrade P.
University of Córdoba Montería
Córdoba, Colombia

Andrew C. Clark
School of Agricultural and Wine Sciences
Charles Sturt University
New South Wales, Australia

Giovanni A. Escamilla García
Departamento de Ingeniería Química
Instituto Tecnológico de Celaya
Guanajuato, México

Maria C. Giannakourou
Department of Food Technology
Technological Educational Institute of Athens
Athens, Greece

V. Giannou
School of Chemical Engineering
National Technical University of Athens
Athens, Greece

Ioannis K. Kookos
Department of Chemical Engineering
University of Patras
Rio, Greece

Joong-Ho Kwon
School of Food Science and Biotechnology
Kyungpook National University
Daegu, Korea

German J. Narvaez G.
University of Sucre
Sucre, Colombia

Carmen E. Pérez C.
University of Santiago
Santiago, Chile

Leigh M. Schmidtke
School of Agricultural and Wine Sciences
Charles Sturt University
New South Wales, Australia

Hafiz Muhammad Shahbaz
School of Food Science and Biotechnology
Kyungpook National University
Daegu, Korea

Eleazar M. Escamilla Silva
Departamento de Ingeniería Química
Instituto Tecnológico de Celaya
Guanajuato, México

Nikolaos G. Stoforos
Department of Food Science and Human Nutrition
Agricultural University of Athens
Athens, Greece

Petros S. Taoukis
School of Chemical Engineering
National Technical University of Athens
Athens, Greece

Peter J. Torley
School of Agricultural and Wine Sciences
Charles Sturt University
New South Wales, Australia

Theofania N. Tsironi
School of Chemical Engineering
National Technical University of Athens
Athens, Greece

Constantina Tzia
School of Chemical Engineering
National Technical University of Athens
Athens, Greece

Petros Tzias
National Technical University of Athens
Piraeus, Greece

Theodoros Varzakas
Department of Food Technology
Technological Educational Institute of Peloponnese
Kalamata, Greece

Jorge F. Vélez-Ruiz
Chemical, Food and Environmental Engineering Department
Universidad De Las Américas Puebla
Puebla, Mexico

Niall W.G. Young
DuPont Nutrition and Health
Physical Food Science

N. Zogzas
Technological Educational Institute of Athens
Athens, Greece

1 Introduction

Theodoros Varzakas and Constantina Tzia

The primary aim of the *Handbook of Food Engineering* is to address food engineering issues. The most recent and advanced information required for the efficient design and development of processes that are used in the manufacturing of food products has been described. The audience for this handbook includes practicing engineers in food and related industries, students preparing for careers as food engineers or food technologists, and other scientists and technologists seeking information about design and development of processes.

Although the first three chapters focus primarily on mass and energy balances, thermodynamics of foods, and food formulation, the chapters that follow are organized according to traditional unit operations associated with the manufacturing of foods. Three key chapters cover the basic concepts of heat transfer, heat exchangers, and steam generation distribution.

Two additional background chapters focus on the basic concepts of diffusion and mass transfer in foods as well as modeling.

More specific unit operations on chilling/freezing, mixing-emulsions, size reduction, evaporation, crystallization, centrifugation/filtration, drying/dehydration, are discussed and analyzed in separate chapters. The chapter on membrane processes deals with liquid food concentration but provides the basis for other applications of membranes in food processing.

Moreover, key chapters include those on irradiation, fluids, rheology, absorption/desorption, extraction, supercritical fluid extraction, distillation, kinetics of chemical reaction in food, and multiphysics modeling of innovative and traditional food processing technologies.

The final chapters of the handbook cover the important topics of fermentation/enzymes, encapsulation, fluidized-bed drying, and innovative methods.

The editors of this handbook hope that the information presented will continue to contribute to the evolution of food engineering as an interface between engineering and food technology/processing. As demands for safe, high-quality, nutritious, and convenient foods continue to increase, the need for the concepts presented will become more critical. In the near future, the applications of new technologies such as nanotechnology in food manufacturing will increase, and the role of engineering in process design and scale-up will be even more visible. Finally, the use of engineering concepts should lead to the highest quality of food products at the lowest possible cost.

The editors wish to acknowledge the authors and their significant contributions to this edition of the handbook. These contributors are among the leading scientists and engineers in the field of food engineering/food processing and their chapters reflect high-quality research currently carried out worldwide.

2 Mass and Energy Balances

N. Zogzas

CONTENTS

2.1 Mass Balances 3
2.1.1 Open and Closed Systems 4
2.1.2 Mass Conservation Law 4
2.1.3 Mass Balance Applications 6
2.2 Energy Balances 18
2.2.1 Heat 19
2.2.2 Energy Conservation Law 20
2.2.2.1 Energy Balance for a Closed (Nonflow) System 20
2.2.2.2 Energy Balance for an Open (or Flow) System 22
2.2.3 Energy Balance Applications 24
Problems 37
List of Symbols 38
Subscripts 39
References 39

Mass and energy balances are powerful tools for the design and optimization of food manufacturing plants. They are based on the application of mass and energy conservation laws to an individual part or the whole food process. The aim is to determine the mass flow rate and composition of any stream of raw material, intermediate or the final product, by-product, waste, or effluent encountered in the process along with the amounts of energy (mainly heat) that must be supplied or rejected. The basic steps that are followed are the construction of the process flow diagram along with any available information, the consideration of the suitable system boundaries, and the establishment and solving of the set of independent equations resulting from the suitable mass and energy balance application.

The above mentioned will be discussed in detail in the following sections along with comprehensive examples and problems collected from a variety of existing food process applications.

2.1 MASS BALANCES

A mass balance is the application of the mass conservation law around or within a system that is a part or the whole of a food process. The law can be applied for the total amount of mass entering, leaving, or accumulating within the system, as well as, for any individual component. The set of equations resulting from this application

is solved to determine the unknown amounts of mass and material composition of the incoming and the outgoing streams of the system. Typical examples of mass balance applications in food processing can be found in mixing, blending, separation, dilution, concentration, drying, evaporation, and crystallization.

2.1.1 Open and Closed Systems

A system can be defined as a collection of matter included within specific boundaries. The boundary can be real or imaginary and separates the system from its surroundings. Let us consider a can in atmospheric air that contains concentrated milk. The outer surface of the can could be considered as the boundary between milk and the atmospheric air. We could also draw an imaginary boundary around the can (Figure 2.1a). Whatever be the case, the system consists of milk and the can walls. In the above example, there cannot be any mass exchange between the system and its surroundings, and this type of system is known as "closed." It must be noted that the consideration of a closed system does not necessarily exclude energy exchange between the system and its surroundings, as well as, any volume changes within the system. In contradiction, an "open" system is the system that allows mass transfer between the system and its surroundings. A typical example is that of a heat exchanger shown in Figure 2.1b. If we draw a boundary around the body of the exchanger, we can easily notice that there are hot and cold fluid streams entering or leaving the system. That is why an open system is also called a "flow" system.

In the majority of food engineering operations, the systems that we deal with are actually open systems, since continuous and semibatch processes are of common practice. Closed systems are rare and can be met mainly in batch processes (i.e., heating or cooling of foods in hermetically closed containers or vessels).

2.1.2 Mass Conservation Law

The law of mass conservation states that "mass can neither be destroyed nor created." This leads to the conclusion that the total mass of a closed system must remain constant over time. The definition does not exclude any component transformation within the system and in the case of a chemical or a biochemical reaction the total mass of the reactants equals the total mass of the products at any time point.

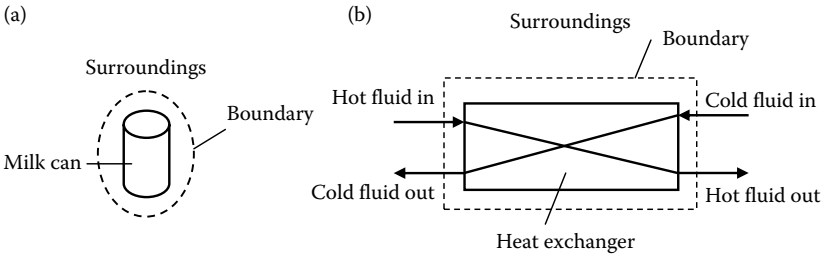


FIGURE 2.1 Examples of (a) closed and (b) open systems.

In open (or flow) systems, mass flows through the boundary and the above law can be expressed in terms of mass flow rates as

Total mass flow rate entering the system	–	Total mass flow rate leaving the system	= Rate of mass accumulation (or mass depletion) within the system

The above word equation can be written in a mathematical form as

$$\dot{m}_{in} - \dot{m}_{out} = \frac{dm_{sys}}{dt} \tag{2.1}$$

where, $\dot{m}_{in}$ and $\dot{m}_{out}$ are the total mass flow rates entering and leaving the system, respectively, and dm_{sys}/dt is the rate of mass accumulation (or mass depletion) within the system at a specific time point in kg/s. Note that in the case of mass depletion the second part of Equation 2.1 is negative producing that $\dot{m}_{out}$ is greater than $\dot{m}_{in}$.

A continuous process is by definition an open system in which the total mass of the feed entering is continuously removed by the form of products and wastes. In this case, there is no accumulation (or depletion) of mass within the system and Equation 2.1 is simplified to

$$\dot{m}_{in} = \dot{m}_{out} \tag{2.2}$$

In steady-state conditions, mass flow rates do not vary with time and the total mass entering or leaving the system for a predefined time period can be easily calculated. The above equation also holds for a batch process in terms of a total mass balance at the beginning and at the end of the process. That is, the total mass of the feed entering the system at the beginning of the process equals the total mass of the products at the end. In general, the total mass flow rate that enters or leaves a system may consist of several streams. Thus, the above equation can be written as

$$\sum_{i=1}^{k} \dot{m}_{i,in} = \sum_{j=1}^{n} \dot{m}_{j,out} \tag{2.3}$$

where, $\dot{m}_{i,in}$ and $\dot{m}_{j,out}$ are the mass flow rates of streams i and j entering and leaving the system, respectively. Equation 2.3 can be applied as well for any individual component that enters with the feed to the system, provided that there are no chemical or biochemical reactions. Under this condition Equation 2.3 can be written as

$$\sum_{i=1}^{k} X_i \dot{m}_{i,in} = \sum_{j=1}^{n} X_j \dot{m}_{j,out} \tag{2.4}$$

where, X_i is the mass fraction of a specific component in the entering stream i and X_j is the mass fraction of the same component in the exiting stream j.

For liquids and gases (including air) mass flow rate can be calculated from volumetric flow rate that is easily measured through flow meters (rotameters, orifice, vanes, anemometers, etc.), provided that the density or the specific volume of the fluid is known.

$$\dot{m} = \rho \cdot \dot{V} \quad \text{or} \quad \dot{m} = \frac{\dot{V}}{v} \tag{2.5}$$

where, $\dot{V}$ is the volumetric flow rate (m^3/s), ρ is the density (kg/m^3), and υ is the specific volume (m^3/kg) of the fluid under processing conditions of pressure and temperature. Physical properties of fluids such as water, steam, air, and other liquid foods are provided.

For an incompressible fluid, that is, for a fluid that does not change its density under the processing conditions, Equation 2.1 can be written in terms of volumetric flow rates by the form

$$\dot{V}_{in} - \dot{V}_{out} = \frac{dV_{sys}}{dt} \tag{2.6}$$

where, $\dot{V}_{in}$ and $\dot{V}_{out}$ are the total volumetric flow rates at the inlet and the outlet of the system, respectively, and dV_{sys}/dt is the rate of volume increase (or volume reduction) within the system at a specific time point in m^3/s. However, this equation is rarely applied to food processing practices since systems are complex involving solid, liquid, and gas mixtures, phase transitions, and material transformations with density change.

2.1.3 Mass Balance Applications

The basic steps that are needed to establish a suitable mass balance over a specific process are

1. Constructing the flow diagram of the process
2. Defining the suitable boundaries
3. Collecting all available data for the streams of materials entering or leaving the boundaries
4. Selecting a basis for calculations
5. Applying of mass balance Equations 2.3 through 2.5
6. Solving the system of equations to estimate the unknowns

There are four types of flow diagrams used in food process design and optimization. The first is the simplest and shows all streams of raw materials, products, side products, and wastes. It is made of blocks that symbolize all individual unit operations needed to complete the process. This type of diagram is called “process block diagram” (PBD). The second type is a more detailed “process flow diagram” (PFD) or “Flowsheet” that shows all the necessary equipment combined together in every

stage of the process. Conventional international symbols are used to depict the various types of equipments along with process parameters such as temperature, pressure, composition, flow rate, level, and any other property necessary to describe the process. The third is a layout of the machinery arrangement on the floor (or in space [3D]) of the plant showing the dimensions of equipment. This type of diagram is useful in estimating the necessary surface and space of the food plant. The fourth diagram is focused on the details of connections and control of process equipment such as piping (including pumps, fans, ducts, regulating and safety valves, steam traps, and other fittings) and instrumentation (such as gauges, sensors of temperature, pressure, level, flow, moisture and others, signal transducers, controllers, and wiring). This type of diagram is called "piping and instrumentation diagram" (PID). Of the above diagrams, the first two types are useful for applying mass and or energy balances. In fact, the PBD is used for overall mass and energy balances across each unit operation and PFD is used for more detailed calculations within a specific operation, for example, estimating the operating conditions, flows, and composition in a triple effect evaporator. A PBD and a PFD for an orange juice concentrate plant are shown in Figures 2.2 and 2.3, respectively.

Boundaries can be drawn around the whole or an individual part of the process. Usually, an overall mass balance along with some selected individual parts is adequate. The choice of the suitable boundaries, as well as, the set of mass balance equations depends on the number of unknowns, the available data, and the easiness of calculations.

Collecting the suitable data such as material compositions, mass (or volumetric) flow rates, process conditions (pressure and temperature), and any other information provided by the flow diagram is essential for solving the set of mass balance equations. Process conditions can be used to estimate thermophysical properties of food materials (including water and air). For example, the pressure of saturated steam is necessary to estimate its temperature, specific volume, and other thermodynamic properties from the available literature steam tables.

In a generalized approach, food materials can be said to consist of water and total solids, with the latter comprising soluble and insoluble matter. In this way, composition can be expressed in a wet or a dry basis. In "wet basis," the composition of a mixture of n constituents is expressed by the mass fractions of all individual components (including water) by the relation

$$X_{i,w.b.} = \frac{m_i}{\sum_{i=1}^{n} m_i} \tag{2.7}$$

where, $X_{i,w.b}$. is the mass fraction of component i in the mixture and m_i its mass in kg. In "wet basis," the sum of all mass fractions of the components of a mixture equals unity. That is,

$$\sum_{i=1}^{n} X_{i,w.b.} = 1 \tag{2.8}$$

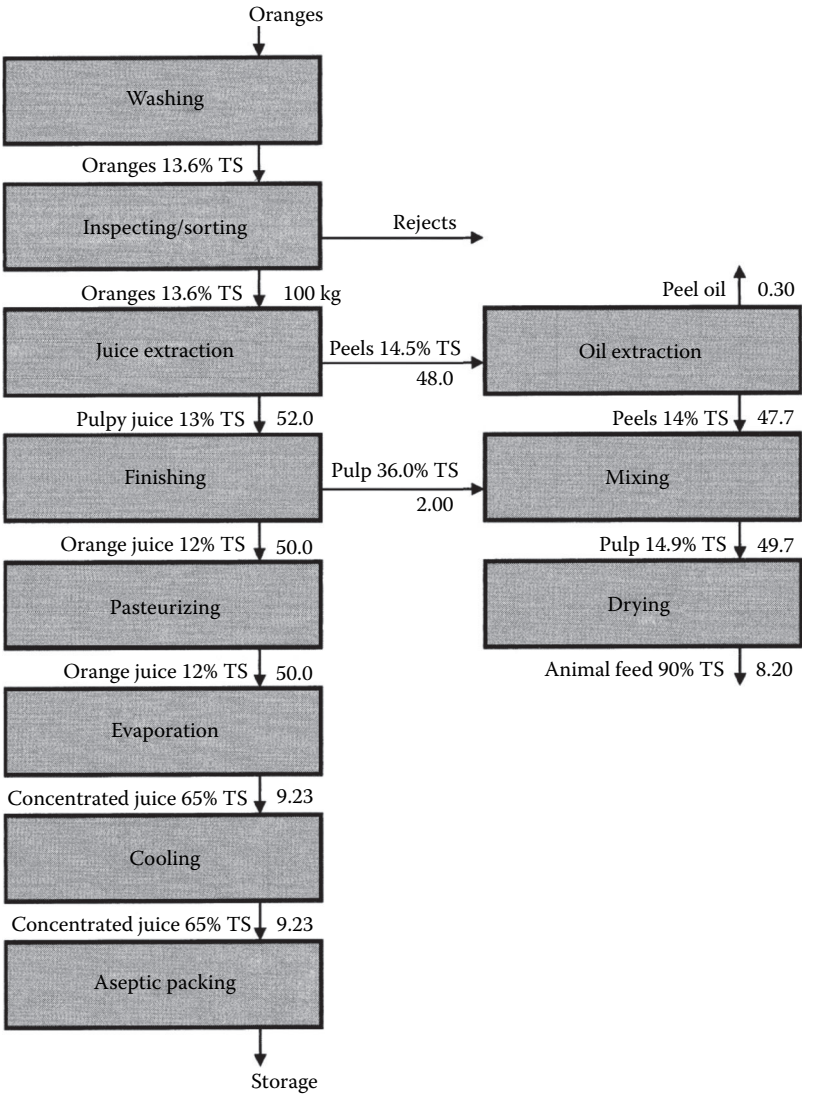


FIGURE 2.2 A PBD and material balance for an orange juice concentrate plant. The basis of calculations is 100 kg of oranges. (Reprinted with permission from Maroulis, B.Z. and Saravacos, D.G., 2008. *Food Plant Economics*, CRC Press, Taylor & Francis Group, Boca Raton, New York.)

In "dry basis" water is not taken into account, thus Equation 2.7 is transformed to

$$X_{i,d.b.} = \frac{m_i}{m_{d.s.}} \tag{2.9}$$

where $m_{d.s.}$ is the mass of dry solids (or dry matter) in kg that is what is left from the total mass when water is excluded (i.e., evaporated). Obviously, Equation 2.8 can no longer

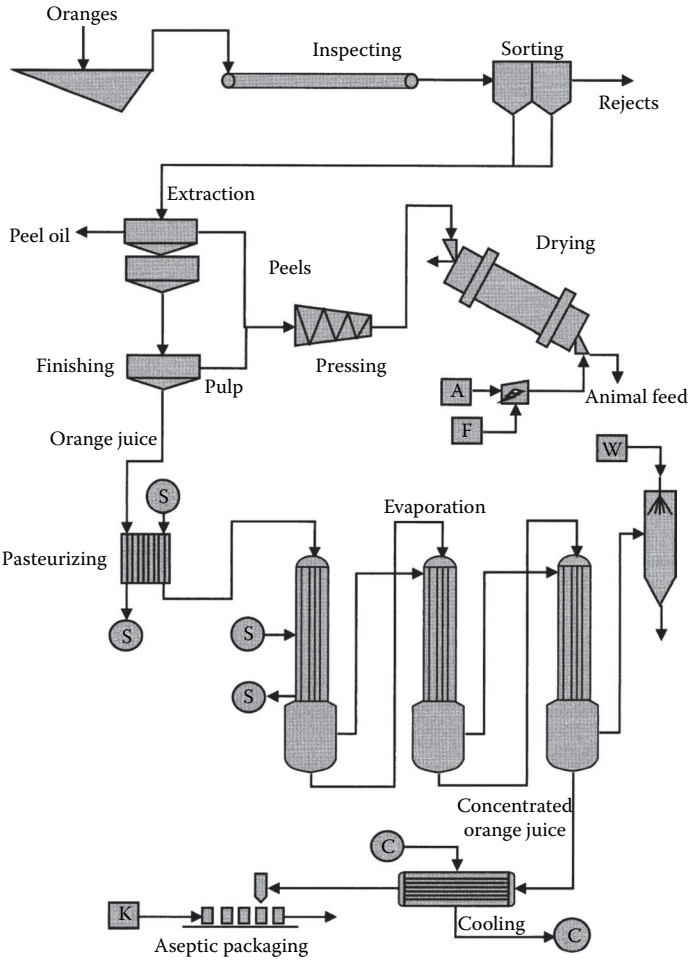


FIGURE 2.3 A PFD for an orange juice concentrate plant. A, air; C, cooling water; F, fuel; K, packaging material; S, steam; W, condenser water. (Reprinted with permission from Maroulis, B.Z. and Saravacos, D.G., 2008. *Food Plant Economics*, CRC Press, Taylor & Francis Group, Boca Raton, New York.)

be justified by the mass fractions in "dry basis." The composition of foods in "dry basis" is often used in food processing where fluctuations of moisture content are significant. For example, the total fat in cheese is expressed as a percentage in dry matter, as well as, the moisture content of dried foods. In the latter, the dry matter of the feed materials entering a dryer remains constant throughout the drying process. Moreover, the use of moisture content in "dry basis" facilitates drying time calculations. Conversion between dry and wet basis moisture content can be done by using the relation

$$X_{d.b.} = \frac{X_{w.b.}}{1 - X_{w.b.}} \tag{2.10}$$

where, $X_{d.b.}$ and $X_{w.b.}$ are the moisture contents in dry and wet basis, respectively. Rearranging and solving for $X_{w.b.}$

$$X_{w.b.} = \frac{X_{d.b.}}{1 + X_{d.b.}} \tag{2.11}$$

Equations 2.10 and 2.11 may be easily deduced from Equations 2.7 and 2.9 considering that the mass of the food material is consisted of water and dry solids.

Another important parameter in applying mass balances is the basis for calculations. An obvious choice that has an economic importance would be the quantity of the final product produced during a specified time period (e.g., an hour, a day, a month, or a year). However, this might not be easy, since calculations are facilitated when done concurrently with the flow of the process. An alternative would be the consideration of arbitrary quantities of raw materials resulting through mass balance calculations to specific quantities of the final product and then scaling up (or down) to the real situation. This technique is mostly favored by the use of spread sheet calculations and data tools like the "solver" of MS Excel. Whatever be the case, the basis of calculations must not be changed throughout the process.

Generally, there is more than one choice in establishing the set of mass balance equations. It depends on the specific boundaries considered throughout the flowsheet and on the ease of calculations. However, the number of independent equations has to be equal to the number of unknowns, excluding equations that are identical. Moreover, the mass balances for all intermediate streams must be in accordance with the overall mass balance of the process.

In the following sections typical examples of mass balance applications in food engineering are provided to familiarize with, while at the end of the chapter some unsolved problems are provided for further practice.

EXAMPLE 2.1: MASS BALANCE OVER A MIXING TANK

A concentrated fruit juice with 65% total solids is mixed with pure water to form a beverage with 12% total solids into a cylindrical mixing tank with 2.5 m internal diameter and 3.5 m height. If the feed of the concentrated liquor is 1.2 m^3/h calculate the volumetric flow rate of pure water and the time to fill 4/5 of the tank's volume. The densities of concentrated liquor and product are given as 1.315×10^3 and 1.04×10^3 kg/m^3, respectively.

A flow diagram of the batch-type process is shown in Figure 2.4. A boundary (dotted line) is chosen around the mass of the product accumulated within the tank. For ease of calculations the basis is chosen as 1 h of operation. Let the mass of concentrate that enters the boundary be m_c, the mass of water m_w, and the mass of the product m_p. Since the basis of calculations is 1 h, $m_c = 1.2 \times 1.315 \times 10^3 \approx 1.58 \times 10^3$ kg and the application of Equation 2.1 to the above system gives

$$1.58 \times 10^3 + m_w = m_p$$

The application of Equation 2.4 for the mass of total solids entering and accumulating into the system results in

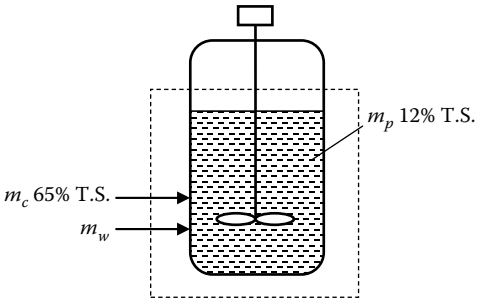


FIGURE 2.4 Mass balance over a mixing tank.

$$0.65 \times 1.58 \times 10^3 = 0.12\ m_p$$

From the above relations m_p and m_w are calculated as 8.56×10^3 and 6.98×10^3 kg, respectively. Thus, the mass flow rate of pure water is 6.98×10^3 kg/h and using Equation 2.5 its volumetric flow rate is found to be 6.98 m^3/h. Where, the density of pure water was considered equal to 1 kg/L or 10^3 kg/m^3.

The volume of the cylindrical tank is

$$V_t = \frac{\pi \cdot 2.5^2}{4} \cdot 3.5 = 17.18\ \text{m}^3$$

The volumetric flow rate of the product accumulated in the tank is calculated from its density as

$$8.56 \times 10^3 / 1.04 \times 10^3 = 8.23\ \text{m}^3/\text{h}$$

Thus, the time to fill 4/5 of the tank's volume is

$$t = \frac{4/5 V_t}{\dot{V}_p} \text{ or } \frac{0.8 \cdot 17.18}{8.23} = 1.67\,\text{h}$$

EXAMPLE 2.2: MASS BALANCE IN AIR DRYING

Potato cubes with 75% (w.b.) initial moisture content are dried in a continuous countercurrent tunnel drier with a production rate of 200 kg/h and final moisture of 19% (d.b.). Air enters with 0.014 kg/$kg_{d.a.}$ specific humidity and 1.01 $m^3/kg_{d.a.}$ specific volume and leaves the drier at a specific humidity of 0.024 kg/$kg_{d.a.}$. Calculate the feed rate of potato cubes and the volumetric flow rate of air at the drier's inlet.

A flow diagram is shown in Figure 2.5 along with a boundary drawn around the drying process. In drying systems the usual basis of calculations is the dry matter of the feed (or the product). As it has been said this dry matter remains constant throughout the drying process. The same happens with air, since air can be considered as a mixture of dry air and water vapor (see chapter 9 (Psychrometrics)), and during drying the water removed from the feed material is absorbed by the air. Thus, the streams entering or leaving the drier can be analyzed in dry solids

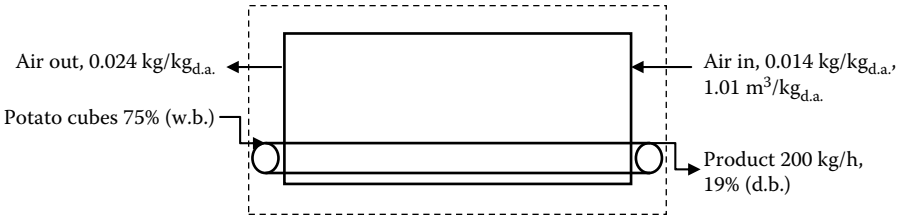


FIGURE 2.5 Mass balance in a tunnel drier.

(of potato cubes), water, and dry air. Applying Equation 2.11 the moisture content of the product in wet basis $X_{p,w.b}$. is

$$X_{p,w.b.} = \frac{0.19}{1+0.19} = 0.16 \quad \text{or} \quad 16\% \ (w.b.)$$

Applying a mass balance for dry solids (Equation 2.4) the mass flow rate of feed $\dot{m}_f$ is calculated

$$0.25 \cdot \dot{m}_f = 0.84 \cdot 200 \quad \text{or} \quad \dot{m}_f = 672 \text{ kg/h}$$

Applying again Equation 2.4 for the water that enters and leaves the drier results in

$$0.75 \cdot \dot{m}_f + 0.014 \cdot \dot{m}_{d.a.} = 0.16 \cdot \dot{m}_p + 0.024 \cdot \dot{m}_{d.a.}$$

where, $\dot{m}_p$ and $\dot{m}_{d.a.}$ are the mass flow rates of product and dry air, respectively, in kg/h. Note that the specific (or absolute) humidity of air is its moisture content in dry basis and psychrometric properties of air are estimated using psychrometric charts. From the above relation the mass flow rate of dry air is calculated as

$$\dot{m}_{d.a.} = \frac{0.75 \cdot 672 - 0.16 \cdot 200}{0.024 - 0.014} \quad \text{or} \quad \dot{m}_{d.a.} = 47{,}200 \text{kg/h}$$

Since the specific volume of air at the drier's inlet is 1.01 m^3/kg$_{d.a.}$, its volumetric flow rate is found using Equation 2.5:

$$\dot{V}_a = 1.01 \cdot 47{,}200 = 47{,}672 \text{ m}^3\text{/h} \quad \text{or} \quad 13.24 \text{ m}^3\text{/s}$$

An important parameter that is useful in the design of air drying systems is the mass of dry air needed per kg of dry solids produced. In the above example, this ratio can be easily found as

$$\frac{\dot{m}_{d.a.}}{\dot{m}_{d.s.}} = \frac{47{,}200}{0.81 \cdot 200} = 291.36 \text{ kg}_{d.a.}/\text{kg}_{d.s.}$$

EXAMPLE 2.3: MASS BALANCE IN JUICE EXTRACTION

Fresh orange juice with 12% total solids (T.S.) is produced in two stages. In the first stage, a juice extractor is fed with oranges containing 13.6% (T.S.) and produces juice at a percentage of 52% of the feed and peels with 15.2% (T.S.). The extracted juice is then fed to the second stage, where a finisher removes 4% of its mass as pulp. Determine the mass and composition in % (T.S.) of every stream in the process.

Figure 2.6 depicts a block diagram of the process along with the boundaries chosen (A, B, C). The basis of calculation will be 1 kg of the finished product. Considering m_f the mass of orange feed in kg, X and Y the mass fractions of total solids for the extracted juice and the pulp, respectively, we may apply a total mass balance around the boundary A as

$$m_f = 0.48 \cdot m_f + 0.04 \cdot 0.52 \cdot m_f + 1$$

Applying mass balances for total solids around boundaries B and C we may write

$$0.136 \cdot m_f = 0.48 \cdot 0.152 \cdot m_f + X \cdot 0.04 \cdot 0.52 \cdot m_f$$

and

$$X \cdot 0.52 \cdot m_f = Y \cdot 0.04 \cdot 0.52 \cdot m_f + 0.12 \cdot 1$$

Solving the above set of equations m_f, X, and Y can be determined. The results of calculations for mass and total solids composition of every stream are shown in Table 2.1. All quantities are based on 1 kg of finished orange juice. If this table is constructed as a spreadsheet (i.e., using MS Excel) it is easy to scale up calculations to a specific quantity of the product, on hourly or an annual basis. This is especially useful in food process design and optimization where we are interested in scaling up, as well as, in the influence of specific process variables to the operation cost.

EXAMPLE 2.4: MASS BALANCE IN MILK CREAM SEPARATION

Milk with 3.7% fat content is centrifuged to produce skim milk and two types of cream, a full fat with 35% and a light with 20% fat content, in equal quantities. The light cream is produced by mixing a portion of the full fat cream that is exiting from the centrifuge, with a suitable portion of the milk feed. Assuming that 6% of

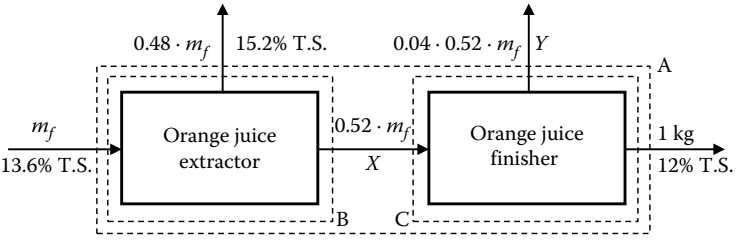


FIGURE 2.6 Mass balance in juice extraction.

TABLE 2.1
Calculations Results for Example 2.3

Type of Stream	Mass (kg)	% (T.S.)
Orange feed	2.00	13.6
Peels	0.96	15.2
Extracted juice	1.04	12.1
Pulp	0.04	15.1
Finished juice	1.00	12.0

the milk stream that enters the centrifuge is separated to full fat cream, determine the mass quantities and fat composition in every stream of the process.

Figure 2.7 depicts a flow diagram of the process along with the boundaries A, B, C, and D (dotted rectangles) chosen for mass balances application. Since the two types of cream are produced in equal quantities we will choose 1 kg of each type as the basis of calculations. Assuming that m_f is the mass of milk entering the centrifuge, m_c is the mass of full fat cream that is mixed with a suitable mass m_s of the feed milk and X is the mass fraction of fat in skim milk, we may apply the mass balance Equations 2.3 and 2.4 as follows.

The total mass and fat balances around boundary A are

$$m_c + m_s = 1$$

$$0.35 \cdot m_c + 0.037 \cdot m_s = 0.2 \cdot 1$$

Similarly, the total mass and fat balances around boundaries B, C, and D are

$$0.06 \cdot m_f = 1 + m_c$$

$$25.33 \cdot 0.037 = 0.06 \cdot 25.33 \cdot 0.35 + 0.94 \cdot 25.33 \cdot X$$

$$m_{tot} = m_f + m_s$$

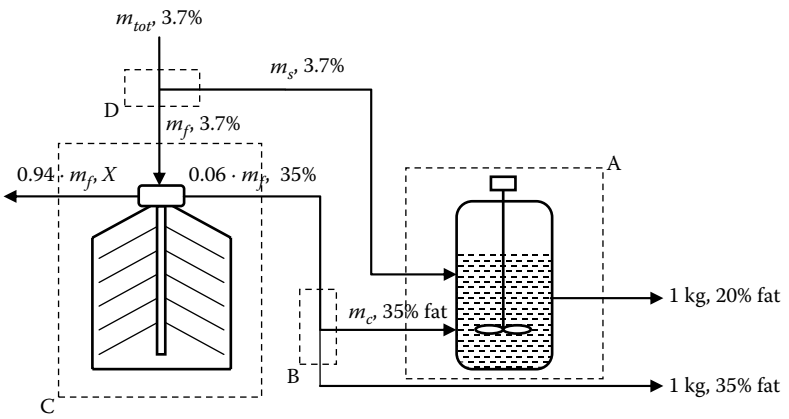


FIGURE 2.7 Mass balance in milk cream separation.

TABLE 2.2
Calculations Results for Example 2.4

Type of Stream	Mass (kg)	Fat (%)
Total milk feed	25,83	3,7
Milk to separator	25,35	3,7
Milk to mixer	0,48	3,7
Skim milk	24,33	1,7
Total cream 35%	1,52	35,0
Cream 35% to mixer	0,52	35,0
Cream product 20%	1,00	20,0
Cream product 35%	1,00	35,0

where, m_{tot} is the total mass of milk feed. From the above equations all five unknowns are easily calculated and the results of calculations are shown in Table 2.2.

Again making all calculations on a spreadsheet, it is easy to scale up the results and to observe the influence of changing the amounts of cream products, or their fat composition, to the rest of process parameters.

EXAMPLE 2.5: MASS BALANCE IN A CRYSTALLIZATION PROCESS

An aqueous solution of 15% solute content is fed into an evaporator/crystallizer, where it is concentrated by evaporation to form a mixture of 65% saturated solution and solute crystals with a proportion of 50%. The mixture is then separated by a centrifuge to a light phase consisting of 65% saturated solution and a dense phase consisting of 92% solute crystals and 8% saturated solution with the same solute content. The light phase is recycled to the evaporator's feed while the dense phase is dried in a rotary drier to produce solute crystals with 0.1% moisture content (w.b.). If the specific humidity of the air at the drier's inlet is 0.01 and 0.02 kg/$kg_{d.a.}$ at its outlet, calculate the mass and composition of each stream of the process per kg of final product.

Figure 2.8 depicts a flow diagram of the above crystallization process. The mixture exiting from crystallizer is called "magma" and it consists of crystals and saturated solution called "mother liquor" (see chapter 4 (Crystallization) for details). The crystals are then separated by centrifugation and the mother liquor is recycled to the evaporator/crystallizer's inlet. Since a small amount of mother liquor is transported along with the crystals, the removal of the excess of water is continued into the rotary drier to produce the final dried crystals.

Let m_f be the mass of feed solution, m_s the mass of steam evaporated in crystallizer, m_m the mass of magma, m_c the mass of crystals separated in centrifuge, m_R the mass of recycled liquor, m_p the mass of the final product, and $m_{d.a.}$ the mass of dry air that enters (or leaves) the drier. The basis of calculations is 1 kg of final product, thus $m_p = 1$ kg. Applying a total mass balance around the rotary drier (boundary A in Figure 2.8) we may write

$$m_c + m_{d.a.} + m_{w,in} = m_p + m_{d.a.} + m_{w,out}$$

or

$$m_c + m_{w,in} = m_p + m_{w,out}$$

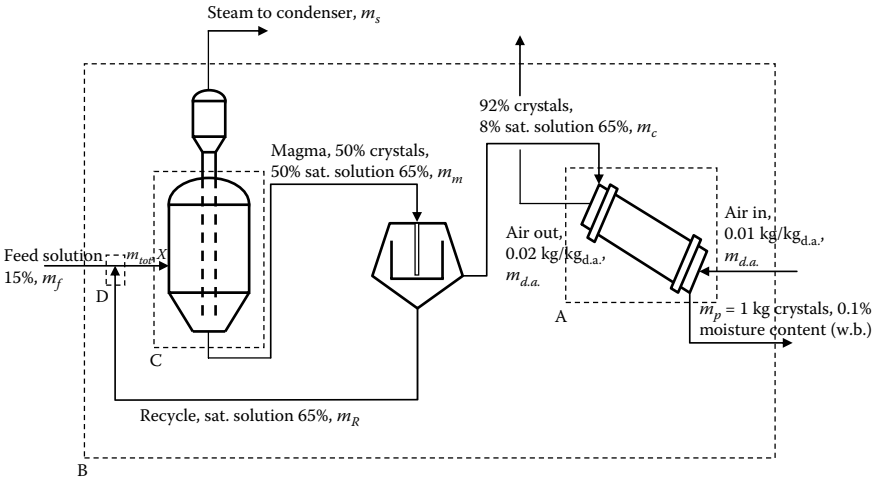


FIGURE 2.8 Mass balance in a crystallization process.

where, $m_{w,in}$ and $m_{w,out}$ are the masses of water vapor contained in the air entering and leaving the drier, respectively. Using the specific humidity of air at the drier's inlet and outlet, the above relation is written as

$$m_c + 0.01 \cdot m_{d.a.} = m_p + 0.02 \cdot m_{d.a.}$$

or

$$m_c = 1 + 0.01 \cdot m_{d.a.}$$

Applying a mass balance for solute around the same boundary

$$0.92 \cdot m_c + 0.08 \cdot m_c \cdot 0.65 = 0.999 \cdot m_p$$

or

$$0.972 \cdot m_c = 0.999$$

or

$$m_c = 1.028 \text{ kg}$$

Substituting,

$$m_{d.a.} = \frac{0.028}{0.01} = 2.8 \text{ kg}$$

Now focusing in boundary B around the total process, the mass balance for solute can be written as

$$0.15 \cdot m_f = 0.999 \cdot m_p$$

or

$$m_f = \frac{0.999}{0.15} = 6.660 \text{ kg}$$

In the same boundary the total mass balance is written as

$$m_f + m_{d.a.} + m_{w,in} = m_p + m_s + m_{d.a.} + m_{w,out}$$

or

$$m_f = m_p + m_s + 0.01 \cdot m_{d.a.}$$

or

$$m_s = 6.66 - 1 - 0.01 \cdot 2.8$$

or

$$m_s = 5.632 \text{ kg}$$

The total mass balance around the crystallizer, boundary C in Figure 2.8, is written as

$$m_f + m_R = m_s + m_m$$

or

$$m_R + 6.66 = m_m + 5.632$$

or

$$m_m = m_R + 1.028$$

The mass balance for solute around the same boundary gives

$$0.15 \cdot m_f + 0.65 \cdot m_R = 0.5 \cdot m_m + 0.5 \cdot 0.65 \cdot m_m$$

or

$$0.15 \cdot 6.66 + 0.65 \cdot m_R = 0.5 \cdot 1.65 \cdot m_m$$

or

$$0.999 + 0.65 \cdot m_R = 0.825 \cdot m_m$$

Solving the above equation systems the masses of magma and recycle are found

$$m_m = 1.89 \text{ kg} \quad \text{and} \quad m_R = 0.862 \text{ kg}$$

The total mass of solution fed to crystallizer m_{tot} is easily found as

$$m_{tot} = m_f + m_R$$

or

$$m_{tot} = 6.66 + 0.862 = 7.522 \text{ kg}$$

while its solute mass fraction X is calculated by applying a solute balance around boundary D as

$$0.15 \cdot m_f + 0.65 \cdot m_R = X \cdot m_{tot}$$

or

$$0.15 \cdot 6.66 + 0.65 \cdot 0.862 = X \cdot 7.522$$

or

$$X = 0.2073 \text{ or } 20.73\%$$

As can be seen from the above example, 45% of magma is recycled to the crystallizer after separation. This is a common practice in food engineering design since recycles are used for raw material and energy conservation increasing the overall efficiency of the process. However, in real situations, the feed solution includes impurities or inert solids and recycling favors accumulation of these substances within the process, thus leading to poor-quality final products. A means to partially overcome this problem is to provide a suitable purge stream, or to separate, or to eliminate (e.g., by a chemical reaction) the unwanted impurities, if this is economically justified.

2.2 ENERGY BALANCES

Energy consumption in food processing is of major importance especially in our days, when the gradual decrease of natural resources has changed the demand of energy conservation to a duty. Thus, the design improvement and optimization of any food process operation not only saves operating and capital cost, but also helps to maintain our planet's heritage. Inevitably, all this has to go through the mass and energy balances, with the latter to be discussed in the following sections.

The main types of energy involved in food process operations are heat, mechanical work, potential, kinetic, chemical, and electromagnetic. Heat is used for heating and cooling (or refrigerating) of raw materials and/or final products, but its major amounts are consumed in water removal processes such as evaporating, drying, and

distillation. It should also be noted that significant amounts of heat are lost through the walls of food process equipment, piping, and effluents. Mechanical work appears when a system moves its boundaries (i.e., a gas that expands (or contracts) behind a piston into a cylinder (Eastop and McConkey, 1986)), or in a rotating shaft (i.e., the work produced by a steam turbine or consumed by a circulating pump) and is mainly met in refrigeration, mixing, circulation, and transportation of process materials. Potential is the energy occupied by an object because of its position in respect to a datum level, while the kinetic energy appears in any moving object due to its velocity. Chemical energy is the energy that is evolved or absorbed by a chemical or a biochemical reaction (i.e., the heat of a fuel combustion), including the heat of dilution and emulsion formation and electromagnetic energy is a type of energy that is met in dielectric heating (i.e., the energy emitted by a magnetron in microwave heating).

From the above types of energy, heat is the most important and it would not be exaggerating to say that it is involved in almost any food processing. Therefore, it will be discussed separately.

2.2.1 Heat

Heat is always transmitted from a body to another at a lower temperature. When thermal equilibrium is reached, that is the temperatures of the two bodies are equal, there is no heat transmission between them. This means that there must be a temperature difference between the two bodies in order to observe heat flowing and that heat (like mechanical work) is a transitory type of energy (i.e., it always appears in transfer from one position to another). Therefore, it is wrong to say that heat is contained or possessed by a body in contradiction to internal, or kinetic, or potential energy that are functions of the body's state (i.e., its pressure and temperature, velocity or position, respectively).

As a consequence of heat flowing from (or to) a body there is a temperature or a phase change. For example, if water is heated, it primarily raises its temperature until it reaches its boiling point and then it is evaporated under constant temperature (provided that its pressure remains constant). The type of heat that raises (or lowers) the temperature of a body is called "sensible" while, the heat that is supplied (or rejected) during phase change is called "latent." The amount of sensible heat Q in J that is transferred to (or from) a body is given by the relation,

$$Q = m\int_{T_1}^{T_2} c\,dT \tag{2.12}$$

where m is the body's mass in kg, c is its specific heat capacity in J/kg K, and T_1, T_2 are its initial and final temperature, respectively, in °C or K. In the case of constant specific heat capacity over the temperature range T_1, T_2 the above relation is simplified to

$$Q = mc(T_2 - T_1) \tag{2.13}$$

It must be noted that if the temperature difference $(T_2 - T_1)$ is positive then heat is transferred (supplied) to the body (heating). If the temperature difference is negative

then heat is rejected from the body (cooling). In general, the specific heat capacity of a substance depends on its temperature and process type. For gases, there are two specific heat capacities, c_p for a constant pressure and c_v for a constant volume process. The specific heat capacity of solids and liquids does not depend on process type. Values for specific heat capacities of food materials are very useful in food engineering calculations and are given in literature as functions of temperature and composition (Choi and Okos 1986), while the composition of foods may be obtained from the USDA (2013) database. Equation 2.13 can also be applied in the case of a temperature-dependent specific heat, where a mean value over the specific temperature range may be used.

The amount of heat that is transferred during phase change is given by the relation

$$Q = m\,L \tag{2.14}$$

where, L is the latent heat of vaporization (in liquid to vapor change), or the latent heat of fusion (in solid to liquid change), or the latent heat of sublimation (in solid to vapor change), in J/kg. Note that the latent heat of vaporization of a liquid is a function of its saturation pressure or temperature. Values for the latent heat of vaporization of water can be found in many handbooks or in saturated water and steam tables as that provided in Haywood, R. W. (1990).

2.2.2 Energy Conservation Law

Similar to mass conservation, the energy conservation law states that "energy can be neither destroyed nor created." According to this law, the total energy of a system and its surroundings remains constant over time, without excluding any changes from one form to another. Applying this principle it leads to the conclusion that the total energy that enters a system equals the total energy that leaves, plus any energy change within it. Or in terms of an equation,

$$E_{tot.in} = E_{tot.out} + \Delta E_{sys} \tag{2.15}$$

2.2.2.1 Energy Balance for a Closed (Nonflow) System

The first law of thermodynamics for a closed (nonflow) system is based on the above law (Equation 2.15) and considers that heat, mechanical work, and internal energy are the main forms of energy that can be interchanged. Thus, Equation 2.15 is transformed to

$$Q = \Delta U + W \tag{2.16}$$

where, Q is the heat supplied to the system, ΔU is the change of its internal energy from an initial to a final state ($U_2 - U_1$), and W is the work done by the system. By convention, the heat supplied to the system and the work done by the system are positive, while the heat rejected and the work consumed by the system are negative. For a constant volume process, the work done by the system is zero and Equation 2.16 is simplified to

$$Q = \Delta U \tag{2.17}$$

while for a reversible constant pressure process Equation 2.16 is transformed to

$$Q = \Delta H \tag{2.18}$$

where, ΔH is the change of the enthalpy of the system from its initial to its final state ($H_2 - H_1$). Enthalpy is related to internal energy by the relation

$$H = U + PV \tag{2.19}$$

where, P is the pressure (N/m^2) and V is the volume (m^3). The above equation can be written in terms of specific values referred to 1 kg of mass of a particular component of the system as

$$h = u + Pv \tag{2.20}$$

where, h and u are the specific enthalpy and internal energy, respectively, (J/kg) and v is the specific volume (m^3/kg). Note that both specific internal energy and enthalpy are properties of the components of a system and are related to its pressure and temperature. Values for specific enthalpy, specific internal energy, and other thermodynamic properties are given for water and steam in various food engineering textbooks, for various ranges of pressure and temperature. Enthalpy values for various foods (including air and water) are very useful in food engineering calculations and may be found in literature (Pham et al., 1994; Fricke and Becker, 2001; Amos et al., 2008 and others). However, they must be used with care, since they are referred to specific food compositions and based on reference values of enthalpy that are not the same in any case. For example, in thermodynamic water and steam tables the reference value of the specific enthalpy of liquid water is 0 at its triple point (0.01°C and 0.611 kN/m^2), while for frozen food materials the reference value of enthalpy is taken as 0 at −40°C. In fact, we are not interested in the absolute values of specific enthalpy but in the changes of it that can be calculated combining Equations 2.13 and 2.18. Thus, for a food material that is heated under constant pressure the enthalpy change from a reference temperature T_{ref} to a temperature T can be calculated by the equation

$$Q = \Delta H = mc(T - T_{ref}) \tag{2.21}$$

where, c is considered constant over the temperature range T_{ref}, T or approximately, a mean value of c may be used. In the case of phase change, the change of enthalpy in Equation 2.18 represents the latent heat that is transferred under constant pressure and combining with Equation 2.14,

$$\Delta H = mL \quad \text{or} \quad L = \frac{\Delta H}{m} \quad \text{or} \quad L = \Delta h \tag{2.22}$$

Equation 2.22 shows that the latent heat L of a material is the change of its specific enthalpy during phase change. For example, the latent heat of vaporization of water equals the difference of its specific enthalpy from saturated liquid to dry saturated vapor.

For the calculation of the specific enthalpy values of moist air we may use the following equations suggested by *(ASHRAE) Handbook-Fundamentals for SI units*.

$$h_{d.a.} \approx 1.006\ T \tag{2.23}$$

$$h_{w.v.} \approx 2501 + 1.86\ T \tag{2.24}$$

where, $h_{d.a.}$ and $h_{w.v.}$ are the specific enthalpies of dry air and water vapor in kJ/kg at temperature T of moist air in °C. It must be noted that the specific enthalpy of dry air is considered zero (reference value) at 0°C, while the number 1.006 denotes the dry air's specific heat capacity at constant pressure in kJ/kg°C, since dry air can be considered ideal at atmospheric pressure. The specific enthalpy of water vapor that is mixed with dry air is calculated by the sum of the specific enthalpy of saturated water vapor (~2501 kJ/kg) at 0°C plus the product of its specific heat capacity at constant pressure (1.86 kJ/kg°C) multiplied by temperature T. The latter represents the specific enthalpy of an ideal gas at temperature T, as water vapor is superheated and considered ideal at atmospheric conditions. The above approximation facilitates energy balance calculations when values of specific enthalpy for water and steam are going to be used along with the ones for moist air, as for example, in the case of air drying of foods.

2.2.2.2 Energy Balance for an Open (or Flow) System

Considering Figure 2.9, a fluid of mass m is entering an open system under steady-state conditions. Work W is produced while heat Q is supplied to the system. The fluid enters with a pressure P_1, a velocity c_1, an internal energy U_1, a volume V_1 corresponding to mass m, and at a height z_1 from a datum level and exits with the respective values of P_2, c_2, U_2, V_2, and z_2. The total energy of the fluid entering (or leaving) the system consists of kinetic, potential, internal, and an amount of energy that causes the fluid to flow. The last is the work necessary to push the volume V of the fluid of mass m into (or out) of the duct and is easily proved to be the product of pressure P and volume V. Since the system is at steady state there is no energy change within it and applying the energy conservation law (Equation 2.15) we have

$$\frac{1}{2}mc_1^2 + mgz_1 + U_1 + P_1V_1 + Q = \frac{1}{2}mc_2^2 + mgz_2 + U_2 + P_2V_2 + W \tag{2.25}$$

Note that heat is supplied and is, therefore, added to the first part, while the work is produced and is added to the second part of the above equation. Considering Equation 2.19 the above equation is simplified to

$$\frac{1}{2}mc_1^2 + mgz_1 + H_1 + Q = \frac{1}{2}mc_2^2 + mgz_2 + H_2 + W \tag{2.26}$$

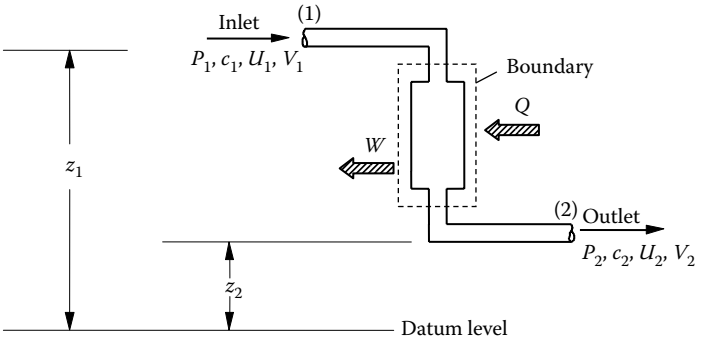


FIGURE 2.9 Energy balance in a flow system.

Equation 2.26 is known as the first law of thermodynamics for flow systems. If the amounts of heat and enthalpy change can be considered negligible the above equation is transformed into Bernoulli's equation that holds for fluid mechanics (see Chapter 8). However, in food engineering applications, the amounts of potential and kinetic energy can be considered negligible compared to heat and mechanical work. Thus, they can be eliminated without considerable error and Equation 2.26 is simplified to

$$Q = \Delta H + W \tag{2.27}$$

Many food process operations can be considered adiabatic (no heat flowing to or from the system) while the work can be neglected. In these situations, the enthalpy change of the system is zero and thus, the total enthalpy of the streams entering the system equals the total enthalpy of the streams leaving it

$$H_{tot.in} = H_{tot.out} \quad \text{or} \quad \sum_{i=1}^{k} H_{i,in} = \sum_{j=1}^{n} H_{j,out} \tag{2.28}$$

where, $H_{i,in}$ and $H_{j,out}$ are the enthalpies of streams i and j entering and leaving the system, respectively. Convective air drying of a food material in a well-insulated drying chamber can be considered as an example of the above equation's application. Equation 2.28 can also be used in adiabatic mixing of food materials or ingredients (including water and air) provided that there are no chemical or physicochemical interactions between them. In the event of such interactions the enthalpy of products formation should be taken into account. On the contrary, there are some food process operations where the work term of Equation 2.27 cannot be neglected. These processes involve milling or grinding, mixing or emulsification, and transportation or circulation of highly viscous materials. In these situations the amounts of mechanical energy are significant and are consumed to overcome frictional losses that are finally converted to heat absorbed by the process materials. Extrusion cooking could be referred as an example of severe mechanical work consumption along with heat.

2.2.3 Energy Balance Applications

The procedure to apply an energy balance is similar to that of applying a mass balance already described in Section 2.1.3. The critical steps are the process flow diagram construction, the selection of the suitable boundaries, and the establishment of the set of equations. In general, a mass balance should precede an energy balance to account for the quantities of the materials that enter or leave the system. However, there are situations where mass and energy balances cannot be carried out independently. In these cases, the input and output mass flow rates depend on the heat supplied (or rejected) and coupled mass and energy balances should be applied. Examples of such processes that involve simultaneous heat and mass transfer are drying, evaporation, and distillation. Following, there are some typical examples of energy balance applications in food processing explaining the way of handling such kind of problems.

EXAMPLE 2.6: ENERGY BALANCE IN ADIABATIC MIXING OF AIR STREAMS

An air stream with 40°C dry bulb temperature, 0.02 kg/kg$_{d.a.}$ specific humidity, and 200 kg/h mass flow rate of dry air is mixed adiabatically under atmospheric pressure with another stream of 25°C dry bulb temperature, 0.01 kg/kg$_{d.a.}$ specific humidity, and 100 kg/h mass flow rate of dry air. Calculate the dry bulb temperature and the specific humidity of the resulting mixture.

Adiabatic mixing of air streams is often met in foods drying where a portion of the air leaving the drier is recycled and mixed with fresh air prior to its heating. The reason is the increase of the process efficiency since the amount of heat supplied is reduced as the ratio of recycled to fresh air is increased. However, recycling increases the air's humidity along with the blower's energy consumption and this must be taken into account for the quality of the final product and the overall system's design and optimization.

The flow process for the above example is shown in Figure 2.10. Taking 1 h as a basis of calculations the mass balance equations for dry air and moisture around boundary A are written as

$$m_{d.a.} = 200 + 100 = 300 \text{ kg}$$

and

$$w \cdot 300 = 0.02 \cdot 200 + 0.01 \cdot 100 \quad \text{or} \quad w = 0.0167 \text{ kg/kg}_{d.a.}$$

where $m_{d.a.}$ is the mass of dry air in the mixture and w its specific humidity.

An energy balance for dry air and moisture can be written by using Equation 2.28 as

$$H_{d.a.in} + H_{w.in} = H_{d.a.out} + H_{w.out}$$

or

$$200 \cdot h_{d.a.1} + 100 \cdot h_{d.a.2} + 0.02 \cdot 200 \cdot h_{w.v.1} + 0.01 \cdot 100 \cdot h_{w.v.2} = 300 \cdot h_{d.a.} + 0.0167 \cdot 300 \cdot h_{w.v.}$$

where, $h_{d.a.1}$, $h_{d.a.2,}$ $h_{d.a.}$ and $h_{w.1}$, $h_{w.2,}$ $h_{w.}$ are the values of specific enthalpies of dry air and water vapor for the entering and exiting streams, respectively (kJ/kg).

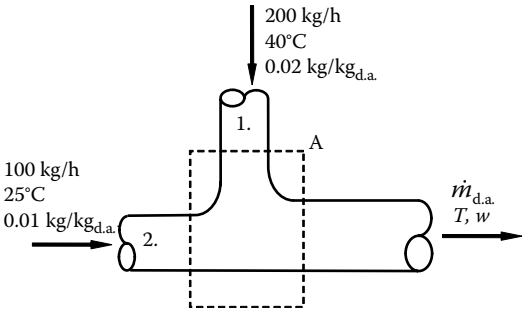


FIGURE 2.10 Adiabatic mixing of air streams.

The calculation of specific enthalpy values can be done through Equations 2.23 and 2.24.

$$h_{d.a.1} = 1.006 \cdot 40 = 40.2 \text{ kJ/kg},\ h_{d.a.2} = 1.006 \cdot 25 = 25.1 \text{ kJ/kg},$$

$$h_{w.v.1} = 2501 + 1.86 \cdot 40 = 2575.4 \text{ kJ/kg}$$

and

$$h_{w.v.2} = 2501 + 1.86 \cdot 25 = 2547.5 \text{ kJ/kg}$$

Substituting in the energy balance equation

$$200 \cdot 40.2 + 100 \cdot 25.1 + 4 \cdot 2575.4 + 1 \cdot 2547.5 = 300 \cdot 1.006 \cdot T + 5 \cdot (2501 + 1.86 \cdot T)$$

Solving for T, the dry bulb temperature of the exiting stream of air is found to be

$$T = 35°C$$

EXAMPLE 2.7: ENERGY BALANCE IN ORANGE JUICE RECONSTITUTION

Orange juice with a mass concentration of 12% in total solids (T.S.) is reconstituted by mixing pure water at 20°C with frozen orange juice concentrate at –15°C containing 48% (T.S.). Calculate the temperature and the required quantities of water and orange juice concentrate per kg of the final product. Consider that the process is adiabatic, the mean specific heats of ice, water, and total solids are 2.0, 4.18, and 1.57 kJ/kg K, respectively, and that the latent heat of fusion of water at 0°C is 333.2 kJ/kg.

A flow diagram of the process is shown in Figure 2.11, where m_c and m_w are the required masses of orange juice concentrate and water, respectively, and T is the temperature in °C of the reconstituted orange juice. The basis of calculations will be 1 kg of the final product, while the reference value of specific enthalpy of water liquid and total solids will be assumed zero at 0°C. We will also assume that there is no freezing point depression of water due to soluble solids concentration. Applying mass balances for total mass and solids we may write the following equations:

$$m_c + m_w = 1$$

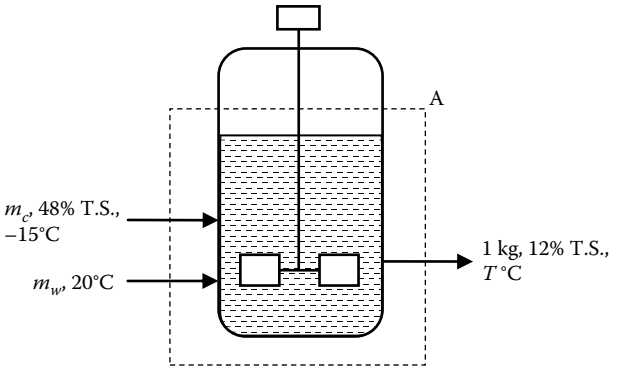


FIGURE 2.11 Energy balance in orange juice reconstitution.

and

$$0.48\, m_c = 0.12 \times 1$$

Thus, $m_c = 0.25$ kg and $m_w = 0.75$ kg.

Note that the mixing mass proportion of juice concentrate to water is 1 per 3 parts.

Since the process is adiabatic (no heat gain or loss) we may use Equation 2.28 for a total energy balance as

$$H_{c,in} + H_{w,in} = H_{p,out}$$

or

$$0.25 \cdot h_{c,in} + 0.75 \cdot h_{w,in} = 1 \cdot h_{p,out}$$

where $h_{c,in}$, $h_{w,in}$, and $h_{p,out}$ are the specific enthalpies of juice concentrate, water, and final product, respectively. Considering that the entering and exiting streams consist of ice, water, and total solids and taking into account the composition of each stream we may write using Equations 2.21 and 2.22,

$$h_{c,in} = 0.52c_{p,ice}(-15 - 0) + 0.48c_{p,T.S.}(-15 - 0) + 0.52\Delta h_{fusion}$$

or

$$h_{c,in} = -0.52 \times 15c_{p,ice} - 0.48 \times 15c_{p,T.S.} - 0.52 \times 333.2$$

and

$$h_{w,in} = c_{p,w}(20 - 0)$$

where, $c_{p,ice}$, $c_{p,w}$, and $c_{p,T.S.}$ are the mean specific heats of ice, water, and total solids, respectively. Note that the latent heat of fusion is taken here to be negative since heat is rejected when water freezes to ice at 0°C. The specific enthalpy of the reconstituted orange juice may be calculated by the equation

$$h_{p,out} = 0.88c_{p,w}(T - 0) + 0.12c_{p,T.S.}(T - 0)$$

Substituting in the above total energy balance equation

$$0.25\ (-0.52 \times 15c_{p,ice} - 0.48 \times 15c_{p,T.S.} - 0.52 \times 333.2) + 0.75c_{p,w}(20) = 1 \times (0.88c_{p,w} + 0.12 \times c_{p,T.S.}) \cdot T$$

or

$$0.25\ (-0.52 \times 15 \times 2 - 0.48 \times 15 \times 1.57 - 0.52 \times 333.2) + 0.75 \times 4.18 \times 20 = (0.88 \times 4.18 + 0.12 \times 1.57) \cdot T$$

Solving for the temperature T of the reconstituted orange juice

$$T = 3.3°\text{C}.$$

EXAMPLE 2.8: ENERGY BALANCE IN MILK PASTEURIZATION

In cheese manufacturing, chilled raw milk at 4°C is pasteurized in a plate heat exchanger at 72°C followed by cooling at 30°C prior to its ripening by the addition of lactic acid bacteria. Calculate the steam consumption and cooling water demand in kg/h. Given, the fresh milk throughput is 4 tons/h, the steam and condensate are saturated at 1.5 bar, the cooling water enters the exchanger at 15°C and leaves at 55°C, the mean specific heats of milk and cooling water are 3.89 and 4.18 kJ/kg K, respectively. If in the above example heat is regenerated by recycling the stream of hot milk, what will be the % economy of steam and cooling water? Assume that there are no heat losses.

A flow diagram of the pasteurization process is shown in Figure 2.12. The unit consists of a heating and a cooling section of the plate heat exchanger (boundaries A and B, respectively). Note that the temperature of steam and condensate is found from the thermodynamic tables 111.4°C since both are saturated at 1.5 bar. For the ease of calculations we will assume that the reference enthalpy values of milk and cooling water are 0 at 0°C (Equation 2.21). Taking 1 h of operation as the basis of calculations and m_s, $m_{c.w.}$, the masses in kg of steam (or condensate) and cooling water, respectively, we may apply Equation 2.28 around the heating section of the heat exchanger (boundary A) as

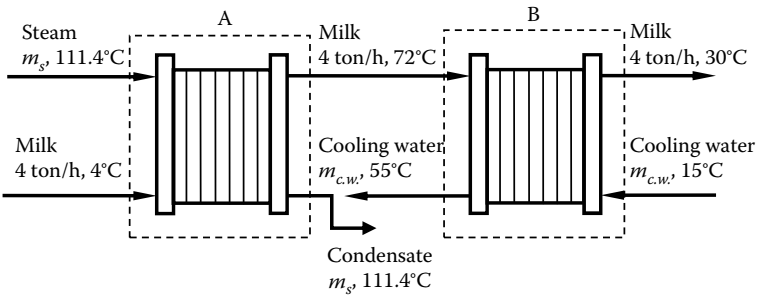


FIGURE 2.12 Energy balance in milk pasteurization.

$$H_{tot.in} = H_{tot.out}$$

or

$$H_{steam,in} + H_{milk,in} = H_{steam,out} + H_{milk,out}$$

or

$$m_s \cdot h_g + 4000 \cdot 3.89 \cdot (4 - 0) = m_s \cdot h_f + 4000 \cdot 3.89 \cdot (72 - 0)$$

or

$$m_s \cdot (h_g - h_f) = 4000 \cdot 3.89 \cdot (72 - 4)$$

or

$$m_s \cdot \Delta h_{fg} = 4000 \cdot 3.89 \cdot (72 - 4)$$

or

$$m_s = \frac{4000 \cdot 3.89 \cdot (72 - 4)}{2226} = 475.3 \text{ kg}$$

Thus, the steam consumption is 475 kg/h.

Note that, h_g and h_f are the specific enthalpies of saturated water vapor and liquid, respectively, while the difference Δh_{fg} represents the latent heat of steam condensation found as 2226 kJ/kg from the thermodynamic water and steam tables.

Now, focusing on the cooling section of the heat exchanger (boundary B) the energy balance can be written as

$$H_{c.w.,in} + H_{milk,in} = H_{c.w.,out} + H_{milk,out}$$

or

$$m_{c.w.}4.18 \cdot (15 - 0) + 4000 \cdot 3.89 \cdot (72 - 0) = m_{c.w.}4.18 \cdot (55 - 0) + 4000 \cdot 3.89 \cdot (30 \cdot 0)$$

or

$$4000 \cdot 3.89 \cdot (72 - 30) = m_{c.w.} \cdot 4.18 \cdot (55 - 15)$$

or

$$m_{c.w.} = \frac{4000 \cdot 3.89 \cdot 42}{4.18 \cdot 40} = 3908.6 \text{ kg}$$

Thus, the demand for cooling water is 3.908 ton/h.

Note that in the application of the above energy balances the heat losses were neglected. In the case where the heat losses are significant they must be added to the second part of Equation 2.28 (heat rejected from the system).

As it has already been said recycling of streams in food engineering may increase the energy efficiency of the process. The above example is a typical case where heat can be regenerated by recycling the hot stream of milk. Figure 2.13 depicts an arrangement where the hot milk stream of 72°C is used to preheat the entering stream of 4°C. At the same time, the hot stream is cooled to the desired temperature of 30°C without any demand for cooling water. The heat exchanger is divided into the heat regeneration section (boundary A) and the heating section (boundary B). Considering T as the temperature in °C of the milk stream leaving the regeneration section and applying an energy balance around boundary A, we have

$$H_{milk,in,4°C} + H_{milk,in,72°C} = H_{milk,out,30°C} + H_{milk,out,T}$$

or

$$4000 \cdot 3.89 \cdot (4 - 0) + 4000 \cdot 3.89 \cdot (72 - 0) = 4000 \cdot 3.89 \cdot (30 - 0) + 4000 \cdot 3.89 \cdot (T - 0)$$

or

$$T = 72 + 4 - 30 = 46°C$$

The steam consumption can now be found by applying another energy balance around boundary B.

$$H_{steam,in} + H_{milk,in} = H_{steam,out} + H_{milk,out}$$

or

$$m_s \cdot h_g + 4000 \cdot 3.89 \cdot (46 - 0) = m_s \cdot h_f + 4000 \cdot 3.89 \cdot (72 - 0)$$

or

$$m_s \cdot \Delta h_{fg} = 4000 \cdot 3.89 \cdot (72 - 46)$$

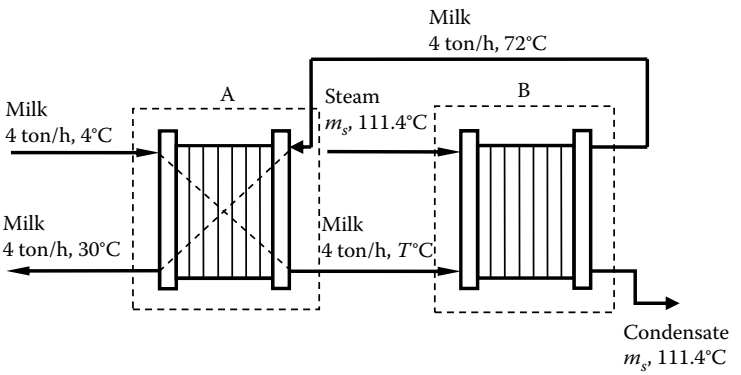


FIGURE 2.13 Energy balance in milk pasteurization with heat regeneration.

or

$$m_s = \frac{4000 \cdot 3.89 \cdot (72 - 46)}{2226} = 181.7 \text{ kg}$$

Thus, the steam consumption is 181.7 kg/h.
The % economy of steam is calculated as

$$\% \text{ steam economy} = \frac{475.4 - 181.7}{475.4} \times 100 = 61.8\%$$

The economy in cooling water is 100% since under the particular conditions of the above example there is no need for it. From the foregoing it is well understood that preheating of the cold streams by recycling the hot ones can be a common practice for heat regeneration in heat exchangers. Although an additional cost may arise by the necessary increase in heat exchanger's surface, this cost is mostly justified by the economy done on heating (and/or cooling) medium's consumption.

In the following sections, examples of coupled mass and energy balances are presented.

EXAMPLE 2.9: ENERGY BALANCE IN DIRECT STEAM INJECTION

A stream of 200 kg/h of tomato pulp with 7% total solids is heated by direct saturated steam injection at atmospheric pressure from 20°C to 90°C. If 8% of the heat supplied by steam is lost to ambient air, calculate the steam consumption, the composition, and the mass flow rate of the final product. Given, the mean specific heat capacities of water and total solids, 4.18 and 1.8 kJ/kg K, respectively.

Figure 2.14 depicts the steam injection flow diagram of the above example. The mass of steam is condensed and mixed with the pulp supplying its heat of condensation for heating the pulp from 20°C to 90°C. The basis of calculations is taken as 1 h of operation and m_s, m_p, are the masses in kg of steam and produced pulp, respectively, with X its total solids mass fraction. The reference value of specific enthalpy for total solids and water liquid is taken as 0 at 0°C (Equation 2.21). Applying mass balances for total mass and water we may write

$$200 + m_s = m_p$$

and

$$200 \times 0.93 + m_s = (1 - X) \cdot m_p$$

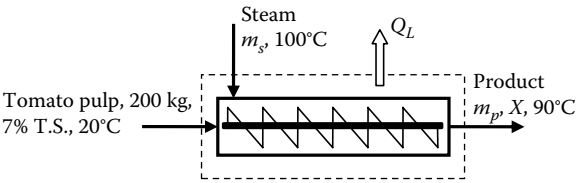


FIGURE 2.14 Mass and energy balance in direct steam injection.

or

$$186 + m_s = (1 - X) \cdot m_p$$

We may also apply Equation 2.27 considering that the mechanical work (for mixing and transportation) is negligible compared to heat.

$$H_{tot.in} = H_{tot.out} + Q_L$$

or

$$H_{steam,in} + H_{pulp,in} = H_{pulp,out} + Q_L$$

where, Q_L are the heat losses added to the second part of the equation since it is by convention negative (heat rejected from the system). Introducing the specific enthalpies of saturated steam h_g, of water h_w and of total solids $h_{t.s.}$ to the above equation we may write

$$m_s \cdot h_g + 0.93 \cdot 200 \cdot h_{w.,20} + 0.07 \cdot 200 \cdot h_{t.s.,20} = (1 - X) \cdot m_p \cdot h_{w.,90} + X \cdot m_p\, h_{t.s.,90} + Q_L$$

$$m_s \cdot 2676 + 186 \cdot 4.18 \cdot (20 - 0) + 14 \cdot 1.8 \cdot (20 - 0) = (1 - X) \cdot m_p \cdot 4.18 \cdot (90 - 0) + X \cdot m_p \cdot 1.8 \cdot (90 - 0) + Q_L$$

or

$$m_s \cdot 2676 + 16053.6 = 376.2 \cdot (1 - \mathrm{X}) \cdot m_p + 162 \cdot X \cdot m_p + Q_L$$

or

$$m_s \cdot 2676 + 16053.6 = 376.2 \cdot m_p - 214.2 \cdot X \cdot m_p + Q_L$$

The amount of heat losses equals the 8% of the heat supplied by the saturated steam that is condensed to water liquid at 90°C under atmospheric pressure. Thus,

$$Q_L = 0.08 \cdot (H_{steam,in} - H_{w.,90})$$

or

$$Q_L = 0.08 \cdot (m_s \cdot h_g - m_s \cdot h_{w.,90})$$

or

$$Q_L = 0.08 \cdot m_s \cdot (h_g - h_{w.,90})$$

or

$$Q_L = 0.08 \cdot m_s \cdot (2676 - 4.18 \cdot 90)$$

or

$$Q_L = 184 \cdot m_s$$

Substituting to the energy balance equation and rearranging,

$$2492 \cdot m_s + 16053.6 = m_p\,(376.2 - 214.2 \cdot X)$$

Solving the set of the three mass and energy balance equations

$$m_s = 26.5, \quad m_p = 226.5, \quad \text{and} \quad X = 0.06$$

Thus, the steam consumption is 26.5 kg/h and the produced pulp rate is 226.5 kg/h with 6% total solids.

EXAMPLE 2.10: ENERGY BALANCE IN MILK POWDER PRODUCTION

Milk powder is produced by spray drying of concentrated milk, at a rate of 100 kg/h with 4% moisture content at 40°C. Fresh air at 25°C and 0.01 $kg/kg_{d.a.}$ specific humidity is heated to 120°C before its entrance to the spray drier and leaves at 75°C. The concentrated milk with 48% in total solids (T.S.) is produced in a vacuum evaporator at 45°C using fresh milk with 12% (T.S.) at 20°C. The evaporator uses saturated steam at atmospheric pressure and the water evaporated is condensed by using cooling water that enters the condenser at 15°C and leaves at 35°C. Calculate the specific humidity of the air leaving the spray drier, the mass flow rate of dry air, the heating load of the air heater, the steam consumption, and the cooling water demand. The specific heat capacities of water and milk total solids are given as 4.18 and 1.8 kJ/kg K, respectively.

A flow diagram of the above process is shown in Figure 2.15. For the ease of calculations the basis will be 1 h of operation. Let m_f be the mass of fresh milk

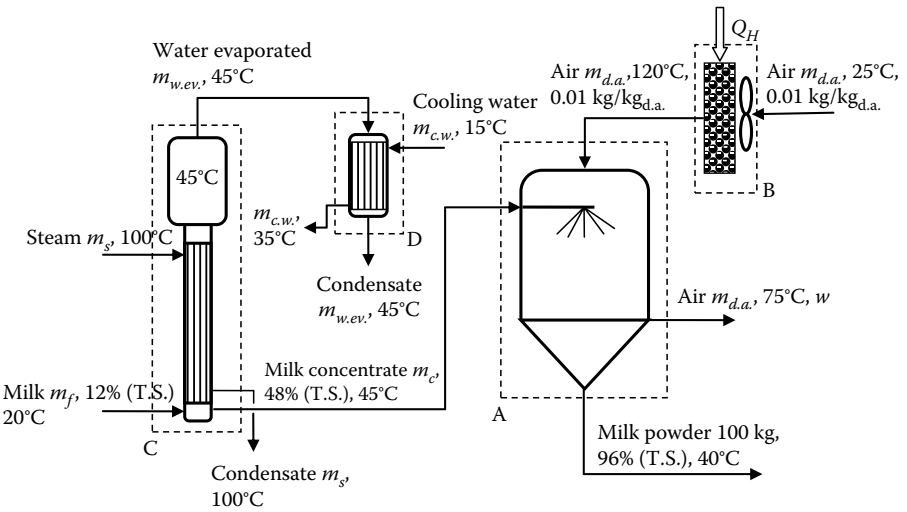


FIGURE 2.15 Mass and energy balance in milk powder production.

entering the evaporator (kg), m_s the mass of steam consumed (kg), m_c the mass of milk concentrate (kg), $m_{w.ev.}$ the mass of water evaporated (kg), $m_{c.w.}$ the mass of cooling water (kg), $m_{d.a.}$ the mass of dry air (kg), w the air's specific humidity (kg/$kg_{d.a.}$) leaving the spray drier, and Q_H the heating load of the air heater (kJ). The reference value of specific enthalpy for milk solids and water liquid is taken as 0 at 0°C (Equation 2.21). We will also assume that there are no heat losses from the evaporator's or the spray drier's units.

The mass balance for total solids of milk around the spray drier (boundary A) leads to

$$0.48 \cdot m_c = 0.96 \cdot 100$$

or

$$m_c = 200 \text{ kg}$$

Applying a mass balance for water in the same boundary

$$0.52 \cdot m_c + 0.01 \cdot m_{d.a.} = 0.04 \cdot 100 + w \cdot m_{d.a.}$$

or

$$m_{d.a.} (w - 0.01) = 100 \tag{2.i}$$

The energy balance around boundary A (Equation 2.28) gives

$$H_{tot.in} = H_{tot.out}$$

or

$$H_{T.S.in} + H_{w.in} + H_{d.a.in} + H_{w.v.in} = H_{T.S.out} + H_{w.out} + H_{d.a.out} + H_{w.v.out}$$

where, $H_{T.S.}$, H_w, $H_{d.a.}$, $H_{w.v.}$ are the enthalpies of milk solids, water, dry air, and water vapor, respectively, in kJ. The enthalpies of milk solids and water can be calculated by applying Equation 2.21, while the enthalpies of dry air and water vapor are calculated through Equations 2.23 and 2.24, respectively. Substituting in the above equation and taking into account that the air's specific humidity does not change with heating,

$$\begin{aligned} &0.48 \cdot 200 \cdot 1.8 \cdot (45 - 0) + 0.52 \cdot 200 \cdot 4.18 \cdot (45 - 0) + m_{d.a.} \cdot 1.006 \cdot 120 \\ &\quad + 0.01 \cdot m_{d.a.} (2501 + 1.86 \cdot 120) = 0.96 \cdot 100 \cdot 1.8 \cdot (40 - 0) \\ &\quad + 0.04 \cdot 100 \cdot 4.18 \cdot (40 - 0) + m_{d.a.} \cdot 1.006 \cdot 75 + w \cdot m_{d.a.} (2501 + 1.86 \cdot 75) \end{aligned}$$

or

$$\begin{aligned} &7776 + 19562.4 + m_{d.a.} \cdot 120.7 + m_{d.a.} \cdot 27.2 = 6912 + 668.8 \\ &\quad + m_{d.a.} \cdot 75.5 + m_{d.a.} \cdot w \cdot 2640.5 \end{aligned}$$

or

$$m_{d.a.} \cdot (2640.5w - 72.4) = 19757.6 \tag{2.ii}$$

Solving the system of equations (2.i) and (2.ii) resulting from the mass and energy balance application

$w = 0.028828$ kg/kg$_{d.a.}$ and $m_{d.a.} = 5311.3$ kg. Accounting for 1 h of operation the mass flow rate of dry air is 5311.3 kg/h.

Now, focusing on the air heater (boundary B) and neglecting the mechanical work of the air blower, Equation 2.27 gives

$$Q_H = H_{air\ out} - H_{air\ in}$$

or

$$Q_H = m_{d.a.}\ h_{d.a.out} + w_{out} m_{d.a.}\ h_{w.v.out} - m_{d.a.}\ h_{d.a.in} - w_{in} m_{d.a.}\ h_{w.v.in}$$

or

$$Q_H = m_{d.a.}\ (h_{d.a.out} + w_{out} h_{w.v.out} - h_{d.a.in} - w_{in} h_{w.v.in})$$

where, $h_{d.a.}$ and $h_{w.v.}$ are the specific enthalpies of dry air and water vapor calculated through Equations 2.23 and 2.24, respectively, while w_{in} and w_{out} are the air's specific humidity at the heater's inlet and outlet, respectively. As mentioned earlier the values of w_{in} and w_{out} are equal to 0.01 kg/kg$_{d.a.}$. Substituting values

$$Q_H = 5311.3(1.006 \times 120 + 0.01(2501 + 1.86 \times 120) \\ -1.006 \times 25 - 0.01(2501 + 1.86 \times 25))$$

or

$$Q_H = 5311.3(1.006(120 - 25) + 0.01 \times 1.86(120 - 25))$$

or

$$Q_H = 5311.3(120 - 25)(1.006 + 0.01 \times 1.86)$$

or

$$Q_H = 516{,}986 \text{ kJ}$$

Since the basis of the calculations was taken at 1 h, the heating load of the air heater is found to be

$$\dot{Q}_H = \frac{516{,}986}{3600} = 143.6 \text{ kW}$$

Now let us pay attention to the evaporator (boundary C). The total milk solids mass balance application gives

$$0.12 \cdot m_f = 0.48 \cdot m_c$$

or

$$m_f = \frac{0.48}{0.12} \cdot 200$$

or

$$m_f = 800 \text{ kg}$$

The total mass balance in the same boundary is written as

$$m_f + m_s = m_c + m_s + m_{w.ev.}$$

or

$$m_{w.ev.} = m_f - m_c$$

or

$$m_{w.ev.} = 800 - 200 = 600 \text{ kg}$$

Applying an energy balance (Equation 2.28) around evaporator (boundary C) we have

$$H_{tot.in} = H_{tot.out}$$

or

$$H_{T.S.in} + H_{w.in} + H_{s.in} = H_{T.S.out} + H_{w.out} + H_{c.out} + H_{w.ev.}$$

where, $H_{T.S.}$, H_w, H_s, H_c, $H_{w.ev.}$ are the enthalpies of milk total solids, water, steam, condensate, and water evaporated, respectively, in kJ. Substituting with the specific enthalpies of entering and exiting components in the above equation

$$0.12m_f 1.8(20 - 0) + 0.88m_f 4.18(20 - 0) + m_s h_{g,100} = 0.48m_c 1.8(45 - 0) + 0.52m_c\ 4.18(45 - 0) + m_s h_{f,100} + m_{w.ev.} h_{g,45}$$

where, $h_{g,100}$ and $h_{g,45}$ are the specific enthalpies of saturated steam at 100°C and 45°C, respectively, and $h_{f,100}$ is the specific enthalpy of saturated water (condensate) at 100°C. The values of these specific enthalpies can be found in saturated water and steam tables as $h_{g,100} = 2676$ kJ/kg, $h_{f,100} = 419.1$ kJ/kg, and $h_{g,45} = 2583.3$ kJ/kg. Substituting values in the energy equation

$$0.12 \times 800 \times 1.8 \times 20 + 0.88 \times 800 \times 4.18 \times 20 + m_s 2676 = 0.48 \times 200 \times 1.8 \times 45 + 0.52 \times 200 \times 4.18 \times 45 + m_s\ 419.1 + 600 \times 2583.3$$

or

$$3456 + 58854.4 + m_s\ (2676 - 419.1) = 7776 + 19562.4 + 1{,}549{,}980$$

or

$$m_s \cdot 2256.9 = 1{,}515{,}008$$

or

$$m_s = \frac{1{,}515{,}008}{2256.9} = 671.28\ \text{kg}$$

Thus, for 1 h of operation the steam consumption will be 671.3 kg/h.

For the calculation of cooling water rate we will apply an energy balance (Equation 2.28) around the condenser (boundary D in Figure 2.15).

$$H_{tot.in} = H_{tot.out}$$

or

$$H_{w.ev.in} + H_{c.w.in} = H_{c.out} + H_{c.w.out}$$

where, $H_{c.w.}$ is the enthalpy of cooling water in kJ. Substituting in terms of specific enthalpies

$$m_{w.ev.}\ h_{g,45} + m_{c.w.}\ 4.18(15 - 0) = m_{w.ev.}\ h_{f,45} + m_{c.w.}\ 4.18(35 - 0)$$

or

$$600(h_{g,45} - h_{f,45}) = m_{c.w.}4.18(35 - 15)$$

or

$$600\Delta h_{fg,45} = m_{c.w.}4.18(35 - 15)$$

where, $\Delta h_{fg,45}$ is the latent heat of evaporation (or condensation) of water at 45°C found as 2394.9 kJ/kg from thermodynamic tables of water and steam. Substituting,

$$600 \times 2394.9 = m_{c.w.}83.6$$

or

$$m_{c.w.} = \frac{1{,}436{,}940}{83.6} = 17188.3\ \text{kg}$$

Thus, the cooling water demand is 17188.3 kg/h or about 17.2 ton/h.

For the simplicity of mass and energy balance calculations in the above example the processing of milk concentrate was chosen to be done in a one-stage vacuum evaporator. In practice, vacuum evaporators of at least three stages (triple effect) are used since the evaporated water from one stage can be used as the heating medium to a subsequent stage at a lower temperature (Brennan et al., 1990).

The increased capital cost of a multiple effect evaporator is thus justified by the significant economy achieved in steam and cooling water consumption. A further decrease in the production cost of the above process can be achieved by recycling the air exiting from the spray drier and mixing with the stream of fresh air at 25°C. Inevitably, a complete process design would require more complex mass and energy balance calculations than the ones presented in the examples of this chapter. The complexity of calculations is further increased by optimizing the operating and capital cost of the process taking into account several technical, economical, and environmental limitations. For further reading please refer to Fryer et al. (1997); Heldman and Lund (2007); Sing and Heldman (2009); Toledo, R.T. (2007); Valentas et al. (1997); Harper, C.J. (1976) and Charm (1971).

PROBLEMS

1. Whole fat milk with 3.5% fat, 3.5% protein, 4.9% carbohydrate, 0.7 ash, and 87.4% moisture is reconstituted by mixing 1 part of milk concentrate with 1.4 parts of water. Calculate the composition of the milk concentrate.
2. In bread manufacturing the dough is made by mixing 58.5% flour, 33% water, 3.5% sugar, 1.5% vegetable oil, 1.5% milk protein, 1% salt, and 1% yeast. If 11% of the water contained in dough is lost during baking and cooling, calculate the required amounts of the above ingredients to produce 1 ton of bread per hour.
3. Tomato paste containing 35% total solids (T.S.) is produced at a rate of 2 ton/h by evaporation. Prior to evaporation, raw tomatoes with 7% (T.S.) are washed and inspected where 1.5% of the feed is rejected and the process continues with pulping and finishing where 4% of the entering stream is removed as skin, cores, and seeds with 32% (T.S.). Calculate the mass flow rate and composition in each stream of the process.
4. Carrot slices with 12% total solids (T.S.) are dried in a continuous tunnel drier to a final moisture content of 4.2% in dry basis (d.b.). Air enters at a rate of 10 m^3/s with 0.01 $kg/kg_{d.a.}$ specific humidity and 1.02 $m^3/kg_{d.a.}$ specific volume, and leaves the drier at a specific humidity of 0.02 $kg/kg_{d.a.}$. Calculate the feed and production rates of carrot slices in kg/h.
5. Hot water at 85°C is made by direct mixing of steam at atmospheric pressure and tap water at 15°C. Calculate the steam consumption in kg of steam per kg of tap water. Assume a mean specific heat capacity of 4.18 kJ/kg K for water and neglect any heat loss.
6. Mashed potatoes with 78% moisture content (w.b.) at 40°C are dehydrated in a drum drier under atmospheric pressure to produce flakes with 7% moisture content (d.b.) at 70°C. If the drum is fed with saturated steam at 2 bar calculate the rate of the water evaporated and the steam consumption considering a production rate of 100 kg/h. The mean specific heat capacities for water liquid and total solids are given as 4.18 and 1.71 kJ/kg K, respectively. Assume negligible heat losses and boiling point elevation.
7. Frozen green peas are produced at a rate of 1 ton/h in the following stages. In the first stage, peeled green peas at 20°C containing 20.4% total solids are blanched by steam at atmospheric pressure in order to deactivate oxidative

enzymes. In the second stage, the green peas are cooled from 90°C to 25°C using 3.2 ton/h of cooling water at 10°C. In the third stage, green peas are frozen in a fluidized-bed freezer at –18°C. Calculate the steam consumption, the cooling load of the freezer in kW, and the final temperature of the cooling water. The mean specific heat capacities for water liquid, ice, and total solids are given as 4.18, 2.0, and 1.81 kJ/kg K, respectively, while the latent heat of steam condensation at atmospheric pressure is 2257 kJ/kg and the latent heat of fusion of water at 0°C is 333.2 kJ/kg. Assume negligible heat losses and freezing point depression.

8. Apricot jam is made by mixing 1 part of crushed fruit containing 11.2% total solids (T.S.) in which 0.7% is pectin, with 1 part of sugar, and an additional amount of pectin. The mixture is then brought to boil under atmospheric pressure until its total solids content becomes 68% in which 1% pectin is included. Considering a jam production rate of 100 kg/h, calculate the mass flow rates of apricot, sugar, pectin, and evaporated water. If the initial temperature of all ingredients is 20°C, calculate the required heat rate in kW assuming negligible boiling point elevation. The mean specific heat capacities for total solids and liquid water are given as 1.65and 4.18 kJ/kg K, respectively.
9. A portion of the air leaving the spray drier in example 2.10 is recycled and mixed with fresh air at 25°C and 0.01 $kg/kg_{d.a.}$ specific humidity. If the specific humidity of the resulting mixture is 0.02 $kg/kg_{d.a.}$ calculate the specific humidity of the air leaving the spray drier, the mass flow rate of dry air, the percentage of the recycled air, the heating load of the air heater, and the % economy done in comparison to the results of the above example. Try to solve the problem using a spreadsheet and observe the change in the percentage of the recycled air and the % economy by changing the value of specific humidity of the mixture. Comment on the results.
10. Calculate the % economy achieved in steam and cooling water consumption if the evaporation of milk in Example 2.10 is done (a) in two stages at 70°C and 45°C or (b) in three stages at 70°C, 57°C, and 45°C, respectively. Comment on the results.

LIST OF SYMBOLS

c	specific heat capacity (J/kg K)
E	energy (J)
H	enthalpy (J)
h	specific enthalpy (J/kg)
L	latent heat (J/kg)
m	mass (kg)
$\dot{m}$	mass flow rate (kg/s)
P	pressure (N/m^2)
Q	heat (J)
t	time (s)
T	temperature (°C) or (K)

U	internal energy (J)
u	specific internal energy (J/kg)
V	volume (m^3)
$\dot{V}$	volumetric flow rate (m^3/s)
v	specific volume (m^3/kg)
X, Y	mass fraction
ρ	density (kg/m^3)

SUBSCRIPTS

c	concentrate
d.a.	dry air
d.b.	dry basis
d.s.	dry solids
f	feed
i	inlet, inside
o	outlet, outside
p	product
ref	reference value
sys	system
T.S.	total solids
tot	total
w.b.	wet basis
w.ev.	water evaporated
w.v.	water vapor

REFERENCES

Amos, N.D., Willix, J., Chadderton, T., and North, M.F., 2008. A compilation of correlation parameters for predicting the enthalpy and thermal conductivity of solid foods within the temperature range of –40°C to +40°C, *Int. Journal of Refrigeration*, 31:1293–1298.

ASHRAE, 2009. *ASHRAE Handbook-Fundamentals,* Published by the American Society of Heating, Refrigerting and Air Conditioning Engineers, Inc., Atlanta, GA.

Brennan, J.G., Butters, J.R., Cowell, N.D., and Lilly, A.E.V., 1990. *Food Engineering Operations*, 3rd ed., Applied Science Publishers, London.

Charm, S.E., 1971. *The Fundamentals of Food Engineering*, 2nd ed., AVI Publishing Co., Westport, Connecticut.

Choi, Y., and Okos, M.R., 1986. Effects of temperature and composition on the thermal properties of foods, *Food Engineering and Process Applications*, 1:93–102, Elsevier Applied Science Publishers.

Eastop, T.D., and McConkey A., 1986. *Applied Thermodynamics for Engineering Technologists*, 4th ed., Longman Group Ltd., London & New York.

Fricke, A.B., and Becker, R.B., 2001. Evaluation of physical property models for foods, *HVAC & R Research*, 7(4):311–330.

Fryer P.J., Pyle, D.L., and Rielly, C.D., 1997. *Chemical Engineering for the Food Industry*, Blackie A. & P., Chapman & Hall, London.

Harper, C.J., 1976. *Elements of Food Engineering*, AVI Publishing Co., Westport, Connecticut.

Haywood, R.W., 1990. *Thermodynamic Tables in SI Units*, 3rd ed., Cambridge University Press, Cambridge, UK.

Heldman, R.D., and Lund, B.D., 2007. *Handbook of Food Engineering*, CRC Press, Taylor & Francis Group, Boca Raton, London.

Maroulis, B.Z., and Saravacos, D.G., 2008. *Food Plant Economics*, CRC Press, Taylor & Francis Group, Boca Raton, New York.

Pham, Q.T., Wee H.K., Kemp R.M., and Lindsay D.T., 1994. Determination of the enthalpy of foods by an adiabatic calorimeter, *Journal of Food Engineering*, 21:137–156.

Sing, R.P., and Heldman, R.D., 2009. *Introduction to Food Engineering*, 4th ed., Academic Press, San Diego.

Toledo, R.T., 2007. *Fundamentals of Food Process Engineering*, 3rd ed., Van Nostrand Reinhold, New York.

USDA, 2013. *National Nutrient Database for Standard Reference, Release 26*, U.S. Department of Agriculture, Washington DC.

Valentas, J.K., Rotstein, E., and Singh R.P., 1997. *Handbook of Food Engineering Practice*. CRC Press, Boca Raton, New York.

3 Fundamental Notes on Chemical Thermodynamics

Petros Tzias

CONTENTS

3.1 Introduction 42
3.2 Scope 42
3.3 Glossary of Basic Thermodynamic Terms 43
3.3.1 System 44
3.3.2 Extensive and Intensive Properties 45
3.3.3 Phase 45
3.3.4 Process 45
3.3.5 Molar Quantities 45
3.3.6 Mole Fraction 46
3.3.7 Molality 46
3.4 Concepts of W, PE, KE, U, Q, and S 46
3.5 Thermodynamic Laws 47
3.5.1 First Law of Thermodynamics 48
3.5.2 Second Law of Thermodynamics 48
3.5.3 Third Law of Thermodynamics 48
3.5.4 Law of Thermal Equilibrium 48
3.6 Thermodynamic Functions and Some Relations for One-Phase Closed System 48
3.7 Fundamental Inequalities 50
3.8 Relations of Thermodynamic Functions in One-Phase Open System 51
3.9 Mixtures 54
3.9.1 Mixing Functions 54
3.9.2 Excess Functions 55
3.9.3 Standard and Reference States of Thermodynamic Functions 55
3.9.4 Dilution Thermodynamic Functions 55
3.10 Gases and Gaseous Mixtures 56
3.10.1 Fugacity 57
3.10.2 The Standard State of a Gas Component 58
3.11 Liquid Mixtures 58
3.12 Equilibrium of Phases 60

3.12.1 Phase Rule 60
3.12.2 Chemical Potential in Phase Equilibria 61
3.12.3 Binary Vapor–Liquid Systems 62
3.12.4 Principle of Corresponding States 64
3.12.5 Enthalpy and Entropy Change in a Two-Phase Transition 65
3.13 Solutions 66
3.14 Electrolyte Solution 68
3.14.1 Debye–Hückel Limiting Law 69
3.15 Thermochemistry: Chemical Reaction Equilibrium 70
3.15.1 Enthalpy of Formation and Enthalpy of Reaction 70
3.15.2 Determination of the Enthalpy of Reaction 71
3.15.3 Equilibrium Constant: Affinity of a Reaction 72
References 73

3.1 INTRODUCTION

Thermodynamics is a very useful tool for scientists and engineers such as chemists, geologists, geophysicists, mechanical and chemical engineers, and so on. Especially for chemists and chemical engineers with mathematics they form the cornerstone for their sciences.

It is very useful when we study a handbook comprising chapters from a certain field of chemical engineering to have some handy notes of thermodynamics because this way we are released from the need at any time to seek and open other textbooks for better understanding of what we read.

This is exactly the intention of this chapter. To provide a brief, elementary review of thermodynamics, reminding the reader of the basic laws, glossary, concepts, and relations of this important branch of science so as to make the study of the current volume much easier and pleasant.

This chapter is addressed, as the content of the whole volume, to chemical engineers or chemists, and for this reason after presenting a few clauses of general interest we will next proceed to clauses dealing with chemical thermodynamics that is with mixtures, solutions, phase equilibriums, chemical reactions, and so on.

Simple definitions of the different thermodynamic functions and quantities have been cited, and we will not enter to any analytical description or philosophical discussion about them. Similarly, we will not prove the mentioned thermodynamic relations, as these are beyond the scope of this chapter.

We will deal only with reversible processes, so far as an interest is in chemical thermodynamics, and we will not refer to statistical, as nuclear and relativistic phenomena.

3.2 SCOPE

Thermodynamics is a branch of physical sciences concerned with the study of the transformation of heat, work, and other kinds of energy (electrical, light energy, etc.) from one form to another, in the different physicochemical phenomena and determines the laws and relations governing and describing these energy transformations.

Historically [1] many scientists have studied the interconversion of heat and work, from N.L.S. Carnot with his famous ideal gas cycle, to Clausius who laid the foundation of the classical thermodynamics with the expression of the first and second law of thermodynamics.

Later, J. Willard Gibbs extended the application of the thermodynamic postulates and relations to chemical reactions and phase equilibriums laying the foundation for the development of the field, which we today call chemical thermodynamics.

Thermodynamics consists of a collection of equalities and inequalities which interrelate physical and chemical properties of substances as well as some physical or chemical phenomena. These relations are deduced in a mathematical way from some laws, the thermodynamic laws, which are derived directly from experience. The physical quantities used are taken either by physics or they are introduced in thermodynamics. Using these relations we can predict the possible direction of chemical reactions or the final result of a physical process.

Thermodynamics is an experimental science [2]. All the physical or chemical quantities used in its relations are independently measurable, but some of them are easier to be measured than others. One very important use of thermodynamics is the possibility to calculate, through its relations, quantities that are measured with difficulty or low accuracy by others measured easily and more accurately.

Another advantage is that, very often, through thermodynamic relations we can calculate the values of physical quantities from existing data of other physical quantities and avoiding by this way, from one part long and difficult experiments and from the other part saving time and money.

Therefore, it becomes obvious that thermodynamics can be a very useful tool to a chemist or a chemical engineer.

3.3 GLOSSARY OF BASIC THERMODYNAMIC TERMS [2–6]

There is a variety of thermodynamic terms, the most common of which are defined below, together with their SI units [3].

The amount of substance [2] N_B of an entity B is a physical quantity proportional to the number N_B of entities B in the system. The SI unit of the amount of substance is the *mol*.

Pressure, Volume, Temperature Pressure and volume are concepts coming from physics.

Pressure is defined as the ratio of a perpendicular force to a surface by the area of this surface. The SI unit of pressure is the Pa.

Volume (m^3) is the three-dimensional space occupied by a substance.

Specific volume (m^3/kg) is the volume per unit mass.

Molar volume is the volume divided by the amount of substance.

Density is the reciprocal of the specific volume.

Temperature is a fundamental concept used in thermodynamics and its definition is a very difficult matter. However, we could simply describe it as the degree of hotness of a substance or as the property of matter which has equal magnitude in systems where thermal flow does not exist [3].

Temperature scales [4]

- The Celsius scale (°C) is established by assigning the value 0.01°C to the triple point of water and the value 100°C to the boiling point of water at an atmospheric pressure of 1 standard atm (760 Torr).
- The absolute temperature scale (T) is a scale which is related to the Celsius scale by the relation:

$$T = t\ (°C) + 273.15$$

  T is given in degrees Kelvin. In this scale it is enough to define just one point and this is the triple of water equal to 273.16 K. The freezing point of water at 1 atm is 273.15 K.
- The ideal gas temperature scale defined as

$$T = 273.16\ K \lim_{P_{273.16} \to 0} \left(\frac{P_T}{P_{273.16}} \right)$$

  where P_T and $P_{273.16}$ are the pressures of a gas trapped in gas thermometer at the temperatures T and 273.16 K. The ideal gas temperature scale is the same with the absolute scale. Constant volume gas thermometers are used to determine the thermodynamic absolute temperatures.
- The International Practical Temperature Scale (IPTS-68).

  This scale gives the temperatures at some reproducible fixed points together with some interpolating instruments and functions, by which we find the temperatures between those points. The fixed points as well as the functions have been determined by constant volume gas thermometers. The IPTS gives the possibility by the above-mentioned instruments and functions to measure the absolute temperature in an easy and accurate way. In the literature [4] we can find temperatures at different fixed points as well as the instruments used to measure the absolute temperature between these points. In the system for the absolute temperature we use the degree K.

3.3.1 System

By *system* in thermodynamics we refer to any part of the real world we choose to study. All the remaining parts of the world are the *surroundings* of the system. By surroundings we consider the part of the world around the system which can interact with it.

A system is *closed* if no matter enters or leaves it during any stage of the process we study. Otherwise it is *open*. A system is called *isolated* if neither matter nor energy enters or leaves it.

The *state* of a system is defined by the values of its properties. *Properties* are physical quantities such as temperature, volume, pressure, and so on, which are related with a system and they have fixed values at any given state of the system. In order to define the state of a system it is not necessary to know the values of all its properties, but only a certain number of them, which are called independent and all the rest (dependent)

can be calculated by the values of the independent ones. Since a property is fixed by the state of a system it is also called a *state function*. A mathematical relationship between thermodynamic state functions is called an "equation of state."

3.3.2 Extensive and Intensive Properties

Considering that we divide a system into different parts, if for one property its value for the whole system is equal to the sum of its values for the different parts, then this property is called *extensive*. Extensive properties are the volume, mass, internal energy, and so on.

If a property has the same value in the whole system as well as in its different parts, then the property is called *intensive*. Intensive properties are the temperature, pressure, molar volume, density, and so on.

3.3.3 Phase

If for a system, throughout all its parts, all its intensive properties have the same value, then the system is a homogenous one and is called a *phase*. One system can consist of more than one phase. In that case, it is heterogeneous and some of its intensive properties have not the same value as all its parts.

One phase can be *open* when it exchanges matter either with its surroundings or with another phase within the system. In the opposite case it is called *closed*.

3.3.4 Process

Process is the pathway through which one system possess from one state to another.

If the volume of the system remains constant, the process is called *isometric* or *isochoric* and if the pressure remains constant the process is called *isobaric*. If during a process the temperature of the system remains constant, the process is called *isothermic,* if the volume of the system remains constant, the process is called *isometric* or *isochoric*, and if the pressure remains constant, the process is called *isobaric*. If no heat enters or leaves a system undergoing one process the system and the process are called *adiabatic*.

A process is called *reversible* if it takes place slowly and in such a way that at any stage of the process the properties of the system differ from equilibrium by infinitesimal amounts. Otherwise, the process is called *irreversible*. All natural processes are irreversible.

3.3.5 Molar Quantities

From any extensive quantity X of a phase it is defined as intensity quantity X_m by the relation:

$$X_m = \frac{X}{\sum_i n_i} \tag{3.1}$$

where $\sum_i n_i$ is the sum of the amounts of the different substances contained in this phase.

3.3.6 Mole Fraction

The mole fraction X_a of a substance a in a phase is defined by the ratio:

$$X_a = \frac{n_a}{\sum_i n_i} \tag{3.2}$$

where n_a is the amount of substance of a and $\sum_i n_i$ the sum of the amounts of all substances in this phase.

It follows immediately from the above definition that

$$\sum_i X_i = 1 \tag{3.3}$$

3.3.7 Molality

Molality *m* is the number of moles of a substance in 1 kg of solvent.

Molarity, *c* is the number of moles of a substance in 1 L of solvent.

Partial molar quantities

From any extensive quantity X of a phase we define an intensive quantity called the partial molar quantity X_a of the substance a in the phase by the relation:

$$X_a = \left(\frac{\partial X}{\partial n_a}\right)_{T,P,n_i \neq a} \tag{3.4}$$

where $n_i \neq a$ means all n's except n_a in this phase.

3.4 CONCEPTS OF W, PE, KE, U, Q, AND S [6–8]

W (work), PE (potential energy), and KE (kinetic energy) are concepts borrowed from physics.

Work (W) is the energy produced by a force (F) acting on a system and replacing it by a distance (ds) in the direction of the force and equals to

$$dW = F \cdot ds$$

In the case of a uniform pressure P acting on a system's wall of surface S and replacing it by a distance x, then

$$dW = -P \cdot s \cdot dx \quad \text{or} \quad dW = -P \cdot dV \tag{3.5}$$

By energy we mean the ability of a system to produce work.

Potential energy (PE) is the energy possessed by a system because of its position.

$$PE = m \cdot g \cdot h \tag{3.6}$$

where m is the mass of the system, g the gravity acceleration, and h the height of the system.

Kinetic energy (KE) is the energy possessed by a system of mass m, because of its velocity (υ) and is equal to

$$KE = \frac{m\upsilon^2}{2} \tag{3.7}$$

Internal energy (U) is the total energy, except potential and kinetic, contained within a system at a certain state. It is a magnitude determined by the state of a system. We cannot measure the absolute value of U, but only differences $\Delta U = U_2 - U_1$ between two states (1) and (2). ΔU depends only on the states (1) and (2) and not on the path followed to pass from one to the other.

Heat (Q) is the amount of energy, transferred from one system to another because of the difference in the temperature of the two systems. The amount of heat depends on the followed path and not on the original and final states of a procedure.

For a system receiving heat Q,

$$Q = C \cdot (T_2 - T_1) \tag{3.8}$$

where C is the heat capacity of the system and T_2, T_1 its final and original temperatures.

*The entropy (*S*)* (6) is an extensive property, depending on the state of a system. It can be defined as

$$dS = \frac{dQ}{T} \tag{3.9}$$

where dS is the heat received by it in reversible way at a temperature T. In natural processes S always increases and

$$dQ \leq T \cdot dS \tag{3.10}$$

The SI unit for W, PE, KE, and Q is the Joule.

The SI unit for S is Joule/K.

3.5 THERMODYNAMIC LAWS [2,5–7]

Thermodynamic laws come from experience and there is no exception to them. There are several expressions for these all equivalent with each other. Below are given the most common ones.

3.5.1 First Law of Thermodynamics

In any process, the total energy is conserved. In other words, there is no device that can create or eliminate energy.

Considering the transformation of heat to work or vice versa in a system the first law can be expressed as

$$dU = dW + dQ \tag{3.11}$$

where dU is the variation of internal energy of the system, dW is the work produced, and dQ is the heat transferred.

dU is an exact differential depending only on the original and final state of the system, but dQ and dW are not exact differentials depending on the pathway of the process.

By substituting Equations 3.5 and 3.9 into Equation 3.11 the first law can be expressed as

$$dU = -P \cdot dV + T \cdot dS \tag{3.12}$$

3.5.2 Second Law of Thermodynamics

It is not possible to transfer heat from a lower temperature to a higher temperature without the expenditure of work. In other words, in any process the total entropy of an isolated system increases.

3.5.3 Third Law of Thermodynamics

The expression of the third law is not possible without reference to statistical mechanics [2]. As expression for the third law we could give Planck's postulate [7]. "At 0 K the entropy of a pure crystalline is zero."

3.5.4 Law of Thermal Equilibrium

"If two systems are in thermal equilibrium with a third one, then they are also in thermal equilibrium between them."

This law is not an independent one but it is derived from the first and second thermodynamic laws [2].

3.6 THERMODYNAMIC FUNCTIONS AND SOME RELATIONS FOR ONE-PHASE CLOSED SYSTEM [6,7]

We have already met the properties P, V, T and the thermodynamic functions U, Q, W, and S for the last two functions: $W = -P \cdot dV$ and $S = dQ/T$.

Furthermore, there are the following very important thermodynamic functions:

$$\textit{Enthalpy}\ H = U + P \cdot V \tag{3.13}$$

$$\textit{Helmholtz free energy} \quad A = U - T \cdot S \tag{3.14}$$

and the Gibbs energy or Gibbs function

$$G = H - T \cdot S = A + P \cdot V = U - T \cdot S + P \cdot V \tag{3.15}$$

All the three functions are state functions and they have the dimensions of energy.

Since they are state functions their differentials are exact differentials and for reversible processes we have

$$dH = T \cdot dS + V \cdot dP \tag{3.16}$$

$$dA = -S \cdot dT + V \cdot dP \tag{3.17}$$

$$dG = -S \cdot dT + V \cdot dP \tag{3.18}$$

By applying the properties at exact differentials we can obtain the following very useful relations:

$$\left(\frac{\partial U}{\partial V}\right)_S = -P, \left(\frac{\partial U}{\partial S}\right)_V = T \tag{3.19}$$

$$\left(\frac{\partial A}{\partial T}\right)_V = -S, \left(\frac{\partial A}{\partial V}\right)_T = -P \tag{3.20}$$

$$\left(\frac{\partial G}{\partial P}\right)_T = V, \left(\frac{\partial G}{\partial T}\right)_P = -S \tag{3.21}$$

$$\left(\frac{\partial H}{\partial S}\right)_P = T, \left(\frac{\partial H}{\partial P}\right)_S = V \tag{3.22}$$

and also the following:

$$\left(\frac{\partial T}{\partial V}\right)_S = -\left(\frac{\partial P}{\partial S}\right)_V \tag{3.23}$$

$$\left(\frac{\partial T}{\partial P}\right)_S = \left(\frac{\partial V}{\partial S}\right)_P \tag{3.24}$$

$$\left(\frac{\partial S}{\partial V}\right)_T = \left(\frac{\partial P}{\partial T}\right)_V \tag{3.25}$$

$$\left(\frac{\partial S}{\partial P}\right)_T = -\left(\frac{\partial V}{\partial T}\right)_P \tag{3.26}$$

$$\left(\frac{\partial P}{\partial T}\right)_V \left(\frac{\partial T}{\partial V}\right)_P \left(\frac{\partial V}{\partial P}\right)_T = -1 \tag{3.27}$$

$$a = \frac{1}{V}\left(\frac{\partial T}{\partial V}\right)_P \text{ is the coefficient of thermal expansion} \tag{3.28}$$

$$K = -\frac{1}{V}\left(\frac{\partial V}{\partial P}\right)_T \text{ is the isothermal compressibility} \tag{3.29}$$

$$K_S = -\frac{1}{V}\left(\frac{\partial V}{\partial P}\right)_S \text{ is the adiabatic compressibility} \tag{3.30}$$

$$C_V = \left(\frac{\partial U}{\partial T}\right)_V \text{ is the heat capacity at constant volume} \tag{3.31}$$

$$C_P = \left(\frac{\partial H}{\partial T}\right)_P \text{ is the heat capacity at constant pressure} \tag{3.32}$$

3.7 FUNDAMENTAL INEQUALITIES

We have already seen (Section 3.4) that although for a reversible process $dQ = T \cdot dS$ for natural processes $dQ \leq T \cdot dS$. Similarly, for natural processes from equalities (3.11), (3.16), (3.17), (3.18) we derive:

$$dU \leq T \cdot dS - P \cdot dV \tag{3.33}$$

$$dH \leq T \cdot dS + V \cdot dP \tag{3.34}$$

$$dA \leq -S \cdot dT - P \cdot dV \tag{3.35}$$

$$dG \leq -S \cdot dT + V \cdot dP \tag{3.36}$$

This means that for a natural process at equilibrium the above functions get the lowest value, except the entropy which gets the maximum.

In other words, for any closed isolated system [2]:

$$\left(\frac{\partial S}{\partial t}\right)_{U,V,n_i} > 0 \tag{3.37}$$

which means that if anything happens in that system then S is increasing, and if

$$\left(\frac{\partial S}{\partial t}\right)_{U,V,n_i} = 0 \tag{3.38}$$

then the system is in equilibrium.

Similarly, from

$$\left(\frac{\partial U}{\partial t}\right)_{S,V,n_i} < 0 \tag{3.39}$$

if anything happens in a system at constant V and S and content then U is decreasing from:

$$\left(\frac{\partial H}{\partial t}\right)_{S,P,n_i} < 0 \tag{3.40}$$

if anything happens in a system at constant S and P and content then H is decreasing from:

$$\left(\frac{\partial A}{\partial t}\right)_{T,V,n_i} < 0 \tag{3.41}$$

that is, if anything happens in a system at constant S and P and content then H is decreasing, and from

$$\left(\frac{\partial G}{\partial T}\right)_{T,P,n_i} < 0 \tag{3.42}$$

if anything happens in a system at constant T and P and content then G is decreasing.

Inequality 3.42 is very important for chemists since most chemical reactions take place at constant T and P.

3.8 RELATIONS OF THERMODYNAMIC FUNCTIONS IN ONE-PHASE OPEN SYSTEM [2,6,7]

We have already seen from Equation 3.12 $dU = -P \cdot dV + T \cdot dS$, which is the expression of the first law of thermodynamics for a change involving only the transformation of energy. If we suppose that in the system under consideration there is also addition or removal of matter, then the above equation should be written under the following form:

$$dU = T\,dS - P\,dV + \sum_i \mu_i dn_i \tag{3.43}$$

where dn_i is the amount of substance of species i transferred and μ_i its molar energy.

In a similar way, from Equations 3.16 through 3.18 we derive:

$$dH = T \cdot dS + V \cdot dP + \sum_i \mu_i dn_i \tag{3.44}$$

$$dA = -S \cdot dT - P \cdot dV + \sum_i \mu_i dn_i \tag{3.45}$$

$$dG = -S \cdot dT + V \cdot dP + \sum_i \mu_i dn_i \tag{3.46}$$

Equations 3.43 through 3.46 are called *Gibbs equations.*

Considering U, H, A, and G as the functions U(S, V, n_i), H(S, P, n_i), A(T, V, n_i), and G(T, P, n_i) we obtain,

$$\mu_i = \left(\frac{\partial U}{\partial n_i}\right)_{S,V,n_{k\neq i}} = \left(\frac{\partial H}{\partial n_i}\right)_{S,P,n_{k\neq i}} = \left(\frac{\partial A}{\partial n_i}\right)_{T,V,n_{k\neq i}} = \left(\frac{\partial G}{\partial n_i}\right)_{T,P,n_{k\neq i}} \tag{3.47}$$

where $n_{k\neq i}$ indicates all the other species n_k except n_i.

The above-defined quantity μ_i is called the *chemical potential* of the substance i; it is an intensive thermodynamic function, it has the dimension of energy per amount of substance, and its unit in the SI system is the Joule per mole.

By definition,

$$\mu_i = R\ T \ln \lambda_i \tag{3.48}$$

where λ_i is called the absolute *activity* of the species i in the multicomponent system.

Integration of Equation 3.43 by keeping P, T, n_i constant [2] leads to,

$$U = S \cdot T - P \cdot V + \sum_i n_i \mu_i \tag{3.49}$$

or

$$G = \sum_i n_i \mu_i \tag{3.50}$$

Differentiation of Equation 3.50 gives,

$$dG = \sum_i n_i \mu_i + \sum_i \mu_i dn_i \tag{3.51}$$

Equating the expressions for dG in Equations 3.46 and 3.47 yields,

$$S \cdot dT - V \cdot dP + \sum_i n_i d\mu_i = 0 \tag{3.52}$$

which is known as the Gibbs–Duhem equation.

Using the above-defined activities and fugacities the Gibbs–Duhem equation takes the form,

$$S \cdot dT - V \cdot dP + \sum_i n_i RT \ln \lambda_i = 0 \tag{3.53}$$

or

$$S \cdot dT - V \cdot dP + \sum_i n_i RT \ln f_i = 0 \tag{3.54}$$

From Equations 3.46 by simple mathematical manipulations we can derive the following useful relations:

$$\left(\frac{\partial \mu_i}{\partial T}\right)_{P,n_i} = -\left(\frac{\partial S}{\partial n_i}\right)_{T,P,n_{k\neq i}} \tag{3.55}$$

$$\left(\frac{\partial \mu_i}{\partial P}\right)_{T,n_i} = \left(\frac{\partial V}{\partial n_i}\right)_{T,P,n_{k\neq i}} \tag{3.56}$$

$$\left(\frac{\partial \mu_i}{\partial n_k}\right)_{T,P,n_{k\neq i}} = \left(\frac{\partial \mu_k}{\partial n_i}\right)_{T,P,n_{k\neq i}} \tag{3.57}$$

$$\left(\frac{\partial \mu_i}{\partial T}\right)_{V,n_i} = -\left(\frac{\partial S}{\partial n_i}\right)_{T,V,n_{k\neq i}} \tag{3.58}$$

$$\left(\frac{\partial \mu_i}{\partial V}\right)_{T,n_i} = -\left(\frac{\partial P}{\partial n_i}\right)_{T,V,n_{k\neq i}} \tag{3.59}$$

$$\left(\frac{\partial \mu_i}{\partial n_k}\right)_{T,V,n_{k\neq i}} = -\left(\frac{\partial \mu_k}{\partial n_i}\right)_{T,V,n_{k\neq i}} \tag{3.60}$$

3.9 MIXTURES [2,6,7]

A system consisting of more than one substance is called mixture. A mixture may exist in gaseous, liquid, or solid phase. We shall confine ourselves to binary mixtures, from which the extension to multicomponent ones is straightforward.

By definition, a mixture is said to be *ideal* if for any component i [6]:

$$\mu_i = \mu_i^0 + R\,T\,\ln X_i \tag{3.61}$$

where μ_i, μ_i^0 are the chemical potentials of component i with a mole fraction X_i in the mixture and of pure i, respectively, both at the same P and T.

In other words, if for any component i in the mixture [2]:

$$\lambda_i = X_i \lambda_i^0 \tag{3.62}$$

where λ_i, λ_i^0 are the absolute activities of the component i with a mole fraction X_i in the mixture and of pure i respectively, again at the same P and T.

A mixture for which Equations 3.61 or 3.62 are not valid is called a *real* mixture.

In an ideal mixture, the interactions between like and unlike species are the same and the components in the mixture behave as in the pure components.

3.9.1 Mixing Functions

For a binary mixture of components A and B with molar fractions $(1 - x)$ and x, respectively, and for any extensive thermodynamic quantity X, such as G, A, H, S, or V the mixing function is defined as

$$\Delta_{mix} X_m = X_m (T, P, x) - (1 - x) X_m (T, P, 0) - x X_m (T, P, 1) \tag{3.63}$$

or

$$\Delta_{mix} X_m = (1 - x) [X_A (T, P, 1 - x) - X_m (T, P, 0)] + [X_B (T, P, x) - X_m (T, P, 1)] \tag{3.64}$$

where X_m (T, P, x) is the molar function of the mixture at T, P, x, X_A (T, P, $1 - x$), X_B (T, P, x) the molar functions of A and B in this mixture at mole fractions $1 - x$ and x and X_m (T, P, 0), X_m (T, P, 1) the molar functions of the pure components A and B, respectively.

From Equations 3.63 and 3.64 using Equations 3.50 and 3.62 and for $X_m = G_m$ we obtain for an ideal mixture

$$\Delta_{mix} G_m^{id} = R\,T[(1 - x) \ln (1 - x) + x \ln x] > 0 \tag{3.65}$$

From Equations 3.21 and 3.65 at constant P, n we obtain

$$\Delta_{mix} S_m^{id} = -R[(1 - x) \ln (1 - x) + x \ln x] < 0 \tag{3.66}$$

From Equations 3.65, 3.66, and 3.15:

$$\Delta_{mix}H_m^{id} = 0 \tag{3.67}$$

and from Equations 3.21 and 3.65:

$$\Delta_{mix}V_m^{id} = 0 \tag{3.68}$$

3.9.2 Excess Functions

By definition excess function X_m^E is the difference between the real $\Delta_{mix}X_m$ and the ideal one. That is,

$$X_m^E = \Delta_{mix}X_m - \Delta_{mix}V_m^{id} \tag{3.69}$$

3.9.3 Standard and Reference States of Thermodynamic Functions [8,9,12]

We define as *standard thermodynamic function* of a component i in a system at any temperature and at a fixed pressure the thermodynamic function of i at a given composition, which is called *standard state.*

Historically, the standard states are defined at the fixed pressure of 1 atm (=101.325 Pa) and in that case the standard thermodynamic functions depend only on the temperature.

Usually, for gases as standard state is accepted the pure ideal gas at 1 atm and for liquids and solids the pure liquids or solids at certain P, T where P can be defined as 1 bar.

As *reference state* is called one state that is used as reference for the calculation of the different thermodynamic function.

Any thermodynamic function can be expressed in function of its standard or reference state.

3.9.4 Dilution Thermodynamic Functions

If in one binary or multicomponent one phase homogenous mixture of nonreacting species, one component is in excess related to the others and this is added to the mixture, this process is called dilution.

The thermodynamic functions of the dilution process are given as the difference of thermodynamic functions of mixing between the final diluted state and the original one, that is

$$\Delta X_{m,dil} = (\Delta X_{m,mix})_2 - (\Delta X_{m,mix})_1 \tag{3.70}$$

3.10 GASES AND GASEOUS MIXTURES [5,6,8]

The PVT behavior of a pure fluid can be expressed by the equation:

$$P \cdot V_m = R \cdot T\,(1 + B \cdot P + C_p^2 + \ldots) \tag{3.71}$$

or

$$P \cdot V_m = R \cdot T \left(1 + \frac{b}{V_m} + \frac{c}{V_m^2} + \ldots\right) \tag{3.72}$$

where V_m is the molar volume of the gas, $V_m = V/n$, V the volume and n the mol of the gas, and R is the gas constant, which in SI units is equal to 8.3144 $J \cdot mol^{-1} \cdot K^{-1}$.

Equations 3.71 and 3.72 are called virial equations of state of a gas and the coefficients b, c, … of Equation 3.72 virial coefficients and they depend on the temperature and on the type of chemical species of the gas. The coefficients B, C, … can be calculated from b, c, …

When

$$P \to 0 \quad \text{then} \quad P \cdot V_m = R \cdot T \tag{3.73}$$

This is the equation of state of an ideal gas. The virial coefficients show the deviation of a real gas from ideality.

The PVT behavior of the gases is also expressed by the compressibility factor:

$$z = \frac{PV_m}{RT} \tag{3.74}$$

For an ideal gas $z = 1$ and $P \cdot V_m = R \cdot T$.

One attempt to express the PVT behavior of the real gases is the Van der Waals equation:

$$\left(P + \frac{a}{V_m^2}\right)(V_m - b) = R \cdot T \tag{3.75}$$

which tries to take into account the volume (coefficient b) of the molecules and the interactions between them.

For an ideal gas we can derive the following relations:

$$\left(\frac{\partial H}{\partial P}\right)_T = V - T\left(\frac{\partial nRT/\partial P}{T}\right)_P = V - \frac{nRT}{P} = 0 \tag{3.76}$$

$$C_P = C_V + n\,R \tag{3.77}$$

Gibbs–Duhem equation at constant T and for a pure gas becomes

$$n\,d\mu = V \cdot dP \tag{3.78}$$

If the gas is ideal, substituting in Equation 3.78 the volume from Equation 3.73 we obtain:

$$n\,d\mu = \frac{nRT}{PdP} \tag{3.79}$$

or

$$d\mu = R\,T\,d\ln P \tag{3.80}$$

and for a change at constant T from P_1 to P_2

$$\mu_2 - \mu_1 = R\,T\ln\left(\frac{P_2}{P_1}\right) \tag{3.81}$$

3.10.1 Fugacity [7,10]

To express the properties of a real gas in the same way with an ideal gas, Lewis and Randall [9] originated the term *fugacity* (f), which has the dimensions of pressure.

So, for a real gas or vapor instead of Equation 3.80 or 3.81 we write [10]:

$$d\mu = R\,T\,d\ln f \tag{3.82}$$

or

$$\mu_2 - \mu_1 = R\,T\ln\frac{f_2}{f_1} \tag{3.83}$$

where f is the fugacity of the gas or vapor.

The ratio

$$\Phi = \frac{f}{P} \tag{3.84}$$

is called *fugacity coefficient*. Since ideal gas behavior is approached as $P \to 0$ then

$$\lim_{P\to 0}\Phi = \lim_{P\to 0}\frac{f}{P} = 1 \tag{3.85}$$

As we will see in the phase equilibrium, the fugacity of a liquid or a solid which is in equilibrium with its vapor is equal to the fugacity of its vapor.

The fugacity of a real pure gas at a given P, T can be evaluated [7] through the relation:

$$\left(\ln\frac{f}{P}\right) = \left[\int_0^P\left(\frac{V_m}{RT} - \frac{1}{P}\right)\right]dP\Bigg]_T \tag{3.86}$$

if we know the equation of state of that gas.

For multicomponent real gases, the partial fugacity f_i of a component i is defined in terms of the chemical potential μ_i as follows:

$$(d\mu_i)_T = R\ T\ d(\ln f_i)_T \tag{3.87}$$

In this case,

$$\lim_{P\to 0}\frac{f_i}{x_i P} = 1 \tag{3.88}$$

where x_i is the mole fraction of component i and P is the total pressure (not the partial pressure P_i).

For multicomponent gases the fugacity f_i can be also evaluated [7] through the relation:

$$\ln f_i = \ln\left(x_i P\right) + \left[\int_0^P\left(\frac{\left(V_m\right)_i}{RT} - \frac{1}{P}\right)\right]dP\Bigg]_T \tag{3.89}$$

where $(V_m)_i$ is the partial molar volume of i, if we know the equation of state of that gas mixture.

3.10.2 The Standard State of a Gas Component [2]

The standard state of a gas component in a mixture of gases is given by

$$\left(g,T,P,x_c\right) = \left(g,T\right) + R\,T\ln\left(x_B\frac{P}{P_0}\right) + \int_0^P\left[V_B(g,T,P,x_C) - \frac{RT}{P}\right]dP \tag{3.90}$$

where μ_B^0 (g, T) is the chemical potential of the pure ideal gas, at temperature T and pressure P_0. Historically, $P_0 = 1$ atm.

3.11 LIQUID MIXTURES [2,8]

All that was mentioned in Section 3.9 and what it will follow are applicable to liquid and to solid mixtures as well.

For a liquid mixture using Equation 3.48 we obtain:

$$\mu_i = \mu_i^0 + R\,T \ln \frac{\lambda_i}{\lambda_i^0} \tag{3.91}$$

or

$$\mu_i = \mu_i^0 + R\,T\,\ln a_i \tag{3.92}$$

where μ_i, μ_i^0 are the chemical potentials of component i with mole fraction x_i and of the pure liquid i at certain P, T, λ_i, λ_i^0 the absolute activities of μ_i and μ_i^0, respectively, and

$$a_i = \frac{\lambda_i}{\lambda_i^0} \tag{3.93}$$

is what we call *relative activity* of i in the mixture. Some authors call a_i simply *activity.*

For the absolute activity, the activity coefficient f_i is defined by the relation:

$$\lambda_i = f_i x_i \tag{3.94}$$

and for the relative activity the corresponding *activity coefficient* γ_i is defined by the relation:

$$a_i = \gamma_i\, x_i \tag{3.95}$$

When $a_i = 1$ from Equation 11.2 we obtain $\mu_i = \mu_i^0$, that is the term $R\,T\,\ln a_i$ gives the difference between μ_i and its reference state μ_i^0 at certain P, T and if P = 1 bar then the difference of μ_i from its standard state.

From Equations 3.92 and 3.93 we get

$$\mu_i = \mu_i^0 + R\,T\,\ln x_i + R\,T\,\ln \gamma_i = \tag{3.96}$$

Since for the case of an ideal mixture $\mu_i = \mu_i^0 + R\,T\,\ln x_i$ (Equation 3.61), then the term $R\,T\,\ln \gamma_i$ expresses the deviation of μ_i from ideality.

After defining the standard state for μ_i the standard states for the other thermodynamic functions can be derived. In particular,

$$S_i^0 = -\frac{d\mu_i^0}{dT} \tag{3.97}$$

$$H_i^0 = \mu_i^0 - T\frac{d\mu_i^0}{dT} \tag{3.98}$$

$$G_i^0 = \mu_i^0 \tag{3.99}$$

3.12 EQUILIBRIUM OF PHASES [2,6,8,11,12]

In many industrial processes there is a coexistence of two or more phases. When there is mass transfer from one phase to the other the phases are not at equilibrium. The study of the mass transfer in these processes requires exact knowledge of the phases at equilibrium. In this clause we will treat liquid–vapor equilibrium states. Similar results can be derived from the treatment of liquid–solid and solid–vapor equilibrium.

We say that two or more phases are in equilibrium regarding several intensive properties, when these properties have the same value in both phases. For example, we have

- Thermal equilibrium when the temperature T is the same in all phases.
- Hydrostatic equilibrium, when the pressure P is the same in all phases.
- Chemical equilibrium, when there is no reaction between the constituents of all the phases.
- Osmotic equilibrium, when P, T, and several μ_i are the same.
- Diffusive equilibrium, when P, T, and all μ_i are the same.

We will deal here with equilibrium states between phases where P, T, μ_i are equal in all phases.

3.12.1 Phase Rule

For a closed, isolated system consisting of several phases a, b, c, … in thermal, hydrostatic, and chemical equilibrium (fixed composition) and where there is no transfer of mass, at macroscopic observation, from one phase to the other, writing the Gibbs–Duhem equations for all the phases, since dP, dT, and dn_i are zero it is derived that, for every component i, $\mu_i^a = \mu_i^b = \mu_i^c = \ldots$

The minimum number of intensive properties (pressure, temperature, mole fractions, etc.) needed so that the state of a closed, isolated nonreacting system is completely defined is called the *degrees of freedom*.

J.W. Gibbs derived a very important rule involving phase equilibriums which connects the degrees of freedom F with the number of phases P and the number of different substances in the system C. This rule is given by the following relation:

$$F = C + 2 - P \tag{3.100}$$

For example, in the P, T diagram of Figure 3.1 for a pure substance we observe that for the regions of only one phase P = 1 and F = 2, which means that both P, T are needed for the definition of the state. For points on the curves we have two phases P = 2 and F = 1 which means that only one of P, T is needed for the definition of the state and finally at the triple point T, that there is no degree of freedom and P = 3 and F = 0 which means only one pair of P, T corresponds to the state of coexistence of three phases.

If a reaction is taking place in the system or we want to take in account a peculiarity of the equilibrium phases, for instance an azeotrope, then the phase rule must be modified.

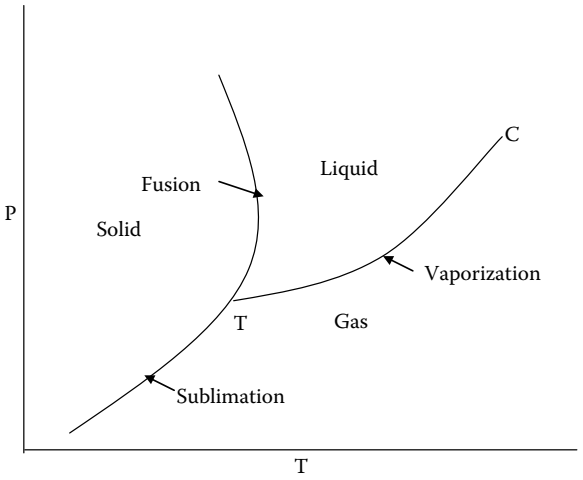


FIGURE 3.1 P–T diagram for a pure substance.

For a single-component two-phase system, following the vaporization curve (Figure 3.1) up to the end point C, we observe that by increasing gradually the temperature of the system we pass to vapor and liquid phases which become more and more similar in density and molar volume and the interphasial separation line become less and less distinct. Finally, at the point C the two phases become identical and their interphasial line disappears. Beyond C there is no liquid or vapor phase, but only one single fluid phase.

At the critical point

$$\left(\frac{\partial P}{\partial V}\right)_{Tc} = 0, \left(\frac{\partial^2 P}{\partial V^2}\right)_{Tc} = 0 \tag{3.101}$$

Point C is called the *critical point* and the corresponding P, T the *critical pressure* P_C and the *critical temperature* T_C of the studying substance.

3.12.2 Chemical Potential in Phase Equilibria [7,11]

In the previous clause, we saw that between two phases a, b in equilibrium for every substance i

$$\mu_i^a = \mu_i^b \tag{3.102}$$

or

$$\mu_i^{0,a} + RTlna_i^a = \mu_i^{0,b} + + RTlna_i^b \tag{3.103}$$

Since the $\mu_i^{0,a}$ and $\mu_i^{0,b}$ are the chemical potentials of the pure i at the same P, T then

$$\mu_i^{0,a} = \mu_i^{0,b} \tag{3.104}$$

and consequently from Equation 3.103

$$a_i^a = a_i^b \tag{3.105}$$

but this does not mean necessarily that the activity coefficients γ_i^a, γ_i^b will be equal since usually $x_i^a \uparrow x_i^b$.

For the case of liquid vapor equilibrium we have seen for the vapor phase that

$$\mu_i^v = \mu_i^{0,v} + R\,T \ln \frac{f_i^v}{f_i^{0,v}} \tag{3.106}$$

while for the liquid phase

$$\mu_i^\ell = \mu_i^{0,\ell} + R\,T \ln \frac{\lambda_i^\ell}{\lambda_i^{0,\ell}} = \mu_i^{0,\ell} R\,T \ln a_i^\ell \tag{3.107}$$

From the previous relations the following relation is obtained, connecting the absolute activity, the relative activity, and the fugacity of a component i in a system in equilibrium

$$\frac{f_i}{f_i^0} = \frac{\lambda_i}{\lambda_i^0} = a_i \tag{3.108}$$

The equations relating the thermodynamic function of phases in equilibrium are very important since from data of one phase we can calculate the properties of the other phase.

3.12.3 Binary Vapor–Liquid Systems [7,9,11]

There are important differences between the behavior of a single component vapor–liquid system and a multicomponent one. For instance, in a single component the vapor and liquid phases have the same composition but not in a multicomponent system.

During the evaporation at constant pressure for a single-component system the temperature remains constant, but in a multicomponent system at constant P the temperature changes during the evaporation. It is obvious that the behavior of a multicomponent system is more complicated than that of a single component. As an example of multicomponent system we study here a two-phase binary system.

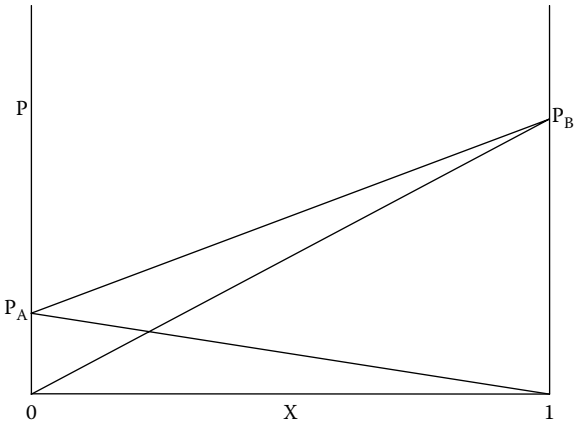


FIGURE 3.2 Vapor–pressure composition diagram for an ideal mixture of two liquids A and B.

Figure 3.2 shows a vapor-pressure-composition (X = mole fraction) diagram for an ideal mixture of two liquids. At any mole fraction between 0 and 1 the vapor pressure of the mixture is

$$P_{mix} = P_A (1 - X) + P_B X \tag{3.109}$$

Figure 3.3 shows the P, X diagram of a real mixture of two component liquids A and B, completely miscible through the whole range of X. At any pressure a composition of the liquid phase X_{liq} corresponds to a different composition X_{vap} of the vapor phase, which is in equilibrium with the liquid. The compositions of the liquid phase form a curve called *bubble point line* and the corresponding compositions of the vapor phase form another curve called *dew point line*. A diagram similar to Figure 3.3 can be drawn relating T with X.

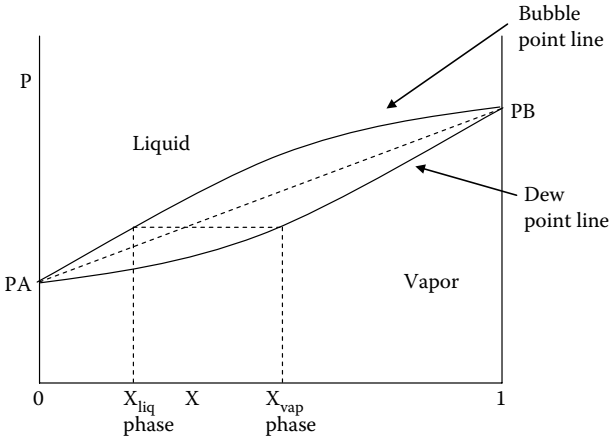


FIGURE 3.3 Vapor–pressure composition diagram for a real mixture of two liquids.

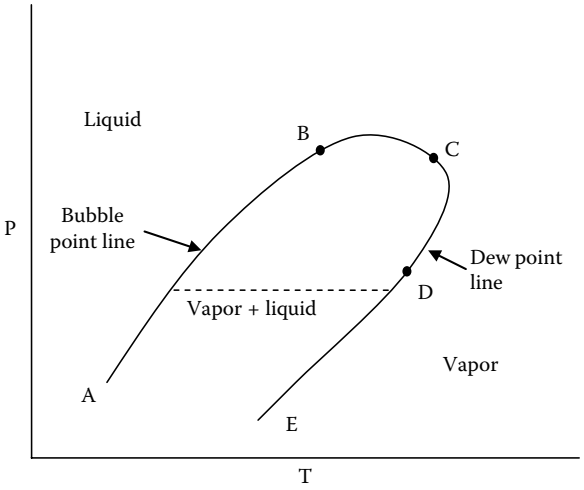


FIGURE 3.4 P–T diagram at constant composition for a mixture of two liquids.

Some binary liquid mixtures at a fixed composition have identical composition in both the liquid and vapor phase. This composition is called azeotropic and the mixture azeotrope.

In these cases although the compositions of the two phases are equal, it does not mean that the mixture is an ideal one.

There are positive azeotropes with azeotropic pressure higher than the vapor pressure of the two pure components and negative azeotropes with P_{az} lower than the vapor pressure of the two pure components of the mixture.

Figure 3.4 shows the P, T diagram of a binary liquid mixture at a constant composition. Since in that case there is one more degree of freedom from the single component system, in order to define the state of the system for the vapor–liquid region we need both P, T (for the single component system it is needed either only P or only T).

In Figure 3.4, the region included inside the ABCDE curve is in the place of the vaporization line of Figure 3.1. To pass from the pure liquid to the vapor under constant pressure the temperature is changing. This passage becomes shorter as we approach the critical point C. The end temperatures of the start and the end of this process are called *bubble point* and *dew point temperatures,* respectively, at the pressure of vaporization. At each composition there is a curve ABCDE and one critical point.

Similar behavior is observed for the processes of fusion and sublimation and it is not necessary to be considered.

3.12.4 Principle of Corresponding States [7,12]

For different real gases at the same pressure and temperature the molar volumes V_m are different. The compressibility factor $z = P V_m/RT$ defined in Section 3.10 expresses the deviations of the real gases from ideality and it is different for the different gases of the same P and T.

However, it has been observed, by defining as reduced pressure P_r, reduced temperature T_r, and reduced molar volume $V_{m,r}$ by the relations

$$P_r = \frac{P}{P_C}, \quad T_r = \frac{T}{T_C}, \quad V_{m,r} = \frac{V_m}{V_{m,C}} \tag{3.110}$$

where P_r, T_r, $V_{m,r}$ are the critical P, T, and V_m that for equal P_C, T_C the $V_{m,r}$ of all gases are approximately the same.

This is known as the Van der Waals *principles of corresponding states.*

The critical compressibility factor

$$z_C = \frac{P_C\ V_{m,C}}{R\ T_C} \tag{3.111}$$

is also found experimentally to be in the narrow range 0.2–0.3, and it can be considered as a universal constant.

So, we finally have

$$z = F\ (P_r, T_r) \tag{3.112}$$

where F is the same function for all the gases.

3.12.5 Enthalpy and Entropy Change in a Two-Phase Transition [2,7,12]

When there is transition from one phase to another we define a property called *change of transition of state* by relation

$$\Delta M_i^{ab} = M_i^b - M_i^a \tag{3.113}$$

Thus, for the case of vaporization we have

$$\Delta V_i^{\ell v} = V_i^v - V_i^\ell \tag{3.114}$$

$$\Delta H_i^{\ell v} = H_i^v - H_i^\ell \tag{3.115}$$

$$\Delta S_i^{\ell v} = S_i^v - S_i^\ell \tag{3.116}$$

where by l and v we mean liquid and vapor, respectively.

Knowing that at equilibrium

$$_i^\ell = \mu_i^v$$

or

$$G_i^{\bullet} = G_i^{v} \tag{3.117}$$

For a two phase, one component, system at each phase

$$G_i = H_i - T\,S_i \tag{3.118}$$

and

$$dG_i = S_i\,dT - V_i\,dP \tag{3.119}$$

From Equations 3.117 through 3.119 it is finally derived

$$\frac{dP_i^{sat}}{dT} = \frac{\Delta S_i^{\ell v}}{\Delta V_i^{\ell v}} \tag{3.120}$$

where the P^{sat} is the vapor pressure at the equilibrium of the two phases.

$$\frac{dP_i^{sat}}{dT} = \frac{\Delta H_i^{\ell v}}{\Delta V_i^{\ell v}} \tag{3.121}$$

From Equations 3.120 and 3.121 we can calculate the entropy and enthalpy change of vaporization.

3.13 SOLUTIONS [2,5,11,13]

For several mixtures it is convenient to distinguish some components from the others, for instance, when one solid, liquid, or gas has a limited solubility in a liquid and its mole fraction in the mixture does not cover the whole range from 0 to 1.

In this case, by convention we call the liquid which covers the whole range of concentration *solvent*, the component with the limited solubility *solute* and the mixture *solution*. When the solvent is in excess and the solute in low concentration the solution is called dilute solution.

For a binary solution the chemical potential of the solvent is given as in mixtures of liquids by the relation

$$\mu_i = \mu_i^0 + R\,T\,\ln d_i = \mu_i^0 + R\,T\,\ln\gamma_i x_i \tag{3.122}$$

where μ_i^0 is the reference chemical potential of pure solvent at certain P, T, a_i, γ_i are, respectively, its relative activity and activity coefficient.

When $x_i \to 1$ then also $\gamma_i \to 1$ and the solvent behaves as an ideal mixture. At these compositions near the pure solvent the partial pressure of fugacity of the solvent is proportional to its mole fraction.

$$P_i = P_i^0 x_i \quad \text{or} \quad f_i = f_i^0 x_i \tag{3.123}$$

where P_i, f_i, x_i the partial pressure, fugacity, and mole fraction of the solvent and P_i^0, f_i^0 are the vapor pressure, fugacity of the pure solvent, respectively, at the temperature of the solution.

In this region, the solvent behaves in an ideal way and the relations (3.123) express what we call as *Raoult's law* (Figure 3.1).

The standard chemical potential of the solvent is that of the pure liquid at 1 atm and the temperature of the solution.

For the solute, however, it is not possible to define a similar standard state since there cannot be solutions with higher solute concentrations.

In this case, it is adopted as standard state for the solute the hypothetical, ideal unit concentration of solute solution at certain pressure and the temperature (reference state) or at the fixed pressure of 1 atm (standard state).

This solute standard state is derived by the extrapolation of the fugacity of the solute at conditions of infinite dilution (the mole fraction of all the solutes in the solution tend to zero), where the fugacity of the solute f_i is proportional to its mole fraction x_i

$$f_i = K\, x_i \tag{3.124}$$

to the hypothetical state of solution with solute mole fraction 1.

Relation (3.124) is called *Henry's law* and K is a constant called Henry's constant.

From the above mentioned analysis the chemical potential of the solute in a solution is given by

$$\mu_i = \mu_i^0 + R\,T \ln \gamma_i x_i = \mu_i^0 + R\,T \ln \frac{f_i}{f_i^0} \tag{3.125}$$

where γ_i, f_i are the activity coefficient and the fugacity of i at a mole fraction x_i and f_i^0, μ_i^0 are the fugacity and the chemical potential of pure i at the reference state of infinite dilution conditions and at the temperature and pressure of the solution.

In the region of very dilute solutions where relation (3.124) is valid the solute behaves in an, by convention, ideal way which is different from near the pure solvent. Figure 3.5 shows the variation of fugacities of the solute and the solvent in function of the molar fractions for a binary ideal or real system at constant P,T.

The standard chemical potential of a solvent is given by the relation [2]:

$$\mu_2^0\left(T, P^0\right) = \mu_2^*\left(T, P\right) + \int_P^{P^0} V_2^*(T,P)\,dP \tag{3.126}$$

where P^0, P are the standard pressure and the pressure of the solution, respectively, *means pure solvent, and V_2^* volume of pure solvent.

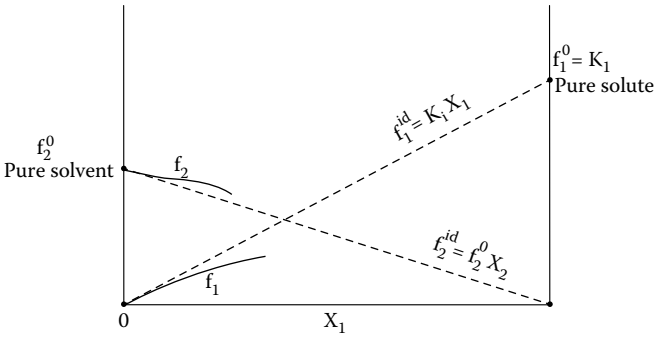


FIGURE 3.5 Fugacities of solute and solvent in function of mole fractions.

The standard chemical potential of a solute is given by relation [2]:

$$\mu_1^0(T) = \left[\mu_1(T,P,m_1) - RT\ln\frac{m_1}{m_1^0}\right]^{\infty} + \int_P^{P^0} V_1^{\infty}(T,P)dP \tag{3.127}$$

where ∞ means conditions at infinite dilution, $\mu_1(T,P,m_1)$ the chemical potential at T, P, m_1, m_1^0 the standard molality, P^0 the standard pressure, and V_1^{∞} the volume of solute at conditions of infinite dilution.

All the other thermodynamic functions and relations for the solution can be derived in a straight mathematical way from the above relations.

3.14 ELECTROLYTE SOLUTION [1,2,8]

Electrolytes are a special class of solute substance, which involve several complications in their thermodynamic study, not found in solutions of nonelectrolytes.

The difficulties arise from the fact that the electrolytes in solution are found under complete or partial dissociation in the ions from which they are constituted. Because of the restriction of electrical neutrality in an electrolyte solution it is not possible to define thermodynamic functions of one ion, for example, its chemical potential, since this would imply the change of the amount of substance of this ion by keeping constant the amount of substance of rest of all the ions, which has no physical meaning.

To overcome this difficulty we consider all the thermodynamic functions with both the anions and the cations of one electrolyte.

For example, for the case of a strong, completely dissociated electrolyte of the type $M_{V+}A_{V-}$, where V_+ and V_- are the number of positive and negative ion, respectively, in the molecule of the electrolyte, we can write

$$\mu_{AB} = V_+\mu_+ + V_-\mu_- \tag{3.128}$$

and using molalities

$$\mu_+(T, P, m) = R\,T\ln m_+ + R\,T\ln\gamma_+(T, P, m) + \mu_+^0(T, P) \tag{3.129}$$

$$\mu_-(T, P, m) = R\,T\ln m_- + R\,T\ln\gamma_-(T, P, m) + \mu_-^0(T, P) \tag{3.130}$$

Substituting Equations 3.129 and 3.130 into Equation 3.128 we obtain

$$\mu_{MA} = R\,T\ln m_+^{V_+} m_-^{V_-} + R\,T\ln\gamma_+^{V_+}\gamma_-^{V_-}\,(T, P, m) + V_+\mu_+^0(T, P) + V_-\mu_-^0(T, P) \tag{3.131}$$

The mean activity coefficient is defined as

$$\gamma_\pm^V = \gamma_+^{V_+}\gamma_-^{V_-} \tag{3.132}$$

and the mean molality

$$m_\pm^V = m_+^{V_+} m_-^{V_-} \tag{3.133}$$

where $V = V_+ + V_-$.

From Equations 3.132, 3.133, and 3.131 and by defining

$$\mu_{MA}^0(T, P) = V_+\mu_+^0(T, P) + V_-\mu_-^0(T, P) \tag{3.134}$$

$$\mu_{MA}(P, T) = V\,R\,T\ln m_\pm + V\,R\,T\ln\gamma_\pm(T, P, m) + \mu_{MA}^0(T, P) \tag{3.135}$$

The $m_\pm$, and $\gamma_\pm$ and $\mu_{MA}^0(T, P)$ have a similar meaning as for the nonelectrolyte solutions when $\gamma_\pm \to 0$ then $\gamma_\pm \to 0$ and $\mu_{MA}^0(T, P)$ is equal to $\mu_{MA}^0(T, P)$ at the reference state.

For the case of weak electrolytes the method to obtain expressions for the chemical potentials are the same for strong electrolytes.

3.14.1 Debye–Hückel Limiting Law [2,6]

In 1923, Debye and Hückel developed a theory about the behavior of strong electrolytes in dilute solutions. This theory was a mathematical treatment of some ideas previously assumed by Arrhenius regarding the dissociation of electrolytes in solution.

By this theory after a series of mathematical calculations we arrive at a formula giving the mean ionic activity coefficient, which for very dilute solutions by approximation takes the form:

$$\ln\gamma_\pm = C\,I^{1/2}\,z_+\,z_- \tag{3.136}$$

where $C = (2 \pi N_0 \rho_s)^{1/2} (e^2/4 \pi \varepsilon K T)^{3/2}$

N_0 = Avogadro's number

ρ_s = density of the pure solvent

e = the charge on a proton

$\varepsilon = \varepsilon_0 \varepsilon_r$, ε_r is the dielectric constant of the solvent and ε_0 is the dielectric constant of a vacuum

T = temperature of solution

$K = R/N_0$, R = gas constant

I is called ionic strength and is given for a 1–1 type electrolytes by

$$I = \frac{1}{2}\left(m_+ z_+^2 + m_- z_-^2\right) \tag{3.137}$$

m_+, m_-, the molalities of the ions

z_+^2, z_-^2, the electrical charges of the ions.

The Debye–Hückel law is very accurate for very dilute solution of strong electrolytes.

For mixed electrolytes the theory is still valid with

$$I = \frac{1}{2}\sum_i m_i z_i^2 \tag{3.138}$$

3.15 THERMOCHEMISTRY: CHEMICAL REACTION EQUILIBRIUM [11,15]

The application of thermodynamics to chemically reacting systems is very important. Together with mass balance the first thermodynamic law under certain conditions gives exactly the energy, absorbed (endothermic) or released (exothermic) by a chemical reaction. For instance, we can calculate the energy needed to produce, from some substances, various other useful substances or the energy released from the combustion of a fuel.

The second thermodynamic law can predict if one chemical reaction will proceed to one direction or to the opposite and at which extent it will stop (equilibrium state).

However, in several cases, although from the second thermodynamic law it results that one reaction should proceed to one direction, this reaction does not start and to overcome this hindrance, they use catalysts or other means.

But still, in these cases thermodynamics is useful, since through the prediction by the second thermodynamic law of the possibility of realization of a reaction, it can allow us or release us from the trouble, to seek the appropriate catalyst for this reaction.

3.15.1 Enthalpy of Formation and Enthalpy of Reaction [4,5]

The heat of formation of any component is the heat required to form that compound from its elements at a certain temperature and pressure. When this formation is

considered under constant pressure then the heat of formation is equal to the enthalpy of formation.

The standard enthalpy of formation, ΔH_F of a compound is defined as the heat required to form the compound in its standard state of 1 atm pressure and 25°C from its elements at the same standard conditions.

$$\Delta H_F = h_{compound} - \sum_i (v_i h_i)_{elements} \tag{3.139}$$

where v_i is the stoichiometric coefficient.

By conversion, the standard enthalpies of formation h_i of all elements of their move stable state is considered as zero, therefore

$$\Delta H_F = h_{compound} \tag{3.140}$$

Tables with standard enthalpies of formation of many compounds are given in many books of thermodynamics.

The heat of reaction is the heat absorbed or rejected by the reaction. If the reaction takes place at constant P, the heat of reaction is equal to the enthalpy reaction.

The standard enthalpy of reaction is defined as the change in enthalpy from a reaction taking place at a constant pressure of 1 atm and constant temperature of 25°C.

The heat of combustion of any compound is defined as the heat of reaction resulting from the oxidation of this compound with oxygen.

The quantities of heat transferred during the vaporization, or fusion which is for a single compound and constant pressure taking place at constant T are called heat effects.

These heat effects together with the heat mixing, the heat of solution (heat of mixing for the case of a solution), as well as the heat of reactions are studied by the branch of thermodynamics, called thermochemistry and the instrument of these function are called calorimeters.

3.15.2 Determination of the Enthalpy of Reaction [4,5,7]

For a reaction under constant P, where variations in potential and kinetic energy are negligible and no work is produced the change in enthalpy is given by

$$H_P - H_r = (H_P - H_{P0}) + (H_r - H_{r0}) \tag{3.141}$$

where H_P, H_r enthalpies of products and reactants at a pressure P, respectively, and H_{P0}, H_{r0} enthalpies of products and reactants at a pressure of 1 atm and temperature of 25°C.

$$\Delta H_R = H_{P_0} - H_{r_0} = \sum_{products} (vh) - \sum_{reactants} (vh) \tag{3.142}$$

where the v's are the stoichiometric coefficients and the h's are the standard molar enthalpies of formation of the compounds in the reaction, is the standard enthalpy of reaction and can be calculated from the standard enthalpies of formation of the products and reactants using existed relative tables.

$(H_P - H_{P_0})$ and $(H_r - H_{r_0})$ can be calculated either from known data, experimentally or by simplification considering, for instance, that the reactants and products behave as ideal gases.

In several cases, we can determine the enthalpy of a certain reaction by simply adding or subtracting other reactions of which we know the enthalpies of reaction.

3.15.3 Equilibrium Constant: Affinity of a Reaction [6,7,11]

Let us consider the reaction

$$v_1c_1 + v_2c_2 \rightleftarrows v_3c_3 + v_4c_4 \tag{3.143}$$

at constant T, P
where c_i are the constituents and v_i the stoichiometric coefficients.

Equation 3.46 at P, T constant gives

$$dG_{T,P} = \mu_1 dn_1 + \mu_2 dn_2 + \mu_3 dn_3 + \mu_4 dn_4 \tag{3.144}$$

and for a reaction

$$-\frac{dn_1}{v_1} = -\frac{dn_2}{v_2} = \frac{dn_3}{v_3} = \frac{dn_4}{v_4} = d\xi \tag{3.145}$$

where ξ is the extent of the reaction.

Based on Equations 3.144 and 3.145 and Equation 3.42 it follows:

$$dG_{T,P} = (\mu_1 dn_1 + \mu_2 dn_2 - \mu_3 dn_3 - \mu_4 dn_4)d\xi \leq 0 \tag{3.146}$$

the sign of the parentheses determines the sign of the ξ and consequently the direction of the reaction.

$$\text{At equilibrium where} \quad dG_{T,P} = 0 \tag{3.147}$$

$$\mu_1 dn_1 + \mu_2 dn_2 = \mu_3 dn_3 - \mu_4 dn_4 \tag{3.148}$$

The quantity $\mu_1 dn_1 + \mu_2 dn_2 - \mu_3 dn_3 - \mu_4 dn_4$ was introduced by De Dander (16) and was called by him as the affinity A_f.

From Equation 3.148 using $\mu_i = \mu_i^0 + RT\ln a_i$ (relation (3.91)) it is obtained:

$$A_f = A_f^0 - RT\ln\left(\frac{a_3^{\nu_3} \cdot a_4^{\nu_4}}{a_1^{\nu_1} \cdot a_2^{\nu_2}}\right) \tag{3.149}$$

where A_f^0 is the affinity for the μ_i^0.

The quantity

$$\left(\frac{a_3^{\nu_3} \cdot a_4^{\nu_4}}{a_1^{\nu_1} \cdot a_2^{\nu_2}}\right) = Q_a \tag{3.150}$$

is called reaction quotient.

At equilibrium where $A_f^0 = 0$ the Q_a depends only on the temperature and on A_f^0 and not on the activities, and is called the equilibrium constant K_a.

Thus, we have

$$A_f^0 = RT\ln K_a \tag{3.151}$$

$$A_f = RT\ln\frac{K_a}{Q_a} \tag{3.152}$$

Since one reaction proceeds only when $A_f > 0$ this means that

when $K_a > Q_a$ the reaction proceeds to the right,
when $K_a < Q_a$ the reaction proceeds to the left,
and when $K_a = Q_a$ there is equilibrium.

REFERENCES

1. SW Angrist, LG Hepler. *Order and Chaos*, New York, USA: Basic Books Inc., 1967.
2. ML Mac Glashan. *Chemical Thermodynamics*. London, UK: Academic Press Inc., 1979.
3. ML MacGlashan. *Physicochemical Quantities and Units*. 2nd Ed., London, UK: The Royal Institute of Chemistry, 1971.
4. TE Daubert. *Chemical Engineering Thermodynamics*. Singapore: McGraw-Hill Book Co, 1985.
5. P Rock. *Chemical Thermodynamics*. California, USA: University Science Books, 1983.
6. CE Reid. *Chemical Thermodynamics*. Singapore: McGraw-Hill Book Co, 1990.
7. JS Hsieh. *Principles of Thermodynamics*. New York, USA: McGraw-Hill, 1975.
8. SE Wood, R Battino. *Thermodynamics of Chemical System*. Cambridge, UK: Cambridge University Press, 1990.
9. JM Smith, HC Van Ness. *Introduction to Chemical Engineering Thermodynamics*. 4th Ed. Singapore: McGraw-Hill Book Co, 1987.
10. GN Lewis, M Randall. *Thermodynamics*. Revised by KS Pitzer, L Brewer. 2nd Ed. New York, USA: McGraw-Hill, 1961, p. 191.

11. DP Tassios. *Applied Chemical Engineering Thermodynamics*. Berlin, Germany: Springer-Verlag, 1993.
12. HC Van Ness, MM Abbott. *Classical Thermodynamics of Non Electrolyte Solutions, with Applications to Phase Equilibria*. New York, USA: McGraw-Hill Inc., 1982.
13. JW Tester, M Modell. *Thermodynamics and its Applications*. 3rd Ed. New Jersey, USA: Prentice-Hall Inc., 1997.
14. JM Prausnitz, RN Lichtenthaler, EG de Azevedo. *Molecular Thermodynamics of Fluid-Phase Equilibria*. 3rd Ed. New Jersey, USA: Prentice Hall, Inc., 1999.
15. MK Karapetyants. *Chemical Thermodynamics*. Trans. by G Leib. Moscow, Russia: MIR Publishers, 1978.
16. Th DeDonder, P Van Rysselberghe. *The Thermodynamic Theory of Affinity*. Stanford, California, USA: Standard University Press, 1936.

4 Heat Transfer

Ioannis K. Kookos and Nikolaos G. Stoforos

CONTENTS

4.1 Introduction 75
4.1.1 Conduction 76
4.1.2 Convection 76
4.1.3 Radiation 76
4.2 Conduction 76
4.2.1 Fourier's Equation 76
4.2.2 Heat Diffusion Equation 77
4.2.3 Commonly Used Boundary Conditions 79
4.2.4 Steady-State 1-D Conduction 80
4.3 Convection 84
4.4 Unsteady-State Conduction 89
4.4.1 Infinite Plane (Slab) 89
4.4.2 Infinite Cylinder 95
4.4.2.1 Infinite Heat-Transfer Coefficient 96
4.4.2.2 Finite Heat-Transfer Coefficient 97
4.4.3 Sphere 98
4.4.4 Newman's Rule for Finite Body Geometries 99
4.5 Cases of Special Interest in Food Engineering 101
4.5.1 Variable Medium Temperature 101
4.5.2 Heat Conduction with Heat Source 103
4.5.3 Semi-Infinite Solid Approximation 104
4.6 Numerical Calculation of the One-Term Solution 106
Nomenclature 109
Greek Letters 110
Subscripts 110
References 111

4.1 INTRODUCTION

In majority of food technology processes, heat transfer is involved to heat, cool, dry, sterilize, and so on, process streams, and this exchange of heat must take place with predetermined rate. In addition, in many cases the objective is to prevent the loss of heat from a hot vessel or pipe system. Given the fact that energy is expensive and can constitute significant part of the operating cost of any process, the study of the ways by which heat is transferred is important in designing energy-efficient systems. When a temperature difference (potential) exists between two parts of a system, heat

transfer will take place in one (or combination) of the following three different ways (Lienhard and Lienhard, 2006).

4.1.1 Conduction

In a motionless fluid, the transfer of heat by conduction is the result of the transfer of vibrational energy or kinetic energy from one molecule to another at microscopic level. Heat transfer by conduction can also be the result of movement of free electrons, a process which is particularly important in the case of metals.

4.1.2 Convection

Heat transfer by convection is related to the mixing of elements of fluid and there is an important distinction between natural (when mixing, for example, is the result of density differences) and forced (mixing imposed by external means) convection. Strictly speaking, convection involves a motionless phase (such as a solid surface) and a moving fluid (such as air) in contact but at different temperatures.

4.1.3 Radiation

All materials radiate thermal energy in the form of electromagnetic waves which, when falling on another body may be partially reflected, transmitted, or absorbed. The fraction that is absorbed appears as heat in the body. Heat transfer with radiation takes place in the absence of an intervening medium.

In this chapter, we will deal with conduction and convection heat transfer. Radiation is the subject of a separate chapter of this volume.

4.2 CONDUCTION

4.2.1 Fourier's Equation

The heat flux $\dot{q}_x''$ is the heat-transfer rate in the x direction per unit area perpendicular to the direction of heat transfer by conduction and is described by the Fourier's equation (Lienhard and Lienhard, 2006; Baehr and Stephan, 2006)

$$\dot{q}_x'' = -k\frac{dT}{dx} \tag{4.1}$$

where $T = T(x)$ is the temperature and k is a transport property called the thermal conductivity. Fourier's equation states that the heat flux is proportional to the temperature gradient and resembles Ohm's law. The negative sign indicates that the temperature gradient is in the opposite direction to the flow of heat, that is, heat flows from higher temperatures to lower temperatures. As far as the thermal conductivity is concerned it should be noted that gases have thermal conductivities in the range 10^{-2}–10^{-1} W m^{-1}K^{-1}, liquids in the range 10^{-1}–10 W m^{-1}K^{-1}, while pure metals in the range 10–10^{3} W m^{-1}K^{-1}. In addition, thermal conductivity is usually a weak function

of temperature and can be assumed constant when small (1–10 K) temperature variations are studied.

4.2.2 Heat Diffusion Equation

One fundamental question that frequently arises is: what is the temperature distribution within a motionless phase (such as solid material) when different temperatures are imposed on its boundaries? In order to simplify the development of the relevant equations we consider the case of heat conduction across a thin flat solid object (such as a glass window) as shown in Figure 4.1. The thickness in the x direction is very small compared to the size of the object in the other directions. The boundaries of the object in the x direction have different temperatures and in effect heat transfer by conduction is taking place in this direction. We further consider a control volume with surfaces located at distances x and $x + dx$ from the left free surface of the object. The energy balance equation when applied to this control volume can be stated as follows: the rate of accumulation of energy within the control volume must be equal to the rate that energy enters the control volume minus the rate at which energy leaves the control volume. As kinetic and potential energy are not important in our case, we can assume that internal energy is the only one important. For the case of solids, internal energy can be expressed as

$$\begin{bmatrix}\text{Internal} \\ \text{energy}\end{bmatrix} = mC_pT \tag{4.2}$$

where m is the total mass and C_p is the heat capacity. All thermophysical properties are assumed constant. The volume of the control volume is Adx, where A is the area available to heat transfer, and if the density of the material is ρ then we obtain

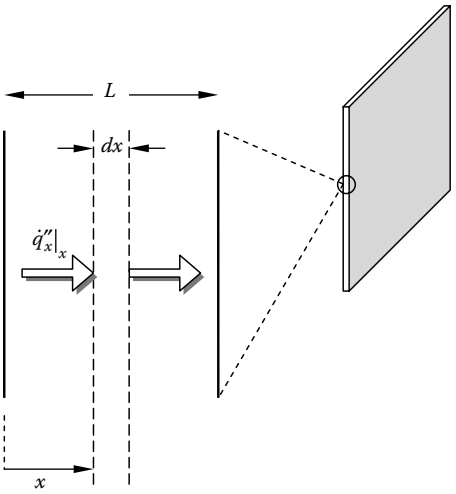


FIGURE 4.1 One-dimensional heat conduction in a solid sheet.

$$\begin{bmatrix} \text{Rate} \\ \text{of energy} \\ \text{accumulation} \end{bmatrix} = \frac{\partial}{\partial t}\left(\rho A dx C_p T\right) = \rho A dx C_p \frac{\partial T}{\partial t} \tag{4.3}$$

As heat (energy) is only transferred by heat conduction we also have that

$$\begin{bmatrix} \text{Rate} \\ \text{of energy} \\ \text{input} \end{bmatrix} = A\dot{q}''_x\Big|_x = -Ak\frac{\partial T}{\partial x}\Big|_x \tag{4.4}$$

$$\begin{bmatrix} \text{Rate} \\ \text{of energy} \\ \text{output} \end{bmatrix} = A\dot{q}''_x\Big|_{x+dx} = -Ak\frac{\partial T}{\partial x}\Big|_{x+dx} \tag{4.5}$$

where the symbol $|_x$ denotes evaluation at x. From Equations 4.3 through 4.5 we obtain

$$\rho A dx C_p \frac{\partial T}{\partial t} = -Ak\frac{\partial T}{\partial x}\Big|_x - \left(-Ak\frac{\partial T}{\partial x}\Big|_{x+dx}\right)$$

or

$$\frac{1}{\alpha}\frac{\partial T}{\partial t} = \frac{\partial}{\partial x}\left(\frac{\partial T}{\partial x}\right) \tag{4.6}$$

where $\alpha = k/(\rho C_p)$ is called the thermal diffusivity and is an important property of any material expressing its capacity to conduct thermal energy relative to its capacity to store thermal energy (small α corresponds to a material with large thermal inertia and the temperature of the material changes in a sluggish way).

When conduction takes place in all directions then $T = T(x,y,z,t)$ and Equation 4.6 becomes

$$\frac{1}{\alpha}\frac{\partial T}{\partial t} = \frac{\partial}{\partial x}\left(\frac{\partial T}{\partial x}\right) + \frac{\partial}{\partial y}\left(\frac{\partial T}{\partial y}\right) + \frac{\partial}{\partial z}\left(\frac{\partial T}{\partial z}\right) \tag{4.7}$$

The right-hand side of Equation 4.7 is defined as the Laplacian of the scalar field of the temperature and in effect Equation 4.7 can be written in the following more compact way (Baehr and Stephan, 2006)

$$\frac{1}{\alpha}\frac{\partial T}{\partial t} = \nabla^2 T = \nabla \cdot \left(\nabla T\right) \tag{4.8}$$

TABLE 4.1
Summary of Heat Diffusion Equation

Heat Diffusion Equation

$$\frac{1}{\alpha}\frac{\partial T}{\partial t} = \nabla^2 T = \nabla \cdot (\nabla T)$$

	3-D	1-D	1-D at Steady State
Rectangular	$\frac{1}{\alpha}\frac{\partial T}{\partial t} = \frac{\partial}{\partial x}\left(\frac{\partial T}{\partial x}\right) + \frac{\partial}{\partial y}\left(\frac{\partial T}{\partial y}\right) + \frac{\partial}{\partial z}\left(\frac{\partial T}{\partial z}\right)$	$\frac{1}{\alpha}\frac{\partial T}{\partial t} = \frac{\partial}{\partial x}\left(\frac{\partial T}{\partial x}\right)$	$\frac{d}{dx}\left(\frac{dT}{dx}\right) = 0$
Cylindrical	$\frac{1}{\alpha}\frac{\partial T}{\partial t} = \frac{1}{r}\frac{\partial}{\partial r}\left(r\frac{\partial T}{\partial r}\right) + \frac{1}{r^2}\frac{\partial^2 T}{\partial \theta^2} + \frac{\partial}{\partial z}\left(\frac{\partial T}{\partial z}\right)$	$\frac{1}{\alpha}\frac{\partial T}{\partial t} = \frac{1}{r}\frac{\partial}{\partial r}\left(r\frac{\partial T}{\partial r}\right)$	$\frac{d}{dr}\left(r\frac{dT}{dr}\right) = 0$
Spherical	$\frac{1}{\alpha}\frac{\partial T}{\partial t} = \frac{1}{r^2}\frac{\partial}{\partial r}\left(r^2\frac{\partial T}{\partial r}\right) + \frac{1}{r^2\sin\theta}\frac{\partial}{\partial \theta}\left(\sin\theta\frac{\partial T}{\partial \theta}\right) + \frac{1}{r^2\sin^2\theta}\frac{\partial}{\partial \varphi}\left(\frac{\partial T}{\partial \varphi}\right)$	$\frac{1}{\alpha}\frac{\partial T}{\partial t} = \frac{1}{r^2}\frac{\partial}{\partial r}\left(r^2\frac{\partial T}{\partial r}\right)$	$\frac{d}{dr}\left(r^2\frac{dT}{dr}\right) = 0$

Equation 4.8 is usually referred to as the heat (diffusion) equation and is important to remember that it expresses the energy conservation principle. Its analytic form in rectangular, cylindrical, and spherical coordinates, as well as some of its more useful special forms are summarized in Table 4.1 (Lienhard and Lienhard, 2006).

4.2.3 Commonly Used Boundary Conditions

As can be observed from Table 4.1 the heat diffusion equation involves first derivative with respect to time and second derivatives with respect to spatial coordinates. As a result for its solution it is necessary to have one initial condition and two boundary conditions for each coordinate necessary to describe physically the system under study. Initial conditions are related to the temperature distribution across all physical space studied at the initial steady-state solution before a change is imposed on the system. Boundary conditions, however, need to describe either the temperature or the heat flow across the boundaries of the system for all times (from the initial to final steady state). The most commonly used boundary condition, and arguably the simplest possible, is to have a fixed temperature distribution across the boundary. This is known as boundary condition of first order. The second possibility is a specification on the heat flux across the boundary with the case of constant heat flux to be the most common

$$-k\left.\frac{\partial T}{\partial x}\right|_{specific\ boundary} = \text{constant} \tag{4.9}$$

In this category belongs the very important case of the insulated surface

$$-k\left.\frac{\partial T}{\partial x}\right|_{specific\ boundary} = 0 \quad \Rightarrow \quad \left.\frac{\partial T}{\partial x}\right|_{specific\ boundary} = 0 \tag{4.10}$$

An equally important case is that of heat transfer by convection in the boundary. In this case, the heat flux by conduction to (from) the boundary must be equal to the heat flux by convection from (to) the boundary. The basic equation for convection is the Newton's equation which simply states that the heat flux by convection is proportional to the temperature difference between the boundary (normally denoted by T_s) and the free body of the fluid (normally denoted by T_∞), that is (Lienhard and Lienhard, 2006; Baehr and Stephan, 2006):

$$\dot{q}''_{x,conv} = h\left(T_\infty - T_s\right) \tag{4.11}$$

h is the heat-transfer coefficient that depends on the fluid properties, geometry, conditions of flow, and so on, and is defined through Equation 4.11. In such cases the boundary condition obtains the following form:

$$k\left.\frac{\partial T}{\partial x}\right|_{specific\ boundary} = h\left(T_s - T_\infty\right) \tag{4.12}$$

4.2.4 Steady-State 1-D Conduction

In this section, the solution of the 1-D heat diffusion equation under steady-state condition will be presented. From Table 4.1 we can observe that the 1-D heat diffusion equation has the following form:

$$\frac{\partial}{\partial x}\left(x^n \frac{\partial T}{\partial x}\right) = 0 \tag{4.13}$$

where $n = 0$ for rectangular coordinates, $n = 1$ for cylindrical coordinates, and $n = 2$ for spherical coordinates.

We will first present the solution of 1-D heat diffusion equation in rectangular coordinates with constant temperature at the boundaries, that is, when the following boundary conditions hold for the case study shown in Figure 4.1

$$\frac{d}{dx}\left(\frac{dT}{dx}\right) = 0 \tag{4.14}$$

$$T|_{x=0} = T_0 \quad \text{and} \quad T|_{x=L} = T_L \tag{4.15}$$

The general solution of Equation 4.14 is the following:

$$T(x) = c_0 + c_1 x \tag{4.16}$$

where c_0 and c_1 are constants that can be determined using the boundary conditions

$$T_0 = c_0 \tag{4.17a}$$

$$T_L = T_0 + c_1 L \Rightarrow c_1 = \frac{T_L - T_0}{L} \tag{4.17b}$$

and therefore

$$\frac{T(x) - T_0}{T_L - T_0} = \frac{x}{L} \tag{4.18}$$

and also

$$\dot{q}''_x = -k \left. \frac{dT}{dx} \right|_{x=0} = k \frac{T_0 - T_L}{L} \tag{4.19}$$

In electricity, resistance (R) is defined through Ohm's law as the potential (V) divided by the transfer rate (current I), that is, $R = V/I$. In a similar way, we can define resistance to heat transfer as the ratio of the potential (temperature difference) to the heat-transfer rate (heat flux times the cross-sectional area) in which case from Equation 4.19 we obtain

$$R_{cond} = \frac{T_0 - T_L}{\dot{q}_x} = \frac{T_0 - T_L}{\dot{q}''_x A} = \frac{L}{kA} \tag{4.20}$$

An important generalization of the results just presented is that of the analysis of a composite wall, an example of which is shown in Figure 4.2. It can be proved that in the case of a composite wall consisting of three layers the following equation holds true:

$$T_0 - T_3 = \dot{q}_x \left(\frac{L_1}{k_1 A} + \frac{L_2}{k_2 A} + \frac{L_3}{k_3 A} \right) \tag{4.21}$$

For a composite wall consisting of N layers, a direct generalization of Equation 4.21 is

$$T_0 - T_N = \dot{q}_x \sum_{i=1}^{N} \left(\frac{L_i}{k_i A} \right) = \dot{q}_x \sum_{i=1}^{N} R_{cond,i} \tag{4.22}$$

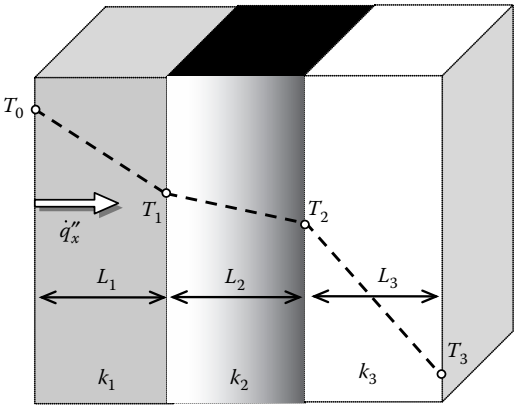


FIGURE 4.2 A composite wall.

When convective boundary conditions are considered, as shown in Figure 4.3, then

$$T_{\infty,H} - T_{\infty,C} = \dot{q}_x \left(\frac{1}{h_0 A} + \frac{L_1}{k_1 A} + \frac{L_2}{k_2 A} + \frac{L_3}{k_3 A} + \frac{1}{h_N A} \right) \tag{4.23}$$

It is important to note that the convective resistance, defined in a similar way to the conductive resistance, is $R_{conv} = 1/(hA)$. We also observe that in the case of a composite wall with convective boundary conditions the overall resistance is the sum of individual resistances.

In the analysis of cases with convective heat transfer at the boundaries it is more convenient to introduce the overall heat-transfer coefficient (U_o). First, we observe that Equation 4.23 for the general case of N layers can be written as

$$T_{\infty,H} - T_{\infty,C} = \dot{q}_x \left(\frac{1}{h_0} + \sum_{i=1}^{N} \frac{L_i}{k_i} + \frac{1}{h_N} \right) \frac{1}{A} \tag{4.24}$$

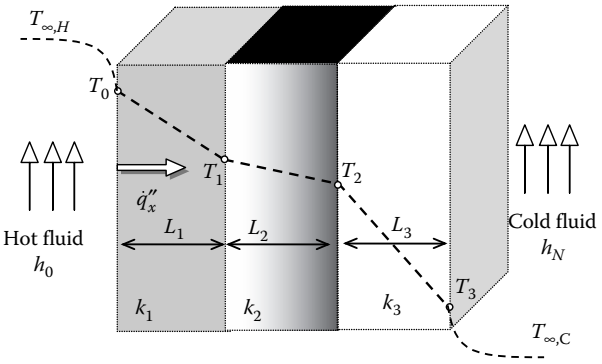


FIGURE 4.3 A composite wall with convective boundary conditions.

The overall heat-transfer coefficient is then defined as

$$\frac{1}{U_o} = \frac{1}{h_0} + \sum_{i=1}^{N} \frac{L_i}{k_i} + \frac{1}{h_N} \tag{4.25}$$

and in effect Equation 4.24 can be written as

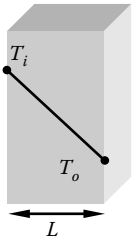
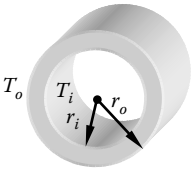
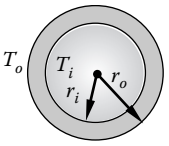
$$\dot{q}_x = U_o A\left(T_{\infty,H} - T_{\infty,C}\right) \tag{4.26}$$

Tables 4.2 and 4.3 summarize the results of this section including the cases of cylindrical or spherical geometries (Lienhard and Lienhard, 2006).

TABLE 4.2
Solution of the Steady-State Heat Diffusion Equation

Steady-State Heat Conduction

$$\frac{d}{dr}\left(r^n \frac{dT}{dr}\right) = 0, T = T_i @ r = r_i,\ T = T_o @ r = r_o$$

Geometry	Temperature Distribution
Cartesian ($n = 0$) 	$\frac{T(x) - T_i}{T_o - T_i} = \frac{x}{L}$
Cylindrical ($n = 1$) 	$\frac{T(r) - T_o}{T_i - T_o} = \frac{\ln(r/r_o)}{\ln(r_i/r_o)}$
Spherical ($n = 2$) 	$\frac{T(r) - T_i}{T_o - T_i} = \frac{1 - (r_i/r)}{1 - (r_i/r_o)}$

Note: Subscript i denotes inside and o outside.

TABLE 4.3
Summary of Equation Applied to Composite Structures with Convective Boundary Conditions

General equation

$$\dot{q}_x = AU_o(T_{\infty,H} - T_{\infty,C})$$

Composite wall

$$\frac{1}{U_o} = \frac{1}{h_0} + \sum_{i=1}^{N}\left(\frac{L_i}{k_i}\right) + \frac{1}{h_N}$$

Composite cylinder

$$\frac{1}{AU_o} = \frac{1}{A_0}\left(\frac{1}{h_0} + r_0\sum_{i=1}^{N}\frac{\ln(r_i/r_{i-1})}{k_i} + \frac{r_0}{r_N}\frac{1}{h_N}\right) = \cdots$$

$$= \frac{1}{A_N}\left(\frac{r_N}{r_0}\frac{1}{h_0} + r_N\sum_{i=1}^{N}\frac{\ln(r_i/r_{i-1})}{k_i} + \frac{1}{h_N}\right)$$

Composite sphere

$$\frac{1}{AU_o} = \frac{1}{A_0}\left(\frac{1}{h_0} + r_0^2\sum_{i=1}^{N}\frac{1}{k_i}\left(\frac{r_i - r_{i-1}}{r_{i-1}r_i}\right) + \frac{r_0^2}{r_N^2}\frac{1}{h_N}\right) = \cdots$$

$$= \frac{1}{A_N}\left(\frac{r_N^2}{r_0^2}\frac{1}{h_0} + r_N^2\sum_{i=1}^{N}\frac{1}{k_i}\left(\frac{r_i - r_{i-1}}{r_{i-1}r_i}\right) + \frac{1}{h_N}\right)$$

4.3 CONVECTION

It has already been mentioned that convection is the mode of heat transfer between a solid surface and a moving fluid. In the absence of fluid motion the heat is transferred by conduction only. The flow conditions (as well as geometry and physical properties) play an important role in conductive heat transfer and the analysis is significantly more complex. The basic equation for heat transfer by convection is the Newton's law of cooling given by Equation 4.11. The objective of the analysis is to determine the heat-transfer coefficient h. To this end there are three approaches that can be followed (Lienhard and Lienhard, 2006; Baehr and Stephan, 2006):

1. Analytical determination of the heat-transfer coefficient. This approach involves the determination of the exact temperature distribution from which the heat-transfer coefficient can be determined through Equation 4.11.
2. Analogy between heat and momentum transfer. Most early work in theoretically predicting the heat transfer in both laminar and turbulent flow cases was done using the analogy between momentum and heat by predicting the approximate results for the heat-transfer coefficient from the momentum transfer or skin friction coefficient.

TABLE 4.4
Most Important Dimensionless Numbers Used in Convective Heat Transfer

Dimensionless Number	Symbol	Definition
Nusselt number	Nu_ℓ	$Nu_\ell = \dfrac{h\ell}{k}$
Reynolds number	Re_ℓ	$\mathrm{Re}_\ell = \dfrac{u\ell\rho}{\mu} = \dfrac{u\ell}{\upsilon}$
Prandtl number	Pr	$\mathrm{Pr} = \dfrac{C_P\mu}{k}$
Peclet number	Pe	$Pe = RePr$
Grashof number	Gr	$Gr = \dfrac{L^3 g\beta\rho^2\Delta T}{\mu^2}$
Rayleigh number	Ra	$Re = GrPr$

Note: ℓ: characteristic dimension.

3. Dimensional analysis. In the cases where the previous two methods fail the heat-transfer coefficient can be obtained by experimental data in terms of appropriate dimensionless numbers obtained by dimensional analysis. The most important dimensionless numbers are summarized in Table 4.4.

Convective heat transfer is classified as natural or forced convection and a characteristic case is shown in Figure 4.4. A hot sphere is located on a flat plate. In the case of natural convection, the air adjacent to the sphere is heated and its density is decreased causing its upward movement. In the case of forced convection a fan is used to force air movement around the hot sphere.

Before presenting some representative equations for convective heat transfer the method of dimensional analysis will be presented briefly. Dimensional analysis is based on dimensional homogeneity, which must be satisfied by variables descriptive of any system. A minimum number of fundamental dimensions are used (as all other dimensions are related to these) and then dimensional analysis can be applied (even without any knowledge of the controlling equations) provided that all variables that are important in the problem under study are included in the analysis. A set of fundamental dimensions, appropriate for studying convective heat-transfer problems, includes mass (M), length (L), time (t), and temperature (T). Some of the most important quantities and their dimensions in the above MLtT system are shown in Table 4.5. In general, the number of dimensionless numbers or groupings of variables that are required to describe a particular problem equals the number of variables considered less the number of independent

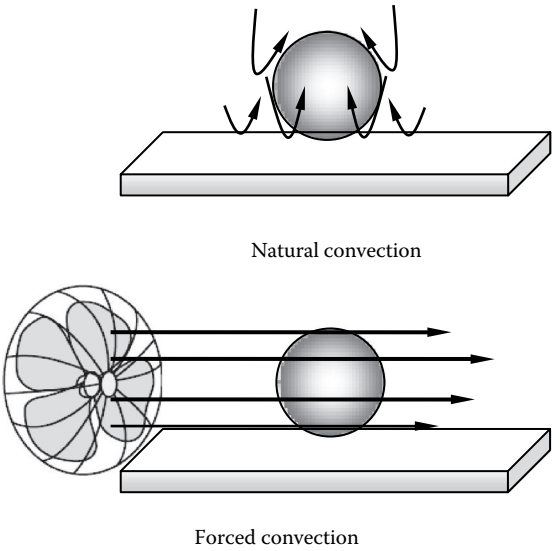


FIGURE 4.4 An example of natural versus forced convection.

TABLE 4.5
Quantities Important to Heat Transfer and Their Dimensions in the Mass, Length, Time, and Temperature Unit System

Quantity	Symbol	Dimensions in MLtT System
Mass	m	M
Length	L	L
Time	t	t
Temperature	T	T
Density	ρ	$M^1 L^{-3} t^0 T^0$
Velocity	u	$M^0 L^1 t^{-1} T^0$
Acceleration	g	$M^0 L^1 t^{-2} T^0$
Force	F	$M^1 L^1 t^{-2} T^0$
Work	w	$M^1 L^2 t^{-2} T^0$
Specific energy	e	$M^0 L^2 t^{-2} T^0$
Specific heat	C_p	$M^0 L^2 t^{-2} T^{-1}$
Absolute viscosity	μ	$M^1 L^{-1} t^{-1} T^0$
Kinematic viscosity	ν	$M^0 L^2 t^{-1} T^0$
Thermal conductivity	k	$M^1 L^1 t^{-3} T^{-1}$
Heat-transfer coefficient	h	$M^1 L^0 t^{-3} T^{-1}$

Source: Baehr, D.B. and Stephan, K. 2006. *Heat and Mass Transfer*, 2nd ed., Springer-Verlag: Berlin, 688 pp.

equations available. Convective heat-transfer coefficient in a circular tube, for instance, depends on:

- The velocity u of the fluid inside the tube
- The density ρ of the fluid
- The specific heat capacity C_p of the fluid
- The thermal conductivity k of the fluid
- The tube diameter D
- The viscosity μ of the fluid

We observe that seven variables (including h) have been identified that involve four fundamental units. It is therefore reasonable to seek for three (seven parameters minus four equations) dimensionless parameters. To find these three dimensionless groups we may consider the following:

$$\text{Constant} = u^a \rho^b C_p^c k^d D^e \mu^f h^g \tag{4.27}$$

where a, b, c, d, e, f, and g are constants to be determined through the homogeneity requirement using Table 4.5:

$$M^0 L^0 t^0 T^0 = \left(\frac{L}{t}\right)^a \left(\frac{M}{L^3}\right)^b \left(\frac{L^2}{t^2 T}\right)^c \left(\frac{ML}{t^3 T}\right)^d L^e \left(\frac{M}{Lt}\right)^f \left(\frac{M}{t^3 T}\right)^g \tag{4.28}$$

From Equation 4.28, we can easily derive the following equations that limit the possible values of the seven exponents

$$M: 0 = b + d + f + g \tag{4.29a}$$

$$L: 0 = a - 3b + 2c + d + e - f \tag{4.29b}$$

$$t: 0 = a + 2c + 3d + f + 3g \tag{4.29c}$$

$$T: 0 = c + d + g \tag{4.29d}$$

We have seven variables and only four equations and we can express any four of them as a function of any three independent exponents. If we select a, c, and g as independent exponents we then can solve Equations 4.29 to obtain:

$$M: b = a \tag{4.30a}$$

$$L: e = a + g \tag{4.30b}$$

$$t: f = c - a \tag{4.30c}$$

$$T: d = -c - g \tag{4.30d}$$

By substituting Equations 4.30 into Equation 4.27 we finally obtain:

$$\text{Constant} = \left(\frac{uD\rho}{\mu}\right)^a \left(\frac{C_p\mu}{k}\right)^c \left(\frac{hD}{k}\right)^g$$

or

$$\text{Constant} = \text{Re}^a\,\text{Pr}^c\,Nu^g \tag{4.31}$$

The particular values of the exponents are determined experimentally. In this particular example if the objective is to determine the local Nusselt number, then it is reasonable to set $g = 1$ and write Equation 4.31 in the following form:

$$Nu = \text{constant}\,\text{Re}^n\,\text{Pr}^m \tag{4.32}$$

Performing experiments at constant Pr number but variable Re number will supply the data necessary to determine n. A similar set of experiments with constant Re but variable Pr can be used to determine m. A formal introduction to the powerful Buckingham π theorem (Buckingham, 1914) can be found at the references given at the end of the chapter. Most equations for convective heat transfer have the following general form (Lienhard and Lienhard, 2006; Baehr and Stephan, 2006):

$$Nu = f(\text{Re, Pr, Gr}) \tag{4.33}$$

Characteristic examples are the following:

1. Local heat-transfer coefficient for turbulent flow over a flat plate

$$Nu_x = \frac{hx}{k} = 0.023\,\text{Re}_x^{0.8}\,\text{Pr}^{0.33}\left(\frac{\mu_\infty}{\mu_w}\right)^{0.14} \tag{4.34}$$

   where the subscript ∞ is used to denote the free (undisturbed) stream of the fluid, w is used to denote calculation at the conditions at the wall, and x is the distance from the edge of the wall. Equation 4.34 applies when $0.6 < \text{Pr} < 60$. For liquid metals such as mercury the following equation can be used:

$$Nu_x = 0.565\sqrt{\text{Re}_x\,\text{Pr}} = 0.565\sqrt{\text{Pe}_x} \tag{4.35}$$

2. Flow over a spherical object with diameter D

$$Nu_D = \frac{hD}{k} = 2 + \left(0.4\,\text{Re}_D^{1/4} + 0.06\,\text{Re}_D^{2/3}\right)\text{Pr}^{0.4}\left(\frac{\mu_\infty}{\mu_w}\right)^{1/4} \tag{4.36}$$

which holds for a wide range of Reynolds numbers ($3.5 < \mathrm{Re}_D < 80000$, $0.7 < \mathrm{Pr} < 380$).

3. Flow over a horizontal cylinder (cross flow) of diameter D

$$Nu_D = \frac{hD}{k} = 0.3 + \frac{0.06\,\mathrm{Re}_D^{1/2}\,\mathrm{Pr}^{1/3}}{\left[1+\left(\frac{0.4}{\mathrm{Pr}}\right)^{2/3}\right]^{1/4}}\left[1+\left(\frac{\mathrm{Re}_D}{282000}\right)^{5/8}\right]^{4/5} \tag{4.37}$$

which holds for a wide range of Reynolds numbers $10^2 < \mathrm{Re}_D < 10^7$ ($\mathrm{Pe} < 0.2$).

4. Flow inside circular tubes (Seider–Tate equation), turbulent fully developed flow with constant temperature of the tube

$$Nu_D = 0.027\,\mathrm{Re}_D^{4/5}\,\mathrm{Pr}^{1/3}\left(\frac{\mu_\infty}{\mu_w}\right)^{0.14} \tag{4.38}$$

which is applicable when $0.7 < \mathrm{Pr} < 16700$, $L/D > 10$, and $\mathrm{Re}_D > 10000$. The Nusselt number is the local Nusselt number and all properties are calculated at the mean fluid temperature.

4.4 UNSTEADY-STATE CONDUCTION

4.4.1 Infinite Plane (Slab)

The problem under consideration consists of a solid slab of thickness L. The other two dimensions of the solid are assumed to extend to infinity, or for practical purposes they are one order of magnitude larger than slab thickness, such as any heat transfer from these sides can be ignored. The slab has initially constant temperature, T_0, throughout, and at time zero ($t = 0$) it is exposed to a medium of temperature T_∞ (Figure 4.5). We are seeking an expression for the temperature evolution, at every point, in the slab, that is, an expression for $T(x,t)$, for x being the distance from the slab center.

Recall the governing partial differential equation in rectangular coordinates (see Table 4.1)

$$\frac{1}{\alpha}\frac{\partial T}{\partial t} = \frac{\partial}{\partial x}\left(\frac{\partial T}{\partial x}\right) \quad \text{or} \quad \frac{1}{\alpha}\frac{\partial T}{\partial t} = \frac{\partial^2 T}{\partial x^2} \tag{4.39}$$

subject to the following initial and boundary conditions:

Initial condition (IC):

$$T(x,t=0) = T_0 = \text{constant} \tag{4.40}$$

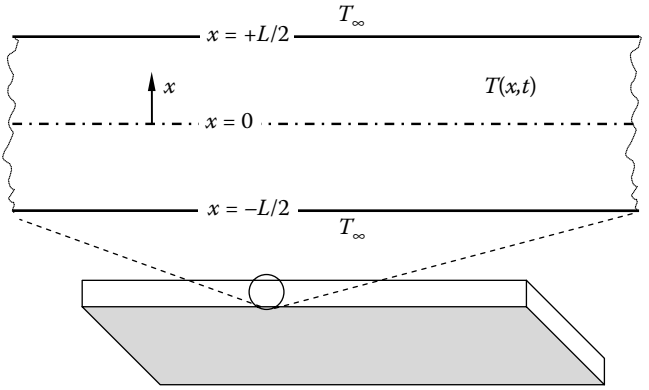


FIGURE 4.5 Unsteady-state, one-dimensional, heat conduction on the slab.

Boundary conditions (BC):

$$k\left.\frac{\partial T}{\partial x}\right|_{x=0} = 0 \tag{4.41}$$

representing symmetry at the centerline, and either

$$T(x = L/2,\ t) = T_\infty = \text{constant} \tag{4.42}$$

indicating instantaneous equilibrium between body surface and medium temperature (implying infinite heat-transfer coefficient h between heating or cooling medium and the solid surface), or

$$k\left.\frac{\partial T}{\partial x}\right|_{x=L/2} = h\left(T_\infty - T(x = L/2,t)\right) \tag{4.43}$$

for finite heat-transfer coefficient, h (which causes a resistance to heat transfer and leads to a lag between body surface and medium temperature).

Infinite heat-transfer coefficient. The solution to Equation 4.39, subject to IC (4.40) and BCs given by Equations 4.41 and 4.42 are explicitly given here by the following equation (Carslaw and Jaeger, 1959):

$$Y_{slab} = \frac{T_\infty - T(x,t)}{T_\infty - T_0} = \sum_{m=1}^{\infty} \frac{2\,(-1)^{m+1}}{\lambda_m} \cos\left(\lambda_m \frac{x}{L/2}\right) e^{-\lambda_m^2 \frac{\alpha\, t}{(L/2)^2}} \tag{4.44}$$

where

$$\lambda_m = (2m - 1)\frac{\pi}{2} \tag{4.45}$$

The distance from the center of the slab, x, and the time, t, are appearing in Equation 4.44 in dimensionless forms as $x/(L/2)$ and $\alpha\, t/(L/2)^2$, the Fourier number, respectively. Fourier number, Fo, is, in general, defined as

$$Fo = \frac{\alpha\, t}{\delta^2} \tag{4.46}$$

for δ being the characteristic dimension for one-dimensional heat conduction solids, that is, the half thickness of a slab ($L/2$ in the case presented) or the radius of an infinite cylinder and a sphere. Results through Equation 4.44 are traditionally presented in the so-called Heisler or Gurney–Lurie charts (Gurney and Lurie, 1923; Heldman and Singh 1981) in graphical form where the dimensionless and normalized temperature (Y) is plotted, on a logarithmic scale, as a function of the Fourier number (Fo), with the dimensionless distance (x/δ) as a parameter. The data presented on these diagrams are for a Fo value greater than approximately 0.3 and they form a set of parallel lines (each line for a different $x/(L/2)$ value as illustrated in Figure 4.6).

Indeed, for long times (for about $Fo \geq 0.3$ for our case) only the first term of the series summation of Equation 4.44 is needed for accurate temperature calculations, since the exponential part of each term in the series summation diminishes very fast. For example, for $Fo = 0.3$ one can consecutively estimate

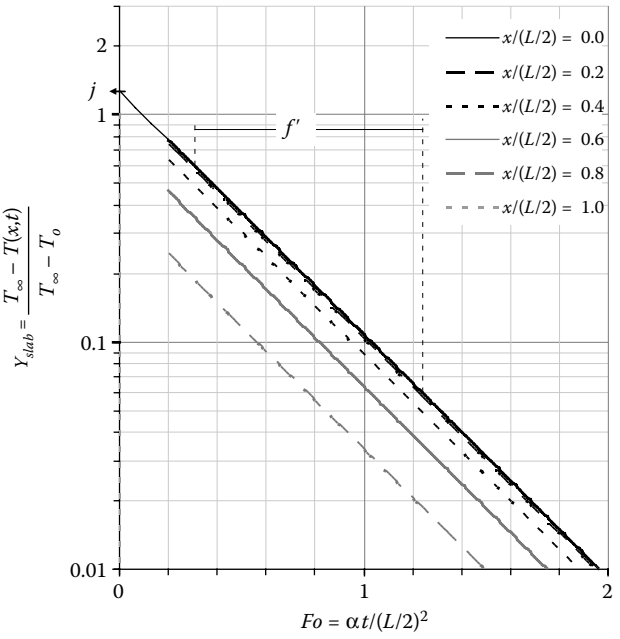


FIGURE 4.6 Temperature evolution at various positions in a conduction-heating slab with infinite heat-transfer coefficient at the surface.

$$\text{for } m = 1 \Rightarrow \lambda_1 = \pi/2, \quad \text{and} \quad e^{-\lambda_1^2 \frac{\alpha\, t}{(L/2)^2}} = e^{-\lambda_1^2 \cdot Fo} = e^{-\left(\frac{\pi}{2}\right)^2 0.3} = 0.4770$$

$$\text{for } m = 2 \Rightarrow \lambda_2 = 3\pi/2, \quad \text{and} \quad e^{-\lambda_2^2 \frac{\alpha\, t}{(L/2)^2}} = e^{-\lambda_2^2 \cdot Fo} = e^{-\left(\frac{3\pi}{2}\right)^2 0.3} = 0.0013$$

$$\text{while for } m = 3, \Rightarrow \lambda_3 = 5\pi/2, \quad \text{and} \quad e^{-\lambda_3^2 \frac{\alpha\, t}{(L/2)^2}} = e^{-\lambda_3^2 \cdot Fo} = e^{-\left(\frac{5\pi}{2}\right)^2 0.3} = 9.19 \cdot 10^{-9}$$

Thus, for long times, the use of one-term approximation to the series summation introduces an error of less than 0.3% on the Y_{slab} values. Using one-term approximation, Equation 4.44 reduces to

$$Y_{slab} = \frac{T_\infty - T(x,t)}{T_\infty - T_0} = \frac{4}{\pi} \cos\left(\frac{\pi\, x}{L}\right) e^{-\frac{\pi^2 \alpha\, t}{L^2}} \tag{4.47}$$

Equation 4.47 can be used instead of Heisler charts or similar diagrams. The fact that Equation 4.47 suggests a straight line diagram when $\log(Y_{slab})$ is plotted against time is shown in Figure 4.6. The distance from the center (x) affects the position of the straight line (as it can be inferred from the pre-exponential term of Equation 4.47) but it does not affect the slope of the line (which is directly related to the factor that multiplies the time variable in the exponential term).

Following the thermal processing literature, an empirical form of Equation 4.47, that simplifies temperature calculations for "long times," will be presented. Each straight line ($\log(Y_{slab})$ vs. Fo) shown in Figure 4.6 can be described by a linear equation of the form:

$$\log(Y_{slab}) = \text{Intercept} + \text{slope} \cdot Fo \tag{4.48}$$

Intercept is traditionally symbolized by the parameter "j," the so-called lag factor, while slope is replaced by its negative reciprocal, the parameter "f" and Equation 4.48 can be written as (Ball, 1923)

$$Y_{slab} = j_{slab}\ 10^{-t/f_{slab}} \tag{4.49}$$

where the parameter f' has been replaced by the parameter f, since Y_{slab}, in Equation 4.49, is given as a function of time instead of Fourier number. The parameter f is formally defined as the time required for Y_{slab} to be reduced by a factor of 10, or, equivalently, as the time required for the straight line of $\log(Y_{slab})$ versus t to traverse a logarithmic cycle. The f value is independent of the position in the slab where temperature is calculated.

Comparing Equation 4.49 with Equation 4.47 we can relate the empirical f and j values with the one-term solution to obtain

$$j = \frac{4}{\pi}\cos\left(\frac{\pi\, x}{L}\right) \tag{4.50}$$

which, for the center of the slab ($x = 0$) reduces to

$$j_c = \frac{4}{\pi} = 1.273240 \tag{4.51}$$

and

$$f = \frac{\ln(10)}{\alpha}\frac{L^2}{\pi^2} \tag{4.52}$$

Finite heat-transfer coefficient. The solution to Equation 4.39, subject to IC (4.40) and BC given by Equations 4.41 and 4.43 is explicitly given by the following equation (Carslaw and Jaeger, 1959):

$$Y_{slab} = \frac{T_\infty - T(x,t)}{T_\infty - T_0} = \sum_{m=1}^{\infty} \frac{2\,\sin(\lambda'_m)}{\lambda'_m + \sin(\lambda'_m)\cos(\lambda'_m)} \cos\left(\lambda'_m \frac{x}{L/2}\right) e^{-\lambda'^2_m \frac{\alpha\, t}{(L/2)^2}} \tag{4.53}$$

where λ'_m is the mth positive root of the following transcendental equation

$$\lambda'_m \tan(\lambda'_m) = Bi \tag{4.54}$$

and Bi is the Biot number defined as (Baehr and Stephan, 2006)

$$Bi = \frac{h(L/2)}{k}, \quad \text{or in general as,} \quad Bi = \frac{h\,\delta}{k} \tag{4.55}$$

As in the case of infinite heat-transfer coefficient the f and j values for the case of finite heat-transfer coefficient can be calculated as

$$j = \frac{2\,\sin(\lambda'_1)}{\lambda'_1 + \sin(\lambda'_1)\cos(\lambda'_1)} \cos\left(\lambda'_1 \frac{x}{L/2}\right) \tag{4.56}$$

$$j_c = \frac{2\,\sin(\lambda'_1)}{\lambda'_1 + \sin(\lambda'_1)\cos(\lambda'_1)} \tag{4.57}$$

and

$$f = \frac{\ln(10)}{\alpha}\frac{L^2}{4\lambda'^2_1} \tag{4.58}$$

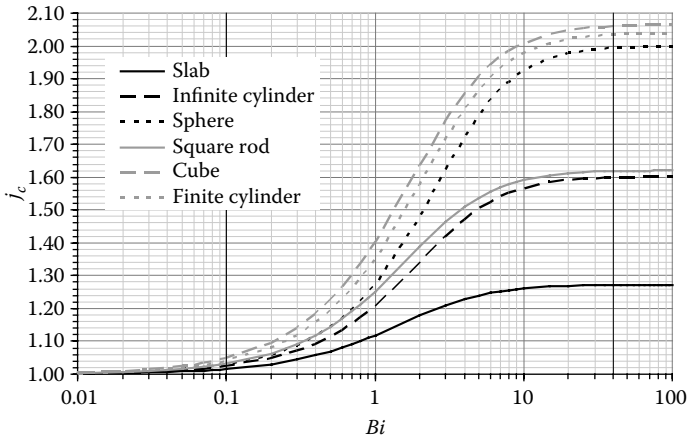


FIGURE 4.7 Effect of Biot number on the center *j* value (j_c) for different geometries.

From Equations 4.56 and 4.58, one can infer that the parameter *j* is a function of Biot number and position, while the parameter *f* is a function of Biot number and body properties. The effect of Biot number on the center *j* value (j_c) is depicted in Figure 4.7 (together with corresponding values for other geometries to be discussed in subsequent paragraphs).

From Figure 4.7 it can be noted that for $Bi \geq 40$, and for all geometries, j_c remains constant. It approaches the value corresponding to the case of infinite heat-transfer coefficient (~1.27 for the case of the slab, see Equation 4.51). Furthermore, note that for large *Bi* values, $\lambda_1' \rightarrow \lambda_1 = \pi/2$. Thus, Equation 4.44 can be thought as a special case of Equation 4.53, for $h \rightarrow \infty$, and can be used when $Bi \geq 40$, due to the simpler calculations involved. Furthermore, for small Biot numbers, that is, for $Bi \leq 0.1$, j_c values approach unity. Under these conditions there is a uniform temperature distribution within the product as it can be inferred from Figure 4.8. In this case, at all positions inside a slab, *j* values coincide (and are equal to unity), indicating uniform temperature throughout a slab and a lumped capacitance model can be used:

$$\frac{T_\infty - T(x,t)}{T_\infty - T_o} = e^{-\left(\frac{hA}{mC_p}\right)t} \tag{4.59}$$

Equation 4.59 is the solution of the following governing ordinary differential equation that results from applying the energy balance to a slab under uniform temperature *T*:

$$mC_p \frac{dT}{dt} = h\,A\,(T_\infty - T) \tag{4.60}$$

subject to the initial condition $T(t = 0) = T_0$. The above discussion is not restricted to the slab geometry or solids; it is also applicable to uniformly heated fluids

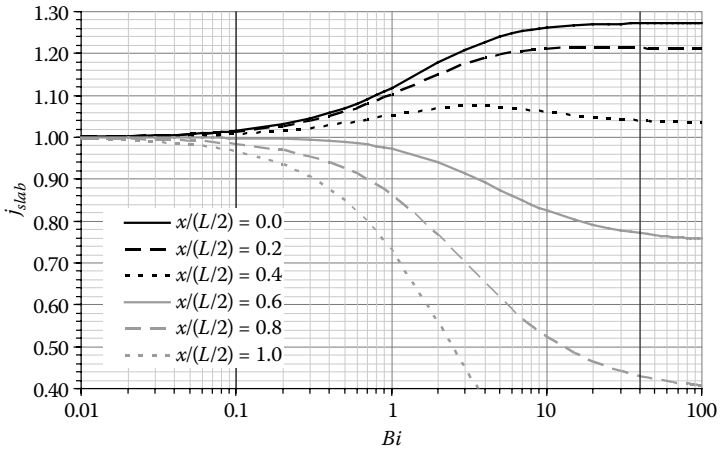


FIGURE 4.8 Effect of Biot number on the *j* value at different positions on a slab.

(forced convection heating) with *h* being replaced by the overall heat-transfer coefficient U_o.

4.4.2 Infinite Cylinder

We will follow the same steps, as for the case of infinite plane (slab), to describe the temperature evolution in a infinite solid cylinder, that is, a cylinder of finite radius *R* but infinite length (see Figure 4.9). Recall the governing partial differential equation in cylindrical coordinates (Table 4.1)

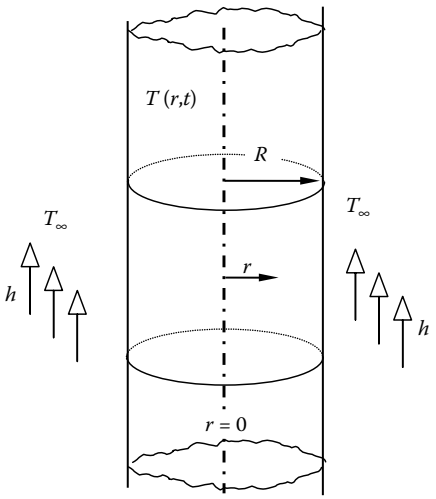


FIGURE 4.9 Unsteady-state, one-dimensional, heat conduction in an infinite cylinder.

$$\frac{1}{\alpha}\frac{\partial T}{\partial t} = \frac{1}{r}\frac{\partial}{\partial r}\left(r\frac{\partial T}{\partial r}\right) \quad \text{or} \quad \frac{1}{\alpha}\frac{\partial T}{\partial t} = \frac{\partial^2 T}{\partial r^2} + \frac{1}{r}\frac{\partial T}{\partial r} \tag{4.61}$$

subject to the following initial and boundary conditions:

Initial condition (IC):

$$T(r,t=0) = T_0 = \text{constant} \tag{4.62}$$

Boundary conditions (BC):

$$k\left.\frac{\partial T}{\partial r}\right|_{r=0} = 0 \tag{4.63}$$

representing symmetry at the central body axis, and either

$$T(r=R,t) = T_\infty = \text{constant} \tag{4.64}$$

indicating instantaneous equilibrium between the cylindrical body surface and medium temperature, or

$$k\left.\frac{\partial T}{\partial r}\right|_{r=R} = h\left(T_\infty - T(r=R,t)\right) \tag{4.65}$$

for finite heat-transfer coefficient, h.

4.4.2.1 Infinite Heat-Transfer Coefficient

The solution to Equation 4.61, subject to IC (4.62) and BC given by Equations 4.63 and 4.64 is given by (Arpachi, 1966)

$$Y_{\substack{infinite\\cylinder}} = \frac{T_\infty - T(r,t)}{T_\infty - T_0} = \sum_{n=1}^{\infty} \frac{2\,J_0(\beta_n(r/R))}{\beta_n\,J_1(\beta_n)}\,e^{-\beta_n^2(\alpha t/R^2)} \tag{4.66}$$

where β_n is the nth positive root of

$$J_0(\beta_n) = 0 \tag{4.67}$$

and J_0 is the Bessel function of the first kind of order zero and J_1 is the Bessel function of the first kind of order one. As for the case of slab, for "long times," that is for about $Fo \geq 0.2$, the following equation, which is equivalent to Equation 4.49, can be used:

$$Y_{\substack{infinite\\cylinder}} = j_{\substack{infinite\\cylinder}}\,10^{-t/f_{\substack{infinite\\cylinder}}} \tag{4.68}$$

TABLE 4.6
Theoretical *f* and *j* Values for Conduction Heat Transfer (Uniform Initial Temperature, Constant Medium Temperature, and Infinite Heat-Transfer Coefficient)

Geometry	*f* Value	*j* Value at any Point	*j* Value at Geometrical Center
Infinite slab	$\frac{\ln(10)}{\alpha}\frac{L^2}{\pi^2}$	$1.273240\cos\left(\frac{\pi x}{L}\right)$	1.273240
Infinite cylinder[a]	$\frac{\ln(10)}{\alpha}\frac{R^2}{\beta_1^2}$	$1.601975J_o\left(\beta_1\frac{r}{R}\right)$	1.601975
Sphere	$\frac{\ln(10)}{\alpha}\frac{R^2}{\pi^2}$	$0.636620\frac{R}{r}\sin\left(\frac{\pi r}{R}\right)$	2

Source: From Abramowitz, M. and Stegum, I.A. 1972. *Handbook of Mathematical Functions with Formulas, Graphs, and Mathematical Tables*. Dover Publications, Inc., New York, 1046 pp.

[a] For $\beta_1 = 2.4048255577$.

with the *f* and *j* values given in Table 4.6 together with the corresponding values for other geometries.

4.4.2.2 Finite Heat-Transfer Coefficient

The solution to Equation 4.61, subject to IC (4.62) and BC given by Equations 4.63 and 4.65 is given by (Arpachi, 1966)

$$Y_{\substack{infinite\\cylinder}} = \frac{T_\infty - T(r,t)}{T_\infty - T_0} = \sum_{n=1}^{\infty} \frac{2\,Bi\,J_0(\beta'_n(r/R))}{\left(\beta'^2_n + Bi^2\right)J_0\left(\beta'_n\right)}\, e^{-\beta'^2_n(\alpha t/R^2)} \tag{4.69}$$

where

$$Bi = \frac{h\,R}{k} \tag{4.70}$$

and β'_n is the nth positive root of

$$\beta'_n\,J_1(\beta'_n) = Bi\,J_0(\beta'_n) \tag{4.71}$$

The *f* and *j* values to be used with the empirical, one-term approximation Equation 4.68, for "long times," that is for about $Fo \geq 0.4$ (depending on the *h* value) are given in Table 4.7 together with corresponding values for other geometries and finite *h*.

TABLE 4.7
Theoretical *f* and *j* Values for Conduction Heat (Uniform Initial Temperature, Constant Medium Temperature, and Finite Heat-Transfer Coefficient)

Product Geometry	*f* Value	*j* Value at any Point	*j* Value at Geometric Center
Infinite slab	$\frac{\ln(10)}{\alpha}\frac{L^2}{4\lambda_1'^2}$	$\frac{2\sin(\lambda_1')}{\lambda_1' + \sin(\lambda_1')\cos(\lambda_1')}\cos\left(\lambda_1'\frac{2x}{L}\right)$	$\frac{2\sin(\lambda_1')}{\lambda_1' + \sin(\lambda_1')\cos(\lambda_1')}$
Infinite cylinder	$\frac{\ln(10)}{\alpha}\frac{R^2}{\beta_1'^2}$	$\frac{2\,Bi\,J_o\left(\beta_1'\frac{r}{R}\right)}{\left(\beta_1'^2 + Bi^2\right)J_0\left(\beta_1'\right)}$	$\frac{2\,Bi}{\left(\beta_1'^2 + Bi^2\right)J_0\left(\beta_1'\right)}$
Sphere	$\frac{\ln(10)}{\alpha}\frac{L^2}{4\zeta_1'^2}$	$\frac{2\,(\sin(\zeta_1') - \zeta_1'\cos(\zeta_1'))}{\zeta_1' - \sin(\zeta_1')\cos(\zeta_1')}\frac{\sin\left(\zeta_1'\frac{r}{R}\right)}{\zeta_1'\frac{r}{R}}$	$\frac{2\,(\sin(\zeta_1') - \zeta_1'\cos(\zeta_1'))}{\zeta_1' - \sin(\zeta_1')\cos(\zeta_1')}$

4.4.3 Sphere

The one-dimensional, unsteady state, temperature distribution for a solid sphere of radius R (see Figure 4.10) is given as the solution of the following differential equation (see Table 4.1):

$$\frac{1}{\alpha}\frac{\partial T}{\partial t} = \frac{1}{r^2}\frac{\partial}{\partial r}\left(r^2\frac{\partial T}{\partial r}\right) \tag{4.72}$$

subject to the following initial and boundary conditions:

Initial condition (IC):

$$T(r,t=0) = T_0 = \text{constant} \tag{4.73}$$

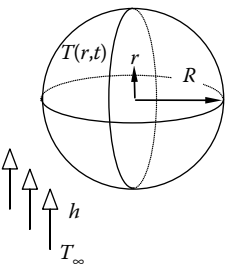


FIGURE 4.10 Unsteady-state, one-dimensional, heat conduction in a solid sphere.

Boundary conditions (BC):

$$k\left.\frac{\partial T}{\partial r}\right|_{r=0} = 0 \tag{4.74}$$

and

$$T(r = R,t) = T_\infty = \text{constant} \tag{4.75}$$

or

$$k\left.\frac{\partial T}{\partial r}\right|_{r=R} = h(T_\infty - T(r = R,t)) \tag{4.76}$$

Infinite heat-transfer coefficient. The solution of Equation 4.72, subject to IC (4.73) and BC given by Equations 4.74, and 4.75 is given by (Carslaw and Jaeger, 1959)

$$Y_{sphere} = \frac{T_\infty - T(r,t)}{T_\infty - T_0} = \frac{2R}{\pi r}\sum_{n=1}^{\infty}\frac{(-1)^{n+1}}{n}\sin\left(\frac{n\pi r}{R}\right)e^{-n^2\pi^2\frac{\alpha t}{R^2}} \tag{4.77}$$

Finite heat-transfer coefficient. The solution to Equation 4.72, subject to IC (4.73) and BC given by Equations 4.74 and 4.76 is given (Carslaw and Jaeger, 1959):

$$Y_{sphere} = \frac{T_\infty - T(r,t)}{T_\infty - T_0} = 2\sum_{n=1}^{\infty}\frac{\sin\left(\zeta_n'\right) - \zeta_n'\cos\left(\zeta_n'\right)}{\zeta_n' - \sin\left(\zeta_n'\right)\cos\left(\zeta_n'\right)}\frac{\sin\left(\zeta_n'(r/R)\right)}{\zeta_n'(r/R)}e^{-\zeta_n'^2\frac{\alpha t}{R^2}} \tag{4.78}$$

where ζ_n' is the nth positive root of

$$\zeta_n'\cot(\zeta_n') = 1 - Bi \tag{4.79}$$

As in the cases studied previously, for "long times," that is for about $Fo \geq 0.2$ to 0.3, Equation 4.78, equivalent to Equation 4.49, can be used in place of Equation 4.77 or 4.78 with the *f* and *j* values given in Tables 4.6 and 4.7, respectively.

4.4.4 Newman's Rule for Finite Body Geometries

For products with geometries that can be obtained as the intersection of two or more infinite bodies, the dimensionless and normalized temperature of such bodies, *Y*, is given as the product of the respective *Y* values of the infinite bodies (Newman, 1931). Thus, for example, the solution for the temperature evolution in a cube (the volume

that lies at the intersection of three infinite slabs of equal thickness, L), governed by the following governing equation (see Table 4.1):

$$\frac{1}{\alpha}\frac{\partial T}{\partial t} = \frac{\partial^2 T}{\partial x^2} + \frac{\partial^2 T}{\partial y^2} + \frac{\partial^2 T}{\partial z^2} \tag{4.80}$$

subject to the following initial

$$T(x,y,z,t=0) = T_0 = \text{constant} \tag{4.81}$$

and boundary conditions

$$k\left.\frac{\partial T}{\partial x}\right|_{x=0} = k\left.\frac{\partial T}{\partial y}\right|_{y=0} = k\left.\frac{\partial T}{\partial z}\right|_{z=0} = 0 \tag{4.82}$$

$$T(x = L/2,t) = T(y = L/2,t) = T(z = L/2,t) = T_\infty = \text{constant} \tag{4.83}$$

or

$$\begin{aligned} k\left.\frac{\partial T}{\partial x}\right|_{x=L/2} &= h\left(T_\infty - T(x = L/2,t)\right) \\ k\left.\frac{\partial T}{\partial y}\right|_{y=L/2} &= h\left(T_\infty - T(y = L/2,t)\right) \\ k\left.\frac{\partial T}{\partial z}\right|_{z=L/2} &= h\left(T_\infty - T(z = L/2,t)\right) \end{aligned} \tag{4.84}$$

is given by (Arpachi, 1966)

$$Y_{cube} = (Y_{slab})^3 \tag{4.85}$$

for Y_{slab} given either by Equation 4.44 for the BC given by Equation 4.83 or Equation 4.53 for the BC given by Equation 4.84.

Of special interest, in the area of food preservation by heat treatment is the knowledge of the temperature evolution in a finite cylinder (a can). This is the volume that lies at the intersection of an infinite slab (of thickness L) and an infinite cylinder (of thickness R), governed by the following form of the heat conduction equation:

$$\frac{1}{\alpha}\frac{\partial T}{\partial t} = \frac{\partial}{\partial x}\left(\frac{\partial T}{\partial x}\right) + \frac{1}{r}\frac{\partial}{\partial r}\left(r\frac{\partial T}{\partial r}\right) \tag{4.86}$$

and subjected to the initial and boundary conditions given by Equations 4.40, 4.41 and either Equation 4.42 or 4.43 for the slab part, and Equations 4.62, 4.63 and

either Equation 4.64 or 4.65 for the infinite cylinder part. The solution can be expressed as

$$Y_{can} = Y_{\underset{cylinder}{finite}} = Y_{slab} Y_{\underset{cylinder}{infinite}} \tag{4.87}$$

for Y_{slab} given either by Equation 4.44 or Equation 4.53 and $Y_{\underset{cylinder}{infinite}}$ by Equation 4.66 or Equation 4.69 depending on the particular boundary conditions related to a particular application. The one-term approximations, applicable for "long times," and expressions in terms of the empirical f and j parameters also hold for finite body geometries:

$$Y_{\underset{body}{finite}} = j_{\underset{body}{finite}} 10^{-t/f_{\underset{body}{finite}}} \tag{4.88}$$

In such cases, the j value for the finite body is equal to the product of the j values of the infinite bodies that their intersection forms the finite body under examination. The inverse of the f value for the finite body is equal to the sum of the inverses of the respective f values. Thus, for the case of the finite cylinder, we have:

$$j_{can} = j_{\underset{cylinder}{finite}} = j_{slab}\, j_{\underset{cylinder}{infinite}} \tag{4.89}$$

and

$$\frac{1}{f_{can}} = \frac{1}{f_{\underset{cylinder}{finite}}} = \frac{1}{f_{slab}} + \frac{1}{f_{\underset{cylinder}{infinite}}} \tag{4.90}$$

For the case of finite heat-transfer coefficient at the body's surface, the effect of Biot number on the j value at the geometric center for different finite geometries, namely, square rod, cube, and finite cylinder, are presented in Figure 4.7.

4.5 CASES OF SPECIAL INTEREST IN FOOD ENGINEERING

4.5.1 Variable Medium Temperature

During the thermal processing of foods a cooling cycle always follows the heating of the product. Microbial destruction that occurs at the early stages of the cooling cycle can be significant and must be taken into account (in addition to that achieved in the heating phase) during thermal process design. Thus, the temperature of the product during both heating and cooling must be known. For such cases, Duhamel's superposition integral can be used to obtain analytical expressions for the temperature evolution throughout the whole thermal process.

According to Myers (1971), "Duhamel's theorem provides a means for solving a problem with a time-dependent boundary condition by using the solution to a corresponding fundamental problem with steady boundary conditions." Duhamel's theorem, applicable for the case of variable medium temperature, can be stated as (Carslaw and Jaeger, 1959; Hildebrand, 1976; Myers, 1971): If $U(t)$ represents the temperature response to a linear homogeneous heat conduction problem initially at $T_0 = 0$ to a single unit step input ($T_\infty = 1$), then the solution, V, to the same problem but when medium temperature becomes a function of time, that is, for

$$T_\infty = \Phi(t) \tag{4.91}$$

is given by

$$V = \Phi(0)U(t) + \int_{\eta=0}^{\eta=t} U(t-\eta)\frac{\partial \Phi(\eta)}{\partial \eta}\, d\eta \tag{4.92}$$

or, equivalently, by

$$V = \int_{\eta=0}^{\eta=t} \Phi(\eta)\frac{\partial U(t-\eta)}{\partial t}\, d\eta \tag{4.93}$$

Thus, as an example, we can apply Equation 4.93 to calculate the temperature distribution in a can filled with solid food, initially at uniform temperature (T_{IT}), undergoing a typical thermal process, consisting of: (a) heating at constant medium temperature (T_{RT}) for time t_h and (b) then cooling at constant medium temperature (T_{CW}). We have that

$$U(t) = U(r,x,t) = 1 - Y_{can} \tag{4.94}$$

where Y_{can} is given by Equation 4.87 and, assuming infinite heat-transfer coefficient between heating or cooling medium and food, Y_{slab} is given by Equation 4.44 and $Y_{\substack{infinite\\cylinder}}$ by Equation 4.66, that is,

$$V(t) = V(r,x,t) = T_{can}(r,x,t) - T_{IT} \tag{4.95}$$

and

$$\begin{aligned} \Phi(t) &= T_{RT} - T_{IT} \quad \text{for } t \le t_f \\ \Phi(t) &= T_{CW} - T_{IT} \quad \text{for } t > t_f \end{aligned} \tag{4.96}$$

Finally, the temperature of the can as a function of time and position is explicitly given as (Flambert and Deltour 1972):

heating cycle ($t \le t_f$)

$$T(r,x,t)_{can} = T_{RT} + \left(T_{RT} - T_{IT}\right)\sum_{m=1}^{\infty}\sum_{n=1}^{\infty}\frac{4(-1)^{m+1}}{\lambda_m} \times \cos\left(\lambda_m \frac{x}{L/2}\right)\frac{J_0\left(\beta_n(r/R)\right)}{\beta_n J_1\left(\beta_n\right)} e^{-((\lambda_m^2/(L/2)^2)+(\beta_n^2/R^2))\alpha t} \tag{4.97}$$

cooling cycle ($t > t_f$)

$$\begin{aligned} T(r,x,t)_{can} = {} & T_{CW} - (T_{RT} - T_{IT})\sum_{m=1}^{\infty}\sum_{n=1}^{\infty}\frac{4(-1)^{m+1}}{\lambda_m} \\ & \times \cos\left(\lambda_m \frac{x}{L/2}\right)\frac{J_0\left(\beta_n(r/R)\right)}{\beta_n J_1\left(\beta_n\right)} e^{-((\lambda_m^2/(L/2)^2)+(\beta_n^2/R^2))\alpha t} \\ & + (T_{RT} - T_{CW})\sum_{m=1}^{\infty}\sum_{n=1}^{\infty}\frac{4(-1)^{m+1}}{\lambda_m} \\ & \times \cos\left(\lambda_m \frac{x}{L/2}\right)\frac{J_o\left(\beta_n(r/R)\right)}{\beta_n J_1\left(\beta_n\right)} e^{-((\lambda_m^2/(L/2)^2)+(\beta_n^2/R^2))\alpha\,(t-t_f)} \end{aligned} \tag{4.98}$$

4.5.2 Heat Conduction with Heat Source

Heat generation due to respiration must be taken into account in assessing product quality as well as designing cooling facilities during cooling storage of fruits and vegetables. Prediction of temperature evolution in such cases involves the solution of the appropriate heat conduction equation (see Table 4.1) with an added heat generation term, that is,

$$\rho C_p \frac{\partial T}{\partial t} = k\nabla^2 T + Q \tag{4.99}$$

where Q is the energy generated per unit volume (compare with Equation 4.8). In rectangular coordinates, Equation 4.99 can be written as

$$\frac{1}{\alpha}\frac{\partial T}{\partial t} = \left(\frac{\partial^2 T}{\partial x^2} + \frac{\partial^2 T}{\partial y^2} + \frac{\partial^2 T}{\partial z^2}\right) + \frac{Q}{k} \tag{4.100}$$

The existence of the Q/k term makes the differential equation nonhomogeneous and its solution procedure more laborious. For the case of one-dimensional, infinite slab, Equation 4.100 reduces to

$$\frac{1}{\alpha}\frac{\partial T}{\partial t} = \frac{\partial^2 T}{\partial x^2} + \frac{Q}{k} \tag{4.101}$$

For the initial and boundary conditions given by Equations 4.40, 4.41, and 4.43, the solution is given by (van Beek and Meffet, 1981)

$$Y_{slab} = \frac{T_\infty - T(x,t)}{T_\infty - T_0} = \frac{Po}{2}\left(1 - \left(\frac{x}{L/2}\right)^2 + \frac{2}{Bi}\right) + \sum_{m=1}^{\infty}\left(1 - \frac{Po}{\lambda_m'^2}\right)\frac{2\sin(\lambda_m')}{\lambda_m' + \sin(\lambda_m')\cos(\lambda_m')}\cos\left(\lambda_m'\frac{x}{L/2}\right) e^{-\lambda_m'^2(\alpha t/(L/2)^2)} \quad (4.102)$$

where Po is the Pomerantsev (dimensionless) number defined as

$$Po = \frac{Q}{k}\left(\frac{L}{2}\right)^2 \frac{1}{T_0 - T_\infty} \quad (4.103)$$

Application of Equation 4.102 includes estimation of the required cooling load through mean (volume average) temperature, Y_m, calculations:

$$Y_m(t) = \frac{\int Y(x,t)\,d\nu}{\int d\nu} \quad (4.104)$$

and

$$Y_{m,slab} = \frac{Po}{3}\left(1 + \frac{3}{Bi}\right) + \sum_{m=1}^{\infty}\left(1 - \frac{Po}{\lambda_m'^2}\right)\frac{2\left(\sin(\lambda_m')\right)^2}{\lambda_m'\left(\lambda_m' + \sin(\lambda_m')\cos(\lambda_m')\right)} e^{-\lambda_m'^2\frac{\alpha t}{(L/2)^2}} \quad (4.105)$$

and a number of cooling criteria based on the particular Po value.

4.5.3 Semi-Infinite Solid Approximation

In the analysis presented in the previous section, it was concluded that the one-term approximation solution is useful for relatively long times. An approximation that is useful for calculating the temperature evolution at short times is that of the semi-infinite solid. When the temperature of the cooling or heating medium in contact with a solid object changes then the temperature of the solid object also changes, but at early times only the areas close to the surface are affected. The temperature of the objects away from the surface is unaffected by the change in the conditions on the medium in contact with the object. Under these conditions one-dimensional, transient conduction is taking place near the surface. The governing equation is the following:

$$\frac{1}{\alpha}\frac{\partial T}{\partial t} = \frac{\partial^2 T}{\partial x^2} \quad (4.106)$$

subject to the following initial and boundary conditions:

Initial condition (IC):

$$T(x,t=0) = T_0 = \text{constant} \tag{4.107}$$

Boundary conditions (BC):

$$T(x \to \infty,t) = T_0 = \text{constant} \tag{4.108}$$

and

$$T(x=0,t) = T_\infty = \text{constant} \tag{4.109}$$

or

$$k\left.\frac{\partial T}{\partial x}\right|_{x=0} = h\left(T_\infty - T(x=0,t)\right) \tag{4.110}$$

Infinite heat-transfer coefficient. The solution of Equation 4.106, subject to IC (4.107) and BC given by Equations 4.108 and 4.109 can be obtained by noting that through the use of the similarity variable (Baehr and Stephan, 2006):

$$\eta = \frac{x}{\sqrt{4\alpha t}} \tag{4.111}$$

the partial differential Equation 4.106 can be written as

$$\frac{d^2T}{d\eta^2} = -2\eta\frac{dT}{d\eta} \tag{4.112}$$

which is an ordinary differential equation. Using the boundary conditions we can obtain the following solution:

$$Y_{Semi-\infty} = \frac{T_\infty - T(\eta)}{T_\infty - T_0} = \frac{2}{\sqrt{\pi}}\int_0^\eta e^{-u^2}\,du = \text{erf}(\eta) \tag{4.113}$$

where erf() is the Gaussian error function a standard mathematical function.

Finite heat-transfer coefficient. The solution to Equation 4.106, subject to IC (4.107) and BC given by Equations 4.108 and 4.110 is given by (Baehr and Stephan, 2006)

$$Y_{Semi-\infty} = \frac{T_\infty - T(\eta)}{T_\infty - T_0} = \text{erf}\,(\eta) + \exp\,(2\eta\xi + \xi^2)\,\text{erfc}\,(\eta + \xi) \tag{4.114}$$

where $\xi = h\sqrt{\alpha t}/k$. The solution of the semi-infinite solid approximation for the case of finite heat-transfer coefficient is presented in Figure 4.11.

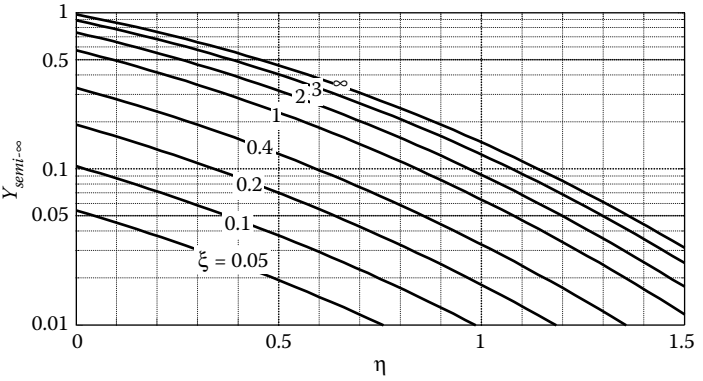


FIGURE 4.11 Solution of the semi-infinite solid approximation for the case of finite heat-transfer coefficient.

4.6 NUMERICAL CALCULATION OF THE ONE-TERM SOLUTION

It is important to stress the importance of the analytic solutions of the transient 1-D conduction given by Equation 4.53 for the slab, Equation 4.69 for the cylinder, and Equation 4.78 for the sphere as well as their one-term approximation valid for "long

TABLE 4.8
A MATLAB Program for Calculating the Positive Roots of Equation 4.54

```
function x = EigSlab(m,Bi,tol)
%
% Positive roots of the transcendental
% equation x tan(x) − Bi = 0
% INPUTS.............................
% m    denotes the m-th root
% Bi   is the Biot number
% tol  is the requested accuracy
% OUTPUTS:...........................
% x    the root requested
%
xL = (m−1)*pi;        eL = xL*tan(xL) − Bi;
xU = (m−1)*pi + pi/2; eU = xU*tan(xU) − Bi;
xM = (xU + xL)/2;     eM = xM*tan(xM) − Bi;
while (abs(eM) > tol)
     if (eL*eM > 0)
          xL = xM; eL = eM;
     else
          xU = xM; eU = eM;
     end
     xM = (xU + xL)/2; eM = xM*tan(xM) − Bi;
end
x = xM;
```

times" (see Table 4.7). They constitute the building blocks for many calculations involving thermal processing of foods. However, as can be observed from Table 4.7, they involve the parameters λ_1', β_1', and ζ_1' which are the first positive roots of the nonlinear Equations 4.54, 4.71, and 4.79, respectively. These parameters (called eigenvalues in the heat-transfer literature and Sturm–Liouville theory) are tabulated in many textbooks as a function of the Biot number. However, the numerical implementation of the one-term approximation of the analytic solution necessitates their numerical evaluation. This can easily be achieved using, for instance, MATLAB®.

In Table 4.8, a MATLAB file is given that can be used to estimate any positive root of the transcendental Equation 4.54 using a simple bisection algorithm. It can be shown that the mth root of Equation 4.54 lies in the interval $[(m-1)\pi, (m-1)\pi + \pi/2]$. More specifically, when $Bi \to 0$ then $\lambda_m' \to (m-1)\pi$ while when $Bi \to \infty$ then $\lambda_m' \to (m-1)\pi + \pi/2$. For the first root it follows that when $Bi \to 0$ then $\lambda_1' \to 0$ while when $Bi \to \infty$ then $\lambda_1' \to \pi/2$. In Tables 4.9 and 4.10, MATLAB programs for estimating the smallest positive roots of Equations 4.71 and 4.79 are given. These programs are then used to determine the smallest positive roots of the three equations as a function of the Biot number and are presented in Table 4.11 for performing hand calculations. The use of computer software is highly recommended for that purpose.

TABLE 4.9
A MATLAB Program for Calculating the Smallest Positive Root of Equation 4.71

```
function x = EigCylinder(Bi,tol)
%%%%%%%%%%%%%%%%%%%%%%%%%%%%%%%%%%%%%%%%%%%%%%%%
% First positive root of the equation
% x J1(x) - Bi J0(x) = 0
%
% INPUTS.............................
% Bi  is the Biot number
% tol is the requsted accuracy
% OUTPUTS:...........................
% x   the root requested
%
xL = 0;          eL = xL*besselj(1,xL) - Bi*besselj(0,xL);
xU = pi;         eU = xU*besselj(1,xU) - Bi*besselj(0,xU);
xM = (xU + xL)/2; eM = xM*besselj(1,xM) - Bi*besselj(0,xM);
while (abs(eM) > tol)
    if (eL*eM > 0)
        xL = xM; eL = eM;
    else
        xU = xM; eU = eM;
    end
    xM = (xU + xL)/2;
    eM = xM*besselj(1,xM) - Bi*besselj(0,xM);
end
x = xM;
```

TABLE 4.10
A MATLAB Program for Calculating the Smallest Positive Root of Equation 4.79

```
function x = EigSphere(Bi,tol)
%%%%%%%%%%%%%%%%%%%%%%%%%%%%%%%%%%%%%%%%%%%%%%%%
% First positive root of the equation
% x cot(x) − (1 − Bi) = 0
%
% INPUTS.............................
% Bi is the Biot number
% tol is the requsted accuracy
% OUTPUTS:...........................
% x the root requested
%
xL = eps;        eL = xL*cot(xL) − (1 − Bi);
xU = pi;         eU = xU*cot(xU) − (1 − Bi);
xM = (xU + xL)/2; eM = xM*cot(xM) − (1 − Bi);
while (abs(eM) > tol)
if (eL*eM > 0)
     xL = xM; eL = eM;
else
     xU = xM; eU = eM;
end
xM = (xU + xL)/2; eM = xM*cot(xM) − (1 − Bi);
end
x = xM;
```

TABLE 4.11
Smallest Positive Root of Equations 4.54, 4.71, and 4.79

	Slab	Cylinder	Sphere
Bi	λ_1'	β_1'	ζ_1'
0.01	**0.09983363**	**0.14124476**	**0.17303198**
0.05	0.22176039	0.31426164	0.38536809
0.10	**0.31105285**	**0.44168178**	**0.54228088**
0.20	0.43284072	0.61697476	0.75930768
0.30	0.52179118	0.74646121	0.92078682
0.40	0.59324193	0.85157843	1.05279429
0.50	0.65327119	0.94077056	1.16556118
0.60	0.70506550	1.01844200	1.26440357
0.70	0.75055806	1.08725428	1.35252233
0.80	0.79103365	1.14897161	1.43203223
0.90	0.82740120	1.20484047	1.50442331
1.00	**0.86033359**	**1.25578371**	**1.57079632**
1.50	0.98824073	1.45694869	1.83659720
2.00	1.07687399	1.59944920	2.02875783
5.00	1.31383772	1.98981471	2.57043156
10.00	**1.42887001**	**2.17949659**	**2.83630038**
50.00	1.54000594	2.35724205	3.07884164
100.00	**1.55524513**	**2.38090166**	**3.11018695**

NOMENCLATURE

A	heat-transfer area, m^2
Bi	Biot number, $Bi = h\delta/k$, dimensionless
C_p	specific heat, J/(kg · K)
D	diameter, m
dx	differential in the x direction, m
dv	differential volume, m^3
f	time required for the difference between the medium and the product temperature to change by a factor of 10, s
f'	the f value based on Fo instead of time, dimensionless
Fo	Fourier number, $Fo = \alpha\, t/\delta^2$, dimensionless
g	acceleration of gravity, m/s^2
h	convective heat-transfer coefficient, $W/(m^2K)$
J_0	Bessel function of the first kind of order zero
J_1	Bessel function of the first kind of order one
j	a temperature "lag" factor, defined as the intercept, with the temperature axis, of the linear portion of the logarithmic Y versus Fo values (see Figure 4.6), dimensionless
k	thermal conductivity, W/(m · K)
L	length of a finite cylinder, thickness of rectangular rod, thickness of infinite slab, m
m	mass, kg
Po	Pomerantsev number, defined by Equation 4.103, dimensionless
$\dot{q}$	heat-transfer rate, W
$\dot{q}$"	heat flux: rate of heat transfer per unit area, W/m^2
Q	energy generated per unit volume, W/m^3
R	cylinder or sphere radius, m resistance to heat transfer (see Equation 4.20)
r	cylinder or sphere radial distance, m
t	time, s
T	temperature, °C or K
T_s	surface temperature, °C or K
T_0	initial or surface temperature, °C or K
T_∞	cooling or heating bulk temperature, °C or K
T_{CW}	cooling (water) medium temperature, °C
T_{IT}	initial product temperature, °C
T_{RT}	heating medium (retort) temperature, °C
t_h	total heating time, s
u	velocity, m/s
U	temperature response to a linear homogeneous heat conduction system initially at zero to a single unit step input, dimensionless
U_o	overall heat-transfer coefficient, $W/(m^2\ K)$
V	temperature response to time-dependent medium temperature, given by Equation 4.92, °C or K
x	x-coordinate, m
y	y-coordinate, m

Y dimensionless, normalized temperature
z z-coordinate, m

GREEK LETTERS

α thermal diffusivity, $\alpha = k/(\rho \cdot C_p)$, m^2/s
β volumetric thermal expansion coefficient, 1/K
β_n nth eigenvalue given by Equation 4.67
β'_n nth eigenvalue given by Equation 4.71
δ characteristic dimension, half thickness ($L/2$) of a slab, radius (R) of a cylinder and a sphere, m
ζ'_n nth eigenvalue given by Equation 4.79
η similarity variable
θ spherical coordinate, rad
λ_m mth eigenvalue given by Equation 4.45
λ'_m nth eigenvalue given by Equation 4.54
μ viscosity, $N \cdot s/m^2$
ν viscosity, $N \cdot s/m^2$
ξ parameter used in the analytic solution of the semi-infinite solid
ρ density, kg/m^3
φ spherical coordinate, rad
Φ time-dependent medium temperature, °C or K

SUBSCRIPTS

c	referring to the geometrical center of the product
C	cooling or cold phase
can	referring to can geometry
cond	conduction
conv	convection
finite cylinder	referring to finite cylinder geometry
finite body	referring to finite body geometries
H	heating or hot phase
i	inside surface
	*i*th layer in a composite structure
infinite cylinder	referring to infinite cylinder geometry
m	referring to mean (volume average) values (see Equation 4.104)
o	outside surface
Semi-∞	semi-infinite solid
slab	referring to slab geometry
sphere	referring to sphere geometry
w	denotes calculation at the conditions at the wall
0	referring to initial conditions (at $t = 0$)
∞	referring to (heating or cooling) medium bulk properties

REFERENCES

Abramowitz, M. and Stegum, I.A. 1972. *Handbook of Mathematical Functions with Formulas, Graphs, and Mathematical Tables*. Dover Publications: Inc., New York, 1046 pp.

Arpachi, V.S. 1966. *Conduction Heat Transfer*, Addison-Wesley: Ontario, 550 pp.

Ball, C.O. 1923. Thermal process time for canned food, *Bulletin of the National Research Council* 37(7), Part 1; Natl. Res. Council: Washington, DC, 76 pp.

Baehr, D.B. and Stephan, K. 2006. *Heat and Mass Transfer*, 2nd ed., Springer-Verlag: Berlin, 688 pp.

Buckingham, E. 1914. On physically similar systems; illustrations of the use of dimensional equations. *The Physical Review*, 2nd Series, 4(4):345–376.

Carslaw, H.S. and Jaeger, J.C. 1959. *Conduction of Heat in Solids*, 2nd ed., Clarendon Press: Oxford, Great Britain, 510 pp.

Flambert, F. and Deltour, J. 1972. Exact lethality calculation for sterilizing process. I. Principles of the method. *Lebensmittel-Wissenschaft und –Technologie*, 5(2):72–73.

Gurney, H.P. and Lurie, J. 1923. Charts for estimating temperature distributions in heating or cooling solid shapes. *Industrial and Engineering Chemistry*, 15(11):1170–1172.

Heldman, D.R. and Singh, R.P. 1981. *Food Process Engineering*, 2nd ed., The AVI Publishing Company, Inc.: Westport, CT, 415 pp.

Hildebrand, F.B. 1976. *Advanced Calculus for Applications*, 2nd ed., Prentice-Hall: Englewood Cliffs, NJ, 733 pp.

Lienhard, J.H. IV and Lienhard, J.H. V 2006. *A Heat Transfer Textbook*, Phlogiston Press: Massachusetts, 749 pp.

Myers, G.E. 1971. *Analytical Methods in Conduction Heat Transfer*, McGraw-Hill Book Company: New York, 508 pp.

Newman, A.B. 1931. The drying of porous solids: Diffusion calculations. *Transactions of the American Institute of Chemical Engineers*, 27:310–333.

van Beek, G. and Meffet, H.F.Th. 1981. Cooling of horticultural produce with heat and mass transfer by diffusion. In: Thorne S. (ed) *Developments in Food Preservation-1*, Applied Science Publishers, Inc: Englewood, NJ, 39–92.

5 Steam Generation *Distribution*

Theodoros Varzakas

CONTENTS

5.1 Introduction 114
5.1.1 Measuring and Control Parameters on the Steam Boiler 114
5.1.2 Capacitance 117
5.1.3 Pipework Sizing 117
5.1.4 Boiler Plant Using Steam Pressurization 117
5.1.5 Boilers Classification 118
5.2 Water-Tube Boilers 123
5.2.1 Cross Drum Boiler 124
5.2.2 Bent Tube or Stirling Boiler 124
5.2.3 Economizers 124
5.2.4 Superheaters 124
5.2.5 Oil Burners 124
5.2.6 Pressure Jet Burners 124
5.2.7 Rotary Cup Burner 125
5.2.8 Gas Burners 125
5.2.8.1 Low-Pressure Burner 125
5.2.8.2 High-Pressure Burner 125
5.2.8.3 Dual Fuel Burners 125
5.2.9 Heat Recovery from Residual Blowdown 125
5.3 Bottom Blowdown 125
5.4 Properties of Steam 126
5.4.1 Superheated Steam 126
5.4.2 Uses of Steam 126
5.4.3 Steam Traps 128
5.4.4 Methods of Estimating Steam Consumption 131
5.4.5 Condensate Recovery 132
5.4.6 Steam Accumulator 133
5.4.7 Steam Injection Equipment 133
5.5 Steam Heating Applications 134
5.5.1 Tri-Generation Systems 135
5.5.2 Computational Fluid Dynamics 137
References 138

5.1 INTRODUCTION

5.1.1 Measuring and Control Parameters on the Steam Boiler

A steam system consists of a steam-supply/generating facility, a steam and condensate return/water piping system, and a steam-use facility (Figure 5.1).

The steam-generating facility, located in the boiler room, consists of boilers, feedwater systems, heat exchangers (e.g., economizers), boiler and system controls, fuel and gas-handling equipment (e.g., fuel trains, stacks), and steam/water treatment equipment and piping. The purpose of the steam-generating facility is to provide energy (in the form of thermal energy of the steam) to drive other processes in the steam-use facility (Cleaver Brooks, 2004).

For steam, the desired operating pressure needs to be determined. Moreover, the steam load characteristics and ultimately the profile of the steam-use facility in its entirety need to be determined. It is important to understand both the steady-state load profile as well as the transient and instantaneous demands. Finally, the desired or necessary steam quality (dryness) or degree of superheat should be determined. Steam quality ranges from 0 to 100% and is defined as the ratio of the amount of saturated steam vapor to the total steam amount (which may consist of both saturated steam vapor and liquid). A 100% steam quality translates to zero amount of saturated steam liquid and, in this condition, the steam is termed to be "dry."

The degree of superheat refers to the amount of thermal energy (heat) added to the steam relative to the saturated steam vapor point of reference, typically expressed in units of degrees Fahrenheit. For example, a degree of superheat of 50°F means that an additional amount of heat has been added to the steam so that the final steam

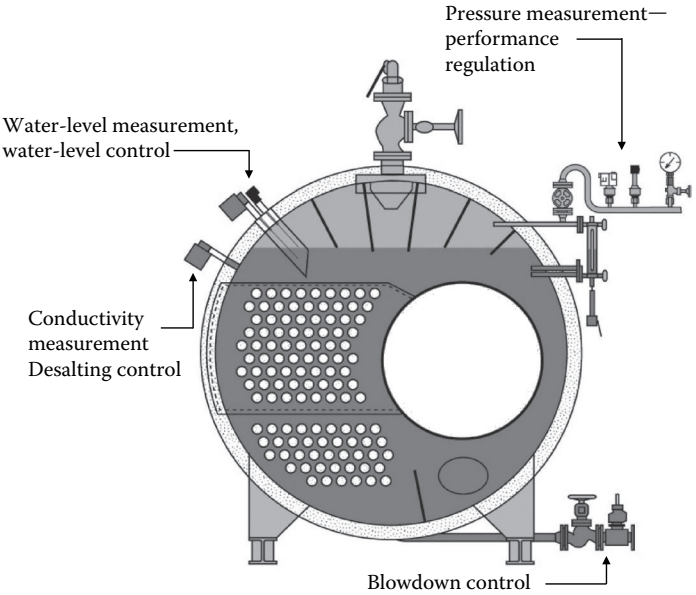


FIGURE 5.1 Steam system.

temperature is 50°F greater than the saturation temperature of the steam at the given operating pressure.

Other operating conditions include condensate return/make-up water conditions focusing on temperature, pressure, and flow rate (% return), water discharge (maximum temperature for water discharge), types of fuel to be combusted within the boiler, that is, natural gas, propane, and fuel oil (although some other alternate fuels may be used), combustion air (ambient air conditions in the boiler area and current fresh air supply (e.g., louvre area), and stack gas (temperature limitations imposed on the stack gas and electrical power.

Oil for boiler fuel is created from the residue produced from crude petroleum after it is distilled to produce lighter oils such as gasoline, paraffin, kerosene, diesel, or gas oil.

Gas is a form of boiler fuel that is easy to burn, with very little excess air. Fuel gases are available in two different forms: *Natural gas* produced (naturally) underground, used in its natural state (except for the removal of impurities), containing a high proportion of methane. *Liquefied petroleum gases* (LPG) produced from petroleum refining and then stored under pressure in a liquid state until used. The most common forms of LPG are propane and butane.

Approximately 42 kg of steam can be produced from 1 Therm of gas (equivalent to 105.5 MJ) for a 10 bar g boiler, with an overall operating efficiency of 80%.

Biomass gasification has emerged as a promising technology to fulfill the increasing world energy demands as well as to reduce significantly the volume of biomass waste generated in developing societies.

Gasification is a thermochemical conversion of solid fuel into syngas having useable heating value. The gases produced by this process can be used to generate electricity by integrated gasification combined cycle (IGCC).

Gasification is carried out by reacting carbonaceous fuel with a restricted amount of oxygen and often in combination with steam. Heat evolved from the exothermic reactions of oxygen with fuel serves to maintain the gasifier operating temperature and drives certain endothermic reactions taking place inside it.

The gasification process can be split into four physicochemical processes. First is drying (>150°C), in which the moisture content of the fuel evaporates. Pyrolysis or devolatilization involves a series of complex physical and chemical processes.

Combustion (700–1500°C) is the most important reaction taking place inside a gasifier, providing practically all the thermal energy needed for the endothermic reactions. Finally, the products of combustion react with the remaining char in the gasification zone. Gasification (800–100°C) involves a series of endothermic reactions supported by the heat produced from the combustion reactions. Gasification yields combustible gases such as H_2, CO, and CH_4 (Basu, 2006).

Ramzan et al. (2011) developed a steady-state computer model for hybrid biomass gasifier using commercial simulation software ASPEN Plus. This model was used to describe the gasification of three different biomass feedstocks. These are food waste (FW), municipal solid waste (MSW), and poultry waste (PW). The effect of operating parameters such as temperature, equivalence ratio (ER), biomass moisture content, and steam injection on syngas composition, high heating value (HHV), cold gas efficiency (CGE), and hydrogen production has been investigated.

Additional control parameters
- Waste gas temperature
- Hot steam temperature

Additional measurement parameters
- Quantity of fuel
- Steam volume
- Feedwater volume
- Waste gas temperature
- Steam temperature

The majority of boiler level controls and level alarms operate on the principle of conductivity or capacitance.

A photo of a boiler in a Greek manufacturing plant is shown in Figure 5.2.

A conductivity probe and controller can be used in a boiler or a tank for on/off pump control and/or alarm duties. It has one electrode for each function, which is cut to the required length on installation. Each probe electrode acts as a simple switch, indicating a low resistance to earth if in water, or a high resistance if out of water.

For example, with a low alarm, the controller senses a change of resistance from low to high as the water level falls below the probe tip. This change in resistance causes the controller to disengage a relay to operate an alarm bell, light, or both, and normally will also cut the power to the burner.

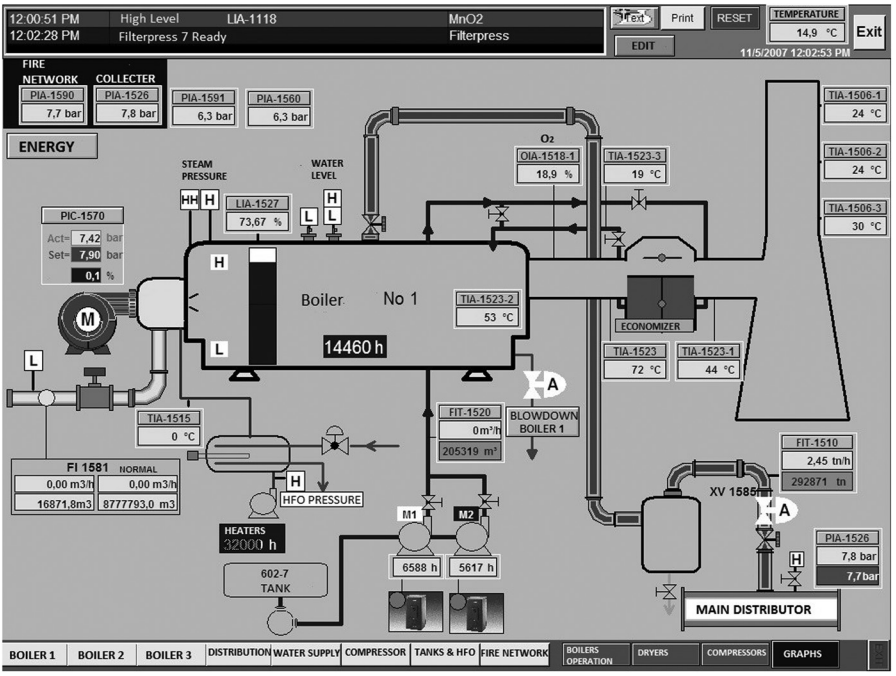


FIGURE 5.2 Depiction of a boiler in a Greek manufacturing plant.

Simple conductivity probes operate on this principle, and have no self-checking facility.

High integrity self-monitoring level alarms (limiters) operate on this same conductivity principle. The probes are designed to detect numerous failure modes and will, for example, sound an alarm if the wiring is damaged. The controller has a cyclic self-test facility which sounds an alarm if it fails to react to a simulated fault. Boilers fitted with alarms of this type in the boiler shell can operate with extended test intervals in most countries, in many cases allowing the boiler house to be demanned (Spirax-Sarco, 2012).

5.1.2 Capacitance

A capacitance probe can be used in a boiler or a tank for modulating or adjustable on/off control. The probe consists of a conductive core completely sheathed in an insulating material. For this reason, capacitance probes cannot be cut to size, and so are available in several different lengths. As the water level rises or falls, the capacitance coupling effect changes.

A high- or a low-level alarm switching point can also be selected. Controllers are available for pneumatic or electrically actuated valves or variable speed pumps.

Used as an on/off adjustable level control, it avoids having to cut probe tips to length, and permits level adjustments to be made at the controller without having to remove the probe from the boiler (Spirax-Sarco, 2012).

5.1.3 Pipework Sizing

The Pole Formula is used for determining the flow of gas in pipes. It is a simplification of the Darcy equation

$$Q = 0.0071\sqrt{\frac{d^5 \times h}{s \times l}} \tag{5.1}$$

Q = flow (m^3/h)
d = diameter of pipe (mm)
h = pressure drop (mbar)
l = length of pipe (m)
s = specific gravity of gas (density of gas/density of air)

Available pressure drop from meter to furthest outlet at 150 Pa, while leaving sufficient pressure at the index point (for pressure loss at the gas appliance)

Steam: water heated to vaporization. At atmospheric pressure, temperature = 100°C.

At higher pressure, vaporization temperature >100°C. A steam phase diagram best illustrates this phenomenon as shown in Figure 5.3.

5.1.4 Boiler Plant Using Steam Pressurization

- Hot water boiler (w/steam maintained inside)
- Boiler feed pump and cistern

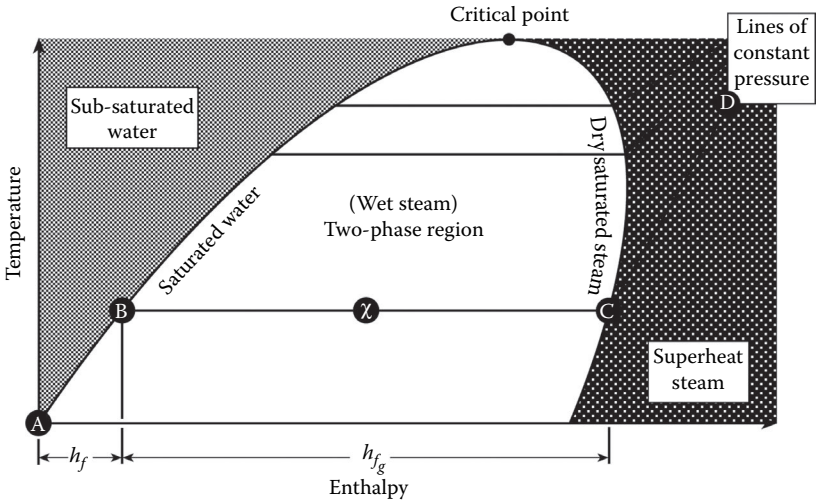


FIGURE 5.3 Temperature enthalpy phase diagram. (Courtesy of Spirax Sarco Limited, 2011. http://www.spiraxsarco.com/resources/steam-engineering-tutorials/steam-engineering-principles-and-heat-transfer/what-is-steam.asp)

- Circulating pump and pipework
- Cooling water bypass (mixing to control the pressure)

Steam and water are at saturation temperatures (Figure 5.4).

Low-pressure steam can be used since it has a higher heat content and causes less risk of noise and wear. Medium or high pressure can be used for large installations with long steam mains and requires pressure-reducing devices for appliances. The operating principle of steam heating is shown in Figure 5.5.

Steam systems can be classified by method of condensate return either by

- Gravity or
- Mechanical

and by pipe layout

- One pipe or two pipes (Figure 5.6 represents one-pipe gravity steam heating system).
- Up-feed or down-feed

Steam distribution can be seen in Figure 5.7.

5.1.5 Boilers Classification

Boilers are classified according to the type of working fluid or heat carrier used such as steam and hot water, physical arrangement of the working fluid (fire tube: flue gas products flow through boiler tubes, water tube: water circulates within boiler tubes),

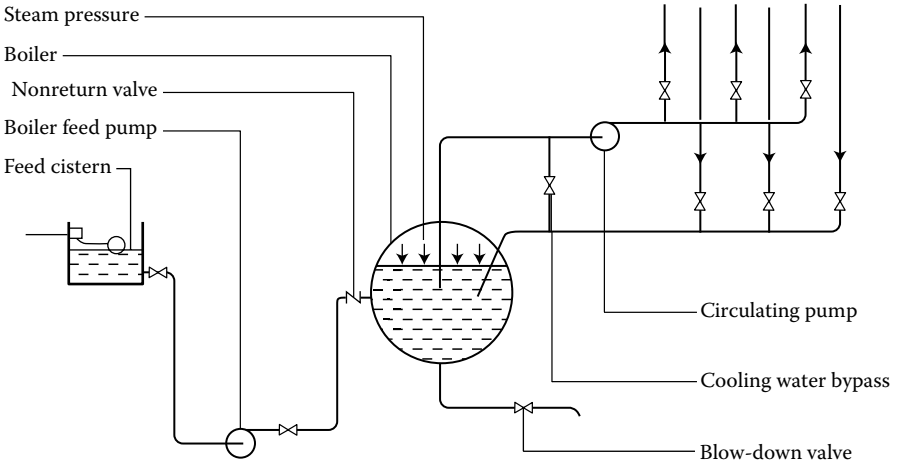


FIGURE 5.4 Boiler plant using steam pressurization. (Adapted from Hall, F. and Greeno, R. 2008. *Building Services Handbook*. UK: Butterworth-Heinemann—An imprint of Elsevier Ltd; Benjamin Ho, 2010. The University of Hong Kong. MEBS6000 Utility Services, http://www.hku.hk/mech/msc-courses/MEBS6000/index.html, Session 4: Fuel Gas Supply and Steam Systems.)

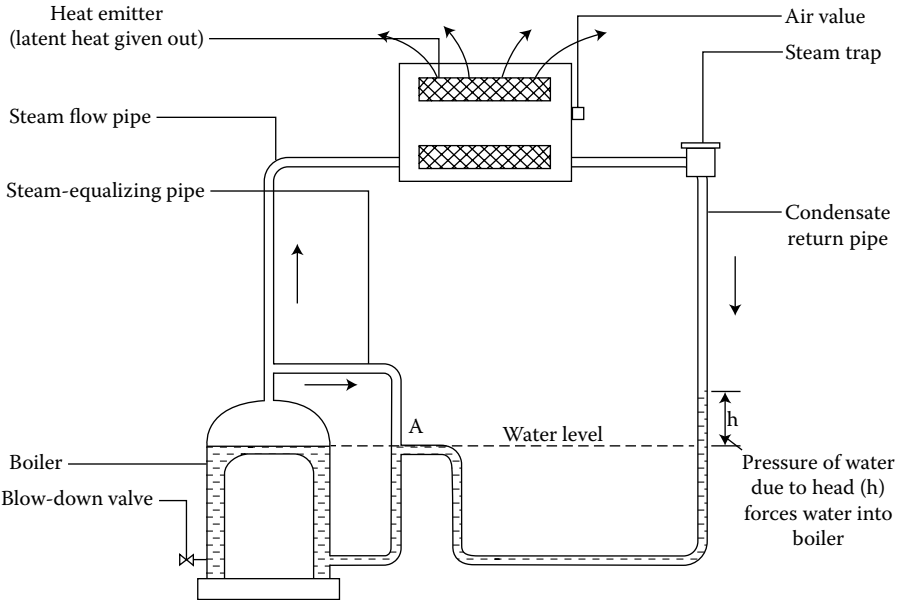


FIGURE 5.5 Operating principle of steam heating. (Adapted from Hall, F. and Greeno, R. 2008. *Building Services Handbook*. UK: Butterworth-Heinemann—An imprint of Elsevier Ltd; Benjamin Ho, 2010. The University of Hong Kong. MEBS6000 Utility Services, http://www.hku.hk/mech/msc-courses/MEBS6000/index.html, Session 4: Fuel Gas Supply and Steam Systems.)

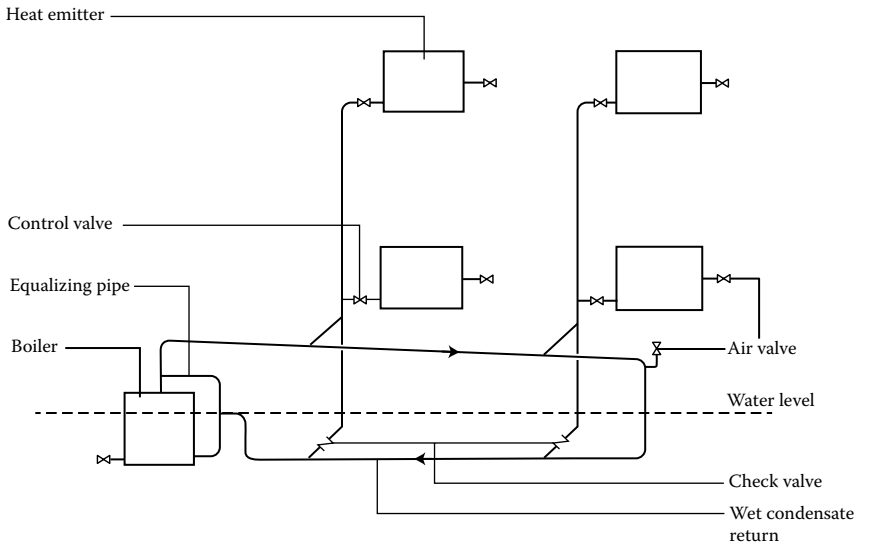


FIGURE 5.6 One-pipe gravity steam-heating system. (Adapted from Hall, F. and Greeno, R. 2008. *Building Services Handbook*. UK: Butterworth-Heinemann—An imprint of Elsevier Ltd.)

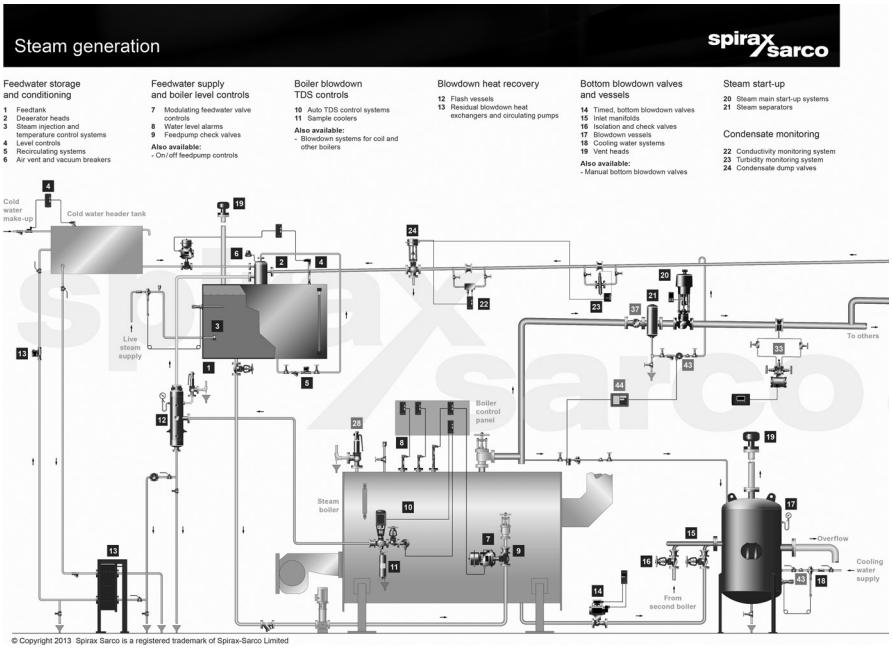


FIGURE 5.7 Steam distribution. (Courtesy of Spirax Sarco Limited, 2011. http://www.spiraxsarco.com/resources/steam-engineering-tutorials/introduction/steam-the-energy-fluid.asp)

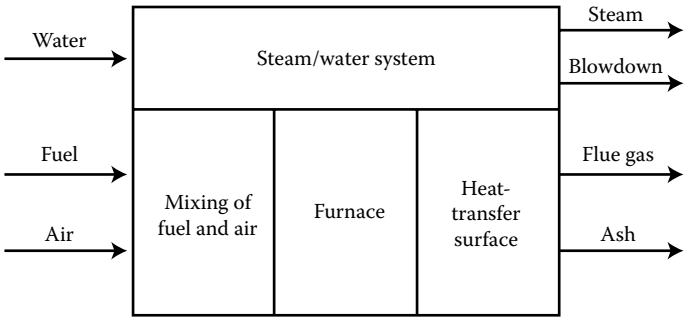


FIGURE 5.8 Basic diagram of a boiler.

and combustion gases/fuels (natural gas, town gas, diesel, etc., gas and oil replace coal for fuel of boiler/furnace) (Figure 5.8).

Blowdown: removal of suspended solids due to chemical dosing of boiler feedwater.

Shell boilers may be defined as those boilers in which the heat transfer surfaces are all contained within a steel shell. Shell boilers may also be referred to as "fire tube" or "smoke tube" boilers because the products of combustion pass through the boiler tubes, which in turn transfer heat to the surrounding boiler water (Figure 5.9). Several different combinations of tube layout are used in shell boilers, involving the number of passes the heat from the boiler furnace will usefully make before being discharged.

The figure shows a typical three-pass wet back shell boiler configuration.

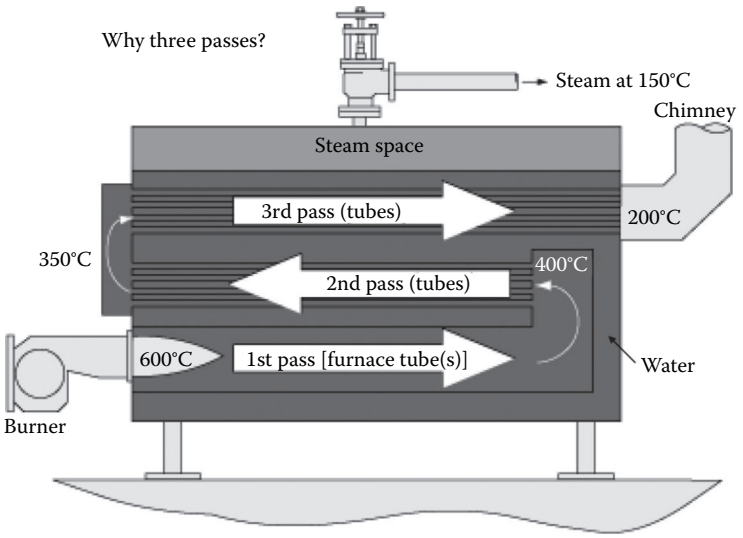


FIGURE 5.9 Typical heat path through a smoke tube shell boiler. Why three passes? (From Spirax Sarco Limited, 2011. http://www.spiraxsarco.com/resources/steam-engineering-tutorials/introduction/the-steam-and-condensate-loop.asp)

A more efficient method of reversing the hot gases is through a wet back boiler configuration. The reversal chamber is contained entirely within the boiler. This allows for a greater heat-transfer area, as well as allowing the boiler water to be heated at the point where the heat from the furnace will be the greatest—on the end of the chamber wall. It is important to note that the combustion gases should be cooled to at least 420°C for plain steel boilers and 470°C for alloy steel boilers before entering the reversal chamber.

Lancashire boilers are examples of shell boilers comprising a large steel shell usually between 5 and 9 m long through which two large-bore furnace tubes called flues pass. Part of each flue was corrugated to take up the expansion when the boiler became hot, and to prevent collapse under pressure. A furnace was installed at the entrance to each flue, at the front end of the boiler. Typically, the furnace would be arranged to burn coal, being either manually or automatically stoked.

Another shell boiler is the two-pass economic boiler, only about half the size of an equivalent Lancashire boiler with a higher thermal efficiency. It had a cylindrical outer shell containing two large-bore corrugated furnace flues acting as the main combustion chambers. The hot flue gases passed out of the two furnace flues at the back of the boiler into a brickwork setting (dry back) and were deflected through a number of small-bore tubes arranged above the large-bore furnace flues.

Finally, packaged boilers are so called because they come as a complete package with burner, level controls, feedpump, and all necessary boiler fittings and mountings. Once delivered at the site they require only the steam, water, and blowdown pipework, fuel supply, and electrical connections to be made to become operational and they use only oil.

Four-pass units are potentially the most thermally efficient, but fuel type and operating conditions may prevent their use. When this type of unit is fired at low demand with heavy fuel oil or coal, the heat transfer from the combustion gases can be very large.

In reverse flame/thimble boilers the combustion chamber is in the form of a thimble, and the burner fires down the center. The flame doubles back on itself within the combustion chamber to come to the front of the boiler. Smoke tubes surround the thimble and pass the flue gases to the rear of the boiler and the chimney.

Steam boilers are differentiated between high and low pressure according to ASTM.

High pressure >100 kPa (gauge) reduces the size of the boiler and steam piping (due to density), but decreases boiler efficiency and is good for heat load at long distance, whereas low-pressure <= 100 kPa (gauge) is simpler in both design and operation with no pressure-reducing valves required and less costly and complex water chemical treatment.

Boiler efficiency simply relates energy output to energy input, usually in percentage terms:

$$\text{Boiler efficiency } (\%) = \frac{\text{Heat exported in steam}}{\text{Heat provided by the fuel}} \times \frac{100}{1}$$

Heat exported in steam is calculated from knowledge of the feedwater temperature, the pressure at which steam is exported, and the steam flow rate.

Heat provided by the fuel may be expressed by "Gross" or "Net" calorific value.

Gross calorific value is the theoretical total of the energy in the fuel including the energy used in evaporating this water.

Net calorific value is the calorific value of the fuel, excluding the energy in the steam discharged to the stack, and is the figure generally used to calculate boiler efficiencies. In broad terms, Net calorific value ≈ Gross calorific value—10%.

Hot water boilers are divided into high and low temperature. High-temperature hot water (HTHW) boilers use water at temperature >121°C or pressure >1100 kPa and carrry greater heat reducing pumping and piping costs, whereas low-temperature hot water (LTHW) boilers use water at temperature <96°C or pressure <= 1100 kPa. Finally, calorifiers provide storage and allow heat exchange (common), whereas nonstorage calorifiers can also be used for providing hot water for space heating.

5.2 WATER-TUBE BOILERS

Water-tube boilers differ from shell-type boilers in that the water is circulated inside the tubes, with the heat source surrounding them.

Water-tube boilers are used in power station applications that require

- A high steam output (up to 500 kg/s)
- High-pressure steam (up to 160 bar)
- Superheated steam (up to 550°C)

However, water-tube boilers are also manufactured in sizes to compete with shell boilers. Small water-tube boilers may be manufactured and assembled into a single unit, just like packaged shell boilers.

Many water-tube boilers operate on the principle of natural water circulation (also known as "thermosiphoning").

Natural Water Circulation in a Water-Tube Boiler Operates as Follows.

- Cooler feedwater is introduced into the steam drum behind a baffle where, because the density of the cold water is greater, it descends into the "downcomer" toward the lower or "mud" drum, displacing the warmer water up into the front tubes.
- Continued heating creates steam bubbles in the front tubes, which are naturally separated from the hot water in the steam drum, and are taken off.

The longitudinal drum boiler was the original type of water-tube boiler that operated on the thermo-siphon principle. Cooler feedwater is fed into a drum, which is placed longitudinally above the heat source. The cooler water falls down a rear circulation header into several inclined heated tubes. As the water temperature increases as it passes up through the inclined tubes, it boils and its density decreases, therefore circulating hot water and steam up the inclined tubes into the front circulation header which feeds back to the drum. In the drum, the steam bubbles separate from the water and the steam can be taken off.

5.2.1 Cross Drum Boiler

The cross drum boiler is a variant of the longitudinal drum boiler in that the drum is placed cross ways to the heat source. The cross drum operates on the same principle as the longitudinal drum, except that it achieves a more uniform temperature across the drum. However, it does risk damage due to faulty circulation at high steam loads; if the upper tubes become dry, they can overheat and eventually fail.

5.2.2 Bent Tube or Stirling Boiler

In the bent tube or Stirling boiler four drums are used. Cooler feedwater enters the left upper drum, where it falls due to greater density, toward the lower, or water drum. The water within the water drum, and the connecting pipes to the other two upper drums, are heated, and the steam bubbles produced rise into the upper drums where the steam is then taken off.

5.2.3 Economizers

The flue gases, having passed through the main boiler and the superheater, will still be hot. The energy in these flue gases can be used to improve the thermal efficiency of the boiler. To achieve this, the flue gases are passed through an economizer.

The economizer is a heat exchanger through which the feedwater is pumped. The feedwater thus arrives in the boiler at a higher temperature than would be the case if no economizer was fitted.

5.2.4 Superheaters

Whatever type of boiler is used, steam will leave the water at its surface and pass into the steam space. Steam formed above the water surface in a shell boiler is always saturated and cannot become superheated in the boiler shell, as it is constantly in contact with the water surface. If superheated steam is required, the saturated steam must pass through a superheater. This is simply a heat exchanger where additional heat is added to the saturated steam. In water-tube boilers, the superheater may be an additional pendant suspended in the furnace area where the hot gases will provide the degree of superheat required.

5.2.5 Oil Burners

The ability to burn fuel oil efficiently requires a high fuel surface-area-to-volume ratio. Experience has shown that oil particles in the range of 20 and 40 μm are the most successful.

A very important aspect of oil firing is viscosity. The viscosity of oil varies with temperature: the hotter the oil, the more easily it flows.

5.2.6 Pressure Jet Burners

A pressure jet burner is simply an orifice at the end of a pressurized tube. Typically, the fuel oil pressure is in the range of 7–15 bar. In the operating range, the substantial

pressure drop created over the orifice when the fuel is discharged into the furnace results in atomization of the fuel.

5.2.7 Rotary Cup Burner

Fuel oil is supplied down a central tube, and discharges onto the inside surface of a rapidly rotating cone. As the fuel oil moves along the cup (due to the absence of a centripetal force) the oil film becomes progressively thinner as the circumference of the cap increases. Eventually, the fuel oil is discharged from the lip of the cone as a fine spray.

5.2.8 Gas Burners

Two types of gas burners are in use namely "low pressure" and "high pressure."

5.2.8.1 Low-Pressure Burner

These operate at low pressure, usually between 2.5 and 10 mbar. The burner is a simple venturi device with gas introduced in the throat area, and combustion air being drawn in from around the outside. Output is limited to approximately 1 MW.

5.2.8.2 High-Pressure Burner

These operate at higher pressures, usually between 12 and 175 mbar, and may include a number of nozzles to produce a particular flame shape.

5.2.8.3 Dual Fuel Burners

These burners are designed with gas as the main fuel, but have an additional facility for burning fuel oil.

5.2.9 Heat Recovery from Residual Blowdown

About 49% of the energy in boiler blowdown can be recovered through the use of a flash vessel and associated equipment; however, there is scope for further heat recovery from the residual blowdown itself.

The accepted method is to pass it through a heat exchanger, heating make-up water en route to the feedtank. This approach typically cools the residual blowdown to about 20°C. This system not only recovers the energy in the blowdown effluent, it also cools the water before discharging into the drainage system.

Plate heat exchangers are preferred for this application, as they are very compact and easily maintained.

5.3 BOTTOM BLOWDOWN

Suspended solids can be kept in suspension as long as the boiler water is agitated, but as soon as the agitation stops, they will fall to the bottom of the boiler. If they are not removed, they accumulate and, given time, will inhibit heat transfer from the boiler fire tubes, which will overheat and may even fail. The recommended method

for removing this sludge is via short, sharp blasts using a relatively large valve at the bottom of the boiler. The objective is to allow the sludge time to redistribute itself so that more can be removed on the next blowdown. For this reason, a single 4-second blowdown every 8 hours is much more effective than 1, 12-second blowdown in the first 8-hour shift period, and then nothing for the rest of the day.

There are two important factors to recognize with bottom blowdown: Energy content of blowdown, that is, the energy contained in the water being blown down is the liquid enthalpy of water at saturation temperature at boiler pressure and change in volume (over a 3 s blowdown period, the amount of water blown down) (Spirax Sarco, 2012).

5.4 PROPERTIES OF STEAM

Three types of heat in steam calculation:

- Specific heat of water (h_f) where liquid water is heated up to vaporization.
- Specific enthalpy of evaporation (h_{fg}) where liquid water changes phase to form vapor (gaseous state), and
- Specific enthalpy of steam (h_g) which is given by $h_g = h_f + h_{fg}$

Heat values of water and steam can be found in Steam Tables to determine various steam properties such as pressure, temperature, specific enthalpy, specific volume (inverse of density), and specific heat capacity.

Published tables are included in databooks, such as CIBSE Guide C, Section 4, or IOP Guide.

Steam often carries tiny droplets of water.

Dryness fraction (χ) = proportion of completely dry steam present in the steam–moisture mixture, $\chi = 1$ for complete dryness

Wet steam has heat content substantially lower than that of dry saturated steam at the same pressure.

5.4.1 Superheated Steam

If the saturated steam produced in a boiler is exposed to further heating, its temperature will increase above the evaporating temperature and will lead to superheated steam. When superheated steam gives up some of its enthalpy (e.g., heat loss to pipes), a fall in temperature will not cause condensation, until the temperature drops to saturation temperature when condensation begins (Figure 5.10).

5.4.2 Uses of Steam

Steam is used

- As a heating medium for industrial process, heating and hot water in buildings, and cooking.
- To produce electrical power in power plants.

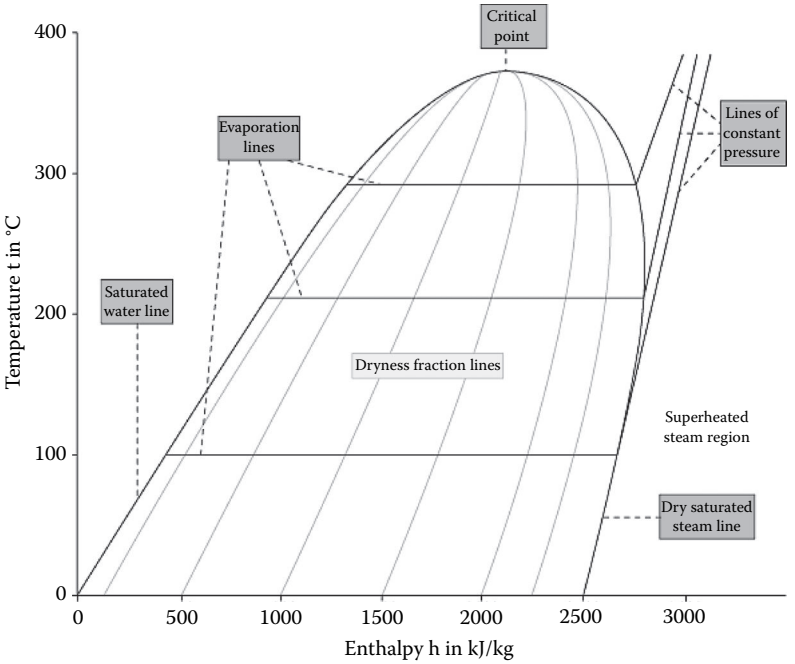


FIGURE 5.10 The temperature/enthalpy diagram. (Courtesy of Spirax Sarco Limited, 2011. http://www.spiraxsarco.com/resources/steam-engineering-tutorials/steam-engineering-principles-and-heat-transfer/entropy-a-basic-understanding.asp)

Common applications include the following:

- As a primary medium for distributing heat in factories—food and drink plants, hospitals, and hotels
- Means of sterilizing, cooking (Chinese restaurants)
- Space heating
- Hot water supply (via calorifiers)

Heat of evaporation for steam OR enthalpy of evaporation = 2257 kJ/kg at atm pressure (slightly higher heat at higher pressure)

- Sensible heat of water = 419 kJ/kg (0 to 100°C)
- Flow at high velocity (24–36 m/s) and high temperature (100–198°C)

Advantages of steam over hot water systems:

- No pumps needed: steam flows through system unaided
- Smaller heat emitters
- Low density: steam can be used in tall buildings where water systems create excessive pressure
- Terminal units can be added/removed easily

- Steam components can be repaired or replaced just by closing the steam supply (no associated draining and refilling a water system)
- Steam system temperature can be controlled by varying either steam pressure or temperature

Disadvantages:

- Higher risk if not properly maintained

5.4.3 Steam Traps

Steam traps are employed to remove/discharge condensate inside appliances, pipelines, or heat exchangers and at the same time do not permit the escape of live steam.

Steam traps are a critical part of the steam and condensate loop.

Condensate returns to boiler by gravity (runs back to boiler), by automatic pump (pumped back to boiler), or by condensate lifting trap.

Condensate must be removed promptly from a plant where maximum heat transfer is sought at all times. The presence of excess condensate in an item of heat-transfer equipment will reduce its efficiency, preventing it from achieving its maximum rated output and may also reduce its service life.

Three main groups of steam traps exist: thermostatic, mechanical, and thermodynamic. Thermostatic traps are operated by variations in fluid temperature. Thermostatic steam traps do not open until the condensate temperature has dropped below steam saturation temperature.

These traps are widely used in applications where it is acceptable to utilize some of the sensible heat in the condensate and reduce flash steam losses, such as noncritical tracing (Spirax Sarco Limited, 2010).

Examples are balanced pressure thermostatic trap, thermostatic trap with an external filter, and thermostatic steam traps (Figures 5.11 through 5.13).

A thermodynamic steam trap is shown in Figure 5.14.



FIGURE 5.11 Balanced pressure thermostatic trap.

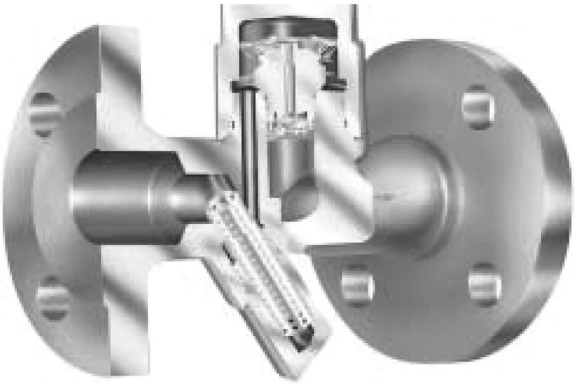


FIGURE 5.12 Thermostatic trap with an external filter.

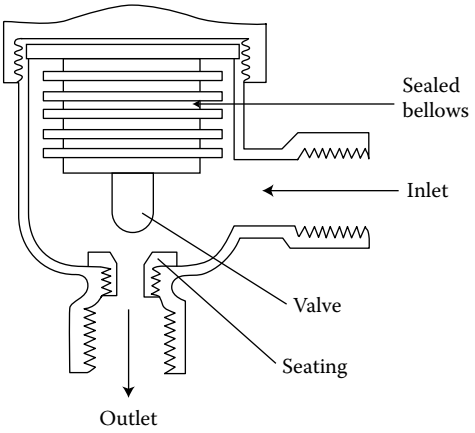


FIGURE 5.13 Thermostatic steam trap. (Adapted from Hall, F. and Greeno, R. 2008. *Building Services Handbook*. UK: Butterworth-Heinemann—An imprint of Elsevier Ltd.)

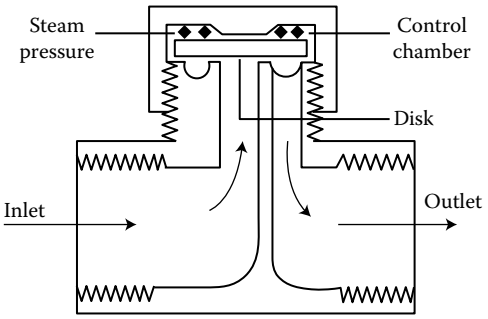


FIGURE 5.14 Thermodynamic steam trap. (Adapted from Hall, F. and Greeno, R. 2008. *Building Services Handbook*. UK: Butterworth-Heinemann—An imprint of Elsevier Ltd.)

Typical applications include tolerance of condensation back-up or removal of excess enthalpy, for example, sterilizers and noncritical tracing.

The closed bellows contain a volatile spirit which has a boiling point suiting the temperature. When steam enters the traps, the volatile spirit expands leading to opening of the bellows and closure of the valve. Water (condensate) enters the traps at a temperature lower than steam, the spirit contracts and closes the bellows hence leading to opening of the valve and allowing water to flow back to boiler.

Typical applications include mains drainage and all tracing applications. Some process applications with light loads such as small presses and cylinders.

The operating principle of the thermodynamic steam trap depends on the fact that steam flows through trap increasing the kinetic energy between disc and seating; hence reducing pressure energy at this point and making the disc move nearer the seating until kinetic energy decreases. Reduction in kinetic energy then increases pressure energy hence lifting the disc from seating (prevented from doing so by the steam pressure acting on the top of the disc in the control chamber). The area at the top of the disc is higher than the area at inlet underneath; hence the upper pressure forces the disc firmly on to its seat.

Following that, water (condensate) enters trap leading to condensation of steam above disc and reduction of pressure with disc forced up and water flow through trap. Water (condensate) then flows through trap at a lower velocity than steam giving insufficient reduction in pressure below the disc and trap remains open until steam enters. Bernoulli principle is obeyed, that is, kinetic pressure + potential energy = constant.

Steam enters the trap, the bucket is lifted, and the valve is closed. Water (condensate) enters trap and bucket fails under its own weight with the result of valve opening leading to steam pressure forcing water out (Figure 5.15).

The latter includes temperature/pressure-controlled applications with fluctuating loads.

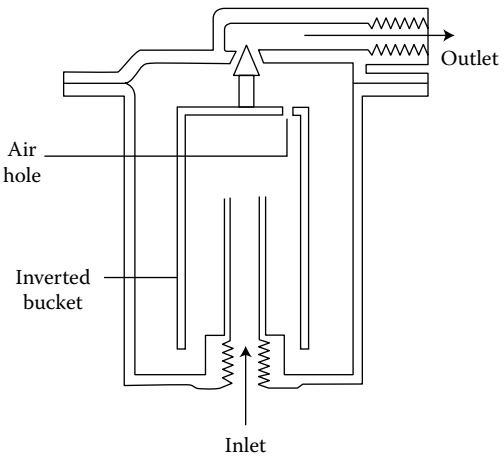


FIGURE 5.15 Inverted bucket steam trap. (Adapted from Hall, F. and Greeno, R. 2008. *Building Services Handbook*. UK: Butterworth-Heinemann—An imprint of Elsevier Ltd.)

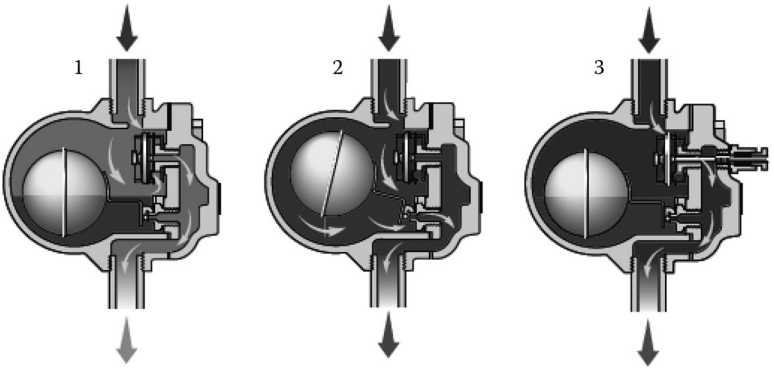


FIGURE 5.16 How a ball float steam trap works. (Courtesy of Spirax Sarco Limited, 2010. http://www.spiraxsarco.com/pdfs/SB/gst_33.pdf)

Ball float (FT) mechanical steam traps have an integral air vent as standard and the options of a manually adjustable needle valve (SLR—steam lock release mechanism) and drain cock tapping.

On start-up, a thermostatic air vent allows air to bypass the main valve (1) which would otherwise be unable to escape (a condition known as "air-binding").

As soon as the condensate reaches the trap, the float is raised and the lever mechanism opens the main valve. (2) Hot condensate closes the air vent but continues to flow through the main valve.

When steam arrives the float drops and closes off the main valve, which remains at all times below the water level, ensuring that live steam cannot be passed.

In syphon dip pipes draining rotating cylinders or long drain lines, a steam pocket may form which can prevent condensate from reaching the trap (a condition known as "steam locking").

A manually adjustable needle valve (SLR mechanism) should be specified to bleed away the steam (3) (Figure 5.16).

Other components include

- Steam separators
- Strainers
- Automatic air vent
- Check valves
- Isolation valves
- Gauges, sight glasses

5.4.4 Methods of Estimating Steam Consumption

Three methods can be employed to estimate steam consumption by calculation (analyzing the heat output on an item of plant using heat-transfer equations), measurement (by direct measurement, using flow-metering equipment (for an existing plant), and thermal rating (design rating displayed on the equipment name-plate (in kW).

The steam consumption required in kg/h will depend on the recommended steam pressure:

Steam flow rate (kg/h) = (Load in kW × 3600)/h_{fg}

Steam pipe sizing data could arise from the following D'Arcy equation:

$$h_f = \frac{f \cdot L \cdot u^2}{2 \cdot g \cdot D} \tag{5.2}$$

where h_f is the head loss to friction (m), f the friction factor (dimensionless), L the length (m), u the flow velocity (m/s), g the gravitational constant (9.81 m/s^2), and D the pipe diameter (m).

Undersized pipes create large pressure drops and high velocities, while oversized pipes are unnecessary and costly. This calculator allows steam and condensate pipes to be sized correctly. Steam pipes can be sized on pressure drop and velocity, and up to three steam trap discharge lines and associated common lines can be sized. Discharge lines from mechanical and electrical condensate pumps can also be sized (http://www.spiraxsarco.com/resources/calculators.asp.).

Friction factor can be difficult to determine, especially for turbulent steam flow. As a result, some graphs, tables, and slide rules are produced to relate steam pipe sizes to flow rates and pressure drops, for example, the "pressure factor" method:

$$F = (P1 - P2)/L \tag{5.3}$$

where F is the pressure factor, P1 the factor based on the inlet pressure, P2 the factor based on the pressure at a distance of L meters, and L the equivalent length of pipe (m).

Other design considerations include condensate recovery, start-up load, and running load.

Volumetric heat release (kW/m^3) is calculated by dividing the total heat input by the volume of water in the boiler. It effectively relates the quantity of steam released under maximum load to the amount of water in the boiler. The lower this number, the greater the amount of reserve energy in the boiler.

Steam release rate (kg/m^2 s) is calculated by dividing the amount of steam produced per second by the area of the water plane. The lower this number, the greater the opportunity for water particles to separate from the steam and produce dry steam.

5.4.5 Condensate Recovery

It is returned to the boiler for reuse as feedwater and can increase heat efficiency of the cycle, reduce make-up water charges, reduce effluent charges and possible cooling costs, keep water-treatment problems to a minimum, and reduce boiler blowdown (less energy is lost).

Start-up load: initial warm up of components and involves the highest steam consumption, whereas the running load is a fairly stable condition.

Other design considerations include flash steam which is formed when high-pressure condensate is discharged to a lower pressure and should be collected and led to a flash vessel as well as suitable collecting legs or reservoirs for condensate, minimum pressure differential across the steam trap, choice of steam trap type, and size and proper trap installation.

5.4.6 Steam Accumulator

The most appropriate means of providing clean dry steam instantaneously, to meet a peak demand is to use a method of storing steam so that it can be "released" when required.

In practice there are two ways of generating steam:

- By adding heat to boiling water, indirectly via a combustion tube and burner, as in a conventional boiler.
- By reducing the pressure on water stored at its saturation temperature. This results in an excess of energy in the water, which causes a proportion of the water to change into steam.

This phenomenon is known as "flashing," and the equipment used to store the pressurized water is called a steam accumulator. There are, in principle, two types of systems available for steam storage; the pressure-drop accumulator and the constant pressure accumulator (Spirax Sarco, 2013).

A steam accumulator is, essentially, an extension of the energy storage capacity of the boiler(s). When steam demand from the plant is low, and the boiler is capable of generating more steam than is required, the surplus steam is injected into a mass of water stored under pressure.

The pressure-drop steam accumulator consists of a cylindrical pressure vessel partially filled with water, at a point between 50% and 90% fully depending on the application. Steam is charged beneath the surface of the water by a distribution manifold, which is fitted with a series of steam injectors, until the entire water content is at the required pressure and temperature.

A steam trap (ball float type) is fitted at the working level and acts as a level-limiter, discharging the small amount of surplus water to the condensate return system.

5.4.7 Steam Injection Equipment

A properly sized steam inlet pipe must feed to well below the water surface level and into a steam distribution header/manifold system. The steam is injected into the water. It is important to remember that the injector capacity will reduce as the pressure in the vessel increases, as the differential pressure between the injected steam and the vessel pressure is reduced. At very low flow rates the steam will tend to issue from the injectors closest to the steam inlet pipe(s). The design of the inlet pipe(s) and the manifold system, together with the placement of the injectors, must provide

even injection of steam throughout the length of the accumulator regardless of actual steam flow rate (Spirax Sarco, 2013).

The discharge from the injectors will be very hot water and steam, possibly with some condensing steam bubbles.

All the injectors should be installed as low down in the accumulator as possible to ensure the maximum possible liquid head above them. It may also be appropriate to install the injectors at a slight angle to avoid erosion of the vessel.

5.5 STEAM HEATING APPLICATIONS

Anderson and Walker (2011) investigated segmented-flow aseptic processing of particle foods. A pilot-scale continuous steam sterilization unit capable of producing shelf stable aseptically processed whole and sliced mushrooms was developed. The system utilized pressurized steam as the heating medium to achieve high-temperature short-time processing conditions with high and uniform heat transfer that will enable static temperature penetration studies for process development. Segmented-flow technology produced a narrower residence time distribution than pipe-flow aseptic processing; thus, whole and sliced mushrooms were processed only as long as needed to achieve the target $Fo = 7.0$ min and were not overcooked. Continuous steam sterilization segmented-flow aseptic processing produced shelf stable aseptically processed mushrooms of superior quality to conventionally canned mushrooms. When compared to conventionally canned mushrooms, aseptically processed yield (weight basis) increased 6.1% (SD = 2.9%) and 6.6% (SD = 2.2%), whiteness (L) improved 3.1% (SD = 1.9%) and 4.7% (SD = 0.7%), color difference (ΔE) improved 6.0% (SD = 1.3%) and 8.5% (SD = 1.5%), and texture improved 3.9% (SD = 1.7%) and 4.6% (SD = 4.2%), for whole and sliced mushrooms, respectively. Segmented-flow aseptic processing eliminated a separate blanching step, eliminated the unnecessary packaging of water and promoted the use of bag-in-box and other versatile aseptic packaging methods.

The continuous steam sterilization segmented-flow aseptic processing system and the aseptic packaging chamber consisted of a sterilization chamber (B), a counterflow, direct-contact water cooling section (C), a double-valve pressure lock system at the inlet (A) and outlet (D) of the processing system, and an aseptic packaging chamber (E) (Anderson 2006). The incline (~45°) of the conveyor and the presence of partitions (or flights), placed approximately every 40 cm along the conveyor belt inside the sterilization chamber, ensured that no particle advanced faster—nor could a large particle advance slower.

To evaluate the effects of processes on physicochemical properties of oat bran soluble dietary fiber (OSDF), the oat bran was processed by steam heating, superfine grinding, and extrusion, and extracted to obtain OSDF as reported by Zhang et al. (2009). The molecular weight distribution, monosaccharide composition, transparency, solubility, structure, and thermal and morphological properties of OSDF were investigated. The yield of OSDF increased after the processing compared to the untreated. The proportion of high molecular weight granules was higher in OSDF from extruded oat bran. The backbone of the OSDF was not changed, but the proportion of the residue linkages in OSDF was varied after the

processing. Solubility and swelling power showed significant positive correlation with molecular weight distribution while transparency showed significant negative correlation with molecular weight distribution. Three processes had great impact on the physicochemical properties of OSDF. The OSDF from superfine ground oat bran showed some physicochemical properties that might be of potential use in the food industry.

The demand for ultra-high-temperature (UHT) processed and aseptically packaged milk is increasing worldwide. A rise of 47% from 187 billion in 2008 to 265 billon in 2013 in pack numbers is expected. Selection of UHT and aseptic packaging systems reflect customer preferences and the processes are designed to ensure commercial sterility and acceptable sensory attributes throughout shelf life. Advantages of UHT processing include extended shelf life, lower energy costs, and the elimination of required refrigeration during storage and distribution. Desirable changes taking place during UHT processing of milk such as destruction of microorganisms and inactivation of enzymes occur, while undesirable effects such as browning, loss of nutrients, sedimentation, fat separation, cooked flavor also take place. Gelation of UHT milk during storage (age gelation) is a major factor limiting its shelf life. Significant factors that influence the onset of gelation include the nature of the heat treatment, proteolysis during storage, milk composition and quality, seasonal milk production factors, and storage temperature. Chavan et al. (2011) focused on the types of age gelation and the effect of plasmin activity on enzymatic gelation in UHT milk during a prolonged storage period. Measuring enzyme activity is a major concern to commercial producers, and many techniques, such as enzyme-linked immunosorbent assay, spectrophotometery, high-performance liquid chromatography, and so on, are available. Extension of shelf life of UHT milk can be achieved by deactivation of enzymes, by deploying low-temperature inactivation at 55°C for 60 min, innovative steam injection heating, membrane processing, and high-pressure treatments.

High-quality standards in blueberry juice can be obtained only taking into account fruit compositional variability and its preservation along the processing chain. Brambilla et al. (2008) processed five highbush blueberry cultivars from the same environmental growing conditions into juice after an initial blanching step and the influence was studied of the cultivar on juice phenolic content, distribution, and relative antioxidant activity, measured as scavenging capacity on the artificial free-radical 2,2-diphenyl-1-picrylhydrazyl (DPPH•). A chromatographic protocol was developed to separate all main phenolic compounds in berries.

An aliquot (1 kg) of fruit for each blueberry cultivar was steam-blanched (85°C) for 3 min and tap-water-cooled in a pilot steam-blanching tunnel (Ghizzoni Dante and Figlio, Felino, Parma, Italia), before being processed into juice.

5.5.1 Tri-Generation Systems

The food industry, both food manufacturing and retailing has a need for heating and electrical power as well as refrigeration. Invariably, the plant is installed, which consists of heating systems employing low-pressure hot water, high-pressure hot water or steam, vapor compression refrigeration systems and an electrical

power supply derived from the National Grid network as is the case in the United Kingdom. The overall utilization efficiency of these processes is low, because of the relatively low electricity generation efficiency in power stations and distribution losses in the grid.

A way of increasing the energy utilization efficiency of food manufacturing and retail facilities is through tri-generation. Tassou et al. (2007) considered tri-generation technology and the feasibility of its application to the food retail industry and examined the economics and environmental impacts of the technology compared to conventional systems. The results indicate that the economic viability of these systems is dependent on the relative cost of natural gas and grid electricity. The system investigated can provide payback periods of less than 4.0 years when the relative cost of gas to electricity is below 0.3.

A major opportunity to reduce energy consumption and improve food processing efficiency is to employ local combined heat and power (CHP) generation. For combined heat and power to be economically attractive, however, there should be coincident demand for electrical power and heat.

Several researchers have investigated the application of tri-generation systems. Bassols et al. (2002) presented several examples of the tri-generation process in the food industry involving ammonia–water absorption plants. Santoyo and Cifuentes (2003) reported the design of a tri-generation system based on a regenerative combined cycle and a lithium bromide absorption system. The design would use the cooling from the absorption refrigeration system to cool the intake air of the compressor of the gas turbine to improve overall efficiency. A similar application was reported by Mohanty and Paloso (1995), where a single shaft gas turbine system was coupled to a double-effect lithium bromide absorption chiller to provide colder intake of air for the compressor.

Hwang (2004) investigated and presented potential energy benefits from the integration of a microturbine and an absorption chiller. The cooling from the absorption chiller would be used to reduce the temperature of the air entering the condenser and subcool the liquid refrigerant leaving the condenser of a vapor compression refrigeration system, as well as pre-cool the microturbine intake air.

A new anaerobic digester design for the treatment of diluted (<2% solids) flush dairy manure was evaluated by Zaher et al. (2008). The new design was developed as an economic alternative for enhancing the performance of anaerobic lagoon systems in cold weather areas. The digester employed used automobile tires as fixed-bed media to improve bacterial retention. The digester was heated by steam injection and built underground to enhance insulation. The tires were sorted in a unique pattern for improving mixing and uniform temperature distribution. The system was tested on a pilot scale. The treatment mechanism was explored by mathematical modeling. The observed treatment efficiency of the new design was comparable to that of conventional digesters operating at higher total solids concentrations (>4%). With a hydraulic retention time (HRT) of 17 days, the measured removal rates were 30–50% and 40–60% of TVS and COD, respectively.

Other benefits of such treatment system are biogas production for heat and power generation (US EPA, 2007).

Temperature of the reactor was maintained at 35°C using steam injection through evenly distributed points in the reactor.

Cocoa butter was steam refined in a packed column at temperatures ranging between 170°C and 260°C, with 1–3% steam injected, in order to verify the impact of refining conditions on the crystallization properties (Calliauw et al., 2008).

Even at 260°C, no significant changes in the TAG distribution of the cocoa butter could be detected. The observed FFA removal during packed column stripping can be well predicted by the simplified Bailey equation, however, for very high vapor pressures, an extended Bailey equation can be considered.

Based on crystallization experiments with SAXS/WAXD and DSC, it has been suggested that the removal of FFA invokes marginally higher crystallization of both the meta-stable polymorphs (α and β') of cocoa butter at 20°C. The amounts of solid fat at equilibrium and the induction time of the isothermal crystallization showed a strong linear correlation with the residual acidity. Upon tempering at 24°C, the generally observed crystal structures evolved from feathery spherulites to larger platelet crystals as more FFA was being removed by the refining, but this could not be unambiguously related to the polymorphic behavior.

Vila Ayala et al. (2007) have recently shown that temperatures up to 220°C in packed column steam refining of cocoa butter did not invoke any changes in the TAG profile. It was also observed that changes in physical properties of cocoa butter after steam refining were highly correlated with the removal of FFA.

5.5.2 Computational Fluid Dynamics

Flow pattern, temperature distribution, and shapes of the slowest heating zone during heating of solid–liquid food mixture (pineapple slices saturated with its moisture) in a cylindrical can of 84 mm diameter and 82 mm height are predicted by Ghani and Farid (2006). The partial differential equations describing the conservation of mass, momentum, and energy are solved numerically using commercial computational fluid dynamics (CFD) software (PHOENICS), which is based on a finite volume method of analysis. Saturated steam at 121°C is used as a heating medium, where the metal can is heated from all sides. The model liquid is assumed to have constant properties except for the viscosity (temperature dependent) and density (Boussinesq approximation). Two methods of analysis are adopted in the simulation. In one of the methods, the pineapple slices are assumed permeable to natural convection flow in its pores, while in the second method, the pineapple slices are assumed impermeable. The results of the simulations of both cases are very similar.

The simulations show, the action of natural convection on the rate of heating, liquid flow pattern, and on the shape and movement of the slowest heating zone (SHZ). The SHZ eventually stays in a region that is about 30–35% of the can height from the bottom.

For liquid food heated in a can, natural convection of fluid occurs due to density differences within the fluid caused by the temperature gradient within the can. For solid food with conduction heating, the location of the SHZ can be determined experimentally (Pflug, 1975), since it lies always at the geometric center of the can.

REFERENCES

Abdul Ghani, A.G. and M.M. Farid. 2006. Using the computational fluid dynamics to analyze the thermal sterilization of solid–liquid food mixture in cans. *Innovative Food Science and Emerging Technologies* 7: 55–61.

Anderson N.M. 2006. Continuous steam sterilization segmented flow aseptic processing of particle foods [PhD diss]. Univ. Park, Pa.: The Pennsylvania State Univ., Dept. of Agricultural and Biological Engineering.

Anderson, N.M. and P.N. Walker. 2011. Quality comparison of continuous steam sterilization segmented-flow aseptic processing versus conventional canning of whole and sliced mushrooms. *Journal of Food Science* 76(6): E429–E437.

Bassols J., B. Kuckelkorn, J. Langreck, R. Schneider, and H. Veelken. 2002. Trigeneration in the food industry. *Appl. Therm Eng* 22:595–602.

Basu, P. 2006. *Combustion and Gasification in Fluidized Beds*. Boca Raton, FL: Taylor & Francis.

Brambilla, A., R. Lo Scalzo, G. Bertolo, and D. Torreggiani. 2008. Steam-blanched highbush blueberry (*Vaccinium corymbosum* L.) juice: Phenolic profile and antioxidant capacity in relation to cultivar selection**.** *J. Agric. Food Chem.* 56*,* 2643–2648.

Calliauw G., J. Vila Ayala, V. Gibon, J. Wouters, W. De Greyt, I. Foubert, and K. Dewettinck. 2008. Models for FFA-removal and changes in phase behavior of cocoa butter by packed column steam refining. *Journal of Food Engineering* 89: 274–284.

Chavan, R.S., S.R. Chavan, C.D. Khedkar, and A.H. Jana. 2011. UHT milk processing and effect of plasmin activity on shelf life: A review. *Comprehensive Reviews in Food Science and Food Safety* 10: 251–268.

Cleaver Brooks, 2004. Steam systems.

Hall, F. and Greeno, R. 2008. *Building Services Handbook*. UK: Butterworth-Heinemann—An imprint of Elsevier Ltd.

Ho B. 2010. The University of Hong Kong. MEBS6000 Utility Services, http://www.hku.hk/mech/msc-courses/MEBS6000/index.html, Session 4: Fuel Gas Supply and Steam Systems.

Hwang Y. 2004. Potential energy benefits of integrated refrigeration system with microturbine and absorption chiller. *Int J Refrig*. 27: 816–829.

Mohanty B. and G. Paloso. 1995. Enhancing gas turbine performance by intake air cooling using absorption. *Heat Recov Sys & CHP*. 15(1): 41–50.

Pflug, I. J. 1975. *Procedures for Carrying Out a Heat Penetration Test and Analysis of the Resulting Data*. Minneapolis, MN: Environmental Sterilization Lab.

Ramzan, N., A. Ashraf, S. Naveed, and A. Malik. 2011. Simulation of hybrid biomass gasification using Aspen plus: A comparative performance analysis for food. *Municipal Solid and Poultry Waste Biomass and Bioenergy* 35: 3962–3969.

Santoyo J.H. and A.S. Cifuentes. 2003. Tri-generation: An alternative for energy savings. *Appl Energy*, 76: 219–227.

Spirax Sarco Limited. 2011. The Steam and Condensate Loop (CM Issue 4 ed.).

Spirax Sarco Limited. 2010. Steam Trapping an overview. SB-GST-33.

Spirax-Sarco, 2012. Steam boiler water level controls and alarms-an overview. http://www.spiraxsarco.com/learn Spirax Sarco Learning Centre.

Tassou, S.A., I. Chaer, N. Sugiartha, Y.-T. Ge, and D. Marriott. 2007. Application of tri-generation systems to the food retail industry. *Energy Conversion and Management* 48: 2988–2995.

The Steam and Condensate Loop http://www.engineeringtoolbox.com/steam-condensate-properties-t_28.html Steam and Condensate [Engineering ToolBox] (web sites).

US EPA, 2007. AgSTAR Handbook. AgSTAR program, http://www.epa.gov/agstar/

Vila Ayala, J., G.H. Calliauw, I. Foubert, K. Dewettinck, B. Dyer, and W.F.J. De Greyt. 2007. Impact of bleaching and packed column steam refining on cocoa butter properties. *Journal of American Oil Chemists' Society* 84(11): 1059–1067.

Zaher, U., C. Frear, P. Pandey, and S. Chen. 2008. Evaluation of a new fixed-bed digester design utilizing large media for flush dairy manure treatment. *Bioresource Technology* 99: 8619–8625.

Zhang, M., Y. Liang, Y. Pei, W. Gao, and Z. Zhang. 2009**.** Effect of process on physicochemical properties of oat bran soluble dietary fiber. *Journal of Food Science* 74(8): C628–C636.

6 Heat Exchangers

Theodoros Varzakas

CONTENTS

6.1 Introduction 141
6.1.1 Conduction 141
6.1.2 Thermal Resistance 142
6.1.3 Convection 142
6.2 Heat Exchangers 145
6.2.1 Rate of Heat Transfer Q 145
6.2.2 Comparing Plate and Tubular Exchangers 150
6.2.3 Plate Heat Exchangers 151
6.3 Flow Inside a Typical Plate Heat Exchanger 156
6.3.1 Tubular Exchangers 156
6.3.2 Scraped-Surface Exchangers 158
6.4 Nusselt Equation 162
6.4.1 Temperature Distribution in Concentric Tube Exchangers 164
6.4.2 Logarithmic Mean Difference 165
6.4.3 Method Number of Transfer Units-Effectiveness for the Analysis of a Heat Exchanger 165
6.5 Forced Convection: Lower-Viscosity Liquids in Turbulent Flow 166
6.5.1 Flow Inside Tubes 166
6.6 Heating or Cooling in an Agitated Cylindrical, Jacketed Vessel 166
6.7 Sieder and Tate Viscosity Correction Factor 169
6.8 Forced Circulation with Streamline (Laminar) Flow 170
6.9 Laminar Flow Inside Tubes 170
6.10 Flow in Tube Bundles 170
6.11 Case Studies 171
References 173

6.1 INTRODUCTION

Heat is the energy produced due to temperature difference. Heat transfer occurs when there is a temperature difference between two or more mediums. There are three different heat transfer processes: conduction, convection, and radiation.

6.1.1 CONDUCTION

Conduction is the heat transfer process through solids and stationary fluids. Energy diffusion is the physical transfer mechanism originating from the molecules in the

medium. The rate of heat transfer is given by Fourier's law. Heat transfer is given by the following equation for a one-dimensional (1-D) and stationary case:

$$q = -KA\frac{(T_2 - T_1)}{x} \tag{6.1}$$

where q = heat transfer rate (J/s)
K = thermal conductivity of the wall (J/ms°C)
A = cross-sectional area to the heat flow direction (m^2)
x = thickness of the wall (m)
T_2 = temperature in the cold surface of the wall (°C)
T_1 = temperature in the hot surface of the wall (°C)

This equation is for an infinite slab; however, it can be used for finite slabs if the length is higher than the thickness.

The solution to temperature in an infinite slab with finite internal and surface resistance to heat transfer is given by Incropera et al. (2007).

Example:

Calculate the rate of heat transfer for a stainless-steel slab, thickness 4 mm, area 1 m^2, with one face at −15°C and the other face at 25°C. Thermal conductivity of stainless steel is 21 J/ms°C.

6.1.2 Thermal Resistance

Thermal resistance is very useful in the evaluation of heat transfer. There is an analogy between heat transfer and electric load or thermal and electrical resistance. Thermal resistance can be associated with heat conduction.

Thermal resistance can be defined as

$$R_t = \frac{T_1 - T_2}{q} \tag{6.2}$$

where $T_1 - T_2$ is the temperature difference and q is the heat transfer rate, and from Equation 6.1, the thermal conduction resistance is

$$R_{cond} = \frac{x}{KA} \tag{6.3}$$

If there is conduction by two solids in series with individual thermal resistances, then the total thermal resistance is the sum of the two individual thermal resistances. The same applies to resistances offered by convection and radiation.

6.1.3 Convection

Convection is the heat transfer between a surface and a fluid in motion at different temperatures. It is the result of two different physical phenomena, that is, energy

by the random movement of molecules (diffusion) and energy by the macroscopic movement of the fluid.

Heat transfer by convection is divided into forced convection and natural convection (Lewis, 1987; McCabe et al., 2008; Reynolds, 1986).

Forced convection is produced when external mediums such as fans, pumps, or atmospheric winds cause the flow.

Natural convection takes place when the heat flow is induced by floating forces, a consequence of density differences caused by temperature differences in the fluid as elements of the hotter, less dense fluid move and mix with elements of the more dense cooler liquid (Earle, 1983).

Owing to the fluid–surface interaction, a region is formed called hydrodynamic limit layer in which velocity varies from zero at the surface to an infinite value associated with the fluid. Ninety-nine percent of the heat transfer between the surface and the fluid takes place in this thin layer.

The first thing in heat transfer by convection is the determination of the hydrodynamic or turbulent nature of the limit layer.

In the laminar regimen, fluid movement is ordered in such a way that flux lines in which particles move may be identified. This laminar fluid flow is associated with low Reynolds numbers, that is, the ratio between the inertial and viscosity forces is low. Hence, disturbances in the fluid, originating from the surface roughness, are quickly dissipated, maintaining an ordered laminar flow. If Reynolds number is high, inertial forces are high enough to magnify the disturbances produced in the flow, generating vortexes that indicate a turbulent regimen in the fluid. Irregular movement and random fluctuations in the velocity characterize the turbulent regimen.

Velocity and temperature profiles in the limit layer are more uniform in the turbulent regimen and hence, temperature and velocity gradients are much higher because diffusion in the twisters is much higher than molecular diffusion in the laminar regimen. Consequently, heat transfer rate is much higher in turbulent flow than in laminar flow.

The only disadvantage in the turbulent regimen is that pressure drop increases in the flow direction. This higher pressure drop will require a higher power of pumps and fans.

In a laminar or turbulent regimen, the heat transfer rate by convection between a surface and a fluid is determined by Newton's cooling law, which is as follows:

$$q = Ah(T_s - T_f) \tag{6.4}$$

where

q = heat transfer rate (J/s)
h = heat transfer coefficient by convection (w/m^2°C)
A = heat transfer area (m^2)
T_s = temperature in the surface (°C)
T_f = temperature in the fluid (°C)

The thermal limit layer is the area in contact with the surface through which heat transfer is produced. This layer shows resistance to heat flow.

Forced convection is where hotter and cooler fluids are mixed by mechanical means such as pumping or agitation. It should be noted that during forced convection,

natural convection still takes place, although its effect is small and often neglected (Brennan et al., 1990; Coulson and Richardson, 1978).

Finally, radiation is the transmission of thermal energy in the form of electromagnetic waves. When radiation from a hot source falls on a body, the fraction absorbed appears as heat in the body.

The heat transfer coefficients can, in principle, be estimated by three methods: (1) analysis of experimental product temperature histories; (2) lumped capacity thermal analysis using an aluminium analog; and (3) Nusselt number correlations.

Successful modeling of the thermal behavior of food products requires accurate knowledge of both the thermal properties of the product and the cooling media to which it is exposed to and a correct approach to validation of the model output against experimental temperature histories. This procedure is complicated where there is uncertainty in the location at which temperature is measured in the product. The cooling of a soft cylindrical cheese product that is partially immersed in brine and air is examined by Cronin et al. (2010). As the cheese is very deformable, it is not possible to exactly identify the measurement location of the temperature-recording thermocouples. The uniform and exponential probability distributions were found to best represent the variability in thermocouple location at the center and surface of the product, respectively.

Expressions for the mean measured temperature at the center and surface that result from the distributed nature of thermocouple location were obtained. These expressions were used to derive equivalent locations in the cheese, which should be used when comparing model and experimental temperature predictions. The theoretical approach was also checked against Monte Carlo simulations and there was excellent agreement between them. It was shown that when validating model temperature histories against experimental readings, this phenomenon must be taken into account.

During processing of canned mixtures of solid–liquid foods, conduction and convection occur simultaneously. The literature lacks in a complete simulation study where a large number of solids are dispersed in the liquid phase, for example, canned peas. Therefore, Kiziltas et al. (2010) determined temperature changes inside a can containing solid–liquid food mixtures. For this purpose, dispersed stationary solids (canned peas in water) in a two-dimensional (2-D) (axi-symmetrical) configuration were applied. Ansys V11 was used to solve continuity, energy, and momentum equations. For experiments, canned pea samples were prepared in 500-g cans, and heating process was conducted in a retort under pasteurization conditions at approximately 98°C. Temperature changes were measured using needle-type thermocouples, and simulation results were validated against experimental data. This study is expected to be a significant contribution to the literature for further optimization studies and to form the basis of an industrial project to improve the canning process of solid–liquid mixtures.

Attia et al. (2012) reported experimental data and scaling analysis for forced convection of foams and microfoams in laminar flow in circular and rectangular tubes as well as in tube bundles. Foams and microfoams are pseudoplastic (shear thinning) two-phase fluids consisting of tightly packed bubbles with diameters ranging from tens of microns to a few millimeters. They have found applications in separation processes, soil remediation, oil recovery, water treatment, food processes, as well as in fire fighting and heat exchangers (Schweitzer, 1979). First, aqueous solutions of

surfactant Tween 20 with different concentrations were used to generate microfoams with various porosity, bubble size distribution, and rheological behavior.

These different microfoams were flowed in uniformly heated circular tubes of different diameter instrumented with thermocouples. A wide range of heat fluxes and flow rates were explored. Experimental data were compared with analytical and semiempirical expressions derived and validated for single-phase power-law fluids. These correlations were extended to two-phase foams by defining the Reynolds number based on the effective viscosity and density of microfoams. However, the local Nusselt and Prandtl numbers were defined based on the specific heat and thermal conductivity of water. Indeed, the heated wall was continuously in contact with a film of water controlling convective heat transfer to the microfoams.

Overall, good agreement between experimental results and model predictions was obtained for all experimental conditions considered. Finally, the same approach was shown to be also valid for experimental data reported in the literature for laminar forced convection of microfoams in rectangular minichannels and of macrofoams across aligned and staggered tube bundles with constant wall heat flux.

6.2 HEAT EXCHANGERS

A heat exchanger is a device for heat transfer between two fluids at different temperatures separated by a solid wall. In the case of fluids, heat is transferred from the hotter to the cooler fluid. Fluids may flow in the same direction through the heat exchanger (cocurrent flow) or may flow in the opposite direction (countercurrent flow). These surface heat exchangers can vary from simple tubular condenser (concentric or double-pipe) to modern and sophisticated heat exchangers used in evaporators for the concentration of highly heat-sensitive biological material.

One of the uses of heat exchangers is in the condensation of water vapor removed from concentrating aqueous solutions in evaporators. The hot water–vapor contacts a falling spray of cold water and no wall intervenes to resist the heat transfer.

Tube and shell heat exchangers are widely used in chemical processing. Plate heat exchangers (PHEs) are also used in bioprocessing due to their versatility and ease of cleaning.

In a concentric tube heat exchanger, there are two concentric tubes, where fluids move in the same direction (parallel flow) or in opposite direction (countercurrent flow). In parallel flow, the hot and cold water go in and out through the same end. In countercurrent flow, fluids go in and out through opposite ends and circulate in opposite directions (Figure 6.1).

6.2.1 Rate of Heat Transfer Q

The rate of entry or exit of heat, Q (J/s), needs to be controlled in the design and operation of process systems requiring heating or cooling.

In a conventional heat exchanger, heat has to pass across a wall separating the two fluids; hence, the greater the area of the wall, A, the greater the rate of heat transfer, Q.

Q is also proportional to the difference in temperature, ΔT, between the two streams.

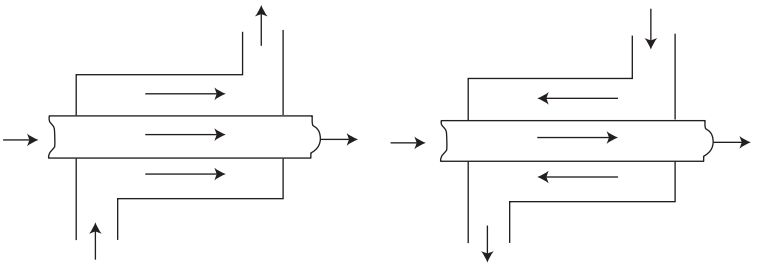


FIGURE 6.1 Concentric tube heat exchanger in parallel flow (left) and countercurrent flow (right).

If a proportionality constant, U, is introduced, then

$$Q = UA\Delta T \tag{6.5}$$

where Q is the rate of heat transfer, A is the area of the heat exchanger surface, ΔT is the temperature difference between the two streams, and U is the overall heat transfer coefficient (OHTC).

Values of U for common types of heat exchangers are listed in the chemical engineering literature. These values vary widely for different products and depend on the different physicochemical and flow characteristics (Table 6.1).

In heat exchanger applications, the significance of the overall resistance to heat transfer takes into account the individual resistance to heat transfer. The solid wall separating the two fluids is one barrier and frictional drag forces take place at the wall and boundary layers. Moreover, the thermal resistance of fouling layers needs to be included in the analysis of OHTC values if surfaces of the heat exchanger are scaled.

Impurities of fluids adhere to surfaces and form layers, increasing the total thermal resistance. This contamination resistance can vary from a null value when the exchanger is new to a maximum value at the end of its useful life.

In steady-state heat flow across a heat exchanger, the value of ΔT is different at different positions. If some mean values of ΔT can be found, then Equation 6.5 can be used to predict the approximate heat transfer area for a steady-state heat transfer rate.

Two expressions for mean values of the temperature difference exist across industrial heat exchangers, the logarithmic mean temperature difference (LMTD) and the arithmetic mean temperature difference (AMTD).

Hence, if ΔT_1 is the terminal temperature difference between the two fluids at one end of the heat exchanger and ΔT_2 that at the other end, then the LMTD is given by

$$\Delta\Theta_m = \frac{\Delta T_1 - \Delta T_2}{\ln(\Delta T_1/\Delta T_2)} \tag{6.6}$$

TABLE 6.1
Approximate Overall Heat Transfer Coefficients U for Shell and Tube Equipment

Hot Side	Cold Side	Overall U (w/m²K)
	Evaporators	
Steam	Water	2000–4250
Steam	Organic solvents	570–1140
Steam	Light oils	455–1020
Steam	Heavy oils	140–425
Water	Refrigerants	425–850
Organic solvents	Refrigerants	170–570
	Heat Exchangers	
Water	Water	850–1700
Organic solvents	Water	280–850
Gases	Water	17–280
Light oils	Water	340–910
Heavy oils	Water	60–280
Organic solvents	Light oil	115–400
Water	Brine	570–1140
Organic solvents	Brine	170–510
Gases	Brine	20–280
Organic solvents	Organic solvents	115–340
Heavy oils	Heavy oils	45–280

When ΔT_1 and ΔT_2 differ only by a few degrees, that is, when the ratio $\Delta T_1/\Delta T_2$ approaches unity, the AMTD is given by

$$\Delta T_{AM} = \Delta T_1 + \Delta T_2/2 \tag{6.7}$$

If ΔT is replaced by $\Delta\Theta_m$, then Equation 6.5 becomes

$$Q = UA\Delta\Theta_m \tag{6.8}$$

If the value of OHTC is known, then the size of the heat exchanger, that is, the heat transfer area can be estimated. Equation 6.8 is used frequently in heat exchanger selection. In this case, the product stream flow rate and operating temperatures are fixed by the process. For a concentric tube exchanger of length, L, in which the hot fluid circulates through the interior tube and the cold fluid through the space between the interior and exterior tube, A_h is given by $\pi D_{int}L$ and $A_c = \pi D_{ext}L$, where D_{int} and D_{ext} are the interior and exterior diameters of the exchanger, respectively. Conduction resistance is expressed in cylindrical coordinates because the wall has a cylindrical shape. In heat exchangers of multiple paths, flow can be parallel or countercurrent in other areas. In these cases, a correction factor F_G is defined. When this factor is multiplied with LMTD for countercurrent flow, the product is the real temperature fall (Figure 6.2).

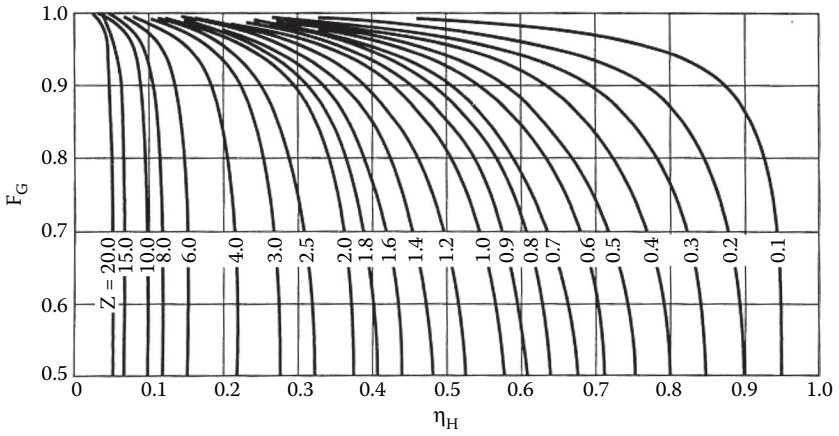


FIGURE 6.2 Correction of LMTD. (From Bowman, R.A., Mueller, A.C., and Nagle, W.M., 1940. *Trans. ASME*, 61: 283, courtesy of American Society of Mechanical Engineers.)

Z factor is defined as the ratio of the fall in temperature of the hot fluid to the increase in temperature of the cold fluid:

$$Z = (T_{ha} - T_{hb})/(T_{cb} - T_{ca}) \tag{6.9}$$

$$n_H = (T_{cb} - T_{ca})/(T_{ha} - T_{ca}) \tag{6.10}$$

n_H denotes the effectiveness of heating, that is, the ratio of the actual increase in temperature of the cold fluid to the maximum possible increase in temperature that could be achieved if the temperature approach at the hot end was zero. From the values of Z and n_H, F_G factor can be estimated. This factor is always less than unity.

Modeling of the heat sterilization of canned food in continuous rotary sterilizers entails knowledge of two parameters. which are the overall heat transfer coefficient (U) between the external heating medium and the can fluid, and the fluid-to-particle heat transfer coefficients h_{fp} between the can fluid and particles (Sablani and Ramaswamy, 1996).

An empirical methodology was developed by Dwivedi and Ramaswamy (2010a) for evaluating the fluid-to-particle heat transfer coefficient (h_{fp}) and overall heat transfer coefficient (U) in biaxially rotating cans. Conventional particle temperature measurement during thermal processing is generally difficult in cans undergoing agitation processing and is even more difficult in cans going through biaxial free rotation as in continuous flow turbo cookers. Thin wire flexible thermocouples have helped in gathering temperature data of both particle and liquid in end-over-end (EOE) batch processes. Wireless temperature loggers have been developed for liquid temperature measurements in continuous flow systems, which can be used to estimate U. Evaluation of h_{fp} is still difficult in these systems due to difficulty in gathering particle temperatures.

The proposed method involves developing correlations between h_{fp} and U using real-time temperature data gathered from test cans in fixed axial mode and then

coupling them with experimentally evaluated U from fluid temperature gathered with wireless sensors to compute h_{fp} for biaxially rotating cans. The methodology is based on the assumption that within a can, factors that influence U will also influence h_{fp}, and therefore, h_{fp} and U are generally interrelated. A three-factor, five-level central composite rotatatable design and a response surface methodology was used to develop the correlation models for the U and h_{fp} in fixed axial mode with retort temperature (111.6–128.4°C), glycerin concentration (80–100%), and rotational speed (4–24 rpm) as the main factors.

Glycerin concentration and rotation speed were highly significant (<0.001), while temperature was marginally significant ($p < 0.05$) with respect to U, while all factors were significant with h_{fp}.

Agitation during thermal processing is an effective means of providing induced convection, which provides higher and uniform heating rates to the product. Canned food products may be heated by conduction, convection, or a combination of both. With convection heating, the rate of heat penetration in the product can be increased by mechanical agitation (Anantheswaran and Rao, 1985a,b) and the product movement within these agitated containers increases the heat transfer within such products.

Some common types of agitation used are EOE and axial agitation. Clifcorn et al. (1950) suggested the use of EOE rotation to increase the heat transfer in canned food products. In EOE rotation, the sealed can is rotated around a circle in a vertical plane. As the can rotates, the headspace "bubble" moves along the length of the can and brings about agitation of the can's contents.

By comparison, the continuous container handling types of retorts are constructed with two cylindrical shells, in which processing and cooling takes place and cans are subjected to axial agitation. The shell can be used for pressure processing in steam or cooling with or without pressure. The Sterilmatic (FMC Corp., San Jose, CA) is an extensively used continuous agitating retort in which an entering can is carried on and advanced by a revolving reel. The Steritort is a pilot-scale simulator of the thermal process in the Sterilmatic series. The motion of a can in a Steritort takes place in three phases consisting of fixed reel, transitional reel, and free reel motion across the bottom of the retort (Dwivedi and Ramaswami, 2010b).

Thermal processing under conditions enabling container agitation are attractive to food processors since they provide higher rates of heat transfer and more uniform temperature due to product mixing. Two common types of agitations are EOE and axial agitation. While EOE agitation is common in batch retorts, axial agitation is predominant in continuous cookers in which the cans roll in a helical path along the retort shell. Dwivedi and Ramaswami (2010b) evaluated heat transfer rates to canned Newtonian fluids in endover-end and axial modes of rotation in the same retort. A single basket rotary retort was retrofitted to accommodate simultaneously both EOE and two types of axial modes of rotation, free axial and fixed axial. In the free axial rotation, the cans were allowed to rotate on their own axis as they rolled along the retort shell during the bottom third of the rotation, while in the fixed axial mode, the cans in the axial direction were held stationary in the rotating basket. The overall heat transfer coefficient U, heating rate index, lag factor, and cook values associated with cans filled with Newtonian fluids were evaluated using a central composite

rotatable design of experiments with glycerin at five concentration level (no glycerin to all glycerin), heating medium temperature (111.6–128.4°C) and five basket-rotational speeds (4–20 rpm). Higher U, and lower heating rate index, lag factor, and cook values were associated with higher rotational speed and retort temperatures for all modes of agitation. The heat transfer parameters associated with free axial rotation were significantly higher than in the endover-end mode, which was higher than in the fixed axial mode. Axial rotation (Berry and Dickerson, 1981; Merson et al., 1980; Quast and Sioza, 1974, Soule and Merson, 1985) has also been used for the heating of canned foods.

A recently developed method of freezing called hydrofluidization (HF) essentially consists in using a circulating system that pumps the refrigerating liquid upward through orifices or nozzles, in a refrigerating vessel, thereby creating agitating jets, and thus evoking extremely high surface heat transfer coefficients (Fikiin, 1992, 2008; Fikiin and Fikiin, 1998). If the process is adequately controlled, it represents a potential application with advantages: to use equipments of small size and to improve the freezing of individual pieces of food, besides the advantages related to the immersion chilling and freezing process.

HF enhances the transfer coefficients involved. The combination of these high coefficients with the use of small food samples leads to processes in which the transport phenomena within the food is affected by the fluid flow over the food samples (Fikiin, 2008).

Peralta et al. (2010) developed a model to estimate the fluid flow and heat and mass transfer in an HF system. A case study of modeling and validating the heat transfer to a single stationary copper sphere of 20 mm diameter impinged by a single round jet of liquid was carried out using computational fluid dynamics. The simulations were performed using parameters such as velocity of the liquid at the orifice exit (2.36–7.07 m/s), temperature of the liquid refrigerant (–5 to –15°C), and distance between the orifice and the stagnation point of the sphere (1 and 5 cm). In general, the errors of the model were in the order of magnitude of the uncertainty of the experimental data of Nusselt number averaged over the sphere surface. Also, the simulated heat transfer and flow field parameters were comparable with those obtained in the literature for similar systems.

6.2.2 Comparing Plate and Tubular Exchangers

In forming a comparison between plate and tubular heat exchangers, the following needs to be taken into account, which will generally assist in the selection of the optimum exchanger for any application:

1. For liquid/liquid duties, the PHE usually has a higher overall heat transfer coefficient and often the required pressure loss will be no higher.

   The shell side of a tubular exchanger is basically a poor design from a thermal point of view. Considerable pressure drop is used without much benefit in heat transfer due to the turbulence in the separated region at the rear of the tube. Additionally, large areas of tubes even in a well-designed tubular unit are partially bypassed by liquid. Thus, low heat transfer areas are created.

2. The effective mean temperature difference is usually higher with the PHE.
3. Although the tube is the best shape of flow conduit for withstanding pressure, it is entirely the wrong shape for optimum heat transfer performance since it has the smallest surface area per unit of cross-sectional flow area.
4. Because of the restrictions in the flow area of the ports on plate units, it is usually difficult to produce economic designs when it is necessary to handle large quantities of low-density fluids such as vapors and gases.
5. A PHE usually occupies considerably less floor space than a tubular exchanger for the same duty.
6. From a mechanical viewpoint, the plate passage is not the optimum, and gasketed plate units are not made for operating pressures much in excess of 300 PSIG.
7. For most materials of construction, sheet metal for plates is less expensive per unit area than tube of the same thickness.
8. The plate is usually more economical than the tube when materials other than mild steel are required.
9. When mild steel construction is acceptable and when a close temperature approach is not required, the tubular heat exchanger will often be the most economic solution since the PHE is rarely made in mild steel.
10. PHEs should have an elastomeric gasket. Even compressed asbestos fiber gaskets contain about 6% rubber. The maximum operating temperature therefore is usually limited to 264°C (APV, 2000).

6.2.3 Plate Heat Exchangers

PHEs are widely used in the food industry and consist of a series of vertical-shaped steel plates separated by gaskets and held in a metal press, which form parallel corrugated channels through which liquid food and heating media can be passed. Plates are designed to enhance fluid mixing. They limit the flow of fluids through the path of the exchanger and provide the surface area for heat transfer. The surface is corrugated to improve heat transfer. Corrugations break the limit layer causing turbulence with low Reynolds numbers, increasing heat transfer coefficient significantly. Moreover, corrugations between adjacent plates form flow channels and increase the stiffness of the thin plates. Most of the plates have chevron-patterned corrugations. According to the angle of chevron, a higher or lower heat transfer coefficient may be obtained. Plates at the edges are not thermal plates and simply contain the fluid preventing contact with pressure plates that are generally made of tempered steel (Edibon, 2012) (Figure 6.3).

Joints prevent both fluids from mixing and prevent losses. They allow fluids to distribute between alternate plates. Joints are made of just one piece to be adjusted in the slots around the perimeter of the plate and around the holes of the ports. Ports are input and output areas for fluids. Pressure plates provide pressure to keep spaces with joints. Tightening or compression poles are tightened to keep the unit intact and in optimum working conditions.

There are also two guide bars, one at the top and the other at the bottom. Plates slide over them maintaining a proper position. These are longer than the plates allowing

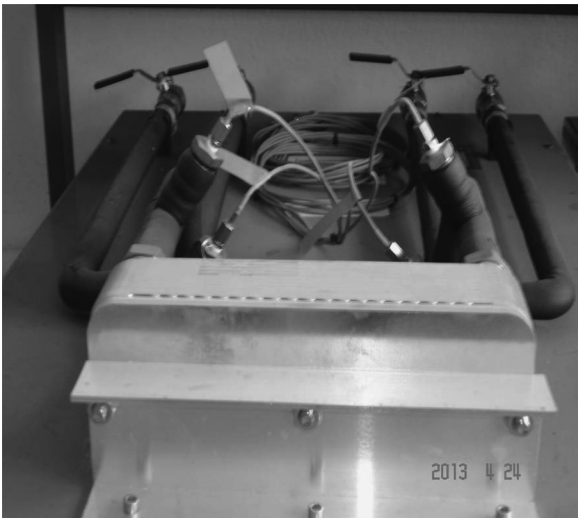


FIGURE 6.3 Plate heat exchanger. (Supplier Edibon, Varzakas lab.)

for loosening and sliding of the plates so that they are inspected and cleaned. PHEs are used because of their high energy recovery. The model for flow in a PHE can be serial flow where the flow passes through each plate and changes directions in the adjacent plate. This model is feasible only for small flows and is rarely used. In connected flow model, fluid divides into subflows that mix before leaving the exchanger. It is used for great volumes of liquid.

In simple section flow configuration, the fluid goes through the unit just once in configuration, the flow goes through some sections of the exchanger arranged in series and is formed by closing intermediate ports of some plates. Hence, the velocity of the fluid and the heat transfer coefficient increase. When both fluids go through the unit twice, we have a 2/2 configuration (Edibon, 2012).

Milk-fouling phenomena of PHEs result in an increase of energy consumption, extra maintenance, higher labor costs, and a decrease in the productivity. In addition, fouling deposits can cause the growth of unwanted microorganisms on the corrugated surfaces of PHEs.

PHEs have been mostly used to pasteurize liquid food products such as milk and fruit juice in the field of food processing. The heat transfer in PHEs leads to fouling, which makes the deposit layer thicker and heat transfer from hot water to milk weaker.

Many liquid food industries have spent a significant amount of time and money on the fouling removal during the cleaning-in-place process (Georgiadis et al., 1998; Gillham et al., 2000). Van Asselt et al. (2005) reported that the dairy industry spent about 80% of the total production costs to clean the processing equipment.

Whey protein beta-lactoglobulin (b-Lg) denatured by heat at 90°C plays a major role in the formation of fouling (de Jong, 1997; Visser et al., 1997). Influenced by high-processing temperature, whey protein chains (native) unfold, resulting in the

formation of protein aggregation and deposit attached to the surface of PHEs. Also, material properties such as roughness, wettability, and charge density of PHE surfaces play a critical role to determine the fouling rate and protein adsorption of skimmed milk.

There have been numerous simulation studies based on typical Arrhenius models for milk fouling phenomenon in 1-D environment (Georgiadis and Macchietto, 2000; Grijspeerdt et al., 2004; Nema and Datta, 2006; Sahoo et al., 2005) and 2-D environment (De Bonis and Ruocco, 2009; Jun et al., 2004; Jun and Puri, 2006; Mahdi et al., 2009).

In particular, the antifouling mechanism associated with plate corrugation profiles causing the extreme turbulent flow scheme and surface coatings to reduce the surface energy is uncertain. Choi et al. (2013) developed a computational fluid dynamics (CFDs) model in three-dimensional (3-D) environment, which could estimate antifouling performances of PHEs during the milk pasteurization process. It was the first attempt to simulate the fouling and temperature distribution patterns on realistic corrugated surfaces of PHE unit with different surface treatments. The conventional stainless-steel surface and stainless-steel plates coated with Lectrofluor 641 and graded Ni-P-polytetrafluoroethylene were compared for their antifouling performances. A transient 3-D fouling model was developed based on heat and mass transfer equations, and fouling kinetics involving diffusion and protein adhesion mechanisms. Pattern and size of corrugations of actual PHE were measured and subsequently used to build 3-D solid geometry using AutoCAD. The geometry file was meshed using Gambit software and further transferred to CFD codes. Fouling predictions based on chemical kinetics and the temperature-dependent parameters accounting for different surface energy values were close to experimental data within a maximum prediction error of 7%. The developed 3-D fouling model is expected to meet the demand of food industries to correlate the surface energy with the self-cleanability of food thermal process equipments and seek the theoretical solution.

Fouling on food contact surfaces (e.g., heat exchangers, work tables, conveyors) during food processing has a significant impact on operating efficiency and can promote biofilm development. Processing raw milk on PHEs results in significant fouling of proteins as well as minerals, and is exacerbated by the wall heating effect. The surface of 316 L stainless-steel heat exchanger plates was modified to resist fouling during food processing. An electroless nickel plating process was used by Barish and Goddard (2013) to codeposit fluorinated nanoparticles onto 316 L stainless steel. The ability to resist fouling was demonstrated on a pilot plant scale PHE. The fluorinated nanoparticle-modified steel reduced surface energy from 41.4 to 24.7 mN/m, and reduced foulant accumulation by 97%. The antifouling coating was demonstrated to improve heat transfer efficiency. Repeatability studies were performed and confirmed that the EN-PTFE surface coating maintained its antifouling properties through 10 independent processing runs. Codeposition of fluorinated particles during electroless nickel plating represents an effective and commercially scalable method to prepare antifouling coatings on stainless steel.

Fouling is unwanted deposit on a (heat transfer) surface. It is a major problem in food and dairy industry because heat transfer to the product decreases, resulting in

reduced product quality and safety. Thus, plant efficiency is reduced, and unsupervised cleaning has to be conducted. This limits processing time and increases plant downtime and costs. Monitoring fouling and cleaning requires high demands for the measuring and analyzing system. Wallhäußer et al. (2012) gave an overview of different fouling monitoring methods in heat exchangers. Experimental (pressure drop, temperature and heat transfer parameters, electrical parameters, acoustic methods), numerical, and computational methods are presented and compared.

In heat exchangers, the pressure between inlet and outlet is measured regularly. When fouling develops, the mean square area in a flow channel decreases, leading to a pressure drop at constant flow rate. This method is standard and can be used as input for other methods, for example, as input in an artificial neural network for fouling detection in a PHE (Riverol and Napolitano, 2005).

Heat transfer parameters such as heat flux, overall heat transfer coefficient, and fouling resistance are based on temperature changes, mass flow rate m, and thermal conductivity of the product, the heating medium, and the fouling layer.

The convective heat exchanger coefficient and fouling thickness in a heat exchanger was determined via transient state estimation by comparing the global response time of a system in fouling and no fouling conditions (Perez et al., 2009). For this, a transient fouling probe was developed using a sensitivity function and the probe was evaluated theoretically and experimentally.

Electrical parameters can be used when electric heating or electrodes are present, for example, a change in salt concentration due to precipitation induces a change in electric conductivity. Usually, electrical resistance and conductivity are chosen.

For determining fouling, a method was developed measuring the electrical and the thermal resistance (heat flux) (Chen et al., 2004). Stainless-steel electrodes were applied to determine the electrical resistance R_{el}, and the thermal resistance R_{th} was calculated with heat flux, backside surface temperature of the fouled wall, and fluid bulk temperature.

Acoustic methods involve ultrasound and vibrational methods. Acoustic parameters change when fouling occurs and can be measured in transmission (one transducer as sender, one as receiver) and in pulse-echo mode (one transducer as sender and receiver).

Acoustic sensors have also been employed. Quartz crystal microbalance is based on the crystal oscillator principle. It consists of a piezoelectric quartz oscillating at its resonant frequency, which changes Δf dependent on deposited material amount. Usually, D_f decreases when material is adsorbed. Guided waves constitute another method. They travel alongside a structure, not through it. Horizontal variation leads to signal reflection and amplitude changes. A tube is excited to oscillate in its resonance frequency, and changes in frequency, velocity, and amplitude are determined. Wave excitation has to be controlled due to different oscillation modes (symmetric, nonsymmetric). This can be done by mechanical impactors (hammer), piezoceramics, or piezopolymers (Wallhäußer et al., 2012).

Usually, two kinds of fouling appear depending on process temperature: chemical reaction at pasteurization (type A or protein fouling, mainly denaturated proteins) and scaling at ultra-high temperature (type B or mineral fouling, mainly salts)

(Bansal and Chen, 2006; Changani et al., 1997; Visser and Jeurnink, 1997). Cleaning is conducted due to the diminished heat transfer with fouling and the risk of unsafe food (Changani et al., 1997; Fryer and Asteriadou, 2009).

The dairy industry is not the only food industry affected by different fouling types. In the beverage industry, particulate/sedimentation fouling during membrane filtration of beer and other fermented beverages plays an important role (Blanpain and Lalande, 1997; Czekaj et al., 2000). In water treatment plants, mostly scaling and biofilms are present and can hinder processing (Laine et al., 2003; Müller-Steinhagen et al., 1999), while in crude oil processing, scaling and chemical reaction occur, reducing heat exchanger performance (Butterworth, 2002; Deshvannar et al., 2010).

Fouling is a cost-increasing problem for a variety of industries, including aerospace, chemical, petroleum, and food. There have been studies on mitigation of fouling some of which recommend the use of lower surface free energy materials, manufactured by different techniques, as an alternative to conventional materials. Although modeling of fouling for a given surface has been an area of interest, there is a lack in the models about correlating the surface free energy with deposit amount computationally. Ozden and Puri (2010) developed a computational model, including the effect of surface energy and operational parameters, and validated it to estimate the amount of foulant deposits and rate of deposition. Four coated surfaces (Microlube/PTFE, TM117P, AMC148, and CNT) were compared with stainless steel (SS316 as control) for flow rates of 3 and 10 g/s and inlet milk temperatures of 40°C and 60°C. The percent error for the decrease in outlet milk temperatures between the experimental data and computed results was between 2% and 18% except for CNT (29.2%). The calculations of deposit amount for each test case and the surfaces tested were in good agreement with the experiments, that is, average percent difference values between measured and calculated values were from 11.1% to 38.1% (except CNT) with an overall average of 21.5%.

The use of PHE as condensers under low pressure is one of the most complicated areas. It is limited mostly because of a relatively high-pressure drop of condensing media. The influence of pressure losses on PHE performance as condensers was discussed by Bobbili and Sunden (2009). The importance of the plate corrugation shape on the thermal and hydraulic performance of PHEs is an established fact. The most recent attempts to generalize correlations for pressure drop and heat transfer in PHE channels were made by Dović et al. (2009) and Khan et al. (2010).

Tovazhnyansky et al. (2010) established the new principle of plate corrugation for low-pressure plate-and-frame condensers. The basic trends on developments of corrugated patterns for low-pressure plate condensers were investigated. The principle of channels with variable geometry was selected for new corrugated pattern development. The proposed plate for condenser has the heat transfer area that consists of several corrugated sections along its length. Shape and dimensions of ridges and valleys of corrugations are variable. The corrugations are inclined to plate vertical axis so that the ridges of two adjacent plate corrugations are in contact. The channel formed by such plates has the variable cross-sectional area. The experimental study of heat transfer and pressure drop for channels of such pattern was carried out. The dependencies for film heat transfer and pressure drop were obtained for each channel

part formed with adjacent sections of the plates. The obtained results were compared with those for plates that are conventionally used. The advantages of proposed corrugation are discussed. The calculation methods based on obtained results were developed for single-phase flow heat exchange and for condensation of pure vacuum vapors. Recommendations on plate surface synthesis are presented.

6.3 FLOW INSIDE A TYPICAL PLATE HEAT EXCHANGER

In this case, the geometry of the flow path is going to be significantly different from that of a circular pipe, so the characteristic linear dimension will be some equivalent diameter, De.

A relationship often used is De = 4 × area for flow/wetted perimeter.

The constant and the indices to the dimensionless groups will also change for this different type of heat exchanger. One form of the Dittus–Boelter equation often seen is

$$hDe/k = 0.28(Deu\rho/\mu)^{0.65}(C\rho\mu/\kappa)^{0.4} \tag{6.11}$$

Again, substitution of the appropriate physical data permits the film heat transfer coefficients, h, for the two fluids to be calculated.

6.3.1 Tubular Exchangers

Simple shell and tube exchangers are limited to low-viscosity foods up to approximately 2 Ns/m^2 in food processing and widely used in boiler or evaporator plants in a food plant. Modification of the conventional design, such as corrugated tubes, gives better heat transfer and does not involve excessive turbulence. Enhanced heat transfer can be obtained by using mixing elements inside the tube; however, these might increase pressure drop through the unit (Fryer, 1992).

Shell and double concentric tube heat exchangers have better performance compared to the classic heat exchangers. The difference is that the simple (or corrugated) tubes, with or without fins, are now replaced by double concentric tubes (Figure 6.4).

In shell and double concentric tube heat exchangers, one sees the shell, the three distributors, the three collectors, and the channel covers with four tube sheets. The two fluids of the same temperature level enter by the first and the third distributor and goes out by the third and the first collector, respectively. The fluid of different temperature level of two other fluids pass by the intermediate collector (or distributor) (Bougriou and Baadache, 2010). They demonstrated that the relative diameter sizes of the two tubes with respect to each other are the most important parameters that influence the heat exchanger size.

The classic conservative approach for thermal process design can lead to overprocessing, especially for laminar flow, when a significant distribution of temperature and of residence time occurs. In order to optimize quality retention, a more comprehensive model is required. A model comprising differential equations for mass and heat transfer is proposed by Kechichian et al. (2012) for the simulation of the

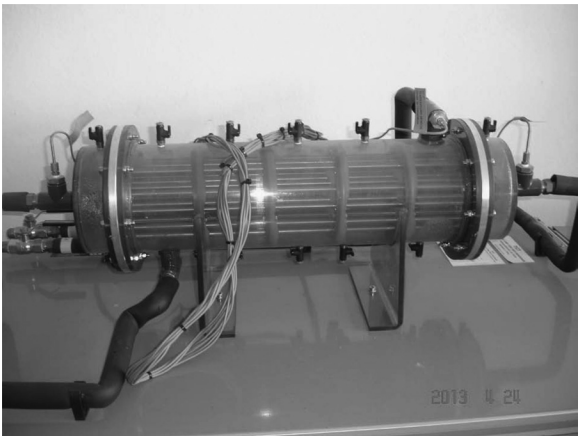


FIGURE 6.4 Shell and tube heat exchanger. (From Edibon, Varzakas lab.)

continuous thermal processing of a non-Newtonian food in a tubular system. The model takes into account the contribution from heating and cooling sections, the heat exchange with the ambient air and effective diffusion associated with nonideal laminar flow. The study case of soursop juice processing was used to test the model. Various simulations were performed to evaluate the effect of the model assumptions. An expressive difference in the predicted lethality was observed between the classic approach and the proposed model. The main advantage of the model is its flexibility to represent different aspects with a small computational time, making it suitable for process evaluation and design.

A tubular ultra-high temperature heat exchanger (Invensys APV, Evreux, France) was used by Alvarez et al. (2010) with 316 stainless-steel tubes, each of them of 6.0 m long and consisting of seven channels that were 14.0 mm in diameter.

The sterilizer included five zones (preheating, heating, recovery 1, recovery 2, and cooling). The study focused on the heating zone (inlet = 80°C; outlet = 128°C), which was the limiting zone because of its sharp fouling increase.

The sterilization was performed in two steps: the launching phase, during which dessert cream flushed water out from the equipment, and the production phase. At the end of the production phase, the cleaning sequence started using a decentralized CIP system. Cleaning solutions and water used during rinses were systematically discharged to the purification station after each use (i.e., it was a single-use system).

Several sensors were installed in the equipment. The flow rate of the milk-based product ($Q = 2.0\ m^3/h$) was measured with an electromagnetic flow meter. A differential pressure sensor was installed in the heating zone. Four 100-Ω platinum temperature sensors were installed at the entrance and outlet of the heating zone, two in the heating fluid and two in the dairy fluid compartments.

The strategy is based on the online and offline use of sensors and tracers, the accuracy, relevance, and robustness of which were evaluated for each phase of the sequence used for cleaning an industrial sterilizer.

The efficient duration of each phase of the cleaning sequence (management of the end of operation) and the sorting of the fluids (management of mixtures and destination of fluids) were determined in real time. As a result, significant reduction in total overall duration of the cleaning sequence, wastewater volume (waste volume was reduced by half), and detergent volume (caustic soda and acid was reduced by up to a few tens of kilograms per cleaning) was achievable (Alvarez et al., 2010).

6.3.2 Scraped-Surface Exchangers

In this type of exchanger, food is passed through a heated chamber that contains a rotating blade. This stirs the food and prevents deposition. Scraped-surface units are widely used for very viscous solid–liquid mixtures and for foods such as ice creams and spreads. In Figure 6.5, a scraped-surface heat exchanger (SSHE) is depicted. There is an outer concentric tube with a fluid flowing inside it. These heat exchangers are double tube with a large concentric tube of diameter 100–300 mm. The inner region through which the other fluid flows from end to end has a rotating shaft (500–700 rpm) with blades attached. This heat exchanger can handle fluids containing solid particles up to 25 mm in size (Hayhurst, 1992).

If temperature of the main volume of liquid in the heat exchanger is T, and the temperature of the heat transfer surface is T_w then heat flows from the surface to the liquid at a time, t, which is the time until the next blade passes from the surface and removes liquid and places new liquid on the surface.

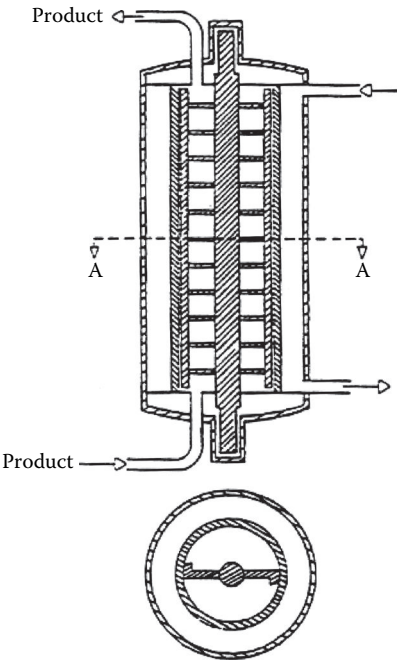


FIGURE 6.5 Schematic diagram of a scraped surface heat exchanger.

According to the following equation

$$Q_T/A = 2k\,(T_W - T)\sqrt{\frac{t}{\pi\alpha}} \tag{6.12}$$

where k is the thermal conductivity of the fluid, α is the thermal diffusivity of the fluid, and A is the surface area for heat transfer

$$h_i = Q_T/tA\,(T_W - T) \quad \text{and} \quad a = k/\rho Cp \tag{6.13}$$

Hence, Equation 6.13 becomes

$$h_i = 2\sqrt{\frac{k\rho Cp}{\pi t}} \tag{6.14}$$

The time to pass successive blades from a surface is t = 1/n B.
n is the velocity of the mixer (r/h) and B is the number of blades on the axis.
Hence, Equation 6.14 becomes

$$h_i = \sqrt{\frac{k\rho CpnB}{\pi}} \tag{6.15}$$

This means that the heat transfer coefficient of a scraped surface depends on the thermal properties of the fluid and the mixing speed and not on the viscosity or the velocity of the liquid in the exchanger (Harriott, 1959).

Evaporators will be described in Chapter 12 of the book.

During heating, solid deposits on heat surfaces can eventually heat up to roasting temperatures, altering the aromatic properties of the treated fluid. Some of these issues can be avoided or minimized by adopting an SSHE in place of classical shell and tubes or double-pipe exchangers.

An SSHE is a double-pipe heat exchanger with a rotor coaxially inserted in the internal tube, known as the stator. The rotor is equipped with scraping blades to clean the inner surface of the stator.

The blades play a double role in the SSHE: on the one hand, they literarily scrape the inner surface of the stator, avoiding particle deposition and cooking; on the other hand, they enhance the heat transfer rates by increasing the fluid velocity near the exchange surface and by generating turbulence. The typical design of an SSHE presents a given number of blades arranged longitudinally on the rotor surface.

Numerical simulations on SSHE have been reported (Baccar and Abid, 1997, 1999; Bongers, 2006; De Goede and De Jong, 1993; Sun et al., 2004; Yataghene et al., 2008). Experimental studies on C-SSHE (De Goede and De Jong, 1993; Dumont and Fayolle, 2000; Dumont et al., 2000; Yataghene et al., 2009) suffer the lack of reliable techniques and protocols to measure the local values of temperature, pressure, and velocity.

D'Addio et al. (2012) analyzed the performance of an SSHE equipped with a new arrangement of blades to achieve higher thermal efficiencies than the conventional SSHE. This new design of exchanger, named as SSHE with alternate blades, A-SSHE, may be particularly suited to treat highly viscous fluids, such as food pastes. Experimental and numerical tests were carried out on an industrial-scale A-SSHE used to heat hazelnut paste, an intermediate product widely used in Italian confectionery industry. Experimental tests included physical, chemical, and rheological characterization of the hazelnut paste and the evaluation of the overall heat transfer coefficient as a function of rotational speeds and mass flow rates. Three-dimensional axial-symmetric CFD simulations of the A-SSHE were performed by using the software Fluent 6.2. For comparison, the same numerical tests were carried out for an equivalent SSHE with a conventional blade design (C-SSHE). Our studies show that the A-SSHE gives heat transfer coefficient values almost twice that of an equivalent C-SSHE, and that the numerical results are consistent with the experimental observations. The analysis of the fluid dynamics and of the thermal profiles suggests that the higher heat transfer efficiency of A-SSHE may be attributed to the occurrence of backmixing phenomena.

D'Addio et al. (2013) extended a former analysis on the thermal behavior of a new kind of SSHE operated in laminar regime to treat hazelnut paste, a highly viscous non-Newtonian fluid largely adopted in the Italian confectionary industry. This unit, named A-SSHE, presents an alternate arrangement of the scraping blades that allows doubling the exchanger thermal efficiency with respect to conventional SSHE with continuous blades; this is mainly due to backmixing phenomena.

Three-dimensional CFD simulations of the A-SSHE are used to estimate the overall heat transfer coefficient as a function of the main process parameters: blades rotational speed, flow rate, and wall temperature. The heat transfer coefficient results are slightly higher during cooling than during heating and increases much more with blade rotational speed than with mass flow rate. Dimensional analysis provides a correlation among heat transfer coefficient, fluid properties, and easily measurable flow parameters. This correlation is useful to design and operate an A-SSHE treating highly viscous food pastes.

Formation of ice occurs within two stages of the ice cream manufacturing process: after the initial freezing in a continuous SSHE (known as the freezer) and then during the hardening in a blast freezer where air (at around −25°C) is the cooling medium. During hardening, undercooling is not sufficient to allow the nucleation of new crystals (Sutton and Bracey, 1996).

Schwartzberg and Liu (1990) proposed the following mechanism for ice formation in a scraped-surface freezer. Dendritic crystals are formed on the scraped-surface wall; they grow and are scraped off the wall and dispersed into the bulk. They then ripen into the block-shaped crystals seen upon exit from the freezer. The process of such crystallization is complex and involves many coupled interactions among fluid flow, heat transfer, and ice crystal nucleation and growth (Lian et al., 2006).

Amamou et al. (2010) examined the freezing step that occurs in a SSHE during the manufacturing of sorbet. During this step, the product enters the exchanger as a liquid; then it is cooled and partially crystallized before exiting the exchanger as a mixture of liquid and ice, also called sorbet. The freezing step governs the final

quality of the product, particularly its texture. Most existing studies have focused on the product after freezing at the exchanger exit. The authors followed the evolution of the ice crystals' granulometry during the freezing of sorbet in the exchanger and to relate this evolution to process parameters such as refrigeration temperature, scraper speed, and initial sucrose concentration. Few *in situ* sensors exist to follow granulometry, and this fact is especially true for rapid kinetics and concentrated suspensions. Focused-beam reflectance measurement (FBRM), an original tool, was used in this study. FBRM is currently used in the chemical and pharmaceutical industries to follow product granulometry, but it is not used in food-related applications. In their study, an experimental protocol was developed to assure identical initial thermal and crystallization conditions. First, the sensor sensitivity and the repeatability of the results were verified. The measurements performed with the FBRM probe showed that this technique can be used to follow crystal granulometry in a sorbet consisting of up to 30% of ice. The effect of process parameters was then analyzed. It appears that a decrease in refrigeration temperature accelerates ice crystallization and yields slightly smaller crystals. The same effect is observed with increasing scraper speed. Additionally, when the initial sucrose concentration in the solution is increased, the ice fraction increases more slowly but the mean chord length is smaller.

SSHEs are used in the food industry to process highly viscous fluids, and ice cream in particular, but most of the time, the influence of operating conditions on product quality is poorly understood. Fayolle et al. (2013) developed simple tools to help industrials understand and then optimize their fabrication process. Residence time distribution (RTD) has been characterized in an industrial pilot system during real ice cream production, after the method had been validated in an experimental set up with a simple mixture of water and sucrose. It has been shown that in its dimensionless form, RTD depends slightly on flow rate and scraper rotational speed. A simple model of flow pattern applicable to SSHE during crystallization was developed to reproduce the observed RTD. It distinguishes two zones: the volume of fluid near the cooling wall where ice is generated and which is swept by the blades and the volume of fluid near to the rotor. Therefore, the model considers two parallel plug flow reactors with axial dispersion, and which exchange fluid by radial mixing. After adjustment of the model parameters, a good agreement was obtained with experimental results. The flow rate is lower in the zone near the cooling wall; this can be due to a higher ice concentration leading to higher viscosity. This approach can contribute to better understand, optimize, and control SSHE used for ice cream production.

SSHEs are widely used in the food industry for crystallization applications in several food processes, such as the crystallization of margarine (Shahidi, 2005), the tempering of chocolate (Dhonsi and Stapley, 2006), the freeze concentration of milk (Sanchez et al., 2011), and the freezing of sorbet or ice cream (Cook and Hartel, 2010). To a certain degree, all of these food products behave as shear-thinning fluids.

SSHEs are composed of two concentric cylinders: an external stationary cylinder, which is in contact with the refrigerant fluid and therefore represents the heat transfer surface, and an internal rotating cylinder (dasher) that is equipped with scraping blades (Harrod, 1986). The main advantage of SSHEs is the scraping action of the

blades, which continually remove the crystal build-up at the heat transfer cylinder wall, improving the heat transfer rate from the wall to the core of the exchanger.

The final quality of these food products is highly related to crystal size distribution and apparent viscosity, both of which are determined by the operating conditions of the process. During the freezing of sorbet, the increase in the ice volume fraction leads to an increase in the apparent viscosity of the product. This effect modifies the fluid flow behavior, the RTD, and the temperature profile inside the equipment. Marcela Arellano et al. (2013) aimed at studying the influence of the operating conditions on the RTD and the axial temperature profile of the product in an SSHE, so as to characterize the product flow behavior.

RTD experiments were carried out in a continuous laboratory pilot-scale SSHE by means of a colorimetric method. Experiments showed that high product flow rates led to a narrowing of the RTD and thus to less axial dispersion, due to the enhancement of the radial mixing with the decrease in the apparent viscosity of the product. Spreading of the RTD was obtained for lower refrigerant fluid temperatures, due to a higher radial temperature gradient between the wall and the center of the exchanger, leading to a higher gradient of the apparent viscosity. This effect increased the difference in axial flow velocities and thus the axial dispersion. These results can be useful for the optimization and modeling of crystallization processes in SSHEs.

6.4 NUSSELT EQUATION

A generalized form of this important equation for heat transfer across boundary films by conduction and convection can be derived using the methods of dimensional analysis. Nusselt's number (Nu) is the dimensionless temperature gradient in the surface. The Nusselt equation in terms of dimensionless groups is shown below:

$$Nu = C(Re)^{\alpha} \cdot (Gr)^{e} \cdot (Pr)^{f} \tag{6.16}$$

Nu, the Nusselt group, = (hL/k)

Re, the Reynolds group, = (Dup/μ)

ρ is the fluid density (kg/m^3), u is the average velocity of the fluid in a cross section of the tube (m/s), D is the interior tube diameter (m), and μ is the dynamic viscosity of the fluid (kg/ms).

$$\text{Gr, the Grashof group, } = (\beta g \Delta T L^3 \rho^2)/\mu^2 \tag{6.17}$$

$$\text{Pr, the Prandtl group, } = (\nu/\alpha = C_p \mu/K) \tag{6.18}$$

ν is the kinematic viscosity of the fluid (m^2/s), a is thermal diffusion of the fluid (m^2/s), Cp the heating capacity of the fluid (J/kg K), and K the thermal conductivity of the fluid (W/mK).

Notice that it is the Nusselt group that contains the film heat transfer coefficient, h.

Hence, h = NuK/D.

Note that since fluids circulate through tubes, Re and Nu are based on diameter D. If the surface was plane, they would be based on a characteristic length L.

Heat transfer research groups have separated the study into two principal areas:

1. Natural convection (where heat transfer is likely to be a very slow process)
2. Forced convection, where convective heat transfer is enhanced by mechanical means and the overall heat transfer rate is much increased

In the process industries, both areas are important, although forced convection is more common.

Experience has shown for

Natural convection, Nu = f(Gr. Pr)
Forced convection, Nu = f(Re. Pr)

The Grashof group contains β, the coefficient of cubical expansion, and g, the acceleration due to gravity, both important in influencing the slow-moving currents of hot fluid generated in natural convection. Since forced convection is very common, processing this form of heat transfer will be considered first.

For internal flow, which is the case of concentric tube heat exchanger, the following needs to be considered: whether flow is laminar or turbulent and the existence of an inlet zone that is thermal and hydrodynamically developed.

When fluids enter the tube, the limit layer increases as long as it moves forward in the tube. Once the entire cross section of the tube is occupied by the limit layer, the flow zone is totally hydrodynamically developed, where viscous effects are extended along the section and the velocity profile does not change when it goes forward in the tube.

The distance from the inlet until the zone where the flow is totally hydrodynamically developed is called hydrodynamic inlet length ($x_{fd,h}$) (Figure 6.6). To calculate this distance, we need to know whether flow is laminar or turbulent. At the beginning of turbulence in totally developed flows, critical Reynolds number is 2300, whereas at totally turbulent conditions, it is approximately 10,000.

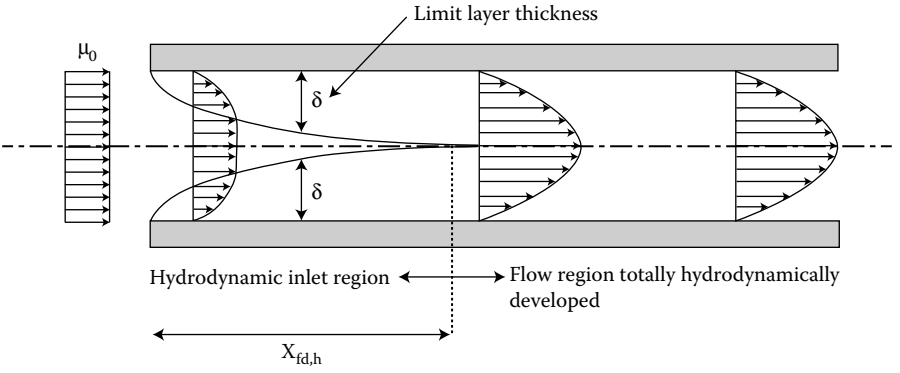


FIGURE 6.6 Formation of the distance from the inlet until the zone where the flow is totally hydrodynamically developed called hydrodynamic inlet length ($x_{fd,h}$). (Courtesy of Edibon, 2012.)

Hence, for a laminar flow, $x_{fd,h} \sim 0.05$ D Re, and for a turbulent flow, $x_{fd,h}$ varies from 10 D to 60 D.

Besides traditional atmospheric frying, high-pressure (superatmospheric) frying might be an alternative approach to the frying of food products. Erdogdu and Dejmek (2010) compared convective heat transfer coefficient during atmospheric and high-pressure frying. For this purpose, a pressure cooker was modified to allow the immersion of a sample into frying oil under pressure and temperature measurement of sample and oil. Heat transfer coefficient versus frying time was determined on potato slabs using changes of total mass of the experimental setup. At the pressure of 2 bar, the results showed an almost doubled heat transfer coefficient compared to the atmospheric pressure frying. The knowledge of heat transfer coefficient during pressure frying is expected to allow accurate determination of temperature distribution and hence the kinetic calculations to lead to the development of an alternative frying process.

6.4.1 Temperature Distribution in Concentric Tube Exchangers

The temperature distribution in a simple concentric tube heat exchanger in parallel (left) and countercurrent flow (right) can be seen in Figure 6.7.

T_{hi} is the temperature of the hot fluid at the inlet of the exchanger.
T_{ho} is the temperature of the hot fluid at the outlet of the exchanger.
T_{ci} is the temperature of the cold fluid at the inlet of the exchanger.
T_{co} is the temperature of the cold fluid at the outlet of the exchanger.

At the beginning, the heat transfer is large due to the maximum temperature difference; however, this difference falls very quickly, approaching asymptotically to zero. In concentric tube exchangers, the outlet temperature of the cold fluid never exceeds the outlet temperature of the hot fluid.

In countercurrent flow, the hot experimental zone of the hot fluid exchanges heat with the coolest zone of the hot fluid. Finally, the outlet temperature of the cool fluid cannot exceed that of the hot fluid.

A photo of a concentric tube exchanger is shown in Figure 6.8.

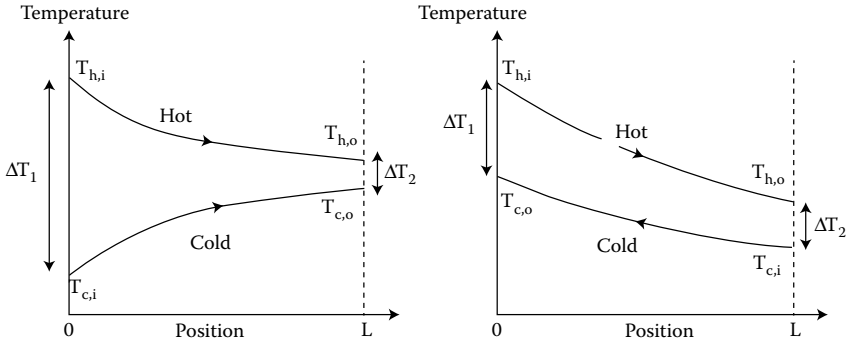


FIGURE 6.7 Temperature distribution in a simple concentric tube heat exchanger in parallel (left) and countercurrent flow (right).



FIGURE 6.8 Concentric tube heat exchanger (Supplier Edibon, Varzakas lab.)

6.4.2 Logarithmic Mean Difference

The average temperature difference is a logarithmic mean difference ΔT_{lm} as reported in Equation 6.6.

$$\text{Hence, the heat transfer rate is } q = UA\Delta T_{lm} \tag{6.19}$$

where $\Delta T_1 = T_{hi} - T_{ci}$ and $\Delta T_2 = T_{ho} - T_{co}$ for parallel flow and $\Delta T_1 = T_{hi} - T_{co}$ and $\Delta T_2 = T_{ho} - T_{ci}$ for countercurrent flow.

For the same inlet and outlet temperatures, ΔT_{lm} for countercurrent flow is higher than for parallel flow. Hence, the required area for heat transfer is lower for countercurrent flow than for parallel flow, assuming the same value of U.

6.4.3 Method Number of Transfer Units-Effectiveness for the Analysis of a Heat Exchanger

The effectiveness is defined as the quotient between the real heat exchanged and the maximum that could be transferred in an infinite area of the exchanger at countercurrent flow.

$$\varepsilon = q_{actual}/q_{max} \tag{6.20}$$

where

$$q_{actual} = C_h(T_{hi} - T_{ho}) = C_c(T_{co} - T_{ci}) \tag{6.21}$$

$$q_{max} = m_hCp_h(T_{hi} - T_{ci}) \quad \text{or} \quad C_{min}(T_{hi} - T_{ci}) \quad \text{if } m_hCp_h < m_cCp_c \tag{6.22}$$

and $q_{max} = m_cCp_c(T_{hi} - T_{ci})$ if $m_cCp_c < m_hCp_h$; hence, the effectiveness varies accordingly.

Combining the last two equations, we have

$$q_{actual} = \varepsilon C_{min}(T_{hi} - T_{ci}) \tag{6.23}$$

The number of transfer units (NTU) is a dimensionless parameter used in the analysis of heat exchangers and is defined as

$$NTU = UA/(mCp)_{min} \tag{6.24}$$

and the capacity coefficient is defined as

$$C_R = (mCp)_{min}/(mCp)_{max} \tag{6.25}$$

6.5 FORCED CONVECTION: LOWER-VISCOSITY LIQUIDS IN TURBULENT FLOW

Dittus–Boelter equations

$$Nu = Const(Re)^{\alpha}(Pr)^{f} \tag{6.26}$$

6.5.1 Flow Inside Tubes

Notice the form of the actual equation if the fluid flows inside a pipe of circular cross section as in the pipe heat exchanger:

hi = inside film heat transfer coefficient, di = diameter, k = thermal conductivity of fluid

$$hi\ di/k = .023(di\ ui\ p/\mu)^{0.8}(Cp\mu/k)^{n} \tag{6.27}$$

n = 0.4 for heating and n = 0.3 for cooling.

The change in value of the index to the Prandtl group, n, arises because of the changes in viscosity brought about by changes in the temperature profile between the mainstream and the wall.

For this inside boundary film, the characteristic linear dimension, L, di is the inside diameter of the pipe, ui is the average velocity of the fluid flowing in the pipe; physical properties are those for this fluid. All the physical properties required for use with this equation are determined at the mean bulk temperature of the fluid, that is, (Ti + To)/2, where Ti and To are the average temperatures at the inlet and outlet of the exchanger, respectively.

6.6 HEATING OR COOLING IN AN AGITATED CYLINDRICAL, JACKETED VESSEL

Stirred reactors, fermenters, and so on often take this form.

A form of Dittus–Boelter equation developed by Chilton is typical for these vessels:

$$h_i D_v/k = 0.36\ (D_a^2 N\ \rho/\mu)^{0.66}(C_p\mu/k)^{0.33} \tag{6.28}$$

where

h_i is the inside surface film heat transfer coefficient
D_v is the inside diameter of cylindrical vessel
D_α is the diameter of agitator
N is the speed of rotation of agitator
k, ρ, μ, and C are properties of the fluid as previously defined.

The similarity of these three forms of the Dittus–Boelter equation for three very different types of heat exchanger is apparent. In the case of the agitated vessel, the Reynolds group, $D\alpha^2N\rho/\mu$, appears to be different.

It is merely the form of Reynolds group used for rotational motion as opposed to that for linear flow over the heat transfer surface.

Helical coil heat exchangers are popular because of compact structure with enhanced heat transfer coefficient by passive heat transfer enhancement technique. Owing to these advantages, helical coil tube heat exchangers are widely used in various applications such as power plants, nuclear reactors, refrigeration and air-conditioning systems, heat recovery systems, chemical processing, and food industries. The analysis of the helical coil heat exchanger with different operating and geometric parameters is presented by Purandare et al. (2013). The analysis shows that both operating and geometric parameters influence heat transfer. The analysis of heat transfer coefficient and Nusselt number with respect to Reynolds number with different correlations and its significance is well discussed in this chapter. The effect of geometric parameter on the performance of helical coiled tube heat exchanger is also presented by the authors.

A photo of a coil vessel heat exchanger is shown in Figure 6.9.

To improve heat transfer performance, the following approaches have been employed. One approach is by using curved tubes to obtain the increased shear stress and heat transfer coefficients. Several materials commonly go through coiled heat exchangers. An attractive feature of a coiled exchanger is that it has a higher

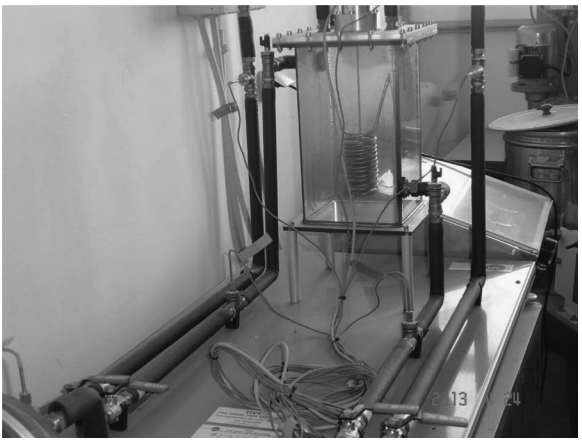


FIGURE 6.9 Coil vessel heat exchanger. (Supplier Edibon, Varzakas lab.)

heat transfer coefficient due to the stresses and wall stresses resulting from secondary flows. It occupies less space than the conventional tube and shell exchangers. However, internal cleaning could be a problem.

Another approach is to induce secondary flow through the use of suitable and appropriate cross sections, such as the square as demonstrated by Hartnett and Kostik (1985) and flattened tubes as conducted by Oliver and Karim (1971).

Scraped-wall heat exchangers have also been successfully used by Bott (2001), Chong (2001), and Tahti (2004). This scraping effect could also be achieved by rotating the exchanger. Vibrations have also been employed successfully by Song (2006, 2008). Electrostatics forces have been employed by Nassauer and Kessler (1986), and chemicals have been used by Jhaveri (2005).

Heat transfer coefficients were obtained for seven copper helical coil heat exchangers with different diameters and diameter ratios. Hot water was used as the heating medium, and dilute polyacrylamide solutions were used to simulate the food solutions. Results showed increased heat transfer coefficients but the magnitudes were lower than those obtained by previous workers (Ismail and Karim, 2012). A unified form of the Graetz–Leveque equation obtained was

$$Nu = 1.75\ Gz^{1/3}[1 + 0.5421Dn^{0.45}(d/D)^{0.54}] \tag{6.29}$$

for water.

Viscoelasticity reduces heat transfer performance.

Heat transfer characteristics for single-pipe and double-pipe helical heat exchangers have been investigated both experimentally (Kumar et al., 2006; Naphon, 2007; Rennie and Raghavan, 2005) as well as numerically (Kumar et al., 2008; Rennie and Raghavan, 2006). Curved tubes offer advantages over straight tubes for heat transfer due to the secondary flows that develop from the centrifugal forces induced by the curvature. The result is two circulating cells that transfer fluid perpendicular to the main axial direction. Fluid in the core of the tube is moved toward the outer wall and then travels back to the inner portion of the tube along the wall.

Aseptic processing of liquid foods is often performed as a continuous operation where the liquid food undergoes heating, holding, and cooling operations just prior to packaging.

Helical coils offer advantages over straight tubes for the heating, holding, and cooling sections of aseptic processing systems. Secondary flows distribute heat more evenly (Ruthven, 1971), and velocity profiles tend to be flatter than in straight tubes (Koutsky and Adler, 1964). Heat transfer in Newtonian and viscoelastic liquids during laminar flow in helical coils has been described by Oliver and Ashar (1976).

A numerical study of a double-pipe helical heat exchanger was performed by Rennie and Raghavan (2010) to ascertain the residence time, temperature, and processing uniformity for food processing applications. A range of laminar flow rates were used, with both parallel flow and counterflow configurations. Both heating and cooling in the inner tube were studied. Heating/cooling uniformity was estimated by using a first-order kinetics model for sterilization. Process uniformity is important in the quest for high-quality product and this report is a first study for the uniformity

in double-pipe helical heat exchangers. RTDs became more uniform with increased flow rates in both the inner tube and in the annulus. Temperature uniformity in the inner tube increased with increasing flow rate. However, it was shown that changing the flow rate in the annulus, for a constant flow rate in the inner tube, affected the uniformity. Similar results were found for the annulus. Heating uniformity in the inner tube tended to increase with increased flow rates. It was also shown that the cooling process was more uniform than the heating process. The findings in this study are important to the design of helical heat exchangers for the processing of liquid foods.

Malaxation has been recognized as one of the most critical points in the mechanical extraction process for virgin olive oil (VOO). It is a low and continuous kneading of olive paste at a carefully monitored temperature. Through this essential technological operation, the small droplets of the oil formed during the milling merge into large drops that can be easily separated with a decanter centrifuge. During this technological phase, a complex and necessary bioprocess takes place in order to determine the quality and composition of the final product. The malaxer is a heat exchanger characterized by a low overall heat transfer coefficient because the ratio of surface area to volume is disadvantageous, so it is important to find an innovative technology to improve heat exchange.

The malaxer was a stainless-steel container (tank volume: 4.5 L) equipped with a helical blade immersed in a water bath at 35°C (rotational speed: 10 rpm).

As matter of fact, the malaxing step is the only discontinuous phase in a continuous extraction process. In the future, the essential challenge of VOO industrial plant manufacturing sector is to design and build advanced machines to transform the discontinuous malaxing step into a continuous phase and to improve the working capacity of the industrial plants. To reduce the malaxing time and thus enhance the quality of the product, two ultrasound-assisted VOO extraction processes were tested against the traditional method (Clodoveo et al., 2013). The sonication treatment was applied on olives submerged in a water bath (before the crushing) and on olive paste (after the crushing). The ultrasound technology provides a reduction of the malaxing duration improving VOO yields and its minor compounds content. Better extractibility and higher minor compounds contents were obtained by sonicating the olives submerged in a water bath than olive paste. After experimental trials, the results were employed to suggest innovative scaling up solutions of the process and new applications of ultrasounds in the VOO industry.

6.7 SIEDER AND TATE VISCOSITY CORRECTION FACTOR

For more viscous liquids, the Dittus–Boelter equations provided earlier lead to unacceptable values for film heat transfer coefficients. This is because of the effect of temperature on fluid viscosities. Measuring the viscosity of the fluids at some mean bulk temperature is not sufficient. After a series of experiments with a variety of more viscous fluids, Sieder and Tate suggested the incorporation of a viscosity correction factor. This is given by

$$(\text{Viscosity of mainstream}/\text{Viscosity at wall})^{0.14} \tag{6.30}$$

This takes into account the difference in viscosity at the wall and at the mainstream conditions. The Dittus–Boelter equation for flow inside circular tubes with more viscous liquids then becomes

$$h_i d_i/k = 0.023(d_i u_i \rho/\mu)^{0.8}(Cp\mu/k)^{0.33}(\mu/\mu_\omega)^{0.14} \quad (6.31)$$

where Cp is specific heat.

6.8 FORCED CIRCULATION WITH STREAMLINE (LAMINAR) FLOW

Although not frequently encountered as turbulent flow in processing, with very viscous liquids, the Reynolds number may be sufficiently low for streamline flow to become established. In streamline flow, heat transfer is by conduction and considerably less research has been reported in this area of heat transfer in fluid flow systems.

6.9 LAMINAR FLOW INSIDE TUBES

Below Reynolds numbers of 10,000, the length-to-diameter ratio for the tube (D/L) has an effect on the film heat transfer coefficient, h. The parabolic velocity distribution established in tubes is influenced by changes in the value of D/L at lower Reynolds numbers and this must be provided for in design equations for film heat transfer coefficients.

For tubes, equations of the form

$$Nu = h_i D/k = 1.62(Re.\ Pr.\ D/L)^{0.33} \quad (6.32)$$

are suggested for less viscous liquids. The Sieder and Tate correction factor $(\mu/\mu_\omega)^{0.14}$ is included when predicting h, for more viscous liquids. Some authors show a slightly higher value for the constant giving

$$h_i D/k = 1.86(Re.\ Pr.\ D/L)^{0.33}(\mu/\mu_\omega)^{0.14} \quad (6.33)$$

6.10 FLOW IN TUBE BUNDLES

Lower-viscosity fluids usually pass through the shell side of tube and shell heat exchangers, and so the mode of heat transfer in tube bundles is mainly by forced convection.

Research for flow at right angles to a single tube suggests a Dittus–Boelter-type equation for outside film heat transfer coefficient, h, as

$$h_o D_o/k = 0.26(Re)^{0.6}(Pr)^{0.3} \quad (6.34)$$

for Re values in the range 1000–100,000.

For Re values below 200, a similar equation gives $h_o D_o/k = 0.86(Re)^{0.43}(Pr)^{0.3}$.

Modified forms of this type of equation include geometric factors to account for more complex "bundles" of tubes fitted with baffles. As well as supporting

the tubes, baffles are fitted to keep the shell-side flow at right angles to the tube, increase the flow velocity, and prevent short circuiting of the fluid. The equations for film heat transfer coefficients for heating and cooling (without change of state) provided earlier indicate the approach used for these values of "h" for incorporation in the equations for the overall heat transfer coefficient, U, for use in heat exchange studies. Many similar equations are available in the heat transfer literature for a variety of different heat exchanger formats as reported by Perry and Green (1997).

6.11 CASE STUDIES

1. A stainless-steel pipe (inside diameter 3 cm, wall thickness 5 mm, length 2 m) carrying a refrigerant is covered by insulating material. Thermal conductivity of steel and insulating material is 45 and 2 J/ms°C.
   a. Calculate the rate of heat transfer through the pipe wall, if the refrigerant temperature is 100°C and ambient temperature is 25°C
   b. Calculate the temperature at the interface between the steel and insulating layer.
   c. If the outside temperature of the pipe is raised to 40°C, how does the rate of heat transfer change?

   Please assume that the outside wall of the pipe is at ambient temperature, except for part c.
2. A thin-walled spherical metallic container is used to store liquid nitrogen at 70 K. The outer diameter of the vessel is 0.4 m and the wall thickness is 5 mm. If the thermal conductivity of the material is 40 J/ms°C and the outer surface of the material is at a temperature of 50 K, evaluate the heat transfer rate by conduction through the walls.

$$r1 = 0.395 \text{ m}, \qquad T1 = 70 \text{ K}$$

$$r2 = 0.4 \text{ m}, \qquad T2 = 50 \text{ K}$$

   Heat transfer rate $= 4\pi k((T1 - T2)/((1/r1) - (1/r2)) = 318$ kJ/s
3. How long will it take for the temperature at the center of a pea to rise to 60°C if a pea initially at a temperature of 20°C is blanched in hot water (100°C).

   Diameter of the pea is 1 cm, specific heat capacity = 3.3 kJ/kgK, density of pea = 950 kg/m^3, thermal conductivity = 0.3 W/mK, surface heat transfer coefficient = 500 W/m^{2}K.

   Diameter of the pea is 0.01 m

   Radius of the pea, L, is 0.005 m

   Specific heat capacity = 3300 J/kgK

$$T = (T - T_{oo})/(T_i - T_{oo}) = (60 - 100)/(20 - 100) = 0.5$$

$$1/Bi = k/h\,L = 0.3/500 \times 0.005 = 0.12$$

From the chart provided in Figure 6.10, $F_o = 0.17$; hence, $0.17 = (k/Cp)(t/L^2)$ and $t = 44.41$ s.

Which is the time taken for temperature at the center of the pea to rise to 60°C?

4. What is the temperature of a rod of material 3 min after immersion in an oil bath, if the temperature of the oil bath is 600 K and the initial temperature of the rod is 300 K. The dimensions of the rod are 60 mm length and 80 mm diameter. Density of the rod is 7900 kg/m^3, thermal conductivity is 17.4 W/mK, specific heat is 526 J/kgK, and surface heat transfer coefficient is 500 W/m^{2}K.
5. A large slab of solid material (thermal conductivity 60 W/mK, thermal diffusivity $a = 1.5 \times 10^{-5}$ m^2/s is 10 cm thick). If the material is initially at a uniform temperature of 20°C and is then suddenly exposed to a heating medium at 200°C (surface heat transfer coefficient is 600 W/m^{2}K), what is the temperature 2 mm below the surface after 5 min of heating?

Thickness required is 0.002 m.

Length, L, is 0.05 m, half the diameter.

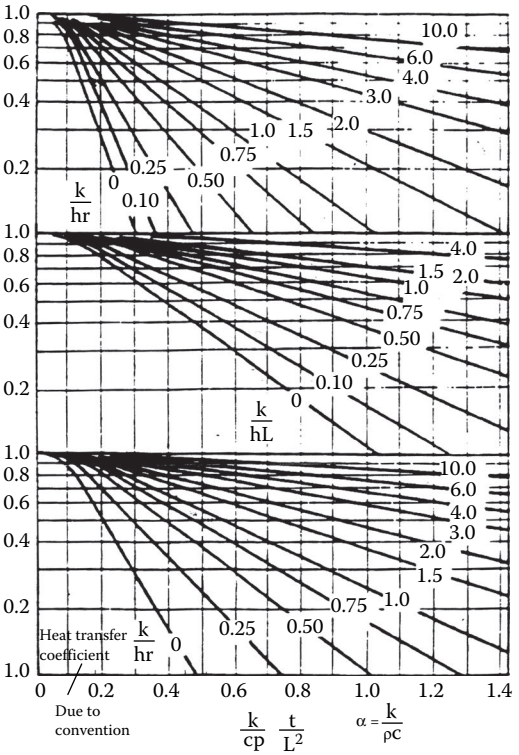


FIGURE 6.10 Heat transfer into a sphere (top), slab (middle), and cylinder (bottom). (Adapted from Henderson, S.M. and Perry, R.L. *Agricultural Process Engineering*, 1995, Copyright Wiley-VCH Verlag GmbH & Co. KGaA.)

Time is $5 \times 60 = 300$ s.

Temperature of heating medium $T_{oo} = 200°C$ and initial temperature of material is 20°C.

$$Fo = (k/Cp)\,(t/L^2) = \alpha\,(t/L^2) = 1.5 \times 10^{-5}\ 300/(0.015)^2 = 1.8.$$

$$m = k/h\ L = 60/600 \times 0.05 = 2$$

$$n = x/L = 0.048/0.05 = 0.96 \text{ approximately } 1$$

$$x = 0.05 - 0.002 = 0.048$$

$$T = (T - T_{oo})/(T_i - T_{oo}) = 0.4;\ \text{hence } (T - 200)/(20 - 200) = 0.4 \text{ and } T = 128.$$

6. In an exchanger of multiple paths, the following temperatures are provided: $T_{ca} = 70°C$, $T_{cb} = 120°C$, $T_{ha} = 240°C$, $T_{hb} = 120°C$. Which is the average fall in temperature in this exchanger?

   F_G factor can be determined by looking at Figure 6.2 and the equations described in that section.

   Hence, $n_H = (120 - 70)/(240 - 70) = 0.294, Z = (240 - 120)/(120 - 70) = 2.4$

   According to these values, F_G is 0.82.

   The fall in temperature at the entrance of the shell is $\Delta T = 240 - 120 = 120°C$.

   At the exit of the shell, $\Delta T = 120 - 70 = 50°C$.

   Hence, $\Delta T_L = (120 - 50)/\ln(120/50) = 80°C$.

   The average fall in temperature is $0.82 \times 80 = 66°C$.

REFERENCES

Alvarez, N., Daufin, G., and Gesan-Guiziou, G. 2010. Recommendations for rationalizing cleaning-in-place in the dairy industry: Case study of an ultra-high temperature heat exchanger. *Journal of Dairy Science*, 93: 808–821.

Amamou, A. H., Benkhelifa, H., Alvarez, G., and Flick, D. 2010. Study of crystal size evolution by focused-beam reflectance measurement during the freezing of sucrose/water solutions in a scraped-surface heat exchanger. *Process Biochemistry*, 45: 1821–1825.

Anantheswaran, R. C. and Rao, M. A. 1985a. Heat transfer to model Newtonian liquid foods in cans during end-over-end rotation. *Journal of Food Engineering*, 4(1): 1–19.

Anantheswaran, R. C. and Rao, M. A. 1985b. Heat transfer to model non-Newtonian liquid foods in cans during end-over-end rotation. *Journal of Food Engineering*, 4(1): 21–35.

APV Corporation. 2000. *Heat Transfer Handbook*, Goldsboro, NC.

Attia, J. A., McKinley, I. M., Moreno-Magana, D., and Pilon, L. 2012. Convective heat transfer in foams under laminar flow in pipes and tube bundles. *International Journal of Heat and Mass Transfer*, 55: 7823–7831.

Baccar, M. and Abid, M. S. 1997. Numerical analysis of three dimensional flow and thermal behavior. *Revue Générale de Thermique*, 36: 782–790.

Baccar, M. and Abid, M.S. 1999. Numerical simulations of hydrodynamic and thermal behaviours in a scraped surface heat exchanger operating in turbulent regime. (Simulation numérique des comportements hydrodynamiques et thermiques des échangeurs racleurs opérant en regime turbulent). *International Journal of Thermal Sciences*, 38(7): 634–644.

Bansal, B. and Chen, X. D. 2006. A critical review of milk fouling in heat exchangers. *Comprehensive Reviews in Food Science and Food Safety*, 5(2): 27–33.

Barish, J. A. and Goddard, J. M. 2013. Anti-fouling surface modified stainless steel for food processing. *Food and Bioproducts Processing*, 91(4): 352–361.

Berry, M. R. and Dickerson, R. W. 1981. Heating characteristics of whole kernel corn processed in a steritort. *Journal of Food Science*, 46(2): 889–895.

Blanpain, P. and Lalande, M. 1997. Investigation of fouling mechanisms governing permeate flux in the crossflow microfiltration of beer. *Filtration & Separation*, 34(10): 1065–1069.

Bobbili, P.R. and Sunden, B. 2009, Pressure drop in multi-parallel channels of corrugated plate steam condensers. *Heat Transfer Engineering*, 30(13): 1024–1032.

Bongers, P. M. M. 2006. A heat transfer model of a scraped surface heat exchanger for ice cream. 16th European Symposium on Computer Aided Process Engineering and 9th International Symposium on Process Systems Engineering, 539–544.

Bott, T. R. 2001. To foul or not to foul. Chemical Engineering Progress Magazine, 30–37. http://people.clarkson.edu/~wwilcox/Design/hxfoul.pdf

Bougriou, C. and Baadache, K. 2010. Shell-and-double concentric-tube heat exchangers. *Heat and Mass Transfer*, 46: 315–322.

Brennan, J. G., Butters, J. R., Cowell, N. D., and Lilly, A. E. 1990. Food engineering operations.

Butterworth, D. 2002. Design of shell-and-tube heat exchangers when the fouling depends on local temperature and velocity. *Applied Thermal Engineering*, 22(7): 789–801.

Changani, S. D., Belmar-Beiny, M. T., and Fryer, P. J. 1997. Engineering and chemical factors associated with fouling and cleaning in milk processing. *Experimental Thermal and Fluid Science*, 14(4): 392–406.

Chen, X. D., Li, D. X. Y., Lin, S. X. Q., and Özkan, N. 2004. On-line fouling/cleaning detection by measuring electric resistance-equipment development and application to milk fouling detection and chemical cleaning monitoring. *Journal of Food Engineering*, 61(2): 181–189.

Choi, W., Jun, S., Nguyen, L. T., Rungraeng, N., Yi, H., Balasubramanian, S., Puri, V. M., and Lee, J. 2013. 3-D milk fouling modeling of plate heat exchangers with different surface finishes using computational fluid dynamics codes. *Journal of Food Process Engineering*, 36(4): 439–449.

Chong, A. 2001. A study of scraped-surface heat exchanger in ice-making applications. MSc. Thesis, University of Toronto.

Clifcorn, L. E., Peterson, G. T., Boyd, J. M., and O'Neil, J. H. 1950. A new principle for agitating in processing of canned foods. *Food Technology*, 4: 450–460.

Clodoveo, M. L., Durante, V., and La Notte, D. 2013. Working towards the development of innovative ultrasound equipment for the extraction of virgin olive oil. *Ultrasonics Sonochemistry*, 20: 1261–1270.

Cook, K. L. K. and Hartel, R. W. 2010. Mechanisms of ice crystallization in ice cream production. *Comprehensive Reviews in Food Science and Food Safety*, 9(2): 213–222.

Coulson, J. M. and Richardson, J. F. (with the collaboration of Buckhurst, J. R., and Harker, J. H.) 1978. *Chemical Engineering Vol. 1, Unit Operations*, Pergamon Press, Oxford, UK.

Cronin, K., Caro-Corrales, J., and Gao, X. 2010. Heat transfer analysis of cheese cooling incorporating uncertainty in temperature measurement locations: Model development and validation. *Journal of Food Engineering*, 99: 175–183.

Czekaj, P., López, F., and Güell, C. 2000. Membrane fouling during microfiltration of fermented beverages. *Journal of Membrane Science*, 166(2): 199–212.

D'Addio, L., Carotenuto, C., Di Natale, F., and Nigro, R. 2012. A new arrangement of blades in scraped surface heat exchangers for food pastes. *Journal of Food Engineering*, 108: 143–149.

D'Addio, L., Carotenuto, C., Di Natale, F., and Nigro, R. 2013. Heating and cooling of hazelnut paste in alternate blades scraped surface heat exchangers. *Journal of Food Engineering*, 115: 182–189.

De Bonis, M. V. and Ruocco, G. 2009. Conjugate fluid flow and kinetics modeling for heat exchanger fouling simulation. *International Journal of Thermal Sciences*, 48: 2006–2012.

De Goede, R. and De Jong, E. J. 1993. Heat transfer properties of a scraped-surface heat exchanger in the turbulent flow regime. *Chemical Engineering Science*, 48: 1393–1404.

De Jong, P. 1997. Impact and control of fouling in milk processing. *Trends in Food Science and Technology*, 8: 401–405.

Deshvannar, U. B., Rafeen, M. S., Ramasamy, M., and Subbaro, D. 2010. Crude oil fouling—A review. *Journal of Applied Science*, 10: 3167–3174.

Dhonsi, D. and Stapley, A. G. F. 2006. The effect of shear rate, temperature, sugar and emulsifier on the tempering of cocoa butter. *Journal of Food Engineering*, 77(4): 936–942.

Dović, D., Palm, B., and Švaić, S. 2009. Generalized correlations for predicting heat transfer and pressure drop in plate heat exchanger channels of arbitrary geometry. *International Journal of Heat and Mass Transfer*, 52(19–20): 4553–4563.

Dumont, E. and Fayolle, F. 2000. Electrodiffusional wall shear rate analysis in scraped surface heat exchanger. *AIChE Journal*, 46: 1138–1148.

Dumont, E., Fayolle, F., and Legrand, J. 2000. Flow regimes and wall shear rates determination within a scraped surface heat exchanger. *Journal of Food Engineering*, 45: 195–207.

Dwivedi, M. and Ramaswamy, H. S. 2010a. An empirical methodology for evaluating the fluid to particle heat transfer coefficient in bi-axially rotating cans using liquid temperature data. *Food and Bioprocess Technology*, 3: 716–731.

Dwivedi, M. and Ramaswamy, H. S. 2010b. Comparison of heat transfer rates during thermal processing under end-over-end and axial modes of rotation. *LWT—Food Science and Technology,* 43: 350–360.

Earle, R. L. 1983. *Unit Operations in Food Processing*, Second edition. Pergamon Press, Oxford, UK.

EDIBON International, C/ Del Agua, 14. Polígono San José de Valderas. Leganés 28918. Madrid. Spain, Technical teaching equipment. 2012. http://www.edibon.com/products/?area=thermodynamicsthermotechnics&subarea=heatexchange, Supplier notes on heat exchangers.

Erdogdu, F. and Dejmek, P. 2010. Determination of heat transfer coefficient during high pressure frying of potatoes. *Journal of Food Engineering*, 96: 528–532.

Fayolle, F., Belhamri, R., and Flick, D. 2013. Residence time distribution measurements and simulation of the flow pattern in a scraped surface heat exchanger during crystallisation of ice cream. *Journal of Food Engineering,* 116: 390–397.

Fikiin, A. G. 1992. New method and fluidized water system for intensive chilling and freezing of fish. *Food Control*, 3(3): 153–160.

Fikiin, K. A. 2008. Emerging and novel freezing processes. In: Evans, J. A. (ed.), *Frozen Food Science and Technology*, Blackwell Publishing Ltd., Oxford, UK.

Fikiin, K. A. and Fikiin, A. G. 1998. Individual quick freezing of foods by hydrofluidisation and pumpable ice slurries. In Advances in refrigeration systems, food Technologies and the cold chain. In: Fikiin, K. (ed.), *Proceedings of IIR Conference, Sofia, Bulgaria. Refrigeration Science and Technology, International Institute of Refrigeration*. Also published in *AIRAH Journal* 2001, 55 (11): 15–18.

Fryer, P. 1992. *Heat Transfer in Food Products*. *Chemical Engineering for the Food Industry*, University of Cambridge, Program for the Industry, Department of Chemical Engineering, 7–11 September, Cambridge, UK.

Fryer, P. J. and Asteriadou, K. 2009. Aprototype cleaning map: A classification of industrial cleaning processes. *Trends in Food Science & Technology*, 20(6–7): 255–262.

Georgiadis, M. C. and Macchietto, S. 2000. Dynamic modeling and simulation of plate heat exchangers under milk fouling. *Chemical Engineering Science*, 55: 1605–1619.

Georgiadis, M. C. Rotstein, G. E., and Macchietto, S. 1998. Optimal design and operation of heat exchangers under milk fouling. *AIChE Journal*, 44: 2099–2111.

Gillham, C. R., Fryer, P. J., Hasting, A. P. M., and Wilson, D. I. 2000. Enhanced cleaning of whey protein soils using pulsed flows. *Journal of Food Engineering* 46: 199–209.

Grijspeerdt, K., Mortier, L., De Block, J., and Van Renterghem, R. 2004. Applications of modeling to optimize ultra high temperature milk heat exchangers with respect to fouling. *Food Control*, 15: 117–130.

Harriott, P. 1959. Heat transfer in scraped-surface exchangers. *Chemical Engineering Progress Symposium Series*, 54: 137–139.

Harrod, M. 1986. Scraped surface heat exchangers—a literature survey of flow patterns, mixing effects, residence time distribution, heat transfer and power requirements. *Journal of Food Process Engineering*, 9: 1–62.

Hartnett, J. P. and Kostik, M. 1985. Heat transfer to a viscoelastic fluid in laminar flow through a rectangular channel. *International Journal of Heat and Mass Transfer*, 28(6): 1147–1155.

Hayhurst, A. 1992. *Introduction to Heat Transfer*, Chemical engineering for the food industry. University of Cambridge, program for the industry, Dept. of Chemical Engineering, 7–11 September, Cambridge, UK.

Henderson, S.M. and Perry, R.L. 1955. *Agricultural Process Engineering*, Wiley, New York.

Incropera, F. P., DeWitt, D. P., Bergman, T. L., and Lavine, A. S. 2007. *Fundamentals of Heat and Mass Transfer*, 6th ed. John Wiley and Sons, Inc., New York.

Ismail, Z. and Karim, R. 2012. Consolidation of heat transfer coefficients of viscoelastic simulated food solutions in helical exchangers. *Journal of Food Engineering,* 108: 122–127.

Jhaveri, Y. 2005. Chemical cleaning of finned coils. *Air Conditioning & Refrigeration Journal*, (ISHRAE Jnl II: Oct–Dec Issue).

Jun, S. and Puri, V. M. 2006. A 2D dynamic model for fouling performance of plate heat exchangers. *Journal of Food Engineering*, 75: 364–374.

Jun, S., Puri, V. M., and Roberts, R. F. 2004. A dynamic 2D model for thermal performance of plate heat exchangers. *Transactions of ASAE*, 47: 213–222.

Kechichian, V., Crivellari, G. P., Gut, J. A.W., and Tadini, C. C. 2012. Modeling of continuous thermal processing of a non-Newtonian liquid food under diffusive laminar flow in a tubular system. *International Journal of Heat and Mass Transfer,* 55: 5783–5792.

Khan, T. S., Khan, M. S., Chyu, M-C., and Ayub, Z. H. 2010, Experimental investigation of single phase convective heat transfer coefficient in a corrugated plate heat exchanger for multiple plate configurations. *Applied Thermal Engineering,* 30(8–9): 1058–1065.

Kızıltas, S., Erdogdu, F., and Palazoglu, T. K. 2010. Simulation of heat transfer for solid–liquid food mixtures in cans and model validation under pasteurization conditions. *Journal of Food Engineering*, 97: 449–456.

Koutsky, J. A. and Adler, R. L. Minimization of axial dispersion by use of secondary flow in helical tubes. *Canadian Journal of Chemical Engineering*, 42(1964): 239–245.

Kumar, V., Faizee, B., Mridha, M., and Nigam, K. D. P. 2008. Numerical studies of a tube-intube helically coiled heat exchanger. *Chemical Engineering and Processing*, 47: 2287–2295.

Kumar, V., Saini, S., Sharma, M., and Nigam, K. D. P. 2006. Pressure drop and heat transfer study in tube-in-tube helical heat exchanger. *Chemical Engineering Science*, 61: 4403–4416.

Laine, J. M., Campos, C., Baudin, I., and Janex, M. L. 2003. Understanding membrane fouling: A review of over a decade of research. *Water Supply*, 3(5–6): 155–164.

Lewis, M. J. 1987. *Physical Properties of Foods and Food Processing Systems*, Ellis Horwood, UK.

Lian, G., Moore, S., and Heeney, L. Population balance and computational fluid dynamics modelling of ice crystallisation in a scraped surface freezer. *Chemical Engineering Science*, 2006: 61:7819–7826.

Mahdi, Y., Mouheb, A., and Oufer, L. 2009. A dynamic model for milk fouling in a plate heat exchanger. *Applied Mathematical Modelling*, 33: 648–662.

Marcela Arellano, H., Benkhelifa, G. Alvarez, and Flick, D. 2013. Experimental study and modelling of the residence time distribution in a scraped surface heat exchanger during sorbet freezing. *Journal of Food Engineering*, 117: 14–25.

McCabe, W. L., Smith, J. C., and Harriott, P. 2008. *Unit Operations of Chemical Engineering*, 6th ed. McGraw-Hill, New York.

Merson, R. L., Leonard, S. J., Mejia, E., and Heil, J. 1980. Temperature distributions and liquid-side heat transfer coefficients in model liquid foods in cans undergoing flame sterilization heating. *Journal of Food Process Engineering*, 4(2): 85–98.

Müller-Steinhagen, H., Hartnett, J. P., Irvine, T. F., Jr., Cho, Y. I., and Greene, G. A. 1999. Cooling-water fouling in heat exchangers (pp. 415–496) In: Hartnett, J., Irvine, T., Cho, Y., and Greene, G. Series Editors. *Advances in Heat Transfer*, Vol. 33, Academic Press, USA.

Naphon, P. Thermal performance and pressure drop of the helical-coil heat exchangers with and without crimped fins. *International Communications in Heat and Mass Transfer*, 34(2007): 321–330.

Nassauer, J. and Kessler, H. G. 1986. The effect of electrostatic phenomena on the cleaning of surfaces. *Chemical Engineering and Processing*, 20(1): 43–52.

Nema, P. K. and Datta, A. K. 2006. Improved milk fouling simulation in helical triple tube heat exchanger. *International Journal of Heat and Mass Transfer*, 49: 3360–3370.

Oliver, D. R. and Ashar, S. M. 1976. Heat transfer in Newtonian and viscoelastic liquids during laminar flow in helical coils. T.I. *Chemical Engineering*, 54: 218–224.

Oliver D. R. and Karim, R. B. 1971. Laminar-flow non-newtonian heat transfer in flattened tubes. *The Canadian Journal of Chemical Engineering*, 49(2): 236–240.

Ozden, H. O. and Puri, V. M. 2010. Computational analysis of fouling by low energy surfaces. *Journal of Food Engineering*, 99: 250–256.

Peralta, J. M., Rubiolo, A. C., and Zorrilla, S. E. 2010. Mathematical modeling of the heat transfer and flow field of liquid refrigerants in a hydrofluidization system with a stationary sphere. *Journal of Food Engineering*, 99: 303–313.

Perez, L., Ladevie, B., Tochon, P., and Batsale, J. C. 2009. A new transient thermal fouling probe for cross flow tubular heat exchangers. *International Journal of Heat and Mass Transfer*, 52(1–2): 407–414.

Perry, R. H. and Green, D. W. (eds.) 1997. *Perry's Chemical Engineers' Handbook*, 7th edition, McGraw-Hill, New York, p. 11–4ff, 11–9.

Purandare, P. S., Lele, M. M., and Gupta, R. 2013. Effect of geometric and operating parameters on performance of helicalcoiled tube heat exchanger. *International Review of Mechanical Engineering*, 7(1): 105–109.

Quast, D. C. and Sioza, Y. Y. 1974. Heat transfer rates during heating of axially rotating cans. *Proceedings of the IV International Congress of Food Science and Technology*, 4: 458–468.

Rennie, T. J. and Raghavan, V. G. S. 2010. Numerical analysis of the lethality and processing uniformity in a double-pipe helical heat exchanger. *Chemical Engineering and Processing*, 49: 672–679.

Rennie, T. J. and Raghavan, G. S. V. 2005. Experimental studies of a double-pipe helical heat exchanger. *Experimental Thermal and Fluid Science*, 29: 919–924.

Rennie, T. J. and Raghavan, G. S. V. 2006. Numerical studies of a double-pipe helical heat exchanger. *Applied Thermal Engineering*, 26: 1266–1273.

Reynolds, T. D. 1986. *Unit Operations and Processes in Environmental Engineering*, Texas University.

Riverol, C. and Napolitano, V. 2005. Estimation of fouling in a plate heat exchanger through the application of neural networks. *Journal of Chemical Technology & Biotechnology*, 80(5): 594–600.

Ruthven, D. M. 1971. The residence time distribution for ideal laminar flow in a helical tube. *Chemical Engineering Science*, 26: 1113–1121.

Sablani, S. S. and Ramaswamy, H. S. 1996. Particle heat transfer coefficients under various retort operating conditions with endover-end rotation. *Journal of Food Process Engineering*, 19(4): 403–424. doi:10.1111/j.1745-4530.1996.tb00402.x.

Sahoo, P. K., Ansari, I. A., and Datta, A. K. 2005. Milk fouling simulation in helical triple tube heat exchanger. *Journal of Food Engineering*, 69: 235–244.

Sanchez, J., Hernandez, E., Auleda, J. M., and Raventos, M. 2011. Review: Freeze concentration technology applied to dairy products. *Food Science and Technology International*, 17(1): 5–13.

Schwartzberg, H. G. and Liu, Yc. Ice crystal growth on chilled scraped surfaces. In: Summer National Meeting, Paper No. 2 g. American Institution of Chemical Engineers; 1990.

Schweitzer, P. A. (ed.) 1979. *Handbook of Separation Techniques for Chemical Engineers*, McGraw-Hill, New York.

Shahidi, F. 2005. *Edible Oil and Fat Products: Processing Technologies*, Wiley-Interscience, John Wiley & Sons, Inc, New Jersey, USA, and Canada.

Song, L. 2006. Mitigation of in-tube fouling in heat exchangers using controlled mechanical vibration. Free Patent on Line, Patent Application: 20070267176.

Song, L. 2008. Vibration actuation system with independent control of frequency and amplitude. Free Patent on Line, Patent Application: 20100193159.

Soule, C. L. and Merson, R. L. 1985. Heat transfer coefficient to Newtonian fluids in axially rotating cans. *Journal Food Process Engineering*, 8: 33–46.

Sun, K. H., Pyle, D. L., Fitt, A. D., Please, C. P., Baines, M. J., and Hall-Taylor, N. 2004. Numerical study of 2D heat transfer in a scraped surface heat exchanger. *Computers & Fluids*, 33: 869–880.

Sutton, R. and Bracey, J. 1996. The blast factor. *Dairy Industries International*, 61(2): 31–33.

Tahti, T. 2004. Suspension melt crystallization in tubular and scraped surface heat exchangers. PhD Thesis, Martin-Luther-Universitat.

Tovazhnyansky, L., Kapustenko, P., Perevertaylenko, O. Y., Arsenyeva, O. P., and Khavin, G. L. 2010. The New Corrugation Pattern for Low Pressure Plate Condensers Chemical Engineering Transactions 21: 223–228, DOI: 10.3303/CET1021038 Editor J. J. Klemeš, H. L. Lam, P. S. Varbanov, http://www.aidic.it/cet/10/21/038.pdf.

van Asselt, A. J., Vissers, M. M. M., Smit, F., and De Jong, P. 2005. In-line control of fouling. *Proceedings of Heat Exchanger Fouling and Cleaning—Challenges and Opportunities*, Kloster Irsee, Germany.

Visser, H. and Jeurnink, T. J. M. 1997. General aspects of fouling and cleaning. *Bulletin of IDF*, 328: 5–6.

Visser, J. and Jeurnink, T. J. M. 1997. Fouling of heat exchangers in the dairy industry. *Experimental Thermal and Fluid Science*, 14(4): 407–424.

Wallhäußer, E., Hussein, M. A., and Becker, T. 2012. Detection methods of fouling in heat exchangers in the food industry. *Food Control*, 27: 1–10.

Yataghene, M., Fayolle, F., and Legrand, J. 2009. Experimental and numerical analysis of heat transfer including viscous dissipation in a scraped surface heat exchanger. *Chemical Engineering and Processing*, 48: 1445–1456.

Yataghene, M., Pruvost, J., Fayolle, F., and Legrand, J. 2008. CFD analysis of the flow pattern and local shear rate in a scraped surface heat exchanger. *Chemical Engineering and Processing*, 47: 1550–1561.

7 Rheology in Use
A Practical Guide

Niall W.G. Young

CONTENTS

7.1 Introduction 179
7.2 What Is Rheology? 180
7.3 Empirical versus Scientific 181
7.4 Viscosity 183
7.5 Measuring Geometries 184
7.6 Factors Affecting Viscosity Values 185
7.7 Flow Equations 189
7.8 Yield Stress 193
7.9 Dynamic (Small Deformation Oscillatory) Measurements 196
7.10 Accessing and Grasping the Moduli 197
7.11 Viscoelastic States of Matter 200
7.12 Case Studies 203
7.13 Fruit Gummy Filling 203
7.14 Fat Blend Crystallization 206
7.15 Fruit Spreads 209
7.16 Conclusions 213
References 214

7.1 INTRODUCTION

Much has been written on this daunting subject, and various methods have been employed in presenting the fundamentals of rheology to audiences and students, where practitioners tend to approach the subject from a technical, mathematical basis. This chapter will deal with rheology from a practical standpoint and offer the reader a guided tour through rheology's use in real food application systems; by first taking a look at the basic theory and following with case studies. While always remembering and accounting for necessary scientific rigor, within food science it is not always possible to wait for steady state or to ensure that the sample is "clean" ahead of measurement. Active food rheology tolerates these vagaries and therefore represents a useful innovation driver within research and development. Indeed, the role of the application rheologist is to create value by transforming data into understanding and by being aware of the tenet that for many industries, "rheology is not a key business, but is key to the business" (Young, 2011).

7.2 WHAT IS RHEOLOGY?

A relatively new science, rheology has developed greatly from its classical roots where Heraclitus is credited as uttering, παντα ρει, everything flows, to the 1920s when Bingham coined the word and outlined it formally as the study of deformation and flow of materials. Today, potential students or users are "frightened" by the mathematical and mechanical implications the subject holds and although true, rheology holds much more to the user who approaches it openly and with practical application in mind. When viewed from this perspective, with a "What's in it for me?" approach one finds that rheology is basically all encompassing. It is rooted just as much in life as it is in the mathematical sciences and one is served well by remembering that time and temperature are key players in being able to interpret rheology's offerings. Rooted in life, one can define oneselves as highly tuned walking rheometers full of a wide-ranging library of results that we call experience. We perform rheological experiments everyday while cleaning ourselves, eating, and many more such activities, each time matching the result we receive with the perception we had the last time we carried out the measurement. One example is shampoo (Young, 2011). Why is shampoo always viscous? It is certainly not because viscous shampoo cleans hair better than runny shampoo. Shampoo is viscous because it conforms to the correct rheological perception we have of the material, namely that it should be thick and substantial while still be sufficiently fluid and homogeneous such that we find it pleasant to use. Already here we are using rheology to make qualified judgments about products and materials around us.

Carrying that principle further into more scientific disciplines we could be prompted to ask about the aim of what we are doing with our given material: Why perform the measurement? What is its purpose? Are there any special considerations to be aware of? (This could be effects of pH changes, temperature, time, etc.) How will the information be used, and how should it be communicated? Can the outcome of the experiment be predicted?

To answer the first of these questions, the measurement may be performed because of the need to understand or describe a process such as gelling, pumping, extruding, filling, or indeed be related to properties such as pouring, spreading, and mouth feel. The results of this measurement will provide data which will allow access to the material properties and on how they change subject to the conditions of the experiment. It is still not possible to see the molecules in action but in essence what one is looking at and interpreting is the action and movement of molecules. Pictured coyly, rheology can be thought of as being an extremely large, delicate, powerful, and perhaps translucent molecular magnifying glass allowing glimpses of the behavior of the material's structural components without actually seeing them.

Consideration then has to be given to the communication of the results. The same results are likely to be communicated very differently depending on who should receive them and to what purpose they are being used. The art of the rheologist is to be able to disseminate their results such that not only the essence but also the knowledge and the understanding are conveyed. Only by securing this ethos does the whole impact of the results come forth and therefore be capable of generating value.

Finally, being able to predict what the outcome of a given experiment represents is a useful piece of experience. It allows the rheologist to monitor the experiment underway and ascertain whether it is proceeding as planned. It also allows confirmation that the measurement chosen is correct and that no untoward occurrences have taken place. If one's predicted result does not conform to the measured results then basically one of two things is wrong: (1) the theory behind the experiment is faulty, or more commonly (2) the experimental set up is wrong. Being able to establish quickly whether the measurement is proceeding as predicted saves not only time and effort but builds fingertip experience which is the life blood of the applicational rheologist.

7.3 EMPIRICAL VERSUS SCIENTIFIC

Before beginning to describe viscosity it would be useful to dwell a little on some of the different methods used to measure rheological parameters, typically viscosity, and also the viscoelastic entities. Basically, two types of method are routinely used, some being more maligned than others, but if the conditions of use are followed and erroneous extrapolations avoided, then each method is acceptable and useful. One simply has to be aware of the limits. The two methods are often referred to as; empirical and scientific.

Empirical methods are typically used to measure viscosity and tend to be simple in mode of operation and style. They tend to measure flow as a function of time, that is, how much material has passed through a given contraction in a given set of seconds. Therefore, the shear rate experienced by the material is governed by the material itself. This should be understood such that more viscous materials will experience a lower shear rate than less viscous material passing through the same system. The only way to change the shear rate is to change the temperature or exit diameter, but control over the shear rate is not within the experimenter's domain. Examples of standard empirical methods include the Ford Cup (Figure 7.1), Bostwick

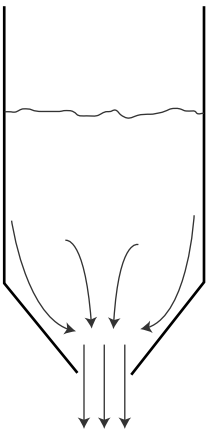


FIGURE 7.1 Schematic representation of a Ford Cup.

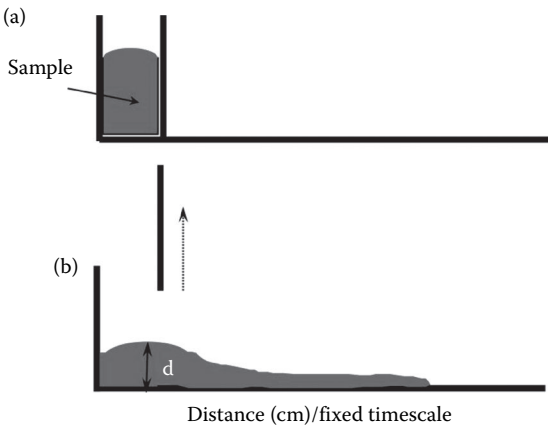


FIGURE 7.2 Schematic representation of Bostwick Consistometer, (a) loaded sample ready to run and (b) sample under measurement.

Consistometer (Figure 7.2), and the Din Cup, although many more exist and can be easily constructed to suit a range of applications.

The criteria for the Ford Cup is that the measurement value is seconds/fixed volume and here, over and above temperature, the viscosity is dependent on elasticity, stickiness, and the size of the drain hole.

Figure 7.2 shows a similar schematic representation of the Bostwick Consistometer, where again apart from temperature the viscosity is dependent on the yield stress and elasticity. Also, the shear rate that could be expected can be approximately calculated by velocity (m/s)/distance (m).

Other examples can also include the capillary viscometers otherwise known by their trade names; Ubbelohde and Ostwald which provide extremely accurate data for low viscous dilute solutions. They are routinely used to access molecular weight data from hydrocolloid solutions but need to be kept scrupulously clean and have the surrounding temperature rigorously controlled, usually to ±0.01°C.

In between the empirical and scientific methods lie the semiempirical and this is best characterized by the traditional Brookfield-type viscometer, which can operate with a T-spindle running in a helipath-type motion, if the sample is a gel. This means the spindle moves gradually down into the sample, always contacting new sample as it moves. Otherwise, traditional bob-like geometries can be used along with discs depending on the nature of the material. For the bob and disc geometries the operating field is typically what is known as an "infinite sea," in other words the measuring geometry does not "see" the walls of the sample container. There are no wall effects. In the case of Brookfield viscometers the experimenter can control the speed with which the measuring geometry rotates, but not the shear rate—that is still under the control of the sample. Thus, for quality control where a sample of the same viscosity is measured again and again this is fine, but for research purposes where samples of different viscosity are normal potential error can arise if conclusions are drawn from Brookfield-type measurements alone.

Finally, the domain of the scientific instruments is that of the controlled stress rheometers, or absolute rheometers. When using a rheometer it is the experimenter who is in full control, being able to choose which shear rate to operate at irrespective of the material. Also, given the same experimental conditions, results from one instrument should be the same as those gained from another. Therefore, rheometers are the pride of the research labs.

7.4 VISCOSITY

Viscosity, perhaps the most common and popular rheology parameter is the resistance of a material to flow. In other words, the more resistance to flow the material exerts, the more viscous the material. However, viscosity is not something that can be measured—it is rather calculated. When performing a viscosity "measurement" one controls either the stress, and measures the resulting strain, or vice versa. Figure 7.3 gives a typical box diagram indicating how viscosity is calculated.

Figure 7.3 shows a fictive box, in solid lines in which the bottom rests on a stationary plate. The top of the box is in contact with an upper surface which is allowed to move, usually by rotation, and separated by a defined gap, given here as (d). When the top surface moves it applies a force (F) to the material, spread out over a surface of area (A). The speed at which the force is applied or the velocity is given by (μ). These are all the parameters required to calculate viscosity as shown by the aid of three simple equations.

$$\sigma = \frac{F}{A} \tag{7.1}$$

where σ is stress, F is force, and A is the area.

$$\dot{\gamma} = \frac{\mu}{d} \tag{7.2}$$

where $\dot{\gamma}$ is shear rate, μ is velocity, and d is the gap. This then allows calculation of the viscosity according to the expression in Equation 7.3.

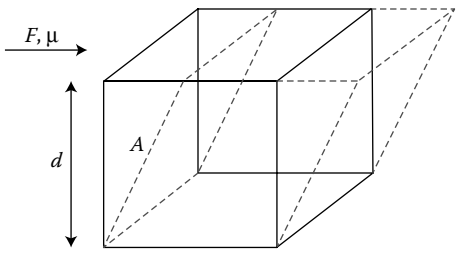


FIGURE 7.3 Box diagram showing the theory behind viscosity calculation.

$$\eta = \frac{\sigma}{\dot{\gamma}} \tag{7.3}$$

where η is viscosity, σ is stress, and $\dot{\gamma}$ is shear rate.

The units for these terms are as follows: stress is given in Pascal (Pa), shear rate in reciprocal seconds (s^{-1}), and viscosity in Pascal seconds (Pa.s). An older unit for viscosity is also still routinely used, Poise (P); although this is more commonly expressed as centipoise (cP). The relationship between Poise and Pascal seconds is governed by a factor of 10 such that 10 Poise is equivalent to 1 Pascal second, and this fits with 1 centipoise is equivalent to 1 millipascal second—this is the viscosity of water at ambient temperature. Similar and often more rigorous mathematical explanations of the above are available from other authors (Barnes, 2000; Rao, 2007; Zhong and Daubert, 2007; Miri, 2011).

7.5 MEASURING GEOMETRIES

The main measuring geometries used in rotational rheometers are the concentric cylinders, or cup and bob, cone and plate, and plate and plate (Figure 7.4). There are of course many others, including variations on these already mentioned.

However, the cup/bob and the cone/plate represent two mathematically defined and proven geometry systems. As such, they will give absolute answers as opposed to the average apparent values stemming from other measurement geometries with incomplete mathematical understanding behind them. In order to run with these two geometry systems properly the conditions of the narrow gap must be satisfied, and this related to the assumption that the calculations of the shear rate and the shear stress result in a linear speed gradient. This is not the case and therefore under large gap conditions the difference can be marked. The smaller the gap, the less the deviation from linear, as outlined in Figure 7.5.

It is this gap relationship which is responsible for one of rheology's rules of thumb, any gap should be 10 times larger than the maximum particle size. Failure to adhere

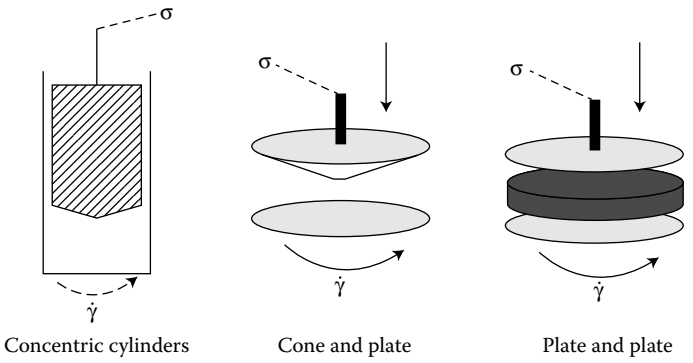


FIGURE 7.4 Schematic diagrams of the three main measuring geometries for rotational rheometers.

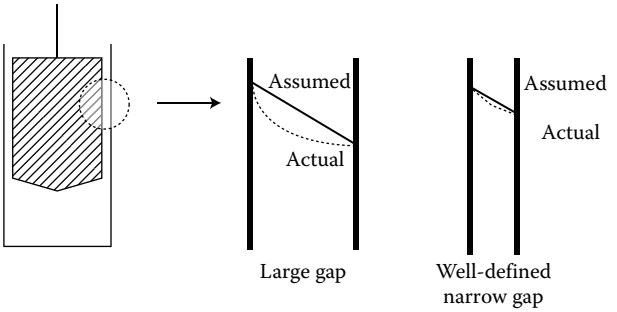


FIGURE 7.5 Giving the approximation of the speed gradient between shear rate and shear stress as a function of large and small gaps.

to this rule may result in error due to the particles potentially blocking the gap, causing a build up, and then rupturing at higher stresses. This will give an unexpected kink or deviation in the normal curve profile.

For the cone/plate, the tip of the cone is truncated and this "missing" part is the gap, thus the gap in cone/plate geometries can be very small, which similarly places demands of the type of samples able to be run. Basically, they must be homogenous solution like in nature; any hint of significant particulate material and the cone/plate geometry will be invalid. Should this be the case, choice of the plate/plate system may be made. Unlike the cone/plate, where the shear rate gradient is the same over the entire surface of the cone, the shear rate gradient on the plate increases from the center to the edge. The software controlling the rheometer is therefore programmed to record the measurement at the edge of the plate, where the shear rate is greatest. This means that care must be taken when loading such a sample to ensure that the sample reaches to the edge around the entire circumference, and that untoward evaporation or material changes at the edge does not occur during the measurement. Another consideration is the size of the gap to be set; of course, it still has to conform to the 10× rule above, and can reach up to 3 mm in certain cases. Care must be taken though to maintain contact between top and bottom plates such that the sample experiences shear and not torsion.

7.6 FACTORS AFFECTING VISCOSITY VALUES

The next step to be aware of is where on the shear rate range one should measure in order to obtain meaningful valid data. Obtaining data is easy, but the rheologist is required to tailor the measurement to maximize the data in the area that best describes the process under investigation. Depending on the nature of the process, vastly different shear rates are to be considered. Table 7.1 provides an indication of the typical shear rate ranges of a list of different processes.

Thus, no useful information will be recorded if when gathering data for chewing, one measures at shear rates only below 10 s^{-1}. It can equally be important to have a feel for the level of viscosity of a range of systems. These are outlined in Table 7.2, which covers, with the exception of air and glass, a range of food substances.

TABLE 7.1
List of Different Processes and Their Accompanying Typical Shear Rates

Process	Shear Rate Range (s^{-1})
Rubbing	10,000–100,000
Stirring/mixing	10–1000
Pumping/pipe flow	1–1000
Dip coating	10–100
Chewing	10–100
Extruding	1–100
Pouring	1–10
Drain off surfaces	0.1–10
Sedimentation	0.000001–0.001

Before continuing further it would be worth considering the range of extrinsic factors that exert influence on viscosity and therefore will have a large effect on the result if they are not accounted for, or at least appreciated. These include, as outlined in Table 7.1, shear rate, time, pressure, and temperature. The effects of shear rate will be dealt with when flow properties are considered. Time plays a critical role in the response of a material to the stress it is exposed to during the measurement, or indeed at conditions of rest. The classic way of describing the effects of time on a substance is to look at the Deborah number, a dimensionless value given by the materials relaxation time and experiment time thus;

$$\mathrm{De} = \frac{\lambda}{t_0} \tag{7.4}$$

TABLE 7.2
List of Typical Food Substance Viscosity Values Together with Air and Glass

Material	Viscosity (Pa s)
Air	10^{-5}
Water	10^{-3}
Olive oil	10^{-1}
Glycerol	10^{0}
Yoghurt	10^{2}
Corn syrup	10^{3}
Gelatin gel	10^{6}
Ice cream	10^{8}
Cheddar	10^{10}
Glass	10^{20}

Note: The values should be thought of as being zero shear viscosity values.

where De is the Deborah number, λ is the relaxation time, and t_0 is the time of the experiment. Knowledge therefore of the Deborah number indicates the predominant property of the material:

$De \ll 1$	Viscous material
$De \gg 1$	Solid material, that is, elastic
$De \approx 1$	Viscoelastic material

The real answer lies with the nature of the experiment, or the situation the material finds itself in. Water is recognized as a liquid, which indeed it is, but when contacted at high speed the vastly shorter timescale of the experiment gives water the feeling of a solid. This can be felt as pain if a belly flop is made in a swimming pool, or can result in death if one jumps from a high suspension bridge over water. Most of the materials within the food science world are viscoelastic in nature and therefore other rheological methods to probe their structure are utilized.

Pressure will also play a role in the viscosity value recorded, and generally, increases in pressure in concomitant increases in viscosity. It is possible to purchase specific pressure cells to fit to commercially available rotational rheometers to run at higher than atmospheric pressure.

Temperature too plays a considerable role affecting viscosity; typically, the hotter something becomes the less viscous it appears and vice versa. The effect of temperature on a material is governed by the Arrhenius equation:

$$\eta = A \exp^{\frac{Ea}{RT}} \tag{7.5}$$

where η is viscosity, A is a constant, *Ea* is the activation energy for flow, *R* is the universal gas constant, and *T* is absolute temperature.

The data (squares) in Figure 7.6 shows the viscosity versus temperature profile for an emulsifier over a temperature range from 20°C to 30°C, and the dotted line is the software-fitted Arrhenius plot. The figure demonstrates just how important it is to have control over the temperature when making rheological measurements; here, it is seen that viscosity drops in a predictable manner with temperature, and that the drop can represent a significant change in consistency and therefore possibly also material functionality.

With an appreciation of the most important and common extrinsic factor affecting viscosity, examination of the flow property types themselves can be undertaken. These fall into two basic categories; Newtonian and non-Newtonian. Newtonian refers to liquids which have the same viscosity irrespective of the shear rate which they are exposed to, provided turbulent conditions are absent. In the presence of turbulence, viscosity tends to increase. Non-Newtonian materials can be split into two groups: time independent, which can either show shear thickening, that is, viscosity increases as shear rate increases, or shear thinning where viscosity decreases with increasing shear rate; and time dependent, which covers material that recover their viscosity at rest after the removal of shear. Again time-dependent materials can be

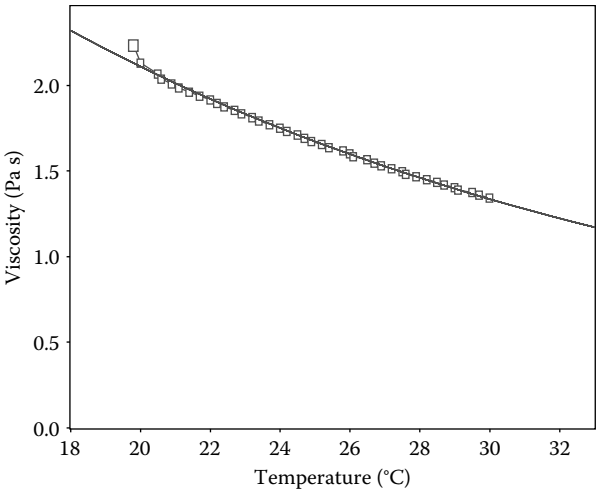


FIGURE 7.6 Arrhenius plot for relifier emulsion, ($r^2 = 0.996$).

split into two groups covering the shear thickening type, such that viscosity increases during shearing and then falls back to the rest viscosity when the shear is reduced—rheopexy; and the shear thinning type where viscosity falls with shearing and recovers back to the rest viscosity again—thixotropy. Materials showing shear thinning or thixotropy are the most common. Examples of shear thickening systems include particulate materials, for example, a slurry of nongelatinized starch. Graphically, these concepts can be expressed as given in Figure 7.7.

Figure 7.7c introduces the concept of pseudoplastic materials, which are characterized as fluids with significant intermolecular interactions, concentrated hydrocolloid solutions being just one example type, and also two hitherto unexplained symbols (η_o) and (η_∞) which represent zero shear viscosity and infinite shear viscosity, respectively, which are used to characterize the viscosity profile of such materials. The intermolecular interactions of these pseudoplastic materials involve the entanglements between the individual polymer or hydrocolloid chains, and are dynamic in nature, that is, they continually break and reform. It is this continual breakage and reforming coupled with the mode of measurement that gives rise to the classic shear thinning viscosity versus shear rate profile of Figure 7.7c. Starting at low shear, let us suppose that we have four entanglements to deal with which are continually breaking and reforming. Since the shear rate value is low, the timescale of the experiment is sufficiently long that the entanglements have time to break and reform before the rheometer "takes a reading." Over a period of gradually increasing shear rates, and thereby decreasing experiment time all four of the entanglements are still "perceived" by the rheometer to be in place. The result is a Newtonian-like curve parallel to the x-axis at low shear rates—as seen in Figure 7.7c, and when this is extrapolated back to zero it is termed the zero shear viscosity. At some critical point, the shear rate will be increased such that the timescale of the experiment is no longer sufficient that all four of our entanglements can reform, only three do so.

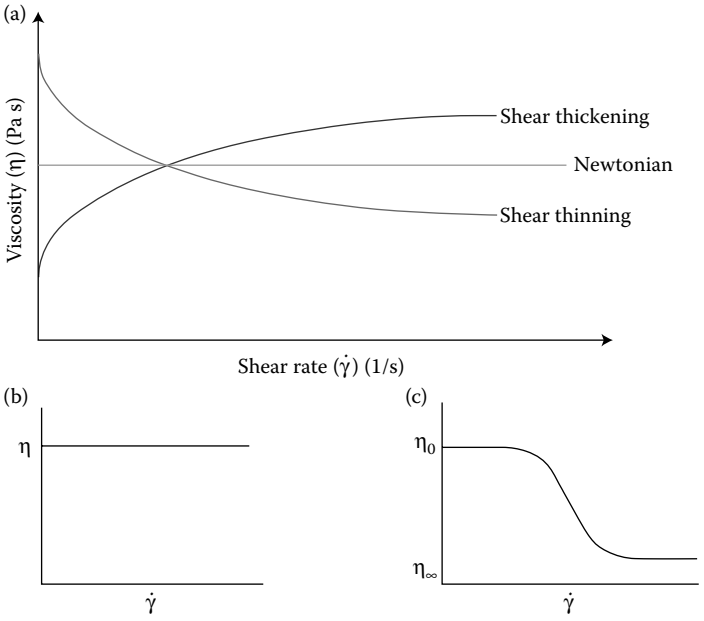


FIGURE 7.7 Schematic representation of Newtonian and non-Newtonian flow behavior, (a) linear scales, (b) Newtonian on double-log scale, and (c) non-Newtonian (pseudoplastic) on double-log scale.

Therefore, a drop in viscosity is recorded. In other words, the resistance to flow is less. This process carries on until finally the shear rate has increased to such a rate that the time of the experiment does not allow for any entanglement to be reformed. When this occurs, the viscosity recorded shows another Newtonian-like plateau at high shear rates and this is known as the infinite shear viscosity. Typically, this is the viscosity of whatever the solvent material, in the case of hydrocolloid solutions—water. The change brought on by the application of shear can affect the material, depending on its properties in a number of ways causing unfolding of polymers, orientation of particles, deformation of spherical particles, or disruption of flocculated particles (Figure 7.8).

7.7 FLOW EQUATIONS

There are a wide range of various flow equations that serve the rheologist but the main ones to become familiar with include the Cross (1965) model, the Carreau (1972) model, and the power-law model. The Cross and the Carreau models were developed to describe the entire pseudoplastic flow curve and are given by Equations 7.6 and 7.7, respectively (Rao, 2007).

$$\eta_a = \eta_\infty + \frac{\eta_0 - \eta_\infty}{1 + \left(\alpha_c \dot{\gamma}\right)^m} \tag{7.6}$$

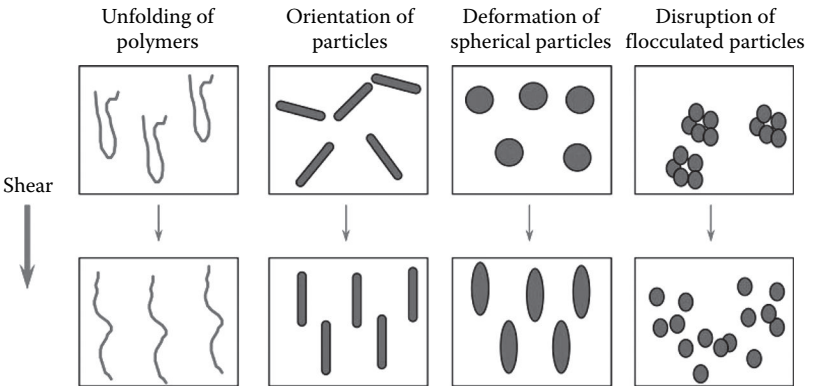


FIGURE 7.8 Possible outcomes of shear being applied to flexible polymers, discrete particles, spherical particles, and flocculated particles.

$$\eta_a = \eta_\infty + \frac{\eta_0 - \eta_\infty}{\left[1 + (\lambda_c \dot{\gamma})^2\right]^N} \tag{7.7}$$

where η_a is apparent viscosity, η_∞ is infinite viscosity, η_0 is zero shear viscosity, α_c and λ_c are time constants related to the relaxation time of the polymer in solution, and m and N are dimensionless exponents. Use of both these equations is basically interchangeable, although it is worth being aware, without descending into mathematical semantics that the Carreau model is considered to be more robust than the Cross model (Raju et al., 1993). Schematically, this can be represented for the Cross model in Figure 7.9.

In order to fit either the Cross or the Carreau models one requires data covering the low-shear Newtoninan plateau and a good portion of the shear thinning section. It is generally unlikely that data from the high-shear Newtonian plateau will be

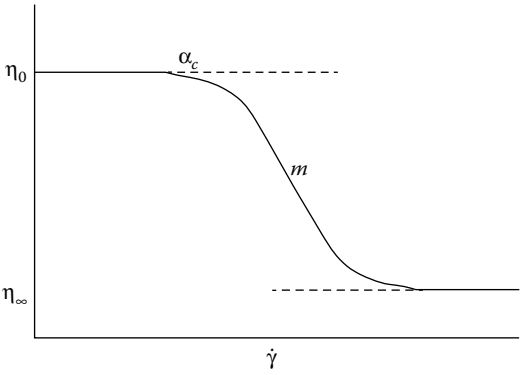


FIGURE 7.9 Schematic graphical representation of pseudoplastic viscosity versus shear rate profile containing Cross-model parameters.

available since this usually requires shear rates that are too high for most rotational rheometers to access. However, if one only has access to the midshear data, or shear thinning data, useful and robust rheological data can still be accessed via the power-law model, given by Equation 7.8

$$\sigma = K\dot{\gamma}^{n} \tag{7.8}$$

where σ is the shear stress, K is the consistency index with units given in Pa s^n, and n is a dimensionless constant, the power-law index and reflects a concept that can be thought of as being the "closeness to Newtonianness." When the power-law index is 1 then the material in question is Newtonian, if the power-law index is <1 then the material is shear thinning. The closer to zero the power-law index, the greater the degree of shear thinning. If the power-law index is >1, the material is shear thickening, and similarly, the greater the value of the power-law index away from 1 the greater the degree of shear thickening. Thus, from a limited range of data, which is available almost every time from pseudoplastic material measurements, two important pieces of information are obtained; a measure of the consistency, the greater the value of K, then the thicker and more full of substance the material will be, and the power-law index which will indicate the material's closeness to Newtonianness. Gaining control over the viscosity profile measurements allows the rheologist to begin an understanding of the material being examined, and in particular for food materials knowledge of the degree of shear thinning can provide insight into the likely flavor release characteristics. A greater degree of shear thinning will result in a greater degree of mixing, and thereby a faster release of flavor. Equally, gaining an understanding of the zero shear viscosity can present information on the likely stability of a material to properties like creaming or sedimentation, both of which are key attributes that food materials must usually guard against.

Dealing exclusively with thixotropy, since that is the property most often observed, concerns structure recovery after the removal of shearing forces. As a material is exposed to increasing shear under processes such as pumping, pouring, extruding, stirring, and so on, the viscosity of the material often decreases. Unless the material quickly recovers its original viscosity and structure again after the shearing is stopped, the drop in viscosity can have adverse consequences on the stability of the product where previously suspended particles now have a tendency to cream or sediment depending on their now relative density difference in relation to the new viscosity in which they find themselves. Traditionally, the most popular method to determine thixotropy has been via the hysteresis loop, an "up–down" curve where shear rate is first increased and then decreased. The area between the up curve and the down curve for viscosity versus shear rate is then an expression for the amount of time required in order for the material to recover. In the case of time-independent materials, this difference is zero. However, perhaps a more intuitive way of measuring this phenomenon is via step change measurements where a low shear rate measurement, for example, such that the material is on the low shear Newtonian plateau, although this is not a prerequisite, is made followed by a high shear measurement which ensures material breakdown and finally followed by another measurement at

the same low shear rate as originally used. The operator has control over the timescale of the low shear rate measurement windows, where each should be of the same length, and the stable plateau viscosity of the first measurement is taken as 100% viscosity of the sample. After the period of high shear breakdown, the recovery is monitored by returning to the same low shear rate as before and observing how much viscosity is regained. When the low shear stable plateau is again reached, a percentage of the original viscosity can be calculated and expressed as the degree of thixotropy or structure recovery (Young et al. 2003; Figure 7.10).

The level of structure recovery for Figure 7.10 was found to be 80% for the pectin/alginate blend, 48% for the pectin, and 23% for the alginate.

The graph of Figure 7.10 was measured at two distinct shear rates, 0.01 s^{-1} and 40 s^{-1}, for the low and high shear rate values, respectively. Often, one is asked what the viscosity of something is, and as was hinted at in Table 7.2, unless the material is Newtonian in behavior this has to be qualified by reporting at what shear rate the measurement was made. Equally and again hinted at in Table 7.1 making sure one measures in the correct shear rate range is vitally important when trying to apply value to the results obtained. Failure to follow these simple principles can lead to far-reaching and costly errors, especially if the viscosity is turned into a "one-point" result. Figure 7.11 highlights the dangers of presenting viscosity as a one-point result—at least for pseudoplastic materials.

If by chance, the viscosity at shear rate x was recorded for both materials A and B, then the value would be the same. If however, the use of the materials were to take place at a lower shear rate process, then material A would be considerably more viscous than B and vice versa. This simply serves to demonstrate that quoting viscosity

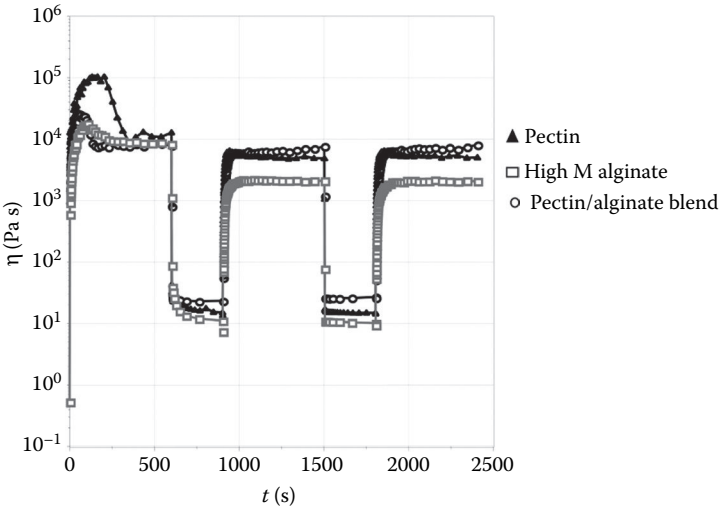


FIGURE 7.10 Stepwise thixotropy graph isolating initial viscosity during the first 600 s followed by two breakdown/recovery steps for three systems; pectin, high M alginate, and a blend of the pectin and alginate. (Adapted from Young, N.W.G, Kappel, G., and Bladt, T. 2003. *Food Hydrocolloids*, 17, 407–418.)

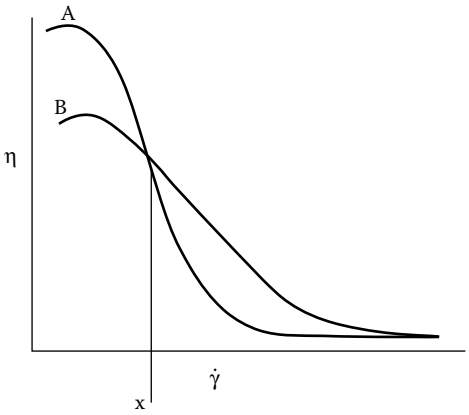


FIGURE 7.11 Fictive viscosity versus shear rate curves for two products A and B.

of non-Newtonian materials should always be accompanied by a shear rate at which the measurement was made, and where possible construction of a viscosity versus shear rate curve would alleviate any grounds for confusion or misunderstanding. The trivial miscommunication even at this simple level does happen on a routine basis and causes many a delay in projects and commercial processes.

7.8 YIELD STRESS

The yield stress is a concept that was believed to be standard until about 40 years ago when instrumentation began to improve such that access to the low shear rate range really became possible. This opened an often polarized debate about its existence (Dzuy and Boger, 1983) or not (Barnes and Walters, 1985) until it was effectively closed in 2004 (Watson, 2004). However, having hinted at the vitriol which pervaded the rheological community, the whole matter was effectively solved some 80 years ago, when Scott Blair in 1933 defined the yield stress as, "that stress below which no flow can be observed—under the conditions of the experiment" (Scott Blair, 1933, p. 114). Taking this as a starting point, the access to the low shear rate range during the 1970s and more so today where shear rates as low as 10^{-8}, 10^{-9} s^{-1} are possible have simply established methods of accurately determining where the onset of flow begins. Thinking back to the entanglements from the viscosity section we can think of the yield stress as being the point at which the first entanglement cannot reform within the experiments timescale as being the yield point. Classically, it has been defined by the Hershel–Bulkley equation for estimating the yield stress.

$$\sigma = \sigma_0 + K\dot{\gamma}^n \tag{7.9}$$

where σ_0 is the estimated yield stress, the rest of the equation is the same as Equation 7.8 for the power law. This would be seen graphically as in Figure 7.12.

Accurate measurement of the yield stress is not, in itself, difficult, but it does demand care from the rheologist and there are pitfalls to be avoided; perhaps, the

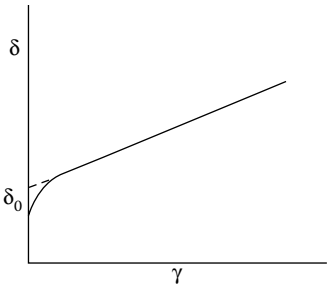


FIGURE 7.12 Classical schematic graphical representation of the yield stress, showing shear stress on the y axis and shear strain on the x axis.

largest of these is to ensure that slip is not present. If slip exists between the material and the measurement geometry, then either false, the so-called pseudo yield stresses can be recorded, or if low enough shear rates are not accessed simply erroneous yield stresses can occur (Figure 7.13).

The factors which can greatly contribute to slip include, (a) smooth wall material, (b) fluid samples within the sensitive concentrated viscosity region, and (c) particles within the system being large compared to the gap, that is, less than the 10× rule. When these conditions are accounted for through either using rough walled systems or more correctly a specific geometry type designed for this purpose, the vane and basket (Dzuy and Boger, 1985), then accurate measurements of yielding conditions can be guaranteed (Figure 7.14).

The measurement of the yield stress is best achieved under conditions of controlled stress, and with the vane geometry the elastic deformation at the vane edge is seen as a linear torque response, which can be associated with network stretching. This network stretching can be understood as the entanglements previously discussed, and when the system ruptures it is said to have yielded. The problem of slip is avoided completely with the vane geometry due to the fact that it effectively sets up an internal slip layer between the sample, between the blades of the vane, and

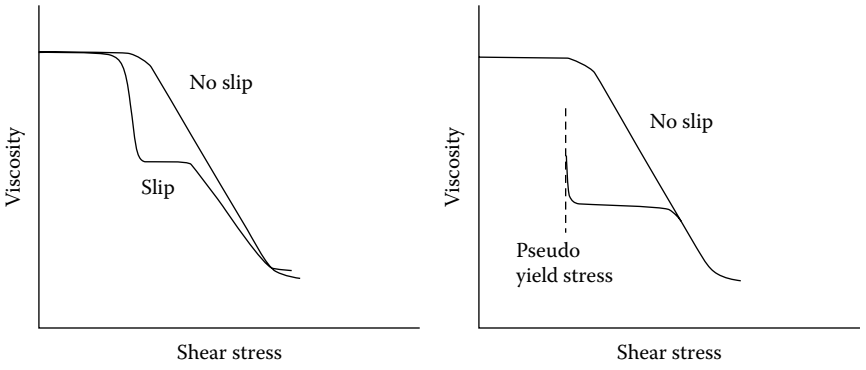


FIGURE 7.13 Schematic graphical representation of slip affecting the reading of yield stress measurement.

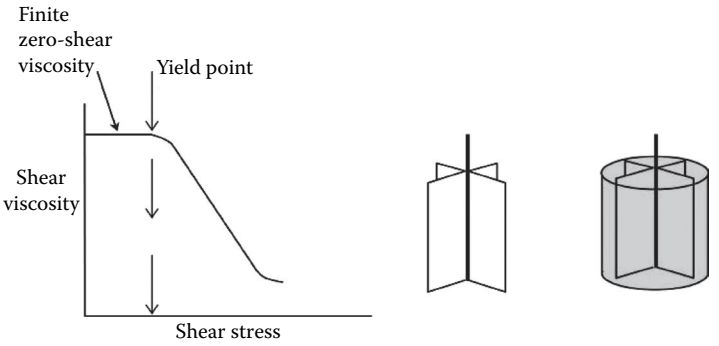


FIGURE 7.14 Typical viscosity versus shear stress curve (left) showing finite zero-shear viscosity plateau and the yield point when measured with a vane–basket geometry (right).

the sample outside the blades. Thus, the wall against which the sample is being measured is effectively itself! In order to secure the measurement access to the low-shear rate range is essential and here shear rates of 10^{-5} s^{-1} and below are basically prerequisites, but also well within the capabilities of modern rheometers.

Using this principle, measuring the yield stress coupled with viscosity data and calculations of the particle properties a matrix may contain, predictions of system stability toward creaming or sedimentation that can be easily achieved. This can then give indications on whether a particular food product will match the expectations of shelf-life the producer demands, and is achieved by first measuring the yield stress with vane geometry where access to the low-shear Newtonian plateau is also gained. From this it is possible, building on the schematic graph from Figure 7.14, to attribute areas of stability and instability for a given system containing particles (Figure 7.15).

Establishing, via Figure 7.14, that the yield point is the same critical point found in the Cross and Carreau equations (Equation 7.6 and 7.7), this can in conjunction with a concept known as the gravitational stress be used to predict system stability. The gravitational stress is the stress exerted upon a particle by the Earth's gravity when the system is standing at rest, and is given by Equation 7.10.

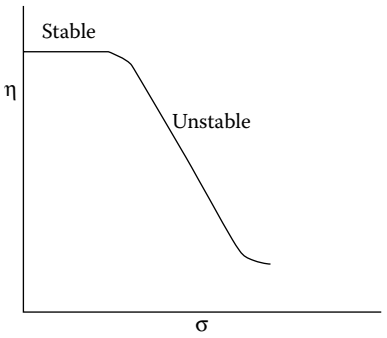


FIGURE 7.15 Attributing areas of stability and instability to viscosity versus shear stress curves.

$$GS = \frac{ag\Delta\rho}{3} \tag{7.10}$$

where GS is the gravitational stress, a is particle size, g is acceleration due to gravity, and $\Delta\rho$ is the difference in density of the particle and the suspending matrix. Briefly then, if the gravitational stress of a system is less than the yield stress under the conditions of the measurement then the system containing particles will be stable. If however, the opposite is true then the product will experience creaming or sedimentation of its particles, depending on the density difference. This leads to an easy and simple way of calculating stability and therefore projected shelf-life of a product, where with an extension, the speed of the moving particle can also be calculated (Young, 2002).

7.9 DYNAMIC (SMALL DEFORMATION OSCILLATORY) MEASUREMENTS

To access viscoelastic data, that is, data containing components of viscosity and elasticity, or fluidity and solidity, measurements in the small deformatory oscillatory mode are required to be made. These are delicate, nondestructive tests that can be used to shed light on gelling, melting, and stability; and are subject to influence by time, temperature, frequency, and strain, that is, by how much the sample is deformed. Figure 7.16 gives a conceptual view of the fundamentals of small deformation oscillation measurements, where the left-hand figure broadly resembles the viscosity explanation of Figure 7.3.

Several equations and definitions are required to explain the right-hand diagram of Figure 7.16, where the general defining equation can be given as

$$G^* = G' + iG'' \tag{7.11}$$

where G^* is termed the complex modulus and is made up of G' and G'', G' is the elastic modulus, or storage modulus, G'' is the viscous modulus or loss modulus, and i is the complex number related to the square root of negative 1. Thus, any material where G' dominates over G'' will have properties dominated by the elastic or solid

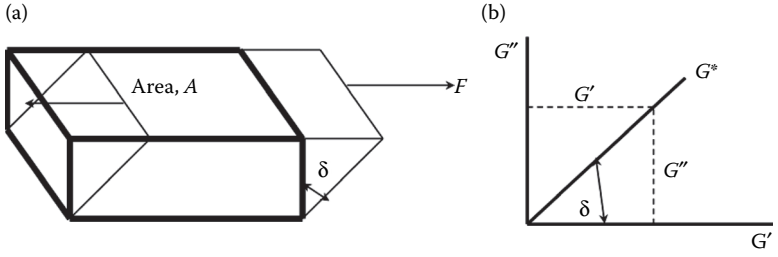


FIGURE 7.16 Conceptual visualization of small deformation oscillation principles: (a) an imaginary piece of material of Area A being oscillated by Force F to a deformation supported by the angle delta; and (b) what the rheometer actually measures.

like behavior, whereas any material dominated by G'' contra G' will possess properties more viscous and fluid like. Constructing G' and G'' from Figure 7.16 is achieved via the following equations:

$$G' = \cos \delta G^* \tag{7.12}$$

$$G'' = \sin \delta G^* \tag{7.13}$$

Equally, utilizing the concepts given above we can access information regarding what is termed the degree of elasticity of the material. This can be achieved through the simple relationship given in Equation 7.14.

$$\tan \delta = \frac{G''}{G'} \tag{7.14}$$

Thus, when the value of tan δ is 1, there is an even contribution between elastic and viscous responses and the material can be thought of as loosely being at its gel point. As tan δ becomes <1 then the material is dominated by elastic forces, its degree of elasticity is greater and therefore it can be described as being more structured, and more solid like. As tan δ becomes >1 the material is dominated by viscous forces, its degree of elasticity is less, and therefore it can be described as being less structured, and more fluid like.

Also, as the name of G' and G'' imply, storage and loss modulus, respectively; a material which is dominated by the elastic modulus will store the energy, much the same way as an elastic band stores the energy when stretched. When the stretching or applied stress is removed, the elastic band snaps back to its rest position and returns the energy stored. So too does any material dominated by G' and therefore this type of deformation is termed reversible. A material thereby dominated by G'' can have the same energy input via the applied stress, but here the energy is not stored, rather lost as heat. When the applied stress is removed from such a material it does not recover its original position, and therefore this type of deformation is irreversible.

7.10 ACCESSING AND GRASPING THE MODULI

In the case of materials undergoing rheological analysis on a commercially available rotational rheometer the applied stress is in the form of a sinusoidal wave form. The rheometer then measures the response of the material to this wave which sends back a similar sinusoidal wave. The two extreme ends of the response scale are given in Figure 7.17, which shows the applied wave, and the response for a perfect solid, and a perfect Newtonian liquid, when measured in the linear viscoelastic region (LVR), a concept which will be explained later.

At any point on the response curve for the perfect solid the resultant strain is directly proportional to the magnitude of the applied stress. Therefore, maximum strain coincides with maximum amplitude in the applied stress, or expressed another way the response curve for a perfect solid is in phase with the applied

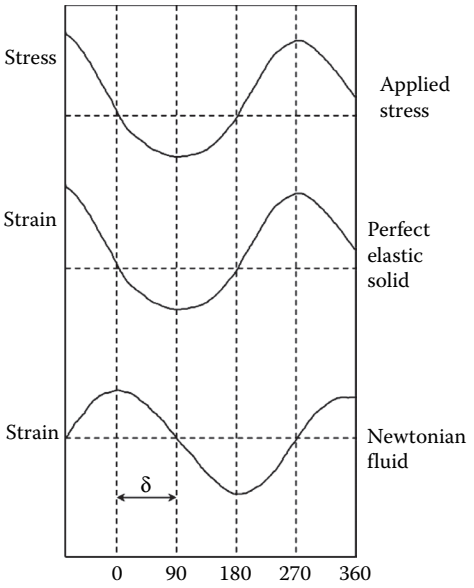


FIGURE 7.17 Conceptual diagram showing applied stress wave (top), response wave for perfect solid (middle), and response wave for Newtonian fluid (bottom).

stress. For Newtonian fluids, however, the point of zero deformation corresponds with a maxima in amplitude of the applied wave in either direction. This leads to the consideration that Newtonian fluids are out of phase with the applied stress. Discussion of in-phase or out-of-phase relates to the angle depicted in Figure 7.17, δ, often referred to as the phase angle. This has an upper and lower limit of 90° and 0° for Newtonian fluids and perfect solids respectively, and therefore similar to the degree of elasticity seen in Equation 7.14; knowledge of the phase angle alone can tell much about the characteristic nature of a material. When the phase angle is 45°, G' and G'' have the same value and therefore any phase angle value above 45° indicates predominantly fluid-like behavior, whereas any phase angle below 45° indicates, predominantly solid-like behavior. The above principle translated to a viscoelastic material would therefore look something like the conceptual process shown in Figure 7.18; in this case a material which displays a predominantly fluid-like behavior given the high phase angle.

Measurement of the viscoelastic properties of a material requires that the rheometer is set up to oscillate to and fro, and can either be done as a function of strain (i.e., deformation) or stress, and as a function of frequency (f, measured in Hertz) or angular velocity (ω, given in rad/s), and of course temperature. It is also important to uphold the mathematical understanding of the results, to measure within the linear viscoelastic region (LVR), which ensures that we can maintain the measurement ethos as being nondestructive. The LVR can be found by first conducting a simple stress or strain sweep at a single frequency or angular velocity on the material in question. Here, a low strain or stress is gradually ramped up to high strain or stress

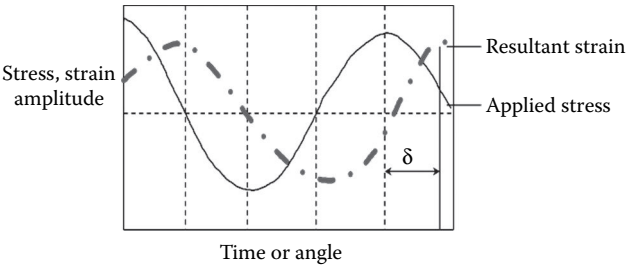


FIGURE 7.18 Applied stress wave (solid line) and response wave (dotted line) for a viscoelastic material.

and the response of G', G'' or phase angle are followed. Using only G', Figure 7.19 shows the LVR as a result of a strain sweep measurement, where at initial low strain rates the response of G' is unaffected by the increasing strain. Here, the profile is parallel to the strain axis and appears akin to the low shear Newtonian plateau seen earlier for viscosity. At some strain, deemed here as the critical strain, G' is seen to decrease in value and continues to do so until a high strain plateau has been reached. The LVR is shown as being the area which conforms to the low strain plateau where G' is largely unaffected; it is within this strain range that the oscillatory measurements to probe viscoelasticity should be made. Basically, anywhere in this region is good, but caution must be exercised. The strain sweep has only been made at one single frequency, thus choosing a strain rate for the subsequent frequency sweep close to the critical point could result in the higher frequency measurements descending into the nonlinear region. Therefore, it is highly recommended to choose a strain rate as far away from the critical point as possible.

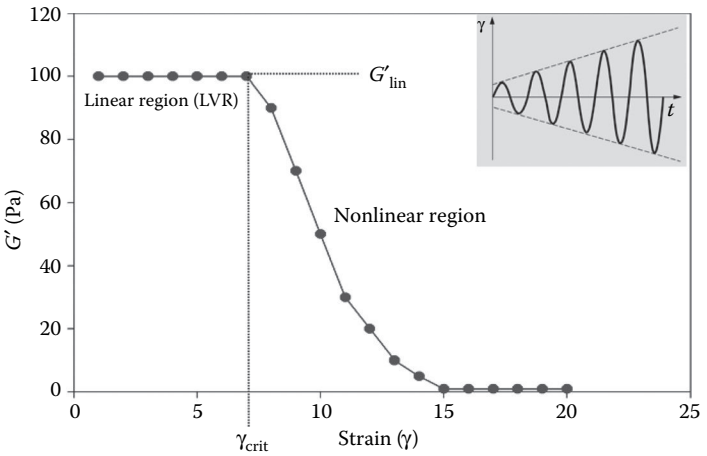


FIGURE 7.19 G' versus strain profile in the form of a strain sweep, outlining the LVR and the nonlinear region. The inset shows the effect of the increasing strain or stress where the deformation or amplitude increases.

Alternatively, a range of strain sweeps could be performed at varying frequency values to eliminate this possibility.

Complementing the elastic and viscous moduli there are corresponding moduli which describe viscosity, in much the same way as Equation 7.11, and these can be used to further characterize and probe the viscoelastic material properties.

$$\eta^* = \eta' - i\eta'' \tag{7.15}$$

where η^* is the complex viscosity, η' is the dynamic viscosity, η'' is an imaginary component, and i is the square root of negative 1.

7.11 VISCOELASTIC STATES OF MATTER

Applying the principles above a range of viscoelastic "fingerprints" can be made which characterize the four main material states that cover the general categories of dilute polymer solution, concentrated polymer solution, weak gel, and strong gel. Figure 7.20 is representative of dilute polymer solutions, typically below the critical coil overlap concentration—a point below which the individual polymer molecules exist in the solution in isolation, effectively "unaware" of their neighbors. Run over a frequency or angular velocity range, at low frequency the viscous modulus, G'', dominates over the elastic modulus, G', and the dynamic viscosity η' appears as a low-frequency Newtonian-like plateau. Specifically, when run as a function of angular velocity, at low values, $G' \propto \omega^2$ and $G'' \propto \omega$. This leads to the observation that with $G'' \gg G'$ the material is dominated by a viscous response. Invoking the phase angle and tan δ values they would be above 70° and $\gg$1, respectively. At higher frequency or angular velocity however, there is a crossover of G'' and G' such that G' becomes greater. This is due to the timescale of the experiment becoming shorter and shorter and thus the material behaves, for this short time, as a more solid-like material before immediately relaxing back to its fluid state. This is akin to hitting water when jumping off a high bridge, and hence is not to be recommended.

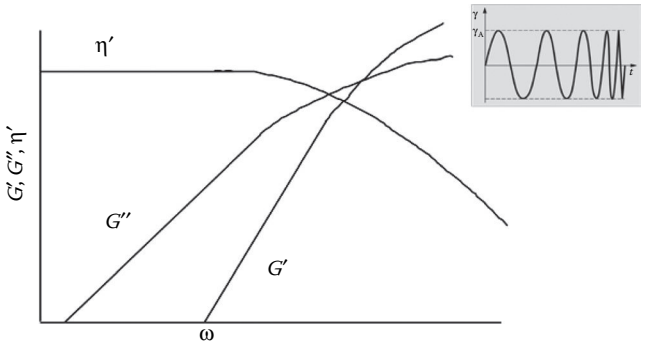


FIGURE 7.20 Viscoelastic fingerprint for a classic dilute polymer solution showing $G'' \gg G'$ and η' with a plateau at low angular velocity values before crossing and decreasing respectively at high angular velocity values. The inset shows the effect of the increase of frequency or angular velocity while maintaining the amplitude.

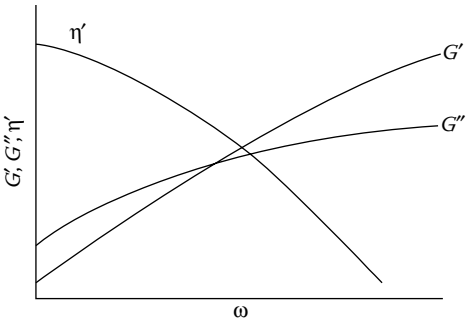


FIGURE 7.21 Viscoelastic fingerprint for a classical concentrated polymer solution showing $G'' > G$ initially, the $G'-G''$ crossover, and the high-frequency area where $G' > G''$.

Increasing the concentration to give a concentrated polymer solution (Figure 7.21), the viscoelastic fingerprint changes such that the crossover point between G' and G'' occurs at lower frequency or angular velocity. Although popularly thought of as the gel point, the crossover of G' and G'' more correctly reflects that lifetime of the entanglements within the system. There are other methods to more fully describe the gel point itself (Winter and Chambon, 1986). The concentrated solution, under a classical frequency sweep is, therefore, characterized by two distinctly different areas; first, a low frequency of predominantly viscous flow behavior, and then at higher frequencies, above the G'–G'' crossover, as more solid like. At the low frequency end there is a hint of a plateau for the dynamic viscosity, but not as marked as for the dilute solution.

Raising the concentration further, the system moves into the weak gel (Figure 7.22) area, where $G' > G''$ over the entire frequency range investigated, but still dependent on frequency. Thus, as frequency increases so too does G' and G''. No crossover of these parameters is visible within this experiment and the values for dynamic viscosity are essentially decreasing across the profile with little hint of a low-frequency Newtonian-like plateau.

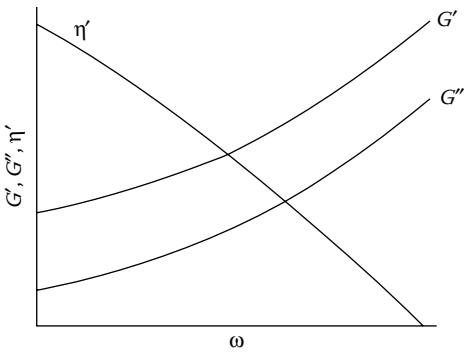


FIGURE 7.22 Viscoelastic fingerprint for a classical weak gel, showing $G' > G''$ over the entire frequency range.

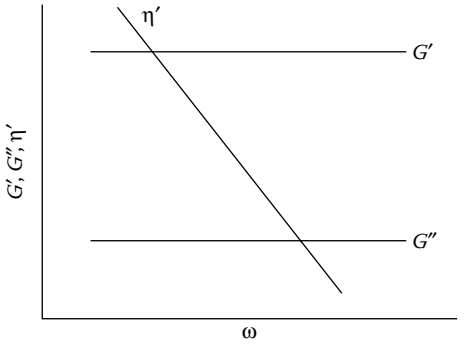


FIGURE 7.23 Viscoelastic fingerprint of a classical strong gel, showing $G' \ggg G''$ over the entire frequency range and no inkling of a low-frequency Newtonian-like plateau for the dynamic viscosity.

Finally, there is the realm of the strong gel (Figure 7.23), not something that is routinely observed at least in the food world with perhaps the exception of some hard cheeses. Here $G' \ggg G''$ over the entire frequency range and both moduli are independent of frequency. Concerning the dynamic viscosity, no suggestion for any Newtonian-like low-frequency plateau is evident.

There is a direct relation between shear viscosity and complex viscosity as expressed by the Cox–Merz rule (Cox and Merz, 1958), which states that the frequency dependency of the complex viscosity and the shear rate dependence of shear viscosity are closely superimposible for isotropic solutions. Basically, this means that if the material is Newtonian-like in character, or predominantly fluid, then the Cox–Merz rule will be obeyed; whereas if the material is pseudoplastic or viscoelastic in nature, predominantly elastic, the Cox–Merz rule will be disobeyed (Figure 7.24).

Knowledge of the Cox–Merz conditions will provide insight into the material characteristics of the sample under investigation and allow practical judgment to be discussed about issues involving flavor release.

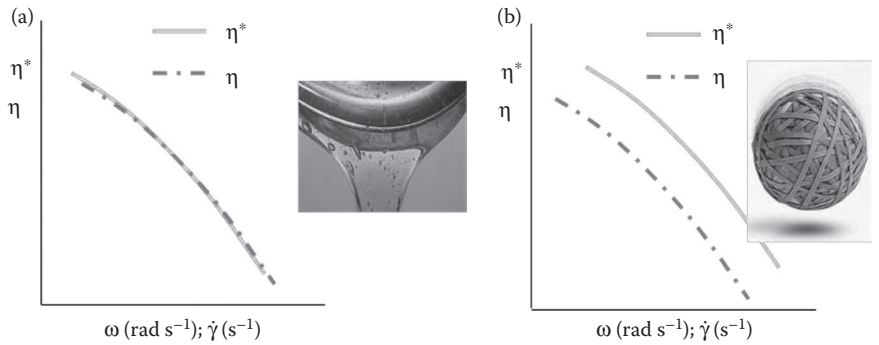


FIGURE 7.24 Depicts Cox–Merz rule being obeyed (a) for Newtoninan-like material without significant structure and being disobeyed (b) for elastic system with structure.

7.12 CASE STUDIES

This section will focus on three separate case studies, looking at real data on real food systems where the investigations are not only led by rheology, but also supported and confirmed with other technologies. They serve to illustrate that successful use of rheology is but one tool on the research scientist's palate. The case studies themselves feature fruit gummy fillings, fat-based systems, and fruit spreads. It is through case studies such as these that experience in rheological theory and adroit interpretation of the data can lead to significant understanding of one's system and create real value at the academic and commercial level.

7.13 FRUIT GUMMY FILLING

Fruit gummy fillings can be made from a range of hydrocolloids, but in this case high ester pectin is the gelling agent of choice, and common for all types is that they set as a function of cooling from a boiling process. This makes the prospect of putting a nongelled gummy mass into a chocolate mould difficult. In order to appreciate the role that temperature plays on the setting of a pectin gummy mass, Figure 7.25 shows the cooling curve performed under oscillatory conditions, where the experiment was run in controlled strain mode and here only the phase angle is shown.

Figure 7.25, read from right to left, starts with the material showing a phase angle around 80°, indicating the predominantly fluid-like nature. As cooling begins there is a clear Newtonian-like plateau where decreasing the temperature has no effect on the structure. This continues to a temperature of around 76°C where the phase angle begins to drop. This is the critical point which is attributed as the onset of setting, that is, the point where structure build-up as a function of cooling begins. The decrease in the

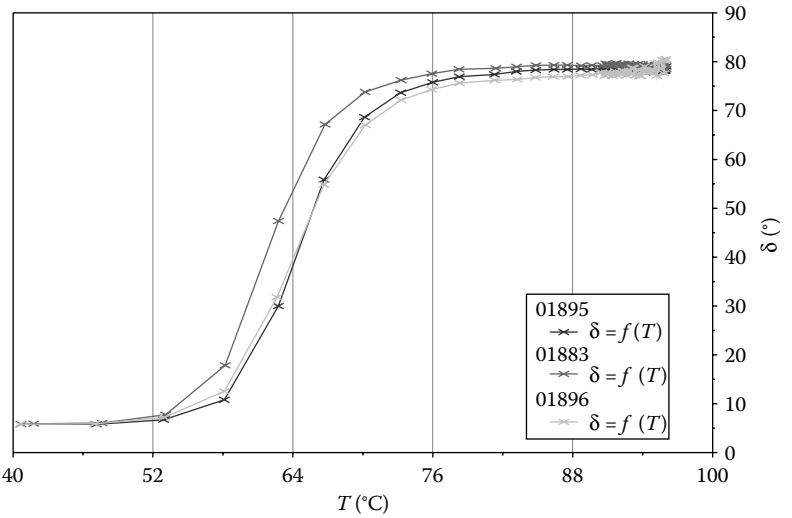


FIGURE 7.25 Cooling profile of three pectin-based gummy masses from 96°C to 40°C depicted as a function of phase angle.

phase angle then proceeds rapidly such that it reaches a value of 45° (the "gel" point) at a temperature between 63°C and 65°C, before ultimately reaching a stable plateau again at a phase angle of around 7° from a temperature of around 50°C. Thus, the graph in Figure 7.25 shows a state change process for the material, moving from a liquid to a solid-like nature over the temperature range studied—for typical gummy masses. Every temperature here is above the melting point of chocolate, and therefore the challenge was to transpose this profile such that it could be achieved under cold conditions.

High-ester pectin gels as a consequence of three specific conditions; the soluble solids must be in the correct range (>55%), the pH must be correct (2.8–3.8), and the temperature must be controlled—as can be seen from Figure 7.25. In Figure 7.25 it may be observed that the pectin had the correct soluble solids level and pH in order to gel, only the temperature was wrong, being initially too high. But as it cooled, it placed the pectin in the gelling window and the gel state resulted. Using this knowledge of high-ester pectin's gelation characteristics it was quite simple to change the gelling conditions such that the soluble solids and temperature were in the favorable gelling window but pH was kept high and therefore outside the gelling window. This resulted in a thick viscous but crucially cold syrup-like mass. Gradually reducing the pH *in situ* then brought the pH progressively into the gelling window and gave the gelling which was being sought. The method chosen was to produce the pectin gummy mass with the correct soluble solids and keep it cold, ambient, and therefore within the gelling window. The pH of this solution was 4.5, too high to gel. However, addition of a specific concentration of glucono delta lactone (GDL) reduced the pH over time from 4.5 to 3.5. Naturally, the greater the dosage of GDL the faster the reduction in pH and the quicker the gelation process occurred. The results of this method are shown in Figure 7.26 showing a double determination where the experiment is started at time zero, corresponding to the GDL addition, and is run under ambient temperature conditions (23°C), and for a duration of two and a half hours. The phase angle, G' and G'' are shown here. Starting at time zero we see a similar Newtonian-like plateau of the phase angle as we did in Figure 7.25, this time with a value approaching 70°, but still sufficiently high to indicate that the material is behaving as a fluid. This is confirmed by the G' and G'' profiles where $G'' > G'$. The plateau region of the phase angle lasts for the first 1800 s, or 30 min, of the graph before the critical "onset of setting" point is reached. Here, the phase angle is seen to decrease and the G' profile begins to lessen the gap toward G''. Structure is being formed. This reduction of phase angle together with the converging G' and G'' profiles continues to the gel point at 45° and the G'–G'' crossover after some 5500 s (about one and a half hours). Structure then continues to form and one can imagine that extending the experiment to say 12,000 s, the phase angle would have settled out at a constant value of around 30°.

From a process point of view, the data in Figure 7.26 leads to the following suggestions with regard to practical use of this material. During the first 1800 s the material is not affected by the reduction of pH, therefore no structure is being disrupted by processes such as pumping, pouring, or filling. After 1800 s and up to 5500 s the onset of structure build-up toward the gelling point occurs—here it would be recommended not to move the mass or expose it to shear, which may disrupt the structure that would be formed. Above 5500 s the product has gelled and is becoming essentially solid like. It should be *in situ*, that is, the chocolate cup and not disrupted

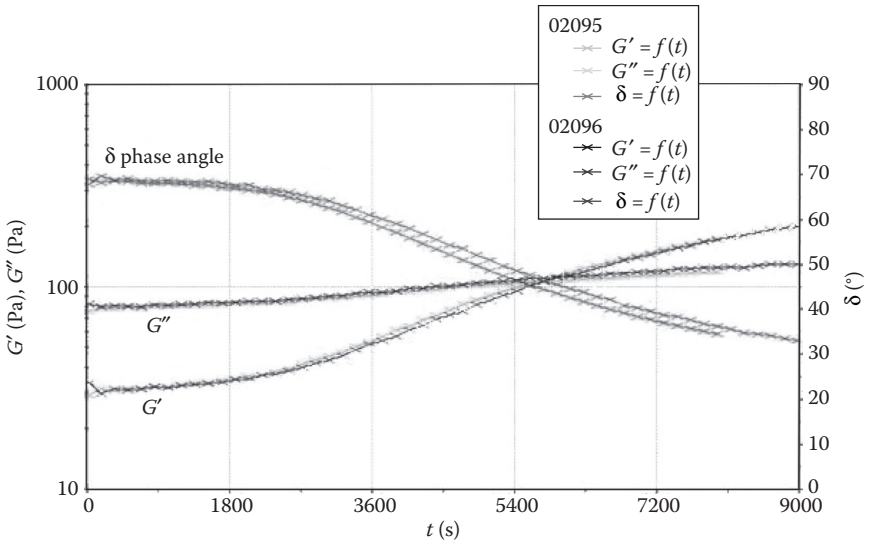


FIGURE 7.26 Gelling profile of pectin gummy mass under ambient temperature conditions where pH is reduced by use of GDL. (Adapted from Young, N.W.G. 2011. *Practical Food Rheology—An Interpretive Approach*, Wiley Blackwell, Oxford, UK, pp. 1–6.)

further. Equally, it now has sufficient structure to allow an entity to be placed on top without it sinking into the mass. These represent some of the key processing conclusions that can be drawn from this simple rheological measurement, however, it is not certain that every pectin gummy manufacturer has access to a controlled stress rheometer beside their production line, or even in their development labs. In order for this piece of rheology to be truly useful and to bring value, it must be able to be translated and followed by other means. Here, following pH as a function of time is the easiest method, as shown in Figure 7.27.

Figure 7.27 shows the pH measurement recorded over time of the drop in pH of the pectin-based gummy mass at four different GDL concentrations under ambient temperature (23°C). The data start at time zero with a pH of around 4.5, and time zero also corresponds to the simultaneous start of the measurement on the rheometer. Hence, by following the rheology curves where onset of gelation and gel points occur as a function of time, it is possible to obtain the pH of the system at which these processes happen. Thus, the state of the gummy mass can be followed completely by only knowing the pH as a function of time once the initial rheological measurements have been made. Different timescales to match particular production conditions can also be easily calculated by using the sliding scale of the increasing GDL concentrations where onset of setting can vary between 20 and 45 min, and time to gel point can vary between 55 and 150 min when going from GDL concentrations of 3.0–1.5%, respectively.

In summary, a simple rheological measurement based initially on cooling curves, and then transposed to time curve built up around small deformation oscillation within the LVR was successfully utilized to shed light and understanding on a cold gelation of pectin-based gummy mass for application in chocolate cups. By following

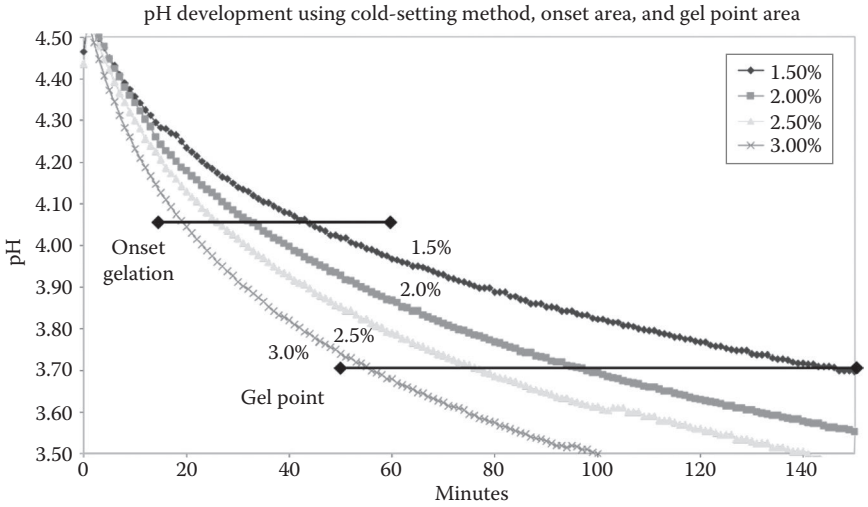


FIGURE 7.27 pH versus time curves for the pectin-based gummy mass at four different GDL concentrations, 1.5%, 2.0%, 2.5%, and 3.0% showing areas of onset of gelation and gel point after confirmation by rheology measurements. (Adapted from Young, N.W.G. 2011. *Practical Food Rheology—An Interpretive Approach*, Wiley Blackwell, Oxford, UK, pp. 1–6.)

the phase angle and G' and G'' curves, material characteristics could be described and related to practical process conditions which would improve and guide the production of the gummy mass commercially. Coupling this rheological measurement with pH versus time curves allowed the material characteristics of the gummy mass to be followed exclusively by changes in pH, therefore facilitating a cheap and easy transfer of the method into a manufacturing environment where access to controlled stress rheometers was absent. The challenge was met, the results were documented, and tested to be robust; the method was transferred to a simpler system and value was created.

7.14 FAT BLEND CRYSTALLIZATION

The need to structure low fat-based systems without *trans* fatty acids (Wassell and Young, 2007) and with a much lower concentration of saturated fatty acids (Wassell et al., 2010a) has been documented. During these investigations, confirmation of the addition of a small amount of a very long chain of saturated fatty acid, behenic acid (C_{24}), building on the work of Sakamoto et al. (2003), into a fat blend gave a significant boost to the level of structure which was possible. This case set about to prove this via conventional rheometry and also to ascertain that the effect was similarly present under dynamic processing conditions with the aid of another technique which could reveal true in-line rheological parameters, ultrasound velocity profiling with pressure difference (UVP-PD). Traditional rheology, run at a constant shear rate as a function of temperature shows a range of fat blends being cooled from 70°C to 40°C (Figure 7.28). All samples with the exception of the one containing 1% of Crystalliser® 110

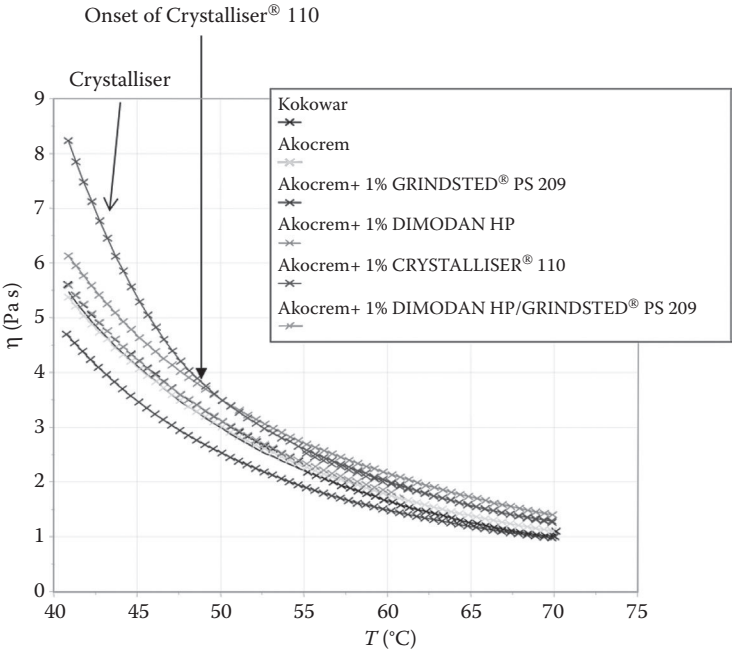


FIGURE 7.28 Viscosity as a function of temperature for fat blends measured off-line. (Adapted from Young, N.W.G. et al. 2008. *International Journal of Food Science and Technology*, **43**(11), 2083–2089.)

essentially follow the same increasing viscosity profile. However, the sample containing Crystalliser® 110, which contains Behenic acid, shows a distinct change in the viscosity increase around 48°C, which for this system is taken as being the onset of the structuring due to the crystallization of the long chain behenic fatty acid molecules. This is a temperature much higher than shorter chain fatty acids would begin to crystallize and results in the Crystalliser® 110 functioning as either a templating or a scaffolding agent, where it builds a fat crystal structure which allows the shorter chain fatty acids to crystallize onto, and thereby boosts the viscosity or structure that would otherwise have been present. Utilizing this scaffolding principle it becomes possible to reduce the overall saturated fat in a recipe and yet still maintain the structure, texture, and eating qualities of the given food material. The challenge now was to prove that this was still the case under the dynamic conditions experienced under processing.

Utilizing the new UVP-PD technique (Wiklund et al. 2007; Young et al., 2008; Wassell et al. 2010b), fully capable of measuring in-line viscosity of opaque systems, the same fat blend was processed through a pilot plant equipped with the UVP-PD instrumentation and run under standard operating conditions. The aim was to observe a similar trend to that shown in the off-line, static measurements of Figure 7.28 where a difference in viscosity approaching a factor of 2 was recorded. The raw data from the UVP-PD is shown in Figure 7.29 for a fat blend alone (Figure 7.29a) and a fat blend with 1% of Crystalliser® 110 (Figure 7.29b). The white shadow-like profile

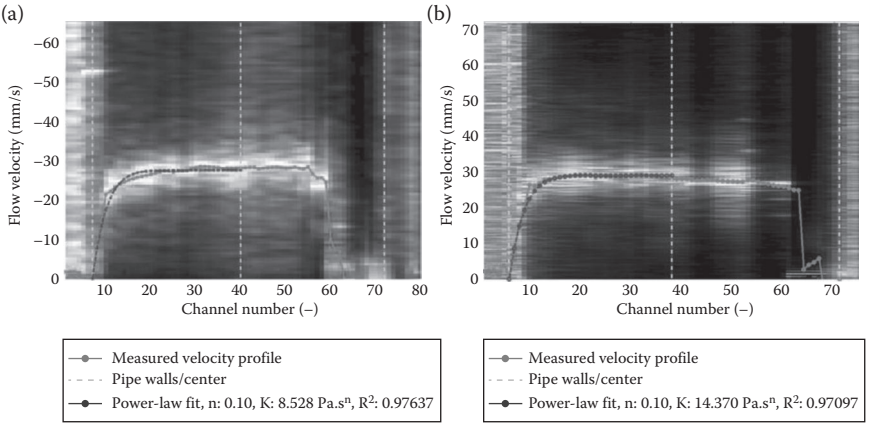


FIGURE 7.29 Spectral plot (white), measured arithmetic average plot (whole plot), and power law fit (half-plot) for fat blend without Crystalliser® 110 (a) and fat blend with Crystalliser® 110 (b). (Adapted from Young, N.W.G. et al. 2008. *International Journal of Food Science and Technology*, **43**(11), 2083–2089.)

is the actual velocity profile, termed the spectral plot and highlighted in green; and the red line is the fit to the data of the power-law model, giving access to the consistency index and the power-law index indicating the degree of shear thinning. The first thing to notice about the spectral plots is their shape; both are fairly flat and snub nosed as opposed to parabolic. If they had been parabolic this would have indicated that the material was predominantly fluid-like in nature with little overall structure. Thus, it can already be concluded that the fat blends here both contain significant amounts of structure because to the plug flow spectral plot shape.

In each case the power-law index is 0.1, indicating that the material is very shear thinning, and the consistency index K is calculated at 8.5 (Figure 7.29a) and 14.4 (Figure 7.29b), which is sufficient to confirm the static data shown from Figure 7.28 where the viscosity increased by a factor of approximately 2. To highlight the difference between the samples instead of relying on the spectral plots and calculated consistency index values, Figure 7.30 presents photographic imagery of the two samples. The sample without Crystalliser® 110 is on the left, and that with Crystalliser® 110 on the right.

When translated into viscosity versus shear rate profiles the data of Figure 7.31 is obtained, from which one can better appreciate the level of difference the Crystalliser® 110 has on the structure and viscosity of the fat blend. Taken at an arbitrary shear rate of 10 s^{-1} the difference between the samples is marginally over a factor of 2.

In summary, addition of a small amount of behenic acid, a long-chain saturated fatty acid, to fat blends has been shown in both static off-line and dynamic in-line measurements using large deformation viscosity measurement and fitting the data to power-law models to have a dramatic effect on the viscosity of the system. The equipment is highly specialized, but the principles are simple, and the results obtained confirm that value and understanding can be brought at the academic as well as commercial level.

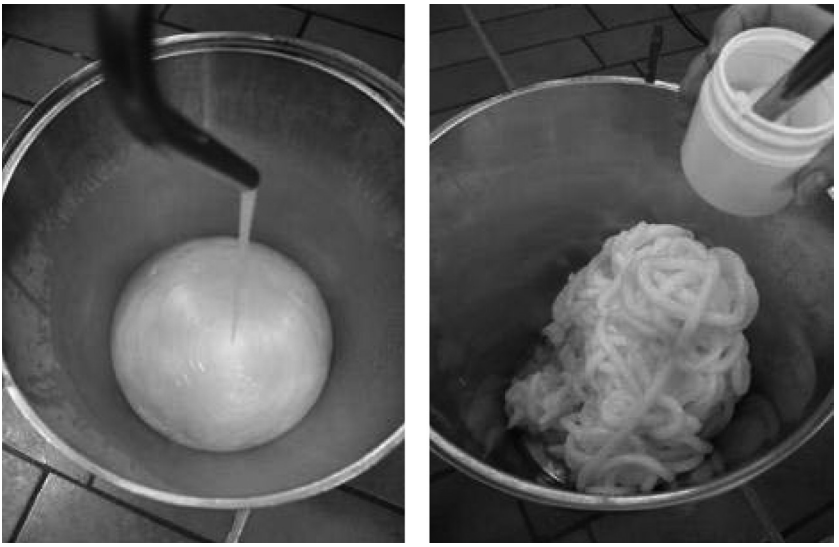


FIGURE 7.30 Fat blend without Crystalliser® 110 (left) and with Crystalliser® 110 as run through the pilot plant and measured with UVP-PD—data are shown in Figure 7.29.

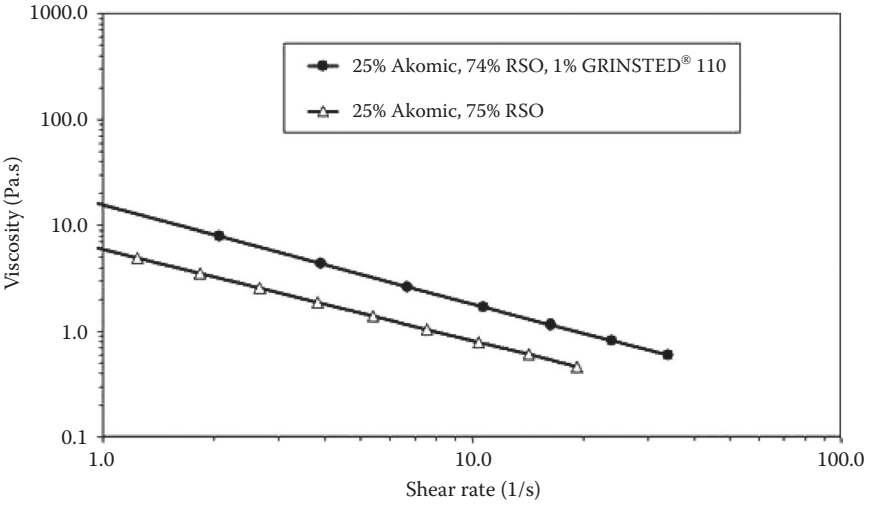


FIGURE 7.31 Viscosity shear rate data for the two fat blends with and without Crystalliser® 110, calculated from measurements performed with the UVP-PD equipment. (Adapted from Young, N.W.G. et al. 2008. *International Journal of Food Science and Technology*, 43(11), 2083–2089.)

7.15 FRUIT SPREADS

The challenge with this case was to document that a new pectin type was an improvement over the then standard in terms of flavor release and spreadability of low-sugar fruit spreads, which are noted for their often poor flavor release. The techniques used

here comprise creep recovery testing, where the sample is exposed to a constant stress for a given time before being allowed to relax back over the same time interval. This is a method that can be used to probe the extreme low-shear rate range and obtain a viscosity value very close to the zero shear value. Also used was classical sensory analysis and proton transfer reaction—mass spectrometry (PTR-MS). A standard low ester amidated (LA) pectin is compared to the new pectin, GRINDSTED® Pectin SF 369 Extra where the first test is to ascertain the low shear viscosity of fruit spreads made at the same sugar level with each of their pectin. In each case, the pectin dosage is 0.6%, the fruit content is 60%, and the sugar level is 35% (Lynenskjold et al., 2008). Figure 7.32, outlining the creep recovery tests carried out on the fruit spreads made with the different pectin types shows a clear and significant difference between them.

The calculated viscosity for each of the fruit spreads were in round figures; 17,000 Pa s GRINDSTED® Pectin SF 369 Extra and 67,000 Pa s for the standard LA pectin, thus a difference approaching a factor of four! This result not only confirms that the viscosity of the fruit spread with GRINDSTED® Pectin SF 369 Extra is considerably less than the standard pectin, but that the likelihood of improved flavor release will be high. This postulation is based on the knowledge that flavor

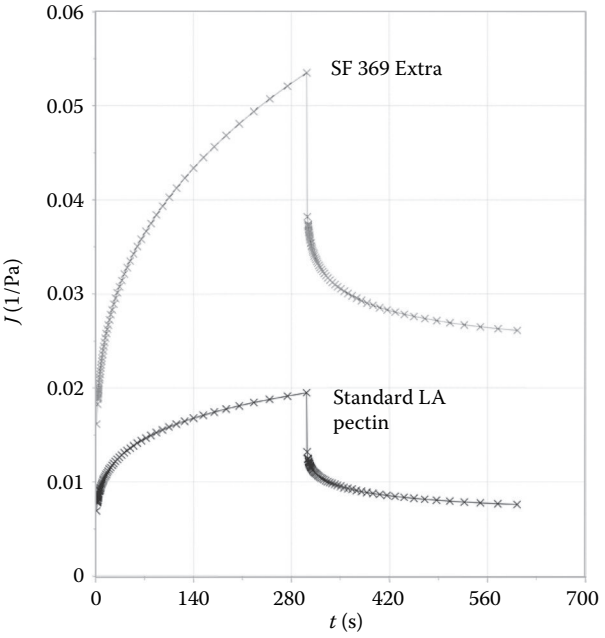


FIGURE 7.32 Shows the creep compliance versus time for the creep recovery profiles of fruit spread with pectin dosage 0.6%, fruit content 60%, and sugar 35% made each with either standard LA pectin or GRINDSTED® Pectin SF 369 Extra. (Adapted from Lynenskjold, E., Butler, I., and Young, N.W.G. 2008. Effect of texture on flavour release in fruit spread applications. In *Gums and Stabilisers for the Food Industry* 14, Royal Society of Chemistry, Cambridge, pp. 181–194.)

release is not diffusion controlled, that is too slow a mechanism; but rather controlled by convective processes, that is, mixing (Morris, 1995). The easier a sample is to mix and break down in the mouth the faster the flavor release will be perceived. Therefore, given that the fruit spread with GRINDSTED® Pectin SF 369 Extra is approximately four times less viscous than the fruit spread with the standard pectin, the ease of mixing should also be correspondingly higher. To test this, use of PTR-MS was made whereby the headspace of the nasal cavity of a subject who ate both fruit spreads was sampled to capture the volatile components released from the fruit spreads. In order to experience flavor these volatile aroma compounds must reach the olfactory receptors. Figure 7.33 represents the experimental setup to find the level or concentration of the main volatile flavor esters which correspond to strawberry, the fruit of choice. These are ethyl butanoate, ethyl hexanoate, and ethyl-2-methylbutanoate.

The results from the PTR-MS for the fruit spread made with GRINDSTED® Pectin SF 369 Extra are given in Figure 7.34, and show the profile for ethyl butanoate at three distinct time points; mouth entry, first swallow, and second swallow. Immediately on entering the mouth, the profile for ethyl butanoate reaches a value of some 16–18, and maintains a value of 15 through the first swallow. Only at the second swallow does the value recede back to baseline levels.

The corresponding results for the fruit spread made with the standard pectin are given in Figure 7.35, where it is obviously apparent of a significant difference. Here, there is simply baseline response as soon as the fruit spread enters the mouth as compared to the sharp increase seen in Figure 7.34. Only by the time of the first swallow does the profile of ethyl butanoate rise above the baseline, but only to level

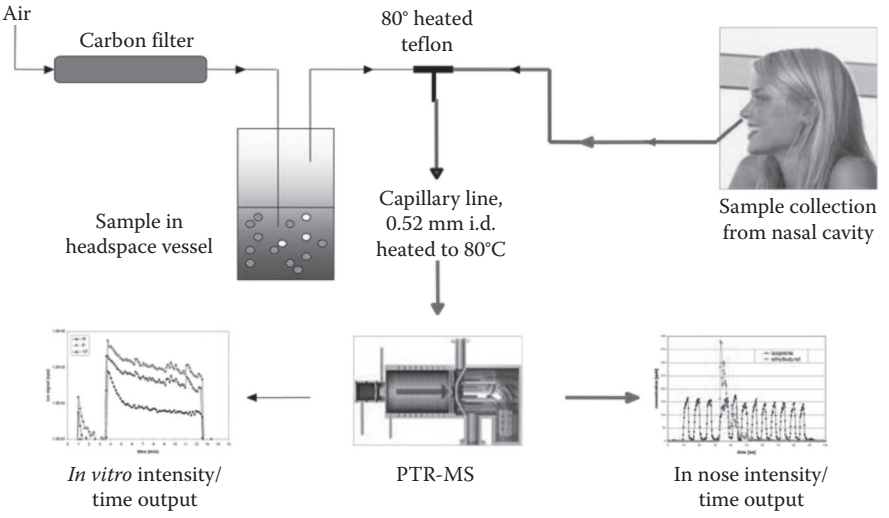


FIGURE 7.33 Experimental setup for *in vitro* and "in nose" analysis by PTR-MS. (Adapted from Lynenskjold, E., Butler, I., and Young, N.W.G. 2008. Effect of texture on flavour release in fruit spread applications. In *Gums and Stabilisers for the Food Industry* 14, Royal Society of Chemistry, Cambridge, pp. 181–194.)

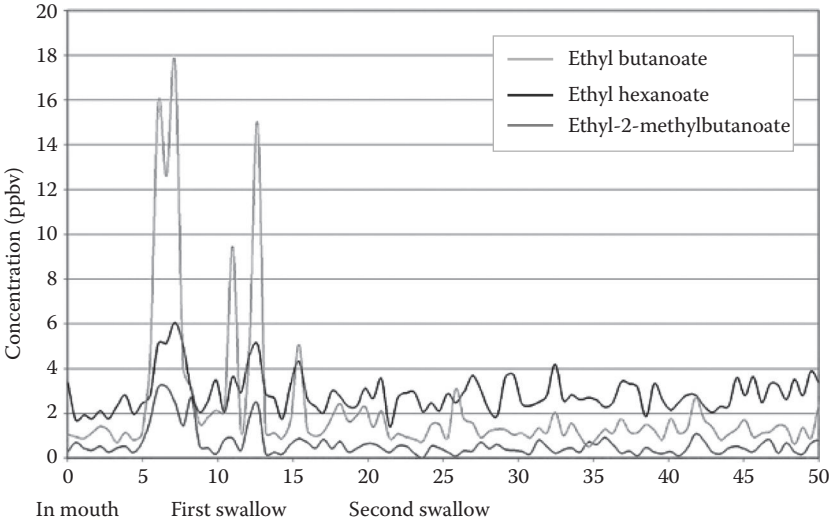


FIGURE 7.34 Flavor release over time profiles for the three main volatile components of strawberry for fruit-spread sample with GRINDSTED® Pectin SF 369 Extra, containing 35% soluble solids. (Adapted from Lynenskjold, E., Butler, I., and Young, N.W.G. 2008. Effect of texture on flavour release in fruit spread applications. In *Gums and Stabilisers for the Food Industry* 14, Royal Society of Chemistry, Cambridge, pp. 181–194.)

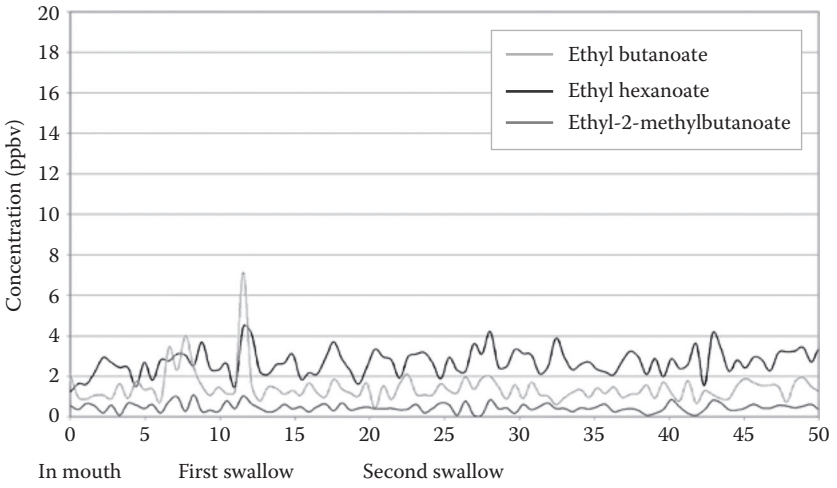


FIGURE 7.35 Flavor release over time profiles for the three main volatile components of strawberry for fruit-spread sample with standard LA pectin, containing 35% soluble solids. (Adapted from Lynenskjold, E., Butler, I., and Young, N.W.G. 2008. Effect of texture on flavour release in fruit spread applications. In *Gums and Stabilisers for the Food Industry* 14, Royal Society of Chemistry, Cambridge, pp. 181–194.)

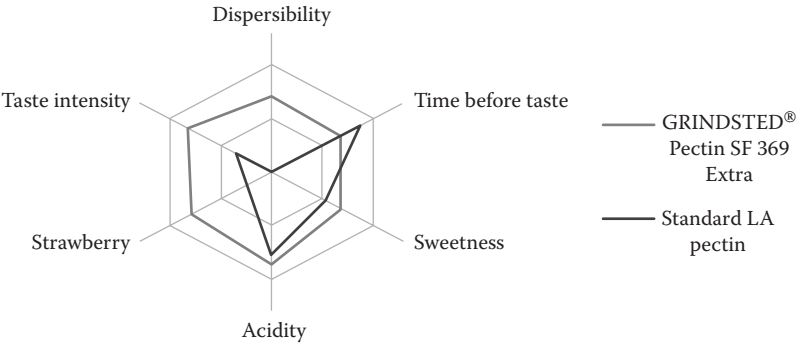


FIGURE 7.36 Sensory attribute profiles for 35% SS strawberry fruit spreads containing either GRINDSTED® Pectin SF 369 Extra or standard LA pectin. (Adapted from Lynenskjold, E., Butler, I., and Young, N.W.G. 2008. Effect of texture on flavour release in fruit spread applications. In *Gums and Stabilisers for the Food Industry* 14, Royal Society of Chemistry, Cambridge, pp. 181–194.)

of 7, fully half the level from Figure 7.34. Thereafter, the profile quickly descends to baseline levels again.

The results agree well with the postulate of lower viscosity samples being able to undergo a faster degree of mixing and therefore a faster release of their volatile aroma compounds (Baines and Morris, 1987). As a final check to confirm the rheology and the PTR-MS results, the fruit spreads were evaluated by a sensory panel for the following parameters: time before taste, sweetness, acidity, strawberry, taste intensity, and dispersibility (in mouth). These results are given in Figure 7.36, which shows that the fruit spread with GRINDSTED® Pectin SF 369 Extra out performs the standard LA pectin fruit spread in all parameters. There is a shorter time before taste, therefore a faster flavor release. The fruit spread is perceived as being sweeter with a more acidic, fresh taste. There is a dramatic increase in the perception that a strawberry fruit spread is being eaten as well as a large increase on the taste/flavor intensity, and finally the dispersibility (degree of mixing) difference is significant.

In summary, the three techniques used to ascertain the flavor release and spreadability of the fruit spread all confirmed the same result: a lesser viscosity boosted considerably the flavor release and taste intensity perception through the system's greater ability to mix and disperse. Equally, this observation can be carried over into the function of spreadability whereby a more easily dispersible system will also be able to be spread out more easily compared to a thicker, more viscous, and in this case gelled one.

7.16 CONCLUSIONS

The theory presented in this chapter is basic and allows a grasp of rheology to be gained quickly and easily; explaining the construction of flow curves to describe the viscosity characteristics of the material. Qualitative and quantitative expressions and evaluations of stability are also demonstrated as being possible. Instrumental

methods to characterize mouth feel and potential flavor perception are discussed as well as how to carry out and utilize the nondestructive small oscillation deformation techniques. This exploratory exposure to rheological theory is then backed up by three short case studies of real systems which illustrate the role rheology can play in actual product development. The results highlight the fact that the value created via rheology can be applied both to commercial and academic ends. Therefore, picking up on the introductory sentence that "rheology is not a key business, but is key to the business," the chapter demonstrates how its guided use coupled with experience and a multidisciplinary approach leads to a complex understanding of one's material from a series of simple rheological measurements. Walking down rheology's path truly represents a step in the right direction.

REFERENCES

Baines, Z.V. and Morris, E.R. 1987. Flavour/taste perception in thickened systems: The effect of guar gum above c*. *Food Hydrocolloids*, **1**(3), 197–205.

Barnes, H.A. 2000. *A Handbook of Elementary Rheology*. University of Wales, Institute of Non-Newtonian Fluid Mechanics, Aberystwyth.

Barnes, H.A. and Walters, K. 1985. The yield stress myth. *Rheologica Acta*, **24**, 323–326.

Carreau, P.J. 1972. Rheolgical equations from molecular network theories. *Transactions of the Society of Rheology*, **16**, 99–107.

Cross, M.M. 1965. Rheology of non-Newtonian fluids: A new flow equation for pseudoplastic systems. *Journal of Colloid Science*, **20**, 417–437.

Cox, W.P. and Merz, E.H. 1958. Correlation of dynamic and steady flow viscosities. *Journal of Polymer Science*, **28**, 619–622.

Dzuy, N.Q. and Boger, D.V. 1983. Yield stress measurement for concentrated suspensions. *Journal of Rheology*, **27**, 321–329.

Dzuy, N.Q. and Boger, D.V. 1985. Direct yield stress measurement with the vane method. *Journal of Rheology*, **29**, 335–347.

Lynenskjold, E., Butler, I., and Young, N.W.G. 2008. Effect of texture on flavour release in fruit spread applications. In *Gums and Stabilisers for the Food Industry* 14, Eds., Williams, P.A. and Phillips, G.O., Royal Society of Chemistry, Cambridge, New York, pp. 181–194.

Miri, T. 2011. Viscosity and oscillation rheology. In *Practical Food Rheology—An Interpretive Approach*, Eds. Norton, I.T., Spyropoulos, F., and Cox, P., Wiley Blackwell, Oxford, UK, pp. 7–28.

Morris, E.R. 1995. Polysaccharide rheology and in-mouth perception. In *Food Polysaccharides and Their Applications*, Ed., Stephens, A.M., Marcel Dekker Inc., New York, pp. 517–546.

Raju, K.V.S.N., Krishna, D., Rama Devi, G., Reddy, P.J., and Yaseen, M. 1993. Assessment of applicability of Carreau, Ellis and cross models to the viscosity data of resin solutions. *Journal of Applied Polymer Science*, **48**, 2101–2112.

Rao, M.A. 2007. *Rheology of Fluid and Semisolid Foods*, 2nd Ed. Springer, New York.

Sakamoto, M., Maruo, K., Kuiryama, J., Kuono, M., Ueno, S., and Sato, K. 2003. Effects of adding polyglycerol behenic acid esters on the crystallisation of palm oil. *Journal of Oleo Science*, **52**, 639–645.

Scott Blair, G.W. 1933. On the nature of yield-value. *Physics*, **4**, 113–118.

Wassell, P. and Young, N.W.G. 2007. Food applications of *trans* fatty acid substitutes. *International Journal of Food Science and Technology*, **42**(5), 503–517.

Wassell, P., Bonwick, G., Smith, C.J., Almiron-Roig, E., and Young, N.W.G. 2010a. Towards a multidisciplinary approach to structuring in reduced saturated fat based

systems—A review. *International Journal of Food Science and Technology*, **45**(4), 642–655.

Wassell, P., Wiklund, J., Stading, M., Bonwick, G., Smith, C., Almiron-Roig, E., and Young, N.W.G. 2010b. Ultrasound Doppler based in-line viscosity and solid fat profile measurement of fat blends. *International Journal of Food Science and Technology*, **45**(5), 877–883.

Watson, J.H. 2004. The diabolical case of the recurring yield stress. *Applied Rheology*, **14**(1), 40–45.

Wiklund, J., Shahram, I., and Stading, M. 2007. Methodology for in-line rheology by ultrasound Doppler velocity profiling-and pressure difference techniques. *Chemical Engineering Science*, **62**, 4277–4293.

Winter, H.H. and Chambon, F. 1986. Analysis of linear viscoelasticity of a crosslinking polymer at the gel point. *Journal of Rheology*, **30**, 367–382.

Young, N.W.G. 2002. The yield stress phenomenon and related issues: An industrial view. In *Gums and Stabilisers for the Food Industry* 11, Eds. Williams, P.A. and Phillips, G.O., Royal Society of Chemistry, London, pp. 226–234.

Young, N.W.G, Kappel, G., and Bladt, T. 2003. A polyuronan blend giving novel synergistic effects and bake-stable functionality to high soluble solids fruit fillings. *Food Hydrocolloids*, **17**, 407–418.

Young, N.W.G., Wassell, P., Wiklund, J, and Stading, M. 2008. Monitoring struturants of fat blends with ultrasound based in-line rheometery (ultrasonic velocity profiling with pressure difference). *International Journal of Food Science and Technology*, **43**(11), 2083–2089.

Young, N.W.G. 2011. Introduction—Why the interpretive approach? In *Practical Food Rheology—An Interpretive Approach*, Eds. Norton, I.T., Spyropoulos, F., and Cox, P., Wiley Blackwell, Oxford, UK, pp. 1–6.

Zhong, Q. and Daubert, C. 2007. Food rheology. In *Handbook of Farm, Dairy and Food Machinery*, Ed. Kutz, M., Willliam Andrew Inc., London, pp. 391–414.

8 Fluid Mechanics in Food Process Engineering

Ricardo D. Andrade P., Carmen E. Pérez C., and German J. Narvaez G.

CONTENTS

8.1 Introduction 218
8.2 Properties of Liquids 219
8.2.1 Pressure 219
8.2.2 Density 220
8.2.3 Specific Weight 220
8.2.4 Specific Gravity 220
8.2.5 Surface Tension 221
8.2.6 Viscosity 222
8.2.7 Apparent Viscosity 225
8.2.7.1 Shear-Thinning Fluids 225
8.2.7.2 Shear-Thickening Fluids 226
8.2.7.3 Plastic Fluid 227
8.2.7.4 Time-Independent Non-Newtonian Fluids 227
8.2.7.5 Rheological Models to Describe the Behavior of Non-Newtonian Fluids 227
8.3 Fluid Statics 229
8.3.1 Pressure Measurements 231
8.3.1.1 Barometer 231
8.3.1.2 Piezometer 232
8.3.1.3 U-Tube Manometer 233
8.3.1.4 Inclined-Tube Manometer 235
8.3.2 Buoyant Force and Archimedes' Principle 237
8.4 Fluid Dynamics 238
8.4.1 Continuity Equation 239
8.4.2 Bernoulli Equation 240
8.5 Flow in a Circular Pipe 242
8.5.1 Reynolds Number 243
8.5.2 Critical Reynolds Number 244
8.5.3 Kinetic Energy Correction Factor 244
8.5.4 Energy Losses in Flow 245
8.5.5 Friction Factor for Laminar Regimes 246
8.5.5.1 Newtonian Fluids 247

8.5.5.2 Power Law Fluids 247
8.5.5.3 Bingham Plastic Fluids 247
8.5.6 Friction Factor for Turbulent Regimes 247
8.5.6.1 Newtonian Fluids 248
8.5.6.2 Power Law Fluids 248
8.5.6.3 Bingham Plastic Fluids 249
8.5.7 Minor Losses 250
8.5.7.1 Loss Coefficient Due to Sudden Contraction 250
8.5.7.2 Loss Coefficient Due to Sudden Expansion 251
8.5.7.3 Loss Coefficient Due to Pipe Fittings 251
8.6 Pumps 252
8.6.1 Pump Characteristics 252
8.6.1.1 Overall Efficiency 253
8.6.1.2 Net Positive Suction Head 253
8.6.2 Types of Pump 259
8.6.2.1 Centrifugal Pumps 259
8.6.2.2 Positive-Displacement Pumps 260
8.6.2.3 Screw Pumps 260
References 260

8.1 INTRODUCTION

Fluid mechanics is the area of physics that mathematically describes the behavior of fluids at rest (fluid statics) or in motion (fluid dynamics) and the subsequent effects of the fluid upon its boundaries, which may be either solid surfaces or interfaces with other fluids. From the point of view of fluid mechanics, all matter consists of only two states: fluid and solid. The difference lies in the reaction of the two to an applied shear or tangential stress.

A solid tends to shatter when subjected to very large stresses, but it can withstand moderate shear stress for an indefinite period. To be more exact, when a shear stress is first applied to a rigid material, it deforms slightly, but then springs back to its original shape when the stress is relieved. Conversely, a fluid is a substance that deforms continuously when acted on by a shear stress of any magnitude. Incidentally, this does not preclude the possibility that such an element may offer resistance to shear stress; however, any resistance must be incapable of preventing a change in shape from eventually occurring, which implies that the force of resistance disappears with the rate of deformation (Çengel and Cimbala, 2010; Munson et al., 2009). Furthermore, the fluids are conventionally classified as either liquids or gases.

Moreover, molecules of any substance exhibit at least two types of force; an attraction force that diminishes with the square of the distance between the molecules and a force of repulsion that strengthens as the molecules move very close together. In solids, the force of attraction is so dominant that the molecules essentially remain fixed in position, while the resisting force of repulsion prevents them from collapsing into each other. In a liquid, the molecules remain sufficiently close together that the force of attraction maintains some coherence within the substance. However, the

molecules of a gas are so far apart, and move with such high velocity, that the forces of attraction are relatively small (Rao et al., 2005; Sahin and Sumnu, 2006). A gas will expand to fill any closed vessel within which it is contained.

In any commercial food processing plant, the movement of liquid foods from one location to another becomes an essential operation. Moreover, powders and small particulate foods are more easily handled as fluids by fluidization. The range of liquid foods encountered in a processing plant is extremely wide, encompassing foods with distinctly different flow properties, from milk to tomato paste. Various types of systems are used for moving raw or unprocessed liquid foods as well as processed liquid products before packaging (Singh and Heldman, 2009).

Fluids (liquids and gases) in food processing plants are typically transported in closed conduits commonly called pipes if they are round. Although sometimes used in processing plants, open drains are generally avoided for reasons of sanitation. Within the design of these systems in food processing is the need for sanitation to maintain product quality. The transport system must comply with the principles of hygienic design and operation. The equipment surfaces coming into contact with the food should be made of corrosion-resistant stainless steel, and should be cleanable with a cleaning system in place (Hoogland and Vlaardingen, 2005; Maroulis and Saravacos, 2003; Singh and Heldman, 2009).

8.2 PROPERTIES OF LIQUIDS

The study of fluid mechanics by necessity includes a statement on the basic laws governing fluid motion. These laws include Newton's laws of motion, the conservation of mass, and the first and second laws of thermodynamics. Before we can proceed, however, it will be necessary to define and discuss certain fluid properties that are essential for the understanding of flow or static condition of fluids. In the following sections, the properties that play an important role in the analysis of fluid behavior are considered.

8.2.1 Pressure

Pressure is one of the elements normally calculated in fluids problem. Pressure is the force per unit area applied in a direction perpendicular to the surface of an object (Equation 8.1). The standard unit for pressure is the pascal (Pa), which is a newton per square meter (N/m^2). Pressure can be expressed in two different ways; it can be expressed as gage pressure, and an absolute pressure. Gage pressure is the pressure relative to the local atmospheric or ambient pressure.

$$P = \frac{F}{A} \tag{8.1}$$

EXAMPLE 8.1

A Bourdon pressure gage connected to a tank reads 500 kPa at a location where the atmospheric pressure is 100 kPa (see Figure 8.1). Determine the absolute pressure in the tank.

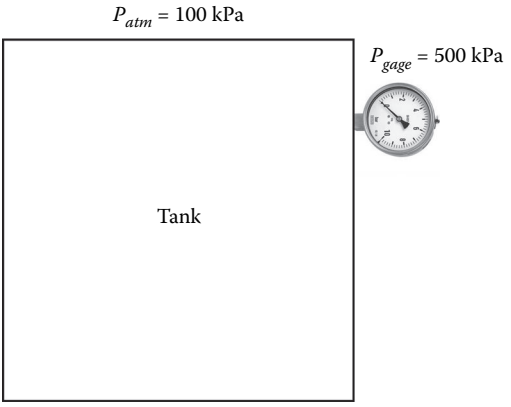


FIGURE 8.1 Example 8.1.

The absolute pressure in the tank is determined from

$$P_{abs} = P_{gage} + P_{atm} = 500\,\text{kPa} + 100\,\text{kPa} = 600\,\text{kPa}$$

8.2.2 Density

The density of a fluid (ρ) is defined as its mass (m) per unit volume (V). In SI units, ρ has units of kg/m^3. Density is an indication of how matter is composed in a body. Materials with more compact molecular arrangements have higher densities. In general, liquids are about three orders of magnitude denser than gases at atmospheric pressure. The density of a gas is strongly influenced by both pressure and temperature. Unlike gases, in liquids, variations in pressure and temperature generally only have a small effect on the value of ρ, for example, the density of water increases by only 1% if the pressure is increased by a factor of 220 (White, 2003). Thus, most liquid flows are treated analytically as nearly "incompressible."

$$\rho = \frac{m}{V} \tag{8.2}$$

8.2.3 Specific Weight

The specific weight of a fluid (γ) is its weight per unit volume. The SI unit for specific weight is N/m^3, while the English unit is lb$_f$/ft^3. Density and specific weight are simply related by gravity:

$$\gamma = g\,\rho \tag{8.3}$$

8.2.4 Specific Gravity

Specific gravity (SG) is the ratio of a fluid density to a standard reference fluid, water (for liquids), and air (for gases):

$$SG_{liquid} = \frac{\rho_{liquid}}{\rho_{water}} \tag{8.4}$$

$$SG_{gas} = \frac{\rho_{gas}}{\rho_{air}} \tag{8.5}$$

Usually, the specified temperature is taken as 4°C.

8.2.5 Surface Tension

You may have noticed water in spherical droplets emerging from a tap; this can be explained by surface tension. A molecule in the bulk of the liquid will be subjected to forces of attraction from all directions. These effectively cancel each other out. However, a molecule at the surface of a liquid will be subjected to a net attraction by the molecules in the bulk of the liquid. Therefore, the surface of the liquid is in a state of tension. Molecules at the surface of the liquid are attracted inward because of van der Waals intermolecular attractions. This creates a force in the surface that tends to minimize the surface area, and this force is known as surface tension (Lewis, 2006; Sahin and Sumnu, 2006). Hence, surface tension (σ) is measured as the energy required to increase the surface area of a liquid by a unit of area, and it is expressed in units of force per unit length, that is, in N/m in SI units.

Among common phenomena associated with surface tension is the rise of a liquid in a capillary tube. Capillarity is the property of exerting forces on fluids by fine tubes or porous media; it is due to both cohesion and adhesion (Finnemore and Franzini, 2002). When the cohesion is of a lesser effect than adhesion, the liquid will wet a solid surface it touches and rise at the point of contact (Figure 8.2a); if cohesion predominates, the liquid surface will depress at the point of contact (Figure 8.2b).

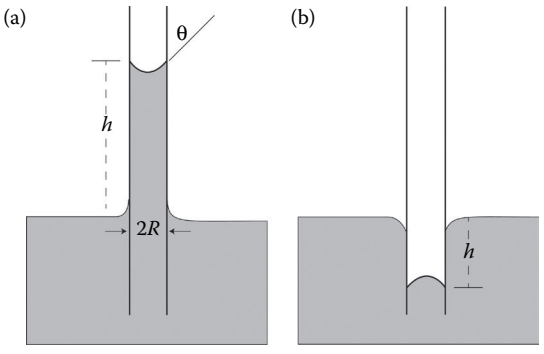


FIGURE 8.2 Effect of capillary action in small tubes.

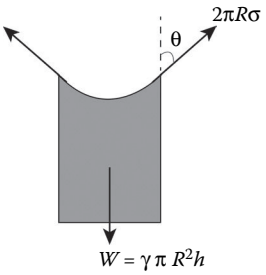


FIGURE 8.3 Free-body diagram for calculating column height.

From the summation of forces in the free-body diagram (Figure 8.3), it can be seen that the vertical force due to surface tension ($2\pi R\sigma\cos\theta$) for equilibrium must balance the weight ($\rho g \pi R^2 h$). Thus

$$\sum F_y = 2\pi R\sigma\cos\theta - mg = 0 \tag{8.6}$$

$$2\pi R\sigma\cos\theta = \rho g \pi R^2 h \tag{8.7}$$

$$h = \frac{2\sigma\cos\theta}{\rho g R} \tag{8.8}$$

EXAMPLE 8.2

A hollow glass tube, having a diameter of 2 mm, is inserted vertically into a container of mercury at 20°C (see Figure 8.2b). How far will the column of mercury in the tube be depressed?

Given data:
D = 2 mm ⇒ R = 1 mm = 1×10^{-3} m, θ = 130°
Mercury at 20°C: ρ = 13,600 kg/m^3, σ = 0.465 N/m

Substituting the numerical values (Equation 8.8), the capillary drop is determined to be

$$h = \frac{2(0.465\ \text{N/m})(\cos 130^\circ)}{(13{,}600\ \text{kg/m}^3)(9.8\ \text{m/s}^2)(1\times 10^{-3}\ \text{m})}$$

$$h = -4.485\times 10^{-3}\ \text{m} = -4.485\ \text{mm}$$

8.2.6 Viscosity

When you pour yourself a glass of milk, the liquid flows freely and quickly, but when you pour honey on your pancakes, that liquid flows slowly. The difference is fluid friction, both within the fluid itself and between the fluid and its surroundings. This

property of fluids is called viscosity. Viscosity is the second most important variable, which characterizes specific fluid-mechanical behavior (White, 2003). This relates the local stresses in a moving fluid to the strain rate of the fluid element. When a fluid is sheared, it begins to move at a strain rate inversely proportional to a property called its coefficient of viscosity.

Consider a hypothetical experiment in which a fluid is placed between two parallel plates, sufficiently large that it can neglect edge conditions, a small distance Y apart. The lower plate is stationary, while the upper plate is moved parallel to the lower one with a velocity U due to a force F corresponding to some area A of the moving plate. Particles of fluid in contact with each plate will adhere. The action is much as if the fluid were made up of a series of thin sheets, each of which slips slightly relative to the next (Figure 8.4a). Thus, the fluid velocities must be U when in contact with the plate at the upper boundary and zero at the lower boundary. If the velocity U is not too high, and if there is no net flow of fluid through the space, the velocity profile will be linear (Figure 8.4b).

For a large class of fluids in laminar flow, the force per unit area that should be applied is proportional to the velocity and distance ratio, according to the following equation:

$$\frac{F}{A} \propto \frac{U}{Y} \tag{8.9}$$

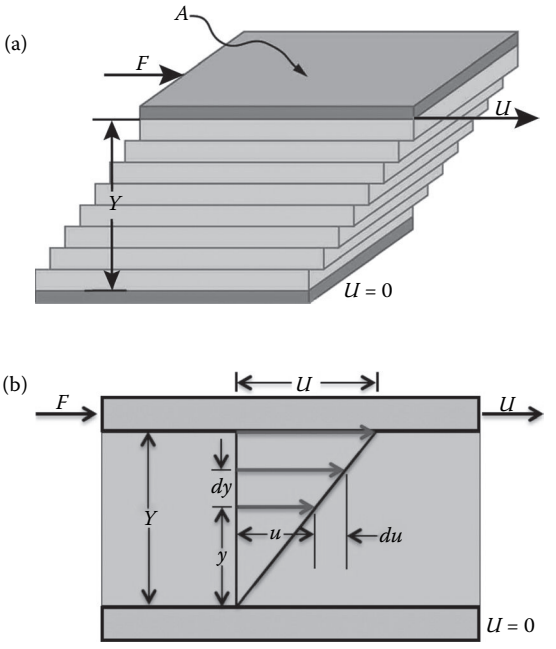


FIGURE 8.4 Schematic diagram showing flow of a fluid between two plates.

For certain applications, it is convenient to express the latter equation in a more explicit way. It can be seen from similar triangles (see Figure 8.4b) that it can replace *U/Y* by the velocity gradient *du/dy*. If we now introduce a constant of proportionality μ, the shear stress τ between any two thin sheets of fluid can be expressed as

$$\tau \equiv \frac{F}{A} = -\mu \frac{du}{dy} \tag{8.10}$$

where μ is the coefficient of viscosity, the absolute viscosity, the dynamic viscosity, or simply fluid viscosity.

Equation 8.10 is called Newton's law of viscosity, and states that "the shear stress between adjacent fluid layers is proportional to the negative value of the velocity gradient between the two layers." All fluids that follow this law are called Newtonian fluids. Fluids that do not obey Newton's law of viscosity (Equation 8.10) are, by definition, non-Newtonian.

The dimensions of viscosity are force per unit area divided by the velocity gradient. In SI the unit of viscosity is Ns/m^2 whereas in CGS, the unit of viscosity is the poise (P), named after Jean Louis Poiseuille (1799–1869). Handbooks commonly quote viscosity in centipoise (1 cP = 0.01 P), which is a very convenient unit of viscosity because the viscosity of water at 20°C is 1 cP.

Viscosity may be further subdivided into two distinct forms: dynamic viscosity and kinematic viscosity. Dynamic viscosity (μ), a property representing shear stress as proportional to the strain rate, has an SI unit Pa.s. Kinematic viscosity ($\nu = \mu/\rho$) describes shifts in momentum and has SI units of m^2/s, but is also commonly represented by the Stoke (cm^2/s).

EXAMPLE 8.3

A block of mass of 6 kg slides down an inclined plane (30°) while lubricated by a thin film of oil (μ = 0.40 Pa.s), as in Figure 8.5. The film contact area is 30 cm^2 and its thickness is 1 mm. Assuming a linear velocity distribution in the film, calculate the terminal velocity of the block.

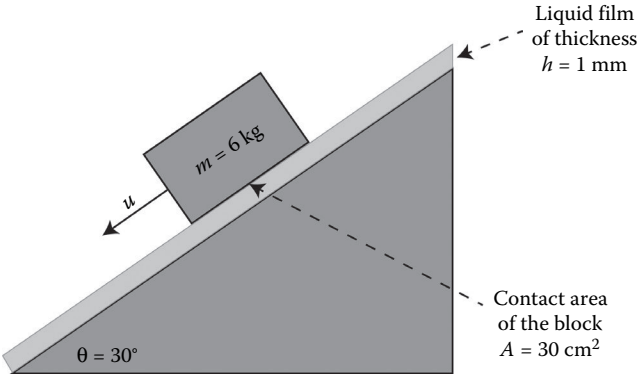


FIGURE 8.5 Example 8.3.

Given data:
$m = 6$ kg, $\theta = 30°$, $\mu = 0.40$ Pa.s $= 0.40$ kg/m.s, $A = 30$ cm$^2 = 3 \times 10^{-3}$ m^2, $h = 1$ mm $= 1 \times 10^{-3}$ m

Let "x" be down the incline, in the direction of u. Terminal velocity (u_t) means constant velocity, and acceleration is zero. Then a force balance in the x direction gives

$$\sum F_x = mg \sin\theta - F_\tau = 0$$

where F_τ is shearing force, $F_\tau = \tau A$, and substituting Equation 8.10, $F_\tau = \mu\, u_t\, A/h$. Therefore

$$\sum F_x = mg\sin\theta - \mu \frac{u_t}{h} A = 0$$

Solving for the terminal velocity

$$u_t = \frac{hmg\sin\theta}{\mu A}$$

Replacing the values

$$u_t = \frac{(1 \times 10^{-3}\text{ m})(6\text{ kg})(9.8\text{ m/s}^2)(\sin 30°)}{(0.40\text{ kg/m.s})(3 \times 10^{-3}\text{ m}^2)}$$

$$u_t = 24.5\text{ m/s}$$

8.2.7 Apparent Viscosity

Many liquid foods are non-Newtonian, including emulsions, suspensions, and concentrated solutions that contain starches, pectins, gums, and proteins. For a non-Newtonian fluid, the flow curve (shear stress vs. shear rate) is nonlinear and does not pass through the origin, that is, the apparent viscosity (η_{app}), the shear stress divided by the shear rate, in such systems is different at each point on the shear stress versus shear rate curve (see Figure 8.6).

The properties of non-Newtonian fluids can be classified as time-independent and time-dependent. There are three important types of time-independent non-Newtonian fluids, namely, shear-thinning fluids (pseudoplastic), shear-thickening fluids (dilatant), and plastic fluids (Bingham or Casson plastic). Figure 8.7 illustrates the shear stress versus shear rate curve for a time-independent non-Newtonian fluid.

8.2.7.1 Shear-Thinning Fluids

A pseudoplastic, or shear-thinning, fluid is characterized by an apparent viscosity that decreases with increasing shear rate. This behavior is assumed to be caused by decreasing molecular interactions within the molecular structure of the fluid during flow. In the case of flowing macromolecules, additional effects of the unfolding and reorientation of molecules may occur (Ibarz and Barbosa-Cánovas, 2003;

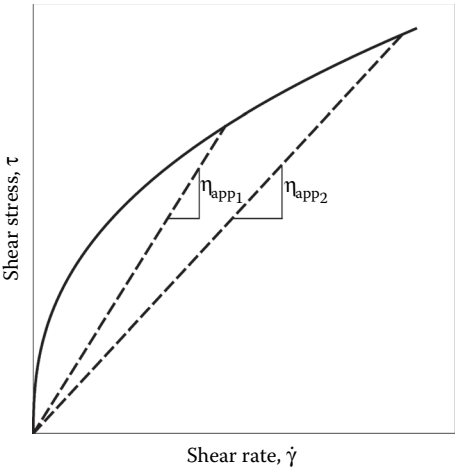


FIGURE 8.6 Determination of apparent viscosity from plot of shear stress versus shear rate.

Rao, 2005). Shear-thinning is a common behavior and is exhibited by emulsions, and suspensions such as concentrated fruit juices and purees.

8.2.7.2 Shear-Thickening Fluids

A dilatant, or shear-thickening, fluid increases the apparent viscosity with increasing shear rate. The accepted mechanism of dilatancy depends on four factors that increase the particle interaction; these are concentration, anisotropy of shape, size, and density. In systems of high concentration, the application of shear produces a

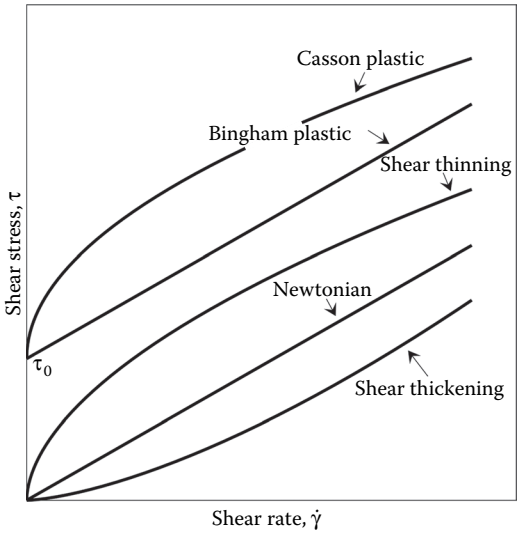


FIGURE 8.7 Rheograms for time-independent fluids.

rearrangement of the solids, causing a mechanical "jam." Nonspherical particles process when subjected to shear; this effectively increases the occupied volume and the effective concentration. Large or denser particles possess greater inertia, and when shear is applied, they are momentarily retarded, then accelerated. The energy expenditure required to accomplish this result brings an additional resistance to flow or a higher apparent viscosity than the usual (Braun and Rosen, 2008). Shear-thickening behavior is less common but is found in liquid chocolate and corn flour suspension.

8.2.7.3 Plastic Fluid

Plastic fluid is characterized by the existence of a yield stress (τ_0), which must be exceeded before the fluid deforms or flows. Once the magnitude of the external stress has exceeded the value of the yield stress, the response of these liquids can be similar to a Newtonian liquid; in that case, they are called Bingham plastic. However, if the response of a liquid, after the yield stress is applied is similar to a shear-thinning flow, then these liquids are called Casson plastic. These fluids consist of three-dimensional structures of sufficient rigidity to resist any external stress less than τ_0. For stress levels greater than τ_0, however, the structure breaks down and the substance behaves like a viscous material (Chhabra and Richardson, 2011; Singh and Heldman, 2009).

Strictly speaking, it is virtually impossible to ascertain whether any real material has a true yield stress or not, but nevertheless the concept of a yield stress has proved to be convenient in practice because some materials closely approximate this type of flow behavior. Furthermore, it is interesting to note that a plastic fluid also displays an apparent viscosity, which decreases with increasing shear rate. It is thus possible to regard these materials as possessing a particular class of shear-thinning behavior (Chhabra and Richardson, 1999; Chhabra and Richardson, 2011).

In the preparation of certain foods, it is important to achieve a required yield stress. For example, whipped cream must have a sufficiently high yield stress in order to hold its shape as a decorative dessert topping.

8.2.7.4 Time-Independent Non-Newtonian Fluids

In some non-Newtonian foods, the apparent viscosity varies with time when the shear rate is held constant. Two different types of fluid behavior can be distinguished: thixotropic and rheopectic (see Figure 8.8). In thixotropic fluids, at a fixed shear rate, the viscosity decreases with time, whereas the viscosity of a rheopectic fluid increases with time. The reason for this variation with t is related to breaking bonds between particles or molecules or in changes to the at-rest shape of long molecules. Thixotropic behavior has been noted in condensed milk, mayonnaise, and egg whites. Rheopectic behavior is observed in gelatinized cross-linked waxy maize starch dispersions (Rao, 2005; Steffe, 1996).

8.2.7.5 Rheological Models to Describe the Behavior of Non-Newtonian Fluids

For non-Newtonian fluids, nonlinear models are needed to describe the changes in viscosity with shear rate or shear stress. Many phenomenological and empirical

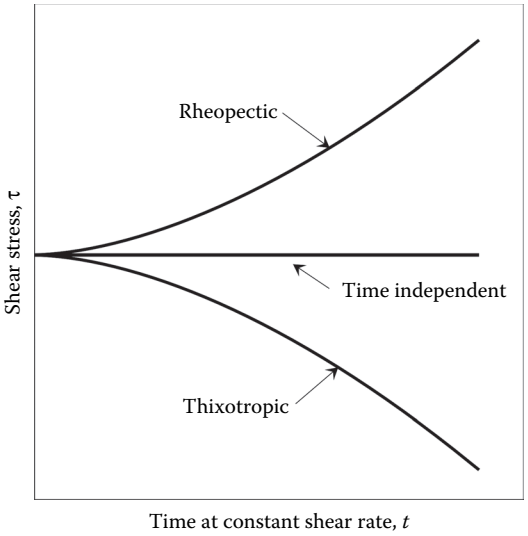


FIGURE 8.8 Rheograms for time-dependent fluids.

models have been reported in the literature. Table 8.1 presents the most used models to characterize rheological behavior time-independent fluids.

The simplest of these nonlinear models is a power law or Ostwald–de Waele relationship. In this model, if $n < 1$, the fluid exhibits shear-thinning properties, for $n = 1$, the fluid shows Newtonian behavior, and if $n > 1$, the fluid shows shear-thickening behavior. The Bingham plastic model is the simplest equation for describing the flow behavior of a fluid with a yield stress and in steady one-dimensional shear. The Casson model has been adopted by the International Office of Cocoa and Chocolate (IOCC) for interpreting chocolate flow behavior. The Casson and Bingham plastic models are similar because they both have a yield stress. A general relationship to describe the behavior of non-Newtonian fluids is the Herschel–Bulkley model. This model is very convenient because Newtonian, shear-thinning, shear-thickening,

TABLE 8.1
Rheological Models to Describe the Behavior of Time-Independent Fluids

Model	Equation
Power law	$\tau = K\dot{\gamma}^n$
Bingham plastic	$\tau = \tau_0 + K\dot{\gamma}$
Casson	$\sqrt{\tau} = \sqrt{\tau_0} + K\sqrt{\dot{\gamma}}$
Herschel–Bulkley	$\tau = \tau_0 + K\dot{\gamma}^n$

Bingham plastic, and Casson plastic behaviors may be considered special cases (Ibarz and Barbosa-Cánovas, 2003; Steffe, 1996).

8.3 FLUID STATICS

Many fluid problems do not involve motion; they concern the pressure distribution in a static fluid and its effect on solid surfaces and on floating and submerged bodies. A static fluid is one that is at rest and, therefore, is not accelerating. Such a fluid is in equilibrium, and Newton's second law is the cornerstone for analyzing its properties. According to the second law, there is no net force acting on any object in equilibrium. In this condition, for equilibrium, the pressure is related to the density of the liquid, the gravity, and the depth. Pressure forces are called surface forces. The gravitational force is called the body force as it acts on the whole body of the fluid (Munson et al., 2009; Nakayama and Boucher, 1998; White, 2003).

Consider an infinitesimal volume element in rectangular parallelepiped shape, as shown in Figure 8.9.

A force balance in the x direction gives

$$\rho\, dx\, dy\, dz + P\, dy\, dz - \left(P + \frac{\partial P}{\partial x} dx\right) dy\, dz = 0 \tag{8.11}$$

Simplifying

$$\frac{\partial P}{\partial x} = \rho\, x \tag{8.12}$$

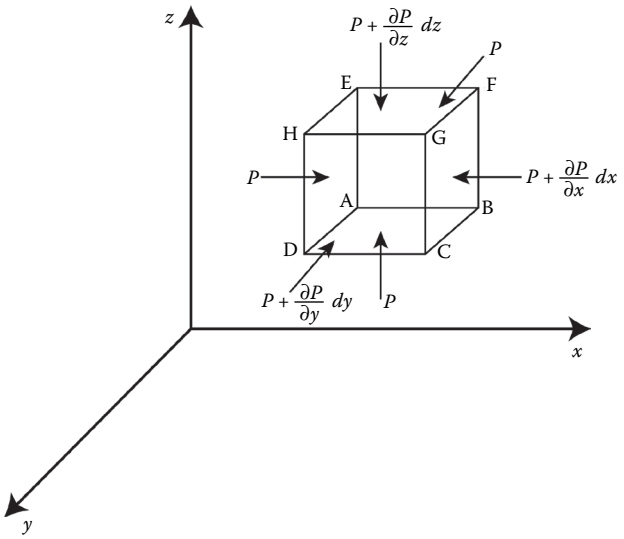


FIGURE 8.9 Pressure variable for an infinitesimal volume element.

For the y and z axis

$$\frac{\partial P}{\partial y} = \rho y \tag{8.13}$$

$$\frac{\partial P}{\partial z} = \rho z \tag{8.14}$$

Multiplying Equations 8.12, 8.13, and 8.14 for dx, dy, and dz, respectively, and adding them, gives

$$\frac{\partial P}{\partial x}dx + \frac{\partial P}{\partial y}dy * \frac{\partial P}{\partial z}dz = \rho\,(xdx + y\,dy + z\,dz) \tag{8.15}$$

or

$$dP = \rho(xdx + ydy + zdz) \tag{8.16}$$

In a fluid at rest, the only external force acting is that of gravity. The pressure gradient is zero along any horizontal line, that is, planes normal to the direction of gravity. Therefore, $x = 0$, $y = 0$, and $z = -g$.

$$dP = -\rho g\,dz \quad \text{or} \quad dP = -\gamma\,dz \tag{8.17}$$

Equation 8.17 is the fundamental equation for fluids at rest and can be used to determine how pressure changes with elevation. The integration of this equation requires an assumption about the gravity distribution and density. For most engineering applications, the variation in g is negligible. In addition, for liquids, the variation in density is usually negligible (incompressible fluids). Gases and liquids are usually treated differently. For liquids, which are generally incompressible fluids, Equation 8.17 gives

$$P_2 - P_1 = -\rho g\,(z_2 - z_1) \quad \text{or} \quad P_2 - P_1 = \gamma h \tag{8.18}$$

This equation indicates that the pressure gradient $(P_2 - P_1)$ in the vertical direction is negative; that is, liquids at the base of a vessel are at a higher pressure than at the surface, owing to the weight of the liquid above (the hydrostatic head). This is important in the design of holding tanks and processing vessel, to ensure that the vessels are constructed using materials of adequate strength. A large hydrostatic head also affects the boiling point of liquids, which is important in the design of some types of evaporation equipment (Fellows, 2000). Furthermore, the pressure will be the same at the same level in any connected static fluid whose density is constant or a function of pressure alone. A consequence is that the free surface of a liquid will seek a common level in any container, where the free surface is universally exposed

to the same pressure. Finally, in view of the fact that the pressure in a fluid depends on the depth and on the value of P_0, any increase in pressure at the surface must be transmitted to every other point in the fluid. This concept is called Pascal's law.

Moreover, gases are compressible, with a density nearly proportional to pressure. Thus, density must be considered as a variable in Equation 8.17 if the integration carries over large pressure changes. For an ideal gas

$$\rho = \frac{PM}{RT} \tag{8.19}$$

where M is molar mass and R is the universal gas constant. In SI units, R has the value 8.314 J/mol K. Substituting this density into Equation 8.17

$$dP = -\frac{PMg}{RT}dz \tag{8.20}$$

Separate the variables and integrate between points 1 and 2.

$$\int_1^2 \frac{dP}{P} = -\frac{Mg}{R}\int_1^2 \frac{dz}{T} \tag{8.21}$$

The integral over z requires an assumption about the temperature variation $T(z)$. One common approximation is that the temperature is assumed to be constant. Performing the integration and solving for P_2

$$P_2 = P_1 \exp\left[-\frac{Mg}{RT}(z_2 - z_1)\right] \tag{8.22}$$

8.3.1 Pressure Measurements

Pressure is an important variable in fluid mechanics, and many instruments have been devised for its measurement. Many devices are based on hydrostatics such as barometers and manometers (piezometer tube, U-tube manometer, and inclined-tube manometer), that is, determine the pressure through measurement of a column of a liquid using the pressure variation with elevation equation for an incompressible fluid (Equation 8.18).

8.3.1.1 Barometer

A barometer is an instrument for measuring atmospheric pressure; thus, atmospheric pressure is often referred to as barometric pressure. The mercury barometer consists of a glass tube closed at one end with the open end immersed in a container of mercury, as shown in Figure 8.10. This causes a near vacuum in the closed upper end because mercury has an extremely small vapor pressure at room temperature (0.16 Pa at 20°C).

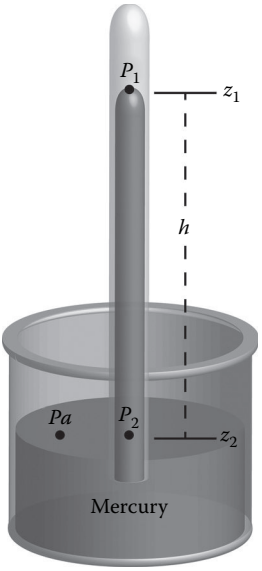


FIGURE 8.10 Mercury barometer.

The pressure at point 2 (P_2) is equal to the atmospheric pressure (P_{atm}), and the pressure at 1 (P_1) can be taken to be zero since there is only mercury vapor above point 1 ($P_1 \approx 0$). Writing a force balance in the vertical direction gives

$$P_2 = -\rho_{Hg}\, g\, (z_2 - z_1) \quad \text{or} \quad P_{atm} = \rho_{Hg}\, g\, h \tag{8.23}$$

Atmospheric pressure is sometimes expressed in terms of the height, h, in millimeters or inches of mercury. Mercury is used because it is the heaviest common liquid and it has an extremely small vapor pressure. Note that if water were used instead of mercury, the height of the column would have to be approximately 10.3 m rather than 760 mm of mercury (mm Hg) for standard atmospheric pressure at sea level. The unit mmHg is also called the torr in honor of Evangelista Torricelli (1608–1647), who invented the barometer. Therefore, 1 atm = 760 torr = 101.325 kPa.

8.3.1.2 Piezometer

A piezometer is one of the simplest forms of manometers. It consists of a fluid reservoir and a tube opened to the atmosphere (see Figure 8.11). As the tube is open to the atmosphere, the pressure measured is relative to atmospheric pressure, so it is a gage pressure. A piezometer is a device used to measure static liquid pressure in a system by measuring the height to which a column of the liquid rises against gravity. Although the piezometer is a very simple and accurate pressure-measuring device, it has several disadvantages. It is only suitable if the pressure in the container is greater than atmospheric pressure, and the pressure to be measured must be relatively small so the required height of the column is reasonable. Also, gas pressures cannot be measured with piezometers, because a gas forms no free surface.

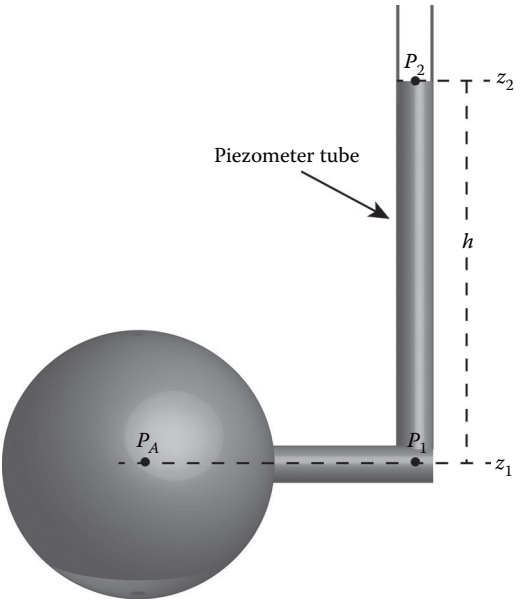


FIGURE 8.11 Piezometer.

The application of Equation 8.18 to the piezometer in Figure 8.11 indicates that the pressure at point A (P_A) can be determined by measuring the height to which the liquid rises in the tube (h) through the relationship $P_A = \rho\, g\, h$. Note that $P_A = P_1$, because point 1 and point A within the container are at the same elevation. Furthermore, the tube is open at the top, thus P_2 can be set equal to zero (gage pressure).

8.3.1.3 U-Tube Manometer

A device for measuring the pressure of both liquids and gases contained in a vessel is the open-tube manometer illustrated in Figure 8.12. One end of a U-shaped tube containing a liquid is open to the atmosphere, and the other end is connected to a system of unknown pressure (P_A). In the U-tube manometer, the fluid whose pressure is being measured should have a density less than that of the manometric fluid, and the two fluids must be immiscible. Furthermore, it should be noted that capillarity due to surface tension at the various fluid interfaces in the manometer is usually not considered, since for a simple U-tube with a meniscus in each leg, the capillary effects cancel out, or capillary rise can be made negligible by using tubes with diameters of about 1.3 cm or larger.

Again, the equation for hydrostatics (Equation 8.18) is used to calculate the unknown pressure (P_A). Consider the right side (P_2) and the left side (P_3) of the manometer separately:

$$P_2 = P_1 + \rho_1\, g\, h_1 \tag{8.24}$$

$$P_3 = P_4 + \rho_2\, g\, h_2 \tag{8.25}$$

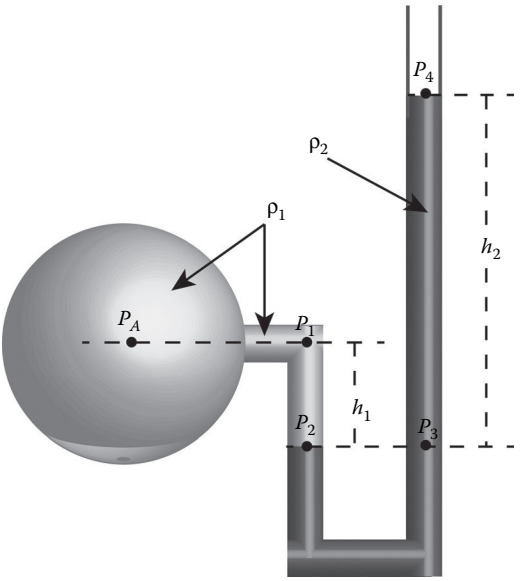


FIGURE 8.12 U-tube manometer.

Since both points A-1 and 2-3 are at the same elevation in the same fluid, they are at equivalent pressures ($P_A = P_1$ and $P_2 = P_3$). The two equations above can be equated and solved for P_A:

$$P_A = P_4 + \rho_2 g h_2 - \rho_1 g h_1 \tag{8.26}$$

Note that point 4 is exposed to atmospheric pressure; thus $P_4 = P_{atm}$ (or 0 gage pressure). Equation 8.26 reduces to

$$P_A = \rho_2 g h_2 - \rho_1 g h_1 \tag{8.27}$$

Finally, when calculating hydrostatic pressure changes, engineers work instinctively by simply allowing the pressure to increase downward and decrease upward. Thus, they use the following mnemonic device:

$$P_{down} = P^{up} + \rho g|\Delta z| \tag{8.28}$$

Applying Equation 8.28 to the U-tube manometer shown in Figure 8.12, the unknown pressure P_A can be calculated according to the following procedure: one can begin at A ($P_A = P_1$), down to P_2 (h_1), jump across fluid 2 to the same pressure P_3 ($P_2 = P_3$), and up to level P_4 (h_2):

$$P_A + \rho_1 g h_1 - \rho_2 g h_2 = P_4 = P_{atm} \tag{8.29}$$

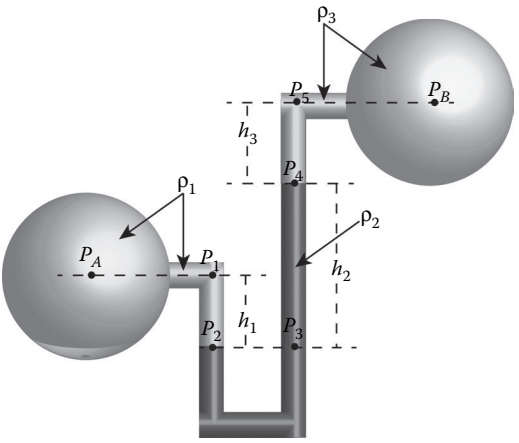


FIGURE 8.13 Differential U-tube manometer.

The U-tube manometer is also widely used to measure the difference in pressure between two containers (see Figure 8.13).

Using our up–down concept as in Equation 8.28, start at (A), evaluate pressure changes around the U-tube, and end up at (B):

$$P_A + \rho_1 g h_1 - \rho_2 g h_2 - \rho_3 g h_3 = P_B \tag{8.30}$$

or

$$P_A - P_B = \rho_2 g h_2 + \rho_3 g h_3 - \rho_1 g h_1 \tag{8.31}$$

8.3.1.4 Inclined-Tube Manometer

For situations where the pressure difference is very small, engineers invented more sensitive measuring devices, for example, the inclined-tube manometer. In this manometer, the tube leg is inclined relative to gravity (see Figure 8.14). The movement of the meniscus over a distance x along the inclined tube is much greater than the corresponding vertical distance h, and it can be read more accurately. Changing the angle of inclination can change the sensitivity of the manometer. However, angles less than 5° are not usually satisfactory, because it becomes difficult to determine the exact position of the meniscus. Normally, it requires a 10–30° inclined tube.

The pressure A can be found by again starting at one end of the system and working around to the other end. Thus

$$P_A = -\rho_1 g h_1 + \rho_2 g h_2 = -\rho_1 g h_1 + \rho_2 g L \sin\theta \tag{8.32}$$

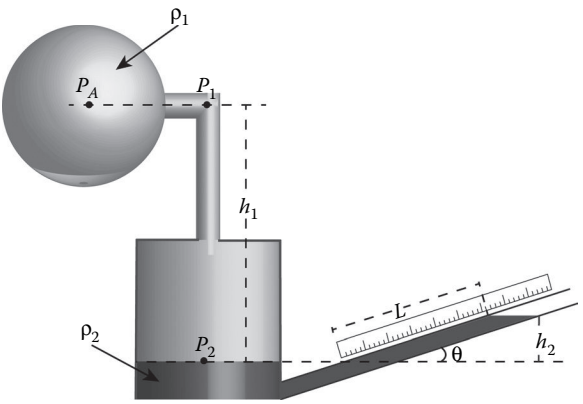


FIGURE 8.14 Inclined-tube manometer.

EXAMPLE 8.4

Piezometer of Figure 8.11 is used to estimate the pressure P_A in the tank by measuring the 15 cm height of liquid. The fluid is water at 20°C. Calculate the percent error due to capillarity if diameter tube is (a) 1 mm and (b) 0.5 mm.

Given data: $h = 15$ cm, $\theta \approx 0°$
Water at 20°C: $\rho = 1000$ kg/m^3, $\sigma = 0.0728$ N/m

a. $D = 1$ mm $\Rightarrow R = 0.5$ mm $= 5 \times 10^{-4}$ m

$$h = \frac{2\,\sigma \cos\theta}{\rho\, g\, R}$$

$$h = \frac{2(0.0728\ \text{N/m})(\cos 0^{o})}{(1000\ \text{kg/m}^3)(9.8\ \text{m/s}^2)(5 \times 10^{-4}\ \text{m})} = 0.0297\ \text{m}$$

$$\Delta h_{true} = 0.15\ \text{m} - 0.00297\ \text{m} = 0.1203\ \text{m}$$

$$\%\ \text{error}\ h = \frac{0.15\ \text{m} - 0.203\ \text{m}}{0.1203\ \text{m}} \times 100\% = 24.69\%$$

b. $D = 0.5$ mm $\Rightarrow R = 0.25$ mm $= 2.5 \times 10^{-4}$ m

$$h = \frac{2(0.0728\ \text{N/m})(\cos 0^{o})}{(1000\ \text{kg/m}^3)(9.8\ \text{m/s}^2)(2.5 \times 10^{-4}\ \text{m})} = 0.0594\ \text{m}$$

$$\Delta h_{true} = 0.15\ \text{m} - 0.0594\ \text{m} = 0.0906\ \text{m}$$

$$\%\ \text{error}\ h = \frac{0.15\ \text{m} - 0.0906\ \text{m}}{0.0906\ \text{m}} \times 100\% = 65.56\%$$

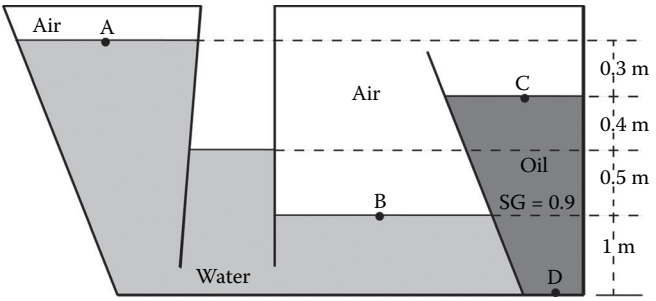


FIGURE 8.15 Example 8.5.

EXAMPLE 8.5

Calculate the pressure at A, B, C, and D in Figure 8.15.

$$P_A = -(0.3\text{ m} + 0.4\text{ m})(9800\text{ N/m}^3) = -6860\text{ Pa}$$

$$P_B = (0.5\text{ m})(9800\text{ N/m}^3) = 4900\text{ Pa}$$

$$P_C = (0.5\text{ m})(9800\text{ N/m}^3) - P_{air} = 4900\text{ Pa} \quad \text{or} \quad P_B = P_C$$

$$P_D = (0.5\text{ m})(9800\text{ N/m}^3) - P_{air} + (0.4\text{ m} + 0.5\text{ m} + 1\text{m})(0.9)(9800\text{ N/m}^3) = 21{,}658\text{ Pa}$$

or

$$P_D = P_C + (0.4\text{ m} + 0.5\text{ m} + 1\text{m})(0.9)(9800\text{ N/m}^3) = 21{,}658\text{ Pa}$$

8.3.2 Buoyant Force and Archimedes' Principle

You know from experience that some objects float in water and other objects sink. Archimedes (287–211 BC) realized that an object immersed in fluid would be lighter by an amount equal to the weight of the fluid it displaces. When a solid is introduced into a liquid, there may be three cases:

- Partially submerged, when the weight of the object is less than the weight of fluid that can be displaced by the object (see Figure 8.16a)
- Fully submerged, when the weight of the object equals the weight of the fluid displaced by the object (see Figure 8.16b)
- Sinks, when the weight of the object is greater than the weight of fluid displaced by the object (see Figure 8.16c)

According to the Archimedes' principle, when an object is immersed in a fluid, the fluid exerts a force on the object whose magnitude is equal to the weight of the

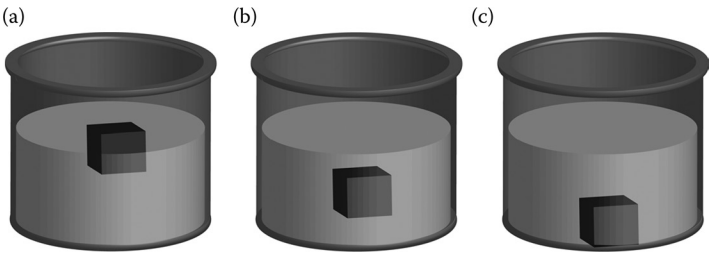


FIGURE 8.16 Buoyancy of a solid submerged in a liquid.

displaced fluid and whose direction is opposite to the force of gravity. This upward force exerted on an object by a fluid is known as the buoyant force:

$$F_B = \rho_f \, g \, V \tag{8.33}$$

where F_B is the buoyant force on the object, g is the acceleration due to gravity, ρ_f is the density of the fluid, and V is the volume of the object immersed in a fluid.

EXAMPLE 8.6

A cube with 15 cm sides is suspended in a fluid by a wire. The top of the cube is horizontal and 20 cm below the free surface. If the cube has a mass of 1 kg and the tension in the wire is T = 225 N, compute the fluid density.

Given data: $L_{cube} = 15$ cm = 0.15 m, $m = 1$ kg, $T = 225$ N = 225 kg.m/s^2
Consider a free-body diagram of the cube:

$$\sum F_y = T + F_B - mg = 0$$

where F_B is the buoyancy force (Equation 8.33). Hence

$$T + \rho_f \, gV = mg$$

$$\rho_f = \frac{mg - T}{gV}$$

$$\rho_f = \frac{(30\,\text{kg})(9.8\,\text{m/s}^2) - (225\,\text{kg.m/s}^2)}{(9.8\,\text{m/s}^2)\,(0.15^3\,\text{m}^3)}$$

$$\rho_f = 2086.17\,\text{kg/m}^3$$

8.4 FLUID DYNAMICS

As was discussed in the previous section, there are many situations involving fluids in which the fluid can be considered stationary. However, in the food industry, it is often necessary to pump fluids over long distances from storage to various processing

units and from one site to another. To understand the interesting phenomena associated with fluid motion, one must consider the fundamental laws that govern the motion of fluid particles (Ramaswamy and Marcotte, 2006; Sahu, 2012; Toledo, 2007). Such considerations include the balances of mass, momentum, energy, and mechanical energy that allow one to obtain the continuity and Bernoulli equations.

8.4.1 Continuity Equation

All the laws of mechanics are written for a system, which is defined as an arbitrary quantity of mass of fixed identity. One of the fundamental principles used in the analysis of uniform flow is known as the continuity of flow. This principle is derived from the fact that mass is always conserved in fluid systems, regardless of the pipeline complexity.

Consider a fluid flowing through a fixed volume, as shown in Figure 8.17. If the mass is steady so that there is no additional accumulation of fluid within the volume, the law of the conservation of mass can be used (Equation 8.34).

$$\dot{m}_1 = \dot{m}_2 \quad \text{or} \quad \rho_1 u_1 A_1 = \rho_2 u_2 A_2 \tag{8.34}$$

If the density remains constant, then $\rho_1 = \rho_2$, and the above becomes the continuity equation for incompressible flow (Equation 8.35):

$$u_1 A_1 = u_2 A_2 \quad \text{or} \quad Q_1 = Q_2 \tag{8.35}$$

where Q is flow rate.

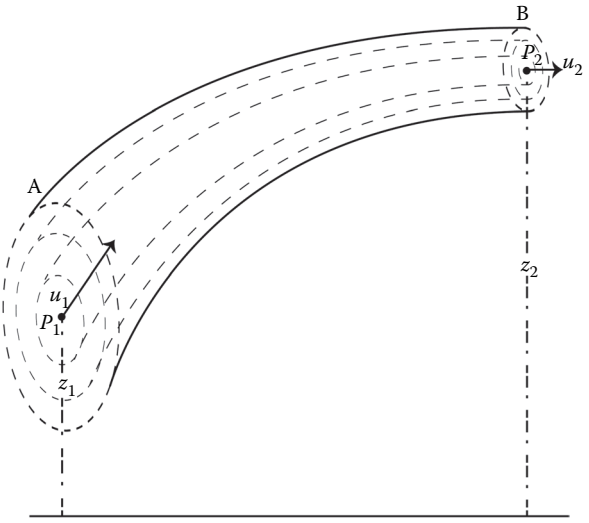


FIGURE 8.17 Two points joined by a streamline.

8.4.2 Bernoulli Equation

Let us consider a particle of fluid moving along a streamline from location (1) to (2), as shown in Figure 8.17. The mechanical energy balance for a steady flow and an incompressible and inviscid fluid may be written as

$$P_1 + \frac{\rho u_1^2}{2} + \rho g z_1 = P_2 + \frac{\rho u_2^2}{2} + \rho g z_2 \tag{8.36}$$

This is the celebrated Bernoulli equation for steady frictionless incompressible flow along a streamline. It is one of the equations most widely used to solve problems in fluid dynamics. To use the Bernoulli equation correctly, note the main assumptions used in deriving this equation (Munson et al., 2009; White, 2003):

- The equation is applicable along a streamline. Strictly speaking, the Bernoulli equation is applicable along a streamline. However, when a region of the flow is irrotational and there is no vorticity in the flow field, the Bernoulli equation also becomes applicable across streamlines.
- Steady flow. Therefore, it should not be used during transient start-up and shut-down periods, or during periods of change in flow conditions.
- The fluid is incompressible. One of the approximations used in the derivation of the Bernoulli equation is that ρ is constant.
- Viscous effects are assumed negligible. Every flow involves some friction, no matter how small, and frictional effects may or may not be negligible. In general, frictional effects are negligible for short flow sections with large cross sections, especially at low flow velocities.
- No shaft work (pumps, turbines, or any other machine) and negligible heat transfer.

The "head" form of the Bernoulli equation is obtained by dividing Equation 8.36 by the specific weight of the fluid ($\gamma = \rho g$):

$$\frac{P_1}{\rho g} + \frac{u_1^2}{2g} + z_1 = \frac{P_2}{\rho g} + \frac{u_2^2}{2g} + z_2 \quad \text{or} \quad \frac{P_1}{\gamma} + \frac{u_1^2}{2g} + z_1 = \frac{P_2}{\gamma} + \frac{u_2^2}{2g} + z_2 \tag{8.37}$$

EXAMPLE 8.7

A tank open to the atmosphere is filled with water to a height of 3 m from the outlet tap (Figure 8.18). A tap near the bottom of the tank is now opened, and water flows out from the smooth and rounded outlet. Determine the maximum water velocity at the outlet.

$P_1 = P_2 = P_{atm}$, $z_1 = 3$ m, $z_2 = 0$, $u_1 \ll u_2$ and thus $u_1 \approx 0$ compared to u_2. For flow along a streamline from 1 to 2, the Bernoulli equation (Equation 8.37) simplifies to

$$z_1 = \frac{u_2^2}{2g}$$

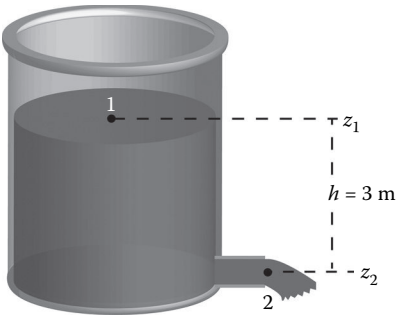


FIGURE 8.18 Example 8.7.

Solving for u_2

$$u_2 = \sqrt{2gz_1}$$

This relation is called the Torricelli equation. Substituting

$$u_2 = \sqrt{2\,(9.8\ \text{m/s}^2)(3\ \text{m})} = 7.67\ \text{m/s}$$

EXAMPLE 8.8

Milk flows steadily through the pipe shown in Figure 8.19 such that the pressures at sections 1 and 2 are 300 kPa and 100 kPa, respectively. Determine the diameter of the pipe at section 2, D_2, if the velocity at section 1 is 12 m/s and viscous effects are negligible.

Given data: $P_1 = 300$ kPa, $P_2 = 100$ kPa, $D_1 = 0.1$ m, $u_1 = 12$ m/s, $z_1 = 10$ m, $z_2 = 0$
Milk: $\rho = 1032\ \text{kg/m}^3$

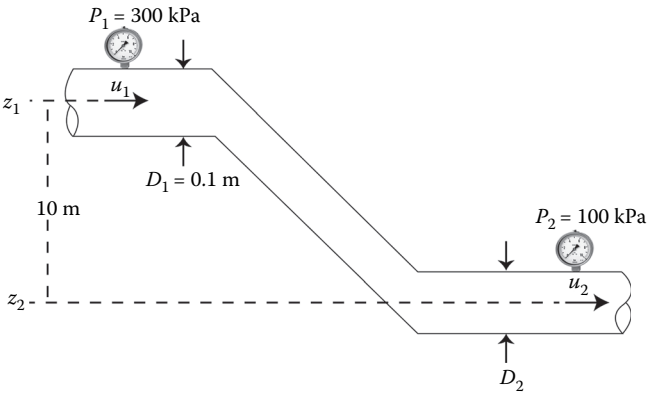


FIGURE 8.19 Example 8.8.

With the assumptions of steady, inviscid, incompressible flow, for flow along a streamline from 1 to 2, the Bernoulli equation (Equation 8.37) simplifies to

$$\frac{P_1}{\rho g} + \frac{u_1^2}{2g} + z_1 = \frac{P_2}{\rho g} + \frac{u_2^2}{2g}$$

Solving for u_2

$$u_2 = \sqrt{2g\left(\frac{P_1}{\rho g} + \frac{u_1^2}{2g} + z_1 - \frac{P_2}{\rho g}\right)}$$

Substituting

$$u_2 = \sqrt{2\,(9.8\ \text{m/s}^2)\left[\frac{300{,}000\ \text{N/m}^2}{(1032\ \text{kg/m}^3)(9.8\ \text{m/s}^2)} + \frac{(12\ \text{m/s})^2}{2\,(9.8\ \text{m/s}^2)} + 10\ \text{m} - \frac{100{,}000\ \text{N/m}^2}{(1032\ \text{kg/m}^3)\,(9.8\ \text{m/s}^2)}\right]}$$

$$u_2 = 26.97\text{m/s}$$

Apply the continuity equation for incompressible flow (Equation 8.35) to estimate the diameter of the pipe at section 2, D_2:

$$\frac{\pi D_1^2}{4} u_1 = \frac{\pi D_2^2}{4} u_2$$

Solving for D_2

$$D_2 = \sqrt{\frac{D_1^2 u_1}{u_2}}$$

Substituting

$$D_2 = \sqrt{\frac{(0.1\text{m})^2(12\ \text{m/s})}{(26.97\ \text{m/s})}}$$

$$D_2 = 0.0667\ \text{m} = 6.67\ \text{cm}$$

8.5 FLOW IN A CIRCULAR PIPE

Fluids in food processing plants are mostly transported in closed conduits; these are usually round and called pipes. The flow of a fluid in a pipe may be laminar or it may be turbulent. Fluids that have a low flow rate or high viscosity may be thought of as a series of layers that move over one another without mixing (laminar flow). Above a certain flow rate, the layers of fluid mix together and irregular behavior occurs along the streak (transitional flow). However, large enough flow rates produce turbulent flow and hence thinner boundary films (Sahu, 2012; Singh and Heldman, 2009; Steffe, and Singh, 1997).

8.5.1 Reynolds Number

Laminar and turbulent flows can be characterized and quantified using the Reynolds number (ratio of inertial to viscous forces):

$$Re = \frac{\rho u D}{\mu} \tag{8.38}$$

In the case of non-Newtonian fluids, the Reynolds number cannot be uniquely defined because of the different choices of characteristic viscosity. For power law fluids (pseudoplastic and dilatant fluids) flowing through circular tubes, five different definitions for the Reynolds number have been proposed by various investigators (Madlener et al., 2009):

- A generalized Reynolds number (Re_{LP}) introduced by Metzner and Reed (1955)
- A Reynolds number based on the apparent viscosity at the wall
- A generalized Reynolds number derived for a power law fluid from the nondimensional momentum equation
- A Reynolds number based on the solvent viscosity
- A Reynolds number based on the effective viscosity

This use of different Reynolds numbers from one investigator to another makes the comparison of different sets of data quite difficult. In fluid flow applications in the food industry, the proposal by Metzner and Reed is the most used (Equation 8.39):

$$Re_{PL} = \left(\frac{\rho u^{2-n} D^n}{K 8^{n-1}}\right)\left(\frac{4n}{3n+1}\right)^n \tag{8.39}$$

With the Bingham plastic model, μ is commonly called the plastic viscosity (μ_{pl}) and the Bingham–Reynolds number is defined by the following equation:

$$Re = \frac{\rho u D}{\mu_{pl}} \tag{8.40}$$

Finally, for non-Newtonian fluids that fit the Herschel–Bulkley model, the generalized Reynolds number can be written as follows:

$$Re_{HB} = \frac{\rho u^{2-n} D^n}{(\tau_0/8)(D/u)^n + 8^{n-1} K\left[(3m+1)/(4m)\right]^n} \tag{8.41}$$

where

$$m = \frac{n K (8u/D)^n}{\tau_0 + K(8u/D)^n} \tag{8.42}$$

8.5.2 Critical Reynolds Number

The point of transition from laminar to turbulent flow is known as the critical Reynolds number. For Newtonian fluids, a Reynolds number of less than 2100 describes laminar flow. A Reynolds number between 2100 and 4000 signifies transitional flow. A Reynolds number greater than 4000 indicates turbulent flow, denoting a small influence of viscous forces on the energy dissipation (Munson et al., 2009; Singh and Heldman, 2009). It should be noted that by minimizing ambient disturbances Pfenniger (1961) maintained laminar pipe flow up to a Reynolds number of 100,000. In the case of non-Newtonian fluids, in particular for fluids with a viscosity characteristic following the Ostwald–de-Waele or power law equations, the critical Reynolds number can be determined according to Equations 8.43 and 8.44 proposed by Hanks (1963) and Mishra and Tripathi (1971), respectively.

$$Re_{PL,critical} = \frac{6464n\,(2+n)^{(2+n)/(1+n)}}{(1+3n)^2} \tag{8.43}$$

$$Re_{PL,critical} = \frac{2100\left(4n+2\right)(5n+3)}{3\,(1+3n)^2} \tag{8.44}$$

For Bingham plastic fluid, the critical Reynolds number can be expressed as follows (Hanks, 1963):

$$Re_{B,critical} = \frac{He}{8c_c}\left(1 - \frac{4c_c}{3} + \frac{c_c^4}{3}\right) \tag{8.45}$$

where He is the Hedstrom number (Equation 8.46) and c_c is the critical value of c (Equation 8.47).

$$He = \frac{D^2 \rho \tau_0}{\mu_{pl}^2} \tag{8.46}$$

$$\frac{c_c}{(1-c_c)^3} = \frac{He}{16800} \tag{8.47}$$

8.5.3 Kinetic Energy Correction Factor

Note that Equations 8.36 and 8.37 assume that the fluid velocity is uniform across the entire cross section. However, in real flow conditions, we cannot neglect the effect of viscosity. Viscosity generates shear stresses acting between the layers or particles of flowing fluid. The interaction between the fluid layers and particles and the interaction of fluid with the boundary of the conduit makes the velocity of flow nonuniform

TABLE 8.2
Kinetic Energy Correction Factor for Laminar Flow

Fluids	α (Dimensionless)
Newtonian	2
Power law	$\frac{4\,(2n+1)(5n+3)}{3\,(3n+1)^2}$
Bingham plastic	$\frac{4}{2-c}$
Herschel–Bulkley	$2\exp(0.168c - 1.062nc - 0.954n^5 - 0.115c^5 + 0.831)$ for $0.06 \le n \le 0.38$
	$2\exp(0.849c - 0.296nc - 0.600n^5 - 0.602c^5 + 0.733)$ for $0.38 \le n \le 1.60$

across the section of flow. Therefore, a correction factor, α, must be used and the kinetic energy term modified as follows:

$$\frac{P_1}{\gamma} + \frac{\alpha_1 u_1^2}{2g} + z_1 = \frac{P_2}{\gamma} + \frac{\alpha_2 u_2^2}{2g} + z_2 \tag{8.48}$$

where α is a dimensionless correction factor that depends on the flow regime and on the type of fluid transported. For turbulent regimes the value of α is always approximated to one, regardless of the type of fluid. However, under laminar regimes the value of α depends on the type of fluid (Metzner, 1956; Osorio and Steffe, 1984; Steffe, 1996) (see Table 8.2).

8.5.4 Energy Losses in Flow

When a fluid flows through pipes or processing equipment, there is a loss of energy and a drop in pressure, which are due to the frictional resistance to flow. Furthermore, pipe systems come with valves, bends, pipe diameter changes, and elbows, which also contribute to this loss. To overcome this loss in energy, it is necessary to apply power by using pumps or turbines to transport the fluid. To apply the Bernoulli equation to these systems, it should take into account that one restriction in this equation is that the flow is inviscid (Çengel and Cimbala, 2010; Earle, 1983). If viscous effects are important, the system is nonconservative and energy losses occur. Another basic restriction on the use of the Bernoulli equation is that there are no mechanical devices in the system between the two points along the streamline for which the equation is applied. Therefore, in order to extend the application of the Bernoulli equation, two additional terms are introduced into the equation:

$$\frac{P_1}{\gamma} + \frac{\alpha_1 u_1^2}{2g} + z_1 = \frac{P_2}{\gamma} + \frac{\alpha_2 u_2^2}{2g} + z_2 + \sum h_f - h_w \tag{8.49}$$

where h_w is the shaft work done on the fluid by the pump. The overall head loss Σh_f is divided into two parts: major loss h_L and minor loss h_m. The major loss comes from the viscosity (in a straight pipe) while minor loss is due to energy loss in the accessories (valves, bends, elbows, tees, sudden contractions, and the pipe entrance, among others). Such losses may not be so minor, for example, a partially closed valve can cause a greater pressure drop than a long pipe.

One way to evaluate such mechanical energy losses is from the fluid's properties and the particular characteristics of the pipe, involving the so-called friction factor. The friction factor (f) is defined as the relation between the stress exerted by the fluid on the pipe wall (τ_w) and the kinetic energy per volume unit:

$$f = \frac{2\tau_w}{\rho u^2} \tag{8.50}$$

Substituting the definition of the shear stress at the wall of a pipe ($\tau_w = (\Delta P)D/(4L)$) into Equation 8.50 gives

$$f = \frac{(\Delta P)D}{2\rho L u^2} \tag{8.51}$$

where $\Delta P = P_2 - P_1$, L is the pipe length, and f is called the Fanning friction factor. In chemical engineering and food engineering textbooks, the Fanning friction factor is more commonly used, while many civil and mechanical engineering textbooks refer to the Darcy friction factor (f_D), which is equal to four times the Fanning friction factor ($f_D = 4f$). In this text, it will only use the Fanning friction factor.

Solving for ΔP in Equation 8.51

$$\Delta P = 2f\frac{L\rho u^2}{D} = \rho g h_L \tag{8.52}$$

and the friction head loss h_L is given as

$$h_L = 2f\frac{L}{D}\frac{u^2}{g} \tag{8.53}$$

The friction factor is a function of the flow regime (laminar or turbulent), type of fluid (Newtonian, pseudoplastic, dilatant, or plastic), and the surfaces roughness (ε) of the pipe. The surfaces roughness is a parameter that depends on the type and characteristics of the material with which the pipe is manufactured (see Table 8.3).

8.5.5 Friction Factor for Laminar Regimes

In laminar flow, f values can be determined from the equations describing the relationship between the pressure drop and flow rate for a particular fluid (Güzel et al., 2009; Steffe, 1996).

TABLE 8.3
Surface Roughness for Pipes of Different Materials

Material	ε (mm)
Stainless steel	0.03
Carbon steel (new)	0.02–0.05
Riveted steel	0.91–9.1
Flexible rubber tubing smooth	0.006–0.07
Flexible rubber tubing wire reinforced	0.3–4
Wrought iron (new)	0.045
Cast iron (new)	0.25
Galvanized iron	0.025–0.15
Sheet metal ducts (with smooth joints)	0.02–0.1
Water mains with tuberculations	1.2
Concrete very smooth	0.025–0.2
Aluminum	0.0015
PVC and plastic pipes	0.0015
Copper	0.0015

8.5.5.1 Newtonian Fluids

$$f = \frac{16}{Re} \tag{8.54}$$

8.5.5.2 Power Law Fluids

$$f = \frac{16}{Re_{PL}} \tag{8.55}$$

8.5.5.3 Bingham Plastic Fluids

$$f = \frac{16\,(6\,Re_B + He)}{6\,Re_B^2} \tag{8.56}$$

8.5.6 Friction Factor for Turbulent Regimes

For completely turbulent flow, the laminar sublayer is so thin that the surface roughness completely dominates the character of the flow near the wall. Hence, the pressure drop required is a result of an inertia-dominated turbulent shear stress rather than the viscosity-dominated laminar shear stress normally found in the viscous sublayer. For flows with moderate values of *Re*, the friction factor is indeed dependent on both the Reynolds number and relative roughness. In cases of transitional and turbulent flow conditions, the mathematical derivations become highly complex

(Munson et al., 2009; White, 2003). Friction factors may be determined from empirical and semiempirical equations.

8.5.6.1 Newtonian Fluids

For the transition regime or turbulent flow, the equation universally adopted is that of Colebrook and White (1937) (Equation 8.57).

$$\frac{1}{\sqrt{f}} = -4\log\left[\frac{1.256}{Re\sqrt{f}} + \frac{1}{3.7}\frac{\varepsilon}{D}\right] \tag{8.57}$$

Note that even for smooth pipes ($\varepsilon = 0$), the friction factor is not zero. That is, there is a head loss in any pipe, no matter how smooth the surface is. This is a result of the no-slip boundary condition that requires any fluid to stick to any solid surface it flows over.

In the food and beverage industry, highly exacting hygienic demands are imposed on surfaces that come into contact with the product being manufactured. Surfaces must therefore be smooth, continuous, and free from cracks, crevices, scratches, and pits, which can harbor and retain soil and/or microorganisms after cleaning. Although good cleanability is the key requirement for surfaces rather than smoothness, a maximum roughness is specified for food contact surfaces since cleaning time required increases with surfaces roughness. Both the American 3-A organization and the European Hygienic Equipment Design Group (EHEDG) specify a maximum roughness for contact surfaces. In particular, DIN 11850-10/99 specifies a maximum surfaces roughness of 0.8 μm for tubing, and the maximum for a weld area is 1.6 μm. Since in the food and beverage industry sanitary piping systems with low roughness values are required, Equation 8.58 can be used (Hoogland and Vlaardingen, 2005; Singh and Heldman, 2009).

$$\frac{1}{\sqrt{f}} = 4\log\left[Re\sqrt{f}\right] - 0.4 \tag{8.58}$$

A practical way of calculating the friction factor is from the Moody diagram (Figure 8.20). The Moody chart or Moody diagram is a graph in nondimensional form that relates the friction factor ($4f$ or f_D), Reynolds number, and relative roughness (Moody and Princeton, 1944). This diagram allows the calculation of the friction factor under laminar or turbulent regime, as well as in the transition zone.

8.5.6.2 Power Law Fluids

The calculation of the friction factor can be performed by the following implicit equation (Dodge and Metzner, 1959):

$$\frac{1}{\sqrt{f}} = \frac{4}{n^{0.75}}\log\left[Re_{PL}\, f^{1-n/2}\right] - \frac{0.4}{n^{1.2}} \tag{8.59}$$

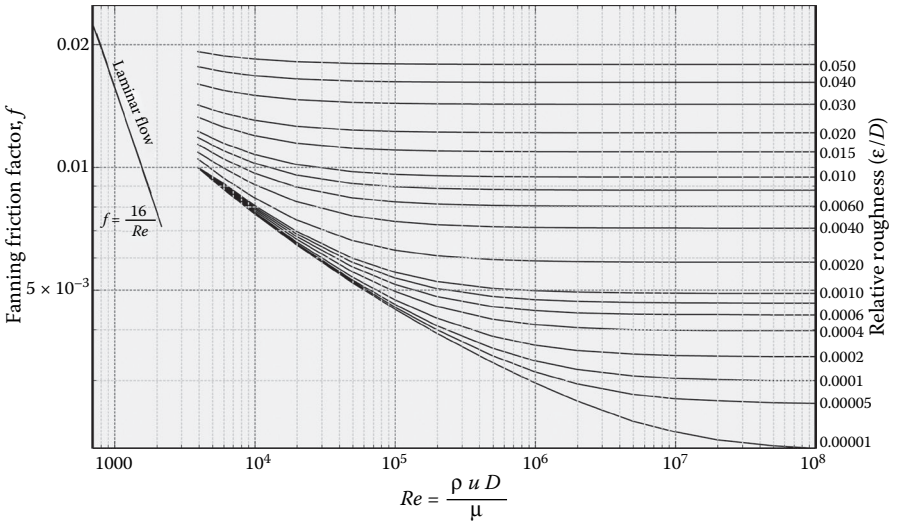


FIGURE 8.20 Moody diagram for pipe friction with smooth and rough walls.

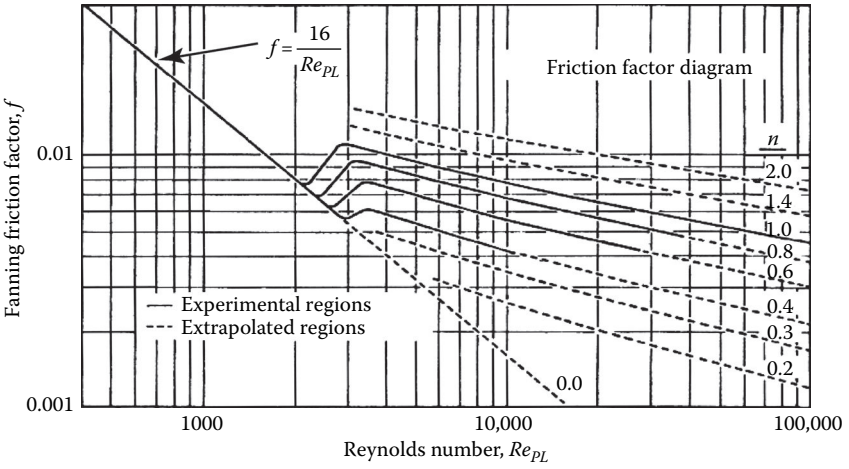


FIGURE 8.21 Fanning friction factors for power law fluids. (From Dodge, D. W. and Metzner, A. B. 1959. *AIChE Journal*, 5(2):189–204.)

In the same way as for Newtonian fluids, the friction factor for power law fluids can be graphically determined by the chart (Figure 8.21) developed by Dodge and Metzner (1959).

8.5.6.3 Bingham Plastic Fluids

The Fanning friction factor for the flow of Bingham plastic fluids in smooth pipes can be written in terms of the Bingham–Reynolds number and c as follows (Steffe, 1996; Sablani et al., 2003):

$$\frac{1}{\sqrt{f}} = 4.53\log(1-c) + 4.53\log\left[Re_B\sqrt{f}\right] - 2.3 \tag{8.60}$$

where

$$c = \frac{2\tau_0}{f\rho u^2}.$$

8.5.7 Minor Losses

For any pipe system, in addition to the Moody-type friction loss computed for the length of pipe, there are additional so-called minor losses due to additional components (valves, bends, tees, elbows, and the like). Since the flow pattern in these components is quite complex, the theory is very weak. Therefore, the losses are commonly measured experimentally and correlated with the pipe-flow parameters. The most common method used to determine these head losses or pressure drops is defined as

$$K_f = \frac{h_L}{u^2/2g} = \frac{\Delta P}{\frac{1}{2}\rho u^2} \tag{8.61}$$

where K_f is the friction loss coefficient.

Minor losses are sometimes given in terms of an equivalent length, l_{eq}. The head loss through a component is given in terms of the equivalent length of pipe that would produce the same head loss as the component. This is calculated by the following relation:

$$h_L = 2f\frac{l_{eq}}{D}\frac{u^2}{g} \quad \text{or} \quad l_{eq} = \frac{k_f D}{4f} \tag{8.62}$$

Minor losses have three components: contraction, expansion, and fittings.

8.5.7.1 Loss Coefficient Due to Sudden Contraction

The loss coefficient for a sudden contraction ($K_{f,c}$) is calculated in terms of the small and large pipe diameters.

$$K_{f,c} = 0.4\left[1.25 - \left(\frac{D_{small}}{D_{large}}\right)^2\right] \quad \text{where} \left(\frac{D_{small}}{D_{large}}\right)^2 < 0.715 \tag{8.63}$$

$$K_{f,c} = 0.75\left[1 - \left(\frac{D_{small}}{D_{large}}\right)^2\right] \quad \text{where} \left(\frac{D_{small}}{D_{large}}\right)^2 > 0.715 \tag{8.64}$$

8.5.7.2 Loss Coefficient Due to Sudden Expansion

The losses for sudden expansion ($K_{f,e}$) or an exit are determined as

$$K_{f,e} = \left[1 - \left(\frac{D_{small}}{D_{large}}\right)^2\right]^2 \tag{8.65}$$

8.5.7.3 Loss Coefficient Due to Pipe Fittings

Friction loss coefficients (K_f) for many fittings are summarized in Table 8.4.

TABLE 8.4
Friction Loss Coefficients for Pipe Fittings

Fittings	K_f
Elbows	
Regular 90°, flanged	0.3
Regular 90°, threaded	1.5
Long radius 90°, flanged	0.2
Long radius 90°, threaded	0.7
Long radius 45°, flanged	0.2
Regular 45°, threaded	0.4
180° Return Bends	
180° return bend, flanged	0.2
180° return bend, threaded	1.5
Tees	
Line flow, flanged	0.2
Line flow, threaded	0.9
Branch flow, flanged	1.0
Branch flow, threaded	2.0
Union, threaded	0.08
Valves	
Globe, fully open	10
Angle, fully open	2
Gate, fully open	0.15
Gate, 1/4closed	0.26
Gate, 1/2closed	2.1
Gate, 3/4closed	17
Swing check, forward flow	2
Ball valve, fully open	0.05
Ball valve, 1/3 closed	5.5
Ball valve, 2/3 closed	210

For non-Newtonian fluids, Steffe (1996) reported that you must modify the friction loss coefficients ($K_{f,NN}$) when the Reynolds number is less than 500. The $K_{f,NN}$ is calculated by the expression

$$K_{f,NN} = \frac{500K_f}{Re_g} \tag{8.66}$$

where Re_g is Re_{LP} or Re_B depending on the type of fluid in question.

EXAMPLE 8.9

Olive oil at 25°C ($\rho = 920$ kg/m^3 and $\mu = 56.5$ cP) is flowing through a 2 cm diameter, 10 m long horizontal pipe steadily at an average velocity of 1 m/s. Determine the head loss.

Given data: $D = 2$ cm $= 0.02$ m, $L = 10$ m, $u = 1$ m/s
Olive oil: $\rho = 920$ kg/m^3, $\mu = 56.5$ cP $= 0.0565$ kg/m.s

First, it must determine the flow regime. The Reynolds number is

$$Re = \frac{\rho u D}{\mu} = \frac{(920\ \text{kg/m}^3)(1\ \text{m/s})(0.02\ \text{m})}{0.0565\ \text{kg/m.s}} = 325.7$$

The Reynolds number is less than 2100. Therefore, the flow is laminar. For Newtonian fluids (Equation 8.54)

$$f = \frac{16}{Re} = \frac{16}{325.7} = 0.049$$

The head loss (h_L) can be determined by Equation 8.53

$$h_L = 2f\frac{L}{D}\frac{u^2}{g} = 2(0.049)\frac{10\ \text{m}}{0.02\ \text{m}}\frac{(1\ \text{m/s})^2}{9.8\ \text{m/s}^2} = 5\ \text{m}$$

8.6 PUMPS

When a fluid is transported along a pipe, a certain amount of energy is needed to overcome the frictional forces. Pumps are usually used for this purpose.

8.6.1 Pump Characteristics

Different parameters are used to characterize a pump, among which are suction head, impelling head, total head, power, overall efficiency, and net positive suction head (NPSH).

- Suction head: The suction head is the value of energy that the fluid has at the suction point.

- Impelling head: The impelling head represents the available energy that the fluid has at the exit of the pump to circulate until reaching the final point of the system.
- Total head: The total head, also called the total dynamic head (TDH), that can be developed by a pump is defined as the difference between the impelling and suction heads. TDH is the value used in the power calculations.
- Power: The power, $\mathcal{P}_f$, gained by the fluid is given by Equation 8.67.

$$\mathcal{P}_f = \gamma Q h_w \tag{8.67}$$

where h_w is calculated with Equation 8.49.

8.6.1.1 Overall Efficiency

Pump overall efficiency is the ratio of power actually gained by the fluid from the shaft power supplied (Equation 8.68). The overall pump efficiency is affected by hydraulic losses in the pump, and by mechanical losses in the bearings and seals.

$$\eta = \frac{\mathcal{P}_f}{W_{shaft}} \tag{8.68}$$

where W_{shaft} is the total power applied to the shaft of the pump.

8.6.1.2 Net Positive Suction Head

On the suction side of a pump, low pressures are commonly encountered, with the possibility of cavitation occurring within the pump. Cavitation occurs when bubbles of gas or vapor, present in the liquid, collapse in the high-pressure region of the pump. This will cause wearing and mechanical damage to the blades. Bubbles occur for two major reasons. Sometimes the pressure of the liquid may be below atmospheric pressure and air may be sucked in through leaking joints. Also, the saturated vapor pressure of the liquid may exceed the local pressure in the pipe and the liquid will boil, thereby forming bubbles of vapor. The correct position of the pumps and take care of such details help to reduce the incidence of cavitation. The NPSH is used to determine the correct positioning of pumps (Çengel and Cimbala, 2010; Munson et al., 2009). This is defined as the difference between the suction head and the vapor pressure of the liquid, P_v (Equation 8.69).

$$NPSH = \frac{P_s}{\gamma} + \frac{u_s^2}{2g} - \frac{P_v}{\gamma} \tag{8.69}$$

There are in fact two values of *NPSH* of interest. The first is the available net positive suction head ($NPSH_A$), which represents the head that actually occurs for a particular flow system. This value can be determined experimentally, or calculated if the system parameters are known. The second is the required net positive suction head ($NPSH_R$) that must be maintained, or exceeded, so that cavitation will not

occur. $NPSH_R$ is characteristic of each pump, and the data are specified by the manufacturer, being a function of the pumps design and its rotation velocity, in the case of centrifugal pumps. For proper pump operation, it is necessary that

$$NPSH_A \geq NPSH_R \tag{8.70}$$

EXAMPLE 8.10

A liquid food is being pumped at a rate of 4 m³/h from a tank A to a tank B (Figure 8.22), through a sanitary pipe with 0.0457 mm of surface roughness. The suction line is 1 m of long (50 mm diameter nominal, DN) and the discharge line of the pump is 10 m of long (DN = 25 mm) with two elbows and one globe valve. Calculate the power requirement for the pump for the following two cases:

a. Water: $\rho = 1000$ kg/m³, $\mu = 1$ cP
b. Tomato juice (5.8°Brix): $\rho = 1030$ kg/m³, $n = 0.59$, $K = 0.22$ Pa.s$^{0.59}$

Given data: $Q = 4$ m³/h $= 1.111 \times 10^{-3}$ m³/s, $\varepsilon = 0.0457$ mm $= 4.57 \times 10^{-5}$ m, $P_1 = P_2 = P_{atm}$, $z_1 = 2$ m, $z_2 = 7$ m, $L_{section1} = 1$ m, $L_{section2} = 10$ m, $DN_{section1} = 50$ mm → $D_{section1} = 0.04749$ m, $DN_{section2} = 25$ mm → $D_{section2} = 0.02291$ m

Calculate the mean velocity in suction line (section 1) and discharge line (section 2):

$$Q = u_1 A_1 = u_2 A_2$$

$$u_1 = \frac{Q_1}{\pi D_1^2/4} = \frac{1.111 \times 10^{-3}\,\text{m}^3/\text{s}}{\pi\,(0.04749\,\text{m})^2/4} = 0.6273\,\text{m/s}$$

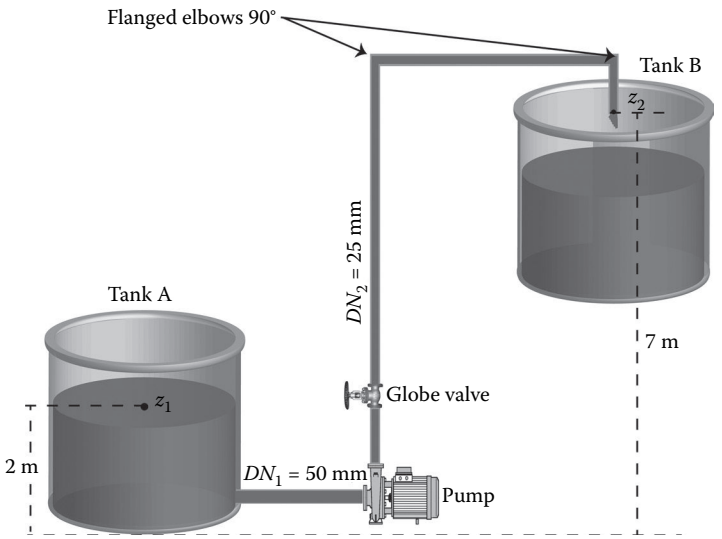


FIGURE 8.22 Example 8.10.

$$u_2 = \frac{Q_2}{\pi D_2^2/4} = \frac{1.111 \times 10^{-3}\ \text{m}^3/\text{s}}{\pi\ (0.02291\text{m})^2/4} = 2.695\ \text{m/s}$$

a. Water: $\rho = 1000\ \text{kg/m}^3$, $\mu = 1\ \text{cP} = 1 \times 10^{-3}\ \text{kg/m.s}$

i. Suction Line (Section 1)

Calculate the Reynolds number and energy losses in suction line:

$$Re_1 = \frac{\rho u_1 D_1}{\mu} = \frac{(1000\text{kg/m}^3)\ (0.6273\text{m/s})\ (0.04749\text{m})}{1 \times 10^{-3}\ \text{kg/m.s}} = 29{,}790$$

In turbulent flow ($Re > 2100$), Fanning friction factor is calculated from Equation 8.57

$$\frac{1}{\sqrt{f_1}} = -4\log\left[\frac{1.256}{29790\sqrt{f_1}} + \frac{1}{3.7}\frac{4.57 \times 10^{-5}\ \text{m}}{0.04749\ \text{m}}\right] \Rightarrow f_1 = 6.48 \times 10^{-3}$$

$$\sum h_{f,section1} = h_{L1} + \sum h_{m,section1}$$

$$\sum h_{f,section1} = 2f_1\frac{L_1}{D_1}\frac{u_1^2}{g} + \frac{k_{f,c}u_1^2}{2g}$$

Calculate the friction loss coefficient in the sudden contraction from Equation 8.63.

$$K_{f,c} = 0.4\left[1.25 - \left(\frac{D_{small}}{D_{large}}\right)^2\right]$$

$$D_{small}/D_{large} \cong 0 \qquad \text{since } D_{small} \ll D_{large}.$$

Thereforre, Kf,c = 0.5

$$\sum h_{f,section1} = 2(6.48 \times 10^{-3})\frac{1\text{m}}{0.04749\ \text{m}}\frac{(0.6273\ \text{m/s})^2}{9.8\ \text{m/s}^2} + \frac{0.5\ (0.6273\text{m/s})^2}{2\ (9.8\text{m/s}^2)}$$

$$\sum h_{f,section1} = 0.011\text{m} + 0.010\ \text{m} = 0.021\text{m}$$

ii. Discharge Line (Section 2)

Calculate the Reynolds number and energy losses in discharge line:

$$Re_2 = \frac{\rho u_2 D_2}{\mu} = \frac{(1000\text{kg/m}^3)\ (2.695\text{m/s})\ (0.02291\text{m})}{1 \times 10^{-3}\ \text{kg/m.s}} = 61{,}742$$

In turbulent flow ($Re > 2100$), Fanning friction factor is calculated from Equation 8.57

$$\frac{1}{\sqrt{f_2}} = -4\log\left[\frac{1.256}{61742\sqrt{f_2}} + \frac{1}{3.7}\frac{4.57\times10^{-5}\,\text{m}}{0.02291\,\text{m}}\right] \Rightarrow f_2 = 6.50\times10^{-3}$$

Alternatively, the Fanning friction factor can be found from the Moody chart (Figure 8.20). For $\varepsilon/D_2 \approx 2\times10^{-3}$ and $Re = 61{,}742$, from the Moody chart read $f_2 \approx 6.0\times10^{-3}$.

$$\sum h_{f,section2} = h_{L2} + \sum h_{m,section2}$$

$$\sum h_{f,section2} = 2f_2\frac{L_2}{D_2}\frac{u_2^2}{g} + \frac{(2k_{f,elbow} + k_{f,valve})u_2^2}{2g}$$

Friction loss coefficients (flanged elbows 90° and globe valve) are determined from Table 8.4.

$$\sum h_{f,section2} = 2(6.50\times10^{-3})\frac{10\,\text{m}}{0.02291\,\text{m}}\frac{(2.695\,\text{m/s})^2}{9.8\,\text{m/s}^2} + \frac{(2(0.3) + 10)(2.695\,\text{m/s})^2}{2(9.8\,\text{m/s}^2)}$$

$$\sum h_{f,section2} = 4.21\text{m} + 3.93\,\text{m} = 8.14\,\text{m}$$

$$\sum h_f = \sum h_{f,section1} + \sum h_{f,section2} = 0.021\text{m} + 8.14\,\text{m} = 8.161\,\text{m}$$

$P_1 = P_2 = P_{atm}$, $z_1 = 2$ m, $z_2 = 7$ m, $u_1 \ll u_2$, and thus $u_1 \approx 0$ compared to u_2. For flow along a stream line from 1 to 2, the mechanical energy balance equation (Equation 8.49) simplifies to

$$z_1 = \frac{\alpha_2 u_2^2}{2g} + z_2 + \sum h_f - h_w$$

$$h_w = z_2 - z_1 + \frac{\alpha_2 u_2^2}{2g} + \sum h_f$$

In turbulent flow ($Re_2 = 61{,}742$), the kinetic energy correction factor is equal to 1.

$$h_w = z_2 - z_1 + \frac{\alpha_2 u_2^2}{2g} + \sum h_f = 7\,\text{m} - 2\,\text{m} + \frac{1(2.695\,\text{m/s})^2}{2(9.8\,\text{m/s}^2)} + 8.161\text{m} = 13.53\,\text{m}$$

The power requirement for the pump is calculated by Equation 8.67:

$$\mathcal{P}_f = \gamma Q h_w = (9800\ \text{N/m}^3)(1.111\times10^{-3}\ \text{m}^3/\text{s})(13.53\ \text{m}) = 147.3\ \text{J/s} = 147.3\ \text{W}$$

b. Tomato juice (5.8°Brix): $\rho = 1030\ \text{kg/m}^3$, $n = 0.59$, and $K = 0.22\ \text{Pa.s}^{0.59}$

i. Suction Line (Section 1)

Calculate the critical Reynolds number (Equation 8.44):

$$Re_{PL1,critical} = \frac{2100(4n+2)(5n+3)}{3(1+3n)^2} = \frac{2100[4(0.59)+2][5(0.59)+3]}{3[1+3(0.59)]^2} = 2367$$

Calculate the Reynolds number (Equation 8.39) in suction line:

$$Re_{PL1} = \left(\frac{\rho u^{2-n} D^n}{K\,8^{n-1}}\right)\left(\frac{4n}{3n+1}\right)^n$$

$$Re_{PL1} = \left(\frac{(1030\ \text{kg/m}^3)(0.6273\ \text{m/s})^{2-0.59}(0.04749\ \text{m})^{0.59}}{(0.22\ \text{Pa.s}^{0.59})8^{0.59-1}}\right) \times \left(\frac{4(0.59)}{3(0.59)+1}\right)^{0.59} = 857.6$$

In laminar flow ($Re_{PL1} < Re_{PL1,critical}$), the friction factor can be calculated from Equation 8.55

$$f = \frac{16}{Re_{PL}} = \frac{16}{857.6} = 0.0187$$

$$\sum h_{f,section1} = h_{L1} + \sum h_{m,section1}$$

$$\sum h_{f,section1} = 2f_1\frac{L_1}{D_1}\frac{u_1^2}{g} + \frac{k_{f,c}u_1^2}{2g}$$

Calculate the friction loss coefficient in the sudden contraction from Equation 8.63. $K_{f,c} = 0.5$

$$\sum h_{f,section1} = 2(0.0187)\frac{1\,\text{m}}{0.04749\,\text{m}}\frac{(0.6273\ \text{m/s})^2}{9.8\ \text{m/s}^2} + \frac{0.5(0.6273\ \text{m/s})^2}{2(9.8\ \text{m/s}^2)}$$

$$\sum h_{f,section1} = 0.032\,\text{m} + 0.010\,\text{m} = 0.042\,\text{m}$$

ii. Discharge Line (Section 2)

$$Re_{PL1,\,critical} = 2367$$

Calculate the Reynolds number (Equation 8.39) in discharge line:

$$Re_{PL2} = \left(\frac{(1030\ \text{kg/m}^3)\,(2.695\ \text{m/s})^{2-0.59}\,(0.02291\text{m})^{0.59}}{(0.22\ \text{Pa.s}^{0.59})\,8^{0.59-1}}\right) \times \left(\frac{4\,(0.59)}{3\,(0.59)+1}\right)^{0.59} = 4356.5$$

In turbulent flow ($Re_{PL2} > Re_{PL2,critical}$), Fanning friction factor is calculated from Equation 8.59

$$\frac{1}{\sqrt{f_2}} = \frac{4}{n^{0.75}}\log\left[Re_{PL2}\,f_2^{1-n/2}\right] - \frac{0.4}{n^{1.2}}$$

$$\frac{1}{\sqrt{f_2}} = \frac{4}{0.59^{0.75}}\log\left[4356.5\,f_2^{1-0.59/2}\right] - \frac{0.4}{0.59^{1.2}} \Rightarrow f_2 = 7.1\times10^{-3}$$

Alternatively, the Fanning friction factor can be found from Figure 8.21. For $n = 0.59$ and $Re = 4356.5$, from the chart, read $f_2 \approx 0.007$

$$\sum h_{f,section2} = h_{L2} + \sum h_{m,section2}$$

$$\sum h_{f,section2} = 2f_2\frac{L_2}{D_2}\frac{u_2^2}{g} + \frac{(2k_{f,elbow} + k_{f,valve})u_2^2}{2g}$$

Friction loss coefficients (flanged elbows 90° and globe valve) are determined from Table 8.4.

$$\sum h_{f,section2} = 2(7.1\times10^{-3})\frac{10\ \text{m}}{0.02291\text{m}}\frac{(2.695\ \text{m/s})^2}{9.8\ \text{m/s}^2} + \frac{(2(0.3)+10)(2.695\ \text{m/s})^2}{2(9.8\ \text{m/s}^2)}$$

$$\sum h_{f,section2} = 4.59\ \text{m} + 3.93\ \text{m} = 8.52\ \text{m}$$

$$\sum h_f = \sum h_{f,section1} + \sum h_{f,section2} = 0.042\ \text{m} + 8.52\ \text{m} = 8.562\ \text{m}$$

Apply the mechanical energy balance equation (Equation 8.49) between points 1 and 2 (see Figure 8.22). $P_1 = P_2 = P_{atm}$, $z_1 = 2$ m, $z_2 = 7$ m, $u_1 \ll u_2$, and thus $u_1 \approx 0$ compared to u_2.

$$z_1 = \frac{\alpha_2 u_2^2}{2g} + z_2 + \sum h_f - h_w$$

$$h_w = z_2 - z_1 + \frac{\alpha_2 u_2^2}{2g} + \sum h_f$$

Since the flow is turbulent ($Re_{PL2} = 4356.5$), $\alpha_2 = 1$

$$h_w = z_2 - z_1 + \frac{\alpha_2 u_2^2}{2g} + \sum h_f = 7\text{m} - 2\text{ m} + \frac{1(2.695\text{ m/s})^2}{2(9.8\text{ m/s}^2)} + 8.562\text{ m} \cong 14\text{ m}$$

The power requirement for the pump is calculated by Equation 8.67:

$$\mathcal{P}_f = \gamma Q h_w = (1030\text{ kg/m}^3)(9.8\text{ m/s}^2)(1.111 \times 10^{-3}\text{ m}^3\text{/s})(14\text{ m}) = 157\text{ J/s} = 157\text{ W}$$

8.6.2 Types of Pump

There are numerous types of pump used in the industry. In particular, consideration is given to centrifugal, positive-displacement, and screw pumps.

8.6.2.1 Centrifugal Pumps

The most common type of pump used in the chemical industry is the centrifugal pump although its performance deteriorates rapidly with an increasing viscosity of fluids, even with Newtonian fluids. The use of a centrifugal force to increase the liquid pressure is the basic concept associated with the operation of a centrifugal pump. Centrifugal pumps consist of a motor-driven impeller enclosed in a case. Fluid enters the eye of the impeller, which rotates at a fixed speed. The impeller is designed to convert kinetic energy into pressure energy. As the fluid is forced to the periphery of the blades, the cross-sectional area available for flow increases and the velocity falls, resulting in a decrease in kinetic energy. This is converted to pressure energy. The efficiency of conversion of kinetic energy to pressure energy will depend on the shape and size of the impeller and the number of blades.

Centrifugal pumps are most efficient with low-viscosity liquids such as milk and fruit juices, where flow rates are high and pressure requirements are moderate. They are also used for pumping liquids containing solid particles (grains in water). The simple design of the centrifugal pump makes it easily adaptable to cleaning-in-place functions. Centrifugal pumps are not self-priming and need to be filled with fluid prior to operation. For these reasons it is advisable to install pumps at ground level or below the level of the fluid being pumped.

8.6.2.2 Positive-Displacement Pumps

By application of direct force to a confined liquid, a positive-displacement pump produces the pressure required to move the liquid product. Product movement is related directly to the speed of the moving parts within the pump. Thus, flow rates are accurately controlled by the drive speed to the pump. The mechanism of operation also allows a positive-displacement pump to transport liquids with high viscosities. For a positive-displacement pump the volume of fluid delivered is largely independent of the discharge pressure. The two major types are the piston pump and the rotary pump.

Positive-displacement pumps are extremely useful for viscous fluids, fluids sometimes containing suspended solids, and for generating high pressures. They tend to be fairly expensive and require more frequent servicing, particularly piston pumps. Most positive pumps are self-priming and will fill with liquid when they are switched on.

8.6.2.3 Screw Pumps

Screw extruders form a most important class of pumps for handling highly viscous non-Newtonian materials. The basic function of the screw pump or extruder is to shear the fluid in the channel between the screw and the wall of the barrel. The mechanism that generates the pressure can be visualized in terms of a model consisting of an open channel covered by a moving plane surface. The fluid path in a screw pump is, therefore, of a complex helical form within the channel section. The velocity components along the channel depend on the pressure generated and the resistance at the discharge end (Chhabra and Richardson, 2011).

Finally, in selecting a pump for a particular application many factors have to be taken into account. The most important are summarized as follows:

- The pressure or head required
- The volumetric flow rate
- The physical properties of the fluid, that is, density, viscosity, suspended solids, and vapor pressure
- Intermittent or continuous service
- Hygiene considerations
- Susceptibility of product to shear damage

REFERENCES

Braun, D. D. and Rosen, M. R. 2008. *Rheology Modifiers Handbook: Practical Use and Application*. New York: William Andrew Publishing.

Çengel, Y. and Cimbala, J. 2010. *Fluid Mechanics: Fundamentals and Applications*. Boston: McGraw-Hill.

Chhabra, R. and Richardson, J. 1999. *Non-Newtonian Flow in the Process Industries. Fundamentals and Engineering Applications*. Oxford: Butterworth-Heinemann.

Chhabra, R. and Richardson, J. 2011. *Non-Newtonian Flow and Applied Rheology. Engineering Applications*. Oxford: Butterworth-Heinemann, 2nd edition.

Colebrook, C. F. and White, C. M. 1937. Experiments with fluid friction in roughened pipes. *Proceedings of the Royal Society of London. Series A, Mathematical and Physical Sciences*, 161(906):367–381.

Dodge, D. W. and Metzner, A. B. 1959. Turbulent flow of non-Newtonian systems. *AIChE Journal*, 5(2):189–204.

Earle, R.L. 1983. *Unit Operations in Food Processing*. Oxford: Pergamon Press, 2nd edition.

Fellows, P. 2000. *Food Processing Technology. Principles and Practice. Food Technology*. Cambridge: CRC Press and Woodhead Publishing Limited, 2nd edition.

Finnemore, E. and Franzini, J. 2002. *Fluid Mechanics with Engineering Applications*. Boston: McGraw-Hill, 10th edition.

Güzel, B., Frigaard, I., and Martinez, D. 2009. Predicting laminar-turbulent transition in Poiseuille pipe flow for non-Newtonian fluids. *Chemical Engineering Science*, 64(2):254–264.

Hanks, R. W. 1963. The laminar-turbulent transition for fluids with a yield stress. *AIChE Journal*, 9(3):306–309.

Hoogland, H. and Vlaardingen, D. 2005. Improving the hygienic design of pipes. In Lelieveld, H., Mostert, M., and Holah, J., editors, *Handbook of Hygiene Control in the Food Industry*. Cambridge: Woodhead Publishing Limited.

Ibarz, A. and Barbosa-Cánovas, G. 2003. *Unit Operations in Food Engineering. Food Preservation Technology Series*. Boca Raton: CRC Press.

Lewis, M. 2006. *Physical Properties of Foods and Food Processing Systems*. Cambridge: Wood-head Publishing Limited.

Madlener, K., Frey, B., and Ciezki, H. 2009. Generalized Reynolds number for non-Newtonian fluids. *Progress in Propulsion Physics*, 1:237–250.

Maroulis, Z. and Saravacos, G. 2003. *Food Process Design. Food Science and Technology*. New York: Marcel Dekker Inc.

Metzner, A. 1956. Non-Newtonian technology: Fluid mechanics, mixing, heat transfer. In Drew, T. and Hoopes, J., editors, *Advances in Chemical Engineering*, volume 1, pages 77–153. New York: Academic Press.

Metzner, A. B. and Reed, J. C. 1955. Flow of non-Newtonian fluids-correlation of the laminar, transition, and turbulent-flow regions. *AIChE Journal*, 1(4):434–440.

Mishra, P. and Tripathi, G. 1971. Transition from laminar to turbulent flow of purely viscous non-Newtonian fluids in tubes. *Chemical Engineering Science*, 26(6):915–921.

Moody, L. and Princeton, N. 1944. Friction factors for pipe flow. *Transactions of the A.S.M.E.*, 66(8):671–684.

Munson, B., Young, D., Okiishi, T., and Huebsch, W. 2009. *Fundamentals of Fluid Mechanics*. Boston: John Wiley & Sons Inc.

Nakayama, Y. and Boucher, R. 1998. *Introduction to Fluid Mechanics*. Oxford: Butterworth-Heinemann.

Osorio, F. A. and Steffe, J. F. 1984. Kinetic energy calculations for non-Newtonian fluids in circular tubes. *Journal of Food Science*, 49(5):1295–1296.

Pfenniger, W. 1961. Transition in the inlet length of tubes at high Reynolds numbers. In Lachman, G., editor, *Boundary Layer and Flow Control*. Oxford: Pergamon Press.

Ramaswamy, H. S. and Marcotte, M. 2006. *Food Processing. Principles and Applications*. Boca Raton: Taylor & Francis Group.

Rao, M. 2005. Rheological properties of fluid foods. In Rao, M., Rizvi, S., and Datta, A., editors, *Engineering Properties of Foods*, pages 41–91. Boca Raton: Taylor & Francis Group, 3rd edition.

Rao, M., Rizvi, S. S., and Datta, A. K. 2005. *Engineering Properties of Foods. Technology*. Boca Raton: Taylor & Francis Group, 3rd edition.

Sablani, S. S., Shayya, W. H., and Kacimov, A. 2003. Explicit calculation of the friction factor in pipeline flow of Bingham plastic fluids: A neural network approach. *Chemical Engineering Science*, 58(1):99–106.

Sahin, S. and Sumnu, S. G. 2006. *Physical Properties of Foods*. New York: Springer.

Sahu, J. 2012. *Fundamentals of Food Process Engineering*. Oxford: Alpha Science Intl. Ltd.

Singh, R. P. and Heldman, D. R. 2009. *Introduction to Food Engineering. Food Science and Technology*, *International Series*. San Diego: Academic Press, 4th edition.

Steffe, J. F. 1996. *Rheological Methods in Food Process Engineering*. East Lansing: Freeman Press.

Steffe, J. F. and Singh, R. P. 1997. Pipeline design calculations for newtonian and non-newtonian fluids. In Valentas, K. J., Rotstein, E., and Singh, R. P., editors, *Handbook of Food Engineering Practice*. Boca Raton: CRC Press.

Toledo, R. T. 2007. *Fundamentals of Food Process Engineering. Food Science Text Series*. New York: Springer, 3rd edition.

White, F. M. 2003. *Fluid Mechanics*. Boston: McGraw-Hill, 5th edition.

9 Diffusion

Theodoros Varzakas

CONTENTS

9.1 Diffusion Phenomena 264
9.1.1 Why Study Diffusion 267
9.1.2 Solute Mass Transfer in Food Systems 270
9.1.3 Usefulness of Effective Diffusivities 270
9.1.4 Prediction of Diffusivities 271
9.1.5 Experimental Considerations and Strategies 271
9.1.5.1 Food Material and Sample Preparation 271
9.1.5.2 Temperature Effect 272
9.1.5.3 Diffusion Liquid Medium 274
9.1.5.4 Agitation 275
9.1.5.5 Sampling for Concentration Determinations 275
9.1.5.6 Different Experimental Techniques and Equipment Used 275
9.1.5.7 Molecular Methods 276
9.1.6 Enzyme Infusion 277
9.1.7 Mathematical Background to the Calculation of Effective Diffusivities 279
9.1.7.1 New Numerical Techniques 286
9.1.8 Diffusion Cell 286
9.1.8.1 Method and Experimental Conditions 287
9.1.8.2 Mathematical Model Used for the Estimation of the Experimental Results 288
9.1.9 Modeling of Hyphal Penetration and Enzymatic Diffusion from a Stationary and a Moving Source 293
9.1.9.1 Kinetics: Diffusion/Adsorption Models 294
9.1.9.2 Mass Transfer Coefficient Approach 296
9.1.9.3 Steady Diffusion from a Sphere 298
9.1.9.4 Transport across a Film 299
9.2 Conclusions 300
Nomenclature 300
Greek Symbols 300
References 301

9.1 DIFFUSION PHENOMENA

Diffusion is a ubiquitous physical process that describes mass transfer purely under the influence of concentration gradients. Molecular diffusion is the transfer of individual molecules through a fluid by means of random individual movements. Diffusion phenomena are particularly significant when they are a limiting step in a sequence of interrelated processes or where diffusion is the principal process taking place. Within the food industry, examples of diffusion-dependent processes include the following: the extraction by leaching of sugar, apple juice, and coffee; vegetable blanching where both diffusion from and into the food may be important such as loss of nutrients by leaching; canning; preservation by salting and pickling; dehydration operations; frying, where the oil uptake and the water loss occur simultaneously; acidification, where the acid is diffused from the solution into the food. In leaching operations, the leachable solids are contained in a framework of insoluble solids, known as the marc, the occluded solution and, in some cases, sparingly soluble solids or solute precursors (Schwartzberg and Chao 1982). Diffusion occurs primarily within the occluded solution but the marc restricts the diffusion process and strongly affects the rate of diffusion. Therefore, when a material is being leached from a dry solid, the solid must first imbibe the solvent, to dissolve the external solute, before diffusion begins (Varzakas 1998a,b; Varzakas et al. 2005a).

Characterization of the diffusion process by concentration versus time profiles and diffusivities (diffusion coefficients) provides a useful way of comparing the effect of important variables on the process.

In a pure solution and under an equimolar concentration gradient the molecular diffusive process can be described by Fick's first law (Equation 9.1):

$$J = -D\frac{\partial c}{\partial x} \tag{9.1}$$

where J represents the flux relative to average molar velocity and $\partial c/\partial x$ is the concentration gradient of the species. The proportionality constant D is known as the molecular diffusion coefficient or diffusivity, which depends on the molecule and its environment and has the units of $m^2\ s^{-1}$. Values of D for gases are of the order of 10^{-5}, for liquids 10^{-9}, and solids 10^{-12}–$10^{-14}\ m^2\ s^{-1}$, respectively.

Fick's law governs many processes in the food and biotechnology industries including extraction processes such as oil from seeds, movement of salt in cheese and solutes in immobilized pellets.

In cheese technology, the mass transfer of small solutes, such as salt, moisture, and metabolites during brining and ripening, is very important for the final quality of the cheese. Floury et al. (2010) reviewed data concerning the diffusion coefficients of solutes in different cheese types; reviewed the experimental methods available to model the mass-transfer properties of small solutes in complex matrices such as cheese; and considered some potential alternative approaches. Numerous studies have reported the transfer of salt in cheese during brining and ripening. Regardless of the type of cheese and its composition, the effective diffusion coefficients of salt have been reported to be between 1 and $5.3 \times 10^{-10}\ m^2\ s^{-1}$ at 10–15°C. However, few

studies have dealt with the mass-transfer properties of other small solutes in cheese. Most of the reported effective diffusion coefficient values have been obtained by macroscopic and destructive concentration profile methods. More recently, some other promising techniques, such as nuclear magnetic resonance, magnetic resonance imaging, or fluorescence recovery after photobleaching, are currently being developed to measure the mass-transfer properties of solutes in heterogeneous media at microscopic scales. However, these methods are still difficult to be applied to complex matrices such as cheese. Further research needs to focus on (i) the development of nondestructive techniques to determine the mass-transfer properties of small solutes at a microscopic level in complex matrices such as cheese; and (ii) the determination of the mass-transfer properties of metabolites that are involved in enzymatic reactions during cheese ripening.

Although salt infusion, through blanching or marinating, has been known to successfully increase the electrical conductivity of solid food components, pretreatment times are long, and in most cases, equilibration between the solid and the liquid is still incomplete. A faster pretreatment method is needed. Previous studies have shown mass-transfer enhancement during electrical treatment. Kusnadi and Sastry (2012) determined the effective diffusion coefficients, D_{seff}, of salt into vegetable (celery, mushroom, and water chestnut) tissue under electric field at three temperatures (25°C, 50°C, and 80°C) and four electric field strengths (0, 658, 1316, and 1842 V/m).

The value of D_{seff} was significantly ($p < 0.05$) increased with temperature and electric field strength for all materials (celery, mushroom, and water chestnut). Activation energies for diffusivity decreased with increasing electric field strength for celery and mushroom, suggesting a diminished role for temperature when field strength was high. No trend was found for water chestnut, implying that it was temperature insensitive. Although in an alternating field the electrophoretic driving force either aligns with or opposes diffusion during each half cycle, the net result is an increase in ion transport over time. This is consistent with the rectification theory as expressed by the Nernst–Planck equation.

The depression of the melting temperature of ice under pressure permits to obtain a rapid freezing of foods. The expected benefit lies in reduced water diffusion from the intra- toward the extracellular media, resulting in a reduced drip loss during thawing. Besides, the modification of the cellular structure induced by ice formation may affect the mass diffusivity of the flesh. Alizadeh et al. (2009) used salmon as a model food. Slabs of salmon (1-cm thick) were frozen using blast air and pressure shift freezing at 200 MPa. The impact of the freezing process on the mass diffusivity of salt was evaluated using an aqueous solution (NaCl, 3% w/w). Results indicated that the effective mass diffusivity was slightly increased in comparison to nonfrozen flesh when a rapid freezing process was used. This may be attributed to a change in the permeability of cell membranes caused by freezing and high pressure.

Predicting microbial evolution in soft cheeses, which suffer the colonization of several pathogens, such as *Listeria monocytogenes*, is a main objective in the improvement of food safety conditions. Noriega et al. (2008a,b) assayed a model that considers diffusional limitations during pathogen's growth in structured foods. To test the feasibility of the model, *Listeria innocua* evolution with time and position was monitored in structured model cheeses prepared to mimic soft cheeses with

different lactic acid contents. The prediction of biomass and substrate evolution requires the kinetics under different aeration conditions. *L. innocua* behavior was also studied in broths prepared with similar composition to model cheeses, evaluating the effect of oxygen concentration on cell growth. The assayed model provided quite accurate results for low concentration of lactic acid, whereas for lactic acid concentrations higher than 3 g L^{-1} cell development in structured media was inhibited.

Experiments to validate the model were conducted measuring the distribution and evolution of *L. innocua* growing in a solid κ-carrageenan model food. Preferential growth on the surface was measured in the solid food, changes inside the medium being much more limited. A good concordance was obtained between the model simulations and the experimental results in the solid food. Some slight differences were nevertheless observed on the surface due to the effect of the different environment surrounding the cells.

Molecular diffusivity can be used to characterize the diffusive process in particular, in determining the effect of solvent viscosity and temperature, which are often the most important variables. Cussler (1984) gives a list of molecular diffusivities in water.

In diffusion processes relevant to food processing, the concentration gradients are usually time dependent and the diffusional process may be better represented by Fick's second law for unsteady-state diffusion. The coefficient is frequently referred to as effective diffusivity D_{eff} (also known as apparent diffusivity, or D_{app}) and describes a net diffusional mass transfer through chemically and structurally complex, heterogeneous systems (Equation 9.2). The molecular and the effective diffusivities must be differentiated. The phenomenon of effective diffusivity appears generally in foodstuffs. Moreover, in a porous medium D_{eff} is smaller than D.

$$\frac{\partial c}{\partial t} = D\frac{\partial^2 c}{\partial x^2} \quad \text{For unidirectional diffusion} \tag{9.2}$$

$$\frac{\partial c}{\partial t} = D\left(\frac{\partial^2 c}{\partial x^2} + \frac{\partial^2 c}{\partial y^2} + \frac{\partial^2 c}{\partial z^2}\right) \quad \text{For multidirectional diffusion} \tag{9.3}$$

where t is the time and x, y, z are the spatial coordinates (Equation 9.3, Gekas 1992). The generalized form of Fick's equation describing the transient-state diffusion of a component with concentration c in a binary system is called Fick's law and may be expressed as in Equation 9.3. This equation holds for an isotropic medium whose structure and diffusion properties in the vicinity of any point are the same in all directions (Crank 1975). The form of Fick's second law (Crank 1975), which refers to unidirectional diffusion across geometrical barriers (Equation 9.4), can be applied to solute diffusion in solid foods:

$$\frac{\partial c}{\partial t} = \frac{1}{x^{\nu-1}}\frac{\partial}{\partial x}\left(x^{\nu-1}D\frac{\partial c}{\partial x}\right) \tag{9.4}$$

where $\nu = 1$ for a slab, $\nu = 2$ for a cylinder, and $\nu = 3$ for a sphere.

General solutions of Fick's second law can be obtained for a variety of initial and boundary conditions. Mathematical solutions are presented by Crank (1975) either as a series of error functions (suitable for small times) or as trigonometric or Bessel function series (suitable for large times).

The diffusion rate is defined as the distance covered by the solute per unit time and its value depends on the specific medium in which a particular process takes place. In gases, the diffusion rate is around 10 cm/min, in liquids about 0.05 cm/min, and in solids it is of the order of 10-5 cm/min (Cussler 1984). In many cases, diffusion occurs simultaneously with other phenomena and since it is a slow step it often limits the overall rate of the process. Diffusion in the solid matrix is more complicated than diffusion in a gas or in a liquid. It might be that diffusion in a solid matrix does not occur and what happens is diffusion in the liquid or gas contained within that porous matrix.

Roques (1987) has reported that the measurements of real diffusion coefficients are always influenced by other interfering phenomena. A great variety of methods have been used for the determination of diffusion coefficients, however, there is a great difficulty in comparing different results as well as systemizing the whole pack of information.

Gekas (1992) has also reported published diffusion coefficients for a wide variety of foods. It is well known that the diffusion coefficient depends on other factors such as temperature, and the relationship between the diffusion coefficient and temperature depends on the diffusional mechanism. This dependence of the diffusion coefficient on temperature in food systems may be determined using the Stokes–Einstein equation presented later in this section (Equation 9.5).

In many cases, the determination of the diffusion coefficient is dependent on accurate determination of the equilibrium value. Oliveira (1988) has discussed the difficulty of predicting equilibrium concentration in food systems and the need to obtain it experimentally or using optimization methods. Partition coefficients may be used to describe equilibrium conditions for a solute diffusing from a solid to an aqueous solution. This is defined as the ratio of solute concentration in the solid to the solute concentration in the medium at equilibrium. Azevedo and Oliveira (1993) obtained partition coefficient values for acetic acid diffusion into potatoes and an agarose gel to be 0.86 and 0.94, respectively.

Moreira (1994) also presented an overview of published diffusional parameters of solutes in foods such as values of selected diffusion coefficients and activation energies, which are shown in Table 9.1.

9.1.1 Why Study Diffusion

Estimation of diffusion coefficients or diffusivity is important since it enables the estimation of the values of rates of mass transfer. In the case of cellular materials, even if the macromolecules are chemically bound to the solid matrix, the overall rates of reaction may be diffusion limited, so further understanding of these processes requires knowledge of the nature and properties of these diffusion-driven events (Berg and Von Hippel 1985). Many theoretical and experimental studies have been carried out on the diffusion of solute through cellular and biological

TABLE 9.1
Overview of Published Diffusional Parameters of Solutes in Food

Reference	Food	Solute	T (°C)	$D \times 10^{-9}$ (m^2s^{-1})	Ea (kJ/mol)
Abdel-Kader (1992)	Peas	Ascorbic acid	50	9.4	18.7
			60	11.9	
			70	13.7	
			80	16.6	
			90	19.4	
Abdel Kader (1991)	Potato	Glucose	60	0.314	29.1
			70	0.394	
			80	0.53	
			90	0.742	
Califano and Calvelo (1983)	Potato	Reducing sugars		1.13	
				0.495	
Garrote et al. (1986)	Potato	Ascorbic acid	50	0.153	49.5
			65	0.932	
			80	1.427	
			100	2.143	
Garrote et al. (1984)	Potato	Glucose	55	0.23	21.2
			65	0.82	
			85	1.25	
Garrote et al. (1988)	Potato	Ascorbic acid	50	1.364	25
			65	1.778	
			80	2.03	
Hashiba et al. (2008)	Egg white	Sodium chloride			
Kincal and Kaymak (1990)	Potato	Ascorbic acid	70	1.15	9.46
			80	1.24	
			90	1.38	
Kozempel et al. (1982)	Potato	Ascorbic acid			
		Thiamine			
		Riboflavin			
		Niacin			
Lathrop and Leung (1980)	Peas	Ascorbic acid		14	
Nicolas and Duprat (1983)	Agarose	Potassium nitrate	30	1.765	11.6
			40	1.926	
			50	2.218	
			60	2.486	
Oliveira and Silva (1992)	Carrots	Reducing sugars	40–100	0.7–1.8	24.1
	Prefrozen			0.4–1.1	14.2
Pflug et al. (1967)	Pickles	Sodium chloride	20–70	0.7–2.8	
Rice and Selman (1984)	Peas	Ascorbic acid	70	0.4	50.1
			85	1.1	
			97	1.4	

TABLE 9.1 (continued)
Overview of Published Diffusional Parameters of Solutes in Food

Reference	Food	Solute	T (°C)	$D \times 10^{-9}$ ($m^2 s^{-1}$)	Ea (kJ/mol)
Selman et al. (1983)	Carrots	Soluble solids	60 70 80 90	0.307 0.413 0.536 0.764	28.2
Turhan et al. (2006)	Carob bean	Soluble solids and phenolic compounds	20, 50, 85		5.84, 0.072 × 10^{-3} at 20°C
Pinelo et al. (2008)	Apple skin	Total phenols		Lower particle size (1.8×10^{-8} to 2.6×10^{-8} m^2/s), larger particles 0.2 to 1.5×10^{-8}	
Li et al. (2012)	Cherry tomatoes	Sucrose and salt	30	1.31	
Kusnadi and Sastry (2012)	Celery, mushroom, and water chestnut	salt	25, 50, 80	2–60 × 10^{-8} m^2 s^{-1}	Decrease with increased electric field strength

Source: Adapted from Moreira, L.A. 1994. Acidification of vegetables during blanching. PhD thesis, Escola Superiora de Biotecnologia, Porto, Portugal; Varzakas, T. et al. 2005b. *Enzyme Microb. Technol*., **37**, 29–41; Varzakas, T. 1998a. Uptake of cell-wall degrading enzymes by soybean preparations. PhD thesis, The University of Reading, Reading, UK.

materials (Fox 1980; Naesens et al. 1981; Guilbert 1985; Gros and Ruegg 1987). Although considerable literature is available on diffusivities of small molecules (like glucose), information relating to larger molecules, such as enzymes is not easily found. These values will be useful to assess the extent of their diffusion during extraction, for example, the amount of pectic substances extracted during the production of apple juice by diffusion (Leach et al. 1995). In cases where enzymes are used to alter extraction values, the values of enzyme infusion can be estimated.

Salting of quail eggs, for their conservation, is usually done by immersion in saline sodium chloride solution (Murakami and Ariki, 1998) and the apparent or effective coefficients of diffusion are determined experimentally (Zorrilla and Rubiolo, 1994). Recently, Hashiba et al. (2008) presented NaCl concentration profiles for one-dimensional diffusion in precooked egg white, at various temperatures, considering the phenomenon of the Languimir-type sorption. As far as it is known, there are no studies using finite element method (FEM) to simulate multicomponent diffusion in whole and pre-cooked eggs, using the Fick generalized equation and

according to Wang and Sun (2003), there are few publications in the area of foods that use FEM for simulation under three-dimensional conditions.

9.1.2 Solute Mass Transfer in Food Systems

Food matrices, whether of plant or animal origin are complex, multicomponent, and frequently anisotropic (Gekas 1992; Vincent 1989). Solute mass transfer may occur through occluded solutions occupying pores in the tissue and is influenced by the volume of the occluded solution, porosity, and the diffusional path tortuosity (Oliveira 1988). Mass transfer also needs to occur through physiological barriers such as cell walls and particularly cell membranes and in this case these barriers provide the dominant resistance (Kays 1991). Other important barriers might be the cytoplasm surrounded by plasmalemma or middle lamella; the vacuole surrounded by the tonoplast. The different membranes constitute the solid phase or the interfaces, holding a liquid phase (vacuole) or the gaseous phase (intercellular spaces) (Moreira 1994). In processing operations involving extraction, conditions are chosen to denature cell membranes removing this resistance to mass transfer. This is usually accomplished by application of sufficiently high temperature (Bruniche-Olsen 1962; Osterberg and Smith-Sorensen 1981; Leach 1993), though freezing could also be used to improve solute mass transfer (Garrote et al. 1986; Oliveira and Silva 1992).

9.1.3 Usefulness of Effective Diffusivities

The effective diffusivity is the key parameter in many situations in food and biotechnology processing. Effective diffusivities are most convenient to describe the process of diffusion through porous solids, which have an intricate network of pores where the diffusing species take a tortuous path. In a porous medium, the effective diffusion coefficient will be significantly smaller than the molecular diffusion coefficient due to tortuosity effects (the more tortuous the region the more devious the route between two points) and hindering effects of the surface of the pores on the molecule's random oscillations (Pyle et al. 1997). Furthermore, Blasinski and Amanowicz (1979) explained this by mentioning two similar reasons. First, the volume of the capillaries in which diffusion occurs is smaller than the volume in which free diffusion into a liquid with the volume occupied by the solid occurs. Second, the motion of particles in capillaries is far slower than in a liquid medium because the capillary walls react inhibitingly on a diffusing particle.

The ratio between the molecular diffusivity of the solute in water and the effective diffusivity from a food material can be characterized by a hindering factor K (Lamberg 1990) accounting for the effects of structural and chemical hindrance of the solute diffusion by the food material. In a porous medium, the measured coefficient will be smaller than the molecular diffusion coefficient due to tortuosity effects (the more tortuous the region, the more devious the route between two points) and hindering effects of the surface of the pores on the molecule's random oscillations.

9.1.4 Prediction of Diffusivities

Molecular diffusivity at a constant temperature may be adequately predicted in very dilute solutions, provided the molecular radius, solvent viscosity, and absolute temperature are known, using the well-known Stokes–Einstein equation (Equation 9.5). The equation neither accounts for intermolecular interactions between solute molecules nor between solvent and solute molecules that may be significant for small solute molecules.

$$D = \frac{k_B T}{6\pi\mu R_0} \tag{9.5}$$

where K_B is the Boltzman constant, T is the absolute temperature, μ is the viscosity of the phase, and R_0 is the radius of the diffusing molecule. However, the equation has little use in the prediction of effective diffusivities from food materials. Various alternative equations have been subsequently developed (Wilkie and Chang 1955; Schwartzberg and Chao 1982) incorporating factors for molecular interactions and physical interferences. However, due to the difficulty in quantifying such factors in heterogeneous food systems and the inherent variability in food materials these equations have limited use in the prediction of effective diffusivities from foods. Moreover, the effective diffusivity should always be determined experimentally in conjunction with the use of fundamental mathematical relationships based on solid geometries as will be discussed subsequently. However, Brune and Kim (1993) predicted molecular diffusion coefficients for proteins in water using a general numerical method. This was applied to rodlike (tobacco mosaic virus) and globular (lysozyme) proteins. Tyn and Gusek (1990) have used a correlation to predict the diffusion coefficients of proteins by adapting the Stokes–Einstein equation to a model for the equivalent hydrodynamic sphere using the radius of gyration which accounts for the size and shape of protein molecules in solution.

9.1.5 Experimental Considerations and Strategies

The primary aim of the experimental component of effective diffusivity determinations is to select and obtain a series of solute content versus time curves which are appropriate to the equation model chosen.

9.1.5.1 Food Material and Sample Preparation

The first consideration is to ensure that solute concentration variations in the solution are only due to the diffusive process. In some cases, the process of slicing or cutting may release some solute. A single variety of the natural material, having consistent maturity, and ideally obtained from the same source, should be used. Plant material should ideally be obtained in a single batch and stored under conditions promoting low metabolic activity (Varzakas et al. 2005a).

Sample preparation is usually required so that the tissue section has the geometric form consistent with the model used. A fixed diameter circular template may

be used to obtain cylinders of consistent dimensions. Moreover, in order to obtain slices (approximating to slab geometry), slices of set thickness from a cylindrical template may be cut, recorded accurately and statistically averaging the thickness. If the experiments are in small particles, then material may be graded using sieves, and a particle size distribution obtained and accounted for in the model.

Where the tissue itself shows structural heterogeneity, care should be taken to avoid regions with a markedly different structure (e.g., the skin and core regions of apple tissue), unless the effects of such regions are the subject of investigation (Stahl and Loncin 1979). If the removal of this area would cause too great a deviation from the actual process, this could apply, for example, if a skin structure would normally be found on one of the infinite surfaces. In the case of an anisotropic structure, care should be taken to apply the template in the same axis each time. Intrinsic variations may still occur between samples. However, this can be reduced further by determining in advance the sample size (base sample) which if chosen repeatedly at random will yield acceptable variation in solute content.

9.1.5.2 Temperature Effect

Many investigations require that the effective diffusivity be determined at a range of precise temperatures. Frequently, the relationship between effective diffusivity and absolute temperature (T) follows a first-order rate process described by an Arrhenius relationship (Equation 9.6), where A is a pre-exponential factor.

$$D_{eff} = A \exp \frac{-E_a}{RT} \tag{9.6}$$

This relationship can then be numerically characterized by an activation energy Ea (kJ mol^{-1}). The activation energy can be readily obtained from a plot of ln D_e versus $1/T$ (Selman et al. 1983; Rodger et al. 1984; Garrote et al. 1986; Kincal and Kaymak 1987, 1990; Tomasula and Kozempel 1989; Rice et al. 1990).

Deviations from the Arrhenius relation were observed by Lazarides et al. (1997), who measured the apparent mass diffusivities during osmotic processing of apple and potato tissues using Fick's second law. Temperature had the largest positive effect on moisture and soluble solids diffusivity. Moisture and solute diffusivities followed Arrhenius kinetics with activation energies ranging between 21.2 and 29.7 kJ mol^{-1} K^{-1} and moderate-to-poor coefficients of correlation. These values are similar to those quoted by Abdel-Kader (1991) and Garrote et al. (1986). There was a stronger dependence of the solute diffusivity than water diffusivity on temperature and this may reflect the different mechanisms of transport for sugars and water in the cell. The transport of sugars is controlled by facilitating protein carriers. Gekas et al. (1993) have shown that these carriers suffer sharp changes at critical temperatures for both apples and potatoes and hence the use of the Arrhenius equation in foods with such a complex structure could be biased through temperature effects on structure.

An accurate thermostat is used either to directly contain an infinite volume of solvent or to maintain flasks containing the appropriate sample size of solids together with the finite volume of the diffusion solvent. In the latter case, it is important to

prevent evaporation losses of the solvent. If the material is of small dimensions or has a relatively open structure, then it will rapidly attain the desired temperature on immersion into the solvent and the time required to alter the measured temperature is minimal. However, some researchers have covered the samples with aluminum foil and heated them to the desired temperature before immersing into the solvent (Kincal and Kaymak 1987).

Pinelo et al. (2008) examined the influence of the extraction conditions, temperature, apple skin particle size, solvent composition, and enzymatic maceration on extraction yields and mass-transfer rates of the main phenolic compounds of apple skins. Mass transfer of the phenolics was assessed by linearization of Fick's second law. Increased temperature, size reduction, and presence of ethanol in the solvent generally increased the mass-transfer rates of phenolics, although each one of these variables had a different effect on the release of each individual phenol compound studied: epicatechin, procyanidin B2, rutin, chlorogenic acid, phloridzin, and a phloridzin derivative. Application of cell wall degrading enzyme preparations, Pectinex Smash (pectinase), Celluclast 1.5 L (cellulase), and Sumizyme (protease) prior to extraction, resulted in a general increase in Fick's module, defined as ($\pi^2 D_{eff}/r^2$). Values of Fick's module for total phenols ranged from 0.0859 to 0.1552 s^{-1} with solvent extraction and from 0.0981 to 0.1834 s^{-1} with enzyme-assisted extraction. Enhanced pectinase and protease dosages thus significantly improved the phenol transfer. This study showed that phenols can be selectively extracted by varying the extraction conditions and by adding cell wall degradation enzymes.

The effective moisture diffusivity of food is known to be either independent or dependent of moisture content (Zogzas et al. 1996; Chen 2007; Loulou et al. 2006; Bourlieu et al. 2008). In the case where it is independent of moisture content, the Arrhenius relation is often used to represent its variation with temperature. However, the dependence of the diffusion coefficient on moisture content is not clearly demonstrated.

There is no general model for describing the relationship between effective diffusivity and moisture content.

Foamed banana product, a crispy snack, can quickly adsorb the moisture from the moist air, leading to loss of textural property. Prakotmak et al. (2011) studied moisture adsorption kinetics of dry banana foam mat and its texture quality change. The adsorption isotherm experiments were carried out with a standard static method using saturated salt solutions over a wide range of relative humidities from 32% to 82% and temperatures of 35°C, 40°C, and 45°C. Three dry banana foam densities of 0.21, 0.26, and 0.30 g/cm^3 adsorbed water vapor under controlled conditions. Fick's second law coupled with an optimization technique was used to estimate the effective moisture diffusivity at sorption conditions.

Empirical equations with two and three constant parameters for describing the dependence of the effective moisture diffusivity on moisture content were tested. The two constant parameters could suitably describe the variation of the effective moisture diffusivity with moisture content. The initial foam density, relative humidity, and temperature significantly affected the effective moisture diffusivity. The banana foam mats for all densities lost their crispy texture at moisture content of 0.078 kg/kg db.

Wiktor et al. (2013) studied the influence of pulsed electric field (PEF) on the drying kinetics of apple tissue. Therefore, mathematical models were applied to describe the process. PEF treatment of the samples was carried out at an intensity of $E = 5–10$ kV/cm and 10–50 pulse numbers.

Subsequently, the apples were convectively dried at 70°C and air velocity of 2 m/s. Based on electrical conductivity measurement, the cell disintegration index Zp was computed. Midilli et al.'s (*Drying Technology*, Vol. 20, pp. 1503–1513, 2001) model was evaluated as the most adequate to describe the moisture transfer in PEF-treated and intact samples. PEF pretreatment induced a reduction in drying time of up to 12% when 10 kV/cm and 50 pulses were applied. For instance, after 60 min of drying, the dimensionless moisture ratio for PEF-treated (10 kV/cm, 50 pulses) samples was 0.18 compared to 0.26 for the untreated apples. The effective moisture diffusivity, calculated on the basis of the Fick's second law, was 1.04×10^{-9} m^2/s for intact samples and from 1.09×10^{-9} to 1.25×10^{-9} m^2/s for PEF-treated samples at 10 pulses at 5 kV/cm and 50 pulses at 10 kV/cm, respectively.

9.1.5.3 Diffusion Liquid Medium

If the material has a density of less than or same as the solvent, there are two important considerations. Primarily, it will need to be held within the bulk of the solvent by some framework (Binkley and Wiley 1981; Leach 1993). Furthermore, the solid may initially imbibe the solvent to such an extent that if solid-phase measurements are made during this period, a decline in solute concentration may be falsely attributed to a diffusive process. It is important to assess the significance of such a decline in advance. Leach (1993), working with apple tissue used a pre-immersion step prior to immersion into the bulk solvent to alleviate this effect. It is desirable to allow a definite time period of contact with the solvent, sufficient to ensure that the solvent has diffused into the air spaces.

To elaborate dehydration and osmotic equilibrium characteristics of cherry tomatoes and to analyze the applicability of Peleg model in prediction of equilibrium moisture content and the methodology of Crank's solution to Fick's diffusion law in calculation of effective diffusivity, cherry tomatoes were osmotically treated in ternary solution (water, sucrose, and NaCl) with or without ultrasound at 30°C as reported by Li et al. (2012).

Results indicated that a time cumulative effect of ultrasound occurred about 30 min for water loss (WL), while for sugar gain it happened after 45 min, which made the dehydration efficiency index best at the ultrasonic power of 150 W for 40 min. As a function of salt content, the equilibrium WL followed well the first-order exponential decay model, and the equilibrium salt content followed well the second-order polynomial. A great relative error (29.13%) between the practical determination and the predicted value indicated that Peleg model was not suitable for prediction of equilibrium moisture content. A great truncation error (865%) occurred when moisture effective diffusivity (6.66×10^{-9} m^2 s^{-1}) was calculated with Crank's solution to Fick's diffusion law by letting $n = 1$ as compared to that (0.77×10^{-9} m^2 s^{-1}) by letting $n = 100$.

Moreover, solubility of polyphenolic compounds and their diffusion to solvent depends on their chemical structure that may vary from simple to highly polymerized

compounds; thus, the choice of solvent is one of the most relevant steps in extraction process. According to literature (Escribano-Bailon and Santos-Buelga 2003), the most frequently used solvents with different efficiency in extraction of plant phenolics are methanol, ethanol, propanol, acetone, ethyl acetate, dimethylformamide, their mixture and their mixture with water.

Bucic-Kojic et al. (2009) investigated the efficiency of four extraction solvents (water and different aqueous solutions of ethanol: 50%, 70%, and 96%) and temperature influence (25°C, 40°C, 50°C, 60°C, 70°C, and 80°C) on extraction of total and individual polyphenolic compounds as well as proanthocyanidins from grape seeds and antioxidant activity of extracts. The relationship of determined compounds with antioxidant activity and extract's color was also estimated.

9.1.5.4 Agitation

The diffusion liquid medium should be agitated in some way to evenly distribute the heat and also to satisfy the key requirement of the model that has no external resistance to mass transfer.

9.1.5.5 Sampling for Concentration Determinations

The extent of diffusion can be monitored by determining the solid or liquid phase concentrations of the solute. Liquid phase concentrations are relatively easier to measure and errors involved are not significant. However, this would imply that the boundary conditions are changing with time and a more complicated model for diffusion should be used.

In practice, a large excess of liquid volume is used so that liquid phase concentration changes over the duration of the experiment are negligible. The extent of diffusion is determined by collecting solid samples and determining the amount of remaining solute. This simplifies the mathematics but there could be errors in sampling due to lack of homogeneity.

9.1.5.6 Different Experimental Techniques and Equipment Used

There is considerable variation in the experimental configurations adopted by various workers. Binkley and Wiley (1981), investigating the effects of different treatments on diffusion from apple, adopted an approach where 10 slices were fixed to a small wire frame immersed in a solvent containing flask placed in a water bath, however, the flasks were only agitated prior to obtaining the sample from the liquid phase. Lenart et al. (1989) and Leach et al. (1995), worked with apples and used effectively infinite volumes of solvent. The former was used a compartmentalized chamber, with two slices corresponding to a given time interval in each chamber. Sufficient agitation was obtained by continuous recirculation of the solvent through the chamber. The latter used a constant temperature shaking water bath to provide temperature control and agitation and a diffusivity frame upon which six subframes were mounted each containing 12 apple slices; individual subframes being removed after appropriate intervals of time.

Djelveh et al. (1989) have reported the use of a diffusion cell to measure the apparent diffusion coefficients of solutes through foodstuffs. A mathematical model was used to obtain the effective diffusion coefficient of NaCl through 3% agar gels. The

diffusion coefficient of Cl^- in gel at 25°C was 1.3×10^{-9} m^2 s^{-1} in less than 110 min. Longo et al. (1992) determined the diffusion of proteases from *Bacillus subtilis* and *Serratia marcescens* within calcium alginate beads. Modeling of data was carried out for diffusion into a finite volume liquid medium. Hulst et al. (1989) determined the D_{eff} of oxygen again using gel materials in relation to gel concentration. Crank's model (1975) was fitted on their data and the model described the solute diffusion from a well-stirred solution into gel beads which are free of solute initially. The results showed a decreasing D_{eff} for agar and agarose at increasing polymer concentration in the gel. The D_{eff} of oxygen for κ-carrageenan, alginate, and gellan gum was in the range of $1.5–2.1 \times 10^{-9}$ m^2 s^{-1}.

The lag-time analysis technique using a diffusion cell has been used by Bassi et al. (1987) to measure diffusion coefficients of lactose and lactic acid through a 3% agarose gel membrane. Average diffusion coefficients were estimated to be 3.97 and 2.9×10^{-10} m^2 s^{-1} for lactose and lactic acid, respectively. The lag time represents the period required to form a steady state in the concentrations of pathway intermediates and enzyme–metabolite complexes. It is a form of the transition time, τ, which is the time that a metabolic system changes from one steady state to another after a perturbation (Welch and Easterby 1994). They also reported that the cytoplasmic diffusion coefficients of macromolecule-sized probes are 10–100 times smaller than the corresponding values in water whereas for metabolite-sized ones, the diffusion coefficients are 2–4 times smaller due to a low viscosity within the interstitial voids.

A diffusion cell and a polysulfone membrane were used for the estimation of the effective diffusion coefficient (D_{eff}) of endoglucanase and lysozyme (Varzakas e al. 1999). D_{eff} was calculated from the slope obtained by fitting the amount of protein transferred through the membrane against time using the appropriate mathematical equation for the steady state. The calculated D_{eff} for endoglucanase was in the order of 10^{-13} m^2 s^{-1}, whereas the calculated D_{eff} for lysozyme was an order of magnitude lower.

9.1.5.7 Molecular Methods

Molecular methods such as pulsed-gradient spin–echo NMR and quasi-electric light scattering studies have also been constructed. In particular, pulsed-field gradient NMR spectroscopy has been used to measure ovalbumin intradiffusion coefficients in polymeric porous gel filtration particles. The protein tracer diffusivity is decreased by 2.2 at all concentrations, consistent with the tortuosity model for transport in pores (Gibbs et al. 1992).

Westrin (1991) measured the diffusion coefficient of ethanol in 4% (w/w) agarose gel at 25°C and found it to be within the range of $8–9.5 \times 10^{-10}$ m^2 s^{-1}. He used the method of unsteady-state diffusion into and out of gel beads dispersed in a solution of finite volume. In his study, NMR and a diaphragm cell were used. NMR techniques have also been used by Kuhn and Lechert (1990) to determine diffusion coefficients of water in slices of potato tissue, whereas they were calculated using the Darken one-dimensional equation (Equation 9.7):

$$D_f = D_s \frac{x}{a_w} \frac{\partial a_w}{\partial x} \tag{9.7}$$

where a_w is the water activity, and x is the moisture content, which are both obtained from the sorption isotherm.

The effective diffusivity of endoglucanase, endoxylanase, pectinase as well as a mixture of endoglucanase and pectinase from *Aspergillus niger* was estimated in food-agarose gels by measuring their diffusion zones and assuming that the Fourier number is unity. The calculated D_{eff} for these enzymes and the mixture was estimated to be of the order of 10^{-9} m^2 s^{-1} (Varzakas 2000).

Diffusion coefficients in gels have recently been measured by holographic interferometry as reported by Gustafsson et al. (1993). This new direct technique avoids sampling and analysis of the solution outside the gel. These workers experimented with ethanol diffusing into and out of an agarose gel. Monte Carlo simulations were used to compare with the standard deviations of the experiment and also to study the effect of random errors in the experiment.

9.1.6 Enzyme Infusion

Enzymes can be applied to intact plant tissue to alter its functional properties or alter albedo structure while other characteristics such as segment integrity are left unaltered (McArdle and Culver 1994). Enzyme infusion is the application of exogenous enzymes to change both surface and interior characteristics such as tissue composition (Steinke and Johnson 1991), morphology (Bruemmer et al. 1978), or texture (Javeri et al. 1991) as well as alter nutritional value (Blanc et al. 1992). Enzyme infusion is a way to create changes in foods or food ingredients without significant processing and simultaneously to discourage consumer concerns already existing over genetically engineered foods. It is difficult, though, to characterize and monitor enzyme movement within and between cells. There are some studies of enzyme production and migration in plant tissues. Aleurone cells of cereal grains secrete enzymes into the germinating seed (Hillmer et al. 1992). Gibbons (1980) used fluorescent immunostaining to show that alpha-amylase in germinating barley seeds migrates by diffusion to and through the endosperm. In a similar study, Beers and Duke (1988) found alpha-amylase in intercellular spaces of pea stem tissue. Migration of small-to-medium proteins was observed in soybean cell-wall channels which were about 66–88 Å in diameter (Baron-Epel et al. 1988). Nicole et al. (1992) and Benhamou and Cote (1992) showed that cell-wall-degrading enzymes were produced by invading fungal hyphae diffuse across cell walls. Biekman (1992) observed that diffusion of the enzyme into potato tissue was the rate-limiting step of tissue degradation during enzymatic potato maceration. Varzakas (1998a,b) and Varzakas et al. (1995a, 2005a) reported a preliminary investigation on the infusion of endoglucanase and endoxylanase from *Aspergillus niger* using fluorescent microscopy and D_{eff} for both enzymes was estimated to be of the order of 10^{-12} m^2 s^{-1}.

Movement of large molecules may occur not only through free liquid present outside cell walls but also through channels or pores in cell walls. It may also be that molecules first diffuse into the liquid that surrounds the cell wall before they attach to the latter. Baron-Epel et al. (1988) estimated soybean cell-wall channels to be approximately 6.6–8.8 nm in mean diameter. Molecules with Stokes radii up to 3.3 nm were found to be unhindered in their movement across the cell wall, whereas

dextrans with a Stokes radius higher than 4.6 nm travelled much slower. According to Baron-Epel et al. (1988), the slow transport of the latter could reflect either a few larger transport channels or a slow process of reptation through a homogeneous population of narrow channels. They also reported that treatment of cultured cells with pectinase but not protease or cellulase increased the channel size.

Salmon et al. (1984) has measured the diffusion coefficient of tubulin in the cytoplasm of embryonic cells of the sea urchin *Lytechius variegatus* by the fluorescence redistribution after photobleaching technique (FRAP). Diffusion coefficient was calculated according to Fick's second law of diffusion and was found to be 5.9 and 8.6×10^{-12} m^2 s^{-1} for tubulin and bovine serum albumin (BSA). The same technique has been used by Metcalf et al. (1986), who incorporated fluorescent lipid and phospholipid probes into the plasma membrane of soybean protoplasts aiming at monitoring their lateral mobility. Diffusion coefficients of the order of 10^{-13} and 10^{-14} m^2 s^{-1} were reported. Two simultaneous diffusion coefficients with a single lipid probe were observed. This showed evidence of lipid domains in the plasma membrane of soybean protoplasts. Dugas et al. (1989) have used fluorescence photobleaching recovery to measure lateral diffusion coefficients and mobile fractions of fluorescent-labeled plasma membrane proteins and lipids from maize protoplasts. The lateral diffusion coefficient and the mobile fraction of the proteins average values of 5 and 0.56×10^{-15} m^2 s^{-1}, respectively. FRAP has also been used to measure the D_{app} for fluorescein-labeled IgG and fluorescein-labeled BSA injected in the cytoplasm of human fibroblasts by erythrocyte-mediated microinjection. These were estimated to be 1×10^{-12} m^2 s^{-1} at 22°C (Wojcieszyn et al. 1981).

Electron spin resonance and fluorescence probes constitute very useful tools. These show values of only 3–5 times that of water for small diffusing molecules (intermediary metabolites) (Westerhoff and Welch 1992). This is due to the fact that most of the cytoplasmic proteins are absorbed to membranous and cytoskeletal elements rather than in solution. High viscosity could facilitate transport by three-dimensional diffusion within cells and might take intracellular diffusion processes more important than in dilute solution. Electron spin resonance has been used by Mastro et al. (1984) to measure diffusion of a small spin label in the aqueous cytoplasm of mammalian cells. An average diffusion coefficient of 3.3×10^{-10} m^2 s^{-1} was estimated.

Stimulus–response tracer techniques are useful for the determination of the mass-transfer characteristics of beds of lignocellulosic materials. Hradil et al. (1993) have used this technique, using glucose as a tracer, to characterize packed beds of untreated, acid pre-hydrolyzed and enzymatically hydrolyzed aspen wood chips. Interparticle and intraparticle void fractions, effective diffusivities, porosities, and tortuosities have been determined.

It is well known that diffusion, adsorption, shear and thermal inactivation of enzymes affect the velocity of the total process. Transport phenomena and adsorption in maceration processes have not attracted great attention. Recently, Biekman and Van Dijk (1992) have modeled the enzymatic maceration of potatoes and concluded not only that there is enzymic diffusion through the tissue but also that blanching affects the effective diffusion in a positive way.

Tanaka et al. (1988) have reported the effect of cellulase pore size on hydrolysis of cellulose fiber by comparing crosslinked with normal cellulase. They tested the hypothesis that when large pores dominate, the catalytic enzymic action becomes high with the effect of an increase in the available surface area. However, the existence of small pores causes limited diffusion of smaller enzyme components into the pores with the immediate result of their inactivation and decrease in the rate of solubilization since there is no synergism with the bigger enzyme molecules and the molecular movement is lowered.

Gekas and Lamberg (1991) determined the diffusion coefficients in systems where volume changes occurred during drying. They applied a modified Crank approach (Crank 1975) to potato drying, for raw and blanched potatoes at two temperatures. D_{eff} values of the order of 10^{-10} m^2 s^{-1} were obtained. Abdel-Kader (1991) estimated the $D_{app.}$ for ascorbic acid losses from peas during water blanching to be within the range of $0.94–1.94 \times 10^{-8}$ m^2 s^{-1} at temperatures varying from 50°C to 90°C. They also concluded the effect of sufficient agitation on the diffusion-controlled leaching of ascorbic acid from peas.

Multicomponent diffusion (where many components diffuse simultaneously) needs to be more carefully examined. Oliveira et al. (1994) have mentioned this problem and that the movement of water should always be analyzed.

9.1.7 Mathematical Background to the Calculation of Effective Diffusivities

Most researchers in this area have adopted diffusion models based on solutions to Fick's second law for various defined geometrical shapes of the solid given in Crank (1975), which is usually based on infinite or semi-infinite geometries of a slab (plane sheet), a cylinder, or a sphere. For example, a slab can be used to describe an apple slice or a sheet of herring muscle; a sphere, coffee beans or particles of cheese curd; and a cylinder, cucumber pickles.

There is some variation in the solutions adopted among various workers, and it is important for any new worker to the field to consider the solution most applicable to the particular diffusion-dependent process. The starting point is to consider the shape of the solid and the nature of the process itself; uptake of solute into the food, leaching of solute from the food or diffusion of solute through the food; and the likely experimental conditions in terms of initial and equilibrium solute concentrations. The solution models usually consider a uniform initial solute concentration throughout the food, no resistance to mass transfer in the diffusion medium and no chemical reaction. However, they vary for a particular geometry depending on the solute concentrations at the surface of the solid, the volume of the solution (and therefore the relative change in solute concentration in the external solvent), and the time period of the experiment.

A representative selection of solutions is given in Table 9.2. For example, Bichsel et al. (1976) and Bressan et al. (1981) investigated solute diffusional loss from coffee beans and cottage cheese curd, respectively; both chose solutions to Fick's second law from Crank (1975) and assumed that the geometry of the solids

TABLE 9.2
Diffusion Phenomena

Authors and Diffusion Process	Diffusion Equation	Experimental Measurements	Calculation of Diffusivity
Biekman and Van Dijk (1992) Effective diffusivity of model proteins though a disk of potato	$M_t = \frac{SD_eC_L1t}{a} + \frac{2aS}{\pi^2}$ $= 1 - \sum_{n=1}^{\infty} \left\langle C_L 1 \cos(n\pi) \exp\left[\frac{-D_e n^2 t}{a^2}\right]\right\rangle$ Modification of equation model for solute flow through a membrane	Protein concentration on the source side initially; at intervals on receiving side	Fitting the experimental values for Mt to the equation by non linear regression.
Bichsel et al. (1976) Diffusion of caffeine from coffee beans	$1 - \frac{M_t}{M_i} = \frac{6}{\pi^2} \sum_{n=1}^{\infty} \frac{1}{n^2} \exp\left[\frac{-D_e n^2 \pi^2 t}{a^2}\right]$ Solution of Fick's 2nd law for solute loss or uptake for spherical geometry	Caffeine content of coffee beans sampled at intervals	Modification of equation model to obtain sigma function correlated to experimental data
Binkley and Wiley (1981) Diffusion of solids from apple disks under different physical and enzymic treatments.	$N = \frac{XAD_e(C - C_L)}{2a}$ A simple lumped parameter equation model	Measurement of soluble solids content in the limited volume of solvent surrounding the slices at intervals	A single effective diffusivity was calculated for each set of data directly from the formula
Bressan et al. (1981). Solids diffusion total solids from cheese curd	$\frac{M_t}{M_\infty} = 1 - \sum_{n=1}^{\infty} \frac{6\alpha(1+\alpha)}{9 + 9\alpha + q_n^2\alpha^2} \exp\frac{-D_e q_n^2 t}{a^2}$ Solution of Fick's 2nd law for solute loss or uptake for spherical geometry but for finite volume of solvent with attainment of equilibrium	Samples of solvent surrounding curd withdrawn at intervals and at equilibrium, solvent assayed	Experimental data fitted to the equation model

Kincal and Kaymak (1987) Solids diffusion from carrot cylinders	$E = \frac{C - C_L}{C_i - C_L}$ $= 1 - \frac{4}{\pi^{\frac{1}{2}}}\left(\frac{D_e t}{a^2}\right)^{\frac{1}{2}} - \frac{D_e t}{a^2} - \frac{1}{3\pi^{\frac{1}{2}}}\left(\frac{D_e t}{a^2}\right)^{\frac{3}{2}}$ Solution of Fick's 2nd law for solute loss or uptake for an infinite cylinder for short time periods. Authors then modify E values to apply to finite cylinder	Carrot samples withdrawn for analysis at intervals	Dimensionless time values calculated for each data point using equation, linear regression of fourier relationship yields *De*
Lamberg (1990) Diffusion of various solutes from potato tissue	$\frac{m_t}{m_i} = \frac{8}{\pi^2}\sum_{n=0}^{\infty}\frac{1}{(2n+1)^2}\exp\left[-\frac{D_e(2n+1)^2}{a^2}\right]\pi^2 t$ Solution of Fick's 2nd law similar to flow through a membrane	Samples of solvent surrounding slices withdrawn and assayed at intervals, material balance used to calculate *Mi* and *Mt*.	Equation model modified by omitting terms $n > 0$ and natural logarithms, linear regression of *ln mi/mt* vrs *t*
Lenart et al. (1989) Solids diffusion from apple tissue	$E = \frac{512}{\pi^6}\exp\left[-\frac{\pi^2 D_e}{4(a^2 + b^2 + c^2)}\right]t$ Equation model adopted considers diffusion in a slab in 3 planes	Apple slices withdrawn for analysis at intervals	Modification of equation model by natural logarithms enables regression of *ln E* vrs *t* to give slope with *De* term
Leach et al. (1995) Diffusion of solids and pectic substances from apple tissue	$E = \frac{C - C_L}{C_i - C_L}$ $= \frac{8}{\pi^2}\sum_{n=0}^{\infty}\frac{1}{(2n+1)^2}\exp\left[-(2n+1)^2\left(\frac{D_e t}{a^2}\right)\frac{\pi^2}{2}\right]$ Solution to Fick's 2nd law for diffusion from an infinite slab developed by Newman (1931)	Apple slices withdrawn for analysis at intervals	A series of dimensionless time values found for data using Newman's tables. *De* calculated by linear regression of Fourier relationship.

continued

TABLE 9.2 (continued)
Diffusion Phenomena

Authors and Diffusion Process	Diffusion Equation	Experimental Measurements	Calculation of Diffusivity
Rodger et al. (1984) Diffusion of salt and acetic acid into herring	$\frac{M_t}{M_\infty} = 1 - \sum_{n=0}^{\infty} \frac{8}{(2n+1)^2\pi^2} \exp\left[\frac{-D_e t(2n+1)^2\pi^2}{4a^2}\right]$ Solution of Fick's 2nd law for diffusion from/or uptake by infinite slab from an infinite solution	Fish withdrawn for analysis at intervals	Experimental data fitted to equation model by successive approximations
Tomasula and Kozempel (1989) Diffusion of various solutes from potato tissue	$\frac{M_t}{M_\infty} = \frac{V_L C_{Li} - V_L C_L}{V_L C_{Li} - V_L C_{L\infty}} = 1 - \sum_{n=1}^{\infty} \frac{2\alpha(1+\alpha)}{1+\alpha+\alpha^2 n^2} \exp\left[\frac{-D_e n^2 t}{a^2}\right]$ Solution of Fick's 2nd law for diffusion from/or uptake by an infinite slab for uptake from a solution of finite volume $\frac{M_t}{M_\infty} = 1 - \sum_{n=0}^{\infty} \frac{8}{(2n+1)^2\pi^2} \exp\left[\frac{-D_e t(2n+1)^2\pi^2}{4a^2}\right]$ Solution of Fick's 2nd law for diffusion from/or uptake by infinite slab	Initial solute content of potato strip and solute contents of solvent surrounding strip at intervals	Minimising the residuals between experimental data theoretical values for Mt/M_∞ obtained from the appropriate equation models

Source: Adapted from Varzakas, T. 1998a. Uptake of cell-wall degrading enzymes by soybean preparations. PhD thesis, The University of Reading, Reading, UK; Varzakas, T. et al. 2005b. *Enzyme Microb. Technol.*, **37**, 29–41.

approximated that of infinite spheres. However, the former workers considered a system in which the solute concentration in the external solvent remains effectively constant and zero throughout the extraction. This can be the case for large infinite solvent volumes and small solute solid concentrations. The latter group of workers considered a process where the concentration of the solute in the surrounding medium changes significantly. This can be the case for small solvent volumes and high solid phase solute concentrations in the case of leaching. However, in the case of solute uptake processes high external solvent concentrations are employed. Consequently, they adopted a different model. Selman et al. (1983), Leach (1993), and Leach et al. (1995) used solutions originally developed by Newman (1931) for drying applications utilizing dimensionless variables for both concentration (E) and time, T (Equation 9.8). E represents a dimensionless solute concentration,

$$E = (C - C_L)/(C_i - C_L). \tag{9.8}$$

T represents the Fourier number (a dimensionless time).

$$T = \frac{D_{eff}t}{a^2} \tag{9.9}$$

Most diffusion problems fall between the limits of diffusion across a thin film and diffusion in a semi-infinite slab. Diffusion across a thin film can usually be treated as a steady-state problem and is mathematically simple. Diffusion in a semi-infinite slab is the unsteady-state problem and is mathematically harder to calculate.

Cussler (1984) has reported that in many cases a simple criterion is necessary to determine which of the two central limits is more closely approached. This criterion depends on the magnitude of the variable (diffusion coefficient) × (time)/(length)^2, which is known as the Fourier number. This variable is a key to all unsteady-state problems. The mass-transfer Fourier number is also very important in leaching (Crank 1975). It is defined as follows:

D_{eff} represents the effective diffusivity of the solute in the solid, t is the contact time and a is a characteristic dimension of the solid.

If Fourier number is much larger than unity an infinite slab is assumed. If it is much less than unity steady-state transport is expected. If it is approximately unity, we may be forced to make a more detailed analysis. In these experiments it has been assumed that a^2 is approximately proportional to time t. This approximation was made in order to aid an easier estimation of the results. In addition to that, the process is significantly advanced when this variable equals unity. A "full" model was not assumed since at the beginning it was not known whether the process was diffusion controlled. In unsteady-state problems, this variable (i.e., the Fourier number) may also be used to estimate how far or how long mass transfer has occurred.

In this work, having started from a concentration of $C = C_0$ and $t = 0$, the concentration C needs to be measured in terms of the diffusion distance, a, and the time, t. Following that, the diffusion coefficients could be estimated. The theory described above will be applied to this problem as follows. Further to the estimation of the diffusion distances from the photographs as well as the UV microscope, graphs of

a^2 need to be plotted against time, t. If a linear relationship is obtained between a^2 and t, this means that a^2 is proportional to t and obedience to Fick's law is observed. Subsequently, D_{eff} could be estimated from the slope of the straight line.

The effective diffusivity, D_{eff}, was estimated from the slope of the graph of the square of the diffusion distance against time (Varzakas et al. 1995b) by assuming that the Fourier number T was approximately unity. Considering the maximum diffusion lengths into the bean, D_{eff} was estimated to be approximately of the order of $1 \times 10^{-12} \pm 1.48 \times 10^{-14}$ m^2 s^{-1} ($\pm$ values represent standard error of the mean values) at 37°C for endoglucanase. The occurrence of the nonzero intercept might indicate very rapid initial absorption of endoglucanase or endoxylanase in soybean due to the high porosity of the tissue. Similarly, effective diffusivity values of endoglucanase based on the minimum penetration lengths was determined to be of the order of 10^{-14} m^2 s^{-1}.

The effective diffusivity of endoglucanase was determined as above (taking into account the maximum diffusion lengths) at higher temperatures and the values were found to be equal to $4 \times 10^{-12} \pm 2 \times 10^{-13}$ and $5 \times 10^{-12} \pm 3 \times 10^{-13}$ m^2 s^{-1} at 50°C and 60°C, respectively, showing an increase in value with temperature. Similarly for endoxylanase, the effective diffusivity was estimated to be equal to $1 \times 10^{-12} \pm 3 \times 10^{-14}$ m^2 s^{-1} at 37°C, $2 \times 10^{-12} \pm 3 \times 10^{-13}$ m^2 s^{-1} at 50°C and $3 \times 10^{-12} \pm 4 \times 10^{-13}$ m^2 s^{-1} at 60°C.

The dependence of the molecular diffusion coefficient on temperature is given by an Arrhenius-type equation as described earlier.

The effect of temperature on maximum effective diffusivity was demonstrated by plotting ln D_{eff} against the reciprocal of absolute temperature for endoglucanase. A straight line fitted to determine the slope indicated that the dependence of diffusivity on temperature followed the Arrhenius relation. Considering the limited number of data points, it was not possible to draw any statistically significant conclusion. However, a preliminary estimate of the activation energy could be made yielding a value of 59.7 kJ mol^{-1} for endoglucanase, comparable to those reported in the literature. Similarly, the activation energy of endoxylanase was found to be 40 kJ mol^{-1} (Varzakas et al. 1997). Rice et al. (1990) reported a value of 41.6 kJ mol^{-1} after having determined the diffusivity in the hot water blanching of potatoes. Temperature also had an effect on the concentration-dependent diffusivity of water into soybean (Hsu 1983). The activation energy for diffusion was found to be between 9 and 13 kcal mol^{-1} and was also found to vary linearly with the water content. The activation energies for diffusion of solutes in food materials are usually within the range of 15–30 kJ mol^{-1} (Pflug et al. 1967; Steffe and Singh 1980; Rodger et al. 1984; Giannakopoulos and Guilbert 1986). Gekas (1992) has also reported activation energy values for the diffusivities in some solid foods.

The Stokes–Einstein equation ($D = K\,T/6\,\pi\,\mu\,R_0$), was also used to compare with the Arrhenius relation.

$$D_{60}/D_{37} = T_{60}\,\mu_{37}/T_{37}\mu_{60} = 0.54 \quad \text{and} \quad D_{50}/D_{37} = T_{50}\mu_{37}/T_{37}\,\mu_{50} = 0.73$$

where D_{60}, D_{37}, D_{50} are the molecular diffusivities at 60°C and 37°C, and 50°C, respectively, T_{60}, T_{37}, and T_{50} are the corresponding temperatures and μ_{60}, μ_{37}, and μ_{50} are the corresponding viscosities. Viscosity values (μ) were obtained from the *Chemical*

Engineers' Handbook (Perry et al. 1984) for viscosities of liquids at 1 atm and corrected for 37°C, 50°C, and 60°C. Viscosity values, expressed in centipoises, had approximate values of 1.4, 2.0, and 2.8 at temperatures of 37°C, 50°C, and 60°C, respectively.

According to the Stokes–Einstein equation, the diffusivity of endoglucanase at 60°C should be only 50% bigger than that at 37°C. However, the results showed that the diffusivity of endoglucanase at 60°C was fivefold bigger than that at 37°C. Similar results were obtained by comparing the diffusivity of endoglucanase at 50°C and 37°C and the diffusivity of endoxylanase at 37°C, 50°C, and 60°C. It was not possible to draw any statistically significant conclusion about whether it is an Arrhenius effect since there was a limited number of data points.

The large difference in magnitude between the diffusivity at 37°C and that at higher temperatures could be explained as a result of the morphology in the soybean cotyledon which was more open/softer at high temperatures. Hence, enzyme penetration was much faster since enzymes could penetrate cracked, softer cells much easier. Another reason could be that it was not a diffusion-controlled process but it was based on a chemical reaction effect. The difference in magnitude at different temperatures might suggest a chemical reaction rather than diffusion.

van der Sman and Meinders (2013) investigated whether moisture diffusion can be predicted for food materials. They focused especially on mixtures of glucose homopolymers and water. The predictions are based on three theories:

(1) The Darken relation, linking the mutual diffusivity to the self-diffusivities, (2) the generalized Stokes–Einstein relation for the solute self-diffusivity, and (3) the free volume theory for water self-diffusivity.

Using literature data obtained for the whole class of glucose homopolymer, they showed that these theories predict the moisture diffusivity for the whole range of volume fractions, from zero to one, and a broad range of temperatures. Furthermore, they showed that the theories equally hold for other hydrophilic biopolymers one finds in food. In the concentrated regime, all experimental data collapse to a single curve. This universal behavior arises because these biopolymers form a hydrogen bonded network, where water molecules move via rearrangement of the free volume.

The free volume theory predicts only the solvent self-diffusion coefficient, which is related to the mean squared displacement of a solvent molecule in the polymer solution. The self-diffusion is different from the mutual diffusion coefficient, which enters Fick's law. Only in the extreme cases of dry polymers or dilute polymer solutions, the mutual diffusivity equals the self-diffusivity. In dry polymers, the mutual diffusivity equals the water self-diffusivity, as follows from the free volume theory. In dilute polymer solutions the mutual diffusivity equals the polymer self-diffusivity, which can be computed using the generalized Stokes–Einstein relation. In this regime the polymer can be viewed as a colloid, with a certain hydrodynamic radius.

According to the Stokes–Einstein relation, the self-diffusion coefficient of small solute depends on the temperature, the viscosity of the solvent, n, and the hydrodynamic radius of the diffusing solute, R. Thus, the D/D_0 ratio, where D is the self-diffusion coefficient of the solute in viscous/gel system and D_0 the onset of pure water, gives information on the impact of solute size and nature, medium viscosity, the presence of macromolecules on diffusion process. Moreover, the average

displacement r of a small solute with a self-diffusion coefficient of D during the diffusion time t is given by $r = (2Dt)^{1/2}$.

The control of flavoring of a food product as well as the flavor perception during consumption is a great challenge for improving food quality.

However, the various ingredient composition and the different textural properties of foods can significantly affect the release of aroma compounds or sapid molecules. It is thus of major importance to determine physicochemical factors that govern diffusion and binding phenomena of these small solutes in food products. In this way, NMR spectroscopy is an efficient tool to characterize these mechanisms at a molecular scale. Diffusion rates of small solutes in aqueous, viscous, and gel solutions can be extracted from relaxation or diffusion NMR experiments. Pulsed-field-gradient (PFG-NMR) experiments are particularly valuable methods to investigate aroma compound self-diffusion and gel microstructure in a noninvasive way. A wide range of methods based on chemical shift, relaxation or diffusion rate changes also provide unique and direct information on binding events of aroma compounds with food macromolecules. Binding site localization, affinity constant, and spatial conformation of complexes can be achieved using conventional 1D- and 2D-NMR spectroscopy (Tavel et al. 2008).

In alloys diffusion is mediated via vacancies, while in liquids it is mediated by the free volume. In the theories of diffusion in these condensed matters the effects of vacancies (free volume) are explicitly taken into account in the thermodynamic and kinetic factors (Jilge et al. 1990).

The "slow mode" theory assumes that the kinetic factor is a harmonic mean of the self-diffusion coefficients, while the "fast mode" theory assumes that the kinetic factor is a linear mean of the self-diffusion coefficients (Jilge et al. 1990).

9.1.7.1 New Numerical Techniques

New computers and softwares have enabled more realistic modeling of mass transfer in food processes (Lombardi and Zaritzky 1996; Welti-Chanes et al. 2005). These advances also permit the application of numerical techniques such as the finite element method (FEM). The FEM is a set of efficient techniques that obtain numerical solutions of differential equations that appear in the most varied fields of science and especially in problems of engineering, physics, and chemistry (Chung 1978; Zienkiewicz and Morgan 1983). According to Puri and Anantheswaran (1993), the main advantages of FEM are as follows: the spatial variation in material properties can be easily manipulated; irregular regions can be modeled with great precision; it is the best for nonlinear problems; the dimensions of the elements can be easily altered; the spatial interpretation is very realistic; and problems with the most diverse boundary conditions can be easily studied.

9.1.8 Diffusion Cell

The diffusion cell (Figure 9.1) used by Varzakas (1998a,b) was made of stainless steel and consisted of two identical chambers, A and B, of known volumes (90 mL), separated by a polysulfone membrane of thickness (L) equal to 50 microns and an effective area (A) equal to ($\pi \times r^2$), where r is the radius of the membrane which is

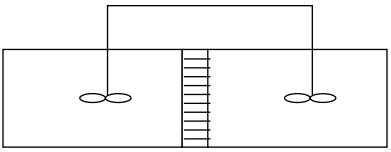


FIGURE 9.1 Schematic representation of the diffusion cell.

equal to 2 cm. The diffusion chambers were held together with screws. Agitation in both chambers was obtained using two stirrers with an approximate speed of 200 rev min^{-1}.

The Stokes diaphragm cell has been used to study diffusion in gases, liquids, or across membranes (Cussler 1984). A similar diaphragm cell was used in these experiments to determine the D_{eff} for lysozyme and cellulase. A calibration of the cell was carried out to make sure that the transfer rate was independent of the stirring speed which was maintained at approximately 200 rev min^{-1}. In liquids, this calibration is commonly made with KCl, water, or urea water. 0.1 M potassium chloride (KCl) was used in this case (Stokes 1951). The concentrations of KCl were obtained by the Volhard method (Williams 1979). For this particular speed used throughout the whole of the experiments, the ratio of S/L was obtained and was found to be equal to 0.4 m, where L is the thickness of the membrane and S is the effective area for diffusion (Stokes 1951). This will be used later to estimate the radius of the pores.

9.1.8.1 Method and Experimental Conditions

At the beginning, lysozyme or endoglucanase dissolved in the buffer solution was pumped into the source chamber A, and the buffer solution without protein was pumped immediately into the receiving chamber B. Samples (1 mL) were withdrawn from each chamber approximately every half an hour. Concentrations in both chambers (C_A, C_B) were estimated. The diffusion cell was left at room temperature (22°C) and all measurements were taken at this temperature.

The effect of the pH on the diffusion coefficient values was tested using different buffer solutions (0.2 M acetate buffer for pH: 4.0, 0.2 M phosphate buffer for pH: 6.0 and 8.0, and 0.1 M glycine-sodium hydroxide buffer for pH: 11.0).

Different concentrations of lysozyme as well as the weights of the membrane were estimated before and after 1 day doing an experiment in flasks. This would help to estimate K_M (the partition coefficient between protein in the membrane and in solution) later. Concentrations were found to be lower and the weights of the membrane were higher after 1 day showing that diffusion and adsorption had occurred. Following this experiment, estimation of C_A and C_B at different initial lysozyme and endoglucanase concentrations (0.5, 1, 3, and 5 mg/mL) and different pH was carried out. Estimated values of the diffusion coefficient (D_M), the partition coefficient (K_M), the flux density (J), the permeability (P), and the membrane concentration (C_M) are presented for different endoglucanase and lysozyme concentrations (0.5, 1, 3, and 5 mg/mL) using two methods (the lag time and the slope).

9.1.8.2 Mathematical Model Used for the Estimation of the Experimental Results

Flux through the membrane in the steady state is described by Equation 9.10 from Fick's second law for diffusion through a plane sheet, assuming the following operating and boundary conditions. The membrane is initially at zero concentration and the concentration at the face through which the diffusing substance emerges is maintained effectively at zero concentration (Crank 1975). The model assumes solubility in the membrane. Accuracy of experiments is within 1% or 2% error.

The following schematic representation (Figure 9.2) shows what is assumed in the diffusion cell.

$$t < 0;\ z = 0;\ C = 0$$

$$t < 0;\ z = L;\ C = 0$$

$$t \geq 0;\ z = 0;\ C = C_{M\,0} = \text{constant},\ C_{M0} = K_M \times C_A$$

$$t > 0;\ z = L;\ C_{ML} = K_M \times C_B = 0,\ K_M > 1$$

C_A = constant with $C_B = 0$ is only considered as an approximation here since C_B is changing and does not have a value equal to zero. However, the following equation can be used for the estimations.

$$Q_t = \frac{D_M C_{M0}}{L}\left(t - \frac{L^2}{6D_M}\right) = \frac{D_M K_M C_A}{L}\left(t - \frac{L^2}{6D_M}\right) = J(t - \tau) \qquad (9.10)$$

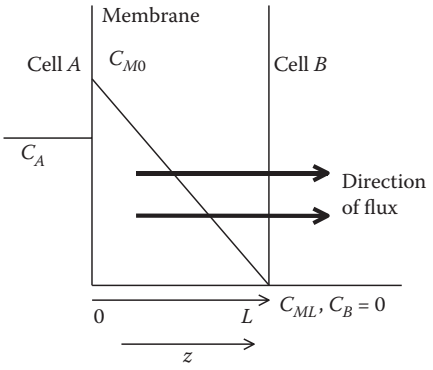


FIGURE 9.2 Schematic representation of what is assumed in the diffusion cell. (Adapted from Varzakas, T., Escudero, I., and Economou, I.G. 1999. *J. Biotechnol.,* **72**, 77–83; Varzakas, T. 1998a. Uptake of cell-wall degrading enzymes by soybean preparations. PhD thesis, The University of Reading, Reading, UK.)

This equation was adopted by Teixeira et al. (1994) and Mulder (1991), where t is the time (s).

D_M is the diffusion coefficient in the membrane (m^2/s).

C_{M0} is the concentration of the solute on the membrane (g/m^3) and is equal to $K_M \times C_A$ at $z = 0$. C_M is higher than C_A since K_M is higher than unity.

L is the thickness of the membrane ($L = 50$ μm).

Q_t is the amount of protein transferred through the membrane area A, in time t, for significantly large times (g/m^2), and from the mass balance, $Q_t = C_B \times V_B/A$; (A is the membrane surface, $= \pi \times (4 \times 10^{-2})^2/4$ m^2).

K_M is the partition coefficient between protein in the membrane and in solution, defined as C_{M0}/C_A.

C_B is the bulk concentration in cell B after C_M is achieved. (The concentration in cell A has been taken after a time $t = 84{,}600$ s.) According to Crank (1975), steady state is achieved when $D\ t/L^2 = 0.45$. In this case it is approximately 3.2 assuming D to be of the order of 10^{-13} m^2 s^{-1}.

J is the flux density of protein (g/m^2s).

P is the permeability of the membrane $= J/C_A$ (m/s).

τ is the lag time (s) representing the intercept of the linear part of the curve obtained by plotting Q_t versus time t. The lag time is the time that the system is in the transient state, before the steady state.

The graph of Q_t versus t in the steady state should be a straight line with slope (J) and intercept (τ) (Crank 1975). These values for both lysozyme and endoglucanase are described by Varzakas (1998a).

There are two methods to calculate D_M. The first one depends on the intercept (the lag-time value) and the second one depends on the slope.

9.1.8.2.1 First Method Based on Lag Time

$$D_M = L^2/6\ \tau \tag{9.11}$$

where L is 50 microns and τ is the measured lag time. As defined earlier,

$$P = J/C_A = Q_t/t\ C_A \tag{9.12}$$

In Equation 9.12, C_A is measured, Q_t is estimated from $Q_t = C_B \times V_B/A$ and J is estimated from the slope of the graph of Q_t against t. Therefore, P and J can be estimated. Now,

$$J = Q_t/t = D_M\ C_{M0}/L = D_M\ K_M\ C_A/L \tag{9.13}$$

In the steady state, J is a constant and represents the slope of the diagram of Q_t versus t. If $\tau = 0$, the steady state is achieved immediately. Therefore, $J = D_M\ C_M/L$ as determined from Equation 9.10. In Equation 9.13, D_M, L, and J are known from previous estimations, hence K_M can be obtained. These equations are described in more detail in Alvarez et al. (1989a,b).

9.1.8.2.2 Second Method Based on the Slope

The slope method is also based on Equation 9.10, therefore, the same boundary conditions are considered (Alvarez et al. 1989a,b).

$$D_M = (J\,L)/(K_M\,C_A) \tag{9.14}$$

To use this equation it is necessary to know K_M. The amount of protein adsorbed on the membrane can be estimated from a mass balance assuming a linear profile and the boundary condition $C_B = 0$ for $t > 0$ and $z = L$ at the interface with cell B.

$$\text{Ads}\ (g) = (C_{M0} + 0)\ LA/2 = C_{A,0}V_{A,0} - V(C_A + C_B) \tag{9.15}$$

This equation states that the amount of protein adsorbed is the difference between the initial and instant quantities (weights times volume) in the membrane, where $C_{A,0}\ V_{A,0}$ is the mass at the initial conditions and $(C_A + C_B)\ V$ is the mass at the time t in the steady state, V is the volume of cells A and B at this time > 0 when the concentrations are C_A and C_B, respectively (it has been assumed that the steady state is well achieved in the first sample after approximately 24 h stirring time as discussed earlier, so that $V = V_0 = 90$ mL). Thus, from the above equation, C_M and K_M can be obtained as follows:

$$C_{M0} = (2/LA)\ [C_{A,0}V_{A,0} - V(C_A + C_B)] \tag{9.16}$$

$$K_M = C_{M0}/C_A \tag{9.17}$$

$$P = J/C_A \tag{9.18}$$

Graphs of the diffusion and partition coefficients against lysozyme concentration and pH have been plotted and a trade-off between K_M and D_M was shown (Varzakas et al. 1999); D_M increases and K_M decreases as lysozyme concentration increases. They also reported that D_M is very much dependent on lysozyme concentration at pH 4.0, 6.0, and 8.0. At pH = 11.0, D_M remains fairly constant showing an independence of lysozyme concentration. K_M seems to be more dependent on lysozyme concentration than D_M at all pH. Moreover, at $C = 1000$ g/m^3, D_M is fairly constant and is therefore independent of pH at this concentration. At all other concentrations D_M seems to be dependent on pH. K_M seems to be dependent on pH more than D.

D_M for endoglucanase was estimated to be of the order of 10^{-13} m^2 s^{-1} compared with a molecular diffusion coefficient value of 10^{-11} m^2 s^{-1}. The estimated value for D_M in this membrane is one order of magnitude slower than that obtained in soybean. This value seems quite reasonable indicating that the enzyme finds a higher resistance in the pores of the membrane compared with the resistance found in the soybean cells. D_M for lysozyme was estimated to be of the order of magnitude of 10^{-14} m^2 s^{-1}, one order lower than that of endoglucanase and three orders of magnitude lower than the value quoted for the molecular diffusion coefficient of lysozyme in water.

The dependence of D_M on endoglucanase and lysozyme concentration and pH was evident. At its isoelectric point, lysozyme appeared to have diffusion coefficients independent of concentration. However, K_M seemed to be more dependent on endoglucanase concentration and pH rather than D_M although major changes could not be observed. The same phenomenon occurred for lysozyme (Varzakas et al. 1999).

Insulin transport phenomena across a series of porous charged membranes were studied by Zhang et al. (2009) at two pH conditions (pH 3.3 and pH 7.4). The membranes were prepared by pore-surface modification of porous poly(acrylonitrile) (PAN) membranes by grafting with weak acidic and basic functional groups. The insulin partition coefficient K between the membrane and solution was estimated from the equilibrium adsorption amount in the batch adsorption experiment. The insulin effective diffusion coefficient D inside the membrane was determined as a fitting parameter by matching the diffusion model with the experimental data of the diffusion measurement. Both K and D correlated well with the charge properties of the insulin and membrane: when the insulin and membrane carried opposite net charge, the partition coefficient showed relatively larger values, while the effective diffusion coefficient was reduced. The insulin permeability coefficient P obtained from the experimental results agreed with that estimated from the partition coefficient and effective diffusion coefficient. These results suggested that the combined effects of the solubility and diffusivity on the permeability coefficient complicated the relationship between the permeability and the charge properties of the insulin and membrane. Additionally, their calculation supported that insulin permeability was reduced by the boundary layer between the membrane and solution.

Static adsorption of serine alkaline protease (SAP) enzyme on hydrophobic polyether sulfone (PES) ultrafiltration membranes in different ionic environments was investigated by Salgin et al. (2006). The amount of SAP adsorbed on membranes was the lowest at its isoelectric point (IEP) where the maximum adsorption was obtained below the IEP of the enzyme. The extent of SAP adsorption in the phosphate buffer solutions including different salts followed the order: $(NH_4)_2HPO_4 > K$ $H_2PO_4 > Na_2HPO_4 - NaH_2PO_4$ (buffer) $> CaCl_2 > ((NH_4)_2HPO_4 + H_2PO_4 + CaCl_2)$, which was consistent with the Hofmeister series. The zeta potentials of membranes contacted with the ionic species were calculated by streaming potential measurements and found that the increase in ionic strength decreased the electrical double-layer thickness leading to a decrease in adsorption.

A model based on mass balance was developed to calculate the diffusion coefficient of SAP in PES membranes. Employing experimental data evaluated in a diffusion cell along with the data of adsorption isotherms, diffusion coefficients of SAP in PES membranes in the presence of different ionic species were calculated. To detect the structural changes that occurred, membrane surfaces were analyzed by Fourier transform infrared attenuated total reflectance (FTIR-ATR) measurements.

Hu et al. (1992) developed a Nernst–Planck diffusion model including intraparticle and film diffusions to study the diffusion of charged proteins in porous particles. The authors allowed hindered diffusion of proteins in the porous media for the model and they first introduced a new concept of coupled mass transfer through a stagnant film. Clark and Lucas (1998) studied the diffusion and partitioning of humic acid into a porous ultrafiltration membrane. They developed a one-dimensional diffusion model

with linear partitioning in porous medium to predict how humic acid diffusivity changes with pH and calcium concentration. They showed that the diffusion coefficient increased with decreasing pH and increasing calcium concentration. Wang et al. (2001) measured the diffusion coefficient of humic acid directly and compared to the predictions of the model developed by Clark and Lucas (1998). The experiments were conducted in a two-chamber diffusion cell separated by a track-etched membrane.

Research to study the phenomena of solution-diffusion in polymeric membranes was started more than a century ago. Some basic insights on the mass transport phenomenon of liquid solution through the membrane layers were derived from the diffusion studies presented by Crank (1975) and Neogi (1996). In a dilute solution, the diffusivity rate derived by Fick's law is expected to be independent of concentration. However, at high concentrations, interaction between the diffusing molecules and the solvent can cause the diffusion coefficient to be dependent on the concentration (Crank, 1975). A typical diffusion coefficient of a dilute solution in polymer can be estimated theoretically, that is at the quantum of 10^{-8} cm^2/s (Cussler 1997).

Lateral flow systems in nitrocellulose (NC) membranes are widely used for transport media applications related to immunoassays. The most important aspect of membranes is their ability to control the diffusion rate of the medium. Ahmad et al. (2010) investigated the effects of membrane pore size on lateral diffusion of protein molecules in an NC membrane. Both experimental work and mathematical modeling were carried out in this study. In modeling, the driving force for transportation of the diffusing molecule was the concentration gradient in lateral diffusion cell under unsteady diffusion. Diffusion experiments for lysozyme and BSA were carried out by using different pore sizes of NC membranes. Good agreement was observed between the developed model and experimental results with correlation coefficients of more than 0.98.

Effects of diffusion length and different diffusing molecules toward the lateral diffusion performance in NC membranes were also discussed extensively. The good fit between the model and experimental results has proven the reliability and flexibility of the lateral diffusion model developed in this study. The understanding of the diffusion phenomenon would be a useful tool for membrane properties design and customization of specific membrane applications in immunoassay.

Experimentally measured changes in solute concentration with time then can be used to calculate dimensionless solute concentrations. Values of dimensionless concentration have been calculated and tabulated for various dimensionless times by Newman (1931). Lenart et al. (1990) adopted a solution to Fick's second law, which unusually considered diffusion in three directions from an apple slice. Simple adaptations of the conventional solutions were considered to account for diffusion from cubular geometries (Rice et al. 1990). Binkley and Wiley (1981), however, adopted a simple model with lumped parameters with no defined geometrical component to calculate the effect of various treatments on the effective diffusivity of soluble solids from apple slices.

Effective diffusivities can then be found by obtaining solute content versus time profiles in either the solid or bulk solvent and then, inserting diffusivity values into any equation model in order to minimize the least-square differences between actual and theoretical concentrations. Other calculation methods usually involve modification

of the Fickian equation model using natural logarithms followed by a linear regression of natural logarithm of dimensionless variable solute concentration against time (Lenart et al. 1989, 1990; Kincal and Kaymak 1990; Lamberg 1990). Selman et al. (1983) calculated the effective diffusivity for each experimental point using the Fourier relationship having first determined dimensionless solute concentrations and subsequently the corresponding dimensionless time values from Newman's tables. Leach (1993) modified this approach and obtained a single effective diffusivity value from a given experimental linear regression of the Fourier relationship.

Nonlinear optimization methods have also been used to minimize residuals between theoretical and experimental concentrations after having taken an estimate for the diffusion coefficient (Oliveira and Silva 1992). The diffusion coefficient obtained corresponds to the best average value over the considered period of time.

However, whichever equation model is chosen it is wise that the applicability of the model to the experimental conditions is checked by recalculating experimental data values from single effective diffusivity obtained from the model (Oliveira 1988; Leach et al. 1995). Moreover, Oliveira (1988), has presented a critical review based on the use of different mathematical methods for the determination of the diffusion coefficients in foods.

9.1.9 Modeling of Hyphal Penetration and Enzymatic Diffusion from a Stationary and a Moving Source

The major stages in growth are summarized here, after having taken into account different models reviewed by Nout and Rombouts (1990). First, extracellular enzymes are assumed to diffuse to the macromolecular substrates (proteins, lipids, cellulose, xylan, and pectin). An enzyme-catalyzed breakdown of substrate into smaller, metabolizable units is followed and these small substrates diffuse back toward the hyphae where they are then taken up by the mold and metabolized to produce hyphal growth (Varzakas 1998a,b). The diffusion of small substrates is faster than enzymic diffusion, since diffusion coefficients are inversely related to the solute size.

For tempe/beans and flour the maximum measured hyphal penetration distances (= a + b in Figure 2.6b) after 40 h were around 2 mm and 5–7 mm, respectively. The molecular diffusion coefficients of protein in solution are typically of the order of 10^{-11} m^2 s^{-1}, which would be consistent with a diffusion distance a from a stationary source of around 1 mm since $a \sim \sqrt{Dt}$. The results, therefore, suggest that the hyphae act as a moving source of enzymes and play a positive role in pushing through the matrix. The enzymes ahead of, and around the growing hyphae, have a dual role: they help to soften the solid structure and liberate small substrate molecules, which provide the necessary source of energy, carbon, and other elements. For fungal growth it is suggested that the greater hyphal penetration distances observed with tempe flour reflect that the cells in flour are not associated with each other. Jurus and Sundberg (1976) revealed hyphal infiltration in 80 h at 25°C to a depth of 742 μm or about 25% of the average width of a soybean cotyledon. Their results would suggest a diffusion coefficient of the order of 10^{-12} m^2 s^{-1}.

As well as enzyme transport, it is necessary for oxygen to diffuse through the matrix in order to help drive oxidative enzyme degradation. Mitchell et al. (1990) proposed

that oxygen diffusion limits the rate of growth of *R. oligosporus* into a model solid substrate. This is due to the fact that oxygen must pass through the actively respiring biomass at the substrate particle surface in order to reach the interior and then diffuse through the aqueous phase within the substratum. The diffusion of enzymes and substrate fragments is very important and more work needs to be done to characterize these extracellular enzymes and their mode of action in degrading the soybean. If the mass-transfer resistance is high this could be the rate-determining step. However, when the porosity of the substrate is low, as is the case with the soybean, the major part of degradation will occur at the outer surface. In contrast, if the porosity is high, the degradation can occur inside the structure and the water-soluble fragments have to diffuse out. In either mode of enzymatic action, the enzymes modify the solid polymeric materials so that they enter the cells and serve as carbon or energy sources.

9.1.9.1 Kinetics: Diffusion/Adsorption Models

Neglecting the external film resistance, the enzyme infiltrates into the bean as a solution. It is hypothesized that its subsequent movement is governed by Fickian diffusion and simultaneous adsorption on the substrate. Hydrolysis is assumed to occur resulting in the breakage of β-glucosidic bonds within the cellulose and hemicellulose matrix. The hydrolysis is followed by enzyme diffusion to the next favorable site (Varzakas 2001; Varzakas et al., 2006).

The main equation for enzyme uptake by soybean cotyledon tissue is given by Crank (1975) assuming no film resistance.

$$\frac{\partial q}{\partial t} = D_{eff} \frac{\partial^2 C_l}{\partial x^2} \tag{9.19}$$

where D_{eff} is the effective diffusivity and q is the total enzyme concentration in the solid.

The boundary conditions are the following:

$$q = 0; \quad t = 0, -L < r < L \tag{9.20}$$

$$C_l = C_0; \quad \text{at } t = 0, x = L \tag{9.21}$$

$$\frac{\partial C_l}{\partial \mathrm{x}} = 0; \quad t > 0, \quad r = 0 \tag{9.22}$$

Differentiating equation $q = C_l + C'_{\text{solid}}$ gives

$$\frac{\partial q}{\partial t} = \frac{\partial C_l}{\partial t} + \frac{\partial C'_{\text{solid}}}{\partial t} \tag{9.23}$$

In order to solve Equations 9.19 and 9.23 it is necessary to know C'_{solid} and C_l. Hence, instantaneous equilibrium in the pore is assumed. Equation representing a Langmuir isotherm

$$C'_{solid} = \frac{BC_l}{K_l + C_l} \tag{9.24}$$

where, B and K_l are isotherm parameters and are functions of the solute and solid concentrations, could be used to solve numerically as Pedersen et al. (1985) have done with their model.

However, it was not possible to solve this equation numerically. Therefore, approximate solutions can be considered for two extreme cases:

Case (i)

If $C_l \ll K_l$ then Equation 9.24 becomes

$$C_{\text{solid}} \cong \frac{BC_l}{K_l} \tag{9.25}$$

This should be true in the diffusion experiments at the "front" of the diffusion wave as well as in uptake experiments when the concentration outside the bean (C_l) is very small (Varzakas 1998a,b).

Therefore, differentiating Equation 9.25 gives

$$\frac{\partial C_{\text{solid}}}{\partial t} = \frac{B}{K}\frac{\partial C_l}{\partial t} \tag{9.26}$$

Substituting Equation 9.26 into Equation 9.23 gives

$$\frac{\partial q}{\partial t} = \frac{\partial C_l}{\partial t}\left(1 + \frac{ma_v B}{K_l}\right) \tag{9.27}$$

Substituting Equation 9.27 in Equation 9.19 gives:

$$\frac{\partial C_l}{\partial t}\left(1 + \frac{ma_v B}{K_l}\right) = D\frac{\partial^2 C_l}{\partial r^2} \tag{9.28}$$

Dividing 28 by $(1 + (ma_v B/K_l))$ gives

$$\frac{\partial C_l}{\partial t} = \frac{D}{1 + (ma_v B/K_l)}\frac{\partial^2 C}{\partial r^2} \tag{9.29}$$

This implies that the effective diffusivity is given by

$$D_{\text{eff}} = \frac{D}{1 + (ma_v B/K_l)} \tag{9.30}$$

which is lower than D, since $ma_v B/K_l$ is >0.

Case (ii)

If $C_l \gg K_l$ which is true for all the experiments at $t = 0$ we have

$$C_{\text{solid}} = B \tag{9.31}$$

a constant. Hence, differentiating gives

$$\frac{\partial C_{\text{solid}}}{\partial t} = 0 \tag{9.32}$$

Therefore, Equation 9.23 simplifies to

$$\frac{\partial q}{\partial t} = \frac{\partial C_l}{\partial t} \tag{9.33}$$

Therefore,

$$\frac{\partial C_l}{\partial t} = D_{eff} \frac{\partial^2 C_l}{\partial r^2} \tag{9.34}$$

In other words, the effective diffusivity is the same as D.

9.1.9.2 Mass Transfer Coefficient Approach

The rate of uptake by soybean can alternatively be expressed in terms of a transfer coefficient as follows:

$$\partial C'_{\text{solid}}/\partial t = K\,(A)\,(C_l - C_l^*) \tag{9.35}$$

where K is the mass-transfer coefficient, A is the area, and $C_l - C_l^*$ is the driving force, which is the difference between the concentration in the liquid at any time and the equilibrium liquid concentration with the bean concentration.

It is expected that this rate should be proportional to this difference in concentrations. This will be tested.

It was also suggested that the rate of uptake should be proportional to (C_l aver. $- C_l^*$). In order to get an estimate of K, the mass-transfer coefficient, a plot of the rate against (C_l aver. $- C_l^*$) needs to be considered. However, units of dC'_{solid}/dt need to be converted into (mol s^{-1}) and units of (C_l aver. $- C_l^*$) into (mol m^{-1}). Following that, fitted linear lines were drawn to estimate the slope and therefore K (Varzakas 1998a,b; Varzakas et al. 2006). K for endoglucanase and endoxylanase was estimated to be approximately equal to 4×10^{-5} m s^{-1}. The fitted lines showed that the model tested required further refinement, as it was unable to fit all data. Extreme data points did not appear to be predicted accurately by this model. However, the best line was fitted to include all these points and the slope was used to give an approximate estimate of an average mass-transfer coefficient. Linear correlation of the data could be made on the rising point of the

error therefore eliminating data falling and associated with different mechanisms. Nevertheless, this would require elimination of most of the data and hence further treatment of these data was not carried out.

K seems to be decreasing over time for both enzymes although for endoxylanase a decrease could only be observed for the enzyme with the highest enzymatic concentrations.

Having obtained values for an average mass-transfer coefficient K, values for D could be estimated assuming a slice and that K is asymptotic with long residence times and t approaches infinity and using the following equation adopted from Spaninks (1979).

$$K = \pi^2 D/4l \tag{9.36}$$

where l is half of the thickness of the slice. The area A is equal to $2\ \pi\ r^2$ where r is the radius of the slice (~2 mm) and 2 because there are 2 sides.

Hence, D for endoglucanase and endoxylanase was estimated to be equal to 4.8×10^{-10} m^2 s^{-1}. These diffusion coefficients are quite high compared with the average diffusion coefficient of a protein in solution, which is of the order of 10^{-11} m^2 s^{-1}. This difference could be attributed to two major factors. First, in this uptake experiment a cotyledon slice was used indicating that most of the cotyledon cells were left quite open for uptake to occur and hence this happened quite fast since the enzymes found no real hindrance on their way to the inside of the cotyledon tissue. Second, the osmotic pressure could be an important factor. There are probably salts and water inside the cotyledon with a low osmotic pressure hence facilitating enzyme movement in the soybean cotyledon.

Diffusion of adsorbed particles and especially enzymes such as endoglucanases and endoxylanases into the solid is a complex process. A detailed description of diffusion should be based on kinetic equations for the transition of enzyme molecules from one solid layer to another. It could be that multimolecular adsorption occurs on soybean. The latter represents a heterogeneous surface consisting of cellulose, hemicellulose and pectin. These soybean polysaccharides form different sites where the enzymes attack and adsorb to.

It is well known that endoglucanases are hydrolytic enzymes able to hydrolyze insoluble cellulose to glucose. They form an endoglucanase system of several distinct enzymes (Klyosov 1990). The three types of enzymes traditionally assigned to the endoglucanase system are: endoglucanases, cellobiohydrolases, and cellobiases. Endoglucanase systems often show only two or three individual components (including at least one endoglucanase) but in many cases 15–20 individual components have been identified (Sprey 1988). Fungal cellobiohydrolases sometimes show the tendency to form aggregates with endoglucanases. These aggregates are very difficult to break up into component parts as reported by Wood et al. (1989). Both endoglucanase and cellobiohydrolase bring about the dispersion of cellulose and this results from hydrolytic and mechanical action on cellulose (Rabinovich 1988). Hydrolysis takes the form of enzymatic cleavage of cellulose molecules whereas the mechanical action is induced by the adsorption of cellulases to cellulose microcracks followed by their penetration into the interfibrillar space. This effect is very important in the

enzymatic degradation of insoluble cellulose. For amorphous cellulose, the entire surface is easily accessible to enzymatic attack. In these experiments, evidence has not been shown for either effects, however, an uptake of endoglucanase by soybean seems to have occurred.

Furthermore, the mechanism by which cellulases break down crystalline cellulose is still poorly understood. Current unsolved problems include the endo- versus exo-classification of cellulases and the molecular origin of the synergy of cellulases. Henrissat (1997) has discussed a slowly emerging mechanism called "processivity" based on the widely accepted concept of multiple attack of endo-acting amylases degrading starch. This mechanism implies a certain amount of endo-attack by enzymes usually considered as exo-acting and could account for some of the presently contradictory experimental observations. He studied the degradation of highly crystalline cellulose from the alga *Valonia ventricosa* by recombinant cellulases from *Humicola insolens* using electron microscopy. The "processivity" hypothesis was tested by preparing oligosaccharides substituted by bulky groups at the extremities and found that the substrates were hydrolyzed by these recombinant cellobiohydrolases and argued against the specific chain end recognition by these enzymes. He also proposed that a different model should be constructed to account for the initial attack of cellobiohydrolases on cellulose. This "processivity" hypothesis seems to be very close and explain some of the contradictory experimental observations derived from this work.

These experiments might indicate that the uptake of endoglucanases (endoglucanases and/or cellobiohydrolases) by soybean is characterized by a multiple attack on cellulose without any desorption from the substrate's surface. Another effect that might take place is that the cellulolytic enzyme desorbs after each scission in order to bind to another site of cellulose. Gonzalez et al. (1989) proposed the presence of two different types of substrate in cellulose differing in their susceptibility for enzymatic attack and formulated a model used to predict the hydrolysis kinetics of different substrates such as microcrystalline cellulose, rice straw, and wheat straw. However, evidence is not provided from this work to support this hypothesis.

Another dimensionless group, analogous to the Nusselt number in heat transfer, can be defined as the Sherwood number defined as

$$\mathrm{Sh} = kL/D \tag{9.37}$$

where L is the film thickness.

9.1.9.3 Steady Diffusion from a Sphere

Steady diffusion into or out of a sphere in an infinite stagnant medium can describe the slow leaching of sugar from a spherical piece of beet or the supply of a nutrient to a microorganism.

The total rate of mass transfer for any radius r is given by

$$J = 4\,\pi\, r^2\, j \tag{9.38}$$

and Fick's law is

$$j = -D\, dc/dr \tag{9.39}$$

hence $j = J/4\pi r^2 = -D\, dc/dr$, which can be integrated to give the total rate of mass transfer between spherical surfaces at r_1 and r_2.

$$J = 4\pi D (c_1 - c_2)/(1/r_1 - 1/r_2) \tag{9.40}$$

If we assume mass transfer from a sphere of radius r_1 into an infinite environment, that is, r_2 approaches infinity we get

$$J/4\pi r_1 = D (c_1 - c_2) \quad \text{and} \quad j = k (c_1 - c_2)/(r_1 - r_2) \tag{9.41}$$

where $K = D/r_1$ is the mass-transfer coefficient and c_1, c_2 the concentrations at the sphere boundary and infinity, respectively.

9.1.9.3.1 Problem Solving

Calculate the max. rate of uptake of glucose to a spherical bacterium of diameter (a) 1 micron and (b) 100 microns in a stagnant medium containing 100 kg m^{-3} glucose. The molecular diffusion coefficient of glucose in aqueous solution is 6×10^{-10} m^2 s^{-1}.

In this situation Sh = 2 hence the mass-transfer coefficient is $k = 1.2 \times 10^{-3}$ m s^{-1} for $d = 1$ micron and $k = 1.2 \times 10^{-5}$ m s^{-1} for $d = 100$ microns.

The rate of mass transfer of glucose is

$$J = \pi d^2 k (100 - c)$$

c is the glucose concentration at the bacterium surface and the max. transfer rate will occur when glucose is simultaneously consumed so that $c = 0$ and is

$$J = \pi d^2 k\, 100 = 1.2\, \pi\, 10^{-13} \text{ kg s}^{-1} \quad \text{for } d = 1$$

and

$$1.2\, \pi\, 10^{-11} \text{ kg s}^{-1} \qquad \text{for } d = 100 \text{ microns.}$$

The mass-transfer coefficient varies with d^{-1} and the absolute rate of transfer varies directly with diameter (Pyle 1992).

9.1.9.4 Transport across a Film

Consider what happens when the transported species is soluble in a film as a gas might be in plastic packaging. Assume that the solubility of the species in the packaging film c_f is related to its composition in the gas adjacent to the film, c_g (with which it is in equilibrium) by the formula

$$c_f = mc_g$$

where the partition coefficient m is smaller than unity.

If we consider steady transport of the component across the packaging film from the interior where concentration is c_1 to the outside environment where it is assumed that the concentration is effectively zero. Hence,

$$j = (D/L)\, mc_1$$

and k the mass-transfer coefficient is mD/L.

The rates of diffusional loss across a film or transfer into the packaged material are proportional to the effective diffusion coefficient of the species in the film and to its solubility in the film while being inversely proportional to the film thickness.

9.2 CONCLUSIONS

Diffusion of solutes in food material is very important since valuable information can be extracted with respect to enzyme move and mechanisms of movement. The estimation of diffusion coefficients helps such accomplishment. Temperature is another crucial factor in the study of diffusion since it will tell us if the process is diffusion controlled or not. The relationship between the diffusion coefficient and temperature depends on the diffusion mechanism.

NOMENCLATURE

a	characteristic linear dimension—half thickness for slab and radius of cylinder and sphere (m)
A	cross-sectional area of sample (m^2)
C_∞	average solute concentrate in sample at equilibrium (mol/m^3)
C	average solute concentration in sample tissue (mol/m^3)
$C1$	concentration on one side of membrane (mol/m^3)
$C2$	concentration on the other side (mol/m^3)
C_i	initial average solute concentration in sample (mol/m^3)
C_L	average solute concentrate in liquid at time t (mol/m^3)
$C_{L\infty}$	average solute concentration in liquid at equilibrium (mol/m^3)
C_{L1}	initial average solute concentration (mol/m^3)
D	molecular diffusivity (m^2/s)
D_e, D_a, D_{app}	effective diffusivity also known as apparent diffusivity
E	dimensionless solute concentration
L	additional thickness—half length of cylinder (m)
M_t	solute uptake at time t (mol)
M_∞	solute uptake at infinite time (mol)
n, m	number of roots
T	dimensionless time ($D_{eff}\, t/a^2$)
t	time (s)
V	volume of liquid (m^3)

GREEK SYMBOLS

β	Bessel function
ε	porosity
τ	tortuosity

REFERENCES

Abdel-Kader, Z.M. 1991. A study of the apparent diffusion coefficient for ascorbic acid losses from peas during blanching in water. *Food Chem.*, **40**, 137–46.

Abdel-Kader, Z.M. 1992. Effect of blanching on the diffusion of glucose from potatoes. *Die Nahrung*, **36(1)**, 15–27.

Ahmad, A.L., Low, S.C., Shukor, S.R.A., Fernando, W.J.N., and Ismail, A. 2010. Hindered diffusion in lateral flow nitrocellulose membrane: Experimental and modeling studies. *Journal of Membrane Science*, **357**, 178–84.

Alizadeh E., Chapleau, N., de-Lamballerie, M., and Le-Bail, A. 2009. Application to salmon (*Salmo salar*) using conventional and pressure shift freezing. *Food Bioprocess Technol*, **2**, 257–62.

Alvarez, M. T., Alvarez, R., and Coca, J. Julio 1989a. Modelos Matematicos para Transferencia en sistemas fluido-membrana-fluido (Membrana homogenea-fluidos no homogeneos y membranas no homogeneas). *Ingenieria Quimica*, 193–197.

Alvarez, M.T., Alvarez, R., and Coca, J. Junio 1989b. Modelos Matematicos para Transferencia en sistemas fluido-membrana-fluido (Membranas y fluidos homogeneos). *Ingenieria Quimica*: 257–262.

Azevedo, I.A.C. and Oliveira, F.A.R. 1993. Validacao experimental de modelos de alimentos para simulacao de processos de acidificacao, Presented at 1st Encontro de Quimica de Alimentos, Santarem, Spain.

Baron-Epel, O., Gharyal, P.K., and Schindler, M. 1988. Pectins as mediators of wall porosity in soybean cells. *Planta*, **175**, 389–95.

Bassi, A.S., Rohani, S., and Macdonald, D.G. 1987. Measurement of effective diffusivities of lactose and lactic acid in 3% agarose gel membrane. *Biotechnol. Bioeng.*, **30**, 794–97.

Beers, E.P. and Duke, S.H. 1988. Localisation of alpha-amylase in the apoplast of pea (*Pisum sativum* L.) stems. *Plant Physiol.*, **87,** 799–802.

Benhamou, N. and Cote, F. 1992. Ultrastructure and cytochemistry of pectin and cellulose degradation in tobacco roots infected by *Phytophthora parasitica* var. *nicotianae. Phytopathology*, **82**, 468–78.

Berg, O.G. and Von Hippel, P.H. 1985. Diffusion-controlled macromolecular interactions. *Ann. Rev. Biophys. Chem.*, **14**, 131–60.

Bichsel, B., Gal, S., and Signer, R. 1976. Diffusion phenomena during the decaffeination of coffee beans. *Food Technol*. **11**, 637–46.

Biekman, E.S.A. and Van Dijk, C. 1992. Measurement of the apparent diffusion coefficient of proteins in potato tissue, Presented in DLO Agrotechnological Research Institute, The Netherlands.

Biekman, E.S.A. 1992. Enzymatic maceration of potatoes for the production of instant dried mashed potato: Modeling of the disintegration process. *Food Biotechnol.*, **6(1)**, 19–33.

Binkley, C.R. and Wiley, R.C. 1981. Chemical and physical treatment effects on solid–liquid extraction of apple tissue. *J. Food Sci.*, **46**, 729–32.

Blanc, P., Loret, M.O., Pareilleux, A., Goma, G., and Baberian, R. 1992. Enzymatic process for deflatulating beans. Poster presented at the International Biotechnology Symposium, August, Crystal City, Vancouver.

Blasinski, H. and Amanowicz, M. 1979. Diffusion in a porous solid. Methods for determining the effective diffusion coefficient. *Int. Chem. Eng*. **19(2)**, 236–9.

Bourlieu, C., Guillard, V., Powell, H., Valles-Pamies, B., Guilbert, S., and Gontard, N. 2008. Modelling and control of moisture transfers in high, intermediate and low aw composite food. *Food Chemistry*, **106(4)**, 1350–58.

Bressan, J.A., Carroad, P.A., Merson, R.L., and Dunkley, W.L. 1981. Temperature dependence of effective diffusion coefficient for total solids during washing of cheese curd. *J. Food Sci.*, **46**, 1958–59.

Bruemmer, J.H., Griffin, A.W., and Onayemi, O. 1978. Sectionizing grapefruit by enzyme digestion. *Proc. Flatul. State Horticult. Soc.*, **91**, 112–14.

Brune, D. and Kim, S. 1993. Predicting protein diffusion coefficients. *Proc. Nat. Acad. Sci. USA*, **90(9)**, 3835–39.

Bruniche-Olsen, H. 1962. *Solid Liquid Extraction*. Copenhagen: NYT Nordisk Forlag, pp. 423–33.

Bucic-Kojic, A., Planinic, M., Tomas, S., Jakobek L., and Seruga, M. 2009. Influence of solvent and temperature on extraction of phenolic compounds from grape seed, antioxidant activity and colour of extract. *International Journal of Food Science and Technology*, **44**, 2394–401.

Chen, X.D. 2007. Moisture diffusivity in food and biological materials. *Drying Technology*, **25(7)**, 1203–13.

Chung, T.J. 1978. *Finite Element Analysis in Fluid Dynamics*. McGraw-Hill, New York.

Clark, M.M. and Lucas, P. 1998. Diffusion and partitioning of humic acid in a porous ultrafiltration membrane. *J. Membr. Sci*., **143**, 13–25.

Crank, J. 1975. *The Mathematics of Diffusion*, 2nd edition, Oxford University Press, Oxford, UK.

Cussler, E.L. 1984. *Diffusion: Mass Transfer in Fluid Systems*. Cambridge University Press, Cambridge, pp. 146–77.

Cussler, E.L. 1997. *Diffusion: Mass Transfer in Fluid Systems*, Cambridge University Press, Cambridge.

Djelveh, G., Gros, J.B., and Bories, B. 1989. An improvement of the cell diffusion method for the rapid determination of diffusion constants in gels or foods. *J. Food Sci.*, **54**(1), 166–169.

Dugas, C.M., Li, Q., Khan, I.A., and Nothnagel, E.A. 1989. Lateral diffusion in the plasma membrane of maize protoplasts with implications for cell culture. *Acta*, **179**, 387–396.

Escribano-Bailon, M.T. and Santos-Buelga, C. 2003. Polyphenols extraction from foods. In: *Methods in Polyphenol Analysis* (edited by C. Santos-Buelga and Williamson G). Royal Society of Chemistry, Cambridge, UK, pp. 1–16.

Floury, J., Jeanson, S., Aly, S., and Lortal, S. 2010. Determination of the diffusion coefficients of small solutes in cheese: A review. *Dairy Science and Technology*, **90(5)**, 477–508.

Fox, J.B. 1980. Diffusion of chloride, nitrite and nitrate in beef and pork. *J. Food Sci.*, **45**, 1740–1745.

Garrote, R., Silva, E.R., and Bertone, R.A. 1986. Losses by diffusion of ascorbic acid during water blanching of potato tissue. *Leb.-Wiss. und Tech.*, **19**, 263–265.

Garrote, R.L., Bertone, R.A., and Silva, E.R. 1984. Effect of soaking-blanching conditions on glucose losses in potato slices. *Can. Inst. Food Sci. and Tech. J.*, **17(2)**, 111–113.

Garrote, R.L., Silva, E.R., and Bertone, R.A. 1988. Effect of freezing on diffusion of ascorbic acid during water heating of potato tissue. *J. Food Sci.*, **53(2)**, 473–474, 487.

Gekas, V. 1992. Characterisation and properties of foods. In *Transport Phenomena of Foods and Biological Materials* (ed. V. Gekas). Chapter 2, Boca Raton, FL: CRC Press, pp. 70–71.

Gekas, V. and Lamberg, I. 1991. Determination of diffusion coefficients in volume-changing systems—Application in the case of potato drying. *J. Food Eng.*, **14(4)**, 317–326.

Gekas, V., Oste, R., and Lamberg, I. 1993. Diffusion in heated potato tissue. *J. Food Sci.*, **58(4)**, 827–831.

Giannakopoulos, A. and Guilbert, S. 1986. Sorbic acid diffusivity in relation to the composition of high and intermediate moisture model gels and foods. *J. Food Technol*., **21(4)**, 477–485.

Gibbons, G.C. 1980. Immunohistochemical determination of the transport pathways of alpha-amylase in germinating barley seeds. *Cereal Res. Commun.*, **8(1)**, 87–96.

Gibbs, S.J., Lightfoot, E.N., and Root, T.W. 1992. Protein diffusion in porous gel filtration chromatography media studied by pulsed field gradient NMR spectroscopy. *J. Phys. Chem.*, **96**, 7458–7462.

Gonzalez, G., Carminal, G., Demas, C., and Lopez Santin, J. 1989. A kinetic model for pretreated wheat-straw saccharification by cellulase. *J. Chem. Technol. Biotechnol*, **44**, 275–288.

Gros, J.B. and Ruegg, M. 1987. Determination of the apparent diffusion coefficient of NaCl in model foods and cheese. In *Physical Properties of Foods*, 2nd edition, (ed. R. Jowitt, T. Escher, F.B. Mckenna, and M. Roquest), Applied Science Publishers Ltd., London.

Guilbert, S. 1985. Effects de la composition et de la structure des aliments sur l' activite et la mobilite de l'eau ou de solutes. These de Doctorat d' Etat, Universite des Sciences et Techniques du Languedoc, France.

Gustafsson, N.O., Westrin, B., Axelsson, A., and Zacchi, G. 1993. Measurement of diffusion coefficients in gels using holographic laser interferometry. *Biotechnol. Prog.*, **9**, 436–441.

Hashiba, H., Gocho, H., and Komiyama, J. 2008. Dual mode diffusion and sorption of sodium chloride in pré-cooked egg white. *Food Science and Technology*, **41**, 1978–1986.

Henrissat, B. 1997. How do cellulases function? In *Carbohydrates and Biotechnology: Structure, Function and Synthesis*. Royal Society of Chemistry Carbohydrate Group. Spring Meeting, University College, Galway.

Hillmer, S., Gilroy, S., and Jones, R.L. 1992. Visualizing enzyme secretion from individual barley (*Hordeum vulgare*) aleurone protoplasts. *Plant Physiol.*, **102**, 279–286.

Hradil, G., Calo, J.M., and Wunderlich Jr., T.K. 1993. Mass transport parameters of aspen wood chip beds via stimulus-response tracer techniques. *Biotechnol. Bioeng.*, **41**, 354–360.

Hu, X., Duong, D.D., and Yu, Q. 1992. Effects of supporting and buffer electrolytes (NaCl, CH_3COOH and NH_4OH) on the diffusion of BSA in porous media. *Chem. Eng. Sci.*, **47(1)**, 151–164.

Hsu, K.H. 1983. Effect of temperature on water diffusion in soybean. *J. Food Sci*., **48**, 1364–1365.

Hulst, A.C., Hens, H.J.H., Buitelaar, R.M., and Tramper, J. 1989. Determination of the effective diffusion coefficient of oxygen in gel materials in relation to gel concentration. *Biotechnol. Tech.*, **3(3)**, 199–204.

Javeri, H., Toledo, R., and Wicker, L. 1991. Vacuum infusion of citrus pectin methylesterase and calcium effects on firmness of peaches. *J. Food Sci.*, **56**, 739–742.

Jilge, W., Carmesin, I., Kremer, K., and Binder, K. 1990. A Monte Carlo simulation of polymer–polymer interdiffusion. *Macromolecules*, **23(23)**, 5001–5013.

Jurus, A.M. and Sundberg, W.J. 1976. Penetration of Rhizopus oligosporus into soybeans in tempe. *Appl. Environ. Microbiol*., **32**, 284–287.

Kays, S.J. 1991. Movement of gases, solvents and solutes within harvested products and their exchange between the product and its external environment. In *Postharvest Physiology of Perishable Plant Products*, ed., S.J. Kays. Chapter 7, New York: Van Nostrand Reinhold, pp. 409–455.

Kincal, N.S. and Kaymak, F. 1987. Modelling dry matter losses from carrots during blanching. *J. Food Proc. Eng.*, **9**, 201–211.

Kincal, N.S. and Kaymak, F. 1990. Simultaneous diffusion and degradation of ascorbic acid in potato blanching. In *Engineering and Food. vol. 1: Physical Properties and Process Ccontrol* (eds. W. Spiess, and H. Schubert). Elsevier Applied Science, London, pp. 512–535.

Klyosov, A.A. 1990. Trends in biochemistry and enzymology of cellulose degradation. *Biochemistry*, **29(47)**, 10577–10585.

Kozempel, M.F., Sullivan, J.F., Monica, E.S.D., Egoville, E.A., Talley, M.J., Jones, W.J., and Craig, J.J.C. 1982. Application of leaching model to describe potato nutrient losses in hot water blanching. *J. Food Sc.*, **47**, 1519–1523.

Kuhn, K. and Lechert, H. 1990. Determination of Fickian diffusion coefficients of water in foods using NMR-techniques and the Darken-equation. *Leb.-Wis. und Tech.*, **23**, 331–335.

Kusnadi, C. and Sastry, S.K. 2012. Effect of moderate electric fields on salt diffusion into vegetable tissue. *Journal of Food Engineering*, **110**, 329–336.

Lamberg, I. 1990. Transport phenomena in potato tissue. PhD thesis, University of Lund, Lund, Sweden.

Lazarides, H.N., Gekas, V., and Mavroudis, N. 1997. Apparent mass diffusivities in fruit and vegetable tissues undergoing osmotic processing. *J. Food Eng.*, **31**, 315–324.

Leach, G.C. 1993. Diffusion of soluble solids in apple tissue. PhD thesis, The University of Reading, Reading, UK.

Leach, G.C., Pyle, D.L., and Niranjan, K. 1995. Effective diffusivity of total solids and pectic substances from apple tissue. *Int. J. Food Sci. and Tech.*, **29**, 687–697.

Lenart, A., Lewicki, P.P., and Dziuda, J. 1989. Changes in the diffusional properties of apple tissue during technological processing. In *Engineering and Food. Vol. 1: Physical Properties and Process Control* (eds. W.E.L. Spiess and H. Schubert), Elsevier Applied Science, London, pp. 531–540.

Lenart, A., Lewicki, P.P., and Dziuda, J. 1990. Changes in the diffusional properties of apple tissue during technological processing. In *Engineering and Food. Vol.1: Physical properties and process control* (eds. W.E.L. Spiess and H. Schubert). Elsevier Applied Science, London, pp. 531–540.

Li, H., Zhao, C., Guo, Y., An, K., Ding, S., and Wang, Z. 2012. Mass transfer evaluation of ultrasonic osmotic dehydration of cherry tomatoes in sucrose and salt solutions. *International Journal of Food Science and Technology*, **47**, 954–60.

Lombardi, A.M. and Zaritzky, N.E. 1996. Simultaneous diffusion of citric acid and ascorbic acid in prepeeled potatoes. *Journal of Food Process Engineering*, **19**, 27–48.

Longo, M.A., Novella, I.S., Garcia, L.A., and Diaz, M. 1992. Diffusion of proteases in calcium alginate beads. *Enzyme Microb. Technol.*, **14(7)**, 586–90.

Loulou, T., Adhikari, B., and Lecomte, D. 2006. Estimate of concentration-dependent diffusion coefficient in drying process from the space average concentration versus time with experimental data. *Chemical Engineering Science*, **61(22)**, 7185–7198.

Mastro, A.M., Babich, M.A., Taylor, W.D., and Keith, A.D. 1984. Diffusion of a small molecule in the cytoplasm of mammalian cells. *Proc. Natl. Acad. Sci. USA*, **81**, 3414–18.

Mcardle, R.N. and Culver, C.A. 1994. Enzyme infusion: A developing technology. *Food Tech.*, **Nov. 94**, 85–89.

Metcalf Iii, T.N., Wang, J.L., and Schindler, M. 1986. Lateral diffusion of phospholipids in the plasma membrane of soybean protoplasts: Evidence for membrane lipid domains. *Proc. Natl. Acad. Sci. USA*, **83**, 95–99.

Mitchell, D.A., Greenfield, P.F., and Doelle, H.W. 1990. Mode of growth of Rhizopus oligosporus on a model substrate in solid-state fermentation. *World J. Microbiol. Biotechnol.*, **6**, 201–208.

Moreira, L.A. 1994. Acidification of vegetables during blanching. PhD thesis, Escola Superiora de Biotecnologia, Porto, Portugal.

Mulder, M. 1991. *Basic Principles of Membrane Technology*. Kluwer Academic Publishers, Dordrecht. Chapters II and V, pp. 46, 174.

Murakami, A.E. and Ariki, J. 1998. Produção de Codornas Japonesas. Finep-SP, pp. 63–67.

Naesens, W., Bresseleers, G., and Tobback, D. 1981. A method for the determination of diffusion coefficients of food components in low and intermediate moisture. *J. Food Sci.*, **46**, 1446–1449.

Neogi, P. 1996. *Diffusion in Polymers*, Marcel Dekker, Inc., New York.

Newman, A.B. 1931. Transcripts. *Am. Inst. Chem. Eng. J.,* **27,** 310. Cited by Selman et al. 1983.

Nicolas, M.G. and Duprat, F. 1983. Determination of potassium nitrate diffusivity in model systems—Preliminaries to extraction study of soluble components during blanching. *Sci. des Alimentes.*, **3(4)**, 615–628.

Nicole, M., Chamberland, H., Geiger, J.P., Lecours, N., Valero, J., Rio, B., and Ouellette, G.B. 1992. Immunocytochemical localisation of laccase L1 in wood decayed by *Rigidoporus lignosus. Appl. Environ. Microbiol*., **58(5)**, 1727–1739.

Noriega, E., Laca, A., and Diaz, M. 2008a. Modelling of diffusion-limited growth for food safety in simulated cheeses. *Food and Bioproducts Processing*, **86**, 122–129.

Noriega, E., Laca, A., and Mario Diaz, M. 2008b. Modelling of diffusion-limited growth to predict *Listeria* distribution in structured model foods. *Journal of Food Engineering*, **87**, 247–56.

Nout M.J.R. and Rombouts F.M. 1990. A review: Recent developments in tempe research. *J. Appl. Bacteriol*., **69**, 609–633.

Oliveira, F.A.R. 1988. Mass transfer analysis for the leaching of water soluble components from food. PhD thesis, University of Leeds, Leeds, UK.

Oliveira, F.A.R. and Silva, C.L.M. 1992. Freezing influences diffusion of reducing sugars in carrot cortex. *J. Food Sci.*, **57(4)**, 932–6.

Oliveira, J.C., Pereira, P.M., and Oliveira, F.A.R. 1994. The role of transport phenomena. In *Minimal Processing of Foods and Process Optimization—An Interface* (eds. R.P. Singh, and F.A.R. Oliveira), CRC Press, Boca Raton, FL, USA.

Osterberg, N.O. and Smith-Sorensen, T.S. 1981. Apple juice extraction in a counter current extractor. *J. Food Tech.*, **16**, 376–402.

Pedersen, H., Furler, L., Venkatasubramanian, K., Prenosil, J., and Stuker, E. 1985. Enzyme adsorption in porous supports: Local thermodynamic equilibrium model. *Biotechnol. Bioeng*. **XXVII**, 961–971.

Perry, R.H., Green, D.W., and Maloney, J.O. 1984. Prediction and correlation of physical and transport properties. In *Perry's Chemical Engineers' Handbook* (ed. R. H. Perry), 6th edition. McGraw-Hill, New York, London, pp. 3–213, 3-246–249.

Pflug, I.J., Fellers, P.J., and Gurevitz, D. 1967. Diffusion rates in the desalting of pickles. *Food Tech.*, **21(II)**, 1634–8.

Pinelo, M., Zornoza, B., and Meyer, A.S. 2008. Selective release of phenols from apple skin: Mass transfer kinetics during solvent and enzyme-assisted extraction. *Sep. Purif. Technol*. **63**, 620–7.

Prakotmak, P., Soponronnarit, S., and Prachayawarakorn, S. 2011. Effect of adsorption conditions on effective diffusivity and textural property of dry banana foam mat. *Drying Technology*, **29**, 1090–100.

Puri, V.M. and Anantheswaran, R.C. 1993. The finite element method in food processing: A review. *Journal of Food Engineering*, **19**, 247–74.

Pyle, D.L. 1992. Mass transfer in food and bioprocesses. University of Cambridge, program for the industry. Chemical engineering for the food industry.

Pyle, D.L., Niranjan, K., and Varley, J. 1997. Mass transfer in food and bioprocesses. In *Chemical Engineering for the Food Industry* (eds. P.J. Fryer, D.L. Pyle, and C.D. Rielly), Chapter 4, Blackie Academic and Professional, London, pp. 160.

Rabinovich, M.L. 1988. In: *Microbiology and Biochemistry of Degradation of Plant Materials* (eds. G.K. Skryabin, E.L. Golovlev, and A.A. Klyosov) Nauka, Moscow (in Russian), pp. 70–108.

Rice, P. and Selman, J.D. 1984. Technical note: Apparent diffusivities of ascorbic acid in peas during water blanching. *J. Food Tech.*, **19**, 121–124.

Rice, P., Selman, J.D., and Abdul-Rezzak, R.K. 1990. Nutrient loss in the hot water blanching of potatoes. *Int. J. Food Sci. Technol.*, **25**, 61–65.

Rodger, G., Hastings, R., Cryne, C., and Bailey, J. 1984. Diffusion properties of salt and acetic acid into herring and their subsequent effect on the muscle tissue. *J. Food Sci.*, **49**, 714–20.

Roques, M.A. 1987. Diffusion in foods: The work of Cost 90bis subgroup. In *Physical Properties of Foods* (eds. R., Jowitt, F. Escher, M. Kent, B. Mckenna, and M. Roques), Elsevier Applied Science, UK, pp. 13–26.

Salgın, S., Takaç, S., and Özdamar, T.H. 2006. Effect of ionic environments on the adsorption and diffusion characteristics of serine alkaline protease enzyme in polyethersulfone ultrafiltration membranes. *Journal of Colloid and Interface Science*, **299**, 806–814.

Salmon, E.D., Saxton, W.M., Leslie, R.J., Karow, M.L., and Mcintosh, J.R. 1984. Diffusion coefficient of fluorescein-labeled tubulin in the cytoplasm of embryonic cells of a sea urchin: Video image analysis of fluorescence redistribution after photobleaching. *J. Cell Biol.*, **99**, 2157–64.

Schwartzberg, H.G. and Chao, R.Y. 1982. Solute diffusivities in leaching processes. *Food Tech.*, **36**, 73–86.

Selman, J.D., Rice, P., and Abdul-Rezzak, R.K. 1983. A study of the apparent diffusion coefficients for solute losses from carrot tissue during blanching in water. *J. Food Tech.*, **18**, 427–40.

Spaninks, J.A.M. 1979. Design procedure for solid liquid extractors and the effect of hydrodynamic instabilities. Ph.D. Dissertation. Wageningen Agriculture University, The Netherlands.

Sprey, B. 1988. Cellular and extracellular localization of endocellulase in Trichoderma reesei. *FEMS Microbiol. Lett*. **55**, 283–294.

Stahl, R. and Loncin, M. 1979. Prediction of diffusion in solid foodstuffs. *J. Food Processing and Preservation*, **3**, 213–23.

Steffe, J.F. and Singh, R.P. 1980. Diffusion coefficients for predicting rice drying behaviour. *J. Agric. Eng. Res*. **27(6)**, 489–493.

Steinke, J.D. and Johnson, L.A. 1991. Steeping maize in the presence of multiple enzymes. I. Static batchwise steeping. *Cereal Chem.*, **68(1)**, 7–12.

Stokes, R.H. 1951. Integral diffusion coefficients of potassium chloride solutions for calibration of diaphragm cells. *J. Am. Chem. Soc.* **73(III)**, 3527–3528.

Tanaka, M., Ikesaka, M., and Matsuno, R. 1988. Effect of pore size in substrate and diffusion of enzyme on hydrolysis of cellulosic materials with cellulases. *Biotechnol. Bioeng.*, **32**, 698–706.

Tavel, L., Guichard, E., and Moreau, C. 2008. Chapter 6 Contribution of NMR spectroscopy to flavour release and perception. Annual Reports on NMR Spectroscopy, **64**, 173–188.

Teixeira, J.A., Mota, M., and Venancio, A. 1994. Model identification and diffusion coefficients determination of glucose and malic acid in calcium alginate membranes. *The Chem. Eng. J*., **56**, B9–B14.

Tomasula, P. and Kozempel, M.F. 1989. Diffusion coefficients of glucose, potassium, and magnesium in Maine Russet Burbank and Maine Katahdin potatoes from 45 to 90°C. *J. Food Sci.*, **54(4)**, 985–989.

Turhan, I., Tetik, N., Aksu, M., Karhan, M., and Certel, M. 2006. Liquid–solid extraction of soluble solids and total phenolic compounds of carob bean (*Ceratonia siliqua* L.). *Journal of Food Process Engineering*, **29**, 498–507.

Tyn, M. and Gusek, T.W. 1990. Prediction of diffusion coefficients of proteins. *Biotechnol. Bioeng.*, **35**, 327–338.

van der Sman, R.G.M. and Meinders, M.B.J. 2013. Moisture diffusivity in food materials. *Food Chemistry*, **138**, 1265–1274.

Varzakas, T. 1998a. Uptake of cell-wall degrading enzymes by soybean preparations. PhD thesis, The University of Reading, Reading, UK.

Varzakas, T. 1998b. *Rhizopus oligosporus* mycelial penetration and enzyme diffusion in soya bean tempe. *Proc. Biochem*., **33(7)**, 741–747.

Varzakas, T.H. 2000. Measurement of diffusivity of cell-wall degrading enzymes in food-agarose gels. *Deutsche Lebens. Rund.*, **96(4)**, 139–142.

Varzakas, T. 2001. Uptake of endoglucanase and endoxylanase from *A. niger* by soybean seeds. *Deutsche Lebensmittel-Rundschau*., **97(12)**, 465–471.

Varzakas, T., Arapoglou, D., and Israilides, C. 2005a. Infusion of an endoglucanase and an endoxylanase from *Aspergillus niger* in soybean. *Lebensmittel Wissenschaft und Technologie*, **38**, 239–247.

Varzakas, T., Arapoglou, D., and Israilides, C. 2006. Kinetics of endoglucanase and endoxylanase uptake by soybean seeds. *J. Biosciences Bioengineering*, **101(2)**, 111–119.

Varzakas, T., Escudero, I., and Economou, I.G. 1999. Estimation of endoglucanase and lysozyme effective diffusion coefficients in polysulphone membranes. *J. Biotechnol.*, **72**, 77–83.

Varzakas, T., Leach, G., Arapoglou, D., and Israilides, C. 2005b. Theoretical and experimental approaches towards the determination of solute effective diffusivities in foods. *Enzyme Microb. Technol.*, **37**, 29–41.

Varzakas, T., Pyle, D.L., and Niranjan, K. 1995a. Diffusion of cellulases in the soybean. Poster presentation. *7th European Congress of Biotechnology*, Nice, France.

Varzakas, T., Pyle, D.L., and Niranjan, K. 1995b. Diffusion of endoglucanases and xylanases in soybean (infusion), determination of their effective diffusivities and the effect of temperature. Poster presentation. *9th World Congress of Food Science & Technology*, Budapest, Hungary.

Varzakas, T., Pyle, D.L., and Niranjan, K. 1997. A preliminary investigation into the infusion of endoglucanases and endoxylanases in soybean. In: Jowitt, R. (ed.). *Engineering and Food at the 7th International Congress on Engineering and Food*. Sheffield Academic Press Ltd., UK. SA 52–55.

Vincent, F.V. 1989. Relationship between density and stiffness of apple flesh. *J. Sci. Food and Agric.*, **47**, 443–462.

Wang, L. and Sun, D. 2003. Recent developments in numerical modelling of heating or cooling processes in the food industry: A review. *Trends in Food Science and Technology*, **14**, 408–423.

Wang, W., Combe, C., and Clark, M.M. 2001. The effects of pH and calcium on the diffusion coefficient of humic acid. *J. Membr. Sci.*, **183**, 49–60.

Welch, G.R. and Easterby, J.S. 1994. Metabolic channeling versus free diffusion: transition-time analysis. *Trends Biochem. Sci.*, **19**, 193–97.

Welti-Chanes, J., Vergara-Balderas, F., and Bermúdez-Aguirre, D. 2005. Transport phenomena in food engineering: Basic concepts and advances. *Journal of Food Engineering*, **67**, 113–128.

Westerhoff, H.V. and Welch, G.R. 1992. Enzyme organisation and the direction of metabolic flow: Physicochemical considerations. *Current Topics in Cellular Regulation—From Metabolite to Metabolism to Metabolon*, **33**, 361–390.

Westrin, B. 1991. Diffusion measurement in gels: A methodological study. PhD thesis, Report LUTKDH/(TKKA-1003)/1–149/, Lund University, Lund, Sweden.

Wiktor, A., Iwaniuk, M., Sledz, M., Nowacka, M., Chudoba, T., and Witrowa-Rajchert, D. 2013. Drying kinetics of apple tissue treated by pulsed electric field. *Drying Technology*, **31**, 112–119.

Wilkie, T. and Chang, S. 1955. Correlation of diffusion coefficients in dilute solutions. *Am. Inst. Chem. Eng. J.*, **1(2)**, 264–270.

Williams, E.J. 1979. *Handbook of Anions Determination.* Butterworth, London.

Wood, T.M., McCrae, S.I., and Bhat, K.M. 1989. The mechanism of fungal cellulase action-Synergism between enzyme components of *Penicillium pinophilum* cellulase in solubilizing hydrogen bond-ordered cellulose. *Biochem. J.*, **260**, 37–43.

Wojcieszyn, J.W., Schlegel, R.A., Wu, E.S., and Jacobson, K.A. 1981. Diffusion of injected macromolecules within the cytoplasm of living cells. *Proc. Nat. Acad. Sci. USA*, **78(7)**, 4407–4410.

Zhang, S., Matsumoto, H., Saito, K., Minagawa, M., and Tanioka, A. 2009. Insulin transport across porous charged membranes: Effect of the electrostatic interaction. *American Institute of Chemical Engineers (AIChE) Biotechnology Progress.*, **25(5)**, 1379–1386.

Zienkiewicz, O.C. and Morgan, K. 1983. *Finite Elements and Approximation*. John Wiley and Sons, London.

Zogzas, N.P., Maroulis, Z.B., and Marinos-Kouris, D. 1996. Moisture diffusivity data compilation in foodstuffs. *Drying Technology*, **14(10)**, 2225–2253.

Zorrilla, S.E. and Rubiolo, A.C. 1994. A model for using the diffusion cell in the determination of multicomponent diffusion coeficients in gels or foods. *Chemical Engineering Science*, **49**, 2123–2128.

10 Absorption

Giovanni A. Escamilla García and
Eleazar M. Escamilla Silva

CONTENTS

10.1 Introduction 310
10.2 Antecedents 310
10.3 Gas Purification 312
10.3.1 Rate of Gas Absorption 314
10.3.2 Stage Equilibrium Gas Absorption 315
10.3.2.1 Single-Component Absorption 316
10.4 Membrane Gas–Liquid Contactors 319
10.4.1 Types of Membrane Contactors 320
10.4.2 Design Considerations for Membrane Gas–Liquid Contactors 322
10.5 Fundamental Aspects in Chemical Absorption 324
10.5.1 Complex Chemical and Phase Equilibrium 325
10.6 Mass-Transfer Fundamentals 326
10.6.1 Mass-Transfer Models 328
10.6.2 Application of Absorption Process 328
10.6.2.1 Vapor–Liquid Equilibrium Model 329
10.6.2.2 Kinetics Model 329
10.6.2.3 Process Simulation Model 330
10.6.3 Resume 333
10.6.3.1 Case of Ammonia Removal from Wastewater through Combination of Absorption Process in the Membrane Contactor and Advance Oxidation Process in Hybride Plasma-Ozone Reactor 333
10.7 Conclusions 336
10.7.1 Effect of Biologically Produced Sulfur on Gas Absorption in a Biotechnological Hydrogen Sulfide Removal Process 337
10.8 Future Prospects 338
References 338

The increasing importance of natural gas as a source of energy poses difficult gas separation design challenges, as the streams recovered from gas fields are at high pressures (typically about 10 MPa) and can contain a high proportion of CO_2 (up to 70%). In addition, as the implementation of the Kyoto protocol would require the capture of large quantities of CO_2, its injection in depleted or near-depleted reservoirs for enhanced oil/gas recovery operations will become increasingly frequent. This is

likely to result in natural gas streams that are even richer in CO_2. Conventional separation techniques are usually restricted to low CO_2 content or low-pressure feeds, and consequently there is a pressing need for an alternative process that is appropriate for such a scenario. However, absorption processes are aimed at the separation of CO_2 if there are a range of applications in various fields of chemical engineering, biochemistry, environmental, metallurgy, biotechnology, and others. Therefore, this chapter also discusses some basic aspects of the absorption process and some general applications show the versatility and usefulness of this ancient and current unitary process.

10.1 INTRODUCTION

Gas absorption is a widely known unit operation in chemical engineering. There are numerous process applications where particular components need to be selectively removed from a gas stream. The type of contacting unit for the feed gas and the absorbing liquid can be tailored to the application along with the choice of the absorbent, which will have a high selectivity for the desired components along with a high capacity for the absorbed components.

Chemical engineers have developed the use of chemically reactive absorption systems as a process that shows high selectivity and capacity as compared to absorbents, which do not chemically react with the absorbing species. There are numerous applications of this approach in the chemical industry. Examples are the removal of ammonia in the Haber process of ammonia synthesis, separation of acid such as CO_2 and H_2S from natural gas, and CO separation from gas mixtures with H_2.

There are numerous types of contactors that have been developed to assure a good contact between the gas and liquid streams. This is important to obtain an efficient separation process that requires a minimal size for the absorber. Many of the contactors are similar to those used in distillation. These include bubble cap trays and columns filled with various packings. Chemical engineers need to be able to design gas absorbers, which produce a treated gas of a desired purity with an optimal size and liquid flow. This can be based on existing correlations and, when required, laboratory and/or pilot plant data.

Industrial and research absorption, its applications and theory are well described in historical and current books, but it is necessary to take some basic concepts. Thus, it is not the intention of this chapter to recapitulate the already known fundamentals but to highlight relevant aspects from the viewpoint of daily industrial absorption work. Among others, absorption is a well-established unit operation with a high level of technical implementation and maturity (Figure 10.1). Therefore, small steps on a high level carry out further development. But the importance in industrial life, moving economical targets and new applications make "old fashioned" absorption attractive and dynamic for everyone, who has to deal with it in his daily work or research.

10.2 ANTECEDENTS

Gas absorption/desorption is a process in which a gaseous mixture is brought into contact with a liquid and during this contact a component is transferred between the gas and liquid streams. The gas may be bubbled through the liquid, or it may pass

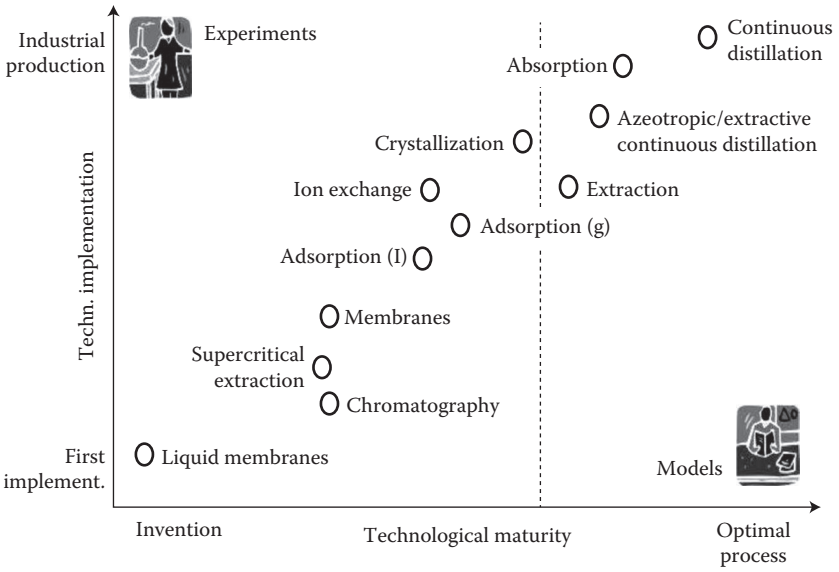


FIGURE 10.1 Applications of fluid separation processes in chemical and petrochemical industries after Górak and Schoenmakers. (Adapted from Górak, A., and Schoenmakers, H., 2004. vadisfluid separation processes—A German perspective, Oral Presentation, *EFCE Working Party on Distiallation, Absorption and Extraction*, September 16, Huelva-E.)

over streams of the liquid, arranged to provide a large surface through which the mass transfer can occur. The liquid film in this latter case can flow down the sides of columns or over packing, or it can cascade from one tray to another with the liquid falling and the gas rising in the counter flow. The gas, or components of it, either dissolves in the liquid (absorption) or extracts a volatile component from the liquid (desorption).

An example of the first type is found in hydrogenation of oils, in which the hydrogen gas is bubbled through the oil with which it reacts. Generally, there is a catalyst present also to promote the reaction. The hydrogen is absorbed into the oil, reacting with the unsaturated bonds in the oil to harden it. Another example of gas absorption is in the carbonation of beverages. Carbon dioxide under pressure is dissolved in the liquid beverage, so that when the pressure is subsequently released on opening the container, effervescence occurs.

An example of desorption is found in the steam stripping of fats and oils in which steam is brought into contact with the liquid fat or oil, and undesired components of the fat or oil pass out with the steam. This is used in the deodorizing of natural oils before blending them into food products such as margarine, and in the stripping of unwanted flavors from cream before it is made into butter. The equilibrium conditions arise from the balance of concentrations of the gas or the volatile flavor, between the gas and the liquid streams. In the gas absorption process, sufficient time must be allowed for equilibrium to be attained so that the greatest possible transfer can occur and, also, opportunity must be provided for contacts between the streams to occur under favorable conditions.

10.3 GAS PURIFICATION

In general, gas purification refers to the removal of impurities from the gas stream. The processes, which are used for this purpose, vary from simple physical techniques to complex hybrid multi-step processes, depending on the nature and concentration of impurities as well as on the treated gas specifications. Usually, the gas purification uses one of the following unit operations:

1. Absorption into liquids
2. Adsorption on solids
3. Separation by membrane
4. Condensation

Although various gas impurities such as H_2S, CO_2, SO_2, NO_x can be separated using these unit operations, the removal of carbon dioxide from the mixtures of gases is an important industrial process in several contexts and will be discussed in detail. The bulk carbon dioxide removal is carried out, for example, in the synthetic ammonia industry and gas-based industries such as natural gas, refinery gas, or coal gas purification, synthesis gas manufacture, and so on. The carbon dioxide separation is also important in the manufacture of synthetic gasoline, industrial organic chemicals such as salicylic acid, cracking of petroleum fractions, and atmosphere control in submarines and spacecrafts.

In recent years, the stringent environmental regulations toward the emissions of carbon dioxide have considerably changed economics of the fossil fuel-fired power plants and energy industries due to the penalty caused by carbon dioxide emissions. However, the use of carbon dioxide has become important in enhanced oil recovery programs. In principle, various methods could be used for the removal of carbon dioxide. The selection of these methods depends on several parameters such as CO_2 concentration in the feed stream, nature of other components present in the feed stream, and pressure and temperature at which the feed stream is available. Figure 10.2 shows the general guidelines for process selection of CO_2 removal technologies [2]. It can be seen from this figure that absorption in a liquid is the most common process used in the industry for CO_2 removal. For economic reasons, the absorbent must have a large capacity for carbon dioxide and must be regenerable. Liquids used for the absorption of carbon dioxide may dissolve the gas physically (e.g., propylene carbonate, selexol, n-formylmorpholine, etc.) or may contain a component, which chemically reacts with dissolved gas (e.g., aqueous carbonate solutions, alkanol amines, etc.). The specific rate of the absorption into physical solvents is, in general, much less compared to that into chemical absorbents. However, as the loading of physical solvents varies with partial pressure they can have a high loading capacity. The regeneration of a physical solvent is usually easy and less expensive. Owing to these properties, physical solvents are mainly used when the concentration of carbon dioxide in the feed stream is very high and only bulk removal is required. However, it becomes necessary to employ chemical absorbents when it is desired to reduce the partial pressure of carbon dioxide to very low levels.

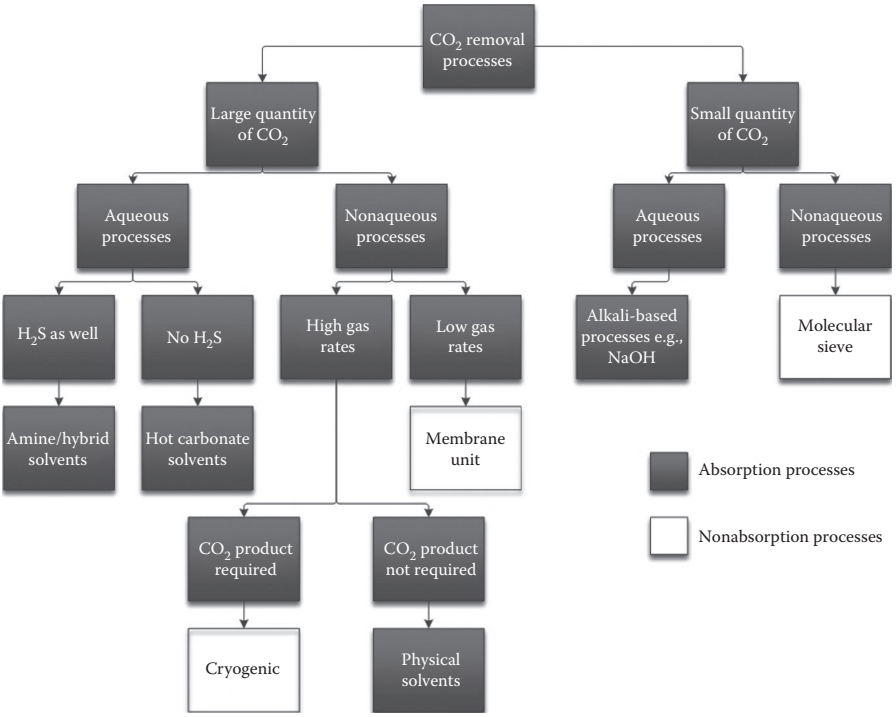


FIGURE 10.2 Guidelines for selection of CO_2 removal processes. (Adapted from Shaw, T.P., and Hughes P.W., 2001. *Hydrocarbon Processing*. May, 53–58.)

Generally, these absorption processes are carried out using conventional gas–liquid industrial contactors. Most of the industrial contactors achieve the gas–liquid mass transfer by direct contact and with dispersion of one phase within another. These industrial contactors can be broadly classified into three categories depending on the dispersing and nondispersing phase [3].

1. Contactors in which the liquid flows as a thin film (e.g., packed column, disccontactors, etc.).
2. Contactors where gas is dispersed into the liquid phase (plate column, bubble column, mechanically agitated contactors, etc.).
3. Contactors where liquid is dispersed into the gas phase (spray column, Venturi scrubbers, etc.).

In any type of gas–liquid contactor, the rates at which components are being transferred from the gas phase to the liquid phase or vice versa depend on the individual mass-transfer coefficients (k_L and k_G) and the gas–liquid interfacial area (a). Hence, the design of gas–liquid contactors is aimed toward increasing the individual mass-transfer coefficients and the interfacial area. Depending on the gas–liquid contactor type and operating conditions, there can be wide variation in k_L, k_G, and the

TABLE 10.1
Salient Features of Conventional Gas–Liquid Contactors

Type of Contactor	Liquid Hold Up	RTD		k_G (m s^{-1})	$k_L \times 10^4$ (m s^{-1})	Interfacial (m^{-1})
		G	L			
Packed column	0.05–0.1	P	P	$1–5 \times 10^{-2}$	0.3–2	20–350
Bubble column	0.6–0.8	P	M	$1–5 \times 10^{-2}$	1–4	25–1000
MAC	0.5–0.8	PM	M	$1–5 \times 10^{-2}$	1–5	200–1000
Spray column	0.05–0.1	PM	P	$1–5 \times 10^{-2}$	0.5–1.5	20–150

Source: Adapted from Doraiswamy, L.K., and Sharma, M.M., 1984. *Heterogeneous Reactions: Analysis, Examples, and Reactor Design. Volume 2: Fluid-Fluid-Solid Reactions*. Singapore: John Wiley.

Note: G, gas; L, liquid; RTD, residence time distribution; P, plug flow; PM, partially mixed; M, mixed; MAC, mechanically agitated contactor.

interfacial area. Table 10.1 shows the range of k_G, k_L, and interfacial area for conventional gas–liquid contactors [3]. In most of the dispersive type of contactors the mass-transfer coefficients and the interfacial area cannot be varied independently since both depend on the process/operating condition and are thus coupled. This interdependence of the mass-transfer coefficient and the interfacial area can lead to unstable and inefficient operation of the dispersive type of gas–liquid contactors under certain operating conditions. For example, under extreme gas and liquid-flow ratios conventional gas–liquid contactors suffer from flooding, weeping or foaming of the contactor. These disadvantages can be eliminated if the gas–liquid interface is immobilized.

10.3.1 Rate of Gas Absorption

The rates of mass transfer in gas absorption are controlled by the extent of the departure of the system from the equilibrium concentrations and by the resistance offered to the mass transfer by the streams of liquid and gas. Thus, we have the familiar expression:

$$\text{Rate of absorption} = \text{driving force/resistance}$$

The driving force is the extent of the difference between the actual concentrations and the equilibrium concentrations. This is represented in terms of concentration differences.

For the resistance, the situation is complicated, but for practical purposes it is adequate to consider the whole of the resistance to be concentrated at the interface between the two streams. At the interface, two films are postulated, one in the liquid and one in the gas. The two-film theory of Lewis and Whitman defines these resistances separately, a gas film resistance and a liquid film resistance. They are treated

very similarly to surface heat coefficients and the resistance of the two films can be combined in an overall resistance similar to an overall heat-transfer coefficient. The driving forces through each of the films are considered to be the concentration differences between the material in the bulk liquid or gas and the material in the liquid or gas at the interface. In practice, it is seldom possible to measure interfacial conditions and overall coefficients are used giving the equation:

$$\frac{dW}{dt} = K_L a(X^* - X) = K_g(Y - Y^*) \tag{10.1}$$

where dW/dt is the quantity of gas passing across the interface in unit time, K_L is the overall liquid mass-transfer coefficient, K_g is the overall gas mass-transfer coefficient, A is the interfacial area and X, Y are the concentrations of the gas being transferred, in the liquid and gas streams, respectively. The quantities of X^* and Y^* are introduced into the equation because it is usual to express concentrations in the liquid and in the gas in different units. With these, X^* represents the concentration in the liquid, which would be in equilibrium with a concentration y in the gas, and Y^* the concentration in the gas stream, which would be in equilibrium with a concentration X in the liquid. Equation 10.1 can be integrated and used to calculate overall rates of gas absorption or desorption. For details of the procedure, reference should be made to works of Perry [4], Charm [5], Coulson and Richardson [6], or McCabe and Smith [7].

10.3.2 Stage Equilibrium Gas Absorption

The performance of counter current stage contact gas absorption equipment can be calculated if the operating and equilibrium conditions are known. The liquid stream and the gas stream are brought into contact in each stage and it is assumed that sufficient time is allowed for equilibrium to be reached. In cases where sufficient time is not available for equilibration, the rate equations have to be introduced and this complicates the analysis. However, in many cases of practical importance in the food industry, either the time is insufficient to reach equilibrium, or else the calculation can be carried out on the assumption that it is and a stage efficiency term, a fractional attainment of equilibrium, introduced to allow for the conditions actually attained. Appropriate efficiency values can sometimes be found from published information, or sought experimentally.

After the streams in a contact stage have come to equilibrium, they are separated and then pass in opposite directions to the adjacent stages. The separation of the gas and the liquid does not generally present great difficulty and some form of cyclone separator is often used. In order to calculate the equipment performance, operating conditions must be known or found from the mass balances. Very often the known factors are as follows:

- Gas and liquid rates of flow
- Inlet conditions of gas and liquid
- One of the outlet conditions
- Equilibrium relationships

The processing problem is to find how many contact stages are necessary to achieve the concentration change that is required. An overall mass balance will give the remaining outlet condition and then the operating line can be drawn. The equilibrium line is then plotted on the same diagram, and the McCabe–Thiele construction applied to solve the problem.

10.3.2.1 Single-Component Absorption

Most absorption or stripping operations are carried out in countercurrent flow processes, in which the gas flow is introduced in the bottom of the column and the liquid solvent is introduced in the top of the column (Figure 10.3). The mathematical analysis for both the packed and plated columns is very similar.

The overall material balance for a countercurrent absorption process is

$$L_b + V_t = L_t + V_b \tag{10.2}$$

where

V = Vapor flow rate
L = Liquid flow rate
t, b = Top and bottom of tower, respectively

The component material balance for species A is

$$L_b x_{A,b} + V_t y_{A,t} = L_t x_{A,t} + V_b y_{A,b} \tag{10.3}$$

where

y_A = mole fraction of A in the vapor phase
x_A = mole fraction of A in the liquid phase

For some problems, the use of solute-free basis can simplify the expressions. The solute-free concentrations are defined as

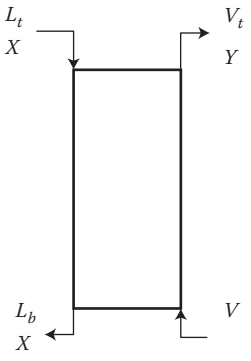


FIGURE 10.3 Counter current absorption process.

$$\overline{X_A} = \frac{x_A}{1 - x_A} \frac{\text{mole fraction of } A \text{ in the liquid}}{\text{mole fraction of non-}A \text{ component in the liquid}} \tag{10.4}$$

$$\overline{Y} = \frac{y_A}{1 - y_A} \frac{\text{mole fraction of } A \text{ in the vapor}}{\text{mole fraction of non-}A \text{ component in the vapor}} \tag{10.5}$$

If the carrier gas is completely insoluble in the solvent and the solvent is completely nonvolatile, the carrier gas and solvent rates remain constant throughout the absorber. Using $\overline{L}$ to denote the flow rate of the nonvolatile and $\overline{V}$ to denote the carrier gas flow rate, the material balance for solute A becomes

$$\overline{L}\ \overline{X}_{A,b} + \overline{V}\,\overline{Y}_{A,t} = \overline{L}\,\overline{X}_{A,t} + \overline{V}\,\overline{Y}_{A,b} \tag{10.6}$$

$$\overline{Y}_{A,t} = \frac{\overline{L}}{\overline{V}}\overline{X}_{A,t} + \left(\overline{Y}_{A,b} - \frac{\overline{L}\overline{X}_{A,b}}{\overline{V}}\right) \tag{10.7}$$

The material balance for solute A can be applied to any part of the column. For example, the material balance for the top part of the column is

$$\overline{Y}_{A,t} = \frac{\overline{L}}{\overline{V}}\overline{X}_{A,t} + \left(\overline{Y}_{A} - \frac{\overline{L}\overline{X}_{A}}{\overline{V}}\right) \tag{10.8}$$

In this equation, $\overline{X}_A$ and $\overline{Y}_A$ are the mole ratios of A in the liquid and vapor phase, respectively, at any location in the column including at the two terminals. Equation 10.8 is called the operation line and is a straight line with slope $\overline{L}/\overline{V}$ when plotted on $\overline{X}_A - \overline{Y}_A$ coordinates.

The equilibrium relation is frequently given in terms of Henry's law constant which can be expressed in many different ways:

$$P_A = H C_A = m x_A = K x_A \tag{10.9}$$

In this equation, P_A is the partial pressure of species A over the solution and C_A is the molar concentration with units of mole/volume. Henry's law constant H and m have units of pressure/molar concentration and pressure/mole fraction, respectively. K is the equilibrium constant or vapor–liquid equilibrium ratio.

The equilibrium relation in the mole fraction coordinates is a straight line while the operating line in the solute-free coordinates is also a straight line. Normally, the equilibrium relation is not a straight line in the mole fraction coordinates. Therefore it is an advantage to use solute-free coordinates because the operating line will always be straight.

The driving force for mass transfer becomes zero whenever the operating line intersects or touches the equilibrium curve. This limiting condition represents the minimum solvent rate to recover a specified quantity of solute or the solvent rate required to remove the maximum amount of solute. In Figure 10.4a, the intersection of the equilibrium and operating lines occurs at the bottom of the absorber. This condition defines the minimum solvent rate to recover a specified quantity of solute. This minimum solvent rate can be calculated from the following expression:

$$\left(\frac{\bar{L}}{\bar{V}}\right)_{min} = \frac{\bar{Y}_b - \bar{Y}_t}{\bar{X}_b - \bar{X}_t} \tag{10.10}$$

In Figure 10.4b, the intersection of the equilibrium and operating lines occurs at the top of the absorber. This condition represents the solvent rate required to remove the maximum amount of solute. This solvent rate can be calculated from the following expression:

$$\left(\frac{\bar{L}}{\bar{V}}\right)_{max} = \frac{\bar{Y}_b - \bar{Y}_t}{\bar{X}_b - \bar{X}_t} \tag{10.11}$$

Equation 10.11 is exactly the same as Equation 10.10 except in this case the bottom compositions are fixed so that the maximum slope of the operating line occurs when the operating line intersects the equilibrium curve at the top of the column.

Figure 10.4c shows the case when the operating line becomes tangent to the equilibrium curve. The minimum liquid-to-vapor ratio for this case can be determined from

$$\left(\frac{\bar{L}}{\bar{V}}\right)_{min} = \frac{\bar{Y}_c - \bar{Y}_t}{\bar{X}_c - \bar{X}_t} \tag{10.12}$$

In this equation, $\bar{X}_c$ and $\bar{Y}_c$ are the coordinates of the tangent point.

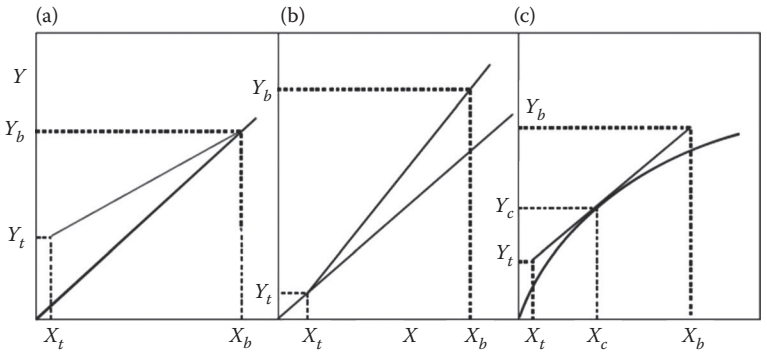


FIGURE 10.4 Limiting conditions for absorption process.

10.4 MEMBRANE GAS–LIQUID CONTACTORS

In recent years, membranes have been frequently proposed for fixing gas–liquid interfacial areas. Such types of nondispersive gas–liquid contactors are generally termed as membrane gas–liquid contactors. Unlike the dense membranes used in gas separation processes, the membranes used in these types of contactors are basically nonselective in nature and the solvent used primarily determines the selectivity aspect. In general, when microporous membranes are used in membrane contactors, the gas–liquid interface is immobilized at the opening of the pores of microporous membrane by careful control of the pressure difference between the two phases. These membrane contactors offer numerous advantages over the conventional gas–liquid contactors. Some of the significant advantages are listed below.

1. The specific gas–liquid interfacial area (area per unit of contactor volume) offered by the membrane gas–liquid contactors is considerably higher, especially in the case of hollow fiber membrane contactors. For commercially available hollow fiber membrane modules, it varies between 1500 and 3000 m^2/m^3 of contactor volume, depending on the diameter and packing density of the hollow fiber. This value is much higher than the contact areas available in conventional contactors (20–1000 m^2/m^3) like stirred tanks, bubble columns, and packed and plate columns [8]. In membrane contactors, the high interfacial area is obtained at the cost of the fiber side mass-transfer coefficient, which is low due to the laminar flow of the fluids inside the fiber. Nevertheless, the overall volumetric mass-transfer coefficient ($k_L a$) is substantially higher, resulting in a considerable reduction in the size of the contactor.
2. The interfacial area for mass transfer in a membrane gas–liquid contactor equals the geometrical membrane surface area. Thus, the interfacial area is constant and not influenced by orientation or change in flow rates. The feature of orientation free area is extremely useful for the offshore applications. In addition, the fixed interfacial area allows trouble-free operation over a wide range of process conditions and easy estimation of the interfacial area. In the conventional gas–liquid contactors, the interfacial area is strongly influenced by the process conditions and for reliable absorber design laborious experimental measurements of the interfacial area are required at different operating conditions.
3. For hollow fiber contactors, the flow within the fibers is usually laminar, thus the fiber side hydrodynamics are well known. This allows the accurate calculation of the fiber side mass-transfer coefficient from first principles.
4. In these contactors, the mass-transfer coefficient and the interfacial area can be varied independently. Thus, the operating limitations such as flooding, loading, weeping, and so on can be eliminated even at extreme gas and liquid flow ratio and at extreme hold-up ratios.
5. The scale-up of the membrane contactor is straightforward and simple due to the modular nature of the contactor.

6. Since for membrane contactors, the direct contact of the two phases is prevented, the contamination due to the mixing of the phases is eliminated. Hence, the requirement of equipment like "demister" (mist-eliminator) used in conventional gas–liquid contactors can be omitted. This feature can be advantageous for the pharmaceutical and clinical applications where sterile process conditions are of high importance.

However, membrane contactors also suffer from the following limitations:

1. The membrane adds an additional mass-transfer resistance to the overall mass-transfer process. The membrane mass-transfer resistance is strongly influenced by the nature of the phase that is present inside the pores of microporous membranes. This feature of the microporous membranes is a critical issue in the design of the membrane contactors.
2. An accurate control of transmembrane pressure is important in the case of microporous membrane contactors. The failure of efficient transmembrane pressure control may induce flow across the membrane (breakthrough), causing unwanted froth, foam and dispersion between the two phases.
3. For hollow fiber contactors, the flow within the fibers is usually laminar, thus the fiber side hydrodynamics are well known. This allows the accurate calculation of the fiber side mass-transfer coefficient from first principles.
4. In these contactors, the mass-transfer coefficient and the interfacial area can be varied independently. Thus, the operating limitations such as flooding, loading, weeping, and so on can be eliminated even at extreme gas and liquid flow ratio and at extreme hold-up ratios.
5. The scale-up of the membrane contactor is straightforward and simple due to the modular nature of the contactor.
6. Since for membrane contactors, the direct contact of the two phases is prevented, the contamination due to the mixing of the phases is eliminated. Hence, the requirement of equipment like "demister" (mist-eliminator) used in conventional gas–liquid contactors can be omitted. This feature can be advantageous for the pharmaceutical and clinical applications where sterile process conditions are of high importance.

10.4.1 Types of Membrane Contactors

Several membrane module configurations are available, both at commercial and laboratory scale, respectively, for the conventional membrane applications such as filtration, gas separation, and so on. These module configurations can be conveniently adopted for the membrane gas–liquid contactors with relatively little modifications. Depending on the type of membranes used in the contactor, these devices can be broadly classified into two groups; the flat sheet membrane contactor and the hollow fiber membrane contactor. Flat sheet membranes are used in plate-and-frame or in spiral wound membrane contactors. Although equally efficient mass-transfer operation can be carried out using flat sheet membrane contactors, hollow fiber membrane contactors are widely used due to the higher interfacial area.

Based on the flow directions of the gas and liquid phase, the hollow fiber membrane contactor can be used in two different modes of operation.

1. *Parallel flows mode*: The flow of both phases is parallel to the axis of the fiber and both fluids flow either in same direction (co-current) or in opposite direction (counter current).
2. *Cross flow mode*: The flow of one of the fluid is perpendicular to the axis of fiber and other fluid flows parallel to the axis of fiber. Thus, the two fluids flow at right angles to each other.

Parallel flow offers the highest average concentration driving force in the case of countercurrent flow and is preferred in situations where membrane or fiber side mass-transfer resistance controls [9]. The choice between the co-current and countercurrent operation is determined by the transmembrane pressure variation. In the case of countercurrent operation the variation in the transmembrane pressure is relatively high, which can interfere with the interface stability and can even lead to breakthrough of one phase into another. In the case of parallel flow, the overall mass-transfer rate can be significantly reduced if the shell-side mass-transfer resistance is significant. In such cases, cross flow configurations are attractive as flow in the direction perpendicular to the fibers leads to higher shell-side mass-transfer coefficients. This is mainly because of the concentration boundary layer break-up due to continuous splitting and remixing of the fluid flowing perpendicular to the fiber. However, the higher mass-transfer coefficient is obtained at the cost of a reduced overall mass-transfer driving force in comparison to countercurrent parallel flow.

The choice of the geometry of hollow fiber membrane contactors in early stages of developments was largely influenced by the simplicity of the module constructions. Conventionally, shell and tube geometry is preferred for membrane contactors due to the ease in the manufacturing of these modules. Later on, several investigators found that uneven packing and uneven flow distribution on the shell side of the shell and tube module resulted in reduced mass-transfer rates. Hence considerable efforts have been made to explore the different module geometries in order to achieve uniform flow distribution on the shell side.

In recent years, it has also been found that the use of fibers woven into a fabric in the membrane module manufacture results in more uniform fiber spacing [10]. The fibers woven into a fabric have been successfully used for the manufacturing of module with different geometries such as rectangular module, helically wound fiber module, baffled shell and tube module, and transverse flow module. Of the various innovative geometries studied by several investigators, only rectangular module and shell and tube transverse flow module have been successfully commercialized. Hoechst Celanese provides shell and tube transverse flow Liqui-Cel® contactors for various gas–liquid contacting applications whereas rectangular cross-flow module is commercialized by TNO Environmental Energy and Process Innovation (The Netherlands) and by Kvaerner Oil and Gas in co-operation with W. L. Gore and Associates GmbH.

10.4.2 Design Considerations for Membrane Gas–Liquid Contactors

The working principle of a microporous membrane contactor is shown in Figure 10.5. The mass-transfer process in the membrane contactor consists of three steps in series, the transfer from gas phase to the membrane surface, transfer within membrane pores and transfer from liquid interface to the liquid bulk. The overall mass-transfer coefficient in the case of membrane contactor is given by the "resistance in series" model [11].

$$\frac{1}{K_{ov}} = \frac{1}{k_G} + \frac{1}{k_m} + \frac{1}{mEk_L} \tag{10.13}$$

Here, k_G, k_m, and k_L are individual mass-transfer coefficients of the gas phase, membrane phase, and the liquid phase, respectively. "m" is the physical solubility of the gaseous species into the liquid bulk and "E" is the enhancement in mass-transfer rate due to chemical reaction (if any). The mass-transfer coefficient of membrane phase, k_m, depends on the type of phase present in the membrane pores. The mass-transfer resistance of the gas filled (non-wetted) pores is usually very small and negligible. However, when the membrane pores are filled with the liquid (wetted), the mass-transfer resistance of the membranes becomes significant [11], resulting in economically unviable operation.

The design strategy of the membrane gas–liquid contactors for CO_2 removal should be aimed at preventing the membrane wetting for long-term application.

In general, the membrane–liquid interactions, decides the wetting of the membrane. Hence, a suitable combination of the absorption liquid and the membrane material is critical for the stability of the membrane gas–liquid contactors. For porous membranes, a minimum pressure is required for the liquid to penetrate into the pores. This minimum breakthrough pressure (ΔP) for ideal cylindrical pores is given by the Laplace equation.

$$\Delta P = -\frac{2\gamma_L \cos\theta}{r_{max}} \tag{10.14}$$

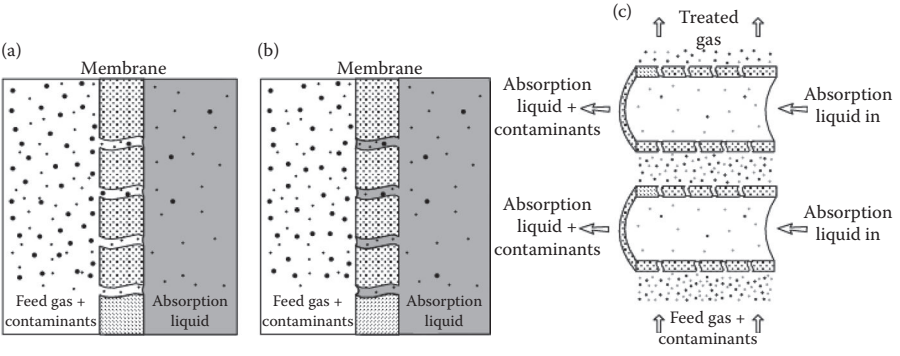


FIGURE 10.5 (a) Nonwetted membrane gas–liquid contactor; (b) Wetted membrane gas–liquid contactor; (c) Cross flow hollow fiber membrane gas–liquid contactor.

The higher breakthrough pressure is a key for the long-term non-wetting application of gas–liquid membrane contactors. It can be seen from Equation10.14 that this objective can be achieved by using solvents with high surface tension (γ_L), reducing the maximum pore size (r_{max}) and increasing the contact angle (θ). However, most of the physical solvents used for bulk CO_2 removal have low surface tensions and the reduction in the membrane pore size beyond certain limit results in reduced transport of the gas through the membrane owing to Knudsen flow. The membrane material having low surface energies favors the higher contact angle for a given solvent. Table 10.2 shows the membrane materials and their surface energies. It can be seen that the PTFE membrane material has a very low surface energy and this material is the most resistant for wetting. However, PTFE hollow fibers are very expensive as compared to the polyolefin fibers and very small diameter (<500 μm) fibers are not commercially available. However, the polypropylene membrane material has sufficiently low surface energy, is inexpensive, and commercially available in very small fiber diameters. Hence, the use of polypropylene membrane in combination with various CO_2 removal solvents had been explored in some works [12].

As discussed earlier, cross flow modules have a higher shell side mass-transfer coefficient and offer higher mass-transfer rates at identical driving force. These modules can be arranged in serial or parallel cascades to give overall countercurrent flow, thereby increasing the overall driving force. In the case of CO_2 removal, using either reactive or nonreactive solvents, liquid side mass-transfer resistance controls the overall mass-transfer process. It seems favorable to have the phase with controlling mass-transfer resistance on the shell side of the cross flow membrane module. However, the mechanical strength of the fibers is limited and the shear by the liquid flowing perpendicular to the fibers is likely to cause buckling and uneven distribution of fibers, resulting in eventual lowering of module performance. In extreme cases of high liquid flow rates complete failure of the module is also possible as observed by Sirkar [13]. Hence for practical reasons, it was decided to use the cross modules with liquid flowing through the fiber and gas flowing on the Shell side. In addition, by using this configuration the effect of variation of local concentration gradients in directions, parallel and normal to flow, for both phases can be analyzed using first principles. The primary focus of the present investigation is on the prevention of the

TABLE 10.2
Surface Energies of Polymer Materials

Polymer	Surface Energy (mN/m)
Polytetraflouroethylene (PTFE)	19.1
Polytriflouroethylene	23.9
Polypropylene	30
Polyvinylideneflouride	30.3
Polyethylene	33.2

Source: Adapted from Mulder, M., 1996. *Basic Principles of Membrane Technology*. 2nd Edition, Dordrecht: Kluwer Academic.

membrane wetting for long-term application and on the performance evaluation of the cross flow membrane module for CO_2 removal using nonreactive as well as reactive solvents. Single fiber studies, focusing on the prevention of wetting and on the liquid side mass-transfer coefficient, with or with reaction, are not only part of the system development but also offer a nice opportunity as a gas–liquid research tool.

The application of hydrophobic microporous membrane as gas–liquid contactor was initially explored in the medical field for the oxygenation of blood as an artificial lung [14,15]. The absorption of a variety of gases in acidic or alkaline medium using membrane hollow fiber modules was initially studied by Cussler and his coworkers [16,17] for industrial applications. Since then, several investigators have studied the membrane-based absorption and desorption method for removal of variety of solutes such as CO_2, SO_2, NO_x, H_2S, VOC, NH_3, and so on using nonreactive as well as reactive solvents. Based on these studies several processes using membrane gas–liquid contactors are successfully commercialized. These industrial processes and the use of membrane gas–liquid contactors for possible applications are reviewed in detail by Sirkar [18] and Gabelman and Hwang [19]. As it is not the intention to review all the applications of the membrane gas absorption process in this section, only the studies related to CO_2 and other removal using this process are discussed.

A significant amount of the published research work on membrane gas–liquid contactors is related to CO_2 removal, due to the enormous scope for application in high volume gas treating processes (e.g., natural gas processing, flue gas processing) as well as low volume CO_2 removal processes (e.g., life support system, supply of CO_2 to greenhouses). In the initial work, Qi and Cussler [16,17] studied the absorption of CO_2 into aqueous alkalis and alkanolamine solutions using polypropylene hollow fiber modules (pore-diameters 0.03 μm). These authors found that the membrane mass-transfer resistance was negligible and the liquid-side mass-transfer resistance controlled the CO_2 absorption in aqueous alkalis and alkanolamine solutions. However, later on Kreulen et al. [20] reported the wetting of the polypropylene membrane with somewhat larger pore diameter (0.2 μm) by aqueous methyl diethanolamine (MDEA) solutions. A similar observation of the wetting of polypropylene membranes (pore diameter 0.03 μm) by aqueous diethanolamine (DEA) and NaOH solutions is also reported by Rangwala [21], who attributed the wetting phenomena to the membrane surface modification by trace impurities.

10.5 FUNDAMENTAL ASPECTS IN CHEMICAL ABSORPTION

Absorption is often carried out with the aid of chemical reactions in the liquid phase in order to increase absorbent capacity and solubility. On the contrary, to typical distillation or physical absorption processes, these cases require the consideration of the occurring chemical reactions. The thermodynamic and mathematical description of such a system is similar to nonelectrolyte systems. It only requires the inclusion of all chemical reactions, their equilibria, and the activity coefficients of all species. The complexity of such a system and the mathematical problems to solve the underlying equations is not only a result of the increased number of components but also due to the highly nonlinear linkage between the relationships for chemical equilibria and activity

coefficients of the different species [22]. Complexity increases when ionic compounds are involved and specific models for electrolyte thermodynamics have to be regarded.

10.5.1 Complex Chemical and Phase Equilibrium

As an example for the complex behavior and equations to be solved in chemical absorption with electrolytes the absorption of CO_2 and H_2S in a mixed amine system is described below. The reactions to be considered are as follows:

Instantaneous reversible reactions:

$$2H_2O \overset{K_1}{\leftrightarrow} H_3O^+ + OH^- \tag{R.1}$$

$$MDEA + H_2O \overset{K_2}{\leftrightarrow} MDEAH^+ + OH^- \tag{R.2}$$

$$MEA + H_2O \overset{K_3}{\leftrightarrow} MEAH^+ + OH^- \tag{R.3}$$

$$HCO_3^- + H_2O \overset{K_4}{\leftrightarrow} CO_3^{2-} + H_3O^+ \tag{R.4}$$

$$H_2S + H_2O \overset{K_5}{\leftrightarrow} HS^- + H_3O^+ \tag{R.5}$$

$$HS^- + H_2O \overset{K_6}{\leftrightarrow} S^{2-} + H_3O^+ \tag{R.6}$$

Kinetically controlled reactions:

$$CO_2 + OH^- \overset{K_7}{\leftrightarrow} HCO_3^- \tag{R.7}$$

$$MEA + CO_2 + H_2O \overset{K_8}{\leftrightarrow} MEACOO^- + H_3O^+ \tag{R.8}$$

The existence of additional electrolytes, for example, NaOH or Na_2CO_3, KOH or K_2CO_3 can be considered by

$$NaOH \overset{K_9}{\leftrightarrow} Na^+ + OH^- \tag{R.9}$$

$$KOH \overset{K_{10}}{\leftrightarrow} K^+ + OH^- \tag{R.10}$$

The occurring reaction $CO_2 + 2H_2O \leftrightarrow HCO_3^- + H_3O^+$ is very slow compared to (R.7), especially in alkaline solutions. Its contribution to the overall rate

of reaction is therefore small and can be neglected. Reactions involving protonation or hydrolysis can be considered as instantaneous compared to the diffusion process. Eigen gives reaction rates for different reactions in aqueous systems [23]. To calculate the exact concentrations of molecular and ionic species in solution the chemical equilibria are expressed with their dissociation constants K_j; that should be based on activities taking nonidealities into account:

$$K_j = \prod_{i=1}^{nc} a_i^{\nu_{i,j}} = \prod_{i=1}^{nc} m_i^{\nu_{i,j}} \gamma_i^{\nu_{i,j}} \tag{10.15}$$

To complete the set of equations, the chemical equilibrium and the concentrations of species in solution, the total mass balances for each apparent component and a charge balance (electro neutrality) for the solution have to be added to the set of equations. For example,

$$m_{CO_2}^{tot} = m_{CO_2} + m_{CO_3^-} + m_{CO_3^{2-}} + m_{MEACOO^-} \text{ (R.2 … R.7)}$$

Electro-neutrality condition:

$$\sum_{i}^{nc} m_i z_i = 0 \tag{10.16}$$

This results in 17 equations for 17 species presuming knowledge of the six total molalities for apparent components. Total mass and concentration of the molecular species water are constant since the concentration measure is molality in mol per kg of solvent (H_2O). If equilibrium exists at the interface the chemical potentials of the molecular components in both phases has to be equal.

$$y_i \varphi_i P = x_i \gamma_i H_{i,H_2O}\ (T, p) \tag{10.17}$$

The Henry coefficient H_{i,H_2O} of the component *i* in water for dissolved diluted gases is used for the standard-state fugacity; the fugacity coefficient φ_i considers the nonideality of the gas phase. The activity coefficient gi has to be calculated by using an adapted electrolyte model, for example, the Pitzer- or electrolyte-NRTL-model [24].

Combining chemistry and thermodynamics, it is important to consider a consistent set of activities. The data calculated on the basis of activity coefficients have to fit the vapor–liquid data as well as the kinetics and chemical equilibria [25]. Unfortunately, considering all these details is often the only way to describe those systems with accuracy needed in industry. These data also have to be combined with the complex equations describing heat and mass transfer that are described below.

10.6 MASS-TRANSFER FUNDAMENTALS

For a nonequilibrium model, the column is divided into stages. In each segment the vapor and the liquid phase is considered separately regarding balances for mass,

components, and enthalpy. Mass transfer between both phases over the interfacial area is evaluated with the film theory, which assumes one-dimensional diffusion in the film and a completely mixed bulk phase. The diffusion in multicomponent systems is often described by the General-Maxwell–Stefan (GMS) approach derived from the kinetic gas theory taking intermolecular friction into account [26]. All simplified models (e.g., Fick's law) can be derived from General–Stefan–Maxwell. The driving force d_i in terms of diffusion fluxes j in GMS is given by

$$d_i = \sum_{j=1}^{nc} \frac{x_i j_j - x_j j_j}{C_t D_{i,j}} \tag{10.18}$$

Assuming electro-neutrality of the entire solution and a constant pressure, the generalized driving force in electrolyte systems is given in [27] and adapted to the one-dimensional case by

$$d_i = \frac{x_i}{RT} \frac{d\mu_i}{dy} + x_i z_i \frac{F}{RT} \frac{d\phi}{dy} \tag{10.19}$$

To calculate the diffusion in the film, Equations 10.18 and 10.19 have to be combined. In electrolyte solutions different diffusivities of ions cause small charge separations leading to electric forces between ions of opposite charge. The diffusivities of hydrogen and hydroxyl ions occurring in the aqueous solution are considerably higher than those of other species [28]. The mass-transfer rate N_i can then be calculated taking into account convection:

$$N_i = J_i + x_i \sum_{j=1}^{nc} N_j \tag{10.20}$$

and that

$$0 = \sum_{i=1}^{nc} J_i \tag{10.21}$$

The solution of the equation system consisting of Equations 10.18 through 10.21 can lead to the so-called cross-effects, such as the "diffusion barrier," "counter diffusion," or "osmotic diffusion," for example, zero diffusion despite a concentration gradient or diffusion of one component against its own concentration gradient or without a gradient. These effects cannot be predicted by the normal Fick's law. However, these effects occur only in concentrated solutions and can often be neglected in diluted systems [29], as they occur typically in absorption processes. Higher concentrations in the vapor phase at the top of desorber might introduce a small influence of these effects.

10.6.1 Mass-Transfer Models

For the calculation of mass transfer between two phases in an absorption process several models exist, such as the film theory, penetration theory, or surface renewal theory. All of these models simplify the hydrodynamic behavior significantly and require a decisive parameter. For the film theory this parameter is the thickness of the boundary layer δ, which can also be expressed in a mass-transfer coefficient β:

$$\beta = \frac{D}{\delta} \tag{10.22}$$

Specific accuracy is needed when mass-transfer coefficients from classical correlations [30] are combined with diffusion coefficients that have been calculated from binary diffusion coefficient [31].

These parameters have either to be determined from laborious experiments and adapted to the particular problem or might also be predicted. Newer approaches use hydrodynamic analogies or CFD calculations [32].

In most chemical absorption problems the chemical reactions are fast enough to influence the mass transfer in the film. Thus, mass transport and reactions occur simultaneously leading to changes in concentration gradients and therefore an enhancement of mass transfer. Several models exist for the consideration of these effects.

The reactions can either be considered as instantaneous and thus equilibrium can be assumed, or can be incorporated into the model using detailed reaction kinetics for both the film and the bulk phase or just for the film assuming that equilibrium of the reaction is achieved in the bulk phase. The simplest modeling approach, the equilibrium model, usually fails to predict chemical absorption processes.

10.6.2 Application of Absorption Process

The absorption process has many years of application in industrial chemical processes, however, currently it is undergoing a revival process because there are many gases that occur in the process which must be controlled to avoid increasing environmental pollution and therefore the atmospheric warming. This has resulted in a series of investigations on the development of scientific studies on innovative systems engineering absorption and desorption. Below there are some novel cases of absorption process applied in the different industrial areas.

Kinetics, modeling and simulation studies were conducted for the absorption of carbon dioxide (CO_2) into highly concentrated and loaded monoethanolamine solutions (MEA) in the temperature range 293–333 K. A new comprehensive mathematical absorption-rate/kinetics model was developed which takes into account the coupling between chemical equilibrium, mass transfer and chemical kinetics of all possible chemical reactions have been used successfully.

Global warming resulting from the emission of greenhouse gases, especially CO_2, has become a widespread concern in recent years. Although various CO_2 capture technologies have been proposed, chemical absorption and adsorption are currently believed to be the most suitable ones for post-combustion power plants. Ahmed Aboudheir et al. [33] studied the kinetics, modeling, and simulation for the

absorption of carbon dioxide (CO_2) into highly concentrated and loaded monoethanolamine solutions (MEA) in the temperature range 293–333 K. A new comprehensive mathematical absorption rate/kinetics model was developed which takes into account the coupling between chemical equilibrium, mass transfer, and chemical kinetics of all possible chemical reactions. The mathematical model is capable of predicting gas absorption rates and enhancement factors from the system hydrodynamics and the physicochemical properties, and can also predict the kinetics of the reaction from experimental absorption data. These results allowed developing a new termolecular-kinetics model for CO_2 reaction with MEA solutions, which proved to be better than previously published kinetic models. As a practical application, the new termolecular kinetics model and the vapor/liquid equilibrium model were integrated with a process-simulation program for CO_2 absorption into an aqueous MEA solution in a packed column. Accurate behavior of CO_2 absorption into this solution in terms of the temperature and concentration profiles was obtained. The results further showed that by using the new kinetics model, the deviation between the predicted and the actual bedheight of the packed column is less than 1.0%.

10.6.2.1 Vapor–Liquid Equilibrium Model

Liquid bulk concentrations of all chemical species are required for the simulation process and the kinetic analysis. A vapor–liquid equilibrium (VLE) model to estimate the CO_2 partial pressure and the liquid bulk concentrations of all the chemical species present in the solution was developed. The input data of the model include the initial concentration of the MEA solution, the initial CO_2 loading of the MEA solution, the equilibrium constants of the reactions, and the solubility of CO_2 into MEA solution.

10.6.2.2 Kinetics Model

In this study a comprehensive absorption rate/kinetics model was developed for interpreting the laminar jet absorption data of CO_2 into MEA solutions from which the kinetics data were extracted. The model takes into account the coupling between chemical equilibrium, mass transfer, and chemical kinetics of all possible chemical reactions. These resulted in a system of unsteady-state partial differential equations referred to as the mathematical model. This mathematical model is capable of predicting gas absorption rates and enhancement factors from the system hydrodynamics and the physicochemical properties, as well as predicting the kinetics of the reaction from experimental absorption data. A rigorous numerical method to solve the system of unsteady-state partial differential equations was developed. The model was validated by comparing its predictions with the experimental data of CO_2 absorption into water and MEA solutions, as well as N_2O absorption into MEA solutions as reported elsewhere [34]. In brief, the diffusion equation in Equation 10.1 is the one most frequently used to represent the absorption of gas into liquid jets. Equation 10.23 governs the variation in time and space of the concentration of the reactants and the products in the liquid phase (one equation for each component or material balance).

$$D_j \frac{\partial^2 C_j}{\partial x^2} = \frac{\partial C_j}{\partial t} + r_i \tag{10.23}$$

where D denotes diffusivity, C denotes the concentration of the chemical species, t denotes the time, r denotes reaction rate, and x denotes the distance normal to the jet surface (independent spatial variable measured from the gas–liquid interface into the liquid bulk), noting that a laminar jet absorber was used to collect the kinetics data.

10.6.2.3 Process Simulation Model

In the gas absorption industry, CO_2 removal from gaseous mixtures with alkanolamine solutions is classified as adiabatic gas absorption with chemical reaction. The first design technique of the gas absorption with chemical reaction in adiabatic packed towers was introduced by Pandya [35]. This design technique accounts for the major heat effects (absorption, reaction, solvent evaporation, and condensation), chemical reaction in the liquid phase, and mass-transfer resistance and heat-transfer resistance in both phases. The main model equations resulting from the mass and energy balance of this model were implemented in this work to obtain the concentration and temperature profiles.

The reliability of the laminar jet absorber was tested as a function of temperature by experimentally determining the temperature effect on the diffusivity of CO_2 in water within the temperature range from 288 to 333 K, the typical temperature range found in gas absorbers. Figure 10.6 shows this experimental diffusivity as well as the predicted diffusivity from the model developed by Versteeg and van Swaaij [36]. The results showed that excellent agreement between the measured and predicted diffusivity was obtained. The average absolute deviation of the measured diffusivity from the predicted diffusivity was 1.7%. This indicates that the behavior of the laminar jet is excellent within this temperature range, the same temperature range for the kinetic data of this work. Points are the experimental data and line is predicted by Versteeg and vanSwaaij model [36].

All experimental absorption rate data obtained in the laminar jet absorber, were interpreted by the numerically solved absorption-rate kinetics model. For each absorption-rate data obtained, the calculated enhancement factor was fitted to the experimentally observed enhancement factor with the apparent reaction-rate constant (k_{app}) as an adjustable parameter. The experimental results of these k_{app} constants are

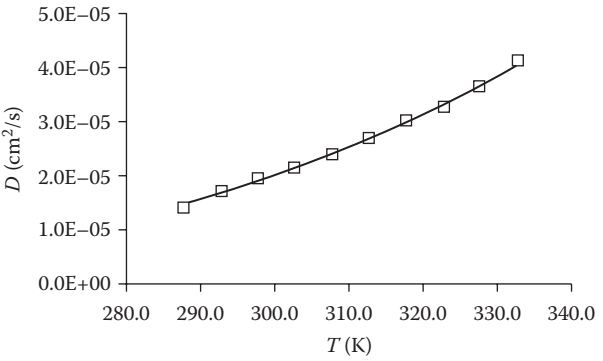


FIGURE 10.6 Diffusivity of CO_2 in water as a function of temperature obtained in laminar jet apparatus.

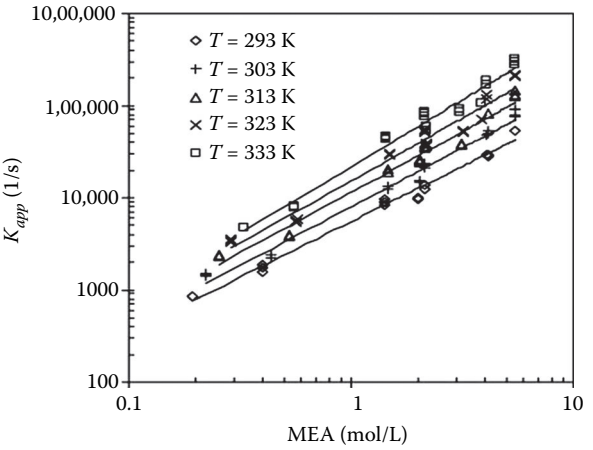


FIGURE 10.7 Experimental results of the apparent reaction-rate constants for CO_2 reaction with MEA solutions.

presented in Figure 10.7. A definite temperature dependence of the overall reaction rate can be observed for the five temperatures studied (293, 303, 313, 323, and 333 K). Numerical calculation of the kinetics of the reaction is usually achieved by assuming a reaction mechanism and interpreting experimental–absorption rate data with the aid of a numerically solved absorption-rate model. The forward reaction rate for termolecular mechanism of Crooks and Donnellan [37], as presented in Equation 10.24, was assumed by the authors.

$$r_{CO_2-MEA} = -\left(k_{RNH_2}\left[RNH_2\right] + k_{H_2O}\left[H_2O\right]\right)\left[RNH_2\right]\left[CO_2\right] \tag{10.24}$$

$$k_{app} = k_{RNH_2}\left[RNH_2\right]^2 + k_{H_2O}\left[H_2O\right]\left[RNH_2\right] \tag{10.25}$$

To calculate the reaction rate constants of Equation 10.24, all the experimental k_{app} constants in Figure 10.7 obtained from the absorption-rate/kinetics model were fitted to the termolecular mechanism expression in Equation 10.25. A linear regression analysis for these data gave the kinetics expressions of Equations 10.26 and 10.27 based on the termolecular reaction rate equation as represented in Equation 10.25.

$$k_{RNH_2} = 4.61 \times 10^9 e^{-\frac{4412}{T}} \tag{10.26}$$

$$k_{H_2O} = 4.61 \times 10^6 e^{-\frac{3287}{T}} \tag{10.27}$$

This new kinetics model was proven to give accurate representation for CO_2–MEA systems for solutions of low and high concentrations as well as for high CO_2-loaded

solutions as documented elsewhere [38]. In this work, the new termolecular kinetics model has been integrated with the process-simulation program in order to verify its applicability and as a demonstration of its practical utilization. The simulation results of this integration are discussed below.

First, the validity of using our new termolecular-kinetics model (Equations 10.25 through 10.27) for the simulation of CO_2 absorption into MEA solutions in packed column was confirmed by comparing the predictions of the column concentration profiles with the experimental data. Figure 10.8 shows the comparison between the experimental results and the model predictions. There is very good agreement between the actual and predicted (solid line in Figure 10.8) CO_2 concentration profile, thereby confirming the validity of using the new termolecular-kinetics model as well as the computer simulation program. In addition, the behavior of the column is also well predicted even with the integration of other published kinetics models with the process simulation program. These include the model of Hikita et al. [37] (the most frequently referenced model), the model of Versteeg et al. [38] (which compiled many kinetics data in literature), and the model of Horng and Li [39] (the most recently published model). The kinetics models of Hikita et al. [37] and Versteeg et al. [39] gave identical and good predictions for the concentration profile along the column as can be seen in Figure 10.8 (dotted line).

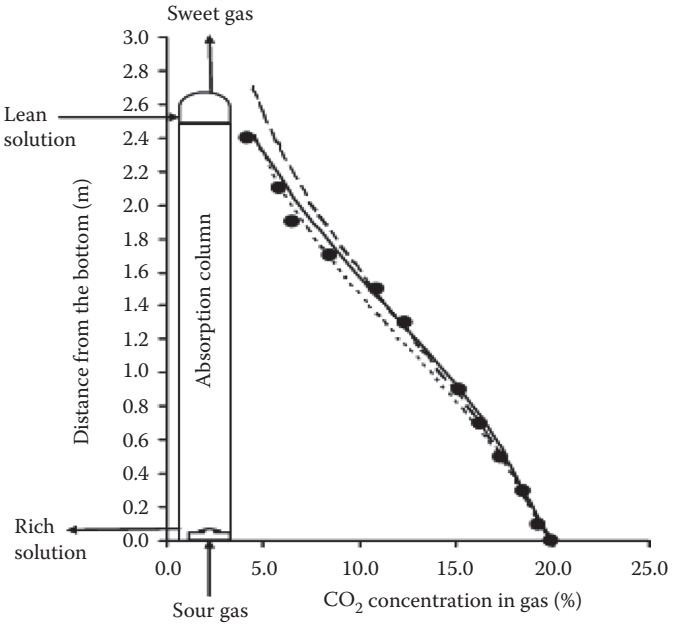


FIGURE 10.8 Measured and predicted CO_2 concentration profiles along the packed column using various kinetics models. Points are measured; solid line is predicted by using the new termolecular-kinetics model, dotted line is predicted by using Versteeg and Hikita kinetics models, and dashed line is predicted by using Horng kinetics model.

10.6.3 Resume

Here we presented a summary of a new termolecular-kinetics model for the reaction of CO_2 with MEA solutions and has been reported for the reaction of CO_2 with highly concentrated and loaded MEA solutions. When this new termolecular-kinetics model and the recently published physicochemical properties correlations were integrated with the process-simulation model, accurate predictions for the concentration and temperature profiles along with the packed columns were obtained for different types of packing materials.

10.6.3.1 Case of Ammonia Removal from Wastewater through Combination of Absorption Process in the Membrane Contactor and Advance Oxidation Process in Hybride Plasma-Ozone Reactor

Wastewater containing high concentrations of ammonia can be harmful to aquatic life and degrades the water quality. Wastewater containing ammonia is usually removed by conventional methods such as aeration in towers, biological treatment, and adsorption of the ammonium ion to the zeolite surface. However, these methods are less effective and relatively expensive. Therefore, there is a need for alternative technologies that can improve the efficiency of ammonia removal from wastewater. This study aims to obtain the process of ammonia removal through a combination of absorption in the membrane contactor and the advance oxidation process in the hybrid plasma-ozone reactor. Wastewater containing ammonia used in the study was a synthetic wastewater with a concentration of about 800 ppm. In the experiment, the wastewater from the reservoir was first passed into the membrane contactor on the shell side, and then mixed with ozone from the ozonizer before entering the plasma reactor, and finally was circulated back to the reservoir. Meanwhile, the absorbent solution was sent to the lumen fiber in membrane contactor. Experimental results showed that the ammonia removal efficiency increases with increasing in circulation rate and temperature of the wastewater. The highest efficiency of ammonia removal obtained from the experimental results was 77%.

Ammonia, even at low concentration, can cause problem to aquatic life and degrades the water quality. Ammonia is usually removed through denitrification in the water treatment plant. There are several conventional methods to remove ammonia from wastewater such as aeration in pack tower, biological treatment [40], and adsorption as ammonium ion into the surface of zeolite [41]. However, these methods almost always depend on relatively high-energy consumption [42]. Therefore, there is a need for alternative technologies that can improve the efficiency of ammonia removal from wastewater with less energy consumption. One technology that can be used for ammonia removal from wastewater is the membrane technology. Membrane contactor is a contactor device for mass transfer in liquid–liquid systems and gas–liquid without mixing of these phases [43]. Membrane contactor used often for such purposes is a microporous hydrophobic hollow fiber membrane contactor. In the case of gas–liquid separation, the membrane will prevent water solution, which has a higher surface tension to penetrate the membrane pores, thanks to the hydrophobic pores of the membrane. Volatile compounds will evaporate from the feed side, and will then diffuse through the gas-filled membrane pores, and will

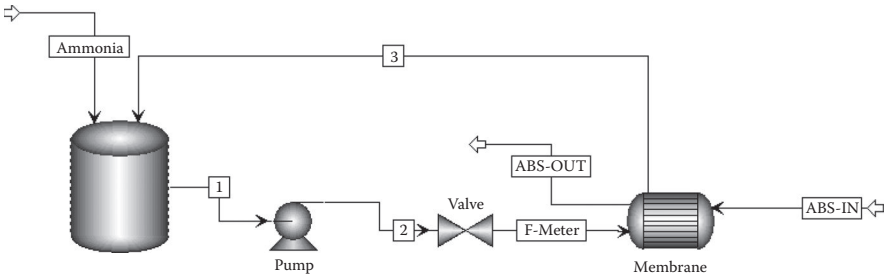


FIGURE 10.9 Schematic diagram of the experimental of ammonia removal through the membrane contactor.

then be swept by a sweep gas, drawn by a vacuum pump, or will react with the absorbing solution [44].

Several studies have been conducted using membrane contactors as a tool for the removal of ammonia from wastewater such as the stripping of ammonia through the membrane contactor using sweep gas [45] and vacuum [46], and the removal of ammonia through the membrane distillation [47,48] and vacuum membrane distillation [49]. This study aims to obtain ammonia removal process through a combination of absorption in the membrane contactor and the advance oxidation process in the hybrid plasma–ozone reactor.

Microporous hydrophobic membrane fibers of polyvinylchloride are used in the experiments sized of 0.8 mm inside diameter and 0.35 mm thickness. The contactor sizes are 3.0, 2.4, and 40.0 cm in outside and inside diameter, and length, respectively. The number of fiber in the contactors are 40, 50, and 60, respectively. Figures 10.9 and 10.10 show a schematic diagram of the ammonia removal process through the membrane and through the combination of membrane and hybrid reactor plasmaozone.

In the ammonia removal process, the pH of the absorbent solutions, wastewater flow rates and temperatures are varied to see their effects on the ammonia removal performance. The mechanism of ammonia transfer through the membrane is shown in Figure 10.11, where first ammonia in the vapor phase diffuses from the bulk

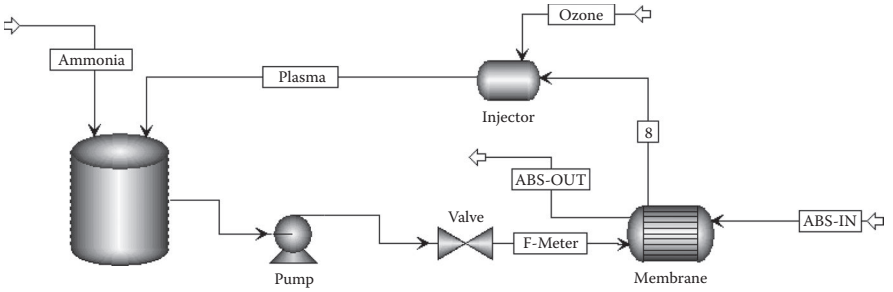


FIGURE 10.10 Schematic diagram of the experimental of ammonia removal through combination of absorption process in the membrane contactor and advance oxidation processes in the plasma-ozone reactor.

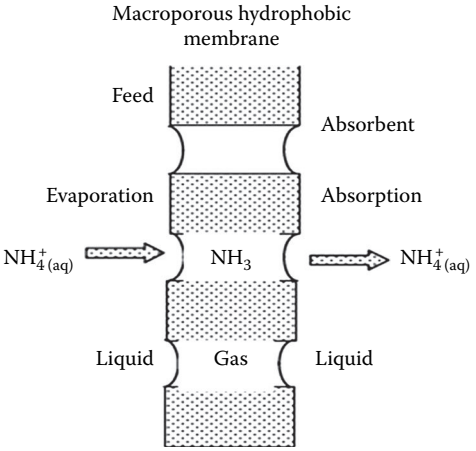


FIGURE 10.11 The mechanism of ammonia absorption from wastewater through membrane (Adapted from Mulder, M., 1996. *Basic Principles of Membrane Technology*. 2nd Edition, Dordrecht: Kluwer Academic.)

wastewater solution to the membrane surface, then diffuses through the membrane pores containing gas, and finally reacts rapidly with sulfuric acid used as an absorbent solution. The effects of pH of absorbent solutions on ammonia removal efficiencies through the membrane process and the combination of the membrane and the plasma-ozone reactor processes are shown in Figures 10.12 and 10.13. The results showed that the lowest pH of the absorbent solution (0.7) gives the highest removal efficiency on both membrane and combination processes. This is due to more sulfuric acid that can absorb ammonia and based on Equation 10.28, the ammonia removal efficiency is increased. The highest removal efficiency of the membrane

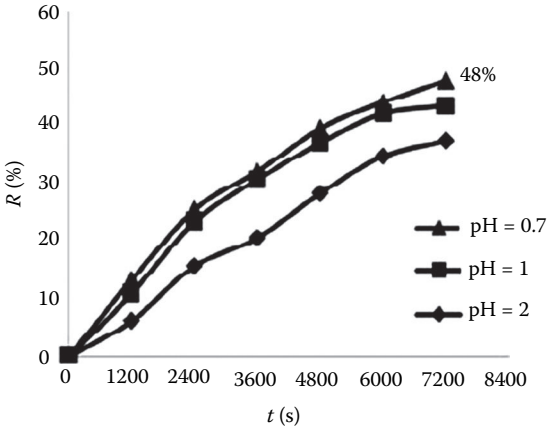


FIGURE 10.12 Variations of removal efficiency, R (%), versus time, t, at various of pH of absorbent solutions for membrane process.

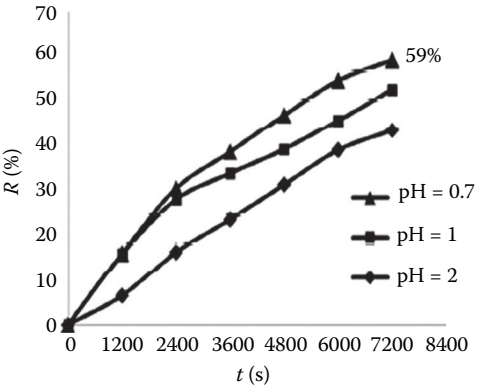


FIGURE 10.13 Variations of removal efficiency, R (%), versus time, t, at various of pH of absorbent solutions for membrane process and combined process of membrane and HPOR.

process is 48%, while the combined process is 59%. An increase in efficiency is due to the amount of ammonia that has been broken down by the hydroxyl radicals to form other compounds. The hydroxyl radical is the result of the decomposition of ozone generated from the ozonizer or the hybrid plasma-ozone reactor (HPOR).

$$2NH_{3(g)} + H_2SO_{4(aq)} \rightarrow \left(NH_4\right)_2 SO_{4(aq)} \tag{10.28}$$

Experiments are also conducted for other ammonia removal processes such as ozonation process, HPOR, combination membrane-ozone, combination of membrane and HPOR, and combination HPOR-ozone. All the processes use pH of the absorbent solution as 1.0. The removal efficiency of all processes is shown in Figure 10.14. HPOR process has the smallest removal efficiency that is 13%. A similar phenomenon is also found for the ozonation process and combination of ozonation-HPOR processes where its removal efficiency values are not much different. However, after the processes are combined with membrane process there are significant increases in removal efficiency and reaches the highest value of 52% for the combination of membrane and HPOR processes. This phenomenon implies that the membrane plays a very important role in the ammonia removal process, while HPOR and ozonizer helps reduce the membrane load on ammonia removal [50].

10.7 CONCLUSIONS

The effect of ammonia removal from wastewater through a combination of hybrid membrane with ozone plasma reactor and ozonator is better when compared with a single membrane processes. Experimental results showed that ammonia removal efficiency increase with an increase in the rate of circulation and temperature of the wastewater and the number of fibers in the contactor, but decrease with increasing pH of the absorbent solution. Ammonia removal efficiency in the combined process can reach 77%, while in the single membrane it is only 48%.

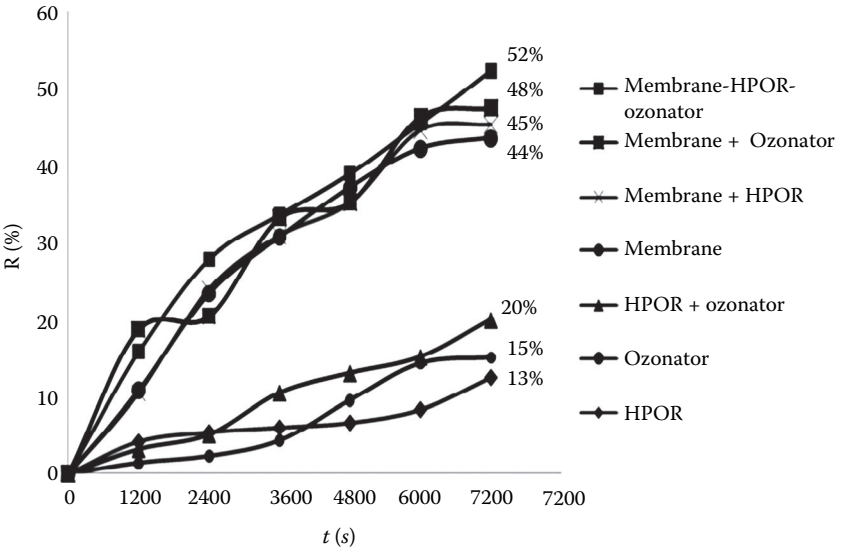


FIGURE 10.14 Variations of removal efficiency, R (%), versus time, t, for various processes using pH of absorbent solution 1.0.

10.7.1 Effect of Biologically Produced Sulfur on Gas Absorption in a Biotechnological Hydrogen Sulfide Removal Process

Absorption of hydrogen sulfide in aqueous suspensions of biologically produced sulfur particles was studied in a batch-stirred cell reactor, and in a continuous set-up, consisting of a lab-scale gas absorber column and a bioreactor. Presence of biosulfur particles was found to enhance the absorption rate of H_2S gas in the mildly alkaline liquid. The mechanism for this enhancement was, however, found to depend on the type of particles used. In the gently stirred cell reactor only small hydrophilic particles were present ($d_p < 3$ μm) and the enhancement of the H_2S absorption rate can be explained from the heterogeneous reaction between dissolved H_2S and solid elemental sulfur to polysulfide ions, S_x^{2-}. Conditions favoring enhanced H_2S absorption for these hydrophilic particles are low liquid side mass transfer (k_L), high sulfur content, and presence of polysulfide ions. In the set-up of gas absorber column and bioreactor, both small hydrophilic particles and larger, more hydrophobic particles were continuously produced (d_p up to 20 μm). Here, observed enhancement could not be explained by the heterogeneous reaction between sulfide and sulfur, due to the relatively low specific particle surface area, high k_L, and low $[S_x^{2-}]$. A more likely explanation for enhancement here is the more hydrophobic behavior of the larger particles. A local increase of the hydrophobic sulfur particle concentration near the gas–liquid interface and specific adsorption of H_2S at the particle surface can result in an increase in the H_2S absorption rate [51].

10.8 FUTURE PROSPECTS

Several new applications of absorption will occur with increasing importance of gas-based techniques and environmental demands. A promising example, as already mentioned, is the CO_2-capture from conventional power plants. Since these power plants contribute to the global anthropogenic CO_2 emissions to a very large extent, the associated flue gas flows from these plants are large and the heat requirements for regeneration of today's available solvents are high. This problem can be considered as one of the most challenging tasks in chemical engineering in this century. Due to the low available partial pressure of CO_2, chemical absorption has to be favored for this task. Using a typical MEAsolvent a loss of 10% efficiency for the power plant is still too high to be commercially feasible [55]. Thus, one of the future aspects is the search for a new solvent. In industrial practice these solvents should possess the following attributes for CO_2 capture:

- Low evaporation and reaction enthalpy to reduce steam requirements for regeneration
- Low vapor pressure to reduce solvent losses
- Fast reaction with CO_2
- Low toxicity
- Little degradation with O_2, NO_x, SO_2
- No corrosion
- No foam

An overview of possible solvents is given in [52]. Tailor-made amine solutions can be an attractive alternative [53]. In this context, the design of ionic liquids (IL) for this specific task is currently carried out [52]. IL's can also be used for gas absorption of other components [54]. Due to their major advantages (no vapor pressure, possibility for tailor-made design) they may become once standard absorbents, if availability and prices in 100 tons scale fit industrial requirements. The sulfate content in turpentine is a source of pollution for the environment when it is used in the α-terpineol process, because it produces mercaptanes and sulfhydric acid; this issue holds good prospects for investigation applying the absorption process. The pharmaceutical and biotechnological industry is another interesting field to study the application of absorption; leaving the biochemistry, biological, agricultural and other areas of interest [55,52]. Regarding its complexity, today's industrial absorption is a well-developed and established unit operation. Commercially, absorption is often the "cash cow" of processes where it is used as a main process step and not only for off-gas treatment. New and exciting challenges especially concerning new applications occur for absorption. Several drawbacks in the existing models and data basis have to be clarified.

REFERENCES

1. Górak, A. and Schoenmakers, H., 2004. Quo vadis fluid separation processes—A German perspective, Oral Presentation, *EFCE Working Party on Distiallation, Absorption and Extraction*, September 16, Huelva-E.

2. Shaw, T.P. and Hughes P.W., 2001. Optimize CO_2 removal, *Hydrocarbon Processing*. May, 53–58.
3. Doraiswamy, L.K. and Sharma, M.M., 1984. *Heterogeneous Reactions: Analysis, Examples, and Reactor Design. Volume 2: Fluid-Fluid-Solid Reactions*. Singapore: John Wiley.
4. Perry, J. H. et al., 1997. *Chemical Engineers' Handbook*, 7th Edition. New York: McGraw-Hill.
5. Charm, S. E. 1971. *The Fundamentals of Food Engineering*, 2nd Edition. Westport: AVI.
6. Coulson, J. M. and Richardson, J. F. 1977, 1978. *Chemical Engineering*, Vol. 1, 3rd Edition. Vol. 2, 3rd Edition. Oxford: Pergamon.
7. McCabe, W. L., Smith, J. C., and Harriott, P., 1975. *Unit Operations of Chemical Engineering*, 3rd Edition. New York: McGraw-Hill.
8. Doraiswamy, L.K. and Sharma, M.M., 1984. *Heterogeneous Reactions: Analysis, Examples, and Reactor Design. Volume 2: Fluid-Fluid-Solid Reactions*. Singapore: John Wiley.
9. Wang, K.L. and Cussler, E.L., 1993. Baffled membrane modules made with hollow fiber fabric. *Journal of Membrane Science*, 85, 265–278.
10. Cussler, E.L., 1994. Hollow fiber contractors. In *Membrane Processes in Separation and Purification*, (eds. J.G. Crespo and K.W. Boddeker), pp. 375–394. Boston: Kluwer Academic Publisher.
11. Kreulen, H., Versteeg, G.F., Smolders, C.A., and van Swaaij, W.P.M., 1993a. Microporous hollow fiber membrane modules as gas–liquid contactors I: Physical mass transfer processes—A specific application—Mass transfer in highly viscous liquids. *Journal of Membrane Science*, 78(3), 197–216.
12. Mulder, M., 1996. *Basic Principles of Membrane Technology*. 2nd Edition, Dordrecht: Kluwer Academic.
13. Wang, K.L. and Cussler, E.L., 1993. Baffled membrane modules made with hollow fiber fabric. *Journal of Membrane Science*, 85, 265–278.
14. Esato, K. and Eiseman, B., 1975. Experimental evaluation of Gore-Tex membrane oxygenator. *Journal of Thoracic and Cardiovascular Surgery*, 69(5), 690–697.
15. Tsuji, T., Suma, K., Tanishita, K., Fukazawa, Z., Kanno, M., Hasegawa, H., and Takashi, A., 1981. Development and clinical evaluation of hollow fiber membrane oxygenator.*Transactions of American Society of Artificial Internal Organs*, 27, 280–284.
16. Qi, Z. and Cussler, E.L., 1985a. Microporous hollow fibers for gas absorption I. Mass transfer in the liquid. *Journal of Membrane Science*, 23, 321–333.
17. Qi, Z. and Cussler, E.L., 1985b. Microporous hollow fibers for gas absorption II. Mass transfer across the membrane. *Journal of Membrane Science*, 23, 333–345.
18. Sirkar, K.K., 1997. Membrane separation technologies: Current developments.*Chemical Engineering Communications*, 157, 145–184.
19. Gabelman, A. and Hwang, S.T., 1999. Hollow fiber membrane contactors. *Journal of Membrane Science*, 159, 61–106.
20. Kreulen, H., Versteeg, G.F., Smolders, C.A., and van Swaaij, W.P.M., 1993b. Microporous hollow fiber membrane modules as gas–liquid contactors II: Mass transfer with chemical reaction. *Journal of Membrane Science*, 78(3), 217–238.
21. Rangwala, H.A., 1996. Absorption of carbon dioxide into aqueous solution using hollow fiber membrane contactors. *Journal of Membrane Science*, 112, 229–240.
22. Luckas, M. and Krissmann, J., 2001. *Thermodynamik der Elektrolytlo¨sungen—Thermodynamics of Electrolyte Systems*. Berlin: Springer-Verlag.
23. Eigen, M., 1963. Protonenu¨bertragung, Sa¨ure-Base-Katalyse und enzymatische Hydrolyse. Teil I: Elementarvorga¨nge—Proton transfer, acid–base catalysis and enzymatical hydrolysis. Part I: Elementary processes. *Angewandte Chemie*, 75, 489–508.

24. Austgen, D.M., Rochelle, G.T., Peng, X., and Chen, C.C., 1989. Model of Vapor-liquid equilibria for aqueous acid gas-alkanolamine systems using the electrolyte-NRTL equation. *Industrial and Engineering Chemistry Research*, 28, 1060–1073.
25. Haubrock, J., Hogendoorn, and Versteeg, G.F., 2005. The applicability of activities in kinetic expressions: A more fundamental approach to represent kinetics of the system CO_2-OH in terms of activities. *International Journal of Chemical Reactor Engineering,* 3, 1–19, article A40.
26. Astarita, G., Savage, D., and Bisio, A., 1983. *Gas Treating with Chemical Solvents*. New York: John Wiley and Sons.
27. Taylor, R. and Krishna, R., 1993. *Multicomponent Mass Transfer*. New York: John Wiley and Sons.
28. Wesselingh, J.A. and Krishna, R., 2000. *Mass Transfer in Multicomponent Mixtures*. Delft: Delft University Press.
29. Cussler, E., 1997. *Diffusion, Mass Transfer in Fluid Systems*, 2nd Edition. Cambridge: Cambridge University Press.
30. Onda, K., Takeuchi, H., and Okumoto, Y., 1968. Mass transfer coefficients between gas and liquid phases in packed columns. *Journal of Chemical Engineering of Japan*, 1,56–62.
31. Asprion, N., 2006. Nonequilibrium rate-based simulation of reactive systems: Simulation model, heat transfer, and influence of film discretization. *Industrial and Engineering Chemical Research,* 45, 2054–2069.
32. Shilkin, A. and Kenig, E.Y., 2005. A new approachto fluid separation modelling in the columns equipped with structured packings. *Chemical Engineering Journal,* 110, 87–100.
33. Aboudheir, A.,Tontiwachwuthikul, P., Idem, R., and Cheminoix, 2007, CCU/09. International Test Centre for Carbon Dioxide Capture (ITC). Faculty of Engineering, University of Regina, Regina, SK, S4S 0A2, Canada.
34. Astarita, G., Savage, D., and Bisio, A., 1983. *Gas Treating with Chemical Solvents*. New York: John Wiley and Sons.
35. P.V. Danckwerts, 1970. *Gas–Liquid Reactions*. NewYork: McGraw-Hill.
36. Versteeg, G.G. and van Swaaij, W.M., 1988. On the kinetics between CO2 and alkanolamines both in aqueous and non-aqueous solutions-I. Primary and secondary amines. *Chem. Eng. Sci.*, 43 (3), 573–585.
37. Gödecke, R., 2006. *Fluidverfahrenstechnik*. Weinheim: Wiley-VCH.
38. PERP Report 03/04s10, Advances in LNG Technologies, New York, Nextant Chem Systems, October 2004.
39. U.S. Departement of Energy, Gasification Technology R&D, http://www.fossil.energy.gov/programs/powersystems/gasification/.
40. Belhateche, D.H., 1995. Choose appropriate wastewater treatment technologies. *Chemical Engineering Progress*, 8, 32–38.
41. Du, Q., Liu, S.J., Cao, Z.H., and Wang, Y.Q., 2005. Ammonia removal from aqueous solution using natural Chinese clinoptilolite. *Separation and Purification Technology*, 44 (3), 229–234.
42. Norddahl, B., Horn, V.G., Larsson, M., du Preez, J.H., and Christensen, K., 2006. A membrane contactor for ammonia stripping, pilot scale experience and modeling. *Desalination*, 199 (13), 172–174.
43. Gabelman, A. and Hwang, S.T., 1999. Hollow fiber membrane contactors. *Journal of Membrane Science*, 159 (1–2), 61–106.
44. Ashrafizadeh, S.N. and Khorasani, Z., 2010. Ammonia removal from aqueous solutions using hollow-fiber membrane contactors. *Chemical Engineering Journal*, 162 (1), 242–249.

45. Mandowara, A. and Bhattacharya, P.K., 2009. Membrane contactor as degasser operated under vacuum for ammonia removal from water: A numerical simulation of mass transfer under laminar flow conditions. *Computers and Chemical Engineering*, 33 (6), 1123–1131.
46. Ding, Z., Liu, L.Y., Li, Z.M., Ma, R.Y., and Yang, Z.R., 2006. Experimental study of ammonia removal from water by membrane distillation (MD): The comparison of three configurations. *Journal of Membrane Science*, 286 (1–2), 93–103.
47. Xie, Z., Tuan, D., Manh, H., Cuong, N., and Brian, B., 2009. Ammonia removal by sweep gas membrane distillation. *Water Research*, 43 (6), 1693–1699.
48. Zhu, Z., Hao, Z.L., Shen, Z.S., and Chen, J., 2005. Modified modelling of the effect of pH and viscosity on the mass transfer in hydrophobic hollow fiber membrane contactors. *Journal of Membrane Science*, 250 (1–2), 269–276.
49. El-Bourawi, M.S., Khayet, M., Ma, R., Ding, Z., Li, Z., and Zhang, X., 2007. Application of vacuum membrane distillation for ammonia removal. *Journal of Membrane Science*, 301 (1–2), 200–209.
50. Kartohardjono, S., Putri, M.H., Fahmiati, S., Fitriasari, E., Ajeng, C., and Bismo, S., 2012. Combination of ozonation process and absorption through membrane contactor using natural hot spring water as absorbent to remove ammonia from wastewater. *Journal of Environmental Science and Engineering*, 1 (4), 428–433.
51. Escamilla, G.A. and García, E. M., 2013. Escamilla Silva. Technical Report. Taloquimia SA de CV.
52. Rolker, J. and Arlt, W., 2006. Abtrennung von Kohlendioxid aus Rauchgasen mittels absorption—Capture of CO_2 from flue gases usingabsorption. *Chemie Ingenieur Technik*, 78, 416–424.
53. SRI-PEP-Report 180A, CO_2-Capture, SRI-Consulting 2009.
54. Authony, J.L., Maginn, E.J., and Brennecke, J.F., 2003. Gas solubilities in 1-n-Butyl-3-methylimidazonium hexafluorophosphate, in Rogers, R.D., Seddon, K.R. (eds.), *Ionic Liquids—Industrial Applicationsfor Green Chemistry*, *ACS Symposium Series* 818, Oxford University Press, 260–269.
55. Kleinjan, W.E., Lammers, J.N.J.J., de Keizer, A., and Janssen, A.J.H., 2006. Effect of biologically produced sulfur on gas absorption in a biotechnological hydrogen sulfide removal process. *Biotechnology Bioengineering*, 94, 633–644.
56. Khayet, M. and Matsuura, T., 2004. Pervaporation and vacuum membrane distillation processes: Modeling and experiments. *AIChE Journal*, 50 (8), 1697–1712.

11 Distillation for the Production of Fortification Spirit

Malcolm S. Allen, Andrew C. Clark, Leigh M. Schmidtke, and Peter J. Torley

CONTENTS

11.1 Introduction 344
11.2 Principles of Distillation 344
11.2.1 Ideal Two-Component Systems 344
11.2.2 Nonideal Two-Component Systems 346
11.2.3 Fractional Distillation 347
11.2.3.1 The Principles behind Fractional Distillation 347
11.2.3.2 Batch and Continuous Fractional Distillation 349
11.2.4 Reflux Conditions 351
11.2.5 Theoretical Plates 352
11.2.6 McCabe–Thiele Diagrams 352
11.3 Distillation Technique 355
11.3.1 Pot Still for Cognac Production 355
11.3.2 Continuous Distillation 357
11.3.2.1 Low Wine Preparation 357
11.3.2.2 Purifying Column 358
11.3.2.3 Rectifying Column 358
11.3.2.4 Pasteurizing (Methanol) Column 359
11.3.2.5 The Overall Process 360
11.4 Minor Components in the Spirit 360
11.4.1 Origin of Volatile Minor Components 360
11.4.2 Quality of Feed Stock 361
11.4.3 Significant Minor Flavor Components 361
11.4.4 Behavior of Minor Flavor Components 361
11.4.5 Minor Components in Fractionating Columns 362
11.4.6 Minor Components in Pot Stills 364
11.5 Assessment of Volatile Aroma Compounds in Spirit 366
References 367

11.1 INTRODUCTION

Distillation can be defined as a process in which the components of a liquid mixture are separated or partially separated by vaporization followed by condensation of the vapor. Distillation has a long and complex history, with reports of its usage in Egypt, China, and India (Bujake 2008) long before the dawn of Christianity. Arab communities are reported to have learned the practice from the Egyptians and made cosmetic paints by heating and volatizing a mixture of natural materials. The residue was used to paint eyelids and was called "kohl." Later, when they performed a similar practice on wine, the product was named "al kohl," and then eventually became alcohol (Bujake 2008). The technique was radically developed in the eleventh century with the invention of a coiled cooling pipe by a Persian philosopher (Avicenna). By the Middle Ages, the knowledge of distillation had spread throughout Europe, and eventually countries developed their own specific beverages. This includes Cognac from France, Schnapps from Germany, Grappa from Italy, Vintage and Tawny Ports from Portugal, and a range of fortified red and white wines including Muscats and Topaques from Australia.

This chapter provides a general description of the principles of distillation with focus on the production of either brandies or high-quality spirit, from grape-derived materials, for use in beverage production. Phase diagrams are described for ideal two-component systems, followed by the nonideal nature of the water–ethanol mixture, along with the corresponding McCabe–Thiele diagrams. The focus of the distillation equipment is confined to pot stills and continuous distillation columns. These techniques are commonly used for commercial distillation and they also provide a good contrast in approaches to distilling ethanol–water mixtures. As well as the distillation of ethanol, the behavior of the minor components during distillation is also described for both pot stills and fractional distillation columns. Comprehensive coverage of other distillation equipment and more complex systems (i.e., three-component mixtures) are beyond the scope of this chapter and are available in Doherty et al. (2008).

11.2 PRINCIPLES OF DISTILLATION

11.2.1 Ideal Two-Component Systems

In this section, a two-component mixture that behaves as an "ideal" system will be examined and the following section will consider the ramifications of a "nonideal" system (such as ethanol–water). An ideal system is one whose components follows Raoult's law:

$$p_i = p_i^* x_i \tag{11.1}$$

p_i = partial pressure of the component
p_i^* = vapor pressure of the pure component
x_i = mole fraction of component in the mixture

If the two pure components of an ideal two-component system have different vapor pressures, the liquid and vapor phases at phase equilibrium will have different

compositions, and the vapor phase will always be enriched in the more volatile component, by comparison with the liquid phase that it is in equilibrium with.

For distillations that are carried out at constant pressure, an isobaric phase diagram is appropriate for representation of the liquid and vapor composition behavior of a two-component system at varying temperatures (Figure 11.1). Such phase diagrams provide a wealth of information about the condition of phase equilibrium in a system. They show whether phase equilibrium exists under a particular set of conditions, and, if it does, they show the composition and relative quantities of the two phases.

If the pressure in Figure 11.1 is atmospheric pressure, then

- Points A and B—correspond to the normal boiling points of the pure components.
- Lines BFCA and BGDA correspond to the liquid and vapor compositions at phase equilibrium, and they show the manner in which composition varies with temperature at phase equilibrium.

Consider a liquid whose composition and temperature correspond to point E. If the liquid is heated, the point on the diagram that corresponds to these parameters of the liquid will rise along line EC toward point C. At point C, the liquid mixture boils, establishing a state of phase equilibrium. The vapor in equilibrium with the liquid phase has the composition indicated by point D, but notice that at the temperature indicated by point C there can be only an infinitesimal portion of the material in the vapor phase. As expected, the vapor of composition indicated by point D is enriched in the component with the lower boiling point. If the temperature is raised further, the extent of vaporization will increase; the vapor becoming less enriched in the more volatile component, and the liquid becoming more enriched in the less volatile

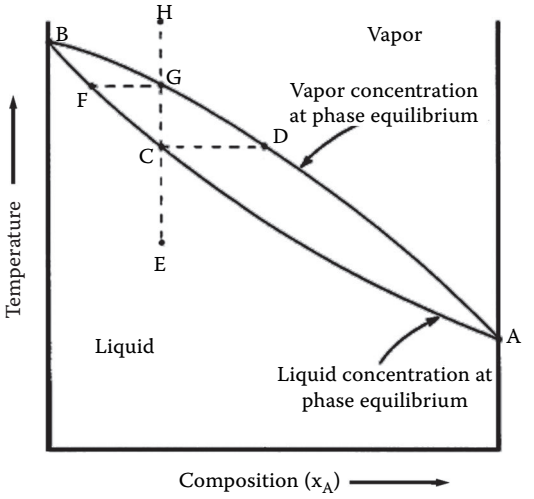


FIGURE 11.1 Isobaric phase diagram for an ideal two-component system.

component. At the temperature corresponding to points F and G, only a small proportion of the total material remains in the liquid phase, and the vapor phase has the composition of the original liquid phase at point E. Raising the temperature further takes the system out of the state of phase equilibrium and into the state of being a single vapor phase, as at point H. The lines CD and FG are referred to as "tie-lines" as they tie together the liquid and vapor compositions at a given temperature.

11.2.2 Nonideal Two-Component Systems

A nonideal system is one whose partial pressure behavior does not follow Raoult's law. The partial pressure of each component approximates to Raoult's law as the mole fraction of that component in the system tends to one, and the partial pressure approximates to Henry's law as the mole fraction tends to zero:

$$p_i = K x_i \tag{11.2}$$

K = Henry's law constant

Deviations from ideal partial pressure behavior may be positive or negative. If deviations from ideal behavior are sufficiently large, the total vapor pressure may exhibit a maximum (for positive deviations) or a minimum (for negative deviations) at some composition. At this maximum or minimum, the liquid and vapor phases will have the same composition at phase equilibrium. The isobaric phase diagram of the nonideal system (Figure 11.2) shows quite marked positive deviations from ideal behavior. In the composition range of the diagram to the left of line CDE, the behavior of the system is analogous to that described earlier for an ideal system.

The enrichment of the vapor phase in the more volatile component cannot proceed beyond point D. At this point, the liquid and vapor phases have the same composition, and this particular composition is called an azeotrope. Azeotropes may be

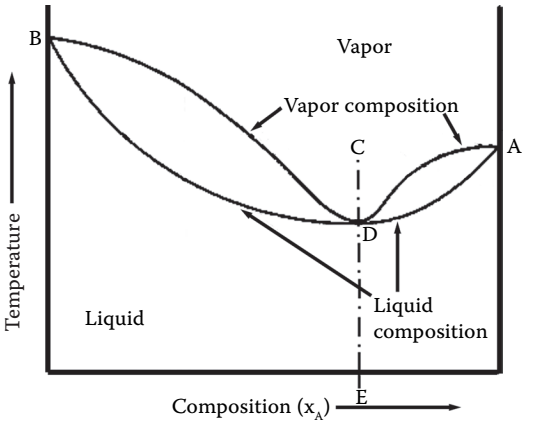


FIGURE 11.2 Isobaric phase diagram for a nonideal two-component system.

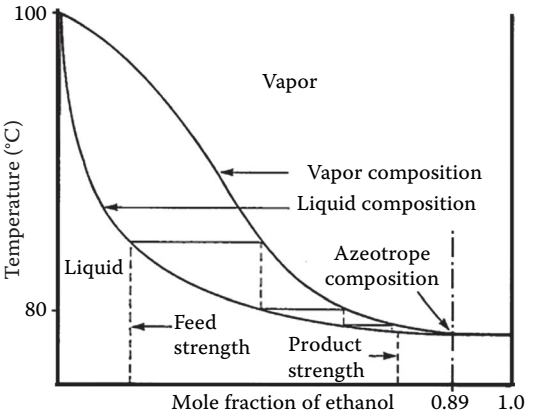


FIGURE 11.3 Isobaric phase diagram for ethanol–water system.

either positive (the boiling point at the azeotrope is lower than either of its constituents), or negative (the azeotrope boiling point is higher than either of its constituents). Fractional distillation of a mixture with a positive azeotrope will produce vapor and distillate phases with the composition of the azeotropic mixture, regardless of the composition of the initial mixture.

The isobaric phase diagram for the ethanol–water system is shown in Figure 11.3. The initial sample to be distilled ("feed strength") corresponds to that of typical wine and the product strength corresponds to that of brandy spirit. Note that the system has deviations from ideal vapor pressure that are only slightly greater than is needed to produce a positive azeotrope (water boils at 100°C; ethanol at 78.4°C; azeotrope mixture [95.6% w/w ethanol; 0.89 mole fraction] boils at 78.2°C).

11.2.3 Fractional Distillation

The type of distillation process that has been considered so far is called equilibrium distillation. In this process, the vapor that is removed from the system is in equilibrium with the total mass of boiling liquid. To completely separate a mixture of two components by equilibrium distillation would be very tedious, as it would require the distillation to be repeated many times. However, this difficulty can be overcome with the use of a fractionating column; the distillation process then being called fractional distillation.

11.2.3.1 The Principles behind Fractional Distillation

Fractional distillation is usually explained in terms of it being continual condensation and re-evaporation of the material, so that there is a gradual change in composition throughout the column. When a vapor is condensed to the corresponding liquid, with no vapor or liquid removed from the system, the condensed liquid must have the same composition as the initial vapor. For example, in an ideal two-component system (Section 11.2.1), when a vapor (temperature and composition at point G) (Figure 11.1) is

condensed (temperature and composition at point C), the process involves a progressive condensation with cooling. Initially, an infinitesimal quantity of liquid of composition F exists in equilibrium with the vapor. As the temperature falls, the proportion of material in the vapor phase decreases, and the variation of the vapor phase composition with temperature is represented by movement along line GD (from G toward D) at the same time the proportion of material in the liquid phase increases, and the variation of the liquid phase composition with temperature is represented by movement along line FC (from F toward C). At the temperature represented by the tie-line CD, all material is in the liquid phase with a composition identical to that of the original vapor. The condensation process that has just been described is exactly the reverse of the vaporization process that was described in Section 11.2.1.

Looking again at the condensation described above, at the temperature that corresponds to the tie-line CD, material has moved entirely into the liquid phase because the composition of the liquid phase at this temperature has become identical to the composition of the system. However, if the composition of the system could be manipulated during the condensation so that it were to move from point G, along line BGDA, toward A (instead of along the line GC toward C) then the system would exist entirely in the vapor phase at the temperature corresponding to tie-line CD, with the vapor having the composition indicated by point D.

This manipulation of the system composition can be achieved by allowing condensation to take place in a vertical column. The liquid phase that is progressively formed, as condensation takes place, drains down the column and away from the site of condensation. Removal of the liquid phase from the site of condensation means that the composition of the system at this site must remain the same as the composition of the vapor. As a result, the vapor becomes progressively enriched in the more volatile component, and conversion to a liquid phase does not occur until the vapor phase contains only the more volatile component, at point A.

Notice the similarity between the process just described (involving removal of liquid phase from the site of condensation as it is formed) to the process of simple distillation described earlier (involving removal of vapor from the site of vaporization as it is formed). To emphasize the similarity, the two processes are summarized below.

- *Vaporization*—vapor is removed from the site of vaporization (in the case of simple distillation this is by condensation of the vapor into a separate receiver). This allows the composition of the system (a liquid in equilibrium with the vapor in contact with it) to remain the same as that of the liquid phase. The liquid will become depleted in the more volatile component but complete vaporization will not occur until the liquid contains only the less volatile component.
- *Condensation*—Liquid is removed from the site of condensation (by allowing it to drain down a column). This allows the composition of the system (a vapor in equilibrium with the liquid in contact with it) to remain the same as that of the vapor phase. The vapor will become depleted in the less volatile component but complete condensation of the vapor phase will not occur until the vapor contains only the more volatile component.

A fractionating column is a device designed to allow establishment of liquid–vapor phase equilibrium over a range of temperatures. It is important to be aware that, at a state of phase equilibrium, material in the system is undergoing condensation and vaporization at all times and the extent of condensation is equal to the extent of vaporization. In a fractionating column, both vaporization and condensation are taking place at sites in the column that are designed to bring about phase equilibrium.

At any particular site in a fractionating column, ascending vapor undergoes some condensation. This produces a liquid phase enriched in the less-volatile component, relative to the original vapor, and leaves the vapor relatively enriched in the more volatile component. Liquid formed by the partial condensation will tend to drain down the column.

At the same site in the fractionating column, descending liquid undergoes some vaporization. This produces a vapor phase enriched in the more volatile component, relative to the original liquid, and will leave the liquid relatively enriched in the less volatile component. Vapor formed by the partial vaporization will tend to rise up the column. Heat is liberated by the partial condensation process, but this heat is absorbed again by the partial vaporization. Overall there is no net gain or loss of heat.

At each site in the column at which phase equilibrium is established, the ascending vapor becomes enriched in the more volatile component while the descending liquid becomes enriched in the less volatile component. If the column has sufficient sites for the establishment of phase equilibrium, the graduation of composition set up can be sufficient to allow the pure more-volatile component to exist at the top of the column.

11.2.3.2 Batch and Continuous Fractional Distillation

Fractional distillation can be achieved by either a batch process or a continuous process (Figure 11.4). Examples of a batch process are typical laboratory fractional distillations and brandy pot-stills.

In the batch process, the liquid mixture to be separated is placed in the pot or boiler (in the case of a brandy pot-still this will be made of copper and heat is usually applied with steam coils). The vapor passes up a vertical fractionation column where refining takes place. Structures within the column such as bubble cap trays and sieve trays are designed to allow vapor to pass up and liquid to flow down the column, while ensuring good contact between the phases to allow their equilibration. Packed columns (e.g., with Raschig rings) can also be used to provide vapor–liquid contact. If an appropriate number of bubble-cap trays are present, the vapor at the top of the fractionating column can be virtually that of the pure more volatile component and can be condensed and collected as product. Eventually, when the entire more volatile component has been removed in this way, the liquid residue in the boiler will contain only the less volatile component. The behavior of a batch process is difficult to assess mathematically because the composition and temperature of the liquid in the boiler, and the liquid and vapor in the fractionating column, is subject to continuous change as the distillation proceeds.

In contrast, a continuous still operates in a state of equilibrium called a steady state. Under steady state the rate at which material is fed into the column is equal to

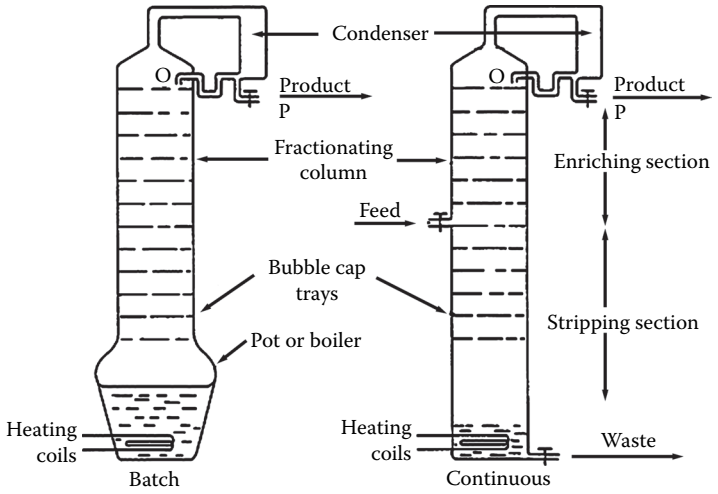


FIGURE 11.4 Batch and continuous distillation columns. Legend: P, product removed from column. O, condensate returned to the column.

the removal rate of the waste and product stream. Also, the heat input to the system is equal to the heat being lost in the waste and product streams. The steady state of a continuous still is particularly amenable to mathematical analysis and automatic control, and because it operates continuously it can handle large quantities of material. The essential components of a continuous fractionating system are shown in Figure 11.4. Notice that the material fed into the column is added at a point some distance up the column.

The least disturbance to the steady-state operating condition of the column and the efficiency of the column is achieved when the feed composition and temperature are identical to the composition and temperature of the liquid phase at the point in the column at which the feed is being added. The heating coils at the base of the column vaporize the liquid at that point in the column and compensate for the removal of heat by condensation of product, withdrawal of the liquid from the bottom of the column, and heat losses.

The fractionating column is divided, in terms of terminology, into two sections. Below the feed inlet is a part of the column called a stripping section; its function is to strip the liquid of its more volatile component. As the feed drains down the column it becomes progressively depleted in the more volatile component, and it is possible for the liquid at the base of the column to be almost entirely made up of the less volatile component. Above the feed inlet is a part of the column called the enriching section; its function is to enrich the vapor phase in the more volatile component. Notice, however, that both processes are identical. The use of different names for the two sections of the column is purely a matter of convenience.

Fractional distillation may be accomplished in a batch or continuous manner. Because the operating compositions and temperatures vary continuously during batch fractional distillation, the process is not particularly amenable to

mathematical analysis or automatic control. In addition, distillation of large quantities of material requires the pot or boiler to be recharged periodically. Continuous distillation operates in a state of equilibrium, called a steady state, in which all inputs to the system (heat and material) are balanced by all outputs from the system.

11.2.4 Reflux Conditions

At the top of the fractionating column, vapor is condensed. Some of the condensate may be removed as product, but some is also returned as liquid to the top of the column (Figure 11.4). Return of some of the condensate to the column is very important to its operation as an increase in the proportion of the condensate being returned results in an increase in the separating ability of the column. The ratio of the liquid that is returned to the column to the liquid that is removed as product is called the reflux ratio:

$$R = \frac{O}{P} \tag{11.3}$$

R = reflux ratio
O = liquid returned to the column
P = liquid removed as product

If there is total reflux ($R = \infty$), no product is removed from the column and all condensate is returned to the column. As the proportion of the condensate that is removed as product increases, the reflux ratio falls and so does the separating ability of the column. The optimum reflux ratio is a balance between the desire for good separating ability (a characteristic that is favored by a high reflux ratio) and good throughput of product (a characteristic that is favored by a low reflux ratio).

If a continuous fractionating column is operating under total reflux ($R = \infty$), no product is being removed. For this to be also a steady-state condition, there must be no feed to the column nor removal of waste from the boiler and no net movement of material up or down the column; in other words, any ascending vapor is balanced by the same quantity of material descending as a liquid phase. If the reflux ratio is less than infinity, some of the vapor is being continually removed as product, and there must be a continual net upward movement of material from the feed point to replace it. Under steady-state conditions, the net upward movement of material must be at a rate that is identical to that at which the product is being removed, and, correspondingly, downward movement of material from the feed point to replace the removal of waste.

The relationship between the reflux ratio and the separating ability of the enriching section of a continuous fractionating still is given by Equation 11.4. For any particular operating condition, R and $x_{A(p)}$ are constant, so Equation 11.4 is a straight line of slope $\frac{R}{R+1}$.

$$y_{A(n+1)} = \frac{R}{(R+1)} x_{A(n)} + \frac{1}{(R+1)} x_{A(p)} \tag{11.4}$$

$y_{A(n+1)}$ = vapor mole faction of component A at theoretical tray n + 1
$x_{A(n)}$ = liquid mole fraction of component A at theoretical tray n
$x_{A(p)}$ = liquid mole fraction of component A in the product

In the stripping section, the relationship between feed and bottoms (waste) liquid flow rates and vapor flow rate and separating ability is given by

$$y_{A(n+1)} = \frac{L}{V} x_{A(n)} - \frac{B}{V} x_{A(w)} \tag{11.5}$$

L = liquid flow rate in the stripping section
V = vapor flow rate in the stripping section
B = bottoms (waste) flow rate
$x_{A(w)}$ = liquid mole fraction of component A in the waste

11.2.5 Theoretical Plates

A theoretical plate is defined as the enrichment or separation associated with one equilibrium stage in a distillation. Thus, the separation arising from a simple equilibrium distillation process corresponds to one theoretical plate, and in a pot still system the vapor immediately above the liquid in the boiler is considered to have an enrichment corresponding to one theoretical plate. Within a fractionating column itself, a theoretical plate corresponds to the enrichment associated with each equilibrium stage in the column.

As the reflux ratio is reduced (throughput increased), more theoretical plates (or equilibrium stages) are needed to achieve a given separation, corresponding to a larger and more costly column. When the liquid and vapor compositions approach the azeotropic composition, the separation associated with each equilibrium stage tends to zero. As a result, the production of good quality SVR (abbreviation for the Latin term spiritus vini rectificatus; rectified spirit of wine), meaning a clean, high-strength spirit, requires many more theoretical plates than the production of brandy spirit, despite the difference in ethanol concentration being relatively small.

11.2.6 McCabe–Thiele Diagrams

The ability of a fractionating column to separate a mixture of components is dependent on both the operating conditions and the phase equilibrium situation within the column. The McCabe–Thiele diagram (Figure 11.5) is a convenient way of expressing both factors diagrammatically and independently. By combining information about the physical properties of the components of the mixture with information based on distillation column operation it is possible to estimate the number of theoretical plates required for the distillation.

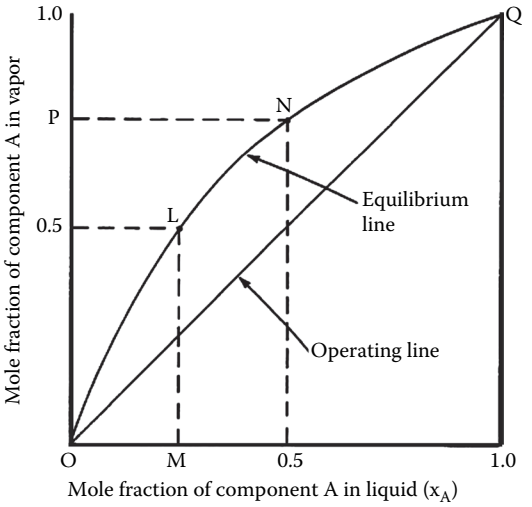


FIGURE 11.5 McCabe–Thiele diagram for a distillation column operating with total reflux.

McCabe–Thiele diagrams are graphs of the mole fraction of a component in the liquid phase (as the x axis) against the mole fraction of the same component in the vapor phase (as the y axis), with the x and y axes having equal length. The phase equilibrium situation for the component (i.e., the mole fraction of the component in the liquid phase against the mole fraction of the component in the vapor phase above the liquid and in phase equilibrium with the liquid) is expressed as a line called the equilibrium line (OLNQ in Figure 11.5). The operating line is the straight line that depicts the steady-state operating condition of the system (i.e., the mole fraction of the component in the liquid phase against the mole fraction of the component in the vapor phase below the liquid).

If an ideal continuous fractional distillation column operates under total reflux (no product removal; $R = \infty$) and steady-state conditions, then Equation 11.4 simplifies to Equation 11.6, which is the operating line on the McCabe–Thiele diagram (Figure 11.5). That is to say that the liquid descending from any tray has the same composition as the vapor ascending to the tray from the tray below.

$$y_{A(n+1)} = x_{A(n)} \tag{11.6}$$

y_A = mole fraction of component A in the vapor
x_A = mole fraction of component A in the liquid

When the column is operating at less than total reflux, the ascending vapor at any point in the enriching column must be richer in the more volatile component than the descending liquid to allow for the removal of product at the top of the column and removal of waste at the bottom of the column (Figure 11.6).

The enriching section operating line is given by Equation 11.4, knowing the reflux ratio, and the product mole fraction, while the stripping section operating

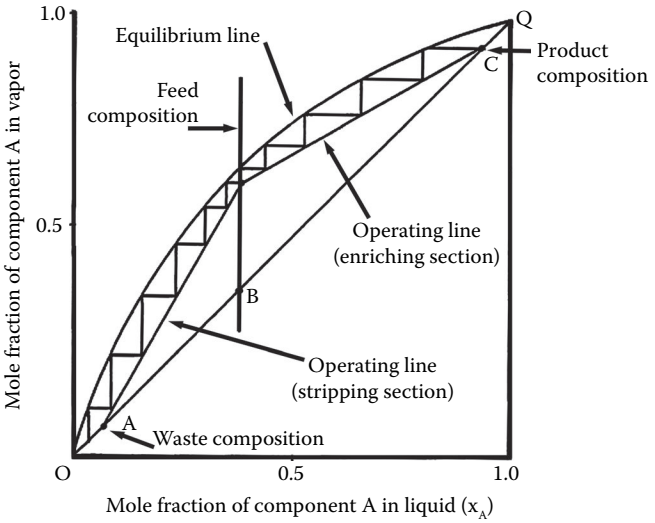


FIGURE 11.6 McCabe–Thiele diagram for a distillation column operating at less than total reflux, and the feed entering the column as a saturated liquid. A, Waste stream composition; B, feed composition; C, product composition.

line is given by Equation 11.5, knowing the liquid, vapor and bottoms flow rate, and the waste mole fraction. The point at which these two lines intersect indicates the state of the feed entering the column. To simplify this discussion, the example assumes that the feed is a saturated liquid (Doherty et al. 2008). The number of theoretical trays is determined by stepping down the region defined by the equilibrium line and the enriching and stripping operating lines, starting at the product mole fraction.

For steady-state operation, removal of product must also be accompanied by removal of waste from the boiler and input of feed to the column. Since removal of product implies also a reflux ratio less than infinity, the operating line in the enriching section must have a slope less than one and that the operating line in the stripping section must have a slope greater than one.

The McCabe–Thiele diagram for the water and ethanol systems is as depicted in Figure 11.7. The feed composition and product composition correspond to those typical of a wine and a brandy spirit, respectively. The equilibrium line meets line OQ at point D. This point corresponds to the composition of the azeotrope, that is, a point at which the vapor phase in equilibrium with a liquid phase has the same composition as the liquid phase. The advantage of the McCabe–Thiele diagrams, with respect to continuous distillation, is that it can account more easily for changes in the operating conditions by allowing adjustment of the operating line. For example, Figure 11.7 shows the case where the reflux ratio is equal to 2. At a reflux ratio of infinity (no product removed), the operating line would become line OQ.

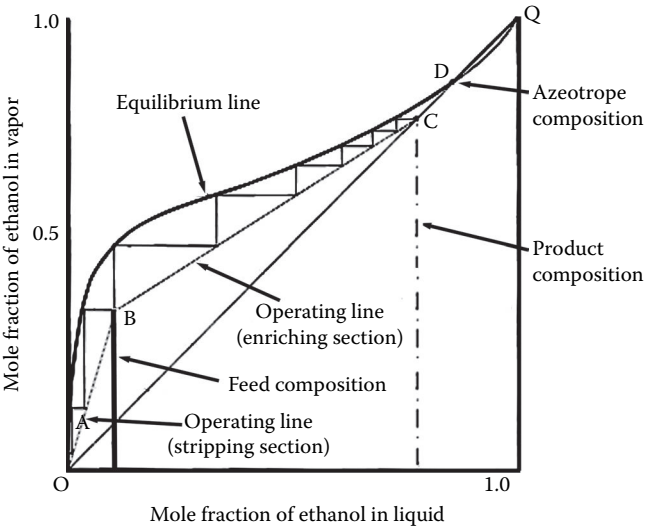


FIGURE 11.7 McCabe–Thiele diagram for water and ethanol (reflux ratio = 2).

11.3 DISTILLATION TECHNIQUE

There are many variations in distillation technique, and in this section two extremes of distillation technique are covered; on the one hand, the process of cognac distillation, and on the other, the complex and intricate process of multi-column continuous still distillation. While the two approaches described represent extremes, the principles underlying both are the same. The behavior of an ethanol–water system and the volatility of minor components play their part in both systems but are put to work in different ways.

Both approaches to distillation have their advantages and disadvantages, and so each is suited to the production of a particular type of product. The poorer separating ability of a pot still is appropriate to the distillation of a brandy with complex flavor, but it requires the wine that is to be distilled to be of corresponding good quality. On the other hand, it will not produce a uniform product from varying feed materials, is less economical of energy, labor, and time than a continuous still, and it cannot produce high strength spirit. In contrast, a continuous still is particularly suited to the removal of minor components that contribute flavor, and can produce high strength neutral spirit, but it cannot provide the depth of flavor required for the best brandies.

11.3.1 Pot Still for Cognac Production

The area covered by the Appellation Contrôlée "Cognac" is north of the Gironde River, adjoining Bordeaux, and is part of the basin of the Charente River (Cognac 2009). The river gives its name to the style of still which is often called the Charente Still (Figure 11.8).

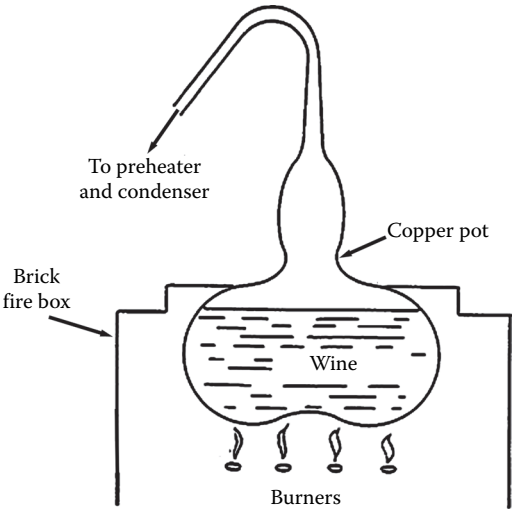


FIGURE 11.8 Drawing of a pot still ("Charente Still") for Cognac production.

Distillation of wine in the area is believed to have begun in the fourteenth century, and was well established by the end of the seventeenth century. The wine used for Cognac production is mostly produced from Ugni Blanc (also known as Trebbiano), though other varieties (e.g., Colombard, Folle Blanche, Montils, Sémillon, and Folignan) can be used. Grapes are picked early for high acidity that inhibits bacterial growth or spoilage, and produce a wine of about 7.5% (by volume; all ethanol concentrations are by volume unless indicated otherwise) ethanol that is distilled as soon as possible after fermentation to minimize both oxidative and microorganism spoilage. Distillation as soon as possible after fermentation, and the low pH, allows relatively low sulfur dioxide use to control microbial spoilage (Iland et al. 2007).

The distillation is carried out in two stages. The first, produces a low wine that contains about 30% ethanol; the second a brandy that is limited by law to a maximum strength of 72.4% ethanol. Although the wine for the first distillation is pre-heated, the low wine is never pre-heated. Over a long time, the pot still design evolved to a shape that would consistently provide good flavor and aroma. Continuous distillation has been tried, but it provided a brandy that lacked the complexity and finesse of the pot still product.

The pot still is made from copper, and has a very characteristic "onion" shape with a concave base. The capacity can be up to 140,000 L (maximum 120,000 L of liquid per distillation) for the first distillation, but the second distillation is always performed in one of 3000 L (maximum 2500 L of liquid per distillation) (Cognac 2009). This requirement has a sound basis because as the size increases the ratio of surface area to volume decreases, changing distillation characteristics, and hence cognac flavor. The appellation laws stipulate that the heating must be by direct fire, which was traditionally fuelled by charcoal, though more recently other fuels such as gas have been used.

The head of the still is important in controlling the degree of reflux, and its volume is 10–13% of the charge capacity. The vapor is led from the still through a pre-heater (where it warms a charge of wine that is the next to be distilled) and a condenser. Freshly distilled Cognac is harsh and is matured in oak from the Forest of Limousin, 130 km to the east. By law, the maturation in wood must be for at least two years; most good brandies have three years, and VSOP (Very Special Old Pale) brandies have five or more.

11.3.2 Continuous Distillation

Production of brandy or spirit with a modern multicolumn continuous still, with sophisticated control equipment, wide use of heat exchangers, and a capacity for high-throughput rates is a remarkable contrast to the simple pot still (Cortella and DaPorta 2003). The following describes a fairly complex multicolumn continuous distillation process (Anderson 1978). There are two important reasons for the complexity of the system:

- It provides the flexibility needed to handle a wide range of starting materials (e.g., wine, lees, fermented marc, heads fractions).
- It allows different columns to be operated under differing conditions.

Although the overall system appears complex, the differing conditions can be broken down into four distinct steps that may be used to produce clean neutral spirit:

- *Analysis column or marc still*—preparation of a low wine from the starting material.
- *Purifying column*—removal of some volatile minor components from the low wine at low ethanol concentration.
- *Rectifying column*—further enrichment of the ethanol to higher ethanol concentration.
- *Pasteurizing (methanol) column*—removal of other volatile minor components from the spirit at high ethanol concentration.

Volatile minor components refer to volatile species other than ethanol and water.

11.3.2.1 Low Wine Preparation

This step enriches the ethanol concentration to that of a low wine (~40–50% ethanol) and separates it from any solids in the starting material, such as grape solids, lees, and skins. Solids in the feed material can cause extensive frothing. This is undesirable because the rising vapor carries trapped liquid with it.

If the starting material is wine or lees, an analyzing column is used. This column has a small number of trays above the feed point, and low wine can be obtained easily with very little reflux giving a high throughput. There are more trays below the feed point to ensure that the waste passing from the column is thoroughly depleted of ethanol.

Some separation from very volatile heads components, such as acetaldehyde and sulfur dioxide can be achieved by collecting the vapor one or two trays from the top. The vapor passes into a condenser, and some of the liquid is returned to the column as reflux while some is directed to low wine storage or the next column in the process. If a clean wine is used as the starting material, a spirit of up to the legally allowable maximum (in Australia) for brandy of 83% ethanol (Anon 2007) can be obtained directly from the column by control of the reflux ratio.

A marc still is used to produce low wine from fermented marc. The marc is passed through the still, for instance by the action of revolving beaters working as an "Archimedean screw" (Da Porto 1998). The ethanol and other volatile components are distilled out by live steam, rather than closed heat. The product is very impure and requires fairly elaborate working if neutral spirit is to be produced from it.

11.3.2.2 Purifying Column

At low ethanol concentrations many components exhibit volatilities that are very much greater than that of ethanol (discussed in Section 11.4.5). Such components are much easier to be separated from ethanol at low ethanol concentrations than high ethanol concentration, allowing them to be separated in a fractionating column provided the ethanol concentration is not allowed to rise while the separation is taking place.

Low wine enters the purifying column at the middle tray and is diluted and carried down the column by hot water that enters the column at the top. "Live" steam is fed in at the base of the column, further diluting the ethanol but driving many of the volatile minor components into the vapor phase. Vapor at the top of the column is condensed, some being returned to the top of the column to maintain reflux, the remainder being run off to the feints receiver. The diluted feed material is removed at the base of the column, and passes to the column that enriches it to the strength of the final spirit. The purifying column is designed to purify the ethanol of other minor components, as its name implies, not to enrich the ethanol concentration.

11.3.2.3 Rectifying Column

After dilution in the purifying column, a rectifying column is used to raise the ethanol concentration to that of the final spirit. To achieve this with a practically useful reflux ratio requires a large number of theoretical plates. As the aim of this column is to separate ethanol from water as efficiently as possible, "live" steam is avoided and steam enclosed in heating coils ("closed" steam) or an external reboiler is used.

The feed tray is well down the column (tray 32 in the 48 tray column). This is to allow a large number of trays in the enriching section to further increase the ethanol concentration at high concentrations at which its volatility is almost one. It is also to allow a number of trays to be present above the collection point (typically four or five trays) to allow the small quantities of remaining heads components to concentrate above the collection point. A portion of the vapors condensed at the collection point are returned to the column to maintain a high reflux ratio (typically $R > 4$) to achieve the required separation. Heads components condensed at the top of the column are removed and returned to the purifying column.

11.3.2.4 Pasteurizing (Methanol) Column

The final purification stage occurs in a pasteurizing (or "methanol") column. This column is not designed to increase the ethanol concentration but rather it separates the heads components. The column is particularly designed to separate methanol, which is a very toxic alcohol. The feed enters at the top of the pasteurizing column and exits at the takeoff point at the bottom of the column. As it passes down the column it is gently heated to vaporize the remaining heads components. The heads components vapor is taken off at the top of the column and run to a feints receiver.

Over most of the composition range of an ethanol–water system, methanol exhibits a volatility that is similar to that of ethanol (Figure 11.9). For this reason it is a component that is particularly difficult to separate. The volatility of methanol is higher than that of ethanol at high ethanol concentrations, as is expected from the smaller size of the methanol molecule and the correspondingly lower boiling point. But at low ethanol concentrations, the rising volatility of methanol is overtaken by that of ethanol because the attractive forces between water and methanol are greater than those between water and ethanol; an effect that is a result of the smaller hydrocarbon component in methanol.

Methanol will always tend to concentrate in heads fractions as its volatility is always greater than one (Figure 11.9). However, there should be a high ethanol concentration for the greatest degree of methanol enrichment in the vapor phase relative to ethanol enrichment in the vapor phase. A high ethanol concentration occurs in the pasteurizing column, and also at the top of the enriching section of the rectifying column and separation of methanol will also be occurring there. The value of the pasteurizing column

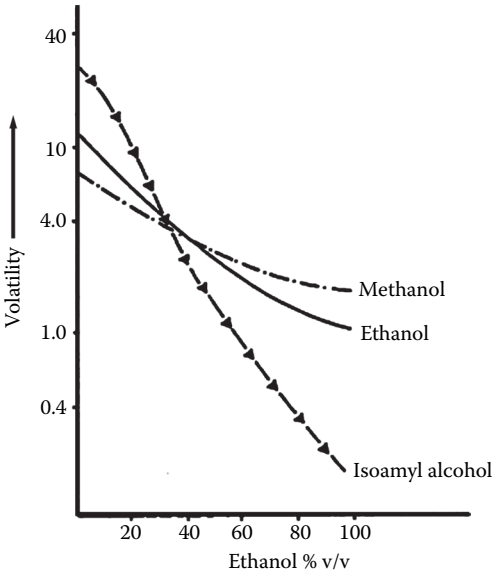


FIGURE 11.9 The volatility of ethanol, methanol, and isoamyl alcohol at different ethanol concentrations. (Adapted from Williams, G. C. 1962. *American Journal of Enology and Viticulture* 13:169–180.)

is that it gives a further opportunity for this separation to occur on a product that has been freed of those heads components that separate in the rectifying column.

11.3.2.5 The Overall Process

The heart of the process is the rectifying column with its stripping and enriching sections. This is the column that does the job of separating water from ethanol, a job that becomes particularly difficult at high ethanol concentrations. Separation of volatile minor components also occurs, and in a simple continuous still this may be the only column and hence the only way of separating minor components. In the system described above, the separation of these minor components is facilitated by two additional columns that are designed to separate ethanol from more volatile components: the pasteurizing (or methanol) column separates components that are more volatile than ethanol at high ethanol concentrations, and the purifying column separates components that are more volatile than ethanol at low ethanol concentrations. An analyzing column is used to provide a low wine, free of any solid material, for the purifying column, and a marc still will be used for this operation if fermenting marc is being utilized.

11.4 MINOR COMPONENTS IN THE SPIRIT

So far, attention has been focused on ethanol and water. However, the difference between good quality spirit and poor quality spirit is not the ethanol concentration but the spectrum of other, less abundant, compounds.

Although the concentration of these additional components is small, they are responsible for "heady" or "taily" character in spirit and for the distinctive flavor of brandy spirit. Their behavior during distillation is both intriguing and remarkable (Faúndez and Valderrama 2004, Osorio et al. 2005), and reveals differences in the characteristics of a pot still and a still with a fractionating column that are not evident with a simple ethanol–water system.

Raoult's law applies to an ideal system, but in our real world, nonideality results in an azeotrope in the ethanol–water system. This nonideality makes the behavior of volatile minor components dependent on the design of the still and the way in which it is operated. First of all, however, the structure and origin of some of these minor components will be considered.

11.4.1 Origin of Volatile Minor Components

There are four main potential sources of these compounds: (i) the grape berries; (ii) the yeast during alcoholic fermentation; (iii) heat-induced chemical changes within the still; and (iv) maturation, particularly oak cask storage. Although all of these sources can be important, the dominant components contributing to aroma and flavor in spirit are minor products of alcoholic fermentation. These components are in the material that is to be distilled before it reaches the still, and the quality of the material for distillation affects the quality of the end product.

Although distillation may recover a reasonable spirit from a poor quality wine, or from lees or marc, the production of good quality spirit is facilitated by undesirable characters of spirit being absent or minimal in the material to be distilled.

11.4.2 Quality of Feed Stock

Production of a clean neutral spirit requires efficient separation of other volatile components from the spirit. This can be achieved with a fractionating column, but it requires a spirit of high strength to be collected, requiring the use of a distillation column with a large number of trays in the enriching section and careful control of the reflux ratio. The limiting ethanol concentration of the ethanol–water azeotrope is 95.5% w/w and typically such neutral spirits are about 95% in alcohol.

In contrast, volatile minor components are essential to brandy spirit. Some can be retained in the spirit by collecting a lower spirit strength from a fractionating column. Alternatively, a simple pot still may be used with the desired strength of 60–80% ethanol being obtained by distilling twice. The production of a good brandy requires the volatile minor components to be harmoniously balanced. Whether this can be achieved depends very much on both the material to be distilled, the still, and its operation.

11.4.3 Significant Minor Flavor Components

Volatile minor components in spirit or brandy are responsible for flavor and aroma (Silva et al. 2000). Important components include:

- *Acetaldehyde*—A normal component of yeast metabolism, and one that is trapped by sulfur dioxide to give a bisulfite addition compound that can regenerate acetaldehyde during distillation. Air contact during or after fermentation can generate acetaldehyde in a wine.
- *Acetaldehyde diethyl acetal*—A product of the reaction of acetaldehyde with ethanol, and a component that is significant at high ethanol concentrations. It can mask the aroma of acetaldehyde in spirit, and the formation of analogous diethyl acetals of higher aldehydes and some ketones in spirit can similarly mask their contribution to flavor.
- *Ethyl acetate*—This is produced by ethanol in wine esterifying acetic acid, and acetic acid can be particularly abundant after bacterial contamination. Some bacterial action can produce ethyl acetate directly.
- *Higher alcohols*—The most abundant minor components in many distilled products; their production by yeast may be stimulated by a number of causes.
- *Higher fatty acid ethyl esters*—Components of yeast cell walls.
- *Higher aldehydes*—Products of the oxidation of grape seed oil fatty acids that were released into the marc during pressing.

11.4.4 Behavior of Minor Flavor Components

The volatility of a minor component can be defined as

$$\text{Volatility} = \frac{\text{Molal concentration in the vapor phase}}{\text{Molal concentration in the liquid phase}} \tag{11.7}$$

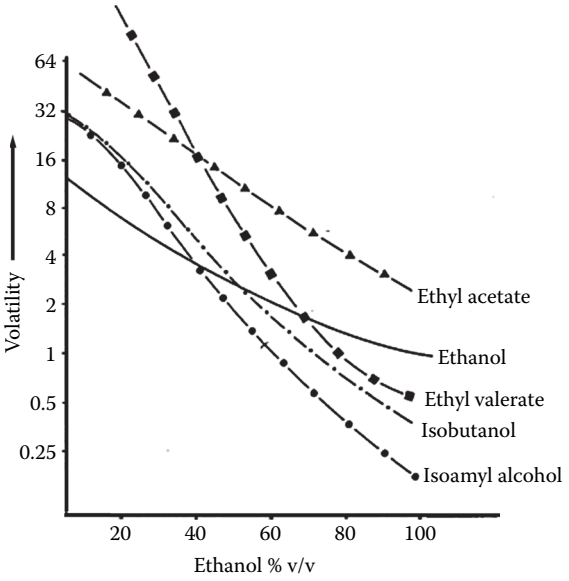


FIGURE 11.10 The volatility of ethanol, ethyl valerate, ethyl acetate, isobutanol, and isoamyl alcohol at different ethanol concentrations. (Adapted from Williams, G. C. 1962. *American Journal of Enology and Viticulture* 13:169–180.)

The volatility of minor components represents the enrichment or depletion of the component in the vapor phase by comparison with the liquid phase. Figure 11.10 shows the variation in volatility of two higher alcohols and two esters when they are present as minor components in an ethanol–water system. The esters and higher alcohols are organic compounds with a large hydrocarbon component to their molecules. As a result, they are poorly solvated by water and much better solvated by ethanol. As these minor components become increasingly surrounded by water molecules rather than ethanol molecules (i.e., as the alcoholic strength of the ethanol–water system decreases) the attractive forces to these surrounding molecules decrease and the ease with which the compound vaporizes increases. Consequently, all of the components exhibit the effects of nonideal behavior as an increase in volatility with a decrease in alcoholic strength. The greater the hydrocarbon portion of the molecule, the greater is the increase in volatility for a given decrease in alcoholic strength.

11.4.5 Minor Components in Fractionating Columns

In fractionating columns the volatile minor components are considered in two groups:

- *Heads*—compounds usually found above ethanol in a fractionating column
- *Tails*—compounds that are usually found below ethanol in a fractionating column

In a fractionating column, which is under steady-state conditions and total reflux ($R = \infty$), a compound will tend to concentrate at an ethanol concentration at which the volatility is equal to one. For example, this would be approximately 60% ethanol for isoamyl alcohol, while isobutanol will be found at around 70% ethanol (Figure 11.10). When the fractionating column is not under total reflux ($R < \infty$), the maximum concentration of a minor component occurs at an ethanol concentration within the column at which the volatility of the component is equal to the internal reflux ratio (Equation 11.8).

$$\text{Internal reflux ratio} = \frac{\text{Mass of liquid descending per unit time}}{\text{Mass of vapor ascending per unit time}} \tag{11.8}$$

When the fractionating column is operating at less than total reflux ($R < \infty$), higher alcohols and fatty acid esters appear in the tails fractions. The actual distribution found for these compounds in a fractionating column having 14 trays in the enriching section is shown in Figures 11.11 and 11.12 (Guymon 1964, 1974, Guymon and Crowell 1969).

The maximum concentration of the amyl alcohols occurs at about 70% ethanol, and that of isobutanol at about 80% ethanol (Figure 11.11). It is evident that the column is being run with an internal reflux ratio of about 0.7. The C_8, C_{10}, and C_{12} fatty acid ethyl esters, which as pure components have boiling points of 208°C, 244°C, and 269°C, respectively, show such a remarkably high volatility in an ethanol–water system because of their long hydrocarbon chains. This means that they collect at a slightly lower ethanol concentration than the higher alcohols (Figure 11.12). An

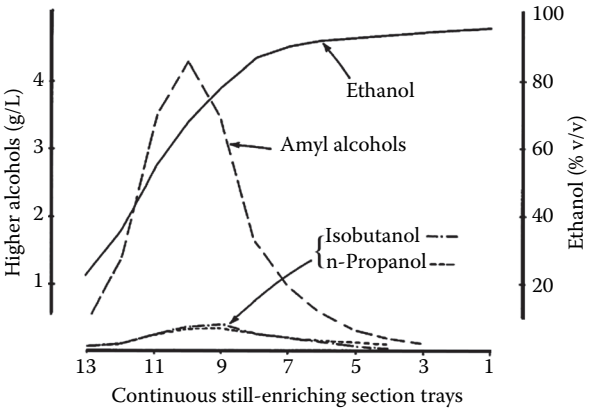


FIGURE 11.11 The concentration of ethanol and higher alcohols (amyl alcohols, isobutanol, n-propanol) within a continuous still-enriching section trays. Trays are numbered from the top of the column; feed to tray 15. (Adapted from Guymon, J. F. 1964. *American Journal of Enology and Viticulture* 11:105–112; Reprinted with permission from Guymon, J. F. Chemical aspects of distilling wines into brandy. In *Chemistry of winemaking*, edited by A. D. Webb. Washington, USA: Copyright 1974, American Chemical Society.)

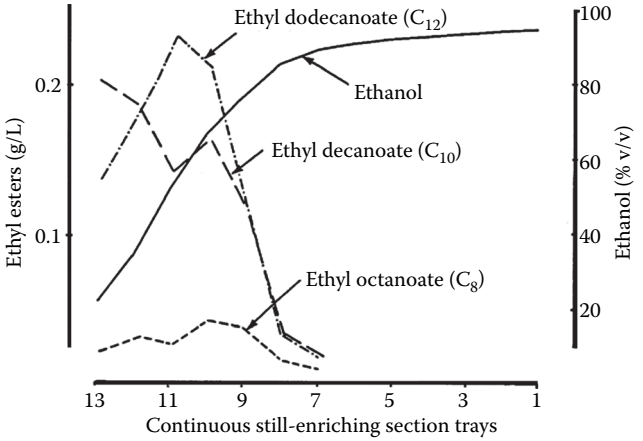


FIGURE 11.12 The concentration of ethanol and fatty acid esters (ethyl dodecanoate, ethyl decanoate, ethyl octanoate) within a continuous still-enriching section trays. Trays are numbered from the top of the column; feed to tray 15. (Adapted from Guymon, J. F. and E. A. Crowell. 1969. *American Journal of Enology and Viticulture* 20:76–85; Reprinted with permission from Guymon, J. F. Chemical aspects of distilling wines into brandy. In *Chemistry of Winemaking*, edited by A. D. Webb. Washington, USA: Copyright 1974, American Chemical Society.)

important aspect is that a large number of theoretical plates are necessary, not so much for increasing the ethanol concentration of the product, but to adequately separate the higher alcohols and fatty acid esters that would provide "taily" character of the spirit. Only at very high ethanol concentration is the volatility of these minor components sufficiently low for a good separation to be obtainable.

It is important to recognize the conflict that attainment of high-quality neutral spirit makes with the demands of rapid throughput and low-energy costs. A reduction of the reflux ratio will provide a faster throughput of material. However, this not only reduces the separation obtained with each theoretical plate, thereby lowering the ethanol concentration at the collection point and increasing the higher alcohol and fatty acid content. It also reduces the internal reflux ratio, driving the maximum concentration of these minor components to higher ethanol concentrations in the column.

11.4.6 Minor Components in Pot Stills

In a pot still, the concentration of volatile minor components in the product reflects their volatility at low ethanol concentrations rather than high ethanol concentrations. The distillate that is first collected is particularly rich in compounds that are more volatile than ethanol, and this is called the heads fraction.

Brandy is often produced using a pot still with two successive distillations of wine, the first of which gives the low wine (26–50% ethanol), while the second gives the brandy (up to 83% ethanol) (Anon 2007). The difference in volatility between

water and ethanol is large at low ethanol concentrations, so despite the lack of a fractionating column, two distillations can provide a useful enrichment.

The volatility of minor components varies with the ethanol concentration (Figure 11.10), and for example, at 30% ethanol both isobutanol and isoamyl alcohol are slightly more volatile than ethanol, and ethyl valerate is much more volatile than ethanol. For the fatty acid esters, the large hydrocarbon component in the molecules would be expected to increase their volatility even more markedly at low ethanol concentrations than for ethyl valerate. Nonideality has made all of these components more volatile than ethanol. In the vapor that is initially formed from the low wine, ethanol is enriched by comparison with its concentration in the liquid. But the higher alcohols are more enriched and the long-chain fatty acid esters are even more so.

An example of this behavior can be seen in Figures 11.13 and 11.14 (Guymon 1974). They show the higher ethanol and fatty acid ester concentrations in successive fractions during the production of 71% ethanol brandy from a 29% ethanol low wine in a 1600 L copper pot still (conditions similar to those used to produce cognac or malt whisky). Figures 11.13 and 11.14 show the concentration of the various components at the same position (the receiver) but at different times, and the early fractions are to the right of the figure and the late fractions are to the left of the figure.

With the pot still, fatty acid esters are collected largely in the heads fraction, with lesser amounts in the first few brandy fractions. The molal concentration of the fatty acid esters in the vapor is so much higher than in the liquid that they are very rapidly distilled over and only appear in the first few fractions. The volatility of the higher alcohols and ethanol is lower. Although the molal concentration of these components in the vapor is higher than in the liquid, it is not so great as to rapidly drive them out of the liquid, and they distill over a greater number of fractions than is the case for

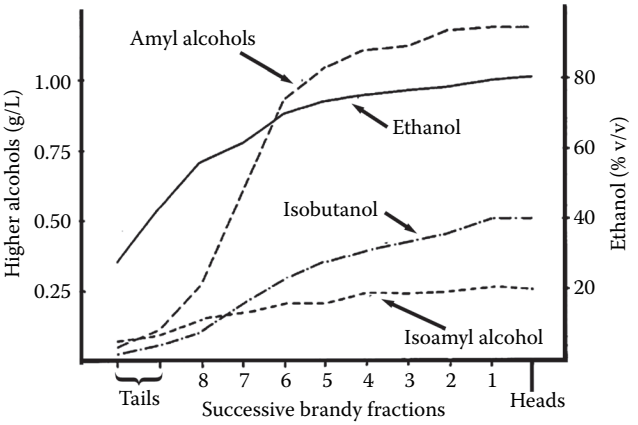


FIGURE 11.13 The concentration of ethanol and higher alcohols (isoamyl alcohol, isobutanol, amyl alcohols) within successive fractions produced by a pot still. (Reprinted with permission from Guymon, J. F. Chemical aspects of distilling wines into brandy. In *Chemistry of winemaking*, edited by A. D. Webb. Washington, USA: Copyright 1974, American Chemical Society.)

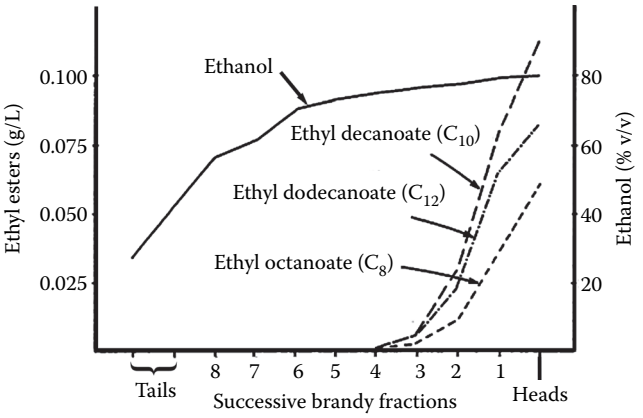


FIGURE 11.14 The concentration of ethanol and fatty acid esters (ethyl decanoate, ethyl dodecanoate, ethyl octanoate) within successive fractions produced by a pot still. (Reprinted with permission from Guymon, J. F. Chemical aspects of distilling wines into brandy. In *Chemistry of winemaking*, edited by A. D. Webb. Washington, USA: Copyright 1974, American Chemical Society.)

the fatty acid esters. At the ethanol concentration found in the low wine, the volatility of isoamyl alcohol is similar to or slightly greater than ethanol, so the two compounds are found together in most fractions with isoamyl alcohol becoming depleted in the liquid in the pot slightly before ethanol.

11.5 ASSESSMENT OF VOLATILE AROMA COMPOUNDS IN SPIRIT

In the assessment of highly concentrated ethanol from continuous stills (~96% ethanol) for the purpose of fortification, consideration of the acetal content of the spirit is important. Acetals are formed by the reaction of aldehyde or ketone compounds in a reversible manner with ethanol. Of the aldehyde and ketones present in wine and spirits, it is usually acetaldehyde that is at the highest concentration, although numerous other types are present (i.e., higher aldehydes) and can significantly impact the aroma profile of wine and/or spirit products (Williams and Strauss 1978).

Figure 11.15 provides an example of the two overall equilibrium steps involved in the acetal formation between acetaldehyde and ethanol, and shows the hemi-acetal intermediate. The equilibrium distribution between the aldehyde, hemi-acetal and acetal will depend on the relative concentrations of water and ethanol, with higher ethanol concentrations favoring the formation of the acetal and low concentrations favoring the aldehyde. Consequently, much acetaldehyde in spirit will be present as its diethyl acetal, particularly at the high ethanol concentrations of high strength SVR from continuous stills, and especially when the spirit has been isolated from heads fractions by redistillation.

If the spirit is used to produce a fortified wine, or is incorporated into a brandy of lower alcoholic strength, the decrease in ethanol concentration of the spirit is accompanied by regeneration of acetaldehyde. Since acetals have a less objectionable

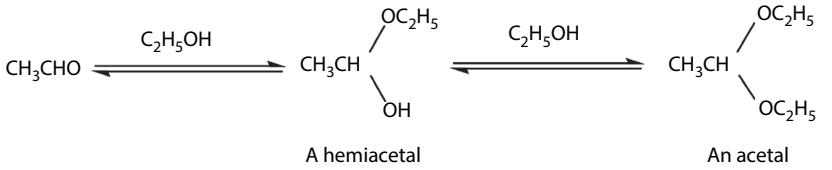


FIGURE 11.15 Equilibrium between acetaldehyde with its hemiacetal and acetal forms.

aroma than the aldehydes they are derived from, an undesirable aroma may arise in the product. This may produce an aroma that was not suspected from appraisal of the spirit itself. The formation of acetals has important organoleptic consequences because the higher aldehydes generally have more obnoxious odors and lower thresholds of detection than acetaldehyde. Acetal formation at the high alcoholic strength of the spirit can lead to a masking of the aroma of these aldehydes and some ketones.

The organoleptic qualities of spirits should be assessed after dilution with water, to the alcoholic strength of the final product. Hydrolysis of acetals to aldehydes or ketones requires acid as a catalyst. Since it is only the aroma that is usually assessed, tartaric or citric acid at a concentration of 1% w/v can be dissolved in the water. Storage in stoppered bottles for two days will ensure that acetal hydrolysis takes place to form the corresponding aldehyde or ketone.

REFERENCES

Anderson, G. L. G. 1978. A review of distillation technology employed in the Australian grape spirit industry. *Technical Symposium on Australian Grape Spirit and Brandy Production, Urrbrae*, Australia, June.

Anon. 2007. Standard 4.5.1 Wine production requirements. Edited by Australian New Zealand Food Authority: Anstat Pty Ltd, South Melbourne.

Bujake, J. E. 2008. Beverage spirits, distilled. In *Food and Feed Technology*, edited by Arza Seidel, 141–173. Hoboken: Wiley.

Cognac, Bureau National Interprofessionel du. 2009. L'encyclopédie du Cognac. Accessed 31/10/2013. http://www.pediacognac.com/.

Cortella, C. and C. Da Porta. 2003. Design of a continuous distillation plant for the production of spirits orginating from fermentated grape. *Journal of Food Engineering* 58:379–385.

Da Porto, C. 1998. Grappa and grape-spirit production. *Critical Reviews in Biotechnology* 18:13–24.

Doherty, M. F., Z. T. Fidkowski, M. F. Malone, and R. Taylor. 2008. Chapter 13. Distillation. In *Perry's Chemical Engineers' Handbook*, edited by R. H. Perry and D. W. Green. New York: McGraw-Hill.

Faúndez, C. A. and J. O. Valderrama. 2004. Phase equilibrium modeling in binary mixtures found in wine and must distillation. *Journal of Food Engineering* 65:577–583.

Guymon, J. F. 1964. The composition of plate samples from distilling columns with particular reference to the distribution of higher alcohols. *American Journal of Enology and Viticulture* 11:105–112.

Guymon, J. F. 1974. Chemical aspects of distilling wines into brandy. In *Chemistry of Winemaking*, edited by A. D. Webb. Washington, USA: American Chemical Society.

Guymon, J. F. and E. A. Crowell. 1969. Gas chromatographic determination of ethyl esters of fatty acids in brandy or wine distillates. *American Journal of Enology and Viticulture* 20:76–85.

Iland, P., P. Grbin, M. Grinbergs, L. Schmidtke, and A. Soden. 2007. *Microbiological Analysis of Grapes and Wine: Techniques and Concepts*. Campbelltown: Patrick Iland Wine Promotions Pty. Ltd.

Osorio, D., J. R. Perez-Correa, L. T. Biegler, and E. Agosin. 2005. Wine distillates: Practical operating recipe formulation for stills. *Journal of Agricultural and Food Chemistry* 53:6326–6331.

Silva, M. L., A. C. Macedo, and F. X. Malcata. 2000. Steam distilled spirits from fermented grape pomace. *Food Science and Technology International* 6:285–300.

Williams, G. C. 1962. Vapor-liquid equilibria of organic homologues in ethanol-water solutions. *American Journal of Enology and Viticulture* 13:169–180.

Williams, P. J. and C. R. Strauss. 1978. Spirit recovered from heap-fermented grape marc: Nature, origin and removal of the off-odour. *Journal of the Science of Food and Agriculture* 29(6):527–533.

12 Food Products Evaporation

Jorge F. Vélez-Ruiz

CONTENTS

12.1 Heat Transfer Fundamentals 370
12.1.1 Heating and Cooling in Food Processing 371
12.1.2 Basic Geometries of Heat Exhangers 371
12.1.3 Overall Heat Transfer Coefficient 372
12.1.4 Performance of a Typical Evaporator 375
12.1.5 Evaporator Types 376
12.1.6 Liquid Food Characteristics 378
12.2 Three Concentrated Food Products 379
12.2.1 Orange Juice 379
12.2.2 Tomato Concentrate 380
12.2.3 Evaporated and Condensed Milks 381
12.3 Evaporation Principles 382
12.3.1 Engineering and Design 382
12.3.1.1 Mass and Energy Balances 383
12.3.1.2 Heat Transfer Coefficients 383
12.3.2 Elements of an Evaporation System 386
12.3.3 One Simple Effect 388
12.3.4 Multiple Effect Operation 389
12.3.5 Engineering Calculation 390
12.3.5.1 Mass Balance on Food Processing 392
12.3.5.2 Boiling Point Rise of Liquid Foods 393
12.3.5.3 Energy Balances on Food Processing 394
12.3.5.4 Evaluation of Heat Transfer Area 396
12.3.6 Practical Solving Criteria 397
12.4 Food Particularities in Evaporation 398
12.4.1 Thermal Sensibility of Foods 398
12.4.2 Physical Properties of Foods 399
12.4.2.1 Flow Properties 399
12.4.2.2 Thermal Properties 399
12.4.2.3 Density 399
12.4.3 Additional Process Limitations 408
12.4.4 Experimental Equipment Utilized in Evaporation Research 408
12.4.5 Computer Simulation 409

12.5 Examples of Application 410
12.6 Final Comments..... 421
References..... 422

12.1 HEAT TRANSFER FUNDAMENTALS

Many liquid foods are concentrated to decrease water content, implying some considerations, such as a significant reduction of volume and weight, enhancement of shelf life, inducing of consistency and flavor changes, and diminishing energy consumption for drying as the next food process operation. The concentration of liquid foods by evaporation is usually utilized for liquid foods such as milk, fruit juices, vegetable purees, soups, and syrups, whereas other concentration processes are applied to a limited extent. Products such as cheese whey, fermentation wastes, molasses residues, and sea water, among others, can also be concentrated by evaporation (APV, 2003).

Food evaporation is the unit operation in which a liquid food is heated by means of high-quality steam, reaching the boiling point of the food system or solution; then the generated vapor, in equilibrium with the liquid food, is separated from the rest of the solution, favored for the vacuum effect; consequently, the rest of the liquid food increases its solids content and a preservative effect is obtained due to water activity lowering.

Thus, the main purpose of the concentration process by evaporation may be one of the following:

1. To reduce the weight and volume from liquid foods having high water content
2. To reduce the need and cost of materials and space during the packaging, storage, and distribution of fresh liquid foods
3. To increase the stability of the fruit juices, milk, soaps, syrups, and vegetable purees by reduction of their water activity
4. To increase the consistency or viscosity of the liquid foods, due to the solids increasing
5. To improve consumer acceptability and convenience
6. To facilitate and economize the dehydration of foods such as coffee, juices, milk, purees, and sugar cane that are nowadays subjected to spray or rotator drying

Evaporation of food items has been extensively utilized and researched, but there is little information on all the engineering aspects of this important food processing operation. Most of the liquid food evaporation is carried out in tubular heat exchangers: single effects are employed for small-scale operations, the scraped surface is used when the food material is very viscous or heat sensitive, and multiple effect evaporators are the commonly used process equipment in which the concentration of milk, fruit juices, and purees is supported. And recently, the design and utilization of plate heat exchangers for evaporation of liquid foods has increased. Thus, an overall approach to this food processing operation is presented in this chapter.

12.1.1 Heating and Cooling in Food Processing

Heat transfer as a part of the engineering science is commonly involved in food processing operations implying heat exchange rates between the food products and the source of heat during the heating or vice versa when a cooling process is present. Pasteurization, canning, cooking, frying, evaporation, dehydration, and distillation are food processes in which heating is involved, whereas refrigeration, freezing, and freeze-drying or lyophilization are examples of treatments in which cooling is involved.

Heating and cooling processes are mainly based on conduction and convection mechanisms that are simultaneously developed throughout the whole transformation, and the radiant energy or radiation is rarely or scarcely present. For that reason, the conductive and convective coefficients of the foods and heating medium need to be known in order to quantify the amount of heat given to or removed from the food products. Both phenomena may be respectively evaluated with the first Fourier's equation and the Newton's relationship (Kern, 1997; Welty et al., 1976, Vélez-Ruiz, 2012).

$$\text{Conduction} \quad dQ = -kA\frac{dT}{dx} \tag{12.1}$$

$$\text{Convection} \quad dQ = -hAdT \tag{12.2}$$

where dQ is the heat flow (W), k is the thermal conductivity (W/m°C), A is the heat transfer area (m^2), dT/dx is the temperature gradient (°C/m) composed of the dT or ΔT as the temperature difference or driving force (°C or K) and dx is the distance or separation between high and low temperatures of the solid body (m), and h is the convective coefficient, also known as the film or superficial heat transfer coefficient (W/m^2°C).

In contrast to thermal conductivity on which there is a complete source of data due to its material nature, data on the convective coefficient are scarce and properly it may be computed from a set of phenomenological correlations.

12.1.2 Basic Geometries of Heat Exhangers

The food industrial equipment or heat exchangers (HE) utilized for the specific processing operations are normally based on two geometries: tubes or hollow cylinders and plates, constituting the tube heat exchangers or plate heat exchangers. The former has been designed and used since many years ago, the plate exchanger a new version of this type of equipment. A couple of figures to illustrate the corresponding diagrams are presented in Figures 12.1 and 12.2.

Whatever be the arrangement, the system has three common situations: (i) there are two fluids: a liquid food and a fluid heating medium (steam or hot water), implying their respective convective coefficients; (ii) there is a solid transfer medium or metal that favors the heat transfer; and (iii) both fluids have their respective pipes for the inlet and the outlet of the stream. Heat transfer convection is part of the fluids and conduction is happening through the metal plate or tube, both mechanisms are being



FIGURE 12.1 External picture (courtesy of GEA Wiegand GmbH) and internal appearance of a shell and tube heat exchanger.

developed at the same time; so for the heat flow one should consider this simultaneous heat transfer with their resistances.

In accordance with technical improvements and historical evolution, the most commonly used equipments for food processing evaporation are the shell and tube geometry (STHE) and the plate geometry (PHE) is being incorporated as an innovative variant.

12.1.3 Overall Heat Transfer Coefficient

As a consequence of the characteristics and particularities developed during the heat exchange between liquid foods as fluid process and steam, hot water or cooling

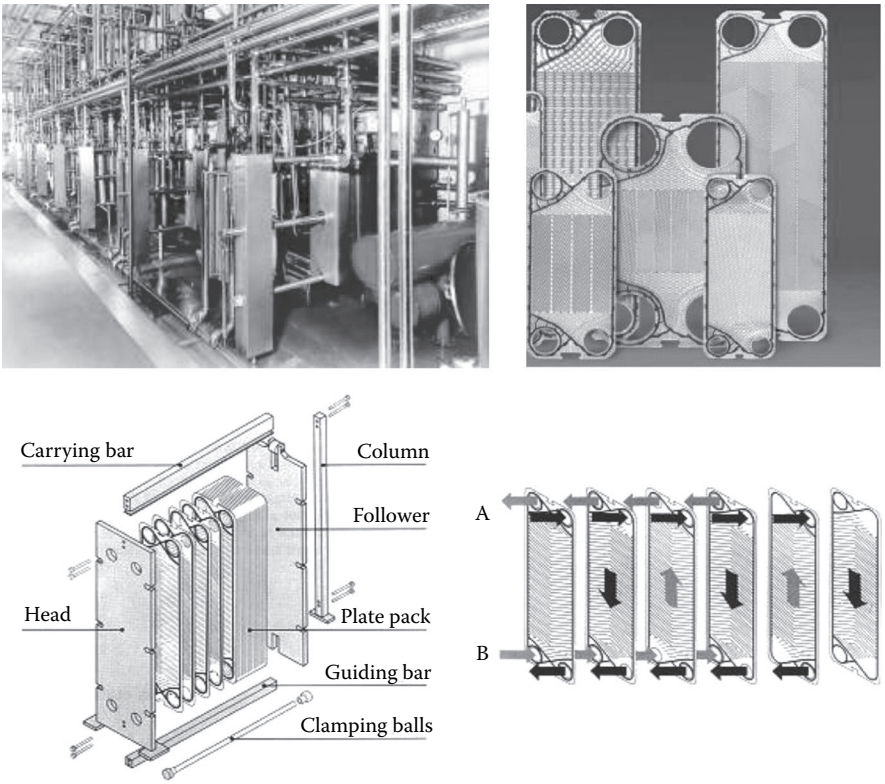


FIGURE 12.2 Picture and outline of a set of individual plates and plate heat exchangers.

fluid as the heating or cooling medium in which a tube or a plate is involved in the indirect heat transfer. Therefore, the heat transfer calculations are based on the overall heat transfer coefficient, on one side, and on the other, due to the flow distribution in the equipment, the average temperature as the driving force should be considered.

$$Q = UA\Delta T_{ML} \tag{12.3}$$

where Q is the total heat flow (W), U is the overall heat transfer coefficient (W/m^2°C), A is the heat transfer surface represented by all the tubes or plates forming the equipment (m^2), and ΔT_{ML} is the average temperature difference (°C or K).

The overall heat transfer coefficient expresses the overall capacity of the system to transfer thermal energy; thus in the equipment or process design a higher value is preferable. It is the inverse of the resistances ($U = 1/\Sigma R$). This coefficient is strongly influenced by the h values; they are related to the momentum transfer phenomenon; in general terms the turbulent flow is preferred and favored in heat exchangers of any design type.

In relation to the aforementioned parameters, some additional details are included below (McCabe et al., 2008) for U and ΔT_{ML}. The difference between the outside and inside coefficients depends on the heat transfer area or surface taken as the basis of the calculation in the case of STHE, whereas for PHE: $U_o = U_i$. Therefore, three different U may be presented:

The overall heat transfer coefficient based on the outside surface (U_o):

$$U_o = \frac{1}{\frac{1}{h_i}\left(\frac{D_o}{D_i}\right) + \frac{\Delta x}{k}\left(\frac{D_o}{D_L}\right) + \frac{1}{h_o}} \tag{12.4a}$$

The overall heat transfer coefficient based on the inside surface (U_i):

$$U_i = \frac{1}{\frac{1}{h_o}\left(\frac{D_i}{D_o}\right) + \frac{\Delta x}{k}\left(\frac{D_i}{D_L}\right) + \frac{1}{h_i}} \tag{12.4b}$$

The overall heat transfer coefficient for the plate (U):

$$U = \frac{1}{\frac{1}{h_i} + \frac{\Delta x}{k} + \frac{1}{h_o}} \tag{12.4c}$$

where h_i is the inside or internal convective coefficient (for the corresponding fluid), D_o is the outside diameter, D_i is the inside diameter, Δx is the metal thickness of the tube or plate, k is the thermal conductivity of the wall, D_L is the logarithmic mean diameter, and h_o is the outside or external convective coefficient (for the other fluid).

Additionally to the convective and conductive resistances, the heat transfer surfaces do not remain clean. Liquid foods and the heating or cooling fluids to a lower degree are continuously forming scales that generate another resistance that should be considered as fouling factors.

For the evaluation of the logarithmic mean temperature difference (ΔT_{ML}), it is necessary to know the temperatures of both fluids at the entrance and at the exit of the equipment. In this parameter the temperature difference at the inlet or outlet places is a function of the type of flow arrangement; that is to say, if the fluids are flowing in the same (parallel) or counter directions. In most of the heat transfer equipment the counter flow is preferred due to higher magnitudes of ΔT_{ML} that produce higher heat flows.

$$\Delta T_{ML} = \frac{\Delta T_1 - \Delta T_2}{ln\left(\Delta T_1 \big/ \Delta T_2\right)} \tag{12.5}$$

where ΔT_{ML} is the average driving force (logarithmic mean) of the heat transfer process, ΔT_1 is the temperature difference at the inlet of the equipment, and ΔT_2 is the temperature difference at the outlet of the heat exchanger.

12.1.4 Performance of a Typical Evaporator

The evaporators are, in essence, heat exchangers with other equipment units that help to complete the main objective: eliminate water from a solution or liquid food. By using steam in the evaporation process, a turbulent film is generated on the heat transfer surface and it becomes the most efficient means for the evaporation phenomena, including conduction and convection heat transfer.

During the process, the phase change takes place in the vicinity of the surface while the vapor generated forms a core within the walls, thus the liquid food or solution, also identified as liquor, is forced to form a thin film in which the large volume in a confined space causes high velocity. Based on the film concept as the fundamental phenomenon of evaporation, a majority of the equipment units have been designed and manufactured. Hall and Hedrick (1971) established that the Reynolds number should exceed a magnitude of 2000, for a good heat transfer in a falling film.

The performance and design of industrial equipment (Figure 12.3) is based on mass and heat balances and transport phenomena that have been well understood, although aspects such as the modeling and evaluation of the heat transfer convective coefficient have been recently studied and researched. Physical properties of foods, such as boiling point elevation, viscosity increase, rheological property changes, and



FIGURE 12.3 Industrial image of a multiple effect evaporator. (Courtesy of GEA Wiegand GmbH.)

thermal property evolution through the whole process, are not completely known, and therefore they are aspects being investigated.

12.1.5 Evaporator Types

With the idea of a brief description, some of the evaporator types and performance characteristics are introduced here. An equipment for the evaporation process includes characteristically three zones: the heating exchange surface zone, the boiling zone and the separator part to avoid product losses and the possibility of contamination of the generated vapor. The existing evaporator types may be grouped into four main categories: batch equipment, tubes arrangements, plate evaporators, and noncommon configurations (Kessler, 1981; Hartel, 1992, Singh and Heldman, 2001; APV, 2003; McCabe et al., 2008; Vélez-Ruiz 2007); they are described next.

Batch-type pan evaporator is one of the simplest and oldest designed equipment for the food industry in which the quality of the concentrated food product is low, due to very long residence times as a consequence of a small heating surface. This type of equipment is still used to concentrate small quantities of liquid foods to produce food concentrates or intermediate products in which a small amount of water has been eliminated. Tube evaporators with natural and forced flows are of three types:

1. Short tubes of horizontal and vertical arrangements (Figure 12.4, Kern, 1997; McCabe et al., 2008). Short tubes are placed in the heating zone, at horizontal or vertical positions; they were widely used in the food industry for many years. These equipment units have been the replacement of the pan type evaporator and lately were substituted by long tube units.
2. Long tubes are the most popular type of industrial evaporator. Long tubes of diameter 1–2 in. for upward flow, and 2–10 in. for downward flow, with 3–15 m length, are used to create the so-called rising and falling film evaporators. These designs are the most popular and commercial equipment for the food industry. Milk industry has utilized these units for many years, to concentrate the fluid to elaborate concentrated and evaporated milks, sweetened condensed milk, and powder milk.
3. Agitated thin-film evaporator for viscous fluids in which the heat transfer is enhanced by a sweeping device or a mechanical agitator. It has a very low processing capacity and it has been used in the tomato industry.

Plate evaporators operate in a similar way to heat exchangers. Liquor flow is a combination of rising and falling films. This is the newest and most expensive equipment, but offers several advantages: good heat transfer rates, low residence times, and flexibility of operation. Even though it is a very innovative design, its utilization for the food industry is scarcely common.

Other configurations: Some evaporators may be constructed with different characteristics to the three aforementioned groups. For instance, a thin film, spinning cone evaporator has been commercialized by FT Industrial (2004) as a single effect with hollow conical discs with certain advantages such as short contact time, low thermal impact, compact installation, and processing flexibility.

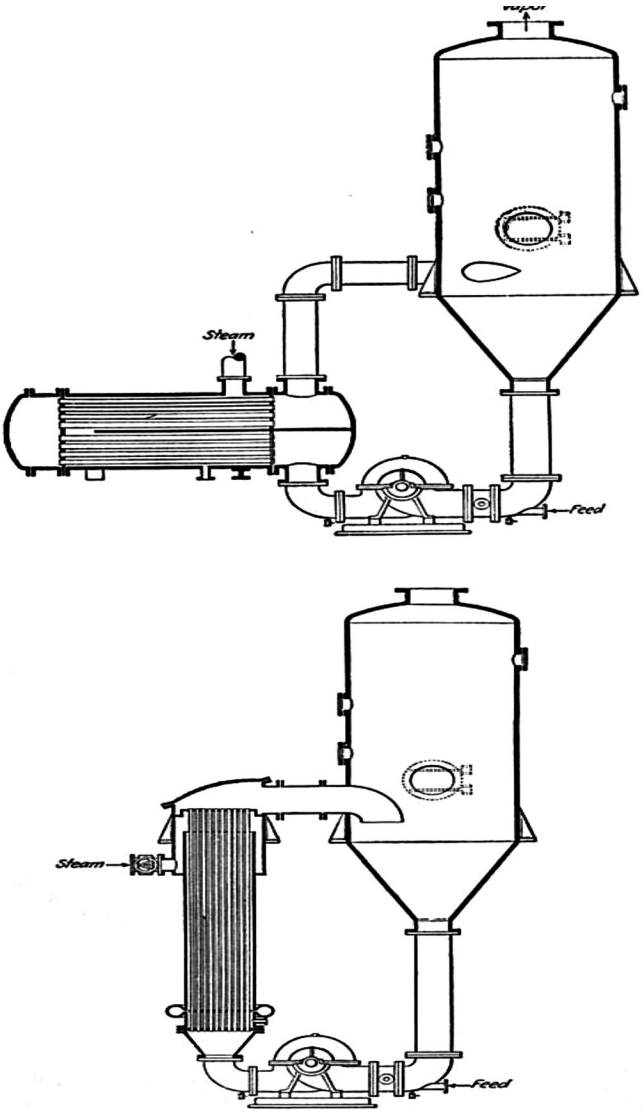


FIGURE 12.4 Outline images of single-effect evaporator (horizontal and vertical tubes).

In the concentration of liquid food products, the equipment is generally arranged to save energy during the evaporation process, whose multistage arrangement leads to a decrease of the steam consumption. Multiple effect equipment may be operated in several configurations: in forward flow, where the fresh stream enters the first evaporator where the steam is supplied, and in reverse flow, also the steam is supplied to the first effect where the concentrated food or product leaves out of the evaporation unit. In parallel flow, the feed is split among all the evaporation units; a combination of these three ways of feed flow may be used. Forward and backward arrangements

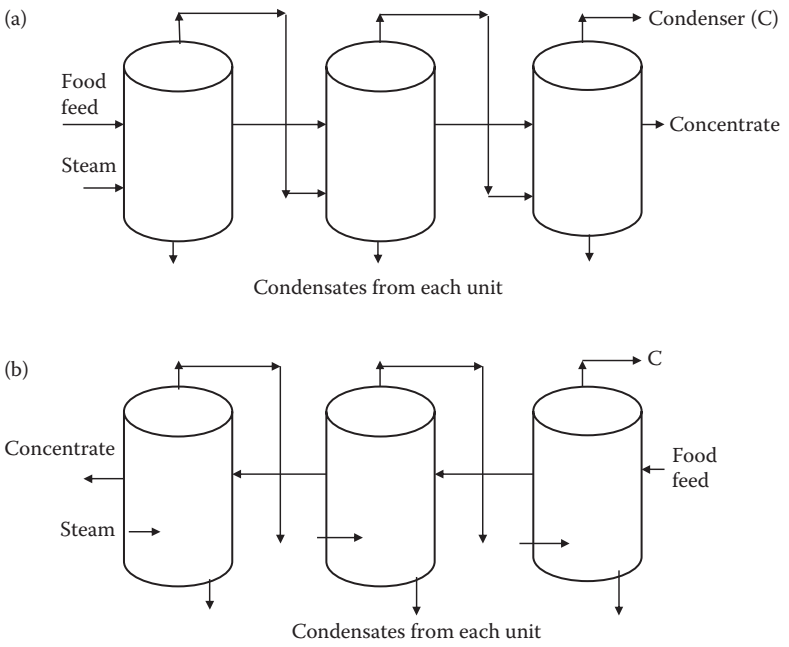


FIGURE 12.5 Outlines of forward and backward evaporator arrangements. (a) Forward feed arrangement and (b) backward feed arrangement.

are outlined below for a triple-effect evaporator (Figure 12.5). Most liquid food concentration is carried out in the forward flow arrangement, and parallel flow has been used in the cane sugar industry, whereas the reverse flow can be applied for not too sensitive liquid foods (Schwartzberg, 1977; Smith, 2008).

In the forward feed, the boiling point decreases from effect to effect implying an important vacuum demand; this arrangement is used for liquid foods with high thermal sensibility. In contrast, backward feed is used with liquid foods showing high viscosity; thus the highest solid concentrate is handled in the effect with the supplied steam. Parallel flow combines limitations, advantages, and disadvantages of the two types of feeding; this arrangement has been used for almost saturated solutions.

12.1.6 Liquid Food Characteristics

The performance and design of evaporation units is importantly affected by the nature and properties of the liquid food to be concentrated. The most important properties of the food item that should be considered are the following:

1. Thermal sensibility of foods, some liquid foods may suffer protein denaturation or vitamins damage like milk, whereas fruit juices may lose part of its nutritional value or flavor due to vitamins or color damage, and aroma volatilization. Vacuum to decrease the boiling point and short processing times are needed in order to avoid these inconveniences.

2. The boiling point, as a colligative property, and density, as a mass to volume relation, increasing are also a consequence of the solids concentration, the boiling point elevation causes more steam consumption, and density augment causes more pump work.
3. Flow properties alter due to the concentration phenomenon; the viscosity of Newtonians fluids increase as the solid content of the concentrate increases, for example, syrups, sugar solutions, and milk, up to certain solids level. Other food items modify its rheological nature from Newtonian to non-Newtonian behavior; thus liquids such as milk, nonclarified juices, and fruit and vegetable purees may develop structural modifications, causing lower heat transfer coefficients, higher energy needs, and particular pump requirements.
4. Fouling of the heat transfer surface may be the result of thermal damage, viscosity and density increasing, or components deposition, which implies a reduction in the overall heat transfer coefficient and a major need for cleaning.
5. Foaming of some food components present in the liquid foods that incorporates air and causes a lower heat flow due to a decrease in the corresponding convective coefficient. Some noncondensable gases may produce the same effect as air incorporation due to a decrease in the convection efficiency.
6. Other liquid food properties, such as the specific heat and thermal conductivity, may be altered.

As a result of this variation in the liquid food properties, many evaporator designs have been developed by the manufacturers, and the selection of the evaporator type depends on the characteristics of the specific food.

12.2 THREE CONCENTRATED FOOD PRODUCTS

Food concentrating is used to eliminate water of liquid item at such levels in which the liquid condition of the food is retained. The evaporation of water in milk and vegetable industries is favored by vacuum application in the equipment.

The utilization of subatmospheric pressures in evaporators performing and the low water activity achieved in food concentrates may imply some risks of microorganisms growing; therefore sanitation is of prime importance. Cleaning in place by circulation of chemical fluids, such as hot detergents, sanitizers, and water, complete with mechanical cleaning when needed, is widely applied in food evaporation industries.

12.2.1 Orange Juice

Orange is widely cultivated around the world. In 2003, the estimated world production of orange, grapefruit, pomelos, lemons, and limes was 60.04×10^6 tons in which Greece contributed with 1.200, China 1.647, Mexico 3.969, and USA 10.473×10^6 tons (Hui, 2006). Concentrated orange juice as a source of nutrients, minerals, and flavor is manufactured by evaporation units under vacuum in pans, circulating evaporators of one or multiple effects, as one alternative to orange juices prepared by freezing. Although the level of concentration for orange juice is normally 62°Bx, this fruit concentrate may be reach up to 65°Bx or 75% total solids concentration (Borgstrom,

1969), or with the aim of increasing savings the juice may be concentrated up to 72°Bx (Crandal et al., 1987); and depending on the final utilization, the concentrate may be combined with fresh juice for human consumption, added with sugar for soft-drinks, added with sodium citrate to prevent jellying, or completed with other ingredients.

A simple description of the orange juice preparation includes the following stages: washing, sorting, spray-rinsing, and conveying of the oranges to the extraction unit, in which the fruits are squeezed to obtain the juice and residual pulp, thus producing a high-quality orange juice with low content of peel oil. In the finishing stage, the extracted juice is separated from the pulp to be pumped to the evaporators. The evaporation unit normally employs a flash concentration at temperatures above 87°C that requires a few minutes to concentrate the juice from 12% to 65% solids. The *concentrated juice* is then cooled down to 15°C or less. In order to recover volatile components the concentrate is blended with fresh or extracted juice to reach a desired level of solids. Some evaporated juices are mixed with recovered essences coming from a distillation unit, but it is more unstable and the volatile gases are lost on storage (Woodroof and Luh, 1986; Hui, 2006).

12.2.2 Tomato Concentrate

Enormous quantities of tomato are consumed as puree, paste, ketchup, and sauce that are concentrated products. Several important aspects, such as tomato variety and pectin retention, will contribute to the final characteristics of the products, particularly to their consistency. In the manufacturing process, great care of the tomatoes should be completed in harvesting, transporting, and storing, because they are not peeled. Some basic ideas of the process of each tomato concentrate in their different presentations are commented next.

Tomato puree follows the following food processing operations: washing and stemming, sorting, some of the vegetables may be trimmed, and all are converted into pulp in the pulping stage. Heating, pumping, and concentration are the next steps for the pulp.

Open kettles and vacuum pans, double and triple effects, are commonly used for the concentration, producing products of less quality if the first equipment is employed, whereas with the reduction of the boiling point (≤71°C) in the second, it will contribute to a better color and flavor of the puree. The *level of concentration* is from 5% to 18% in the first, from 18% to 25% in the second effect, and from 25% to 28–30% in the final evaporator, depending on the definite specific gravity, 1.040–1.045. To prevent foaming and sticking of the pulp on the surface, water is sprayed on the hot zones, or sometimes cottonseed oil may be added on it. Finally, the concentrated pulp flows through the finisher of 0.7–0.8 mm diameter, before the canning and thermal treatment (Luh and Woodroof, 1988; Smith et al., 1997).

Tomato paste is obtained by a similar manufacturing process, in which the concentration operation is longer to reach higher solids content. A concentrated tomato paste must contain around 33% of total solids; the standards of identity require 25% of solids at least.

Tomato ketchup and sauce, in addition to the aforementioned unit operations, in which the most important is the concentration process by evaporation, include a

stage of spicing after the concentration. Garlic and onion powders, salt, spice oils, sugar, and vinegar are some of the more common; they are incorporated as a blend. Ketchup may contain 32–35% of solids, 1.145–1.165 of specific gravity, whereas sauce with similar solids content is characterized by a higher intensity of the added spices, depending on its final presentation such as chili, hot, pizza or spaghetti sauce, among others (Luh and Woodroof, 1988; Smith et al., 1997).

12.2.3 Evaporated and Condensed Milks

Although milk has the appearance of a simple liquid, its structure is very complex, knowledge of it is necessary to better understand those changes through processing and the properties of intermediate and finished dairy products. Chemically, milk is integrated by several hundreds of constituents, some of which have special significance, even though they are present in low concentrations. The components of milk include proteins, lipids, carbohydrates, minerals, pigments, vitamins, enzymes, and miscellaneous compounds.

From the physical–chemical point of view, milk is a complex solution of salts, lactose, and other hydrophilic minor components where whey proteins, casein corpuscular micelles, and fat globules are dispersed. The physical state of the dispersed phase represents two separate colloidal forms: a suspension and an emulsion; this double colloidal system provides milk with more divergent product structures than most other food ingredients. Proteins and lipids are the most important milk components because their physicochemical modifications affect the structure and overall behavior of dairy products (Vélez-Ruiz, 1996; Marcelín and Vélez-Ruiz, 2013). Fresh milk has limited stability; therefore it may be processed to preserve the milk components and to augment its shelf life, and one of the most commonly used techniques is to decrease water content by evaporation and drying in order to lower water activity.

The application of evaporation to fresh milk, in which falling films in multiple evaporators are usually utilized varying from one to seven (Verdurmen and de Jong, 2003), produces concentrated milk with three different products as the more important, namely, evaporated milk, condensed milk, and sweetened condensed milk. Concentration of milk as a preservation method is competitively merchandized in different parts of the world; it may be distributed even in remote zones as one of its main advantages. The milk products most commonly found on the market shelves are the evaporated and sweetened condensed presentations.

The manufacturing process for the concentration of raw milk normally includes the following food processing operations: reception of fresh milk, verification and authentication of milk quality (solid content, microorganism count, and detection of foreign constituents, among others) and cooling, standardization and mass formation to get the needed composition and volume, heating, and homogenization to achieve fracture of milk fat, air elimination, and pasteurization or preheating previous to the concentration process. If three effects necessary with vacuum are involved in the concentration, the *level of concentration* is from 12–15% to 18–21% of solids in the first evaporator, from 18% to 30–33% in the second effect, and from 30% to 42–45% in the final stage; in all the equipments they work with vacuum, contributing to avoid damages to the milk components due to a decrease in the boiling point. In

accordance with Verdurmen and de Jong (2003), the boiling temperatures vary from 70–80°C in the first unit and from 40–50% in the last unit. Contrary to juices concentration, the loss of volatiles in milk evaporation is considered a beneficial aspect.

The concentration process involves water removal by boiling, reducing the interparticle spaces with respect to the fresh milk. As a consequence of high temperatures during the evaporation process, physicochemical changes occur within individual milk components, particularly in whey proteins and casein. The specific structural modifications for the two commercial types of concentrated milk, evaporated and sweetened condensed, have an important influence on their properties and particularly on flow behavior. Thermal treatment causes most of the changes in the structure of milk concentrates. These changes involve fusion of the protein micelles, and sometimes of fat globules and protein bodies, forming entirely new structures. The specific structural modifications for these two types of concentrated milk, evaporated and sweetened condensed, have much relevance to their final characteristics.

Evaporated milk contains all the original milk solids in a reduced water volume. The homogenization and heat processes required for the manufacture of this dairy product to ensure good storage properties strongly affect the colloidal state of proteins and fat components.

Sweetened condensed milk is essentially a suspension of lactose crystals and colloidal proteins in a saturated solution of lactose and sucrose. This kind of dairy product is unlikely to show a simple Newtonian behavior. The most important physical phenomenon in sweetened condensed milk studied by researchers is the age-thickening process. Both consistency and thickening determine the level of consumer acceptability, and are strongly influenced by the elaboration process. The viscosity of this dairy product must be high enough to prevent sedimentation and fat rise but low enough to enable the product to be poured easily from the container. When age-thickening is developed, a slow irreversible change occurs in the size or shape of the casein micelles, but the role of whey proteins in this physical change is not clearly known (Vélez-Ruiz, 1996; Marcelín and Vélez-Ruiz, 2013).

12.3 EVAPORATION PRINCIPLES

Most evaporators for liquid foods operate under vacuum conditions with a boiling temperature in the range of 45–75°C as a function of the reached vacuum at the corresponding evaporator stage. This decreasing in the boiling point of food items minimizes the thermal degradation of food components. Although the vapor generated in each unit is superheated, when it enters the next evaporator, the condensation inside the heat transfer zone happens at that temperature corresponding to the pressure of the unit where it was generated. If negative pressure is not incorporated, the boiling temperature would be high (>100°C, at atmospheric pressure) that is obviously not recommended.

12.3.1 Engineering and Design

In each stage of the evaporator, the concentrating food stays for a time that is governed by the desired concentration, the maintained vacuum and the heat transfer characteristics. The boiling liquid flows up or down along the tube or plate

depending on the specific arrangement and evaporator type. On the outside, the steam condenses on the external surface of the tubes or plates, delivering the heat for water evaporation. The temperature difference between steam and boiling liquid is smaller at the top of the tube or plate than at the bottom due to the pressure losses along the tube.

Mass and energy balances as the basis of the evaporation process are well understood, but the heat transfer and pressure drop in evaporator tubes and plates are complex phenomena (Bouman et al., 1993). Transport phenomena related to momentum and heat transfer through the evaporation process are very complicated as a consequence of the continuous change in water content, solids increasing, apparent viscosity augment, boiling temperature increasing, and flow nature of the concentrated liquid food.

12.3.1.1 Mass and Energy Balances

A reduction of the energy needs for concentration of liquid foods may be reached by adding more evaporative effects (n), the requirements of heat transfer area increases as a function of the number of effects, and consequently the cost of the evaporation equipment increases. According to Smith (2008), from a relation of total costs versus the number of effects in evaporation systems, three stages represent the optimum number in which minor costs are implied.

As a first, quick and ideal approximation for calculation of energy requirements in evaporation equipment of n effects; to evaporate a unit of water mass at each effect it requires a steam consumption of 1/n (kg/h) may be considered. A better estimation is provided by an overall energy balance as will be commented later. In feed forward units, the amount of evaporated water tends to increase successively due to the flashing effect induced by the superheated steam, as a consequence of the pass of one effect with higher boiling temperature to the next evaporator within a lower boiling point. For a reverse flow unit the opposite situation occurs, the amount of evaporated water decreases from effect to effect, because additional steam condensation must be completed to heat up the liquid food to successively higher boiling points.

12.3.1.2 Heat Transfer Coefficients

Both heat transfer coefficients, convective and overall, markedly vary through the evaporation process as a function of several factors, such as liquid food product, concentration, evaporator type, boiling temperature, and temperature difference between boiling and steam temperatures. Ibarz and Barbosa-Cánovas (2003) and McCabe et al. (2008) mention some values for the overall heat transfer coefficient, a range of 1000–5000 W/m^{2}K has been cited for long-tube vertical evaporators, a range of 800–3000 W/m^{2}K for short-tube evaporators, and a range of 600–2000 W/m^{2}K for agitated-film evaporators as a function of the solution viscosity. Kessler (1981) also reported overall coefficients for skim milk of magnitude 1000–2600 W/m^{2}K, whereas for whole milk, the coefficients are 900–2600 W/m^{2}K, corresponding to the higher values of 2000–2600 for the first evaporator, and minor values (900–1200) for the third effect. Some reported data from studies on food evaporation for both heat coefficients, convective and overall, including a diversity of liquid foods and used equipment are shown in Tables 12.1 and 12.2.

TABLE 12.1
Heat Transfer Coefficients (*h* and *U*) Data and Proposed Correlations

Authors/Equipment Characteristics	Food Item	Correlation and Comments[a]
Hall and Hedrick (1971)/Evaporators	Milk	$Nu = 0.11([Re^{a})]^{0.69} Pr^{0.4}$ a: empirical constant, 0.964 for skim, 0.961 for whole milk
Chen et al. (1979)/Rotary steam-coil vacuum	Tomato paste	$Nu = 0.60 X_s^{-2.51} Re^{0.62} Pr^{0.33} \left(\frac{\mu}{\mu w}\right)^{0.14}$ X_s: mass fraction of solids, 20–50%; h: 795–15,000 W/m^{2}K
Muddawar and El-Masri (1986)/Rotary vacuum falling film	Liquid foods	$Nu = 0.042 Re^{0.17} Pr^{0.53}$, $Re > 10^4$
Bourgois and LeMaguer (1987)/Upward liquid film	Pineapple juice	$Nu = 8.5 Re^{0.20} Pr^{0.33} S^{0.67}$ S: slip ratio, 13–62°Bx
Stankiewicz and Rao (1988)/Thin-film wiped surface, simple effect	Sugar solution	$Nu = 0.048 Re_x^{0.59} Pr^{1.05} Fr^{0.12} \left(\frac{\eta}{\eta w}\right)^{-2.93}$ Transition regime, M_f: 58–87 kg/h,10–45%, h: 1800–12,000 W/m^{2}K, N: 150–500 rpm
	Sugar solution	$Nu = 4.14 Re^{0.26} Pr^{0.33} Fr^{0.03} \left(\frac{\eta}{\eta w}\right)^{-0.75}$ Turbulent regime, M_f: 87–133 kg/h, 10–45%, h: 11,100–13,000 W/m^{2}K
Dodeja et al. (1990)/Thin-film scraped surface	Whole milk	$Nu = 6616 GRe^{0.133} Pr^{0.076} \left(\frac{\Delta T}{T_s}\right)^{0.284}$ ΔT (temperature difference), T_s: 19–70%, U: 1270–1530 W/m^{2}K

Jebson and Iyer (1991)/Falling film (multiple)	Skim and whole milks	$h = 2288 - 349\Delta T\mu + 82\Delta TM - 2\Delta T\mu M$
		ΔT: temperature difference,°C μ: cP; M: steam mean kg/s
Abichandani and Sarma (1991)/Horizontal thin-film scraped surface	Cream, milk and water	A multiple correlation for U was proposed, U: 600–1800 W/m²K
Bouman et al. (1993)/Falling film (one effect)	Skim milk	$h = 0.77q^{0.69}\eta^{-0.44}$
		q: heat flux, 0.6–12.7 W/m²K
	Whole milk	$h = 6.05q^{0.47}m^{0.26}\eta^{-0.44}$
		m: wetting rate, 0.06–0.50 kg/m s, η: Pa s
Sangrame et al. (2000)/Thin-film scraped surface	Tomato pulp	$U = 411.4 + 113.4T - 149.3P - 1.6T^2 + 2.4TP - 0.3P^2$
		T: steam temperature, P: feed flow rate, Pulp, 5.9–19%
Hoffman/(2004)/Plates one to four effects	Skim milk	$Nu = 1.25 \times 10^{-4} Pe_x^{0.80} Kp^{0.91} Pr^{-0.12} \left(\frac{L}{de}\right)^{0.13}$
		q: heat flux, <15–20 kW/m², 9.0–48%
	Sugar, waste brines	$Nu = 3.79 \times 10^{-2} Pe_x^{0.33} Kp^{0.62} Pr^{-0.12}$
		$q \geq 22$–25 kW/m²; P_r: 2.3–842, 14–87, 1.9–35%, Kp: pressure criterion, L: plate height: 1 m; d_e: equivalent diameter: 4–32 mm
Prost et al. (2006)/Falling film (three effects)	Sucrose solution	$h = 29804 Re_L^{-0.265} Pr_L^{0.159}$
		9.3–36%, Re: 22.6–2613; P_r: 3.5–200; h: 4358–5401 (first), h: 4823–6168 (second), h: 1908–2995 W/m²K (third effect), L: liquid

[a] Nu: Nusselt number, Pe: Peclet number; Pr: Prandtl number; Re: Reynolds number. μ = η: viscosity; $\mu_w = \eta_w$: viscosity at Tw (wall temperature).

TABLE 12.2
Overall Heat Transfer Coefficients for Evaporation Processes

Reference Food Item	Equipment	U (W/m²K)
Schwartzberg (1977):		
Corn syrup, dextrose	Falling film—one effect	568–1200
Skim milk	Rising film—one pass	980–2150
Sugar	Calandria	1475–3400
	Falling film—one effect	475–2725
Tomato paste	Forced circulation	720–3000
Chen et al. (1979):		
Tomato paste	Rotary steam-coil vacuum	704–4355
Moresi (1985):		
Apple juice	Falling film—multiple effect, six in forward arrangement	492–1540
Apple juice	Falling film—multiple effect six in backward arrangement	874–1135
Jebson and Iyer (1991)		
Skim and whole milk	Falling film—multiple effect	300–3200
Sangrame et al. (2000):		
Tomato pulp	Thin-film scraped surface	626–911

12.3.2 Elements of an Evaporation System

Equipment units utilized to complete the operation of an evaporation unit consist of preheaters, pumps, vapor condensers, compressors (also called thermo compressors), and controls, as the most important processing units (Brown et al., 1965; Hartel, 1992; Singh and Heldman, 2001; Ibarz and Barbosa-Cánovas, 2003; McCabe et al., 2008).

Preheaters: Preheating of a liquid food to be concentrated normally precedes the evaporation process; tubular heat exchangers are normally utilized for this pretreatment. Either a double tube or a shell and a tube are common heat exchangers that may be utilized; which equipment is used depends on the feed mass to be processed.

Pumps: Pumping is needed to feed the raw milk to the evaporation system or when reverse feeding evaporation is handled. Reciprocating pumps together with steam jet ejectors are commonly used to produce vacuum. The concentrate leaving from the last effect should be moved out with a positive pump, and also the condensate water may be removed from the condenser with a centrifugal pump. Reciprocating pumps may also be used to produce vacuum.

Heat exchange zone: This section is constituted by the tubes and shell or by the plates in which the liquid food to be concentrated is constantly distributed forming a thin film that favors the heat transfer. The magnitude of the heat flow is directly proportional to the overall heat coefficient, surface area, and temperature difference (Equation 12.3). In this section, it is very important

to get an even film in each tube or plate that favors a uniform distribution of the liquid food and proper heat transfer.

Boiling zone: It is represented by the space at certain vacuum pressure, where the heated liquid reaches the vapor pressure that generates the boiling temperature; thus the boiling of the liquid food starts the separation of the vapor to the upper part and the concentration of the remaining liquid. Table 12.3 (Hall and Hedrick, 1971; Cengel and Boles, 2006) shows some thermodynamic data related to the boiling and vaporization phenomena.

Vapor–liquid separator: Once the evaporation of the food has occurred, there exists not only the need for separation of the main products, the concentrate and the generated vapor, but also the recuperation of the liquid droplets going with the vapor. These are the functions of the separator.

Condenser: When the vapor is not recycled to the process, the condensation of the vapor generated in the first or the last effect is needed. The condenser is also a shell and a tubular heat exchanger able to cool down the vapor phase and transform it into the liquid phase by removal of the latent heat, in which cold water is normally employed for that purpose; sometimes a process liquid at low temperature may be utilized in order to recover energy. Simultaneously, the vacuum is maintained because the volume occupied by the liquid is considerably lower than the vapor volume. Occasionally, a jet condenser as a direct condenser can be employed instead of the tubular condenser; thus the sprayed water and the condensate are mixed and may be reutilized for other equipment.

Compressors: Vapor recompression increases the efficiency in energy consumption of an evaporation system. Energy is added to the generated vapor by means of two alternative units: a mechanical compressor or a steam jet (thermocompressor). The objective of vapor recompression is to increase the pressure and thereby the temperature of the generated vapor. In the first equipment the compression is accomplished mechanically by using a compressor. In the second case, the released vapor is compressed

TABLE 12.3
Thermodynamic Data of Water Vaporization

T (°C and °F)		P (kPa, psia[a], and mm Hg)			Δh (kJ/kg and BTU/lb)	
0	32	0.612	0.088	4.600	2500.9	1075.8
20	68	2.339	0.339	17.50	2453.5	1055.5
40	104	7.385	1.070	55.30	2406.0	1035.1
60	140	19.95	2.891	149.4	2357.7	1014.3
80	176	47.42	6.873	355.1	2308.0	992.90
100	212	101.4	14.70	760.0	2256.4	970.30
120	248	198.7	28.79	1489.1	2202.1	947.34

T: boiling temperature, P: saturation pressure, Δh: latent heat.

[a] Absolute pressure in pounds per square inch.

by acting on it with a high-pressure steam. Any quantity of liquid incorporated into the vapor stream will decrease the energetic value of the vapor, as well as increase product losses. An efficient separator will avoid or minimize these liquid food losses and, therefore, it will maximize the vapor energy efficiency.

12.3.3 One Simple Effect

The design of evaporators is generally based on the determination of the heat transfer area of one or several units, and also on the calculation of the steam consumption required to reach the concentration of the liquid food product. Depending on the magnitude of the liquid food feeding, the concentration process may be completed by a simple or multiple arrangement. A typical picture of simple evaporation equipment is shown in Figure 12.6.

A single evaporation unit represents the fundamental equipment used for the concentration of liquid foods and solutions. It constitutes the application of a heat exchanger designed with particular characteristics in order to not only support the heating of the liquid, but also favor the evaporation of the food and the separation of the generated vapor and the concentrate. Even though it is a single unit, it may be arranged in forward and backward feedings of the liquid food to be concentrated.

This type of equipment is able to handle lower quantities of feeding and is consequently designed to reach lower evaporation and concentration capacities, which produces lower product flows, basically as a result of the minor area of heat transfer.



FIGURE 12.6 Picture of a single evaporator. (Courtesy of GEA Wiegand GmbH.)

TABLE 12.4
Theoretical Steam Consumption in Evaporation Equipments

Type of Arrangement	Range of steam consumption (kg of steam/kg of vapor)	Average
Single effect	1.00–1.33	1.17
Double effect	0.50–0.63	0.57
Triple effect	0.34–0.40	0.37
Quadruple effect	0.26–0.30	0.28
Quintuple effect	0.22–0.24	0.23
Sextuple effect	0.18–0.20	0.19
Septuple effect	0.16–0.18	0.17
TVR triple effect	0.24–0.27	0.25
TVR four effect	0.17–0.21	0.19
TVR five effect	0.13–0.17	0.15
TVR six effect	0.11–0.13	0.12

TVR: Thermovapor recompression.

The steam consumption for this equipment is in the range of 1.00–1.33. Certainly the concept of multiple evaporator units implies an increase in contact area, in fluid feeding, in evaporation or concentration capacity, and a decreasing in steam needs, as can be observed in Table 12.4 (Hall and Hedrick, 1971; Hartel, 1992; McCabe et al., 2008).

In a single evaporator, in order to augment the economy of the performance, the generated vapor can be utilized by the same unit to preheat the feeding of fresh stream, then the steam needs will be reduced.

For multiple effect operation, the sequence is the same: the vapor generated in the previous unit is supplied to the next evaporator and so on, constituting double, triple, quadruple, quintuple, sextuple, septuple, and octuple evaporators, the more commercial one being a triple-effect arrangement.

12.3.4 Multiple Effect Operation

Multiple effects represent the image of an industrial equipment for concentration of higher quantities of fresh feeding, such as fruit juices, milk, and purees of commercial production; a set of multiple evaporators is presented in Figure 12.7.

The performance of this type of industrial equipment may be summarized into four steps for a forward arrangement, there being a similar operation for other types of feeding (Holland, 1975; Hartel, 1992; McCabe et al., 2008).

First, the liquid food or mixture to be separated is introduced to the first effect as a feed stream with a low content of solids. The energy required to evaporate the water is supplied by the latent heat of condensation coming from the steam upon condensing, the steam flows normally at the external side of the heat exchanging zone and it is removed as a condensate.

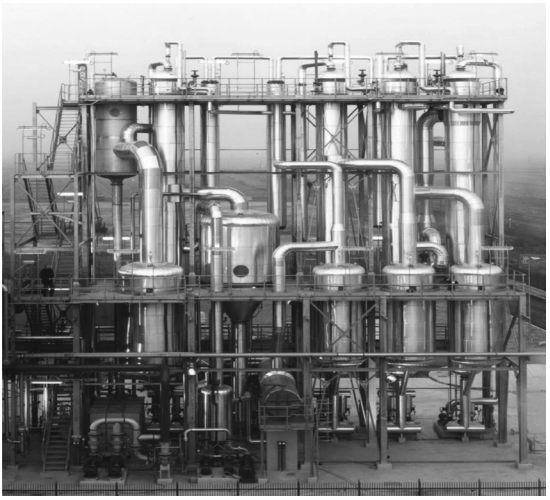


FIGURE 12.7 Picture of a multiple evaporator. (Courtesy of GEA Wiegand GmbH.)

Second, the gravity, vacuum, and/or hydraulic pump forces the liquid food down or up through the tubes or plates at a relatively high velocity of 2–6 m/s and the evaporation phenomenon occurs in each effect.

Third, after the liquid–vapor mixture in equilibrium at the boiling temperature leaves the tubes or plates, it strikes a deflector that favors the separation of the major part of the liquid; then, the concentrated liquid, also known as liquor, is transferred to the next evaporator taking advantage of higher vacuum pressure and sometimes of the pumping work, depending on the arrangement.

Fourth, the vapor generated in the previous evaporator can be pumped to the next unit, to be utilized as the heating medium in the chest to supply the energy needed for vaporization of the liquid food (semiconcentrated), or is withdrawn to the thermocompressor or to the condenser, such as it happens in the last evaporator.

12.3.5 Engineering Calculation

Usually in the design of evaporator units, even as a simple or as a multiple arrangement, the expected prediction results are: (i) the amount of evaporated water or capacity (kg of evaporated water/h), (ii) the boiling point elevation, (iii) the needed amount of steam or consumption (kg of steam/kg of evaporated water), (iv) the approximate boiling temperatures in the different effects (T_n), (v) the quantities of product or intermediate concentrates (kg/h), and (vi) the area of heating surface required at each unit (A_n). Although the following procedure is developed for a triple-effect evaporator, the application to a single evaporator is very similar and simpler. Also, it may be applied to more than three evaporators.

The procedure that is going to be explained was developed for three effects in other times in which the computational tools were more limited, and even though it is limited to the solution of a system of three simultaneous equations, it still represents a very good class exercise. With the passage of time, many software packages

have been introduced; for instance, polymath software is able to solve a system of 30 simultaneous equations. More complete and complex solutions have been analyzed and proposed for more specialized people.

To find out the desired information also identified as unknowns, the application of material and enthalpy balances as well as the heat transfer equation is obligatory; this is an important and particular characteristic of the unit operations or food processing operations. In this development, some assumptions should be considered.

- Liquid solutions, including the fresh feeding (w_F) and intermediate concentrates (w_{S1}, w_{S2}) and product concentrate (w_P), in the evaporator system are composed of nonvolatile solutes and water; they are well mixed.
- The driving force or available temperature difference (ΔT_n) is only reduced by the boiling point rise of the specific liquid food at each effect.
- Incondensable gases do not affect the overall pressure and heat transfer effectiveness in the effect.
- The vapor phase is in equilibrium with the liquid phase; therefore the concentrates and generated vapor have the same temperature (T_n).
- The supplied energy for the heating and boiling process is obtained only from the condensation; it means that steam is saturated as its condensate is saturated liquid.
- The enthalpy of both phases, as well as the enthalpy of phase change, may be found in thermodynamic tables for water.
- The overall heat transfer for each evaporator is constant through the whole evaporation process. All these aspects are considered and outlined in Figure 12.8.

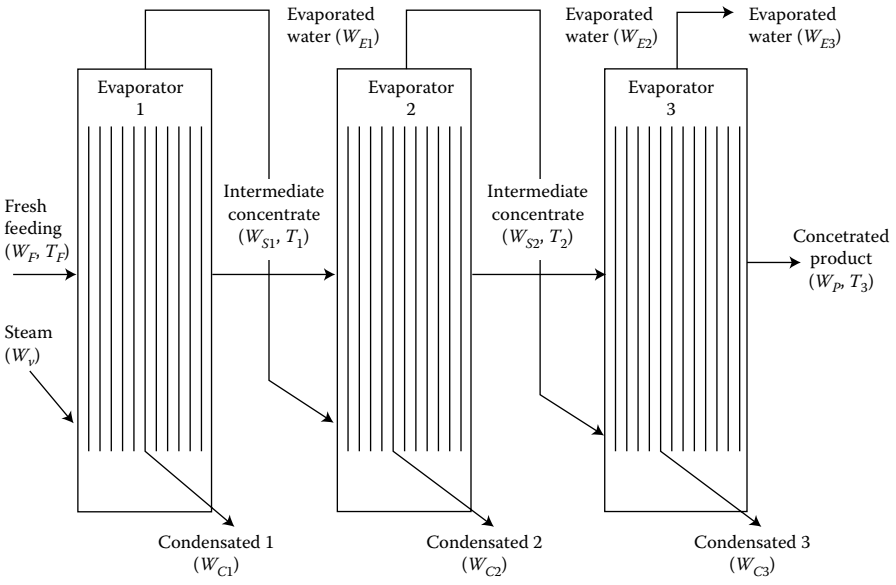


FIGURE 12.8 Outline of a triple-effect evaporator in forward arrangement.

12.3.5.1 Mass Balance on Food Processing

Taking as a basis the triple-effect evaporator schematized by Figure 12.7 and considering a stable system/process in which there is no accumulation, the performance and design equations are developed below.

A total balance of mass for the overall system and for the liquor phase, in which the steam for the first effect is completely condensed, is the following:

$$W_F + W_V = W_{C1} + W_{C2} + W_{C3} + W_{E3} + W_P \tag{12.6a}$$

$$W_F = W_{E1} + W_{E2} + W_{E3} + W_P \tag{12.6b}$$

where W is the mass flow (kg/h) for each one of the streams, F is the feed, V is the steam, C is the condensate at effects 1, 2, and 3, respectively, E is the generated vapor at each of effects 1, 2, and 3, and P is the product or concentrate from the third unit.

In Equation 12.6, W_v is the steam consumption, and W_{E1} (= W_{C1}) + W_{E2} (= W_{C2}) + W_{E3} is the evaporated water, which in conjunction represents the capacity of the triple-effect equipment. Furthermore, taking the flux identity: $W_V = W_{C1}$ as it was mentioned, and doing a balance for the water and solid contents.

$$\begin{aligned} W_F(X_{WF}) &= W_{C2}(1.0) + W_{C3}(1.0) + W_{E3}(1.0) + W_P(X_{WP}) \\ W_F(X_{SF}) &= W_P(X_{SP}) \end{aligned} \tag{12.7}$$

For the first effect, only for the liquor, in which the vapor phase $W_V = W_{C1}$:

$$\begin{aligned} W_F(X_{WF}) &= W_{S1}(X_{SS1}) \\ W_F(X_{WF}) &= W_{S1}(X_{SS1}) \end{aligned} \tag{12.8}$$

Similarly for the second unit, in which the vapor phase $W_{E1} = W_{C2}$:

$$\begin{aligned} W_{S1} &= W_{E2}(1.0) + W_{S2}(X_{WS2}) \\ W_{S1}(X_{SS1}) &= W_{S2}(X_{SS2}) \end{aligned} \tag{12.9}$$

And finally, for the third evaporator (vapor phase $W_{E2} = W_{C3}$):

$$\begin{aligned} W_{S2}(X_{WS2}) &= W_{E3}(1.0) + W_P(X_{WP}) \\ W_{S2}(X_{SS2}) &= W_P(X_{SP}) \end{aligned} \tag{12.10}$$

where X is the mass fraction of solids (dimensionless), for two components, the solids (S) and water (W); and $S1$, $S2$, and $S3$ or P ($P = S3$) are the intermediate concentrated solutions or liquors coming up from each evaporator and expressed as mass flow (kg/h).

12.3.5.2 Boiling Point Rise of Liquid Foods

To consider the effect of the boiling point rise, the simplest case is to consider ΔT as insignificant; in the case of liquid foods, a common correlation establishes that ΔT is a function of the total solids.

If the boiling point of the fluid to be concentrated is unknown, there are two options; the first one is to employ those boiling points of the liquid foods or solutions from Dühring diagrams, such as the example included in Figure 12.9 for tamarindo juice at different concentrations and in Figure 12.10 for sucrose solutions (Ibarz and Barbosa-Cánovas, 2003).

The second option may be to utilize some of the proposed correlations that have been developed in research works, like those included in Table 12.5, relationships that have been obtained from experimental work.

A few reported diagrams have been developed for fruit juices (Moresi and Spinosi, 1980, 1984; Ilangantileke et al., 1991; Camiro-Cabrera et al., 2007), whereas Dühring graphics for some common solutions appear at some books (Holland, 1975; Ibarz and Barbosa-Cánovas, 2003. McCabe et al., 2008, Vélez-Ruiz, 2009).

As a general consideration:

$$\Delta T_{bp} = T_{\text{solution}} - T_{\text{water}} \quad \text{(at the same pressure)} \tag{12.11}$$

where ΔT_{bp} is the boiling point rise (°C), T_{solution} is the boiling point of the corresponding solution (°C), and T_{water} is the boiling point of water (°C) for the same operating conditions at the evaporator.

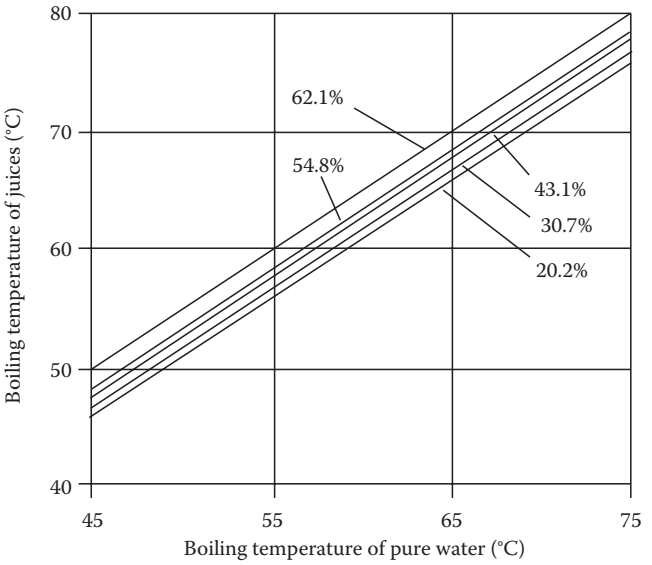


FIGURE 12.9 Dühring diagram for tamarindo juice at different solids contents (% w/w).

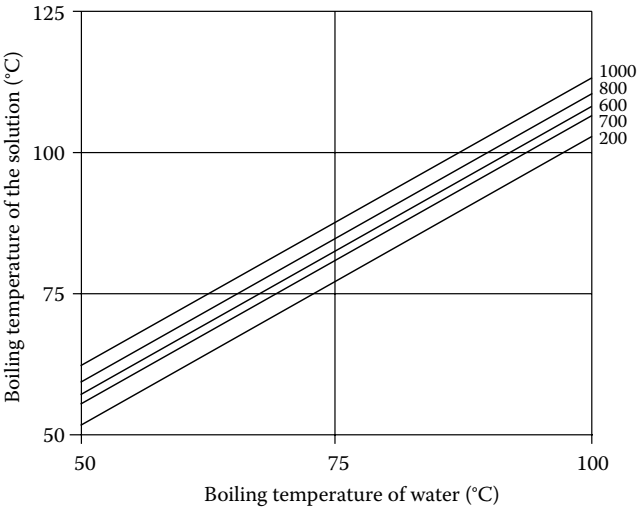


FIGURE 12.10 Dühring diagram for sucrose solutions at different solids contents (g of sucrose/100 g of water).

12.3.5.3 Energy Balances on Food Processing

The energy balance may be applied to the overall system and at each one of the effects, similar to the mass balance. The overall enthalpy balance considering just the sensible part for the solutions or concentrates without phase change and adding the latent heat when a change of phase (evaporation or condensation) is involved.

$$W_F\Delta h_F + W_V\Delta h_V = W_{C1}\Delta h_{C1} + W_{C2}\Delta h_{C2} + W_{C3}\Delta h_{C3} + W_{E3}\Delta h_{E3} + W_P\Delta h_P \quad (12.12a)$$

where W is the mass flow (kg/h), and Δh is the specific enthalpy (kJ/kg) for the corresponding stream, as it was previously specified.

In this case, the difference of energies between the steam ($W_V\Delta h_V$) and the first condensate ($W_{C1}\Delta h_{C1}$) is the enthalpy of condensation due to the implied phase change ($W_V\Delta h_{LV}$). Therefore, the equation may be partially modified:

$$W_F\Delta h_F + W_V\Delta h_{LV} = W_{C2}\Delta h_{C2} + W_{C3}\Delta h_{C3} + W_{E3}\Delta h_{E3} + W_P\Delta h_P \quad (12.12b)$$

With these considerations, the energy balances for the three evaporators are

$$\text{First: } W_F\Delta h_F + W_V\Delta h_V = W_{C1}\Delta h_{C1} + W_{E1}\Delta h_{E1} + W_{S1}\Delta h_{S1} \quad (12.13a)$$

$$\text{Second: } W_{S1}\Delta h_{S1} + W_{E1}\Delta h_{E1} = W_{C2}\Delta h_{C2} + W_{E2}\Delta h_{E2} + W_{S2}\Delta h_{S2} \quad (12.13b)$$

$$\text{Third: } W_{S2}\Delta h_{S2} + W_{E2}\Delta h_{E2} = W_{C3}\Delta h_{C3} + W_{E3}\Delta h_{E3} + W_P\Delta h_P \quad (12.13c)$$

TABLE 12.5
Proposed Relationships for Boiling Point Elevation (ΔT_{bp}) and Related Aspects

Reference	Food Material	Equations/Comments
Moresi and Spinosi (1980)	Orange juice	$\Delta T_{bp} = 3.2y - 2.4y^2 + 14y^3$ y (weight fraction of sucrose): 0.10–0.65
Moresi and Spinosi (1984)	Grape juice	$\Delta T_{bp} = \frac{RT_w^2}{\Delta H_v} x$, R: gas constant, T_w: water boiling point, x: solute molar fraction, ΔH_V: vaporization latent heat, $ln_p = A - \frac{B}{T}$, A and B: characteristic constants, T: absolute temperature, 324–385 K, p: 100–760 mm Hg $A = 20.64 - 0.384y + 1.297y^2 - 2.045y^3$ $B = 5212 - 1375y$, y: weight fractions of equivalent sucrose: 0–0.73
Crapiste and Lozano (1988)	Sucrose	$\Delta T_{bp} = 0.031C^{0.094}P^{0.136}\exp(-0.0533C)$ C: concentration in °Bx, P: pressure in mbar
	Reducing sugar	$\Delta T_{bp} = 0.023C^{0.533}P^{0.119}\exp(-0.0359C)$
	Juices	$\Delta T_{bp} = 0.014C^{0.749}P^{0.106}\exp(-0.0339C)$
Ilangantileke et al. (1991)	Tanger juice	$\Delta T_{bp} = 0.049C^{0.029}P^{0.113}\exp(-0.03889 - 0.00065C^2)$ C: concentration in °Bx, P: pressure in mbar, 35–67°Bx
Tellis-Romero et al. (2007)	Grapefruit juice	$BP_{GJ} = m_0 + m_1 BP_W$ m_0 and m_1 given constants at each concentration (9.3–60.6°Bx), BP_W: boiling point of water. In the range of 9.3–29°Bx, the boiling point elevation was nearly independent of pressure. $m_0 = 0.17$, 0.96, and 3.27°C; $m_1 = 1.00$, 1.01, and 1.02 for 9.3, 34, and 56°Bx.

These three equations may be simplified taking the same consideration, that is to say, the heating medium or steam only supplies the condensing latent heat in each effect. Additionally by considering the heat flux as the energy needed for the liquor phase or the supplied energy from the steam, the energy equations for the three effects, in which the boiling point at each evaporator is taken as the basis temperature, are given below:

First:

$$W_F \Delta h_F + Q_1 = W_{E1}\Delta h_{E1} + W_{S1}\Delta h_{S1}$$
$$W_V \Delta h_V = W_{C1}\Delta h_{C1} + Q_1 \quad (12.14a)$$

Second:
$$W_{S1}\Delta h_{S1} + Q_2 = W_{E2}\Delta h_{E2} + W_{S2}\Delta h_{S2}$$
$$W_{E1}\Delta h_{E1} = W_{C2}\Delta h_{C2} + Q_2 \quad (12.14b)$$

Third:
$$W_{S2}\Delta h_{S2} + Q_3 = W_{E3}\Delta h_{E3} + W_{S3}\Delta h_{S3}$$
$$W_{E2}\Delta h_{E2} = W_{C3}\Delta h_{C3} + Q_3 \quad (12.14c)$$

where Q is the transferred heat in each one of the effects (Q_1, Q_2, and Q_3 in kW or kJ/h).

The corresponding energy of each concentrate ($W\Delta h = \Delta H$) has been canceled at each energy balance, due to the aforementioned comment, in which $\Delta h = \text{Cp}\Delta T$ and ΔT is zero ($T_1 - T_1$, $T_2 - T_2$ and $T_3 - T_3$, respectively), and so on ($\Delta h_s = 0$) in the case of more effects.

12.3.5.4 Evaluation of Heat Transfer Area

The rate of heat transfer is required for designing and sizing the heat transfer area of evaporators: the number of tubes or the number of plates. The heating area is evaluated from Equation 12.15, in which usually U and A are based on the outside surface of the heating tubes; this is not the case of plate evaporators.

$$Q = UA\Delta T \quad (12.15)$$

where Q is the heat flux (kW), transferred from the condensing steam to the liquid food; U is the overall heat transfer coefficient including conduction, convection, as well as the fouling resistances (W/m^{2}K); ΔT is the temperature difference or driving force for each effect (°C), evaluated as the difference between the steam temperature and the corresponding boiling point of each effect (°C); and A is the heat transfer area for each evaporation unit (m^2), which is the main parameter in calculations for evaporator design.

Furthermore, considering each one of the mentioned parameters (resistances):

$$U = \frac{1}{\frac{1}{h_0} + R_{f0} + \frac{\Delta x D_0}{k D_{ML}} + R_{fi} + \frac{D_0}{h_i D_i}} \quad (12.16)$$

where h_o and h_i are the outside and inside heat transfer coefficients (W/m^{2}K) for external and internal convection, respectively; Rf_o and Rf_i are the external and internal resistances for the corresponding fouling (m^{2}K/W); Δx is the tube thickness (m) and k is the thermal conductivity (W/mK), forming the conduction resistance; and D_o, D_i, and D_{ML} are the external, internal, and logarithmic mean tube diameters (m), respectively.

For evaporator plates, the diameter is not considered. Additionally, the heat transfer area A (m^2) may be evaluated for tube or plate heat exchangers, from two geometrical relationships.

$$A = n(\pi D_0 L) = n(L_e a) \tag{12.17}$$

where n is the number of tubes or plates, L is the length of the tubes (m), and L_e and a are the effective length (m) and effective width of the plates (m), respectively.

The thermal potential or driving force (ΔT) at each evaporator unit is

$$\Delta T = T_v - T_n \tag{12.18}$$

where T_V is the steam temperature (°C), which should be modified for multiple evaporators (T_{E1} and T_{E2}), and T_n is the boiling point of the liquid food in the corresponding effect (°C, T_1, T_2, and T_3).

Therefore, the needed heat flow for each one of the evaporators is

First: $$Q_1 = U_1 A_1 \Delta T_1 \tag{12.19a}$$

Second: $$Q_2 = U_2 A_2 \Delta T_2 \tag{12.19b}$$

Third: $$Q_3 = U_3 A_3 \Delta T_3 \tag{12.19c}$$

That includes the proper data and specific conditions of operation at every evaporator unit.

12.3.6 Practical Solving Criteria

For a triple-effect equipment in which the fundamental equations are applied (12.6 through 12.10, 12.12 through 12.14, and 12.19), and considering that typically the fresh flow (w_F), the vacuum or boiling temperature of the third effect (T_3), the final concentration (X_P), and the overall heat transfer coefficients (U_1, U_2, U_3) are known. There will generate seven or more equations with seven or more unknowns (Holland, 1975; Vélez-Ruiz, 2007; McCabe et al., 2008; Vélez-Ruiz, 2009).

Commonly, the unknowns or variables to be solved are: (i) the consumption or steam for the first effect, (ii–iv) the mass flow leaving from each effect: $w_{SI,}$ w_{S2}, and w_p, (v and vi) the boiling temperatures for the first and second effects (T_1 and T_2), and (vii) the heating surface per evaporator, assumed as identical for the three evaporators ($A_1 = A_2 = A_3 = A$).

To solve the general set of equations associated with an evaporation system of three effects, several methods may be used; two of the most common are to solve by some generalized nonlinear numerical procedure, such as the Newton–Raphson method (Holland, 1975), or by linearizing the equations and using integrated iteration loops (Ribeiro and Caño Andrade, 2002), among others.

Although there exist other options, for instance, the utilization of simultaneous equations by polymath software, one simple, iterative, and practical solution that represents a very good exercise for students is importantly based on the assumption

of equal heating areas for the three effects; it is summarized into four steps (Holland, 1975; Vélez-Ruiz, 2007, 2009; McCabe et al., 2008):

1. Guess the boiling points for effects 1 and 2 (T_n), taking as basis the overall heat transfer coefficients of the three effects, and the overall ΔT to get an idea of the magnitude of the temperatures.
2. Develop the enthalpy and mass balances for the three effects, that taking into account the aforementioned assumptions, it will reduce the set of equations to a simultaneous system of three, to evaluate the flow rates.
3. Apply the equations to solve for Q_n, and later, evaluate the surface area of each evaporator.
4. Evaluate the average area (A) to know if the heating area is approximately the same for each effect. If the area is different at 10% or more (this criterion may be fitted to get a more accurate solution), another iteration will be convenient.

With this practical procedure, the number of iterations will be less than three and an error less than 10% will be obtained. This procedure will be exemplified in Section 12.5 with specific situations. Ibarz and Barbosa-Cánovas (2003) mention other iterative procedures for solving evaporator equations when the boiling point rise is neglected or when it is an important consideration.

12.4 FOOD PARTICULARITIES IN EVAPORATION

Concentrated foods normally are not commercial items; the products of a concentration process by evaporation are not stable to microbial attack, and consequently, concentration is completed with other preservative processes. Some of the complementary processes are canning, dehydration, sugaring, and thermal treatment, among others.

Even though the engineering aspects are the more important ones to be considered, there are some additional aspects that should be taken into account in order to perform a good selection of the evaporation equipment for a specific liquid food.

12.4.1 Thermal Sensibility of Foods

Evaporation and other food processing operations involve the transfer of heat to food in which the processing temperature is between ambient and sterilization temperatures (30–120°C). High operation temperatures may affect the nutrient retention of the treated liquid food, causing a loss of nutritional quality that should be avoided as much as possible.

From the kinetic point of view, the heat damage to the food item is caused by a chemical conversion of the thermally sensitive component. Nutrient components such as vitamins and proteins are mainly affected to a different degree, at a low conversion rate of the specific component. In agreement with Thijssen (1970) and Barbana and El-Omri (2012), there is a direct relationship with the residence time and an exponential dependence with the temperature.

The conversion or damage degree (C) may be expressed by a first-order reaction, whereas the conversion rate (k_r) may be related to the Arrhenius equation.

$$C = k_r t \tag{12.20a}$$

$$k_r = k_0 \exp^{-Ea/RT} \tag{12.20b}$$

where k_0 is a constant, Ea is the activation energy, R is the universal gas constant, and T is the absolute temperature.

These relationships have been applied to a good number of kinetic changes for color, vitamins, and, to a lower degree, for proteins, and also for physical properties such as viscosity.

12.4.2 Physical Properties of Foods

Physical properties of liquid foods are required for adequate design and analysis of the evaporation equipment and process, but these properties may be altered during the process.

Some of these properties may be evaluated easily by additive relationships, such as the density, specific heat, and thermal conductivity, while others such as viscosity, apparent viscosity, flow behavior index, and consistency coefficient cannot be predicted with precision. Although several researchers have been conducting studies to determine the physical properties of foods, still there is limited information. Particularly the engineering calculations for evaporation need those involved physical properties as a function of concentration and temperature.

12.4.2.1 Flow Properties

Flow properties, such as viscosity, apparent viscosity, flow behavior index, consistency coefficient, and yield stress as the major known ones, are needed for handling and transporting liquid foods. Due to their physical nature, these properties are strongly dependent on the solids concentration and temperature; therefore several research works have analyzed and modeled the influence of both variables on the flow characteristics. Some representative works are mentioned in Table 12.6, in which a few of the existing correlations and data for flow properties for liquid foods of different origin as a function of the concentration or temperature are included.

12.4.2.2 Thermal Properties

Properties such as the thermal conductivity and diffusivity, as well as the convective coefficient and specific heat, have been studied to a minor extent than the rheological characteristics; however, some of the existing correlations and data for thermal properties of liquid foods of different origin as a function of the concentration or temperature are presented in Table 12.7.

12.4.2.3 Density

Although density is a physical property of easier determination, there is limited information on it. Some of the existing correlations and data for density in liquid foods of different origin as a function of the concentration or temperature are presented in Table 12.8.

TABLE 12.6
Flow Properties and Related Aspects

Reference	Food Material	Equation/Correlation Observations and Comments	Instrument
Chen et al. (1979)	Tomato paste	$\mu_a = 3.62 X_s^{2.4} \exp\left(\frac{1710}{T + 460}\right)$ μ_a: lb/ft h or poise, X_s: mass fraction of solids 20–50%, T: temperature °F	Höppler falling sphere viscometer
Moresi and Spinosi (1980)	Orange juice	$\mu = \alpha T^{\beta}$, μ: cP, α, and β: are two characteristic constants, $\alpha = 34.668 - 0.02024y + 0.0162y^2 - 2.045y^3$, $\beta = -6.1055 + 0.0396y - 0.00268y^2$, y: weight fraction of sucrose 0.10–0.65 (10–65°Bx)	
Moresi and Spinosi (1984)	Grape juice	$n = 1 - 0.25y \quad k = \exp\left(C + \frac{D}{T}\right)$ $\mu_a = f(y,T)$, μ_a: 0.600–1200 mPa s, function of concentration (0–73.1°Bx), and temperature, C and D: characteristic constants $C = -13.38 + 16.93y - 95.74y^2 + 248.5y^3 - 217.6y^4$, $D = 1903 - 1802y + 22960y^2 - 68310y^3 + 66330y^4$, y: weight fractions of equivalent sucrose	Haake rotational viscometer (RV12)
Bayindirli (1992)	Apple juice	$\mu = \mu_w \exp\left(\frac{\left[-0.24 + \frac{917.92}{T}\right]X}{100 - [2.03 - 0.00267T]X}\right)$ μ_a: 0.5–7.2 cP, μ_w: viscosity of water at the same temperature, T: absolute temperature 20–80°C, X: concentration 14–39°Bx	Ostwald–Cannon Fenske viscometer

Bayindirli (1993)	Grape juice	$\mu = \mu_w \exp\left(\frac{\left[-0.24 + \frac{1821.45}{T}\right]X}{100 - \left(0.86 + \frac{0.00044}{T}\right)X}\right)$ μ_a: 0.5–4 cP, μ_w: viscosity of water at same temperature, T: absolute temperature 20–80°C, X: concentration 19–35°Bx	Ostwald–Cannon Fenske viscometer
Hernandez et al. (1995)	Orange juice	K: 0.064–4.27 mPa s^n, n: 0.68–0.85 for 45–65°Bx	Haake rotovisco viscometer (RV-12)
Vélez-Ruiz and Barbosa-Cánovas (1997)	Concentrated milk	$lnK = 9.863 + \frac{2557}{T} + 0.1426X$ K: mPa s^n, X: solids concentration 12.7–40.4%, w/w, T: absolute temperature 20–80°C	Physica UM rheometer (MC20)
Hobani (1998)	Date concentrates	K: 2.00–37.1 mPa s^n, n: 0.63–0.99 for variety Khudary, K: 1.34–13.3 mPa s^n, n: 0.79–0.94 for variety Sufri, K: 3.30–35.9 mPa s^n, n: 0.61–0.99 for variety Serri, T: 25–95°C, 40–70°Bx	Viscotester Haake
Giner et al. (1997)	Cherry juices	$\eta = 1.12 \times 10^{-6} \exp\left(0.094 + \frac{3523}{T}\right)$ η: 1.36–6850 mPa s, T: absolute temperature 5–70°C, C: solids concentration 22–74°Bx	Rotovisco RV12
Vélez-Ruiz and Barbosa-Cánovas (1998)	Concentrated milk	$lnK = -18.22 + \frac{2973}{T} + (0.1278X)$ K: Pa s^n, X: solids concentration 12.6–42.6%, w/w, T: absolute temperature 5–25°C	Physica UM rheometer (MC20)
Cepeda and Villarán (1999)	Clarified apple juice	$\mu = \exp\left(-53.46 + \frac{9458.9}{T} + 0.29C\right)$ μ: 0.003–3300 Pa s, T: absolute temperature 10–60°C, C: solids concentration 17–70°Bx	Rotatory viscometer (Mettler RM 180)

continued

TABLE 12.6 (continued)
Flow Properties and Related Aspects

Reference	Food Material	Equation/Correlation Observations and Comments	Instrument
Vélez-Ruiz and Barbosa-Cánovas (2000)	Concentrated milk	$K = 0.244\exp(0.148X)$ K: mPa s^n, X: solids concentration, 12.5–46.7%, w/w $n = 1.11 - 0.0072X$, or $n = 1.13\exp(-0.0079X)$	Physica UM rheometer (MC20)
Dogan et al. (2003)	Tomato concentrate	K: 1.45–5.08 Pa s^n, n: 0.22–0.17, for 8.75–17.1°Bx	Capillary viscometry and in-line US viscometer
Zuritz et al. (2005)	Clear grape juice	μ: 0.6–18 Pa s for 20–80°C, 22.9–70.6°Bx	Brookfield viscometer (LVDV-II)
Kaya and Sözer (2005)	Sour pomegranate	$\mu = 1.25 \times \square 10\square^{1}(-11)\exp(0.148C + (4398/T))$ μ: 0.014–14.04 Pa s, T: 5–60°C, C: concentration 45–73°Bx	RheoStress rheometer
Nindo et al. (2005)	Blueberry juice	$\mu = 0.056\exp\left(\frac{[7C^2 + 9055]}{8.314T} - 0.0019C^2\right)$ μ: 1.2–150 mPa s, C: solids concentration, 10–65°Bx, T: 20–60°C	TA rotatory rheometer (AR 2000)
	Raspberry juice	$\mu = 0.0206\exp\left(\frac{[6.8C^2 + 11196]}{8.314T} - 0 - 0017C^2\right)$ μ: 1.2–200 mPa s, C: solids concentration 10–65°Bx, T: 20–60°C	
Choi et al. (2006)	Tomato concentrate	K: 5–94.3 Pa s^n, n: 0.32–0.21 at 60°C, variety Heinz, K: 2.4–99.5 Pa s^n, n: 0.39–0.15 at 60°C, variety Orsetti, K: 2.6–55.3 Pa s^n, n: 0.36–0.18 at 60°C, variety AB, for 5–24°Bx	Viscotester Haake (VT24) and in-line US viscometer
Dak et al. (2007)	Mango juice	$K = aC^b$ a and b: characteristic constants, K (Pa s^n), $a = 0.0002$, $b = 3.90–3.99$ (30–40°C), 7.6–26%, $a = 0.0001$, $b = 4.12$ (50°C); $a = 0.00006$, $b = 4.29$ (60°C); $a = 0.00004$, $b = 4.39$ (70°C)	Brokfield viscometer (LVDV-II)
Rodriguez et al. (2007)	Prickly pear juice	$n = -0.949 + 0.083X - 0.001X^2$ $K = 26.24 - 1.263 + 0.208T + 0.015X^2 - 0.005XT$ n: 0.50–0.83, K: 89–3188 mPa s^n, X: solids concentration 42–58°Bx	Brookfield DVI

Akbulut et al. (2008)	Pekmez beverage	$K = 1.67 \times 10^{19} \exp(0.288C + 8463.7/\mathrm{T})$ K: Pa s^n, C: concentration of total solids, % w/w, T: absolute temperature, 10–50°C	Brookfield rotational viscometer
Ferreira et al. (2009)	Cashew juice	$\mu = 1.32 - 3.39 \times 10^{-2}T + 2.78 \times 10^{-4}T^2 + 1.84 \times 10^{-1}C_s - 2.17 \times 10^{-3}TC_s$, T: temperature, 5–80°C, C_s: soluble solids, 0.8–11.2°Bx	Cannon Fenske viscometer
Kumoro et al. (2011)	Noni juice	$K = a_1 \exp\left(a_2 + \frac{a_3}{T + 273}\right)$, $a_1 = 0.0053$, $a_2 = -0.0026$, $a_3 = -0.0030$ $n = b_1 \exp\left(b_2 C + \frac{b_3}{T + 273}\right)$ $b_1 = 0.1984$, $b_2 = -0.1275$, $a_3 = -0.0164$ for C: 5–15°Bx, T: 30–70°C	Brookfield DVIII
Chirife et al. (2011)	Balsamic vinegar dressing	$\log \mu = 0.194e^{0.038*Bx}$ $\log \mu = 0.141e^{0.040*Bx}$, $\log \mu = 0.106e^{0.042*Bx}$ at 15, 25 and 35°C, respectively for C: 31–76°Bx, T: 15–35°C	Brookfield LVDVI
Barbana and El-Omri (2012)	Reconstituted tomato concentrate	n: 0.03–0.28, K: 1.57–38.53 Pa s^n, T: 20–60°C, C: 9.7–26.8% w/w, as a f (T, C) $K = k_1 C^a$, k_1: 0.0024–0.0038, a: 2.62–2.81 $K = k_0 \exp\left(\frac{E_a}{RT}\right)$, k_0: 0.104–9.634, Ea: 3.63–7.36 kJ/mol K	Rheomat RM-180

μ: viscosity; μ_a: apparent viscosity; K: consistency coefficient; n: flow behavior index.

TABLE 12.7
Thermal Properties of Solutions, Concentrates Foods, and Related Aspects

Reference	Food Material	Equations/Correlations Observations	Instrument
Chen et al. (1979)	Tomato paste	$C_p = 1 - 0.67X$, C_p: BTU/lb°F, X_s: mass fraction of solids, k: BTU/hft°F, $k = \frac{(5.75 - 4.8X_s)[993 + 500X_s - 0.317(T - 32)]}{17300[1.1 - 0.002(T - 32)]}$ T: temperature, °F, 20–50%	
Moresi and Spinosi (1980)	Orange juice	$Cp = 4.186 - 2.679y$, Cp: kJ/kg K, y: weight fraction of sucrose: 0.10–0.65, 10–65°Bx	Thermal Analyzer Dupont 990
Choi and Okos (1983)	Tomato juice	$Cp = Cp_sX_s + Cp_wX_s$, $k = k_SX_S + k_WX_s$, Cp: kJ/kg°C, k: W/mK, X_s: mass fraction of total solids, 4.8–80%, X_w: water fraction $Cp_w = 4.188 + 0.001029T$, T: temperature, 20–150°C $Cp_s = 1.727 - 0.000745T + 0.00000959T^2$; $k_w = 0.6192 + 0.00053T_s$	Thermal conductivity probe
Moresi and Spinosi (1984)	Grape juice	$Cp = yCp_s + (1 - y)Cp_w$, $Cp\,y$: weight fraction of equivalent sucrose, 0–0.73, 0–73.1°Bx, $Cp_S = 1.21$, S: pseudosucrose component, W: water	Thermal Analyzer Dupont 990
More and Prasad (1988)	Whole milk	$k = (0.59 + 0.0012T)(1 - 0.0078X)$, k: W/m k, T: temperature, 40–90°C, X: total solids, 37–72.4%	Steady-state, parallel-plate apparatus
Reddy and Datta (1994)	Reconstituted milk	$Cp = 3833.2 - 28.019X - 1.759T - 0.11X^2 + 0.234XT - 0.05^2$ X: concentration, 40–70%, T: temperature, 35–65°C $k = 0.5656 - 0.0027X + 0.00091T - 0.000021X^2$	
Tellis-Romero et al. (1998)	Orange juice	$Cp = 1424.34 + 2673.19X_w + 2.446X_w$, C_p: J/g°C, X_W: water content, 0.34–0.73 w/w, $k_w = 0.0797 + 0.5238X_w + 0.00058T_s$, K: W/m°C, T: temperature, 5–75°C	Two coaxial copper cylinders

Zainal et al. (2000)	Guava juice	$k_w = 0.522 - 0.00002T$ at 9°Bx, K: W/m°C, T: temperature, 65–85°C, 9–11°Bx $k = 0.512 + 0.00002T$ at 11°Bx	
Sobolík et al. (2002)	Soluble coffe	$k_w = 10^{-3}(565.1 + 1.8T - 0.00058T^2)(1 - 0.54w)$ k: W/m°C, w: coffee mass fraction: kg dry coffee/kg solution, 0–0.5	
Zuritz et al. (2005)	Clear grape juice	$\beta = \frac{a_1 + 2a_3T}{a_0 + a_1T + a_2Bx + a_3T^2 + a_4Bx^2}$, β: thermal expansion coefficient (1/K), a_0, a_1, a_2, a_3, and a_4: parameters of the second degree polynomial, T: absolute temperature, 20–80°C, Bx: soluble solids, 23–71%	
Magerramov (2007)	Apple, cherry, and raspberry juices	$Cp = 4.12 - 2.56 \times 10^{-2}C - 9.50 \times 10^{-5}C^2 + 7.73 \times 10^{-4}T + 1.50 \times 10^{-4}$, $CT - 2.40 \times 10^{-6}C^2T$ T: temperature, 10–120°C, C: solids concentration, 13–52%	Adiabatic calorimeter and measuring cells
Ferreira et al. (2009)	Cashew juice	Thermal expansion coefficient, 1.29–7.27 × 10^{-4}°C^{-1}, T: temperature, 5–80°C, Cs: soluble solids, 0.8–11.2°Bx 0.302–3.42 mPa s	
Souza et al. (2010)	Umbu pulp	$Cp = 2192 + 0.021X_a$ $k = -0.706 - 0.277 \times 10^{-1}T + 0.434 \times 10^{-3}T^2 + 0.228 \times 10^{-1}X_a$, $\alpha = -0.675 \times 10^{-8} - 0.129 \times 10^{-7}T + 0.111 \times 10^{-9}T^2 + 0.335 \times 10^{-8}X_a$ $0.649 \times 10^{-10}TX_a$ X_a: moisture content, 65–95%, T: temperature, 5–85°C, Cp: 3.6–4.2 kJ/kg°C, k: 0.5–2.5 W/°C m, α: 1–6 × 10^{-7} m^2/s	
Kumoro et al. (2011)	Noni juice	$k = d_1 + d_2C + d_3T$, k: W/m°C, d_1: 580.8, d_2: −1.771, d_3: −1.028, C: soluble solids, 5–15°Bx, T: temperature, 30–70°C	Thermal conductivity measurement apparatus (cylindrical cell)

Cp: specific heat; k: thermal conductivity, α: thermal diffusivity.

TABLE 12.8
Density of Liquid Foods, Concentrates, and Related Aspects

Reference	Food Material	Equations/Correlations Observations
Chen et al. (1979)	Tomato paste	$\rho = 62.4(0.44X_s - 0.997)$, ρ: lb/ft^3, X_s: mass fraction of solids, 20–50%
Moresi and Spinosi (1980)	Orange juice	$\rho = -09944 + 0.307y - 0.282y^2$, y: weight fraction of sucrose, 0.10–0.6, 10–65°Bx
Moresi and Spinosi (1984)	Grape juice	ρ: g/cm^3, y: weight fraction of equivalent sucrose, 0–0.73, 0–73°Bx, $\rho_{GS} = 1.608$: density of pseudosucrose component, ρ_w: water density
Bayindirli (1992)	Apple juice	$\rho = 0.83 + 0.35\exp(0.01X) - 0.000564T$, ρ: g/cm^3, 1.02–1.17, T: absolute temperature, 20–80°C, X: concentration, 14–39°Bx
Bayindirli (1993)	Grape juice	$\rho = 0.83 + 0.43\exp(0.01X) - 0.000555T$, ρ: g/cm^3, 1.07–1.18, T: absolute temperature, 20–80°C, X: concentration, 19–35°Bx
Ramos and Ibarz (1998)	Fruit juice and puree:	
	For peach juice	$\rho = 1006.6 - 0.5155T + 4.1951C + 0.0135C^2$
	For orange juice	$\rho = 1025.4 - 0.3289T + 3.2819C + 0.017C^2$
	For apple juice	$\rho = 1056.5 - 0.3610T$, ρ: kg/m^3, T: temperature, 5–75°C, C: soluble solids, 10–60°Bx
Tellis-Romero et al. (1998)	Orange juice	ρ range: 1077–1275 kg/m^3, T: 0.5–62°C, concentration: 0.34–0.73 w/w
Cepeda and Villarán (1999)	Crab apple juice	$\rho = 0.0054C + 0.9671$ ρ: g/cm^{3}at 25°C, C: solids concentration, 17–70°Bx
Zainal et al. (2000)	Guava juice	$\rho = 1047 - 0.5293T$ at 9°Bx, ρ: 1002–1012 kg/m^3, T: temperature, 65–85°C $\rho = 1047.9 - 0.45T$ at 11°Bx ρ: 1011–1019 kg/m^3 $\rho = 1053.4 - 1.4421T + 0.2256C + 0.00864C^2$

Tsen and King (2002)	Banana puree	ρ: kg/m^3, T: temperature, 5–75°C, C: soluble solids, 10–80°Bx, $\rho = 1047 - 0.5293T$
Sobolík et al. (2002)	Soluble coffee	$\rho_C = 1654–1.79T–0.0063T^2$; $\rho_W = 1000–0.036T–0.004T^2$ ρ: kg/m^3, w: kg dry coffee/kg solution, 0–0.5, T: temperature, 25–95°C, c: solid coffee
Zuritz et al. (2005)	Clear grape juice	ρ range: 1097.3–1358.4 kg/m^3, ρ for 20–80°C, 22.9–70.6°Bx
Magerramov et al. (2008)	Seven fruit juices: black currant, cherry plum, melon, peach, pear, plum, and tangerine,	ρ: 1.01–1.13 g/c m^3, for 283–403 K, 10.7–70°Bx Standard volumetric pycnometer and magnetic densimeter
Ferreira et al. (2009)	Cashew juice	$\rho = 996.49 - 0.096T - 0.0038T^2 + 4.030C_s$, ρ: 969.08–1040.16 kg/m^3 T: temperature, 5–80°C, C_s: soluble solids, 0.8–11.2°Bx,
Souza et al. (2010)	Umbu pulp	$\rho = 2891.520 - 39.558X_a + 0.209X_a^2 - 0.010T^2$, T: temperature, 5–85°C, X_a: moisture content, 65–95%, 940–1100 kg/m^3 pycnometric method
Enríquez-Fernández et al. (2013)	Concentrated milk	$\rho = 988.1 + 2.8754X$
	Reconstituted milk	$\rho = 944.0 + 3.0999X$ ρ: kg/m^3, X: solids concentration, 44–60% w/w
Kumoro et al. (2011)	Noni juice	$\rho = c + c_2C + c_3T$, ρ: kg/m^3, c_1: 1042, c_2: 1.348, c_3: 0.489, C: soluble solids, 5–15°Bx, T: temperature, 30–70°C Capillary tube pycnometer

Note: ρ is the density.

12.4.3 Additional Process Limitations

From the operational viewpoint, one of the more severe problems in the concentration by evaporation of liquid foods is fouling on the heating surface. It is well known that surfaces of tube and plate heat exchangers do not remain clean after some time of processing. Scaling or deposits form over the interior and exterior surfaces of tubes and plates, and may be considered as an additional thermal resistance; this phenomenon constitutes a gradual buildup of layers of damaged major food components, proteins, carbohydrates, salts, minerals and dirty impurities, among others. The formed deposits can severely affect the heat transfer equipment and process; particularly they affect the overall heat transfer coefficient. When fouling becomes substantial, cleaning needs to be completed in order to eliminate the formed fouling, sometimes taking significant time of the labor process and stopping the normal production.

Fouling minimization requires engineering considerations in equipment and process design and also in deciding operational conditions, such as to modify the fluid flow rate, to reconsider the fluid location, to increase the pumping pressure, and/or the process temperature.

Other problems come from the thermal degradation of nutrients as it was mentioned before; both limitations are minimized in an agitated thin-film evaporator. Some years ago, a thin-film spinning cone evaporator (centritherm) was developed and also represents an alternative for this type of foods (FT Industrial, 2004).

Aroma retention for coffee, fruit juice, and tea extract is also a process limitation. The aromas are organic and gas components characterized by high volatility; thus the removal of water by evaporation results in losses of them. Liquid food materials contain aromas that are complex aqueous mixtures of organic compounds, in which a typical low boiling component in the coffee aroma is methyl mercaptane (6°C), whereas a typical high boiling component in grapes is methyl anthranilate (225°C). The problems of volatile losses have been faced by two alternatives, mixing fresh and concentrated juices, or using an aroma recovery unit (Thijssen, 1970; Karlsson and Trägardh, 1998; Hui, 2006). In the case of fluid milk, the elimination of gases is an advantage, because an important part of the gases or volatiles are absorbed by the liquid food when it passes through the different stages in the milking unit of a ranch or farm.

New technologies based on membrane separation are combined with the evaporation process in order to eliminate or compensate some of the evaporation disadvantages. In juices, processing mainly compensates the volatiles loss, and in milk processing it decreases the fouling problem.

12.4.4 Experimental Equipment Utilized in Evaporation Research

Studies and experiments on evaporation and related properties have utilized a diversity of equipment such as laboratory rotary evaporators (Chen et al., 1979; Bayindirli, 1992; Bouman et al., 1993; Enriquez et al., 2013; Magerramov et al., 2008; Souza et al., 2010; Kumoro et al., 2011), heating mantles (Chirife et al., 2011), using pilot plant scale (Stankiewicz and Rao, 1988; Dodeja et al., 1990; Vélez-Ruiz and Barbosa-Cánovas, 1997, 1998; Hobani, 1998), and with industrial evaporation units (Zuritz et al., 2005), with several arrangements. Falling and climbing evaporators have been

utilized more frequently, either with simple effects (Prost et al., 2006) or multiple effects (Jebson and Iyer, 1991; Hernandez et al., 1995; Tellis-Romero et al., 1998; Zuritz et al., 2005) and a few studies exist on plate (Hoffman, 2004) and scraped surface evaporators (Abichandani and Sarma 1991; Sangrame et al., 2000).

Moreover, for studies of the physical properties affected by the evaporation process, the liquid foods have been reconstituted (Moresi and Spinosi, 1984; Tsen and King, 2002; Dak et al., 2007; Akbulut et al., 2008; Ferreira et al., 2009; Barbana and El-Omri, 2012), reformulated (Zainal et al., 2000), and mostly, they have been concentrated on vacuum (Moresi and Spinosi, 1980; Stankiewicz and Rao, 1988; Bayindirli, 1993; Vélez-Ruiz and Barbosa-Cánovas, 1997; Choi et al., 2006).

Heat treatments have implied the application of mathematical analysis and models for evaluation of heat transfer coefficients (Chen et al., 1979; Stankiewicz and Rao, 1988; Jebson and Iyer, 1991; Prost et al., 2006). Rheological properties have been measured either with viscometers (Moresi and Spinosi, 1980, 1984; Bayindirli 1992, 1993; Cepeda and Villarán, 1999; Sobolík et al., 2002; Zuritz et al., 2005; Akbulut et al., 2008; Enriquez et al., 2013; Ferreira et al., 2009; Chirife et al., 2011; Kumoro et al., 2011) or with rheometers (Hernandez et al., 1995; Giner et al., 1997; Vélez-Ruiz and Barbosa-Cánovas, 1997, 1998; Kaya and Sözer, 2005; Nindo et al., 2005; Barbana and El-Omri, 2012), and even with in-line instruments (Dogan et al., 2003; Choi et al., 2006), whereas the boiling point determination has been measured by a pyrex lab set (Moresi and Spinosi, 1980; Camiro-Cabrera et al., 2007), the density has been measured by means of pycnometers with different characteristics (Magerramov et al., 2008; Ferreira et al., 2009; Souza et al., 2010) and thermal properties with different thermal devices, adiabatic calorimeter (Magerramov, 2007), mixture calorimeter (Souza et al., 2010), cylindrical cells (Tellis-Romero et al., 1998; Souza et al., 2010; Kumoro et al., 2011), parallel plates (More and Prasad, 1988), a line heat source probe (Choi and Okos, 1983), or a thermoanalyzer (Moresi and Spinosi, 1980, 1984).

Finally, the solid content determination has been carried out by measuring the soluble solids with refractometers (Dogan et al., 2003; Kaya and Sözer, 2005), or the total solids by moisture determination in a vacuum oven (Dogan et al., 2003; Rodríguez-Martínez et al., 2007; Enríquez-Fernández et al., 2013).

12.4.5 Computer Simulation

Now in the presence of advanced and personal computers and with the development of commercial simulators, the evaluation of an evaporator performance and its design may be faced with more precision, more control, more detail, more velocity, and of course without experimentation. But it is very important to have the fundamentals and basic knowledge of the evaporation as a food processing operation, mainly applied.

Some works have incorporated simulation techniques and programs that may be very useful; Chuaprasert et al. (1999) utilized a data reconciliation method in Aspenplus to simulate an agitated evaporation by adjusting process measurements and satisfying the mass and energy balances; they found very good results and recognized the short time of process simulation. Cadet et al. (1999) also applied simulation modeling and nonlinear predictive control on cane sugar evaporation with five effects, obtaining very good and promising fittings for the sugar industry. Benne

et al. (2000) demonstrated the reliability of artificial neural networks for modeling and control of an industrial evaporation process for saccharose.

Chawankul et al. (2001) developed a heat exchange-two flash by Aspen Plus software to simulate the concentration of orange juice in agitated thin-film evaporators, obtaining good agreement between the experimental and simulated data. Jemqvist et al. (2001) proposed a simulation program for concentration of salty water; it is designed to be flexible and allows us to get the evaluation of flow rates and to optimize all types of desalination processes, and the simulation has been extended to the food industry. In addition, they separated and modeled by modules, including a base for physical properties and the computation of the heat transfer coefficient. Ribeiro and Caño Andrade (2002) developed a steady-state model for a plate evaporator with successful simulation of six industrial units used for milk concentration of a Brazilian plant. Miranda and Simpson (2005) modeled also a multiple effect evaporator for simulation and control purposes. They developed a dynamic model with differential equations and a parameters sensitivity methodology in which the simulation showed acceptable behavior in the comparison of an industrial plate evaporator for tomato juice and the simulator results.

12.5 EXAMPLES OF APPLICATION

As an illustrative way of applying the aforementioned fundamentals, five examples have been selected and they are solved next with academic purposes (Vélez-Ruiz, 2007; McCabe et al., 2008; Vélez-Ruiz, 2012).

EXAMPLE 12.1 MASS AND ENERGY BALANCES

18,000 kg/h of an *orange juice* fed into an evaporation unit to produce a concentrate. The juice has 24% of solids content at 25°C at the beginning and it should be concentrated up to 72% by utilizing saturated steam at 120°C. Consider a boiling temperature of 75°C. Determine the mass and energy balances and the time of performance of the evaporator to complete this process.

Comment: This liquid food is one of the most commonly subjected to concentration by evaporation. The idea is to evaluate the capacity (rate of evaporated water), the consumption (rate of needed vapor), and the economy (ratio between the capacity and the consumption), just by application of balances.

SOLUTION

1. Mass balance

   Global: $18{,}000 + W_V = W_E + W_P + W_C$

   Liquor: $18{,}000 = W_E + W_P$

   Solids:

$$(0.24)\left(18{,}000\ \frac{\text{kg}}{\text{h}}\right) = W_E(0) + W_P(0.72) \quad \therefore W_P = 6000\left(\frac{\text{kg}}{\text{h}}\right)(\text{product})$$

From the liquor balance: $W_E = 18{,}000 - 6000\,\frac{kg}{h} = 12000\,\frac{kg}{h}$

Therefore, the quantity of fruit concentrate is 6000 kg/h, and the capacity of the evaporation systems is 12,000 kg/h. The concentrate represents a triple of the initial concentration.

2. Energy balance
Knowing the quantity of water to evaporate (12,000 kg/h) as the capacity of the unit, then the time needed to carry out this process is 1.0 h or 60 min, that may be considered as the residence time. Obviously, by augmenting the water removal capacity of the evaporator, the operation time will decrease.

For the evaluation of the capacity, a $T_{base} = 0°C$ and existing data from thermodynamic tables for water (Cengel and Boles, 2006) and computer programs (Vélez-Ruiz and Soriano-Morales 2003). The needed data for the energy balance are: for the evaporated water (sat. vapor at 75°C): 2634.6 kJ/kg; Cp = 3.27 for feeding and 2.22 kJ/kg°C for the concentrate, and for the vapor (condensation heat, for saturated steam at 120°C): 2202.1 kJ/kg.
Liquor:

$$Q + \left(18{,}000\,\frac{kg}{h}\right)\left(3.27\,\frac{kJ}{kg}\right)(25-0)°C = \left(12000\,\frac{kg}{h}\right)\left(2364.6\,\frac{kJ}{kg}\right) + \left(6000\,\frac{kg}{h}\right)\left(2.22\,\frac{kJ}{kg}\right)(75-0)°C$$

$$Q = 27{,}902{,}700\,\frac{kJ}{h}$$

Vapor:
$w_v\Delta h_V = W_C\Delta h_C + Q \quad \therefore Q = W_V(\Delta h_V - \Delta h_C)$, *and* $w_v = w_c$

$$w_V = \frac{Q}{\Delta h_V} = \frac{27{,}902{,}700\,\frac{kJ}{h}}{2202.1\,\frac{kJ}{kg}} = 12{,}670.95\,\frac{kg}{h} \rightarrow \text{that is the consumption.}$$

$$\text{Economy} = \frac{\text{Capacity}}{\text{Consumption}} = \frac{12{,}000\,\frac{kg}{h}}{12{,}670.95\,\frac{kg}{h}} = 0.95$$

Conclusion: From the developed balances, it can be summarized that, for the concentration of 18,000 kg/h of orange juice from 24% to 72% (by weight) at 25°C, the evaporator unit needs to evaporate 12,000 kg/h of water to produce *6000 kg/h of concentrate*. This evaporation unit implies a supply of *12,671 kg/h of steam* at 120°C.

EXAMPLE 12.2 ONE EFFECT WITH BPE

A concentrate *tamarindo solution* (18%) will be concentrated by evaporation to reach 36% w/w of concentration. The solution is fed at a rate of 30,000 kg/h and

18°C that will be concentrated by utilizing saturated steam at 125 kPa. Consider that the evaporation unit will work at 24 in Hg of vacuum and an overall heat transfer coefficient of 2050 W/m^{2}K may be assumed. Estimate the needed requirements of this process in order to buy the equipment.

Comment: This liquid food is not very much consumed; it is utilized in some cultures as a beverage. The idea is to evaluate the capacity (rate of evaporated water), the consumption (rate of needed vapor), the economy (ratio between the capacity and the consumption), and the needed heat transfer area, as well as the number of tubes just by application of balances and heat transfer fundamentals.

Solution

1. Mass balance

   Global: $30{,}000 + W_V = W_E + W_P + W_C$

   Liquor: $30{,}000 = W_E + W_P$

   Solids:

   $$(0.18)\left(30{,}000\ \frac{\text{kg}}{\text{h}}\right) = W_E(0) + W_P(0.36) \quad \therefore W_P = 15{,}000\left(\frac{\text{kg}}{\text{h}}\right)(\text{product})$$

   From the liquor balance: $W_E = 30{,}000 - 15{,}000\ \frac{\text{kg}}{\text{h}} = 15{,}000\ \frac{\text{kg}}{\text{h}}$

   Therefore, the quantity of sugar concentrate is *15,000 kg/h*, and the capacity of the evaporation systems is *15,000 kg/h*. The concentrate represents a double of the initial concentration.
2. Boiling point rise (BPR)
   Knowing that with this vacuum (24 in Hg for an atmospheric pressure of 29.92), implies an absolute pressure of 5.92 in Hg (20 kPa), and a boiling point for water of 60°C. Taking as reference Figure 12.9 to estimate the BPR, the approximate boiling point for the concentrate is 63°C (placed between the second and third lines); in this case *a BPR of 3°C* is taken.
3. Energy balance
   For a $T_{base} = 0$°C and existing data from thermodynamic tables for water (Cengel and Boles, 2006) and computer programs (Vélez-Ruiz and Soriano-Morales, 2003). The needed data for the energy balance are: for the evaporated water (sat. vapor at 63°C): 2459.8 kJ/kg; Cp = 3.81 for feeding (18°Bx) and 3.60 kJ/kg°C for concentrate (36°Bx), and for the vapor (condensation heat, for saturated steam at 125 kPa or 106°C): 2240.6 kJ/kg.
   Liquor:

   $$Q + \left(30{,}000\ \frac{\text{kg}}{\text{h}}\right)\left(3.81\ \frac{\text{kJ}}{\text{kg}}\right)(18 - 0)°\text{C} = \left(15{,}000\ \frac{\text{kg}}{\text{h}}\right)\left(2459.8\ \frac{\text{kJ}}{\text{kg}}\right) + \left(15{,}000\ \frac{\text{kg}}{\text{h}}\right)\left(3.60\ \frac{\text{kJ}}{\text{kg}}\right)(63 - 0)°\text{C}$$

$$Q = 38,241,600\,\frac{kJ}{h}$$

Vapor:
$W_V\Delta h_V = W_C\Delta h_C + Q \quad \therefore Q = W_V(\Delta h_V - \Delta h_C)$

$$W_v = \frac{Q}{\Delta h_v} = \frac{38,241,600\,\frac{kJ}{h}}{2240.6\,\frac{kJ}{kg}} = 17,067.57\,\frac{kg}{h}$$ that is the *consumption*

$$\text{Economy} = \frac{\text{Capacity}}{\text{Consumption}} = \frac{15,000\,\frac{kg}{h}}{17,067.57\,\frac{kg}{h}} = 0.88$$

The BPR consideration and the different operation conditions determine an important difference between the economies of examples 12.1 and 12.2.

4. Heat transfer area
With the existing information, the last and important step is the evaluation of the needed area for the heating-evaporation process and equipment design.

$$A = \frac{Q}{U\Delta T} \rightarrow \textit{the driven force is: } T_{\text{Vapor}} - T_{\text{boiling}} = (106 - 63)°C$$

$$A = \frac{\left(38,241,600\,\frac{kJ}{h}\right)\left(\frac{1000\,J}{1kJ}\right)}{\left(2050\,\frac{w}{m^2k}\right)\left[\frac{1\,\frac{J}{s}}{1w}\right]\left(\frac{3600s}{1h}\right)(43K)} = 120.507\ m^2$$

The required heating area is small due to a small quantity of feeding and the high difference for the driving force between the saturated vapor (106°C) and the boiling point of the concentrate (63°C).

Finally, the heat transfer area is given by tubes of 1.5 in. and 12 ft long; the next consideration is:

$$A_{\text{tube}} = 3.1416 \times \left(1.9\,\text{in}\,\frac{0.0254\,m}{1\,in}\right)\left(12\,\text{ft}\,\frac{0.305\,m}{1\,ft}\right) = 0.555\,\frac{m^2}{\text{tube}}$$

$$\text{Number of tubes} = \frac{120.51 m^2}{0.555\ m^2/\text{tube}} = 218\ \text{tubes}$$

Conclusion: From the developed equations, it can be summarized that, for the concentration of 30,000 kg/h of tamarindo concentrate from 18% to 36% (by weight) at 18°C, the evaporator unit needs to evaporate 15,000 kg/h of water to

produce *15,000 kg/h of concentrate*. This evaporation unit implies a supply of *17,068 kg/h of steam* at 106°C and a heat transfer area of 120.51 m^2.

EXAMPLE 12.3 ONE EFFECT, WITH BPE AND USE OF ENTHALPY–CONCENTRATION TABLES

A single evaporation unit is to be designed to concentrate 36,000 kg/h with 9% (by weight) of a *sodium hydroxide solution*. The dilute solution at 39°C is to be fed to an evaporator to be concentrated up to 45% by utilizing saturated steam at 100°C. On the basis of an overall heat transfer coefficient of 1200 W/m^2K and an operation pressure of 13.5 kPa that is kept inside the equipment, determine the design parameters.

Comment: This liquid was selected due to knowing its Dühring diagram. The design parameters include the capacity, the consumption, the economy, and the heat transfer area.

Solution

1. Mass balance

   Global: $36{,}000 + W_V = W_E + W_P + W_C$

   Liquor: $18{,}000 = W_E + W_P$

   Solids:

$$(0.09)\left(36{,}000\ \frac{\text{kg}}{\text{h}}\right) = W_E(0) + W_P(0.45) \quad \therefore W_P = 7200\left(\frac{\text{kg}}{\text{h}}\right)(\text{product})$$

   From the liquor balance: $W_E = 36{,}000 - 7200\frac{\text{kg}}{\text{h}} = 28{,}800\frac{\text{kg}}{\text{h}}$

   Therefore, the quantity of concentrated product is *7200 kg/h*, and the capacity of the evaporation systems is *28,800 kg/h*. The concentrate represents 1/4 of the capacity.

2. Boiling point rise (BPR)
   Using data for water (P = 13.5 kPa), it corresponds to a saturation temperature of 51.5°C (by interpolation), based on thermodynamic tables (Cengel and Boles, 2006). On the other side, NaOH solution at 45% has a boiling point (from the Dühring diagram) of ~85.5°C (Brown et al., 1965; McCabe et al, 2008); thus,

$$BPR = T_{bsol} - T_{bwater} \rightarrow T_{bsol} = 85.5°C; \quad T_{bwater} = 51.5°C$$
$$\therefore BPR = 85.5 - 51.5°C = 34°C$$

3. Energy balance
   Taking a $T_{base} = 0$°C and using enthalpy–concentration diagrams or tables for NaOH (Brown et al., 1965; McCabe et al, 2008) and thermodynamic tables for water (Cengel and Boles, 2006). Being the needed data for the energy balance: Δh, for NaOH 9% at 39°C: 151 kJ/kg; for the evaporated water (sat. vapor at 85.5°C): 2652 kJ/kg; for NaOH 45% at 85.5°C: 441 kJ/

kg; and for the vapor (condensation heat, for saturated steam at 100°C): 2256.4 kJ/kg.
Liquor:

$$Q + \left(36{,}000\ \frac{\text{kg}}{\text{h}}\right)\left(151\frac{\text{kJ}}{\text{kg}}\right) = \left(28{,}800\ \frac{\text{kg}}{\text{h}}\right)\left(2652\ \frac{\text{kJ}}{\text{kg}}\right) + \left(7200\ \frac{\text{kg}}{\text{h}}\right)\left(441\ \frac{\text{kJ}}{\text{kg}}\right)$$

$$Q = 74{,}116{,}800\ \frac{\text{kJ}}{\text{h}}$$

Vapor:
$W_V \Delta h_V = W_C \Delta h_C + Q \quad \therefore Q = W_V(\Delta h_V - \Delta h_C)$

$$W_V = \frac{Q}{\Delta h_V} = \frac{74{,}116{,}800\ \frac{\text{kJ}}{\text{h}}}{2256.4\ \frac{\text{kJ}}{\text{kg}}} = 32847.37\ \frac{\text{kg}}{\text{h}} \quad \text{that is the consumption}$$

$$\text{Economy} = \frac{\text{Capacity}}{\text{Consumption}} = \frac{28{,}800\ \frac{\text{kg}}{\text{h}}}{32{,}847.37\ \frac{\text{kg}}{\text{h}}} = 0.877$$

4. Heat transfer area
With the existing information, the last and very important step is the evaluation of the required area for the heating-evaporation process and equipment design.
$A = \dfrac{Q}{U\Delta T}$ where the driving force is: $T_{vapor} - T_{boiling} = (100 - 85.5)°C$

$$A = \frac{\left(74{,}116{,}800\ \frac{\text{kJ}}{\text{h}}\right)\left(\frac{1000\ \text{J}}{1\text{kJ}}\right)}{\left(1200\ \frac{\text{W}}{\text{m}^2\text{k}}\right)\left(\frac{1\frac{\text{J}}{\text{s}}}{1\text{W}}\right)\left(\frac{3600s}{1\text{h}}\right)(14.5\ \text{K})} = 1183.22\ \text{m}^2$$

The required heating area is big due to three main aspects: the first is a big quantity of feeding; second, a low feeding temperature; and third, the small difference or a few degrees for the driving force as a consequence of the boiling point elevation.

Conclusion: From the developed calculations, it can be summarized that, for the concentration of 36,000 kg/h of NaOH solution from 9% to 45% (by weight) at 39°C, the evaporator unit needs to evaporate 28,800 kg/h of water to produce *7200 kg/h of concentrate*. This evaporation unit implies a *heating area of 1183.22 m²* and a supply of *32,847.4 kg/h of saturated steam* at 100°C.

EXAMPLE 12.4 DOUBLE EFFECT WITHOUT BPE, FORWARD ARRANGEMENT

A double effect in forward arrangement should be designed to concentrate 75,000 lb/h at 135°F of *fluid milk* from 12% to 45% of solids. Steam at 212°F is available for this process, and knowing that a temperature of 141°F will be kept in the second evaporator, as well as $U_1 = 450$ and $U_2 = 300$ BTU/h ft²°F may be supposed. The Cp may be estimated by Cp = 1 – 0.54SC in BTU/lb°F.

Comment: This example has been selected to include two additional aspects that are not considered in the rest of the examples, first to handle English units and, secondly, to take the boiling points as the reference temperatures instead of 32°F.

Solution

Taking as reference the parameters included in Figures 12.5 and 12.8, with W_F in the first effect and W_P from the third, the algorithm for multiple effect evaporation is followed.

1. Mass balance
   Liquor mass balances: $W_F = W_{E1} + W_{C2} + W_P$

   Solids: $75{,}000\,\frac{\text{lb}}{\text{h}}(0.12) = W_P(0.45) \quad \therefore W_P = 20{,}000\,\frac{\text{lb}}{\text{h}}$

   Capacity: $W_{E1} + W_{E2} = 75{,}000 - 20{,}000 = 55{,}000\,\frac{\text{lb}}{\text{h}}$ (1)

2. Energy balances (BPE = 0)
   To proceed with the energy balances on the three effects, and knowing the boiling point of water at 141°F, Tn must be assumed with an overall ΔT = (212 – 141)°F = 71°F = $\Delta T_1 + \Delta T_2$, and following the aforementioned steps, in which the boiling point assumption of the first evaporator is based on equal heat transfer surfaces:

   $$Q_1 = Q_2 \quad \therefore U_1A_1\Delta T_1 = U_2A_2\Delta T_2 \rightarrow \text{If} \bullet A_1 = A_2$$

   $$U_1\Delta T_1 = U_1\Delta T_2 \quad \therefore \Delta T_2 = \frac{450\,\frac{\text{BTU}}{\text{hft}^2\,°\text{F}}}{300\,\frac{\text{w}}{\text{m}^2\text{k}}}\Delta T_1 = 1.50\Delta T_1;$$

   and

   $$\Delta T_1 + 1.50\Delta T_1 = \Delta T = 71°\text{F}$$

   $$\therefore \Delta T_1 = 28.40 \quad \text{and} \quad \rightarrow \Delta T_2 = 42.60°\text{F}$$

   With this information, the boiling point corresponding to the first effect becomes: $\Delta T_1 = 212 - T_1 = 28.4$, thus $T_1 = 183.6$°F; and $T_2 = 141$°F (= 183.6 – 42.6)°F, which correspond to a $P = 2.895$ psia (lb_f/in^2 absolute).

Therefore, for the energy balances, taking as T_{base} the boiling temperature at each effect, assuming the Cp for the flow to each effect are 0.9352 for 12% and 0.8458 BTU/lb°F for 28%, respectively, and considering the aforementioned assumptions (Sections 12.3.5 and 12.3.6).

First effect balances (T base = 183.6°F, then h for the concentrated solution = 0 and h_{fg} is the heat for the phase change):

$$W_F = W_{E1} + W_{S1}; \quad W_V = W_{C1}$$

$$W_F \Delta h_F + Q_1 = W_{E1} \Delta h_{E1} + W_{S1} \Delta h_{S1} \Leftrightarrow Q_1 = W_V (h_V - h_S) = W_V h_{fg}$$

$$Q_1 = 988.0 \frac{\text{BTU}}{\text{lb}} W_{E1} + \left(75{,}000 \frac{\text{lb}}{\text{h}}\right)\left(0.9352 \frac{\text{BTU}}{\text{lb°F}}\right)(135.0 - 183.6)°\text{C} = W_V \left(970.3 \frac{\text{BTU}}{\text{lb}}\right)$$

$$\therefore 970.3 W_V = 988.0 W_{E1} - 3{,}408{,}804 \rightarrow (2)$$

Both mass flows (W_v and W_{E1}) are in lb/h, while the Q_1 is in BTU/h.

Second effect balances (T base = 141°F, then h for the product = 0 and h_{fg} is the heat for the phase change, as in the previous evaporator, but at different temperatures):

$$W_{S1} = W_{E2} + W_P; \quad W_{E1} = W_{C2}$$

$$W_{S1} \Delta h_{S1} + Q_2 = W_{E2} \Delta h_{E2} + W_P \Delta h_P$$

$$Q_2 = 1014.1 \frac{\text{BTU}}{\text{lb}} W_{E2} - W_{S1}\left(0.8488 \frac{\text{BTU}}{\text{lb°F}}\right)(183.6 - 141.0)°\text{F} = W_{E1}\left(988 \frac{\text{BTU}}{\text{lb}}\right)$$

$$\therefore 988\, W_{E1} = 1014.1 W_{E2} - 36.16\, W_{S1} \rightarrow (3)$$

The three mass flows (W_{E1}, W_{E1}, and W_P) are in lb/h, while the Q_2 is in BTU/h.

Analyzing the previous Equations 2 and 3 there are four unknowns (W_V, W_{E1}, W_{S1}, and W_{E2}), that may be solved by considering the mass balances (Equation 1), and the capacity, generating the next set of equations:

$$W_{S1} = 20{,}000 + W_{E2}$$

$$75{,}000 = W_{S1} + W_{E1}$$

$$W_{E1} + W_{E2} = 55{,}000 \quad \therefore W_{E2} = 55{,}000 - W_{E1}$$

Now, including the same two unknowns in Equation 3 and solving them simultaneously:

$$988 W_{E1} = 1041.1 W_{E2} - 36.16\,(20{,}000 + W_{E2})$$

$$988 W_{E1} = 1050.26 W_{E2} + 723{,}200)$$

$$988 W_{E1} = 1050.26\,(55{,}000 - W_{E1}) + 723{,}200$$

$$2038.26 W_{E1} = 58{,}487{,}500$$

$$\therefore W_{E1} = 28{,}694.82 \frac{\text{lb}}{\text{h}} \quad \therefore W_{E2} = 26{,}305.18 \frac{\text{lb}}{\text{h}}$$

Finally, by substitution of W_{E1} the other two relationships:

$$W_{S1} = 75{,}000 - 28{,}694.82 = 20{,}000 + 26{,}305.18 = 46{,}305.18\ \frac{\text{lb}}{\text{h}}$$

$$970.3W_V = 988\,(28{,}694.82) + 348{,}804 \rightarrow W_V = 29{,}577.75\ \frac{\text{lb}}{\text{h(needed)}}$$

$$\text{Economy (1)} = \frac{28{,}694.82}{29{,}577.75} = 0.97 \rightarrow \text{Economy (2)} = \frac{26{,}305.18}{28{,}694.81} = 0.92$$

3. Heat transfer area
   The heating surface for each evaporation unit is computed below:

$$A_1 = \frac{\left(970.3\ \frac{\text{BTU}}{\text{lb}}\right)\left(29{,}577.75\ \frac{\text{lb}}{\text{h}}\right)}{\left(450\ \frac{\text{BTU}}{\text{hft}^2\,°\text{F}}\right)(212 - 183.6)°\text{F}} = 2245.64\ \text{ft}^2$$

$$A_2 = \frac{\left(988.0\ \frac{\text{BTU}}{\text{lb}}\right)\left(28{,}694.82\ \frac{\text{lb}}{\text{h}}\right)}{\left(300\ \frac{\text{BTU}}{\text{hft}^2\,°\text{F}}\right)(183.6 - 141)°\text{F}} = 2218.35\ \text{ft}^2$$

These heat transfer areas are very similar, they do not differ more than 1% with respect to the mean area of 2233.5 ft^2, and they are not different by more than 2%; therefore, it is not necessary to complete a second iteration.

Conclusion: With these data, the results are: *consumption* (W_V) = *29,578 lb/h*; *overall economy* (55,000/29,577.75) = *1.86*; evaporated water by effect: W_{E1} = *28,694.82*, W_{E2} = *26,305.18*; and heat transfer areas: A_1 = *2246*, A_2 = *2218 m*^{2}.

EXAMPLE 12.5 TRIPLE-EFFECT BACKWARD ARRANGEMENT, WITHOUT BPE

It is desired to design a triple-effect evaporation system to concentrate the solids of *tomato juice* from 6% to 51%. The feed flow is 30,000 kg/h entering the third effect at 24°C by means of forced convection and saturated steam at 115°C is available for heating requirements of the first unit. Considering that the third effect is to be operated to a vacuum pressure of 4 in Hg, and overall heat transfer coefficients of 1800, 1650, and 1500 W/m^{2}K are expected, determine the design parameters for this backward triple evaporator, neglecting the BPR.

Solution

Taking as reference the parameters included in Figure 12.5, with w_F fed to the third effect and W_P coming from the first, the algorithm for multiple effect evaporation is followed.

1. Mass balance
   Liquor mass balances:

$$W_F = W_{E3} + W_{C3} + W_{C2} + W_P \rightarrow (1)$$

Solids:

$$30{,}000\,\frac{\text{kg}}{\text{h}}(0.06) = W_P(0.51) \quad \therefore W_P = 3529.41\frac{\text{kg}}{\text{h}}$$

$$\text{Capacity} = W_{E1} + W_{E2} + W_{E3} = 30{,}000 - 3529.41 = 26{,}470.59\,\frac{\text{kg}}{\text{h}}$$

2. Boiling temperatures and energy balances
To proceed with the energy balances on the three effects, and knowing the boiling point of water (at 4 in Hg) is 53°C; Tn must be assumed with an overall $\Delta T = (115 - 53)°\text{C} = 62°\text{C} = \Delta T_1 + \Delta T_2 + \Delta T_3$, and following the aforementioned steps (previous examples). Thus, the boiling point assumption based on equal heat transfer surfaces:

$$Q_1 = Q_2 = Q_3 \quad \therefore U_1A_1\Delta T_1 = U_2A_2\Delta T_2 = U_3A_3\Delta T_3$$

$$U_1\Delta T_1 = U_2\Delta T_2 = U_3\Delta T_3 \quad \therefore \Delta T_2 = \frac{1800\,\frac{\text{W}}{\text{m}^2\text{K}}}{1650\,\frac{\text{W}}{\text{m}^2\text{K}}}\Delta T_1 = 1.091\Delta T_1;$$

and

$$\rightarrow \Delta T_3 = 1.20\Delta T_1 \quad \therefore \Delta T_1 + 1.09\Delta T_1 + 1.20\Delta T_1 = \Delta T = 62°\text{C}$$

$$\Delta T_1 = 18.84°\text{C} \rightarrow 18.8°\text{C}; \quad \Delta T_2 = 20.55 \rightarrow 20.6°\text{C}; \quad \Delta T_3 = 22.61 \rightarrow 22.6°\text{C}$$

The boiling point corresponding to each effect becomes: $\Delta T_1 = 115 - T_1$; thus $T_1 = 96.2°\text{C}$; $\Delta T_2 = 96.2 - T_2$; thus $T_2 = 75.6°\text{C}$; and $\Delta T_2 = 75.6 - T_3$; thus $T_3 = 53°\text{C}$.

Therefore, the energy balances taking as T_{base} the boiling temperature at each effect (similar to Example 12.4), assuming the Cp for the flows to each effect are 3.99, 3.66, and 3.33 kJ/kg°C, respectively, and considering the same assumptions:

First effect balances:

$$W_{S2} = W_{E1} + W_P; \quad W_V = W_{C1} \rightarrow (2)$$

$$W_{S2}\Delta h_{S2} + Q_1 = W_{E1}\Delta h_{E1} + W_P\Delta h_P \rightarrow (3)$$

$$Q_1 = 2271\,\frac{\text{kJ}}{\text{kg}}W_{E1} - W_{S2}\left(3.33\,\frac{\text{kJ}}{\text{kg°C}}\right)(75.6 - 96.2)°\text{C} = W_V\left(2216\,\frac{\text{kJ}}{\text{kg}}\right)$$

$$\therefore 2216W_V = 2271W_{E1} + 68.598W_{S2} \rightarrow (3^*)$$

Second effect balances:

$$W_{S3} = W_{E2} + W_{S2}; \quad W_{E1} = W_{C2} \rightarrow (4)$$

$$W_{S3}\Delta h_{S3} + Q_2 = W_{E2}\Delta h_{E2} + W_{S2}\Delta h_{S2} \rightarrow (5)$$

$$Q_2 = 2320.6\,\frac{\text{kJ}}{\text{kg}}W_{E2} - W_{S3}\left(3.66\,\frac{\text{kJ}}{\text{kg°C}}\right)(53.0 - 75.6)°\text{C} = W_{E1}\left(2271\,\frac{\text{kJ}}{\text{kg}}\right)$$

$$\therefore\ 2271W_{E1} = 2320.6W_{E2} + 82.716W_{S3} \rightarrow (5^*)$$

Third effect balances:

$$W_F = W_{E3} + W_{S3};\quad W_{E2} = W_{C3} \rightarrow (6)$$

$$W_F\Delta h_F + Q_3 = W_{E3}\Delta h_{E3} + W_{S3}\Delta h_{S3} \rightarrow (7)$$

$$Q_3 = 2375\,\frac{\text{kJ}}{\text{kg}}W_{E3} - W_F\left(3.99\,\frac{\text{kJ}}{\text{kg°C}}\right)(24 - 53)°\text{C} = W_{E2}\left(2320.6\,\frac{\text{kJ}}{\text{kg}}\right)$$

$$\therefore\ 2320.6W_{E2} = 2375W_{E3} + 3,471,300\,\frac{\text{kJ}}{\text{h}} \rightarrow (7^*)$$

Analyzing Equations 3*, 5*, and 7*, there are six unknowns (W_v, W_{E1}, W_{S2}, W_{E2}, W_{S3}, and W_{E3}) that may be solved by considering the mass balances (Equations 2, 4, and 6), generating the next set of equations:

From the capacity, and Equations 6 and 5*:

$$W_{E1} = 26,470.59 - W_{E2} - W_{E3}$$

$$W_{S3} = 30,000 - W_{E3}$$

$$2271(26,470.59 - W_{E2} - W_{E3}) = 2320.6W_{E2} + 82.72(30,000 - W_{E3})$$

$$W_{E3} = 26,337.17 - 2.09827W_{E2} \rightarrow (8)$$

Now, Equations 7* and 8 include the same two unknowns, solving them simultaneously:

$$2320.6W_{E2} = 2375(26,337.17 - 2.098W_{E2}) + 3,471,300$$

$$W_{E2} = 9039.18\,\frac{\text{kg}}{\text{h}}\quad \therefore\ \text{Equation 8} \rightarrow W_{E3} = 7370.53\,\frac{\text{kg}}{\text{h}}$$

$$\text{and substituting in capacity} \rightarrow W_{E1} = 10,060.88\,\frac{\text{kg}}{\text{h}}$$

Finally, by substitution of W_{E1} and W_{S2} (Equation 2: 3429.41 + 10,060.889) kg/h in Equation 3*:

$$2216W_V = 227(10,060.88) + 68.6(13,490.3) \rightarrow W_V = 10,728.2\,\frac{\text{kg}}{\text{h}}$$

3. Heat transfer area
   The heating surface for each evaporation unit is computed below:

$$A_1 = \frac{\left(2216\,\frac{kJ}{kg}\right)\left(10728.2\,\frac{kg}{h}\right)}{\left(1800\,\frac{W}{m^2°C}\right)(115-96.2)°C} = 702.35\,\frac{kJm^2}{Wh}\left(\frac{10^3W}{1kJ}\right)\left(\frac{1h}{3600\,s}\right) = 195.1m^2$$

$$A_2 = \frac{\left(2271\,\frac{kJ}{kg}\right)\left(10060.88\,\frac{kg}{h}\right)}{\left(1650\,\frac{W}{m^2°C}\right)(96.2-75.6)°C(3.6)} = 186.7m^2 \quad A_3 = \frac{2320.6\times 9039.18}{1500\times 22.6\times 3.6} = 171.9\,m^2$$

(iv) Second iteration
In order to get a better accuracy, and even though there exists a small difference between areas (<15%), a second iteration may be completed. It should start from the evaluation of the mean area and, lately, the new difference of temperatures is re-evaluated in the following way:

$$A_m = \frac{(195.1m^2)(18.8°C) + (186.7\,m^2)(20.6°C) + (171.9\,m^2)(22.6°C)}{62°C} = 183.85\,m^2$$

$$\Delta T_{12} = \frac{18.8\times 195.1}{183.85} = 20;\ \Delta T_{22} = \frac{20.6\times 186.7}{183.85} = 20.9;\ \Delta T_{32} = \frac{22.6\times 171.9}{183.85} = 21.1°C$$

Now the boiling temperatures would be modified to 95, 74.1, and 53°C, respectively. As can be observed, only there is a modification on T_1 and T_2.

Conclusion: With these new boiling temperatures, the balances suffer some minor changes. After following the same methodology and solving the equations, it will generate closer and accurate heating surfaces for the three effects with minimal differences between them. Therefore, after the second iteration, the final results are: *consumption* (W_v) = *10,676.33 kg/h; economy* (26,470.59/10,676.33) = *2.48*; evaporated water by effect: W_{E1} = *10,026.41*, W_{E2} = *9052.37*, and W_{E3} = *7391.81 kg/h*; and heat transfer areas: A_1 = *182.6*, A_2 = *183.3*, and A_3 = *184.5* m^2.

Comment: The required heating area is small in comparison to the first example due to a smaller feeding flow and to neglect the boiling point elevation. Comparing the first and the second iteration, there are small adjustments on the solved balances that led to a more accurate solution, taking the heating area as the decision criterion.

12.6 FINAL COMMENTS

Even though industrial applications of evaporation have many years, there are several engineering aspects that have been studied in a limited way. It is very important to apply the fundamental knowledge of this food processing operation at the different sectors of the food industry. The requirements of energy for evaporation are very important (one to five percentage of the total energy of a country). Therefore, it is

remarkable from the ecological and economical viewpoints that evaporators operate at their optimum capacity and efficiency.

Evaporation of food items has been used and researched satisfactorily, but engineering information, covering aspects such as the boiling point elevation, physical properties, and heat transfer coefficients, is still very limited. Only a few scientific works were found on these aspects, with the exception of rheology on which more information is now available.

Information on this important food processing operation has been collected in this chapter to describe different parts of it. Fundamentals of the unit operation, some typical food items, experimental information of researching works, as well as examples of application and a variety of references, have been compiled with the objective of illustrating and helping the different sectors of food science, such as students, food industrial workers, and investigators.

For students it is very important to understand that although there are, and will be, more computer tools, it is fundamental to know the basic principles of food processing operations in order to get the right engineering design. Sometimes the tools are not well applied due to a "hole" in the knowledge, and even without sophisticated computers, the basic calculations can be completed if knowledge of the correct terms are involved.

REFERENCES

Abichandani, H. and Sarma, S.C. 1991. Evaporation in a horizontal thin film scraped surface heat exchanger. *Journal of Food Process Engineering*, 14: 173–187.

Akbulut, M., Coklar, H., and Ozen, G. 2008. Rheological characteristics of *Juniperus drupacea* fruit juice (pekmez) concentrated by boiling. *Food Science and Technology International*, 14(4): 321–328.

APV. 2003. *Evaporator Handbook. Commercial Brochure*. APV Company, New York.

Barbana, Ch. and El-Omri, A. 2012. Viscometric behavior of reconstituted tomato concentrate. *Food and Bioprocess Technology*, 5: 209–215.

Bayindirli, L. 1992. Mathematical analysis of variation of density and viscosity of apple juice with temperature and concentration. *Journal of Food Processing and Preservation*, 16: 23–28.

Bayindirli, L. 1993. Density and viscosity of grape juice as a function of concentration and temperature. *Journal of Food Processing and Preservation*, 17: 147–151.

Benne, M., Grondin-Pérez, B., Chabriat, J.P., and Hervé, P. 2000. Artififcial neural networks for modeling and predictive control of an industrial evaporation process. *Journal of Food Engineering*, 46 (4): 227–234.

Borgstrom, G. 1969. *Principles of Food Science*. The Macmillan Company, USA.

Bourgois, J. and LeMaguer, M. 1987. Heat transfer correlation for upward liquid heat transfer with phase change: Applications in the optimization and design of evaporators. *Journal of Food Engineering*, 6: 291–300.

Bouman, S., Waalewijn, R., De Jong, P., and Van der Linden, H.J.L.J. 1993. Design of falling–film evaporators in the dairy industry. *Journal of the Society of Dairy Technology*, 46(3): 100–106.

Brown, G.G., Foust, A.S., Katz, D.L., Schneidewind, R., White, R.R., Wood, W.P., Brown G.M. et al. 1965. Operaciones Básicas en la Ingeniería Química. Ed. Marín, Spain. pp. 499–517.

Cadet, C., Touré, Y., Gilles, G., and Chabriat, J.P. 1999. Knowledge and nonlinear predictive control of evaporators in cane sugar production plants. *Journal of Food Engineering*, 40: 59–70.

Camiro-Cabrera, M., Torres-Pacheco, R.A., Enriquez-Fernandez, B.E., Vélez-Ruiz, J.F., and Sosa-Morales, M.E. 2007. Physical properties of concentrated mango and orange juices (008-23). *IFT Annual Meeting*, Chicago, IL, USA.

Cengel, Y.A. and Boles, M.A. 2006. *Thermodynamics. An Engineering Approach*. McGraw-Hill, Singapore.

Cepeda, E. and Villarán, M.C. 1999. Density and viscosity of *Malus florinda* juice as a function of concentration and temperature. *Journal of Food Engineering*, 41: 103–107.

Chawankul, N., Chuaprasert, S., Douglas, P., and Luewisutthichat, W. 2001. Simulation of an agitated thin film evaporator for concentrating orange juice using AspenPlus™. *Journal of Food Engineering*, 47: 247–253.

Chen, C.S., Lima, V.M., and Marsaioli, A. 1979. A heat transfer correlation for rotary steam-coil vacuum evaporation of tomato paste. *Journal of Food Science*, 44(1): 200–203.

Chirife, J., Sansiñena, M., Galmarini, M.V., and Zamora, M.C. 2011. Physicochemical changes and sensory characterization of a balsamic vinegar dressing at different Brix. *Food and Bioprocess Technology*, 4: 1505–1511.

Choi, Y. and Okos, M.R. 1983. The thermal properties of tomato juice concentrates. *Transactions of the ASAE*, 26(1): 305–311.

Choi, Y.J., Milczarek, R.R., Fleck, C.E., Garvey, T.C., McCarthy, K.L., and McCarthy, M.J. 2006. In-line monitoring of tomato concentrate physical properties during evaporation. *Journal of Food Process Engineering*, 29: 615–632.

Chuaprasert, S., Douglas, P., and Nguyen, M. 1999. Data reconciliation of an agitated thin film evaporator using Aspen plus. *Journal of Food Engineering*, 39: 261–267.

Crandal, P.G., Chen, C.S., and Davis, K.C. 1987. Preparation and storage of 72°Bx orange juice concentrate. *Journal of Food Science*, 52(2): 381–385.

Crapiste, G.H. and Lozano, J.E. 1988. Effect of concentration and pressure on the boiling point rise of apple juice and related sugar solutions. *Journal of Food Science*, 53(3): 865–868.

Dak, M., Verma, R.C., and Jaaffrey, S.N.A. 2007. Effect of temperature and concentration on rheological properties of "Kesar" mango juice. *Journal of Food Engineering*, 80: 1011–1015.

Dodeja, A.K., Sarma, S.C., and Abichandani, H. 1990. Heat transfer during evaporation of milk to high solids in thin film scraped surface heat exchanger. *Journal of Food Process Engineering*, 12: 211–225.

Enríquez-Fernández, B.E., Camarillo-Rojas, C.R., and Vélez-Ruiz, J.F. 2013. Influence of reconstituted milk properties on spray dried milk and parameters design. *Journal of Food Process Engineering*, 36 (1): 87–94.

Enríquez-Fernández, B.E., Camarillo-Rojas, C.R., and Vélez-Ruiz, J.F. 2011. Influence of reconstituted milk properties on spray dried milk and parameters design. *Journal of Food Process Engineering*, 36: 87–94.

Ferreira, R.C, da Costa, R., Sant, T., de Sousa, A. Martins, C., Teixeira, M.F., and de Souza, S. 2009. Thermophysical properties of carshew juice at different concentrations and temperatures. *Revista Brasileira de Produtos Agroindustriais. Camplina Grande*, 11(1): 35–42.

FT Industrial. 2004. *Centritherm. Commercial Brochure*. FT Industrial Company, Australia.

Giner, J., Ibarz, A., Garza, S., and Xhian-Quan, S. 1997. Rheology of clarified cherry juices. *Journal of Food Engineering*, 30: 147–154.

Hall, C.W. and Hedrick, T.I. 1971. *Drying of Milk and Milk Products*. The AVI Pub. Co. Westport, CT, USA. pp. 17–46.

Hartel, R.W. 1992. Evaporation and Freeze Concentration. In *Handbook of Food Engineering* (D.R. Heldman and D.B. Lund, Eds). Marcel Dekker, Inc. New York, NY, USA.

Hernandez, E., Chen, C.S., Johnson, J., and Carter, R.D. 1995. Viscosity changes in orange juice after ultrafiltration and evaporation. *Journal of Food Engineering*, 25: 387–396.

Hobani, A.I. 1998. Rheological behavior of date concentrates. *Journal of Food Engineering*, 36: 349–357.

Hoffman, P. 2004. Plate evaporators in food industry-theory and practice. *Journal of Food Engineering*, 61: 515–520.

Holland, C.D. 1975. Evaporation. In *Fundamentals and Modeling of Separation,* C.D. Holland (ed). Prentice-Hall, Englewood Cliffs, NJ, USA. pp. 5–42.

Hui, Y.H. 2006. *Handbook of Fruits and Fruit Processing*. Blackwell Publishing, Ames Iowa, USA.

Ibarz, A. and Barbosa-Cánovas, G.V. 2003. *Unit Operations in Food Engineering*. CRC Press, Boca Raton, FL, USA. pp. 625–670.

Ilangantileke, S.G., Ruba, A.B., and Joglekar, H.A. 1991. Boiling point rise of concentrated Thai tangerine juices. *Journal of Food Engineering*, 15: 235–243.

Jebson, R.S. and Iyer, M. 1991. Performances of falling film evaporators. *Journal Dairy Research*, 58: 29–38.

Jemqvist, A., Jemqvist, M., and Aly, G. 2001. Simulation of thermal desalinisation process. *Desalinisation*, 134(1–3): 187–193.

Karlsson, H.O.E. and Trägardh, G. 1998. Aroma recovery during beverage processing. *Journal of Food Engineering*, 34: 159–178.

Kaya, A. and Sözer, N. 2005. Rheological behavior of sour pomegranate juice concentrates (*Punica granatum* L.). *International Journal of Food Science and Technology*, 40: 223–227.

Kessler, H.G. 1981. *Food Engineering and Dairy Technology*. V.A. Kessler, Germany. pp. 208–238.

Kern, D.Q. 1997. *Process Heat Transfer*. CECSA, México D.F. (In Spanish).

Kumoro, A.C., Retnowati, D.S., and Budiyati, C.S. 2011. Influence of temperature and solid concentration on the physical properties of noni (*Morinda citrifolia* L.) juice. *Food and Bioprocess Technology*, 4: 1482–1488.

Luh, B.S. and Woodroof, J.G. 1988. *Commercial Vegetable Processing*. AVI Pub. Co. Inc., Westport, CN, USA.

Magerramov, M.A. 2007. Heat capacity of natural, fruit juices and of their concentrates at temperatures from 10 to 120°C. *Journal of Engineering Physics and Thermophysics*, 40(5): 1055–1063.

Magerramov, M.A., Abdulagatov, A.I., Azizov, N.D., and Abdulagatov, I.M. 2008. Pressure- and temperature-dependent density change of juices during concentration. *Food and Bioprocess Technology*, 1: 254–269.

Marcelín, M. and Vélez-Ruiz, J.F. 2013. Development of a sweetened condensed milk with addition of low caloric sweeteners and gums: Flow properties analyses. Julio 13–16, Chicago, Illinois, EU. IFT 2013.

McCabe, W.L., Smith, J.C., and Harriot, P. 2008. Evaporation. In *Unit Operations of Chemical Engineering,* W.L. McCabe, J.C. Smith, and P. Harriot (eds). McGraw-Hill, Tokyo, Japan. pp. 473–503.

Miranda, V. and Simpson, R. 2005. Modeling and simulation of an industrial multiple effect evaporator: Tomato concentrate. *Journal of Food Engineering*, 66: 203–210.

More, G.R. and Prasad, S. 1988. V.R.N. Thermal conductivity of concentrated whole milk. *Journal of Food Process Engineering*, 10: 105–112.

Moresi, M. 1985. Design and optimization of falling-film evaporators. In *Developments in Food Preservation*, Vol. 3 (S. Thorne, Ed.). Elsevier Applied Science Publishers, Barking, UK. pp. 183–244.

Moresi, M. and Spinosi, M. 1980. Engineering factors in the production of concentrated fruit juices. I. Fluid physical properties of orange juices. *Journal of Food Technology*, 15: 265–276.

Moresi, M. and Spinosi, M. 1984. Engineering factors in the production of concentrated fruit juices. II. Fluid physical properties of grape juices. *Journal of Food Technology*, 19: 519–533.

Muddawar, I.A. and El-Masri, M. 1986. Momentum and heat transfer across freely falling turbulent liquid films. *International Journal of Multiphase Flow*, 12(5): 771–790. Cited by Hernandez E., Chen C.S., Johnson J. and Carter R.D. 1995. Viscosity changes in orange juice after ultrafiltration and evaporation. *Journal of Food Engineering*, 25: 387–396.

Nindo, C.I., Tang, J., Powers, J.R., and Singh, P. 2005. Viscosity of blueberry and raspberry juices for processing applications. *Journal of Food Engineering*, 69: 343–350.

Prost, J.S., González, M.T., and Urbicain, M.J. 2006. Determination and correlation of heat transfer coefficients in a falling film evaporator. *Journal of Food Engineering*, 73: 320–326.

Ramos, A.M. and Ibarz, A. 1998. Density of juice and fruit puree as a function of soluble solids content and temperature. *Journal of Food Engineering*, 35: 57–63.

Reddy, C.S. and Datta, A.K. 1994. Thermophysical properties of concentrated reconstituted milk during processing. *Journal of Food Engineering*, 21: 31–40.

Ribeiro, C.P. and Caño Andrade, M.H. 2002. A heat transfer model for the steady-state simulation of climbing-falling-film plate evaporators. *Journal of Food Engineering*, 54: 309–320.

Rodríguez-Martínez, V., Sosa-Morales, M.E., and Vélez-Ruiz, J.F. 2007. Physicochemical and flow characterization of prickly pear concentrates. *VI Congreso Ibero Americano de Ingeniería de Alimentos (CIBIA VI)*, November 5–8, Ambato, Ecuador.

Sangrame, G., Bhagavathu, D., Thakare, H., Ali, S., and Das, H. 2000. Performance evaluation of a thin film scraped surface evaporator for concentration of tomato pulp. *Journal of Food Engineering*, 43(4): 205–211.

Schwartzberg, H.G. 1977. Energy requirements for liquid food concentration. *Food Technology*, March: 67–76.

Singh, R.P. and Heldman, D.R. 2001. *Introduction to Food Engineering*. Academic Press, Glascow, Great Britain, UK. pp. 625–670.

Sobolík, V., Zitný, R., Tovcigrecko, V., Delgado, M., and Allaf, K. 2002. Viscosity and electrical conductivity of concentrated solutions of soluble coffee. *Journal of Food Engineering*, 51: 93–98.

Souza, M., Ferreira, R., da Costa, R., Minim, L.A., dos Reis, J.S., and Bonomo, P. 2010. Thermophysical properties of umbu pulp. *Brazilian Journal of Food Technology*, 13(3): 219–225.

Smith, R. 2008. *Chemical Process Design and Integration*. John Wiley and Sons, Ltd., Chichester, England.

Smith, D.S., Cash, J.N., Nip, W-K., and Hui, Y.H. 1997. *Processing Vegetables. Science and Technology*. Technomic Pub. Co. Inc., Lancaster, PE, USA.

Stankiewicz, K. and Rao, M.A. 1988. Heat transfer in thin-film wiped-surface evaporation of model liquid foods. *Journal of Food Process Engineering*, 10: 113–131.

Tellis-Romero, J., Cantú-Lozano, D., Telis, V.R.N., and Gabas, A.L. 2007. Thermal evaporation: Representation of rise in boiling point of grapefruit juice. *Food Science and Technology International*, 13(3): 225–229.

Tellis-Romero, J., Telis, V.R.N., Gabas, A.L., and Yamashita, F. 1998. Thermophysical properties of Brazilian orange juice as affected by temperature and water content. *Journal of Food Engineering*, 38: 27–40.

Thijssen, H.A.C. 1970. Concentration processes for liquid foods containing volatile flavors and aromas. *Journal of Food Technology*, 5: 211–229.

Tsen, J.H. and King, V.A.E. 2002, Density of banana puree as a function of soluble solids concentration and temperature. *Journal of Food Engineering*, 55: 305–308.

Vélez-Ruiz, J.F. 1996. Rheological Properties of Concentrated Milk. Doctoral Thesis. WSU, Pullman WA, USA.

Vélez-Ruiz, J.F. 2007. *Notes of Food Engineering II*. Universidad de las Américas Puebla. Unpublished document. Puebla, Mexico.

Vélez-Ruiz, J.F. 2009. Evaporation of liquid foods. In *Food Processing and Engineering Topics*, M.E. Sosa-Morales and J.F. Vélez-Ruiz (eds). Nova Science Publishers, Inc., New York, USA. pp. 179–214.

Vélez-Ruiz, J.F. 2012. *Notes of Food Transport Phenomena*. Universidad de las Américas Puebla. Unpublished document. Puebla, Mexico.

Vélez-Ruiz, J.F. and Barbosa-Cánovas, G.V. 1997. Effects of concentration and temperature on the rheology of concentrated milk. *Transactions of the ASAE*, 40(4): 1113–1118.

Vélez-Ruiz, J.F. and Barbosa-Cánovas, G.V. 1998. Rheological properties of concentrated milk as a function of concentration, temperature and storage time. *Journal of Food Engineering*, 35: 177–190.

Vélez-Ruiz, J.F. and Barbosa-Cánovas, G.V. 2000. Flow and structural characteristics of concentrated milk. *Journal of Texture Studies*, 31: 315–333.

Vélez-Ruiz, J.F. and Soriano-Morales, A.L. 2003. Evaluación de Propiedades Físicas de Alimentos Utilizando un Programa de Computadora. *Revista Internacional Información Tecnológica*, 14(4): 23–28.

Verdurmen, R.E.M. and de Jong, P. 2003. Optimising product quality and process control for powdered dairy products. In *Dairy Processing. Improving Quality*, G. Smith (ed). CRC Press, Boca Raton, FL, USA.

Welty, J.R., Wicks, Ch.E., and Wilson, R.E. 1976. *Fundamentals of Momentum, Heat, and Mass Transfer*. John Wiley and Sons, New York, USA.

Woodroof, J.G. and Luh, B.S. 1986. *Commercial Fruit Processing*. AVI Pub. Co. Inc., Westport, CN, USA.

Zainal, B.S., Rahman, R.A., Ariff, A.B., Saari, B.N., and Asbi, B.A. 2000. Effects of temperature on the physical properties of pink guava juice at two different concentrations. *Journal of Food Engineering*, 43: 55–59.

Zuritz C.A., Muñoz Puntes E., Mathey H.H., Pérez E.H., Gascón A., Rubio L.A., Carullo C.A., Chernikoff R.E., and Cabeza M.S. 2005. Density, viscosity and coefficient of expansion of clear grape juice at different soluble solid concentrations and temperatures. *Journal of Food Engineering*, 71: 143–149.

13 Food Irradiation Processing

Joong-Ho Kwon, Jae-Jun Ahn, and Hafiz Muhammad Shahbaz

CONTENTS

13.1 Introduction 428
13.2 Energy and Process 429
13.2.1 Energies Used and Their Characteristics 429
13.2.2 Process and Terminology 430
13.2.3 Irradiation Facilities and Operations 431
13.2.4 Dosimetry 433
13.2.5 Food Irradiation and HACCP 434
13.3 Biological Effects of Ionizing Radiations 435
13.3.1 Direct and Indirect Theory of Radiations 435
13.3.2 Microbial Inactivation 438
13.3.3 Effect of Irradiation on Food Components 440
13.4 Application Fields 444
13.4.1 Growth Control: Sprout/Root/Shoot/Stem Growth Control 445
13.4.2 Shelf Life Extension 447
13.4.3 Disinfestations 448
13.4.4 Microbial Decontamination 450
13.4.5 Sterilization of Special Foods 453
13.4.6 Novel Applications 454
13.4.7 Cold Process Characteristics 454
13.5 Safety Evaluation of Irradiated Food 455
13.6 Regulation and Legislation 457
13.7 Consumer Acceptance 459
13.8 Approval and Commercialization 463
13.9 Irradiation Identification Methods 467
13.9.1 Physical Methods 467
13.9.1.1 Photostimulated Luminescence 467
13.9.1.2 Thermoluminescence 471
13.9.1.3 ESR Spectroscopy 472
13.9.2 Chemical Methods 475
13.9.2.1 Hydrocarbons Analysis 475
13.9.2.2 2–Alkylcyclobutanones 477

13.9.3 Biological Methods 478
13.9.3.1 DNA Assays 478
13.9.3.2 Direct Epifluorescent Filter Technique and Aerobic Plate Count 479
13.9.3.3 Limulus Amebocyte Lysate/Gram-Negative Bacteria 479
13.9.3.4 Germination and Half Embryo Test 480
References 480

13.1 INTRODUCTION

Food supply must meet certain basic requirements for both maintaining stable quantities and securing safety features. There have been many conventional technologies and techniques used for preserving and/or improving food quality and safety, such as heat or cold treatment, chemicals, and atmospheric modification to control microbes, pests, and biochemical changes. It is generally understood, however, that an increasing demand for safer foods as well as for convenience/processed foods requires new technologies in order to solve or complement the limitations of existing methods (WHO 1988; FAO/WHO 2003).

As one of the alternative methods, food irradiation is attracting much attention mainly because none of the processes used in the food industry currently has had its safety and technical efficacy investigated as thoroughly and over such a long period of time as food irradiation (Loaharanu et al. 2007). In particular, the safety of irradiated food has been thoroughly studied and comprehensively evaluated for more than 50 years, which includes systematic evaluation by panels of experts in the field of toxicology, radiation chemistry, nutrition, microbiology, and packaging (Loaharanu et al. 2007; Roberts 2014). Furthermore, interest in food irradiation is increasing in connection with persistent problems including over 25% of postharvest food losses from infestation, contamination, and spoilage; undiminished concerns over foodborne diseases; and growing international trade in food products that must meet strict import standards of quality and quarantine (Byrne 1996; FAO/WHO 2003).

In addition, with increasingly restricted regulations or appointed prohibition on the use of various chemical fumigants for insect and microbial control in food, food irradiation is recognized as a prospective alternative to protect food against insect damage and as a quarantine treatment for fresh produce (ICGFI 1999; UNEP 2000; WHO 2003). Food irradiation is a physical method of processing foods by exposing them to ionizing energy from approved radiation sources, which can be compared with heating or freezing (WHO 1988). Irradiation treatment has received approval for different food categories from national health authorities and/or international organizations (FAO/IAEA) concerned, which was based on its scientific evidence as an effective food safety measure with over 60 years of research and development (IAEA website 2013). It has two distinct advantages in connection with human health and well-being: one is the inactivation of certain foodborne pathogens and quarantine pests, thereby making the food safer, and the other is the extension of shelf life of the food by both destroying spoilage organisms and delaying the deterioration process, thus increasing food availability (Josephson and Peterson 1983; Kwon

1998; Stewart 2001). However, there is still controversy in consumer acceptance of irradiated foods, limiting its wider acceptance and use (Eustice and Bruhn 2006).

This chapter introduces food irradiation processing dealing with the energies applied and the processes involved, the biological effect of ionizing radiation, the application fields, the safety evaluation, regulations and approvals, consumer acceptance, commercialization, and the identification methods for irradiated foods.

13.2 ENERGY AND PROCESS

13.2.1 Energies Used and Their Characteristics

Food is routinely processed with different wavelengths of radiant or electromagnetic energy. These include infrared waves used in traditional baking and broiling, microwaves used for quick cooking, and sunlight used for drying (Figure 13.1) (Ryser 2009). In a narrow sense, however, radiation energies approved for food irradiation are gamma rays emitted from radioisotopes, machine-generated x-rays with a maximum energy of 5 million electron volts (MeV; an electron volt is the amount of energy gained by an electron when it is accelerated by a potential of 1 V in a vacuum), and electrons with a maximum energy of 10 MeV (CAC 1984; 2003).

These three principal types of radiation energy are ionizing radiations because their energy is high enough to dislodge electrons from atoms and molecules and to convert them to electrically charged particles called ions and thus can be used in food irradiation processing according to the Codex Alimentarius General Standard (CAC 1984).

1. Gamma radiation from radionuclides, such as ^{60}Co or ^{137}Cs
2. Machine sources of bremsstrahlung (x-rays) with electron energies up to 5 MeV
3. Machine sources of electron beams with energies up to 10 MeV

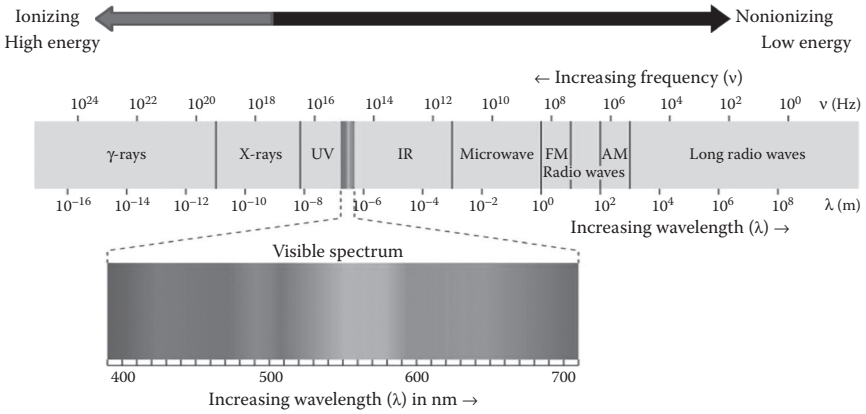


FIGURE 13.1 Elecromagnetic radiation energy spectrum. (From Ryser, E.T. 2009. Novel x-ray irradiation technology for the food industry. Paper presented at annual meeting of Korean Society of Food Science and Nutrition, Changwon, Nov. 4–6).

TABLE 13.1
Energy Characteristics of Gamma Rays, X-Rays, and Electrons

	Gamma Rays (Co-60)	X-Rays	Electrons
Energy	Electromagnetic 1.33 Mev, 1.17 MeV	Electromagnetic <5 MeV	Beam <10 MeV
Energy efficiency	Low (<30%)	Low (converting)	High (<85%)
Penetration	High (60~80 cm)	High	Low (<10 cm)
Source	Radionuclide	Electricity (on/off)	Electricity (on/off)

Gamma rays and x-rays, such as microwaves and ultraviolet and visible light, are included in the electromagnetic spectrum (Figure 13.1) and occur in the short-wavelength, high-energy region of the spectrum having the greatest penetrating power (Cleland 2006). They have the same nature and effects on materials except for their origins; gamma rays with specific energy come from the spontaneous disintegration of radionuclides (^{60}Co or ^{137}Cs), but x-rays of varying energies are usually produced by a machine in which a beam of fast electrons in a high vacuum bombards a metallic target, resulting in the conversion to x-rays (bremsstrahlung). The gamma rays used in food processing, mainly obtained from large ^{60}Co radionuclide sources, have essentially monoenergetic photons; ^{60}Co emits simultaneously two photons per disintegration with energies of 1.17 and 1.33 MeV. The machine-generated bremsstrahlung x-rays with a maximum energy of 5 MeV can be used in food irradiation even though the efficiency of conversion from electrons to x-rays is low, and this has hindered its use so far (Table 13.1) (Cleland 2006).

In gamma processing, a resulting depth–dose distribution in the food products usually resembles an approximately exponential curve. Irradiation from both sides (two-sided irradiation), obtained either by turning the process load or by irradiation from two sides of a plaque source, is often employed to increase the dose uniformity in the process load (Cleland 2006).

Electrons with high energy up to 10 MeV are produced from machines capable of accelerating electrons to near the speed of light by means of a linear accelerator. Compared with gamma ray or x-rays, electrons have limited penetration power and thus can be used only for the treatment of thin packages of food and free flowing or falling grains. Electrons are also emitted by some radioactive materials; in this case, they are called "beta rays" (Cleland 2006).

13.2.2 Process and Terminology

Food irradiation is defined as the treatment of food by a certain type of energy. The process involves exposing the food, either packaged or in bulk, to carefully controlled amounts of radiation energy for a specific time to achieve certain desirable objectives, such as a reduction of microbial populations, inactivation of pathogens and pests, and shelf life extension of fresh commodities. The type of energy used in processing food materials is limited to radiations such as high-energy gamma rays, x-rays, and accelerated electrons, as mentioned above. As far as the penetrating

capability is concerned, gamma rays or x-rays may be used for the processing of relatively thick packages, or dense products over a prolonged period of time, while high-power electron beams may provide a higher throughput for large amounts of products only when a shallow penetration is acceptable in treating the foods. Electrons normally have a fairly narrow spectral energy that limits their penetration (Cleland 2006). One-side irradiation of 4-cm-thick water-equivalent products (most foods) can be performed by a 10 MeV accelerator with acceptable dose uniformity. In contrast, products as thick as 9 cm of water equivalent material can be treated through two-sided irradiation with 10 MeV electrons (Cleland 2006).

The gamma rays used are mainly obtained from ^{60}Co radionuclide, which is called as radioactive isotopes or radioisotopes. The becquerel (Bq) is a unit of radioactivity and 1 Bq equals one disintegration per second. The time taken by a radionuclide to decay to half the level of radioactivity originally present is known as its half life: ^{60}Co is 5.6 years and 137Cs is more than 30 years (Cleland 2006). In food irradiation processing, food is exposed to certain amounts of radiation energy, and the amount of ionizing radiation absorbed is called the radiation-absorbed dose and measured in units of rads (1 rad = 100 erg/g) or grays (1 Gy = 100 rads), with 1 Gy equal to 1 J/kg and 1000 Gy equal to 1 kiloGray (kGy) (IAEA 1982; Cleland 2006).

13.2.3 Irradiation Facilities and Operations

The common features of commercial irradiation facilities are composed of three parts that include radiation sources, an irradiation room, and a conveyer system to transport the food into and out of the room (Figures 13.2 and 13.3). The main difference in the structures of irradiation plants is the shielding largely with concrete (1.5–1.8 m thick) surrounding the irradiation room, which is to protect people from radiation exposure originating from the irradiation sources (WHO 1988; Cleland 2006).

A gamma irradiator uses a radionuclide source, which continuously emits radiation and should be stored in a water pool (usually 6 m in depth) when not being used

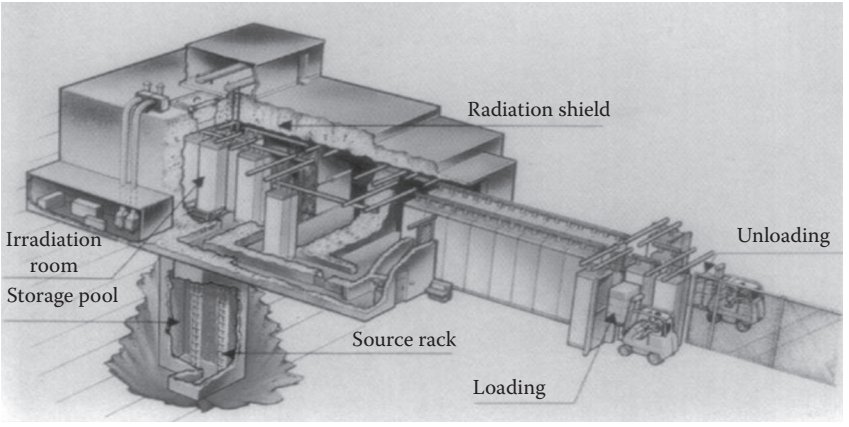


FIGURE 13.2 Gamma irradiation facility (pallet carrier type).

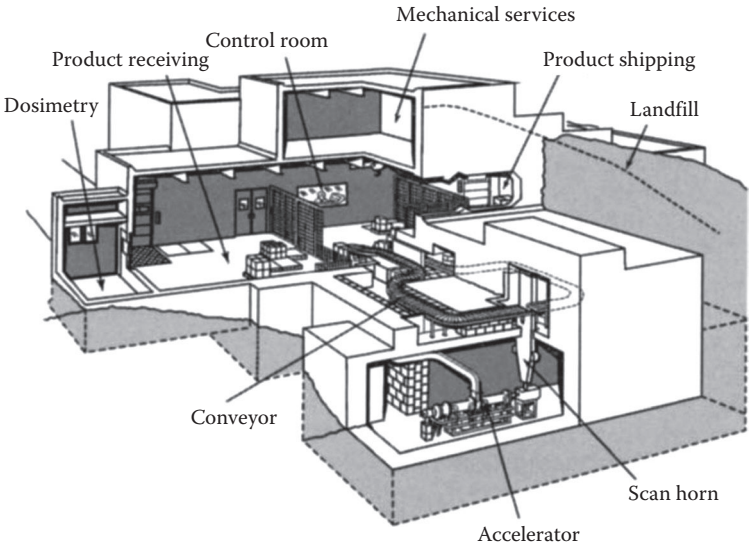


FIGURE 13.3 Electron beam irradiator.

to treat food. Water, known as one of the best shields against various radiations, absorbs radiation energy and protects workers from radiation exposure when they enter the irradiation room. In contrast to gamma irradiators, the machines producing high-energy electrons operate by electricity and can be switched off (Josephson and Peterson 1983; Cleland 2006).

The transporting system used in a large food irradiation facility is similar to that employed for the radiation sterilization of medical products and can be either a conveyor or rail system. In a gamma irradiator, the size of the containers in which the food is moved through the irradiation room can vary and pallets up to 1 m^3 can be used. However, with machines, the volume or thickness of a product to be treated should be much less because there is a fundamental difference in the penetration of the radiation energies (Cleland 2006). Industrial irradiation facilities for treating food should be licensed, regulated, and inspected by the national radiological safety and health authorities concerned. Most countries have established their rules based on irradiation standards and codes of practice jointly established by international organizations. The Codex General Standard for Irradiated Foods and an associated International Code of Practice for the Operation of Radiation Facilities Used for the Treatment of Foods were adopted in 1983 by the Codex Alimentarius Commission of the FAO and WHO, which state that irradiated foods should be accompanied by shipping documents identifying the irradiator, date of treatment, lot identification, dose, and other details of treatment (CAC 1984, 2003).

Commercial application of irradiation technology requires several assessments to determine the suitability of its use and to justify the investment and operating costs. More than 200 such irradiators are operated around the world (Cleland 2006). The plants, which must be approved by governmental authorities before construction, are

subject to regular inspections, audits, and other reviews to ensure that they are safely and properly operated. These types of governmental controls would also be valid for irradiation facilities processing food and the principle of lot traceability is an essential part of the process controls, whether a product is medical supplies or food (Cleland 2006). At the international level, provisional guidelines for good manufacturing practices (GMPs) and good irradiation practices for various kinds of foods have been documented (ICGFI 1994), which cover all aspects in the implementation of irradiation processing on a commercial scale. The guidelines require that, as with all food technologies, effective quality control systems be established and adequately monitored in terms of critical control points at the irradiation facility. Foods should be handled, stored, and transported according to GMPs before, during, and after irradiation. Only high-quality food should be accepted for irradiation.

13.2.4 Dosimetry

Dosimetry in food irradiation is the measurement of the absorbed dose in food treated with ionizing radiations, which is essential for successful implementation of the processing by providing details of the dosimetry procedures on process validation and process control. A well-characterized reliable dosimetry system that is traceable to recognized national and international dosimetry standards can help to establish the required documentary evidence with regard to dose. Besides, dosimetry is necessary for scaling up processes from the research level to the industrial level. Thus, accurate dosimetry is indispensable (IAEA 1982, 2002).

The dosimetry methods and procedures should be accurate, easy to use, reasonable in price, and acceptable to national regulations associated with the control of irradiated foodstuffs. It is also required that the dosimetry personnel at the irradiation facility be sufficiently trained in dosimetry-related activities (IAEA 2002).

The success of radiation processing of food depends to a large extent on the ability of the processor in terms of reliable dosimetry by measuring the absorbed dose delivered to the food product, determining the dose distribution patterns in the product package (through process qualification procedures) and controlling the routine radiation process (through process control procedures). In the processing of foodstuffs by irradiation, reliance is placed on the radiation quantity "absorbed dose" to obtain accurate and meaningful information about the relevant radiation effects (IAEA 2002).

Dosimetry systems can be classified based on their intrinsic accuracy and applications into four classes of dosimeter (ASTM 2000): (a) primary standard dosimeters, (b) reference standard dosimeters, (c) transfer standard dosimeters, and (d) routine/working dosimeters. Primary standard dosimeters enable an absolute measurement of the absorbed dose to be made with reference only to the SI base units (mass, length, time, electric current, etc.) and fundamental physical constants. Reference standard dosimeters are of high metrological quality that can be used as reference standards to calibrate other dosimeters. In turn, they need to be calibrated against a primary standard, generally through the use of a transfer standard dosimeter that are being used for transferring dose information from an accredited or national standards laboratory to an irradiation facility in order to establish traceability to that

TABLE 13.2
Example of Routine Dosimetry Systems

Dosimeter	Measurement Instrument	Usable Dose Range (Gy)
Alanine	EPR spectrometer	$1–10^5$
Dyed PMMA	Visible spectrophotometer	$10^2–10^5$
Clear PMMA	UV spectrophotometer	$10^3–10^5$
Cellulose acetate	Spectrophotometer	$10^4–4 \times 10^5$
Lithium borate, lithium fluoride	Thermoluminescence reader	$10^{-4}–10^3$
Lithium fluoride (optical grade)	UV/Visible spectrometer	$10^2–10^6$
Radiochromic dye films, solution, optical waveguide	Visible spectrophotometer	$1–10^5$
Ceric-cerous sulfate solution	Potentiometer or UV spectrophotometer	$10^3–10^5$
Ferrous cuprie sulphate solution	UV spectrophotometer	$10^3–5 \times 10^3$
ECB solution	Spectrophotometer, color titration, high-frequency conductivity	$10^{-2} \times 10^6$
Amino acids	Lyoluminescence reader	$10^{-5}–10^4$
Polymeric plastic (M center)	Fluorescence reader	$50–5 \times 10^5$

standards laboratory. Routine (or working) dosimeters are used in irradiation processing facilities for dose mapping and for process monitoring for quality control. They must be frequently calibrated against a reference or transfer dosimeters (IAEA 2002). Commonly used routine dosimeters include PMMA, radiochromic and cellulose triacetate (CTA) films, ceric-cerous, and ECB dosimeters (Table 13.2)

One of the fundamental aspects of process control is dosimetry. Dosimetry forms the key element for the success of the treatment, for the safety of the process, and for the wholesomeness of the products. Thus, reliable routine dosimeters—in accordance with national or international standards—are a prerequisite of good irradiation practice (GIP). Moreover, with the increased trade in irradiated products, traceable dosimetry has become crucial for certifying the dose applied to the food, which provides a reliable system to ensure that imported products have been treated according to legal requirements. The choice of routine dosimetry systems should take into account the characteristics of the radiation source and the product. Additionally, they should be selected based on convenience of use and cost (IAEA 2002; Cleland 2006).

13.2.5 Food Irradiation and HACCP

Hazard analysis critical control points (HACCP) was originally developed to invigorate hygienic concepts in food production, which can be easily adapted to food irradiation processing. The following seven principles of HACCP have been designed to locate and define potential hazards and specify measures for their control in radiation processing of food products (Mortimore and Wallace 1992; Pierson and Corlett 1992; IAEA 2002).

Principle 1, Conduct a hazard analysis—the analysis of possible hazards results in identifying "the failure to achieve the desired effects of radiation processing" as the key point.

Principle 2, Identify the critical control points—it is determined that the particular critical control point (CCP) in radiation processing is the dose that has been imparted. In addition, several other CCPs apply during the process but are not specific to radiation processing alone.

Principle 3, Establish critical limits—the critical limits, minimum and maximum acceptable doses are derived.

Principle 4, Establish monitoring requirements—a monitoring system is established to control this critical point, which results in documentation of all process parameters as well as the dosimetry results. Recent trends have been for quality assurance methodology, that is, preventing problems from occurring rather than for quality control, which implies testing of the product to ensure that a problem has not already occurred. However, dosimetry should not be used solely as a system for product release. Routine product dosimetry is the final step in the overall control system to ensure that the correct dose has been applied.

Principle 5, Establish corrective actions—a corrective action is established that needs to be taken when monitoring indicates that a particular CCP is moving out of control.

Principle 6, Establish record keeping procedures—documentation pertaining to the procedures and records appropriate to these principles and their application are established. Because traceability is so critical in food irradiation control, documentation forms a key part of any dosimetry system.

Principle 7, Establish verification procedures—procedures are established to verify that the HACCP system is working correctly and that the established procedures are adhered to during routine and prolonged operations.

13.3 BIOLOGICAL EFFECTS OF IONIZING RADIATIONS

13.3.1 Direct and Indirect Theory of Radiations

Ionizing radiations will produce some biological damage, whether the radiation source is natural or man-made. The effect of irradiation on living organisms can be divided into two categories: direct and indirect effects. The direct effect is, as a consequence of striking atoms with radiation, creating an ejection of electrons from the atoms. The indirect effects are due to the formation of free radicals during radiolysis (radiation-induced splitting) of water molecules. There is a considerable quantity of water in living tissues. The radiolysis of water molecules produces hydroxyl radicals, which are highly reactive species that interact with the organic molecules present in foods (Figure 13.4).

The effect of irradiation is related to the nature and complexity of organisms (Table 13.3). However, the correlation of radiation sensitivity is inversely proportional to the size of microorganism. Viruses are the smallest living organisms and are most resistant to radiation, some surviving as many as 100 kGy. Therefore, radiation only at high doses can inactivate viruses. Furthermore, many factors contribute

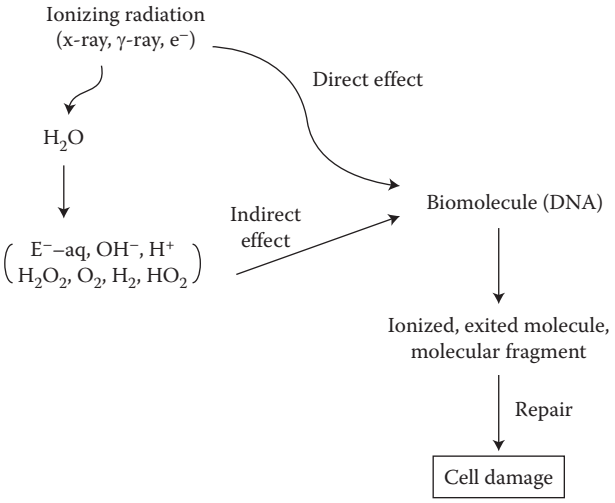


FIGURE 13.4 Direct damage and indirect damage in food matrix by irradiation.

to the action of radiation on bacteria, including the irradiation dose; amount of bacteria; species and strain of bacteria; physical state and chemical composition of the medium; and storage conditions after the irradiation treatment. The sensitivity of an organism to radiation can be expressed in terms of the number of grays required to destroy a specific fraction of the population.

$$D_{10}\text{value} = \frac{\text{Dose(kGy)}}{(\log N_0 - \log N)} = \log_{10}\frac{N}{N_0} = -\frac{1}{D_{10}}D$$

The radiation resistance of a pathogen is often represented as D_{10} values, which are the amounts of radiation energy required to inactivate 90% of the pathogenic population in a sample (IAEA 1982). The D_{10} value, however, is affected by the environment in which the microorganisms are present. It has been reported that

TABLE 13.3
Approximate Doses to Kill Various Organisms

Organisms	Doses (Gy)[a]
High animals, including mammals	5–10
Insects	10–100
Nonsporulating bacteria	500–10,000
Sporulating bacteria	10,000–50,000
Viruses	10,000–200,000

[a] To convert to rad, multiply by 100.

Salmonella enteritidis has a D_{10} value 0.70 kGy and 0.49 kGy in low-fat and high-fat beef, respectively. If the food has high water content, then the indirect action of radiation is important and the bacteria have a lower D_{10} value than in dry foods. Thus, higher doses are required to produce the desired microbial kill in dry foods such as spices. The water phase is immobilized, so the radicals are unable to move and cause indirect damage. Similarly, higher doses are needed to produce the same microbial kill as in nonfrozen products. The D_{10} of *Escherichia coli* 0157:H7 in chicken meat was 0.27 kGy at +5°C and 0.42 kGy at –5°C. Such effects need to be taken into consideration while deciding on an effective radiation dose (Lund et al. 1999). The effects of radiation will also vary depending on the timing of irradiation with respect to the stage of development of the organism. For example, irradiation application during the growth stage of an organism can affect its maturation and could cause alterations in the normal structure, metabolism, reproduction, and so on. Figure 13.5 shows a plot relating dose to surviving fraction of microorganisms. The $\log_{10}(N/N_0)$ plotted against the dose is a straight-line relationship, provided the radiation effect is the direct effect and one ionizing causes a kill. Such an effect would be independent

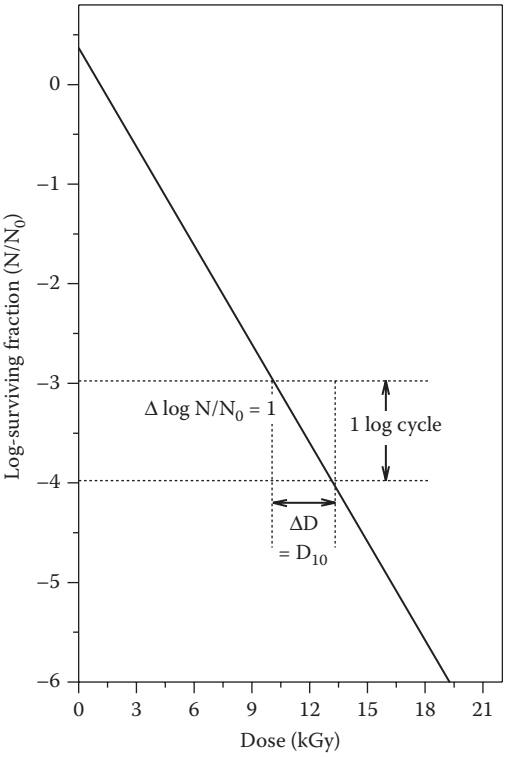


FIGURE 13.5 Relationship between radiation dose and surviving fraction of microorganisms. (From IAEA. 1982. Training Manual on Food Irradiation Technology. 2nd ed., Joint FAO/IAEA Division of Isotope and Radiation of Atomic Energy for Food and Agricultural Development. Technical Report Series No. 114, IAEA, Vienna, Austria.)

of dose rate, temperature, concentration of microorganisms, and the physical state and composition of the medium. The efficiency of the given type of radiation would depend on the target size and would relate to the number of ionizations produced per unit volume (IAEA 1982).

13.3.2 Microbial Inactivation

Ionizing radiation treatment is highly effective to reduce the microbial load in various foods. It offers a safe alternative method to improve the safety and shelf-stability of food products without affecting nutritional or sensory quality (Yun et al. 2012). However, a definite dose of irradiation will destroy a certain amount of pathogens, regardless of the initial concentration of microorganisms present in that sample (Figure 13.6). Radiation can also do nothing if spoilage has already been initiated. Irradiation is advantageous in that a temperature increase of the food products is either none or minimized (Chawla et al. 2003).

Radiation treatment at doses of 2–7 kGy—depending on condition of irradiation and the food—can effectively eliminate potentially pathogenic nonspore-forming bacteria from food products with no effect on sensory, nutritional, and technical qualities. Radiation decontamination is mainly applied to poultry and red meat, egg products (Álvarez et al. 2006), and fishery products. It is a unique feature of radiation decontamination that it can also be performed when the food is in a frozen state. Microorganisms surviving low- and medium-dose radiation treatment are more sensitive to environmental stresses or subsequent food processing treatments than the microflora of unirradiated products (Farkas 1998).

The ability of ionizing radiation to destroy microorganisms has been studied since the late nineteenth century (Aziz et al. 1997). Different scientists have reviewed the industrial application of ionizing energy to preserve different foods (Klinger et al. 1985; El-Zawahry et al. 1991). Pietranera et al. (2003) reported that 3 kGy gamma irradiation significantly reduced the microbial load of ice creams without affecting the quality. Jo et al. (2007) reported that low-dose irradiation can improve the microbial quality and reduce the risk by the foodborne pathogens in ice cream, which has

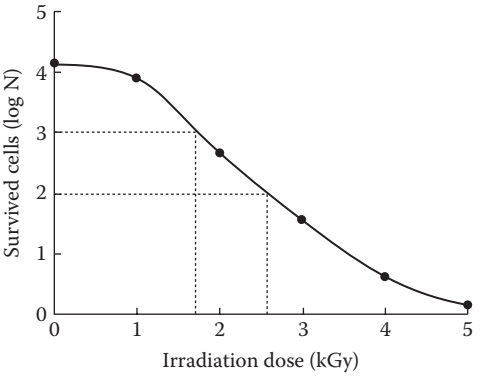


FIGURE 13.6 Typical microbial survive curve of irradiated foods.

limited alternative sterilization methods due to the temperature characteristics of the products. Aziz et al. (1998) found that a gamma ray dose of 10 kGy is capable of eliminating actinomycetes in food and animal feed products. El-Zawahry et al. (1991) reported that gamma irradiation treatment of 5–10 kGy was able to completely inhibit the fungal and bacterial population contaminating different Egyptian and Saudi Arabian foods.

Viruses seem to be significantly more resistant to irradiation than more complex microorganisms. They are different from true organisms in that they do not respire and depend on the host for food and enzymes. Radiation can inactivate viruses only at high doses. Thirty kGy have been reported to inactivate foot-and-mouth disease virus suspended in an aqueous medium. However, 40 kGy was required to inactivate this virus in dry state (IAEA 1982).

Mallett et al. (1991) irradiated clams and oysters with a gamma source and found that they could significantly reduce virus numbers without affecting the survival rate of the shellfish or negatively impacting the taste or texture. Hepatitis A was determined to have a D-value of 2 kGy, while rotavirus SA11 had a D-value of 2.4 kGy. Husman et al. (2004) used animal calciviruses as a substitute for noroviruses in studies of inactivation by gamma irradiation. They found that the presence of solutes, such as proteins, in the medium in which the viruses were irradiated increased the resistance of the viruses to inactivation by irradiation. For a 3-log reduction in low protein content stocks, the feline calcivirus needed 0.5 kGy, and the canine calcivirus needed 0.3 kGy; no level was determined for the norovirus. In the high protein stocks, both calciviruses were highly resistant to gamma irradiation. Comparing the D-values for the viruses to those of the pathogenic bacteria, it can be seen that significantly more radiation would be needed to inactivate the viruses. Lamuka et al. (1992) used gamma irradiation of dose 2.5 kGy for whole chickens. They found that this dose completely eliminated naturally occurring *Salmonella* from the poultry carcasses.

Yeast and molds show sensitivity to radiation comparable with some nonspore-forming bacteria. However, there is a substantial variation according to species. The higher doses used to kill the molds may lead to tissue softness in fruits, making them susceptible to handling damage and rotting. Therefore, the effective way to reduce the dose requirement for yeast and mold control is to use a combination of radiation and mild heat.

The combined application of irradiation processing and modified atmosphere packaging (MAP) is beneficial in improving shelf life and retaining sensory quality in minimally processed vegetables. Lacroix and Lafortune (2004) reported the efficiency of gamma irradiation combined with modified atmosphere packaging as an alternative treatment to ensure the innocuity and shelf life extension of precured vegetables.

Research studies during the past few years have proven that irradiation can effectively improve the microbiological quality of dried products (Farkas 1988; Yusof et al. 2007). Zegota and Malolepszy (2008) demonstrated the ability of gamma radiation treatment to decontaminate industrial casein; a milk protein that is utilized as a component of many food and nonfood products. The 5 kGy gamma ray dose was sufficient to reduce the total microflora and coliforms counts to an acceptable

level for food products. Recently, Song et al. (2012) has investigated the potential of gamma radiation to reduce the microbial population of freeze-dried miyeokguk, a seaweed food product recommended as space food, without compromising the sensory quality. The results revealed that a 10 kGy irradiation dose is sufficient to achieve the desired objectives.

Radurization is not always related to simple reduction of a bacterial population. Different organisms show different sensitivities to radiation, and to destroy a population of mixed organisms is not uniform. Irradiation may result in a changed flora and a different outgrowth pattern. Such changes can affect the ultimate spoilage of food and demands careful evaluation to protect consumers against unusual health hazards. In addition, there is no absolute value for the amount of radiation required to destroy all microorganisms present. The microbial destruction follows a statistical pattern, and for sterile products, the objective is to reduce the probability of survival to less than one organism in an initial population of 10^{12} organisms (IAEA 1982).

13.3.3 Effect of Irradiation on Food Components

Food components usually comprises elements, including carbon, hydrogen, oxygen, and nitrogen. These elements consist of characteristic atoms containing a relatively small nucleus and a number of electrons. Ionizing radiation loses energy while passing through matter such as food and so on. At the same time, the energy is absorbed and consequently leads to the ionization or excitation of the atoms and molecules of the matter (Stewart 2001; Kuan et al. 2013). Consequently, this results in chemical changes in food upon irradiation. Irradiation can also produce subsequent changes in food components; particularly in carbohydrates, proteins, lipids, and vitamins (Kempner 2001). Different scientists (Delincée 1983; Houee-Levin and Sicard-Roselli 2001; Stewart 2001) have reviewed the chemistry of food irradiation in detail.

Physicochemical properties and nutritive value of irradiated foods could be preserved for longer time as compared to nonirradiated foods. For example, meat preservation can be safely attained by irradiation (Kanatt et al. 2006). Fats are among the least stable food components, and are very susceptible to ionizing radiation, which may induce autoxidation (Cheng et al. 2011). However, irradiation may induce some biological changes in meat because of the oxidation of unsaturated fatty acids that can influence its quality and nutritive value (Du et al. 2000). Polyunsaturated fatty acids of the phospholipid fraction are most susceptible to irradiation and leads to the development of rancidity in meat during storage (Giroux and Lacroix 1998). Cheng et al. (2011) reported that irradiation processing induced changes in lipid oxidation of chilled pork and increased lipid oxidation and thiobarbituric acid reactive substance values during refrigerated storage.

Radiation chemistry of proteins has been studied for more than 30 years (Houee-Levin and Sicard-Roselli 2001). The effect of irradiation was different on globular and fibrous proteins (Delincée 1983; Stewart 2001). Ionizing radiations affect protein molecules by direct and indirect ways. In liquid solution, indirect interaction is predominant whereas direct effects are minor. On the contrary, when proteins are in solid state, they are largely affected directly (Kempner 2001; Kuan et al. 2013). Under irradiation, primary water free radicals such as hydrated electron, hydrogen

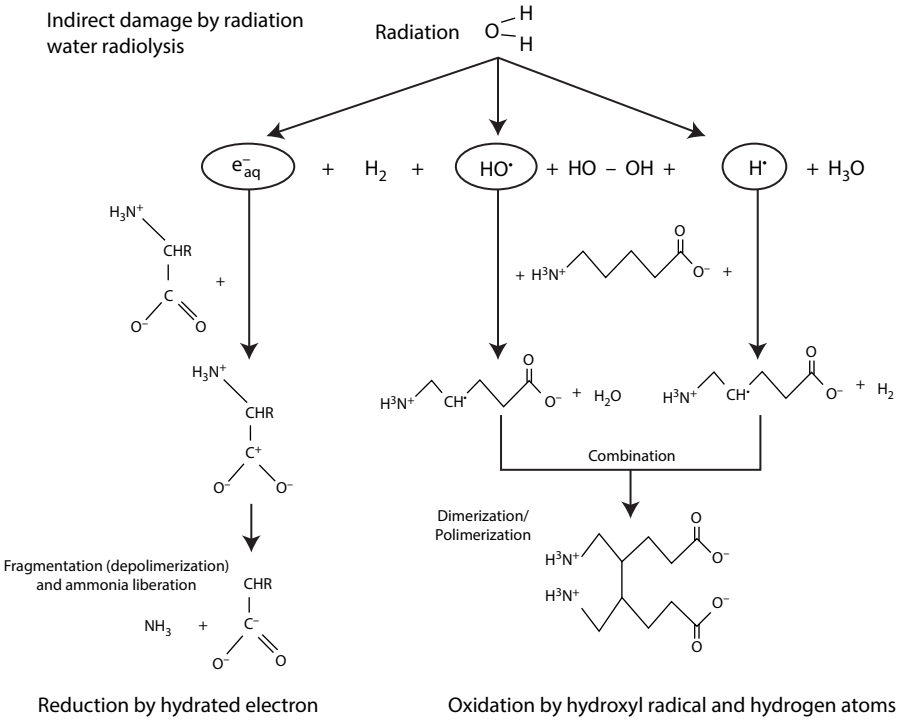


FIGURE 13.7 Effect of irradiation on proteins.

atom, and hydroxyl radical are created, which efficiently reacts with proteins (Figure 13.7). As a result, different types of modifications are possible such as polymerization (dimerization) and fragmentation. Audette-Stuart et al. (2005) have extensively studied these reactions, especially those of OH free radicals as they are important in biological oxidative disorders. As a consequence of these reactions, physicochemical changes in protein foods occur, including the emulsifying and foaming properties of protein emulsion (Song et al. 2009; Kuan et al. 2011), the increase and reduction of viscosity and water solubility of protein pastes (Al-Assaf et al. 2007; Bhat and Karim 2009), and the tensile strength as well as the water vapor permeability of protein films (Micard et al. 2000; Ciesla et al. 2006a,b). In addition, these chemical reactions during the irradiation treatment of proteins depend on various factors such as the structure and state of protein and conditions of irradiation (Kuan et al. 2013).

Lee et al. (2005) investigated the effects of different gamma irradiation doses (0, 4, 16, 32, and 50 kGy) on the film-forming solution of soy protein isolate. SDS-PAGE analysis showed that cross-linking of protein molecules occurred at a dose range of above 16 kGy. In addition, a significant decrease in the viscosity of the gamma-irradiated soya protein isolate solution was observed. This reduction of viscosity was assigned to the conformational change of protein molecules by oxygen radicals generated by the water radiolysis. Gamma irradiation also substantially improved the water vapor permeability of the soy protein film produced; that is,

at 50 kGy, the water vapor permeability decreased by 13%. They also observed an increase in Hunter *b* color value upon increasing of irradiation dose, indicating the occurrence of browning/darkening reaction.

Micard et al. (2000) studied the effects of gamma irradiation (doses of 10, 20, and 40 kGy) on wheat gluten films. It was observed that irradiation increased the tensile strength and decreased the elongation at break; that is, a 10 kGy dose resulted in a 32% decrease in elongation. These changes were attributed to a decrease in insoluble glutenin; that is, depolymerization and/or breakdown of covalent linkages. However, the improvement on the mechanical properties was due to the formation of bityrosine upon irradiation. Moreover, an increase in the water vapor permeability by 19% was recorded on gluten film treated at 10 and 20 kGy.

Song et al. (2009) reported that gamma irradiation (0, 1, 2, and 5 kGy) improved the foaming properties of egg white [liquid egg white (LEW) and egg white powder (EWP)], which led to an increased volume in angel cake produced. However, a significant decrease in viscosity was observed on LEW upon irradiation, whereas that of EWP remained unaffected. Researchers explained that the reduction of LEW was due to the breakdown of protein, and the resistance of change in EWP was due to the low water content that protects the protein from breakdown by radiolytic products of water. The angel cakes produced with irradiated egg white samples showed increased volume than that of control samples. They explained that this effect was contributed by the increased foaming ability of gamma-irradiated LEW and EWP in a dose-dependent manner. Gamma irradiation also resulted in the reduction of hardness, chewiness, and gumminess but Hunter L (lightness) value increased in the angel cakes.

Ionizing radiations are capable of generating free radicals, which can induce molecular changes and fragmentation of starch (Grant and D'Appolonia 1991; Sabularse et al. 1991; Sokhey and Hanna 1993). Physiochemical changes in starch due to irradiation result in the reduction of viscosity and high water solubility (Bao and Corke 2002; Lee et al. 2003). The glycoside bonds are broken down at chain endings in starch granules by irradiation. Bhat and Karim (2009) have comprehensively reviewed the impact of radiation processing (gamma, electron beam, and ultraviolet) on the physicochemical and functional properties of starch (Figure 13.8).

De Kerf et al. (2001) studied the disintegrating properties of starch products (corn, potato, and drum-dried corn starch) irradiated by x-rays and electron beams at 0, 10, 15, and 100 kGy. The disintegration properties of the starches were compared using α-lactose monohydrate tablets containing 5% (w/w) starch as a disintegrant. They found a subsequent increase in starch solubility accompanied by a decrease in the swelling capacity with irradiation dose increment. Irradiation treatments caused modifications in different starches and led to fragmentation of the amylopectin fraction, as these molecules became smaller in molecular weight with irradiation dose and merged with the amylose fraction. Therefore, the decreased swelling capacities of irradiated starch were attributed to the marked decrease in concentration of the amylopectin fraction.

Abu et al. (2005) observed the functional properties of cowpea flours after gamma irradiation at doses 2, 10, and 50 kGy. Some of the starch-related functional properties of cowpea flours and pastes such as the swelling index, and gel strength and viscosity, were found to be significantly reduced at all applied doses. In addition,

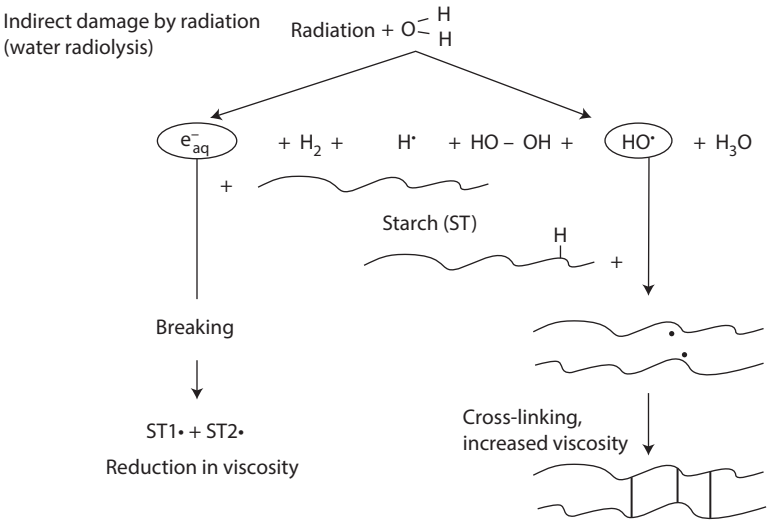


FIGURE 13.8 Effect of irradiation on starch.

the effect was dose dependent, which has been attributed to radiation-induced degradation of the starch. The radiation-induced decrease in the swelling and gel strength has been attributed to the decrease in viscosity owing to starch degradation. Furthermore, the degradation of starch in flours and pastes may have inhibited the ability of the starch granules to trap water and swell during gelatinization, contributing to the decrease upon irradiation.

The effects of irradiation on vitamins have led to different conclusions depending on whether pure solutions or actual food matrices were investigated (WHO 1994). The published studies show that vitamins C and B_1 are the most sensitive water-soluble vitamins, and that E and A are the most sensitive fat-soluble vitamins to irradiation (Kilcast 1994) (Table 13.4). Aqueous and other solutions of vitamins are highly sensitive to irradiation, but this is not true of vitamins in food. Therefore, it is inappropriate to conclude from vitamin losses in solution to food as a result of irradiation (Villavicencio et al. 2000). The sensitivity of vitamins to radiation is unpredictable and food vitamin losses during the irradiation are often substantial (Dionísio et al. 2009).

TABLE 13.4
Sensitivity of Fat- and Water-Soluble Vitamins to Ionizing Radiation

Most Sensitive →→ → →→

Fat-soluble vitamins

Vitamin E → Carotene → Vitamin A → Vitamin D → Vitamin K

Water-soluble vitamins

Vitamin B_1 → Vitamin C → Vitamin B_6 → Vitamin B_2 → Folate, Niacin → Vitamin B_{12}

Source: Adapted from Diehl, J.F. and Josephson, E.S. 1994. *Acta Alimentary* 23: 195–214.

Taipina et al. (2009) evaluated the changes in vitamin E content and sensory properties in Pecan nuts (*Carya illinoensis*) treated with gamma-irradiation at doses of 1 and 3 kGy. The vitamin E content of irradiated pecan nuts measured as α-tocopherol equivalents by a colorimetric method remained stable at these applied doses. Villavicencio et al. (2000) studied the effect of gamma irradiation (0.5, 1.0, 2.5, 5.0, and 10 kGy) and subsequently storage (ambient temperature for 6 months) on the content of several B-vitamins in two varieties of Brazilian beans. The content of vitamin B1, B2, and B6 was analyzed by HPLC. Irradiation slightly affected the thiamine and riboflavin, whereas a dose-dependent decrease was noted for pyridoxine. However, the effect was significant only at the highest doses of 5 and 10 kGy. Dionísio et al. (2009) comprehensively reviewed the published work related to several food products subjected to an irradiation process.

13.4 APPLICATION FIELDS

The range of doses commonly used in food irradiation processing to achieve various effects can be classified into three general applications and dose categories from a practical point of view when foods are treated with ionizing radiation (Table 13.5) (WHO 1988; ICGFI 1999).

TABLE 13.5
Dose Requirements in Various Applications of Food Irradiation Technology

Purpose of Treatment	Dose (kGy)[a]	Products
Low dose (up to 1 kGy)		
• Sprout inhibition	0.05–0.15	Potatoes, onions, garlic, ginger, etc.
	0.25–0.30	Chestnuts
• Insect disinfestation and parasite disinfection	0.15–0.50	Cereals and pulses, fresh and dried fruits, and vegetables, dried fish and meat, Fresh pork, feedstuffs, etc.
• Delay of physiological ripening	0.50–1.00	Fresh fruits and vegetables
Medium dose (1–10 kGy)		
• Shelf life extension	1.0–3.0	Strawberries, fresh fish, etc.
• Elimination of spoilage and pathogenic microorganisms	1.0–7.0	Fresh and frozen seafood, raw and frozen poultry and meat, feedstuffs, etc.
• Improving physical properties of food	2.0–7.0	Dehydrated pulses and vegetables (reduced cooking time), Grapes (increased juice yield)
• Decontamination	3.0–10.0	Spices, herbs, poultry feeds, etc.
High dose (above 10 kGy)	10.0–	Packaging materials, animal diets, enzymes,
• Commercial sterilization		hospital diets, space foods, viruses, etc.

[a] Gy (gray): unit used to measure absorbed dose (100 rad, 1 J/kg).

Low-dose irradiation: up to 1 kGy (sprout inhibition; delay of ripening; insect disinfestation; parasite inactivation).

Medium-dose irradiation: 1–10 kGy (reduction in the numbers of spoilage microorganisms; reduction in the numbers or elimination of nonspore-forming pathogens, i.e., disease-causing microorganisms).

High-dose irradiation: above 10 kGy (reduction in the numbers of microorganisms to the point of sterility).

Probably, the most desirable application of this technique is to improve the safety and quality of food and foodstuffs by ensuring the hygienic quality of solid or semisolid foods, especially those of animal origin, through inactivation of foodborne pathogens. This application is comparable to thermal pasteurization of liquid foods, which is widely applied for milk but is not suitable for foods such as meat, poultry, and seafood in a raw state, which are major sources for food poisoning (WHO 1988).

13.4.1 Growth Control: Sprout/Root/Shoot/Stem Growth Control

The tuber, bulb, and nut crops are normally sprouted after breaking of postharvest dormancy, thereby losing their marketable quality. The sprout and/or root inhibition of these crops during storage enable food industries to provide consumers with a year-round supply of potatoes, onions, garlic, yams, chestnuts, and other plant foods at a reasonable price, which avoids unnecessary shipments from other climatic zones during the off-season. The long-term storage of these crops is possible with the aid of refrigeration, particularly in subtropical and tropical regions. In addition, the desired inhibitory effects can also be obtained using chemical sprout inhibitors, such as maleic hydrazide, propham, and chloropropham. These chemicals, however, have limitations with their treatment effectiveness under tropical conditions and toxic residues in the produce, and thus, many countries have already prohibited their use.

A very low dose of 0.15 kGy or less inhibits sprouting of fresh produce, such as potatoes, onions, garlic, ginger, yams, and so on and 0.25 kGy for chestnuts. It leaves no residues and allows long-term storage at room temperatures (ICGFI 1999). Potatoes are required to be irradiated within 6–7 weeks after harvest to inhibit sprouting (Cho et al. 1982). Proper curing resulted in a reduction of the rotting rate in irradiated potatoes by healing the wounds in the periderms. Irradiated potatoes were more stable in their physicochemical and organoleptic qualities than the nonirradiated control and were superior to the control in their processing properties for potato chips (Byun et al. 1982).

The late-ripening varieties of onions and garlic were suitable for long-term storage by irradiation at 0.10–0.15 kGy, which should be done within 1–2 months after harvest (Figure 13.9). Drying of the outer surface and neck of the bulbs prior to irradiation is essential, together with the proper control of relative humidity during storage (Kwon et al. 1984; Kwon et al. 1985). Sulfur-containing pungent components were resistant to irradiation at the sprout-inhibition dose (Kwon et al. 1985, 1989). Irradiation could be utilized for the root inhibition and insect control of chestnuts, for which irradiation should be done as early as possible after harvest. A dose of 0.25 kGy was needed to preserve the quality of chestnuts for more than 7 months under humidified condition (Cho et al. 1983; Kwon 2005).

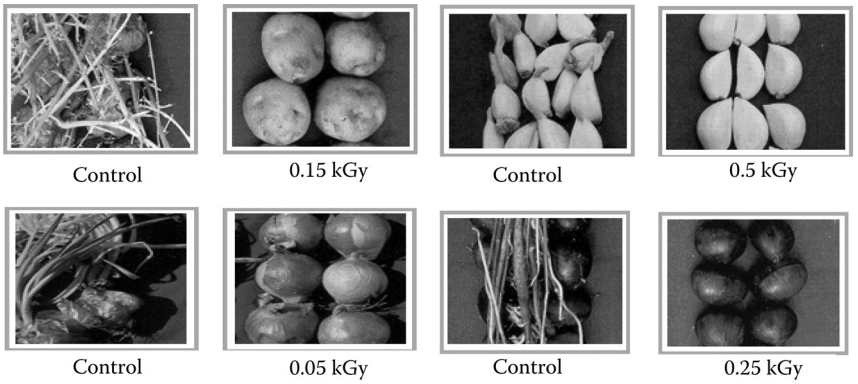


FIGURE 13.9 Sprout or root inhibition of potatoes, onions, garlic, and chestnuts during postirradiation storage.

The first commercial gamma irradiator has been operated for sprout inhibition of potatoes at the Shihoro irradiation center in Hokkaido, Japan, since 1974, which has been performed for more than 30 years with a volume of around 10,000 tons annually (Figure 13.10). The irradiated potatoes have been shown to have a better processing quality compared with nonirradiated potatoes (Kume et al. 2009a).

Sprouts from vegetable seeds have gained popularity in most advanced countries of the world as highly nutritious foods (Waje et al. 2009). However, fresh sprouts are highly susceptible to microbial growth particularly by pathogenic bacteria. Multiple outbreaks of foodborne illness (*Salmonella* and *E. coli* O157:H7) have been reported throughout the world linked to the consumption of raw or slightly cooked sprouts of alfalfa, mung bean, clover, cress, soybeans, radishes, and so on (Neetoo and Chen 2011; Ding et al. 2013). Studies have proven that contaminated seeds are the most significant source of foodborne pathogens in most sprout-related outbreaks (Liao 2008). However, sprouts can also be contaminated with pathogenic bacteria during the sprout germination and distribution process (Waje et al. 2009; Ding et al. 2013).

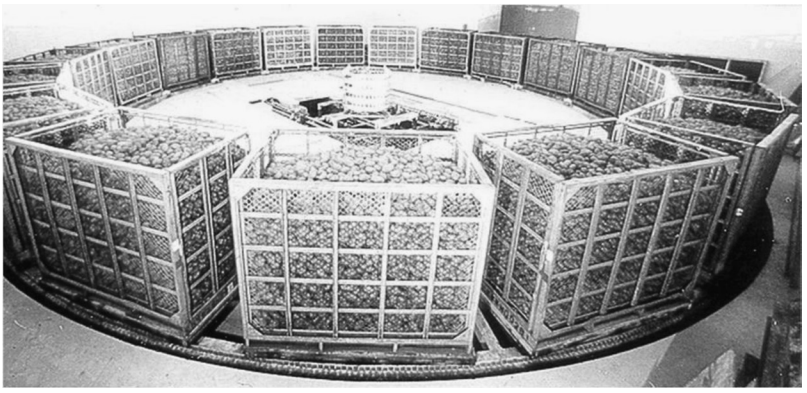


FIGURE 13.10 Gamma irradiator for potatoes in Hokkaido, Japan.

The application of thermal and chemical disinfestation treatments has shown limited effectiveness in eliminating pathogens on sprouts and seeds (Waje and Kwon 2007; Ding et al. 2013). In recent decades, ionizing radiation has been recognized as a safe and effective food-processing technology for reducing spoilage losses and improving their hygienic quality (Yordanov et al. 2006). Furthermore, ionizing radiations have shown the potential to completely destroy various foodborne pathogens from both seeds as well as sprouts (Thayer et al. 2003b; Bari et al. 2004). Ionizing radiations have the ability to penetrate cracks, crevices, and intercellular spaces of seeds and sprouts that contain pathogens (Waje et al. 2009). The US Food and Drug Administration (FDA) has tested and approved irradiation treatment of fresh produce, including sprouts, at a maximum dose of 1 kGy, and of seeds intended for sprout production at doses up to 8 kGy (Code of Federal Regulations 2000; Ding et al. 2013).

13.4.2 Shelf Life Extension

Exposure to a low dose of radiation delays the ripening and/or senescence of some fruits and controls fungal rot in certain vegetables, thereby extending their postharvest shelf life. Gamma irradiation at 1–3 kGy was applied to several fruits and vegetables, such as strawberries, peaches, tomatoes, apples, pears, and so on. Treatment effects on shelf life extension were different according to the radiation tolerance of each commodity, and thus the feasibility of irradiation treatment needs to be studied from a practical point of view (Josephson and Peterson 1983; Molins 2001). The shelf life of fresh mushrooms and fresh ginseng was effectively prolonged by irradiation at 1 or more kGy (Figure 13.11). Irradiation of mushrooms inhibits cap opening and

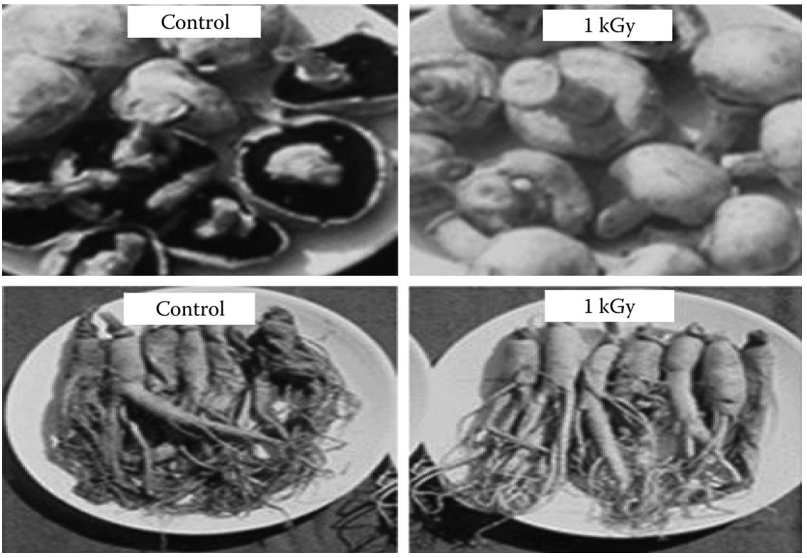


FIGURE 13.11 Shelf life extension of fresh mushrooms and ginseng by irradiation.

stem elongation. A corrugated-paper box/polyethylene-film wrapping was proposed as a packaging method suitable for reducing quality deterioration. The shelf life extension can be increased at least twofold by irradiation and subsequent storage at 10°C compared with the nonirradiated control (Byun et al. 1989). Strawberries are frequently spoiled by molds. Irradiation at 2–3 kGy and subsequent storage at 10°C could result in a shelf life extension up to 14 days, which primarily depends on the initial quality of the fresh food. Not all fruits and vegetables are suitable for irradiation because undesirable changes in color or texture, or both, limit their acceptability. In addition, different varieties of the same fruit or vegetable may respond differently to irradiation. The time of harvest and the physiological state also affects the response of fruits and vegetables to irradiation. To delay ripening in fruits, it is important to irradiate them before ripening starts (Josephson and Peterson 1983; ICGFI 1999).

However, the shelf life of meat, poultry, fish, seafood, and their processed products can be considerably prolonged by treatment with combinations of low-dose irradiation and refrigeration that do not significantly alter the quality. Different spoilage microorganisms, such as *Pseudomonas* spp., are relatively sensitive to irradiation. For instance, irradiation at 2.5 kGy of fresh poultry carcasses processed according to GMPs is enough to eliminate *Salmonella* contamination, and also reduces the populations of spoilage microorganisms, thereby extending the shelf life of the animal food remarkably when stored in a refrigeration condition (ICGFI 1999).

13.4.3 Disinfestations

Irradiation as a commercial insect control technique was applied for the first time in 1929 to cigars to control for *Lasioderma serricorne*, although the x-ray machine used proved to be unsuitable for continuous processing (Diehl 1995). Irradiation is also used to reduce pest populations in stored products (Salimov et al. 2000). Until now, irradiation of some stored products has been permitted in about 33 countries with 14 countries permitting it for all stored products (Hallman 2013).

Ionizing radiations knock electrons out of their orbits, producing ions and radicals. The free electrons collide with other electrons, resulting in an electron shower. The ions and radicals cause further damage to large organic molecules such as DNA inhibiting the development of irradiated organisms. The secondary damage caused by the ions and radicals created by the electron shower may cause more damage to organic molecules than the primary radiation itself. In organisms, radiation most easily affects sites of ongoing cell division, which in the adult insect includes the gonads and midgut. At minimal doses that stop the functions of these organs, insects will not reproduce and will cease feeding because the midgut cannot process food.

Irradiation at certain dose levels can destroy insects in various ways: sterility, lethality, reduced longevity, delayed molting, reduction of eggs hatching, delay in development, respiration inhibition, and so on (Table 13.6). In addition, it is important to note that irradiation causes sterility in insects, particularly at different life stages below the adult. Therefore, if a larva develops from an irradiated egg, it will not develop to the pupa stage. Similarly, an adult will be sterile if it develops from an irradiated pupa.

TABLE 13.6
Absorbed Doses That Might Achieve Quarantine Security of Several Pest Groups

Pest Group	Objective	Dose (Gy)
Aphids and whiteflies	Sterilize actively reproducing adult	50–100
Seed weevils (Bruchidae)	Sterilize actively reproducing adult	70–100
Scarab beetles	Sterilize actively reproducing adult	50–150
Fruit flies (Tephritidae)	Prevent adult emergence from third instar	50–150
Weevils (Curculionidae)	Sterilize actively reproducing adult	80–165
Borers (Lepidoptera)	Prevent adult development from late larva	100–280
Thrips	Sterilize actively reproducing adult	150–250
Borers (Lepidoptera)	Sterilize late pupa	200–350
Spider mites	Sterilize actively reproducing adult	200–350
Stored product beetles	Sterilize actively reproducing adult	50–400
Stored product moths	Sterilize actively reproducing adult	100–1000
Nematodes	Sterilize actively reproducing adult	~4000

The sterile insect technique has been adopted to eradicate pests or suppress their populations from specific regions (Calkins and Parker 2005). For this purpose, irradiation is used to reproductively sterilize reared pests and then released into pest-infested areas to mate with native insect populations to reduce successful reproduction. Similarly, phytosanitary irradiation prevents migration of potentially damaging organisms to new areas (Hallman 2011). Citrus fruits exported to the United States from Mexico are subjected to gamma irradiation at 150 Gy to prevent the entry of tephritid fruit flies (Hendrichs et al. 2009).

A major application of food irradiation is to replace banned fumigants used to meet quarantine requirements. Because insect pests can cause major harvest losses, controls have been legislated around the world to prevent their migration (Kwon 1998). Methyl bromide, the only broad-spectrum fumigant used for agricultural products but to be restricted in future use due to its potential toxicity and ozone-depleting properties, will be phased out globally according to the Montreal Protocol for environmental protection (UNEP 2000). Irradiation has been found as an effective method for pest control in fresh produce and dried food products and a promising alternative to methyl bromide. Unlike methyl bromide, irradiation is a physical treatment that does not leave a residue, and unlike phosphine, the other major fumigant used to control grain pests, irradiation is a fast and cold treatment, and can kill or control phosphine-resistant pests.

Irradiation disinfestation on the order of 1 kGy or less can be used to prevent losses caused by insect pests in stored grains, pulses, cereals, flour, spices, dried fruits, dried nuts, dried fishery products, and other dried food products. A minimum absorbed dose of about 150 Gy results in ensuring quarantine security against various species of tephritid fruit flies in fresh fruits and vegetables, and a minimum dose of 300 Gy can prevent insects from becoming established in noninfested areas. In most cases, irradiation either kills or inhibits further development of different

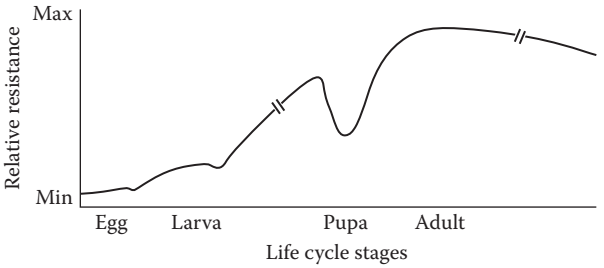


FIGURE 13.12 Generalized pattern of resistance to lethal effects of ionizing radiation in insects.

life-cycle stages of the insect pests. The inactivation of some pathogenic parasites with public health significance, such as tapeworms and trichinae in meat, can be achieved at dose ranging from 0.3 to 1 kGy (Figure 13.12).

Proper packaging is required, however, for irradiated products to prevent insect reinfestation. Radiation disinfestation can facilitate trade in fresh fruits, such as citrus, mangoes, and papayas that often harbor insect pests of quarantine importance. The occurrence of fruit flies, such as the Mediterranean, Oriental, Mexican, or Caribbean fruit flies, has repeatedly disrupted trade among countries. It has been found that low doses of ionizing radiation, 0.15–0.3 kGy, will very effectively control for fruit flies and other insect problems. This makes the use of irradiation for quarantine treatment a very practical possibility. In 1996, the United States Department of Agriculture (USDA)/Animal and Plant Health Inspection Service (APHIS) issued a Notice of Policy accepting irradiation as a quarantine treatment against major species of fruit flies regardless of commodities. Subsequently, in 1997, a final rule was issued by the USDA/APHIS for the irradiation of papayas, carambola, and litchi as a phytosanitary treatment. This rule allows interstate movement of these commodities from Hawaii to the US mainland and permits treatment either in Hawaii or in non-fruit-fly-supporting areas of mainland United States. Small commercial-scale irradiation of fruits from Hawaii has been carried out under special permission of the USDA/APHIS since 1995. Such irradiated fruits have been marketed successfully in the United States.

13.4.4 Microbial Decontamination

Among the different applications of food irradiation, special attention has been given to the inactivation of spoilage or pathogenic microorganisms. This includes irradiation up to 3 kGy to pasteurize poultry, seafood, and beef, which is termed radurization and higher doses (3.0–20 kGy) for sterilization of poultry, red meat and meat products, spices, herbs, and seasonings, which is termed as radicidation and radappertization. Most pathogenic microorganisms show comparatively higher sensitivity to irradiation treatments than to other general treatments (Josephson and Peterson 1983; WHO 1988; Loaharanu et al. 2007).

Ionizing radiations can effectively destroy pathogens present inside the tissues of sprouts or flesh because of their high penetration power. Gamma irradiation ensures

microbiological safety without deteriorating the sensory and nutritional properties of meat and poultry (Hashim et al. 1995; Abu-Tarboush et al. 1997) and that of fresh plant produce (Thayer et al. 2003a; Hajare et al. 2006). Kim et al. (2000) studied the efficacy of gamma irradiation processing at 5–10 kGy compared with conventional methods of decontamination to inactivate contaminating microorganisms present in Korean medicinal herbs.

The incidence of foodborne illness arising from the consumption of food contaminated with pathogenic microorganisms is ever increasing, which leads to a heightened public awareness of the health threat posed by food pathogens. Among these, *E. coli O157:H7, Salmonella, Campylobacter jejuni, Listeria monocytogenes*, and *Vibrio* are of primary concern from a public health point of view because of the severity of the illnesses and the higher number of outbreaks and individual cases of foodborne illness associated with these pathogens. Among these food-poisoning bacteria (Table 13.7) (Thayer 1995), *E. coli* O157:H7 has also been linked to major foodborne disease outbreaks through many sources including meat and dairy products in the United Kingdom, hamburger meat, apple juice, and water in the United States, vegetables in Japan, and seed sprouts in Germany. *Salmonella* and *C. jejuni* are usually associated with poultry. *L. monocytogenes* are associated with dairy products, processed meats, and other foods having a relatively long shelf life under refrigeration. *Vibrio* spp., in turn, have been the causative agents in cholera pandemics and in many outbreaks of disease caused by raw mollusks. Adherence to GMP is obviously essential but this alone may not be sufficient to reduce the number of food-poisoning outbreaks. Pathogens such as those mentioned above are quite sensitive to low doses of ionizing radiations (ICGFI 1999).

Irradiation at 2.5 kGy will virtually eliminate *Salmonella* and *Campylobacter* under proper production conditions for fresh poultry carcasses, which also destroys *E. coli* O157:H7 that can lead to illness or death, with an estimated 20,000 infections and 250 deaths in the United States annually. Irradiation is a unique method for inactivating these pathogens in food in a raw and frozen state. Frog legs heavily contaminated by *Salmonella* and other pathogens can be effectively decontaminated, which

TABLE 13.7
Radicidation Effects on Pathogenic Microorganisms

Pathogen	Temperature (°C)	Substrate	D_{10} Value[a] (kGy)
Aeromonas hydrophila	2	Beef	0.14–0.19
Campylobacter jejuni	0–5	Beef	0.16
Escherichia coli O157:H7	5	Beef	0.28
Listeria monocytogenes	2–4	Chicken	0.77
Salmonella spp.	2	Chicken	0.36–0.77
Staphylococcus aureus	0	Chicken	0.36

Source: From Thayer, D. W. 1995. *Journal of Food Safety* 15: 181–12.

[a] Decimal reduction dose for the initial microbial populations.

can be purchased in some French food markets. Eggs and egg products often contaminated with *Salmonella* can be another candidate for food-irradiation processing at about 2 kGy while still maintaining the sensory and technological properties. Seafood, especially shellfish, is often contaminated with pathogens such as *Vibrio parahaemolyticus* and *Shigella*. Nevertheless, many people like to eat raw shellfish such as oysters and clams. In the case of frozen seafood, the reduction of pathogens to an acceptable level needs about 3 kGy for inactivating *Vibrio* spp., *Salmonella* spp., and *Aeromonas hydrophila*. It is well known that fresh pork should be cooked thoroughly because it may contain *Trichinella spiralis*, *Toxoplasma gondii*, and so on, parasites that may cause illness and death. These parasites can also be inactivated with less than 1 kGy.

Radiation enhances the keeping quality of foods through a substantial reduction in the number of spoilage-causing microorganisms contaminating fresh meat, seafood, and some vegetables. This process of extending the shelf life is called "radurization" and the products are usually stored under refrigerated conditions following irradiation treatment. Pasteurization of solid foods such as meat, poultry, and seafood by irradiation is a practical method to eliminate pathogenic organisms and microorganisms except for viruses, which can be achieved by a reduction in the number of specific viable nonspore-forming pathogenic microorganisms with doses ranging from 2 to 8 kGy. This process of improving the hygienic quality of food by inactivation of foodborne pathogenic bacteria and parasites is called "radicidation." This medium dose application is very similar to heat pasteurization, and is hence also called "radiopasteurization."

On the contrary, spices, herbs, and vegetable seasonings valued for their distinctive colors and flavors are often heavily contaminated with microorganisms because of the environmental and processing conditions for their production. In this regard, the microbial load should be reduced before they are safely incorporated into other food ingredients. Previously, most spices and herbs were fumigated, usually with sterilizing gases such as ethylene oxide, to decontaminate microorganisms contaminating foods. Use of most chemical fumigants has been prohibited worldwide because they were found to be carcinogenic or toxic. Table 13.8 shows the comparative effect of different decontamination methods, on dried spices. Heat treatment, including steaming, can cause significant loss of their flavor and aroma; thus, nonchemical and nonthermal processes are required. Irradiation has since emerged as a viable alternative, by which spices and herbs that are cleaner and have a better quality are available compared with those fumigated with ethylene oxide or treated with hot steaming (ICGFI 1999; Waje et al. 2008). Recently, hot steaming treatment has been utilized in food industries for the decontamination of spices, herbs, and vegetable seasonings. A comparative study undertaken to determine the effects of different methods showed that irradiation at 10 kGy was more efficient than vacuum steaming for 70 min on the microbial, physicochemical, and sensory qualities of black and red pepper powders (Waje et al. 2008). Irradiation of spices and dried vegetables on a commercial scale is practiced in over 20 countries and global production has significantly increased up to 268,000 tons in 2005 (Kume et al. 2009a). The United States has approved irradiation up to 30 kGy for herbs, spices, and vegetable seasonings for the purpose of their microbial control since 1986.

TABLE 13.8
Comparative Effects of Different Decontamination Methods on Dried Spices

		Decontamination Method		
Quality Parameter	**Spice Powder**	**Control**	**Vacuum Steam**	**Irradiation (10 kGy)**
Total plate count (CFU/g)	Black pepper	2.8×10^6	7.0×10^3	3.5×10^2
	Red pepper	2.1×10^6	1.1×10^5	1.8×10^1
Functional components (mg/g d.b.)	Black pepper (piperine)	12.36^a	9.30^c	11.10^b
	Red pepper (capsaicin)	0.56^a	0.50^a	0.55^a
Hunter color difference (ΔE)	Black pepper	0.00	2.08	0.60
	Red pepper	0.00	0.23	0.33
Sensory score (1–5)	Black pepper	3.3^a	3.1^a	3.4^a
	Red pepper	3.8^a	3.4^{ab}	3.1^b

Note: Means followed by the same letters within the row ($^{a–c}$) are not significantly different ($P < 0.05$).

Yun et al. (2012) found that gamma irradiation (1–10 kGy) effectively reduced aerobic bacteria and fungi in soybean. In addition, the applied doses did not significantly affect the sensory attributes. Irradiation at the doses applied did not cause any significant change in the isoflavone content of soybeans, but decreased the tocopherol content. Hocaoglu et al. (2012) evaluated the combined effect of gamma irradiation and different storage conditions on microbiological and physicochemical changes produced in shrimp. The results showed that irradiation and subsequent storage at low temperature (+4°C) significantly reduced the bacterial contamination in the shrimp samples. Furthermore, the combined application proved helpful in stabilizing the chemical characteristics in the shrimp meat samples. However, irradiated foods must be stored and handled with the same safety protocols adopted for nonirradiated or other treated foods.

13.4.5 Sterilization of Special Foods

Radiation sterilization at dose levels from 25 to 70 kGy extends the shelf life of precooked or enzyme-inactivated food products in hermetically sealed containers almost indefinitely at room temperature. This process is similar to thermal canning in achieving shelf-stability and is often called "radappertization" (IAEA 1982), which belongs to the reduction of the number and/or activity of all organisms involved with food spoilage or having public health significance, including their spores to such an extent that none are detectable in the treated products by any recognized methods. Radiation-sterilized foods are served to hospital patients who have immune system deficiencies requiring a sterile diet. These foods are also used by astronauts in the space program because of their special quality and safety, compared with conventionally existing foods treated by other preservation techniques. The limited scale

of various ready-to-eat foods has been commercially high-dose irradiated in South Africa for more than 10 years to serve military personnel and outdoor enthusiasts, such as campers, yachters, and hikers (ICGFI 1999).

13.4.6 Novel Applications

Irradiation is not only used for inactivating undesirable microorganisms and insect pests but is also used to improve the quality of foods by reducing or eliminating toxic or undesirable compounds in food as well as by extending the shelf life of fresh produce. Irradiation is known to reduce the allergenicity of food by modifying the structure of proteins causing allergic reactions. A model study showed that the volatile *N*-nitrosamine could be reduced or eliminated by irradiation and the radiation-induced breakdown products did not recombine under human stomach conditions (pH 2–4, 37°C). The possible reduction of residual chlorophyll b by irradiation was found in a model study, which indicated that irradiation could destroy chlorophyll b in teas (Byun et al. 2007). Further research is urgently needed to identify and evaluate the breakdown products induced by irradiation and its safety for future applications to real food systems (Lee et al. 2012).

13.4.7 Cold Process Characteristics

Food irradiation is a physical method of processing foods by exposing them to ionizing energy from approved radiation sources, which can be compared with heating or freezing. The energy absorbed by the irradiated food is much less than that taken up by heated foods. It is generally understood, therefore, that chemical changes induced by irradiation are much smaller than those by heating.

In terms of energy, 1 Gy equals 1 J of energy absorbed per kilogram of food being irradiated. The maximum dose of 10 kGy (maximum dose to be mostly used for food irradiation), recommended by the Codex General Standard for Irradiated Foods, corresponds to a temperature rise of only 2.4°C in food having the heat capacity of water (4.184 J/°C). This is approximately 3% of the energy needed to raise the temperature of water from approximately 20°C to 100°C (WHO 1981). Therefore, irradiation is often referred to as a cold pasteurization process because it can accomplish the same objective as thermal pasteurization of liquid food such as milk (WHO 1981; ICGFI 1999). It has been reported that radiation pasteurization uses only 21 kJ/kg and radappertization uses 157 kJ/kg, which is much less than the energy used in other food processes. A comparison has also been made with other methods of preserving, distributing, and preparing meat for servings. Food irradiation appears to save significant amounts of energy (Table 13.9) (Brynjoifossn 1981; Annoy 1998).

Meantime, irradiation is known as a process with nonthermal and nonresidue characteristics, being little affected by environmental and processing factors. Table 13.10 shows a comparison of factors influencing sterilization processes and that treatment with radiation is a competitive process among the methods listed (IAEA 1982; Loaharanu 1996).

TABLE 13.9
Comparison of the Energy Consumption in Different Food Processes

Process of Food	Energy (kJ/kg)
Sprouting inhibition (0.10 kGy)	12
Insect disinfestation (0.25 kGy)	7
Radpasteurization (2.5 kGy)	21
Radappertization (30 kGy)	157
Heatappertization (heat sterilization)	918
Blast freezing chicken (4.4°C → –23.3°C)	7552
Storing the product (–25°C for 3.5 wks)	5149
Refrigerated storage (0°C for 5.5 days)	318
Refrigerated storage (0°C for 10.5 days)	396
Cooking the whole thawed chicken (93°C)	2558

TABLE 13.10
Comparison of Factors Affecting the Process in Different Sterilization Methods[a]

Specification	Dried Heat	Humid Heat	Gas Fumigation (EtO)	Irradiation
Temperature	+	+	+	– / +
Time	+	+	+	+
Pressure	–	+	+	–
Humidity	–	NA	+	–
Drying or deaeration after treatment	NA	+	+	NA
Reaction with material	Oxidative degradation	Gaseous degradation	Hydroxyl ethylation	Radiolytic degradation
Toxic residue	No	No	Yes	No
Environmental pollution	No	No	Yes	No
Density	+	+	+	+
Packaging method	Narrow	Narrow	Narrow	Wide
Packaged end product	NA	NA	NA	A
Type of treatment	Batch	Batch	Batch	Continuous

[a] + , affected; –, not affected; NA, not applied; A, applied.

13.5 SAFETY EVALUATION OF IRRADIATED FOOD

It is true that food irradiation is the most studied single technology or technique in terms of its effects on nutritional adequacy as well as toxicological and microbiological safety of the foods when treated with ionizing radiations. This extensive ongoing research for more than 50 years is probably due to the use of radiations emitting

from radionuclide or machine sources, being different from traditional heating and freezing. Since the 1950s, hundreds of short-term or long-term safety and nutritional studies have demonstrated the wholesomeness of irradiated foods, thereby leading to the approval of one or more food for irradiation processing by 57 countries currently (IAEA website).

Among the many comprehensive animal feeding studies on irradiated food, those conducted at the Raltech laboratory in the United States are generally acknowledged from the systematic and statistical points of view. The studies involved using chicken irradiated either by a cobalt-60 source or electron beam up to a dose of 58 kGy. One hundred and thirty-four tons of chicken meat, or nearly a quarter of a million birds, were used in the study to compare high-dose irradiation with heat sterilization of chicken. The study included chronic feeding studies in mice and dogs, teratology studies, and mutagenicity tests, followed by comprehensive reviews by scientists of the US FDA in the 1980s. No adverse effects from consuming chicken treated with even high doses of radiations were demonstrated. Over the last 20 years, millions of mice, rats, and other laboratory animals were bred and reared exclusively on irradiated diets at doses up to 25 or 50 kGy at many institutions in different countries. No transmittable genetic defects—teratogenic or oncogenic—were observed being attributed to the consumption of irradiated diets (ICGFI 1999; Loaharanu 2007).

Nevertheless, there is sometimes concern about the possibility that irradiation might make food radioactive. Irradiation doses (maximum 10 or 30 kGy) permitted to treat foods, however, are far less than the high dose enough to make food radioactive. Every material in our environment, including food, contains trace amounts of radioactivity, which means that trace amount (less than 200 becquerels/kg) of natural radioactivity from elements, such as potassium (K), is unavoidable in our daily diets. Even when foods are exposed to very high doses of radiation, the maximum level of radioactivity would be just one-thousandth of a Bq per kg of food, which is 200,000 times lesser than the level of radioactivity naturally existing in food. Food undergoing irradiation cannot become radioactive any more than luggage passing through an airport x-ray scanner or teeth exposing to x-ray. Food itself never contact directly with the radiation source while they are under processing (ICGFI 1999).

Since irradiation was evaluated as a physical process as early as 1976 by FAO/IAEA/WHO Expert Committee, it was concluded in 1980 that "irradiation of any food commodities up to 10 kGy causes no toxicological hazards, along with no special problems in the nutritional and microbiological aspects" (WHO 1981). The Joint FAO/WHO CAC was satisfied regarding the above evaluations and adopted "the Codex General Standard for Irradiated Food and the Recommended International Code of Practice for the Operation of Radiation Facilities for the Treatment of Food" in 1983, recommending that the Codex be accepted by all its member countries (CAC 1984). The joint evaluation of WHO and IOCU recertified in 1992 the safety of irradiated food and reported that if irradiation processing is strictly used under the GMPs, there is no problem from the nutritional and microbiological point of view. Furthermore, the WHO Golden Rules for Safe Food Preparation (WHO 1981) states that "consumer would better select a fresh irradiated frozen poultry meat." In 1997,

FAO, IAEA, and WHO convened a Joint Study Group to evaluate studies on irradiated food at above 10 kGy and they concluded that food irradiated with any doses is both safe and nutritionally adequate. Thus, no upper-dose limit needs to be imposed as long as food is irradiated based on prevailing GMPs (Loaharanu 2007).

Recently, there has been some misunderstanding between irradiated food and radioactive food. The former is a food that has been intentionally processed with the approved radiation energy to achieve desirable purposes (sprout inhibition, insect/pathogens destruction, microbial inactivation, etc.). The latter, however, is a food that has become accidentally contaminated by radioactive substances from nuclear power plant accidents or weapons testing. The radio-contamination in food is totally different from irradiated food, which is to be improved in its safety and quality in terms of microbiological and physiological points of view (ICGFI 1999).

13.6 REGULATION AND LEGISLATION

The Codex General Standards for Irradiated Foods were first established in 1983 (CODEX STAN 106-1983) and revised in 2003 (CODEX STAN, REV.1-2003). The standards include the scope, general requirements for the process, hygiene of irradiated foods, technological requirements, reirradiation, postirradiation verification, and labeling requirements (CAC 2003).

This standard applies to foods processed by ionizing radiation being used in compliance with applicable hygienic codes, food standards, and transportation codes. It does not apply to foods exposed to irradiation doses imparted by measuring instruments used for inspection purposes. Three types of ionizing radiations may be used for food irradiation: (a) gamma rays from the radionuclides ^{60}Co or ^{137}Cs; (b) x-rays generated from machine sources operated at or below an energy level of 5 MeV; and (c) electrons generated from machine sources operated at or below an energy level of 10 MeV (CAC 2003).

For the irradiation of any food, the minimum absorbed dose should be sufficient to achieve the technological purpose. The maximum absorbed dose should be less than that which would compromise consumer safety and wholesomeness, or would adversely affect the structural integrity, functional properties, or sensory attributes. The maximum absorbed dose delivered to a food should not exceed 10 kGy, except when necessary to achieve a legitimate technological purpose (WHO 1981, 1994, 1999; CAC 2003).

Radiation treatment of foods should be carried out in facilities licensed and registered for this purpose by a competent national authority. The facilities should be designed to meet the requirements of safety, efficacy, and good hygienic practices of food processing. The facilities should be staffed by adequately trained and competent personnel. Control of the process within the facility should include the keeping of adequate records, including quantitative dosimetry. Facilities and records should be open to inspection by appropriate authorities (CAC 2003).

The irradiation of food is justified only when it achieves the technological requirement and it should not be a substitute for good hygienic and GMPs or good agricultural practices. Foods to be irradiated and their packaging materials shall be of suitable quality, acceptable hygienic condition, and appropriate for this purpose

and shall be handled, before and after irradiation, according to GMPs taking into account the particular requirements of the technology of the process. Except for foods with low moisture content (cereals, pulses, dehydrated foods, and other such commodities) irradiated for the purpose of controlling insect reinfestation, foods should not be reirradiated. However, food is not considered as having been reirradiated when (a) the irradiated food is prepared from materials that have been irradiated at low dose levels for purposes other than food safety, for example, quarantine control or the prevention of the sprouting of roots and tubers; (b) the food, containing less than 5% of irradiated ingredients, is irradiated; or (c) the full dose of ionizing radiation required to achieve the desired effect is applied to the food in more than one increment as part of the processing for a specific technological purpose. The cumulative maximum absorbed dose delivered to a food should not exceed 10 kGy as a result of reirradiation except when it is necessary to achieve a legitimate technological purpose, and should not compromise consumer safety or the wholesomeness of the food (CAC 2003).

However, when required and where applicable, analytical methods for the detection of irradiated foods may be used to enforce the authorization and labeling requirements. The analytical methods used should be those adopted by the Codex Commission. For irradiated foods, whether prepackaged or not, the relevant shipping documents shall provide the appropriate information to identify the registered facility, which has irradiated the food, the date(s) of treatment, irradiation dose, and lot identification. The labeling of prepackaged irradiated foods should indicate the treatment and in all aspects should be in accordance with the relevant provisions of the Codex General Standard for the Labeling of Prepackaged Foods (CAC 1985). A declaration of the fact of irradiation should be made clearly on the relevant shipping documents. In the case of products sold in bulk to the ultimate consumer, the international logo (Figure 13.13) and the words "irradiated" or "treated with ionizing radiation" should appear together with the name of the product on the container in which the products are placed (CAC 2003). Subsequent to the 2003 finalization of revised texts especially on sanitary applications of irradiation by the Joint FAO/WHO Codex Alimentarius Commission (Codex), the International Plant Protection Convention has also assigned a high priority to the development of international standards on the use of irradiation for phytosanitary applications to help governments ensure the supplies of safe and wholesome foods and to control insect pests (IPPC 2003; Loaharanu 2007; Griffin, 2008).



FIGURE 13.13 International logo of irradiated food.

13.7 CONSUMER ACCEPTANCE

Consumers are originally conservative in accepting new technologies and their products. Consumer acceptance or rejection of new technology is the result of a complex decision-making process, which involves an assessment of the perceived risks and benefits associated with the new technology and available alternatives (Henson 1995). When milk pasteurization was first introduced as a means of improving the safety of milk in the early 1900s, it was refused by consumers who had perceived concerns about the new technology although it makes milk safer even without changing the taste and color of fresh milk. These public concerns, as a result, delayed the regulatory approval and commercial use of this new technology by nearly 70 years. The arguments against pasteurization were almost similar to those adapted today against food irradiation. They included that heat pasteurization causes quality change, formation of dangerous substances, price increases, accidents occurring, and so on, none of which turned out to be true; however, those campaigns against pasteurization apparently delayed its practical implementation, with the effect of thousands of people suffering from health problems (Hall and Trout 1968). A similar situation has arisen with irradiated food. Although the safety and benefits of food irradiation have been thoroughly documented in terms of its scientific basis and mechanisms with over a half century of research and evaluations, the commercial implementation of food irradiation has been delayed mainly due to the misunderstanding or misconception by the general public on its safety and the conservative position of food industries. Considering the emerging needs for effective alternative technologies to both chemical fumigants that have been used for sanitary and phytosanitory measures in the international trade of fresh food commodities and heat treatments, which have limitations in application to dried foodstuffs and powdered ingredients due to quality changes and treatment effectiveness, the various benefits of food irradiation technology or techniques cannot be overlooked as a green process in the food and health industries (Loaharanu 2007; Kwon 2010). At a time when food poisoning outbreaks is ever increasing, when fumigants are being phased out, and the consumer is looking for safer and higher quality of foods, food irradiation is expected to play an important role in the production of safe and wholesome food just as heat pasteurization has been doing now (Loaharanu 2007; Kwon 2010). In fact, many consumers are unfamiliar with food irradiation. However, education and publicity activities using factual information have shown positive results on changing the attitude of consumers. Consumers have indicated that the endorsements of the wholesomeness of irradiated foods by international and national health authorities concerned have increased their confidence in the safety of this technology.

A number of market studies conducted over the past two decades repeatedly demonstrated that 80–90% of consumers would choose irradiated foods rather than non-irradiated ones in cases where consumers received information and understood the benefits (Eustice and Bruhn 2006). In 2002, Texas A & M University (TAMU) (Aiew et al. 2003) undertook a study on consumer acceptance and willingness to purchase irradiated ground beef before and after educational information. Before given any information, about half of the respondents had no knowledge on food irradiation and 51% would not buy irradiated ground beef. While approximately 88% of them

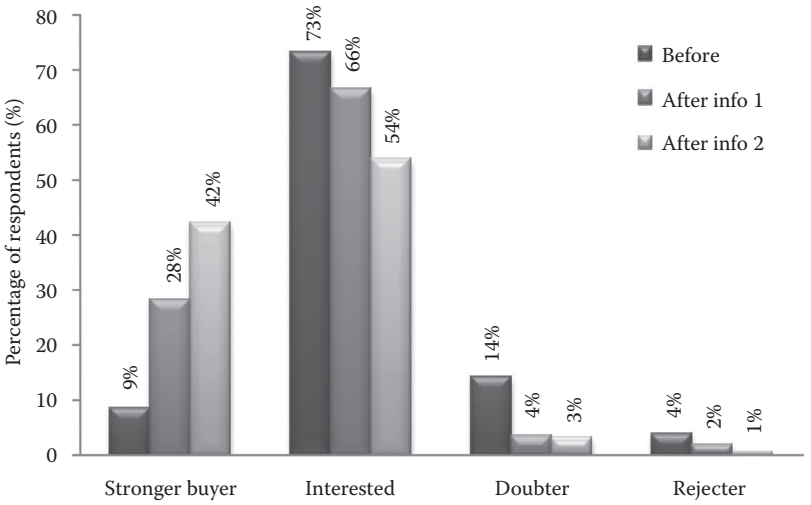


FIGURE 13.14 Consumer willingness to buy irradiated ground beef before and after information about food irradiation. (From Aiew, W., Nayga, R. M., and Nichols, J. 2003. Information effects on consumers' willingness to purchase irradiated products (Working Paper). College Station, TX: Texas A&M University Department of Agricultural Economics).

became willing purchasers after receiving a presentation on irradiated food, more than 94% of the respondents indicated their willingness to buy irradiated ground beef following a second presentation on irradiated food (Figure 13.14). The percentage of strong buyers increased from 9% to 42%, while the percentage of doubters or rejecters decreased significantly from 14% to 3% for doubters and from 4% to about 1% for rejecters (Figure 13.14). This result was higher than the Food Net Report 2000 by the Centers for Disease Control and Prevention (CDC 2000), showing that if given a choice between nonirradiated and irradiated foods, from half to about 80% of consumers would purchase the irradiated one as a result of informative education.

Similarly, Turkish people's (total of 444 respondents) awareness and acceptance, and influence of benefit statements on irradiated foods were investigated (Gunes and Tekin 2006). Consumer awareness of food irradiation was very low (29%) and the majority of consumers (80%) showed uncertainty about the safety of irradiated foods (Figure 13.15) with only 11% expressing that irradiated foods are safe. The results indicated that a positive attitude toward irradiated food increased by more than 60% upon receiving a benefit statement of food irradiation. The informative statement brought about a change in consumer attitudes toward irradiated foods. Sixty-four percent of the respondents who were uncertain about the safety of irradiated food indicated that they would buy irradiated food after receiving information on the benefits of food irradiation (Figure 13.16). Purchase willingness of irradiated food was highest (44%) when the price is same as nonirradiated food, but over 20% of consumers responded to pay a 5% premium price for irradiated food. They also reported that consumer acceptance increased to 66% when highly trusted companies produce irradiated food (Gunes and Tekin 2006).

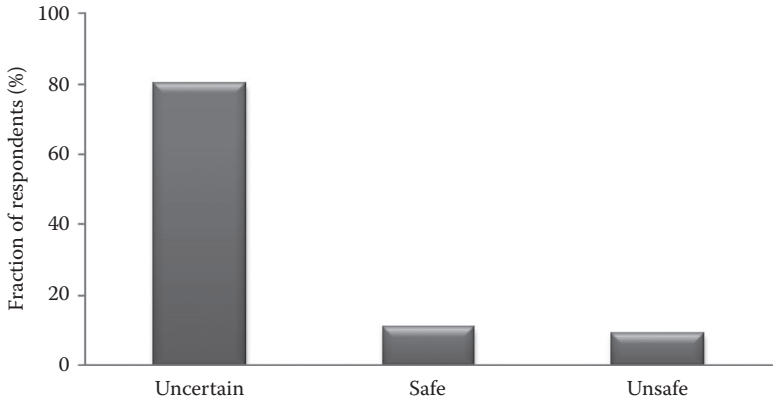


FIGURE 13.15 Consumers' overall opinion about the safety of food irradiation prior to hearing a benefit statement. (Adapted from Gunes, G. and Tekin, M. D. 2006. *LWT-Food Science and Technology* 39: 443–7.)

In a USDA-funded project in California and Indiana regarding the impact of a brief educational program on community leaders' attitudes on food irradiation, a 10-min video on food irradiation resulted in an increased willingness to try irradiated foods from 57% to 82%. In South Africa, a marketing and educational program also indicated that receiving visual information could increase consumer willingness to buy irradiated shelf-stable meat products from initially 15% to 54%. Meantime, both after receiving information and tasting foods, 76% of respondents would purchase irradiated shelf-stable meat products, while 5% of them probably would not buy the products (ICGFI 1999).

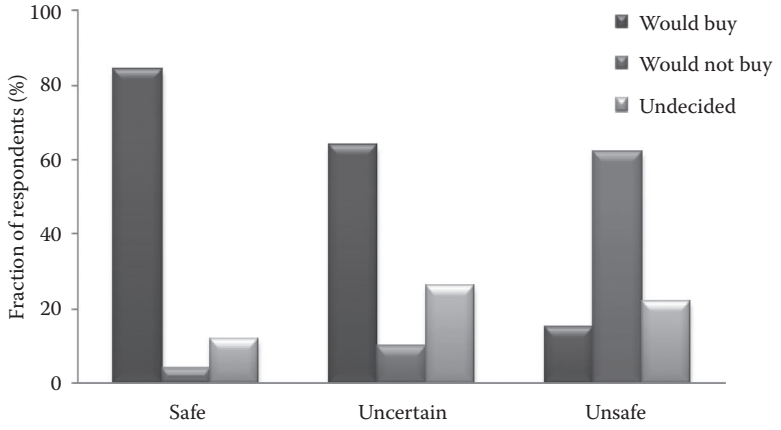


FIGURE 13.16 Consumers' tendency to buy irradiated foods after hearing a benefit statement as categorized by their earlier opinion on the safety of irradiated food. (*X* axis shows consumers' opinion on safety of irradiated foods prior to hearing the benefit statement.)

Numerous marketing tests of irradiated foods have been carried out in different countries during the last few decades, and to date, all have been successful. In the United States, a retailer in the Chicago area featured irradiated strawberries, grapefruit, and oranges in 1992, which outsold the nonirradiated produce by 10 to 1 (ICGFI 1999). Irradiated tomatoes, mushrooms, and onions were later marketed with similar sales success. In 1996, when another test was conducted, the market share increased to 63% when irradiated poultry was priced 10% lower than the store brand, 47% when the price was equally, and 18% and 17% when the price was 10% and 20% higher. This is consistent with other attitude surveys and market place data that show irradiated food is more acceptable in upscale markets. Prior to the first marketing of irradiated onions and garlic in the Buenos Aires area in 1985, consumers were informed about food irradiation by the local media, and consequently, about 10 tons of irradiated products were sold within 3 days. In China, various irradiated foods were tested during the 1980s and the 1990s, which included apples, garlic, potatoes, tomatoes, seasonings, dehydrated vegetables, meat products, sweet potato wine, and so on. Nham, fermented pork sausage consumed in a raw state in Thailand, is often contaminated with *Salmonella* and occasionally with *T. spiralis*. Labeled irradiated Nham was test marketed along with the traditional products in 1986 in Thailand. About 34% of consumers selected irradiated Nham out of curiosity and their satisfaction with the taste was high, showing 95% of the customers expressed their intent to purchase irradiated Nham again. During the 3-month test, irradiated Nham outsold the nonirradiated product by a ratio of 10 to 1 and this product is presently available in Thai markets. Irradiated strawberries, chicken breast meat, and Camembert cheese were test marketed in Lyon, France in 1987, with a 30% higher price than that of the nonirradiated products and sold successfully. Over a 6-year period, different popular dishes, such as grilled chicken, curried chicken, bacon, and curried beef, have been evaluated by a large number of different groups, including hikers and sea voyagers, which indicated high acceptance as well (ICGFI 1999).

Market tests and ongoing sales of irradiated foods are providing the best source of practical information on whether irradiated foods meet consumers' needs, which consequentially provide excellent information on consumer acceptance, thus facilitating the commercialization of food irradiation. On the contrary, an unfavorable description of radiation has a great negative effect on consumer acceptance of irradiated foods although anti-irradiation messages can be counteracted and finally consumer confidence in irradiated food can be restored by factual information on food irradiation (Fox 2002). In general, most consumers have expressed less concern about food irradiation than other food-processing technologies (Bruhn 1998). Irradiation had the least amount of concern among functionally equivalent techniques such as freezing and pasteurization (Figure 13.17) (Gunes and Tekin 2006). Similar results were found in that people had less concern with irradiation than with pesticides, bacteria, additives, and hormones (Resurreccion et al. 1995). Consumer attitude studies have demonstrated that when given science-based information, 60–90% of consumers prefer the benefits of food irradiation. When information is accompanied by samples, consumer acceptance may increase to 99%. Such information on food irradiation requires product benefits, safety endorsements by recognized health authorities concerned, and environmental safety (Bruhn 1998). A successful marketing for

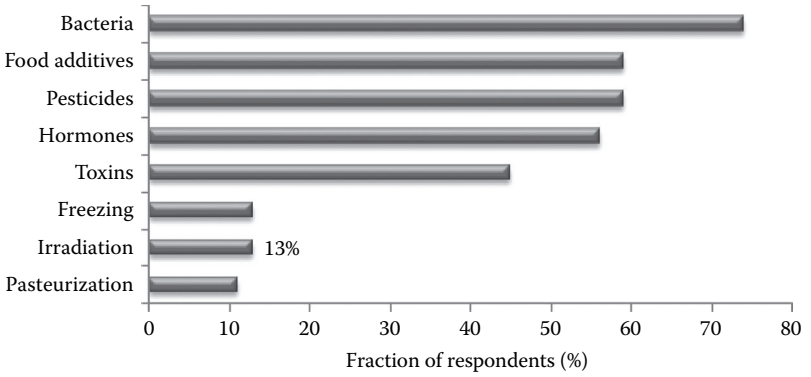


FIGURE 13.17 Consumer concerns about several food processing methods and components potentially harmful to health. (Adapted from Gunes, G. and Tekin, M. D. 2006. *LWT-Food Science and Technology* 39: 443–7.)

irradiated foods can be achieved not only by educating consumers with factual information, but by also providing an opportunity to experience irradiated foods along with their nonirradiated counterparts.

13.8 APPROVAL AND COMMERCIALIZATION

Fifty-seven countries have approved one or more food and food ingredients for irradiation. The Irradiated Food Authorization Database (IAEA website) on country approvals of irradiated foods includes country name, class of food, specific food product, objective of irradiation, date of approval, and recommended dose limit. At the same time, a database on facilities for the irradiation of foods includes country name, facility contact details, type of irradiator, and energy source. They can be accessed at http://nucleus.iaea.org/fitf/ and are maintained by the Food and Environmental Subprogramme of the Joint FAO/IAEA Division of Nuclear Techniques in Food and Agriculture (IAEA website). The Joint Division continues to assist its member states in the implementation of postharvest applications of irradiation in food and agricultural commodities by sponsoring research projects and scientific visits, convening groups of experts to provide independent and authoritative advice, collaborating with the Codex, and other international organizations (IAEA website).

Among the 60 countries that have approved specific applications of food irradiation, approximately 40 countries are actually producing irradiated foods for commercial purposes. Both the number of approvals of food products/applications and the number of countries that have approved food irradiation have been increasing. The recent trend of approvals is based on food classes rather than individual food items presented in Table 13.11 (Anoymous 1998). The foods are classified into eight classes: roots and tubers, fruits and vegetables, cereals and certain pod-bearing plants, fish and seafood, meat and poultry, spices and seasonings, dried food of animal origin, and miscellaneous foods, based on purpose and minimum/maximum dose. The United States and Croatia permitted irradiation doses up to 30 kGy for

TABLE 13.11
Advisory Technological Dose Limit of Irradiation for Different Food Classes on the Basis of Similarity of Chemical Compositions (WHO/FAO/IAEA)

Class of Food	Classes of Food	Purpose	Maximum Dose (kGy)
Class 1:	Bulbs, roots, and tubers	To inhibit sprouting during storage	0.2
Class 2:	Fresh fruits and vegetables (other than Class 1)	To delay ripening	1.0
		Insect disinfestation	1.0
		Shelf life extension	2.5
		Quarantine control[a]	1.0
Class 3:	Cereals and their milled products, nuts, oil seeds, pulses, dried fruits	Insect disinfestation	1.0
		Reduction of microbial load	5.0
Class 4:	Fish, seafood and their products (fresh or frozen)	Reduction of certain pathogenic microorganisms[b]	5.0
		Shelf life extension	3.0
		Control of infection by parasites[b]	2.0
Class 5:	Raw poultry and meat and their products (fresh and frozen)	Reduction of pathogenic microorganisms[b]	7.0
		Shelf life extension	3.0
		Control of infection by parasites[b]	2.0
Class 6:	Dry vegetables, spices, condiments, animal feed, dry herbs and herbal teas	Reduction of certain pathogenic microorganisms[b]	10.0
		Insect disinfestation	1.0
Class 7:	Dried food of animal origin	Disinfestation	1.0
		Control of molds	3.0
Class 8:	Miscellaneous foods, including, but not limited to, honey, space foods, hospital foods, military rations, spices, liquid egg, thickeners	Reduction of microorganisms	>10
		Sterilization	>10
		Quarantine control	>10

Source: From Anoymous. 1998. Present status and guidelines for preparing harmonized legislation on food irradiation in the Near East, Paper presented at Joint AAEA/FAO/IAEA Regional Workshop, Tunis, Tunisia.

Note: 1. Product grouping into classes (except Class 8) is on the basis of similarity of chemical compositions.
2. The maximum dose limits have been set for good irradiation practice and not from a food safety viewpoint.

[a] The minimum dose may be specified for particular pests. For fruit flies, the minimum dose is at least 0.15 kGy.

[b] The minimum dose may be specified depending on the objective of treatment to ensure the hygienic quality of food.

certain food items that include dried vegetables, herbs, spices, and other powdered products. Furthermore, Brazil and South Africa have approved food irradiation without upper dose limits (CAC 2003; IAEA website).

Since the start of potato irradiation in the middle of the 1970s by the first commercial gamma irradiator located in Hokkaido, Japan, some significant progress has been made in the field of food irradiation research and commercial development around the world. Some irradiated foods, such as spices, herbs, and dried vegetable seasonings, and different processing ingredients have entered international markets for use by the food industry. However, other irradiated foods such as ground beef, chicken, and some processed foods are mainly distributed in domestic markets to meet local demands. Starting in April 2007, irradiated mangoes from India entered the United States for the first time, opening the gate for international trade in fresh produce using irradiation. With the recent generic acceptance of irradiation for imported fruits and vegetables, international trade of irradiated food is likely to increase significantly in the near future (Loaharanu 2007).

The commercial status of food irradiation worldwide was reported by Kume and Todoriki (2013) on the regional basis of Asia, the European Union, and the United States. The results show that the quantities of irradiated foods in Asia, the EU, and the United States in 2010 were estimated at 285,200, 9300, and 103,000 tons, respectively. Compared with 2005, the quantity of irradiated foods was about 100,000 tons higher in Asia and 10,000 tons higher in the United States, but 6000 tons lower in the EU. As a result, commercial implementation of food irradiation has apparently increased in Asian regions during the past 5 years (Kume and Todoriki 2013). In particular, irradiation for phytosanitary purposes of fruits and agricultural products, such as sweet potatoes, guava, and tropical exotics such as mangos, longan, dragon fruit, rambutan, and mangosteen, has recently increased in different countries, including Mexico, the United States, Thailand, Vietnam, Australia, and India for their international trade, reaching about 18,500 tons in 2010 (Table 13.12).

Figure 13.18 shows the different countries listed in the order of the quantity of irradiating foods. China and the United States are producing 200,000 and 100,000 tons, respectively, followed by Vietnam with 66,000 tons and Mexico with 10,300 tons. Globally, the number of countries that recorded more than 1000 tons of irradiated foods was sixteen (Kume and Todoriki 2013). Compared with the African region where commercial food irradiation has not progressed, the Asian and Pacific region has been active in the commercialization of food irradiation. Particularly, China and Vietnam have rapidly extended their volume of commercial irradiation. In addition, Thailand, India, the Philippines, and Australia have been recently expanding fruit irradiation for quarantine purposes. However, Latin America countries, such as Mexico, Peru, and Chile, have been trying to implement commercial irradiation for quarantine treatment in exporting fruits and agricultural commodities (Kume et al. 2009b; Kume and Todoriki 2013). The majority of irradiated foods and ingredients are composed of spices and dried vegetables, fruits and vegetables, meat and poultry, and so on (Kume and Todoriki 2013).

Considering both the gradual ban on using chemical fumigants for food and the emerging risk of foodborne diseases in the food industries, irradiation as a nonresidual and nonthermal cold process is expected to be one of the alternative technologies

TABLE 13.12
Export Volumes of Fruit Irradiated for Phytosanitary Purposes

Country	Product	Volume (ton)
Hawaii	Tropical exotics[a]	260
	Papaya	12
	Sweet potatoes	5370
Australia[b]	Mango	460
	Litchi	33
India	Mango	100
Thailand	Longan	595
	Mangosteen	330
	Litchi	18
	Rambutans	8
Vietnam	Dragon fruit	850
Mexico	Guava	9121
	Sweet lime	600
	Mango	239
	Grape fruit	101
	Manzano pepper	257
Total		18,446

[a] Longan, dragon fruit, rambutans, mango, mangosteen.
[b] Exported to New Zealand (2010).

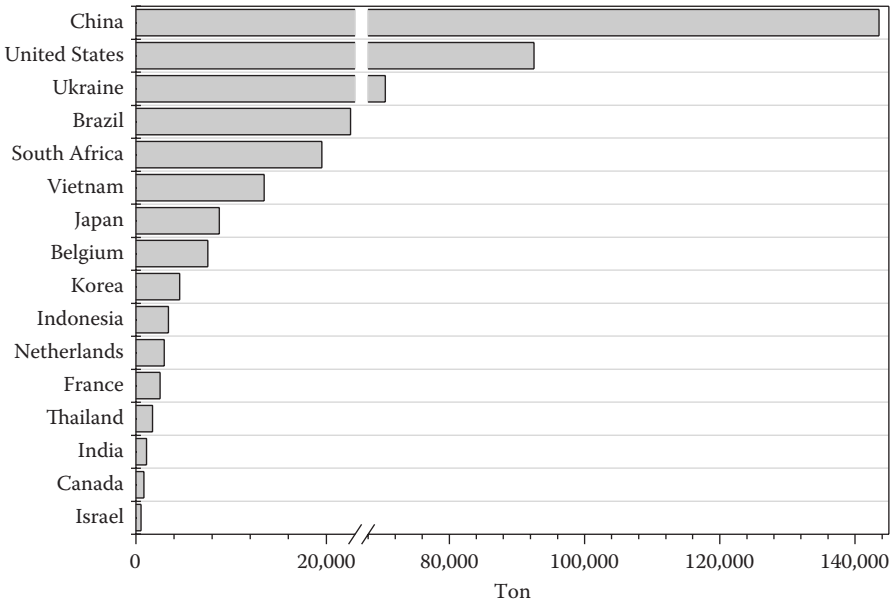


FIGURE 13.18 Quantity of food irradiation in the world in 2010.

to improve the safety and quality of various foods and foodstuffs (Loaharanu 2007). In this respect, further efforts are required to educate the public with factual information on the advantages and disadvantages of food irradiation compared with conventional methods. The WHO views irradiation as a process that has the potential to increase the supply of safe food, and thus contribute to improved public health. The FAO also sees food irradiation as a process to reduce food loss and facilitate international trade. This is because it would be difficult for a country to ban the importation of irradiated foods without the risk of challenge (WHO 1988; FAO/WHO 2003).

New technologies, such as milk pasteurization from 100 years ago and food irradiation now, are difficult to be introduced mainly due to consumer acceptance. Perceived public concerns delay their regulatory approval and commercial use (Hall and Trout 1968). Marketing trials of irradiated foods, however, have demonstrated that consumer reluctance decreases remarkably when consumers have the opportunity to buy irradiated foods and experience their benefits. A more positive and open attitude toward food irradiation is growing in many countries with respect to the commercial applications of food irradiation.

13.9 IRRADIATION IDENTIFICATION METHODS

In view of the fact that the use of food irradiation is increasing, special emphasis has been given to the development of detection methods to differentiate irradiated foods from nonirradiated foods. International trade emphasizes the implementation of various national and international regulations to ensure proper labeling demonstrating the confirmation of specified applied irradiation doses. The consumers' right to enjoy free choice about irradiated products largely depends on correct labeling. Therefore, the need of reliable and convenient methods capable of detecting irradiated foods has increased to enhance the trade and acceptability of irradiated foods (Table 13.13). However, it is unfortunate that none of the current available identification techniques have the potential to recognize all irradiated foodstuffs (Akram et al. 2012).

Several methods based on physical, chemical, biological, and microbiological changes appearing in foods upon irradiation have been approved as standard methods in the Codex Alimentarius Commission in the Codex General Standard for Irradiated Foods in Section 6.4 on "Post-irradiation verification" (FAO/WHO 2003; Akram et al. 2012). The European Committee for Standardization (CEN) approved five methods (EN1784 to EN1788) as European standards for the detection of irradiated foods in 1996, while five more validated standard methods (EN13783, EN13784, EN14569, EN13708, and EN13751) were authorized in 2004 (Chauhan et al. 2009) (Table 13.14).

13.9.1 Physical Methods

13.9.1.1 Photostimulated Luminescence

Mineral dusts, especially silicate materials, present on food can store energy in charge carriers trapped at structural or interstitial sites following irradiation. Photostimulated luminescence (PSL) is a radiation-specific phenomenon based on energy being stored by these trapped charge carriers upon irradiation. Light is used

TABLE 13.13
Technical and Practical Criteria of a Detection Method for Irradiated Food

Technical Criteria

a. *Discrimination*—Parameter measured in the irradiated food should be absent in the nonirradiated food; alternatively, the parameter should be well characterized in the nonirradiated food and changes induced by irradiation should be distinct and separable
b. *Specificity*—Other food processing methods and storage should not induce comparable changes to irradiation
c. *Applicability*—The test should apply throughout the dose range relevant to the irradiation of the food tested
d. *Stability*—The parameter should be useful for at least the storage life of the irradiated food
e. *Robustness*—The measurement should be insensitive to the following effects, or its response should be known with sufficient confidence, for example, dose rate, temperature at any stage of treatment or storage, other storage variables (oxygen, moisture, etc.), further processing, admixture with other food
f. *Independence*—The method should not require samples of the nonirradiated food from the particular batch tested
g. *Reproducibility* and *repeatability*
h. *Accuracy* and proper statistical *validation*
i. *Sensitivity*—The method should be capable of detecting doses below the commercially applicable dose
j. *Dose dependence*—The method should be capable of generating a dose–response curve; this criterion concerns the measurement of dose applied to the food

Practical Criteria

a. *Simplicity*—The method should not demand high levels of technical skills, data interpretation, or specialized equipment
b. *Low cost*
c. *Small sample size*
d. *Speed of measurement*
e. The method should apply to a *wide range* of food and food types
f. *Nondestructive* measurement of the parameter
g. The method should be capable of *easy standardization* and *cross-calibration*
h. Confidence that the method is *resistant to fraud;* it would desirable if the parameters were inherent to food rather than to the associated packaging, for example, mineral dusts

Source: Adapted from McMurray, C. H. et al. 1996. *Detection Methods for Irradiated Foods—Current Status*. pp. 108–118. Cambridge, UK: Royal Society of Chemistry.

rather than heat to stimulate the release of these trapped charge carriers, giving a measurable photon count (Figure 13.19). This method may in principle be applied to detect irradiated foods of any kind, which contain mineral debris, especially silicate mineral and bioinorganic materials such as calcite, which originate from shells or exoskeletons, or hydroxyapatite from bones or teeth (Sanderson et al. 1996; EN13751 2009). PSL was proposed by Sanderson (1991) to resolve the practical limitations of the thermoluminescence (TL) method related to extended mineral separation/

TABLE 13.14
European Standards for the Detection of Irradiated Foods That Are Also Adopted by Codex

Commodity	Principle and Standard No. Method	Commodity	Validated Products	Remark[a]
EN1784	Gas chromatographic (GC) analysis of hydrocarbons	Food containing fat	Chicken, pork, beef, avocados, mangoes, papayas, camembert	Type II
EN1785	GC/MS analysis of 2-alkylcyclobutan-ones	Food containing fat	Chicken, pork, liquid whole egg	Type III
EN1786	ESR spectroscopy of bones	Food containing bone	Chicken, fish, frog legs	Type II
EN1787	ESR spectroscopy of cellulose	Food containing cellulose	Paprika powder, pistachio nut shells, strawberries	Type II
EN1788	Thermoluminescence of silicate minerals	Food containing silicate minerals	Herbs and spices, shrimps	Type II
EN13708	ESR spectroscopy of crystalline sugars	Food containing crystalline sugar	Dried papayas, dried mangoes, dried figs, raisins	Type II
EN13751	Photo-stimulated luminescence	Food containing silicate minerals	Herbs and spices, shellfish	Type III
EN13783	Microbial screening using direct epifluorescent filter technique/aerobic plate count (DEFT/APC)	Herbs, spices and raw minced meat	Herb and spices	Type III
EN13784	DNA comet assay screening	Food containing DNA	Chicken, pork, plant cells, for example, seeds	Type III
EN14569	Microbiological screening for using LAL/GNB procedure		Chicken, pork, beef	

[a] Type II: reference methods; Type III: alternate approved methods.

preparation procedures. Furthermore, the PSL technique is quick without consuming much time with laborious sample preparation or involving a reirradiation step like in the case of TL.

The whole sample is uniformly spread in a small petri dish (50 mm, $n = 2$) or may be divided into pieces to fit in the dish. The samples are loaded in the sample chamber of a SURRC PPSL Irradiated Food Screening System (SURRC; Scottish Universities Research and Reactor Centre, Glasgow, UK) and the PSL signals are recorded for 60 s.

The photon signals can be divided into two threshold limits, that is, an upper and lower one are used to interpret the PSL results. The defined threshold limits for herbs and spices, after various interlaboratory trials are $T_1 = 700$ counts/60 s and $T_2 = 5000$ counts/60 s while for shellfish, the threshold established limits are

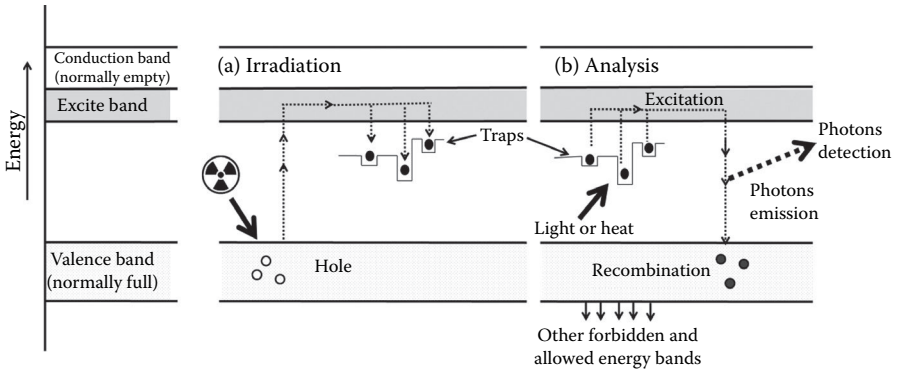


FIGURE 13.19 Principle of photo- and thermo-luminescence of silicate minerals separated from irradiated food materials. (Tsoulfanidis 1995).

T_1 = 1000 counts/60 s and T_2 = 4000 counts/60 s (Figure 13.20). The PSL method can be applied as a screening approach only because it may yield false-positive or false-negative results because of signal bleaching (false-negative) or cross-contamination (false-positive) (Bortolin et al. 2007; Ahn et al. 2012a). Therefore, it can be successfully applied as a rapid screening method for many irradiated foods (Sanderson et al. 1996). However, storage conditions can slightly affect the PSL photon count measurements. Recently, Ahn et al. (2012a) studied the effect of different light conditions such as sunlight, artificial light, and darkness (dark room) on the luminescence characteristics of contaminating minerals separated from irradiated onions. A slight change was observed in PSL PCs under different applied conditions but all the irradiated samples were effectively identified even after a storage time of 2 years. Kim et al. (2012) reported on the limitation of the PSL technique for the identification of spice mixtures containing a small proportion of irradiated components. In a recent study, Yunoki et al. (2012) evaluated the possibility of irradiated packaging material as alternative specimens for the screening detection of irradiated foods. The core of irradiated corrugated fiberboards (CFs) exhibited PSL signals sufficient for differentiating irradiated from nonirradiated samples even after CFs were exposed to light and environmental stresses raised to 50°C for over 6 months postirradiation. However, a difficulty was observed in establishing a well-defined

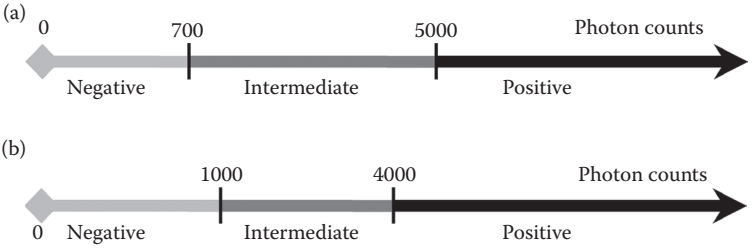


FIGURE 13.20 Threshold value of PSL photon counts (a) spices and herbs; (b) shellfish.

"positive" threshold limit due to the marked variations of the PSL signals among CFs. Kim et al. (2013) reported that dry treatments such as spray drying and vacuum drying may affect the luminescence detection characteristics in different seasoning samples.

13.9.1.2 Thermoluminescence

The thermoluminescence method is used for foodstuffs from which a sufficient amount of silicate minerals can be isolated. The TL method has been applied to a wide range of foods such as herbs, spices, shellfish (shrimps and prawns), fresh fruits, and vegetables, as well as dehydrated fruits and vegetables. The physical process of TL is based on the transition of the electrons located in the excited state to the ground state when they are stimulated by heat. The contaminating inorganic minerals, especially silicate materials, present on the surfaces of foods can absorb energy when exposed to ionizing radiation in the charge carriers trapped at structural or interstitial sites. As the sample is heated, thermal stimulation of these minerals can discharge the stored energy, yielding a measurable luminescence. A thermoluminescence reader measures the amount of light that is emitted during controlled heating (Figure 13.19). The intensity of the emitted light (energy) is related to the radiation dose measured as a function of temperature, and the result is a glow curve.

The silicate minerals are usually more sensitive to applied radiations providing a high TL intensity with good stability of the TL signals upon storage (McKeever 1985). According to EN 1788 (2001), glow 1 curves of irradiated food samples generally produce a peak between the temperature range of 150°C and 250°C, whereas in nonirradiated samples, low natural radioactivity causes TL signals above 300°C (Figure 13.21) (Bayram and Delincée 2004). Silicates, quartz, and feldspars are frequently found in most herbs and spices. These are highly sensitive to ionizing radiation and considered to be responsible for the TL glow curve profiles with high peaks near 200°C (Duller 1997).

The first TL glow (glow 1) of the isolated minerals is measured. Then, a second TL glow (glow 2) of the same sample is recorded after exposure to a fixed dose of radiation to eliminate the effect of varying composition of the minerals and thus the varying shapes and heights of the glow curves. The reirradiation dose (normalization) is 1 kGy or above for herbs, spices, and their mixtures and shellfish and fresh and dehydrated fruits and vegetables for decontamination purpose and 50–250 Gy for potatoes for sprout inhibition. Thus, the TL_1/TL_2 ratio is used for the validation of radiation treatment of the samples because the irradiated samples evidently yield higher TL glow ratios than that of nonirradiated samples (Kyung et al. 2012). Different methods can be adopted to separate the mineral fractions shown in Figure 13.21. However, the typical method usually involves separation of inorganic minerals (density over 2.5 g/cc) through washing of the sample with distilled water and purification from organic matter (density less than 1.1 g/cc) through a density separation approach using heavy liquids, such as sodium polytungstate or carbon tetrachloride. High-temperature exposure may lead to the fading of the TL glow curves (Kitai and Furuta 2009) because temperature can stimulate the entrapped electrons to move to the ground state (Preusser et al. 2009). Ahn et al. (2012b) reported the effect of boiling, roasting, and microwave treatments on the TL characteristics of irradiated

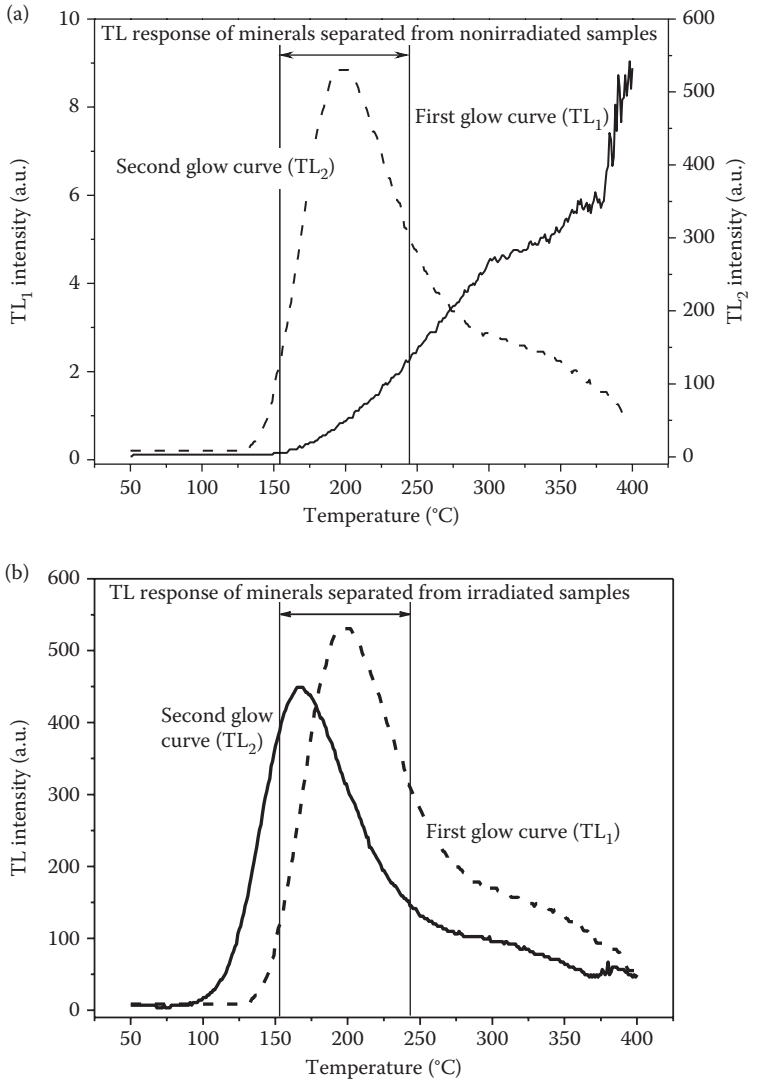


FIGURE 13.21 TL glow curve of silicate minerals separated from irradiated samples (a) nonirradiated; (b) irradiated.

feldspar. Boiling or roasting caused a shift of the TL peak maxima toward higher temperatures.

13.9.1.3 ESR Spectroscopy

Electron spin resonance (ESR) is a spectroscopic technique that permits the detection of unpaired electrons, originating from radicals, including those induced by irradiation or from paramagnetic ions, such as Mn^{2+} (Marcos et al. 2007) (Figure 13.22). In food materials with plant origins, irradiation can generate free radicals in



FIGURE 13.22 Typical ESR spectra of nonirradiated foods (a) ESR silent (no signal); (b) natural signal usually in food of plant origin; (c) effect of Mn^{2+}.

cellulose (Figure 13.23) and crystalline sugars (Figure 13.24), which could serve as irradiation detection markers in ESR analysis (Delincée and Soika 2002). Radiation-induced radicals generally occur in the solid and dry fractions of food. The rigid structure of the matrix is capable of trapping free radicals or excited states of the electrons and inhibits them to react with each other or with food components present in the wet portion of the food. The sample is subjected to the simultaneous action of a magnetic field and an electromagnetic microwave of very high frequency (Raffi et al. 2000; Marchioni 2005). Effective drying techniques are required as pretreatments to reduce the moisture content to obtain clear or improved ESR spectral features (Akram et al. 2012).

ESR has been approved by the European Union as an international standard method for the detection of irradiated foods containing cellulose (EN1787 2000), crystalline sugar (EN13708, 2001), and bone (EN1786 1997). Measurement of the g value of the ESR signal, which represents the frequency to the magnetic field strength value ratio, is used for the identification of irradiated samples. Irradiated bone shows

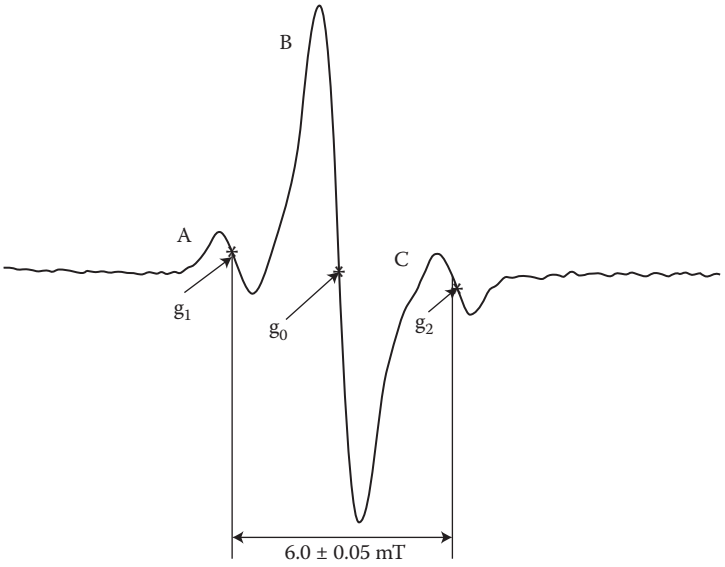


FIGURE 13.23 Typical ESR spectra of irradiated cellulose containing foods.

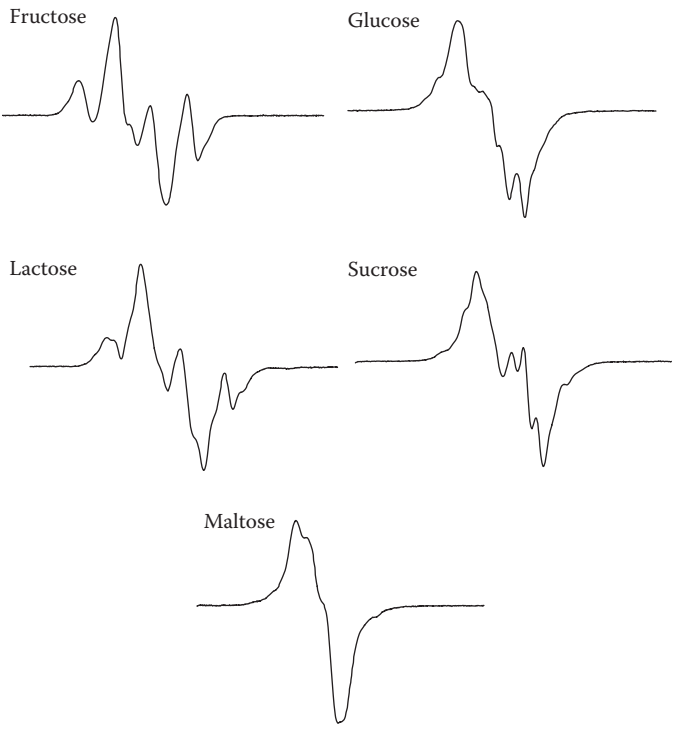


FIGURE 13.24 Typical ESR spectrum of irradiated crystalline sugars.

a characteristic unparalleled ESR signal with g values of 2.002 and 1.998 related to the radiation-induced paramagnetic radicals (Figure 13.25). On the contrary, the ESR spectra of nonirradiated samples show one singlet line ($g_{symm} = 2.005 \pm 0.001$). However, stability of the radiation-induced free radicals is highly dependent on the storage time. In principle, they are sufficiently stable for a long period of storage at room temperature in the solid and dry states. Sample pretreatment may highly influence the clear or improved ESR spectral features (Kwon et al. 2014).

Recently, Akram et al. (2013) reported the significant effects of different sample pretreatments such as freeze-drying, alcoholic extraction, and water and alcoholic extraction to characterize different irradiated sauces using the ESR technique. The alcoholic extraction pretreatment of irradiated sauce samples represents good applicability of the ESR technique compared with the freeze-drying pretreatment. Previously, de Jesus et al. (1999) reported water extraction by alcohol for fruit pulps of kiwi, papaya, and tomato containing high water content. In another study, de Jesus et al. (2000) observed a dose-dependent increase in radiation-induced cellulose radical signals in the flesh of irradiated vegetables analyzed by the ESR technique after different sample pretreatments. Raffi and Stocker (1996) reported on the limitations of ESR spectroscopy for irradiated spices, where storage time significantly influenced the radiation-induced signals. Marcos et al. (2007) reported ESR signals due to Mn^{2+} in nonirradiated soybean samples, where clear radiation-induced cellulose

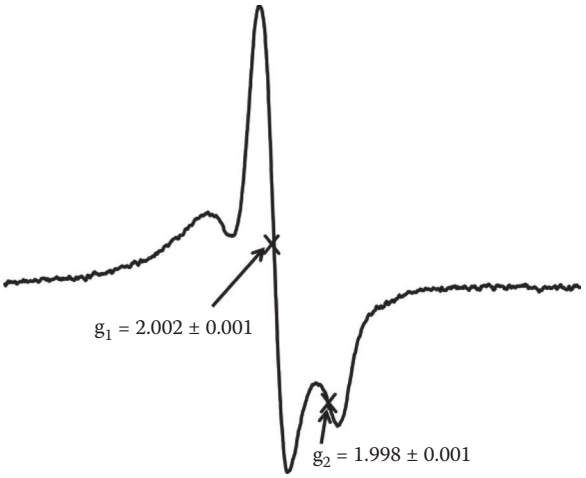


FIGURE 13.25 Typical ESR spectra of irradiated bones.

radical signals were found by selecting a part (hilum) of the bean showing a high ESR response with a smaller effect from Mn^{2+} upon irradiation. Recently, Ahn et al. (2013) found that different nonirradiation-specific paramagnetic species present in irradiated food materials can produce complex ESR spectra during analysis.

13.9.2 Chemical Methods

13.9.2.1 Hydrocarbons Analysis

The European Committee for Standardization (CEN) approved two protocols (EN-1784 and EN-1785) as European standards for the detection of irradiated foods containing lipids. When such foodstuffs containing fats are irradiated, many volatile compounds are formed that may be useful as markers of irradiation treatment (Figure 13.26). This is because when fatty acids are exposed to high-energy radiation, they undergo preferential cleavages, which, unlike other treatments, occur in the ester carbonyl region. Therefore, these compounds can be used as irradiation detection markers for the identification of irradiated foodstuffs. For example, the two main hydrocarbons formed from each fatty acid C [N:M] are those with one carbon less than the parent fatty acid ($C[_{N-1:M}]$) and those with two carbons less and one extra double bond ($C[_{N-2:M+1}]$). The amount of radiolytic compounds from lipids, such as volatile hydrocarbons, aldehydes, or butanones, is directly related to the chemical composition of the lipids (Raffi 1998).

Radiation-induced hydrocarbons in fat-containing foods can be detected by gas chromatography–mass spectrometry (GC/MS) analysis. This method was first introduced by Nawar's group (Nawar et al. 1969; Nawar and Balboni 1970), and has been developed into a detection method for irradiated foods. Through the radiolytic decomposition mechanism, hydrocarbons mainly form two types, C_{n-1} and $C_{n-2:1}$, of hydrocarbons from α- and β-cleavages near the carbonyl group of the fatty acids

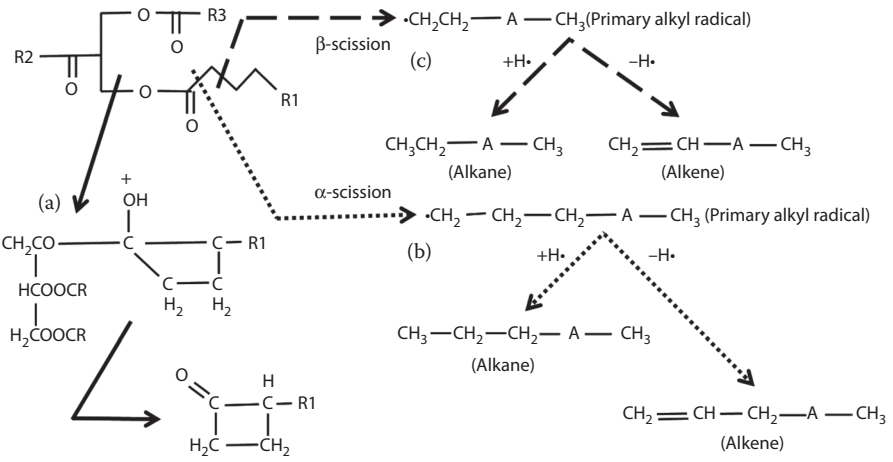


FIGURE 13.26 Radiation-induced cleavage of triglyceride molecule resulting 2-alkylcyclobutanone (a) and hydrocarbons (b and c). (From Marchioni 2006.)

in irradiated foods. The hydrocarbons are known to originate mostly from fatty acids, but are not produced during cooking or as a result of oxidation, indicating that they could be used as specific detection markers for irradiated fat-containing foods (Nawar 1986; Stevenson 1992).

The simple analytical procedure involves the extraction of fat from the sample using hexane, isolation of the hydrocarbons, and their identification by means of GC/MS. Florisil column chromatography (FCC) has a higher reliability and reproducibility for the isolation of hydrocarbons (Schulzki et al. 1995). However, the FCC method takes more time and requires organic solvents in large quantities, along with high running costs (McMurray et al. 1994).

A solid-phase extraction (SPE) method is the most popular technique used for sample pretreatment prior to GC analysis, and has many advantages, such as the use of less organic solvents, ease of automation, reduced time, and cost-effectiveness (Whitcomb and Campiglia 2001; Theodoridis and Manesiotis 2002).

Barba et al. (2012) investigated the production of hydrocarbons upon gamma irradiation in pork, bacon, and ham. Hydrocarbons were analyzed with a sequential procedure for lipid extraction using hexane, FCC, and GC. Hydrocarbons $C_{17:1}$, $C_{16:2}$, $C_{17:2}$, and $C_{16:3}$ were detected in meat samples irradiated at 0.5 kGy or higher but not in nonirradiated samples except for $C_{17:1}$. The detection levels in all irradiated samples were on the order of $C_{16:2}$, $C_{17:1}$, $C_{17:2}$, and $C_{16:3}$ from the highest to the lowest. Kim et al. (2004) analyzed the hydrocarbons produced in beef, pork, and chicken by irradiation (0–10 kGy) using SPE and GC/MS. The detection limit of hydrocarbons was 0.5 kGy, with the exception of $C_{16:3}$ in beef. There was a high correlation between the irradiation dose and the concentration of hydrocarbons in the meat samples. Li et al. (2010) reported the detection of hydrocarbons 1,7-hexadecadiene (1,7-$C_{16:2}$) and 8-heptadecene (8-$C_{17:1}$), as identification markers for chilled beef irradiated at 0.5 kGy or higher by means of a new method using headspace solid-phase microextraction, gas chromatography, and mass spectrometry (HS-SPME–GC–MS).

Hwang et al. (2001) reported the effect of different treatments such as boiling, frying, or heating in an oven, for the analysis of hydrocarbons in shell eggs irradiated at 0.5, 1, and 3 kGy. Hydrocarbons were determined with a sequential procedure using lipid extraction by hexane, FCC, and GC. Hydrocarbons 15:0, 14:1, 17:0, 16:1, 17:1, 16:2, 17:2, and 16:3 were detected in shell eggs irradiated at 0.5 kGy or higher, but not in nonirradiated ones except for 15:0 and 17:0. Boiling for 40 min slightly affected the detection levels of hydrocarbons in nonirradiated or irradiated eggs. Frying the egg yolk of nonirradiated eggs for 5 min produced hydrocarbons 17:1 and 17:2 besides 15:0 and 17:0. Hydrocarbons 15:0, 17:0, 17:1, 17:2, 14:1, and 16:1 were detected in the egg yolk of nonirradiated eggs while heating it in a cooking oven at 170°C for 60 min. Heating of nonirradiated eggs in a cooking oven at 170°C for 60 min resulted in the production of hydrocarbons 15:0, 17:0, 17:1, 17:2, 14:1, and 16:1 in the egg yolk.

13.9.2.2 2–Alkylcyclobutanones

The European Standard protocol EN1785 (2003) specifies a method based on the measurements of 2-alkylcyclobutanones (2-ACBs) produced by the irradiation of foods that contain fat, including meat, fish, shrimp, cheese, liquid egg products, and so on (Morehouse and Ku 1990; EN1785 2003).

The principle is based on the fact that upon irradiation, the acyl–oxygen bond in triglycerides is cleaved and this reaction results in the formation of 2-ACBs containing the same number of carbon atoms as the parent fatty acid, and the alkyl group is located in ring position 2 shown in Figure 13.26. Therefore, if the fatty acid composition is known, the 2-ACBs formed can be predicted (Stewart et al. 2001; EN1785 2003; Crews et al. 2012).

Improvements and optimization is necessary for the detection of hydrocarbons in foods containing a low fat content (<1%) and irradiated at low doses (0.5 kGy) (Ndiaye et al. 1999). Horvatovich et al. (2000) suggested a time-saving (4–5 h) and cost-effective modified method for the detection of fat-containing irradiated foods compared with the reference methods EN1784 (1996) (volatile hydrocarbons) and EN1785 (2003) (2-ACBs). Barba et al. (2012) reported on the capability of SPME, coupled with either GC-ionization flame detector or multidimensional GC–MS for the detection of radiolytic markers or volatile hydrocarbons produced during the irradiation of cooked ham. The proposed screening method provides the potential for the rapid detection of most *n*-alkanes and *n*-alkenes produced during the irradiation of most fatty acids (oleic acid, stearic acid, and palmitic acid) in cooked ham.

Food-processing technologies other than irradiation can also lead to the formation of ACBs. Therefore, to eliminate the possibility of false-positive results, improvements are required in the EN1785 (2003) standard to verify whether 2-ACBs can be detected in nonirradiated foods or foods treated/processed by any means other than irradiation. Furthermore, improvements are required to widen the applicability spectrum of the 2-ACB technique. It may be possible by increasing the sample size to increase the extracted fat, optimizing the chromatographic separation of the 2-ACBs from the extracted fat, improving the sensitivity of the detector, optimizing the injection parameters, and permitting a variety of extraction techniques such as acetonitrile or supercritical fluid extraction (Crews et al. 2012).

13.9.3 Biological Methods

13.9.3.1 DNA Assays

High-energy ionizing radiation causes damage to DNA such as denaturation, fragmentation, strand breaks, and so on. The large molecule DNA is particularly a sensitive target for ionizing radiation. This radiation-induced DNA damage offers potential as a detection method (Chauhan et al. 2009). Considerably increased extension of the DNA from the nucleus toward the anode is exhibited by irradiated cells compared with nonirradiated ones shown in Figure 13.27 (Haine et al. 1995). Microgel electrophoresis is used to study the DNA fragmentation of single cells or nuclei. Leakage of DNA subunits from the nuclei of lysed cells during electrophoresis yields "comet"-like characteristics. On the contrary, nonirradiated samples do not exhibit this feature (Ostling and Johanson 1984; Stevenson 1992). The comet assay has wide application in different research areas and has been modified for the detection of irradiated foods by Cerda et al. (1993). Both alkaline and neutral protocols are available to measure DNA damage (EN13784 2001). This method is cheap and easy to perform in a short time and has been successfully tested for plant foods as well as animal foods with some limitations (Cerda et al. 1993, 1997; Khan et al. 2002, 2005; Verbeek et al. 2007).

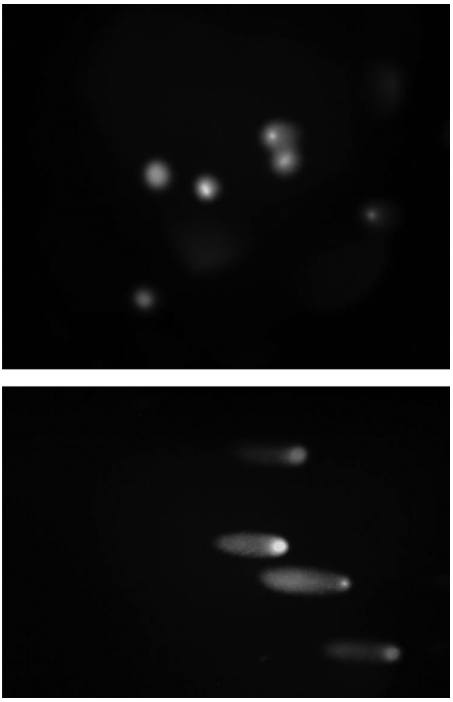


FIGURE 13.27 DNA comet assay results from nonirradiated (above; round and intact) and irradiated samples (with clear tails).

13.9.3.2 Direct Epifluorescent Filter Technique and Aerobic Plate Count

Direct epifluorescent filter technique and aerobic plate count (DEFT/APC) method is based on a comparison of the APC with the count obtained using DEFT. The APC helps to calculate the number of viable microorganisms in a sample after a possible irradiation treatment while DEFT gives the total number of microorganisms, including nonviable cells, present in the sample shown in the microscopic fluorescent image of Figure 13.28 (Betts et al. 1988; EN13783 2001).

Oh et al. (2003) reported the applicability of the DEFT/APC method for the screening of irradiated spices produced in Korea. Araújo et al. (2009) successfully evaluated that the microbiological method DEFT/APC could be satisfactorily applied for the screening and identification of the hygienic status of minimally processed irradiated vegetables. The DEFT microorganism count is generally unaffected by irradiation. Particularly, microorganisms may be inactivated by irradiation and thus undetectable by the APC technique. However, the storage period may affect the DEFT/APC results (Jones et al. 1995).

The method has limitations regarding the use of fumigation or heat as decontamination treatments. In such a case, the DEFT/APC difference in counts can be similar to the difference in counts obtained after irradiation (EN13783 2001; Chauhan et al. 2009).

13.9.3.3 Limulus Amebocyte Lysate/Gram-Negative Bacteria

This microbiological assay is analogous to the DEFT/APC test and not totally specific to irradiated foods just as the DNA comet assay. The EN14569 (2004) protocol specifies its application on whole or different parts of poultry meat.

The technique evaluates the number of viable Gram-negative bacteria present in the sample and the concentration of bacterial endotoxins existing on the surfaces of the Gram-negative bacteria as lipopolysaccharides (LPS). The total amount of

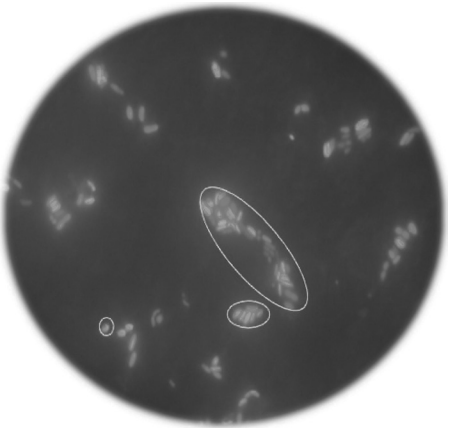


FIGURE 13.28 Microscopic fluorescent image of a DEFT/APC test of spices. (From Betts, R. P. et al. 1988. *Journal of Applied Bacteriology* 64: 329–35.)

Gram-negative bacteria, both viable and dead, is calculated with the LPS. If the difference between the Gram-negative bacteria and the endotoxin is high, it is presumed that the sample was treated most probably with ionizing radiation (Haire et al. 1997; EN14569 2004).

The test is presumptive and economical. It has been validated as a screening method for a variety of foodstuffs (Glidewell et al. 1993; Scatter et al. 1994; EN14569 2004). However, a significant amount of dead microbes in comparison with the viable fraction may be due to other reasons that can limit its useful application.

13.9.3.4 Germination and Half Embryo Test

The basic principle of the germination test depends on the fact that irradiated seeds germinate at a considerably slower rate than control seeds (Stevenson and Stewart 1995). This seedling assay is mainly confined to vegetable seeds. It is easy and cheap but too slow for routine analysis. Kawamura et al. (1989, 1996) worked to reduce the analysis time and to accelerate the germination process. They established an improved germination test called the "half embryo test" for some fruits, particularly for irradiated grapefruit and citrus fruit, in which the embryo was used for germination in place of seeds. This test is based on the inhibition of shoot growth by γ-irradiation.

Kawamura et al. (1992) reported that the germination test can discriminate between γ-irradiated and nonirradiated rice even after long storage. Similarly, Chaudhuri (2002) found that the germination method was efficient and reliable in detecting gamma-irradiated lentil seeds even after 12-month storage. Cutrubinis et al. (2004) successfully evaluated the applicability of the germination test as a detection method for garlic treated with up to 25 kGy in the dormancy period.

REFERENCES

Abu, J. O., Muller, K., Duodu, K. G., and Minnaar, A. 2005. Functional properties of cowpea (*Vigna unguiculata* L.Walp) flours and pastes as affected by γ-irradiation. *Food Chemistry* 93: 103–11.

Abu-Tarboush, H. M., Al-Kahtani, H. A., Atia, M., Abou-Arab, A. A., Bajaber, A. S. and El-Mojaddidi, M. A. 1997. Sensory and microbial quality of chicken as affected by irradiation and post irradiation storage at 4.0 C. *Journal of Food Protection* 60: 761–70.

Ahn, J. J., Kim, G. R., Akram, K., and Kwon, J. H. 2012a. Luminescence characteristics of minerals separated from irradiated onions during storage under different light conditions. *Radiation Physics and Chemistry* 81: 1215–9.

Ahn, J. J., Akram, K., Kwak, J. Y., Jeong, M. S., Jang, Y. D., and Kwon, J. H. 2012b. Radiation-induced thermoluminescence characteristics of feldspar upon different heat and microwave treatments. *Journal of Luminiscence* 132: 1964–8.

Ahn, J. J., Akram, K., Kim, H. K., and Kwon, J. H. 2013. Electron spin resonance spectroscopy for the identification of irradiated foods with complex ESR signals. *Food Analytical Methods* 6: 301–8.

Aiew, W., Nayga, R. M., and Nichols, J. 2003. Information effects on consumers' willingness to purchase irradiated products (Working Paper). College Station, TX: Texas A&M University Department of Agricultural Economics.

Akram, K., Ahn, J. J., and Kwon, J. H. 2012. Analytical methods for the identification of irradiated foods. In: *Ionizing Radiation: Applications, Sources and Biological Effects*. ed. Belotserkovsky, E., and Ostaltsov, Z, 1–36. New York: Nova Science Publishers.

Akram, K., Ahn, J. J., and Kwon, J. H. 2013. Characterization and identification of gamma-irradiated sauces by electron spin resonance spectroscopy using different sample pretreatments. *Food Chemistry* 138: 1878–83.

Álvarez, I., Niemira, B. A., Fan, X., and Sommers, C. H. 2006. Inactivation of *Salmonella* serovars in liquid whole egg by heat following irradiation treatments. *Journal of Food Protection* 69: 2066–74.

Al-Assaf, S., Phillips, G. O., Williams, P. A., and du Plessis, T. A. 2007. Application of ionizing radiations to produce new polysaccharides and proteins with enhanced functionality. *Nuclear Instruments and Methods in Physics Research Section* B 265: 37–43.

Annoy. 1998. Combination Process for Food Irradiation, Panel Proceedings Series, Summary Report, 1–14, Vienna: IAEA.

Anoymous. 1998. Present status and guidelines for preparing harmonized legislation on food irradiation in the Near East, Paper presented at Joint AAEA/FAO/IAEA Regional Workshop, Tunis, Tunisia.

Araújo, M. M., Duarte, R. C., Silva, P. V., Marchioni, E., and Villavicencio, A. L. C. H. 2009. Application of the microbiological method DEFT/APC to detect minimally processed vegetables treated with gamma radiation. *Radiation Physics and Chemistry* 78: 691–3.

ASTM. 2000. American society for testing and materials, standard guide for selection and calibration of dosimetry systems for radiation processing, ASTM E1261, Annual Book of ASTM Standards, Vol. 12.02, Philadelphia: ASTM.

Audette-Stuart, M., Houee-Levin, C., and Potier, M. 2005. Radiation induced protein fragmentation and inactivation in liquid and solid aqueous solutions. Role of OH and electrons. *Radiation Physics and Chemistry* 72: 301–6.

Aziz, N. H., El-Fouly, M. Z., Abu-Shady, M. R., and Moussa, L. A. A. 1997. Effect of gamma-radiation on the survival of fungal and actinomycetal florae contaminating medicinal plants. *Radioactivity and Radiation Measurement* 48: 71–6.

Aziz, N. H., Youssef, Y. A., El-Fouly, M. Z., and Moussa, L. A. 1998. Contamination of some common medicinal plant samples and spices by fungi and their mycotoxins. *Botanical Bulletin of Academia Sinica* 39: 279–85.

Bao, J. and Corke, H. 2002. Pasting properties of gamma-irradiated rice starches as affected by pH. *Journal of Agricultural and Food Chemistry* 50: 336–41.

Barba, C., Santa–Maria, G., Herraiz, M., and Calvo, M. M. 2012. Rapid detection of radiation–induced hydrocarbons in cooked ham. *Meat Science* 90: 697–700.

Bari, M. L., Al-Haq, M. I., Kawasaki, T., Nakauma, M., Todoriki, S., and Kawamoto, S. 2004. Irradiation to kill *Escherichia coli* O157:H7 and *Salmonella* on ready-to-eat radish and mungbean sprouts. *Journal of Food Protection* 67: 2263–8.

Bayram, G. and Delincée, H. 2004. Identification of irradiated Turkish foodstuffs combining various physical detection methods. *Food Control* 15: 81–91.

Betts, R. P., Farr, L., Bankes, P., and Stringer M. F. 1988. The detection of irradiated foods using the direct epifluorescent technique. *Journal of Applied Bacteriology* 64: 329–35.

Bhat, R. and Karim, A. A. 2009. Impact of radiation processing on starch. *Comprehensive Reviews in Food Science and Food Safety* 8: 44–58.

Bortolin, E., Boniglia, C., Calicchia, A., Alberti, A., Fuochi, P., and Onori, S. 2007. Irradiated herbs and spices detection: light-induced fading of the photo-stimulated luminescence response. *International Journal of Food Science and Technology* 42: 330–5.

Bruhn, C. M. 1998. Consumer acceptance of irradiated food: Theory and reality. *Radiation Physics and Chemistry* 52: 129–33.

Brynjoifossn, A. 1981. Food-energy-developing countries—Food irradiation. IAEA-SM-250/26, 421.

Byrne, M. 1996. Irradiation update. *Food Engineering Int'l*, December, 37.

Byun, M.W., Jo, C., and Lee, J. W. 2007. Potential applications of ionizing radiation. In: Food Irradiation Research and Technology, ed. C. H. Sommers and X. Fan. Ames, Iowa: Blackwell Publishing. DOI: 10.1002/9780470277638.ch15.

Byun, M. W., Kwon, J. H., Cho, H. O., Cha, B. S., Kang, S. S., and Kim, J. M. 1989. Effect of ionizing radiation of physiological characteristics of fresh mushrooms (*Agaricus bisporus* L.). *Korean Journal of Food Science and Technology* 21: 669–73.

CAC. 1984. Codex General Standard for Irradiated Foods and Recommended International Code of Practice for the Operation of Radiation Facilties Used for the Treatment of Foods. Codex Alimentarius Commission Vol. XV. FAO, Rome (1984).

CAC. 1985. General standard for the labeling of and claims for prepackaged foods for special dietary uses CODEX STAN 146-1985. Codex Alimentarius Commission.

CAC. 2003. Revised Codex General Standard for Irradiated Foods. CODEX STAN 106-1983, Rev. 1-2003. Codex Alimentarius Commission.

Calkins, C. O. and Parker, A. G. 2005. Sterile insect quality, pp. 269–96. In: *Sterile Insect Technique. Principles and Practice in Area-Wide Integrated Pest Management*, ed. V. A. Dyck, J. Hendrichs, and A. S. Robinson, Dordrecht: Springer.

Centers for Disease Control (CDC). 2000. FoodNet report 2000. Available on the World Wide Web: http://www.cdc.gov/foodnet/annual/2000/2000final_report.pdf.

Cerda, H., Delincée, H., Haine, H., and Rupp, H. 1997. The DNA 'comet assay' as a rapid screening technique to control irradiated food. *Mutation Research* 375: 167–81.

Cerda, H., Hofsten, B. V., and Johanson, K. J. 1993. Identification of irradiated food by microelectrophoresis of DNA from single cells. In: *Recent Advances of New Methods of Detection of Irradiated Food*, ed Leonardi, M., Belliardo, J. J., and Raffi, J. J., Proceedings of the workshop, 401–5. Ancona, 24–26 Sept. 1991, Commission of the European Communities, Luxembourg.

Ciesla, K., Salmieri, S., and Lacroix, M. 2006a. γ-Irradiation influence on the structure and properties of calcium caseinate-whey protein isolate based films. Part 1. Radiation effect on the structure of proteins gels and films. *Journal of Agricultural and Food Chemistry* 54: 6374–84.

Ciesla, K., Salmieri, S., and Lacroix, M. 2006b. γ-Irradiation influence on the structure and properties of calcium caseinate-whey protein isolate based films. Part 2. Influence of polysaccharide addition and radiation treatment on the structure and functional properties of the films. *Journal of Agricultural and Food Chemistry* 54: 8899–908.

Chaudhuri, S. K. 2002. A simple and reliable method to detect gamma irradiated lentil (*Lens culinaris* Medik.) seeds by germination efficiency and seedling growth test. *Radiation Physics and Chemistry* 64: 131–6.

Chauhan, S. K., Kumar, R., Nadanasabapathy, S., and Bawa, A. S. 2009. Detection methods for irradiated foods. *Comprehensive Review in Food Science and Food Safety* 8: 4–16.

Chawla, S. P., Kim, D. H., Jo, C., Lee, J. W., Song, H. P., and Byun, M. W. 2003. Effect of gamma irradiation on the survival of pathogens in Kwamegi, a traditional Korean semidried seafood. *Journal of Food Protection* 66: 2093–6.

Cheng, A., Wan, F., Xu, T., Du, F., Wang, W., and Zhu, Q. 2011. Effect of irradiation and storage time on lipid oxidation of chilled pork. *Radiation Physics and Chemistry* 80: 475–80.

Cho, H. O, Byun, M. W., Kwon, J. H., and Yang, J. S. 1982. Effect of irradiation time after harvesting and irradiation dose on its storability of potatoes. *Korean Journal of Food and Nutrition* 11: 53–9.

Cho, H. O., Yang, H. S., Byun, M. W., Kwon, J. H., and Kim, J. G.1983. Batch scale storage of sprouting foods by irradiation combined with natural low temperature. IV. Storage of chestnuts. *Korean Journal of Food Science and Technology* 15: 231–7.

Cleland, M. R. 2006. Advances in gamma ray, electron beam, x-ray technologies for food irradiation. In: *Consumer Acceptance and Marketing of Irradiated Foods*, ed. C. H. Sommer, and X. Fan, 11–36. Chicago: Blackwell Publishing and IFT Press.

Code of Federal Regulations. 2000. 21 CFR part 179 irradiation in the production processing and handling of food. US Federal Register, 65: 64605–7.

Crews, C., Driffield, M., and Thomas, C. 2012. Analysis of 2-alkylcyclobutanones for detection of food irradiation: Current status, needs and prospects. *Journal of Food Composition and Analysis* 26: 1–11.

Cutrubinis, M., Delincée, H., Bayram, G., and Villavicencio, A. C. H. 2004. Germination test for identification of irradiated garlic. *European Food Research and Technology* 219: 178–83.

de Kerf, M., Mondelaers, W., Lahorte, P., Vervaet, C., and Remon, J. P. 2001. Characterisation and desintegration properties of irradiated starch, *International Journal of Pharmaceutics* 221: 69–76.

de Jesus, E. F. O., Rossi, A. M., and Lopes, R. T. 1999. An ESR study on identification of gamma-irradiated kiwi, papaya and tomato using fruit pulp. *International Journal of Food Science and Technology* 34: 173–8.

de Jesus, E. F. O., Rossi, A. M., and Lopes, R. T. 2000. Identification and dose determination using ESR measurements in the flesh of irradiated vegetal products. *Applied Radiation Isotopes*, 52: 1375–83.

Delincée, H. 1983. Recent advances in radiation chemistry of proteins. In: *Recent Advances in Food Irradiation*, ed. P. S. Elias, and A. J. Cohen, 129–47. Amsterdam: Elsevier Biomedical.

Delincée, H. and Soika, C. 2002. Improvement of the ESR detection of irradiated food containing cellulose employing a simple extraction method. *Radiation Physics and Chemistry* 63:437–41.

Diehl, J. F. 1995. *Safety of Irradiated Foods*. New York: Marcel Dekker.

Diehl, J. F. and Josephson, E. S. 1994. Assesment of wholesomeness of irradiated foods. *Acta Alimentary* 23: 195–214.

Ding, H., Tong-Jen F., and Michelle, A. S. 2013. Microbial contamination in sprouts: How effective is seed disinfection treatment? *Journal of Food Science* 78: 495–501.

Dionísio, A. P., Gomes R. T., and Oetterer, M. 2009. Ionizing radiation effects on food vitamins—A review. *Brazilian Archives of Biology and Technology* 52: 1267–78.

Du, M., Ahn, D. U., Nam K. C., and Sell, J. L. 2000. Influence of dietary conjugated linoleic acid on volatile profiles, color and lipid oxidation of irradiated raw chicken meat. *Meat Science* 56: 387–95.

Duller, G. A. T. 1997. Behavior studies of stimulated luminescence from feldspars. *Radiation Measurements* 27: 663–94.

El-Zawahry, Y. A., Aziz, N. H., and El-Fouly, M. Z. 1991. Incidence of toxic and pathogenic microorganisms in different Egyptian and Saudi Arabian commodities and their decontamination by gamma-irradiation. *Egypt Journal of Medical Microbiology* 26: 267–82.

EN13783. 2001. Foodstuffs—Detection of irradiated food using direct epifluorescent filter technique/aerobic plate count (DEFT/APC). European Committee of Standardization (CEN), Brussels.

EN13784. 2001. Foodstuffs—DNA comet assay for the detection of irradiated foodstuffs. European Committee of Standardization (CEN), Brussels.

EN14569. 2004. Foodstuffs—Microbiological screening for irradiated food using LAL/GNB procedures. European Committee of Standardization (CEN), Brussels.

EN13751. 2009. Foodstuffs—Detection of irradiated food using photostimulated luminescence. European Committee of Standardization (CEN), Brussels.

EN1784. 1996. Foodstuffs—Detection of irradiated food containing fat–Gas chromatographic analysis of hydrocarbons. European Committee of Standardization (CEN), Brussels.

EN1785. 2003. Foodstuffs—Detection of irradiated food containing fat—Gas chromatographic/mass spectrometric analysis of 2–alkylcyclobutanones. European Committee of Standardization (CEN), Brussels.

EN1787. 2001. Foodstuffs—Detection of irradiated food containing cellulose by ESR spectroscopy. European Committee of Standardization (CEN), Brussels.
EN1788. 2001. Foodstuffs—Thermoluminescence detection of irradiated food from which silicate minerals can be isolated. European Committee of Standardization (CEN), Brussels.
EN13708. 2001. Foodstuffs—Detection of irradiated food containing crystalline sugar by ESR spectroscopy. European Committee of Standardization (CEN), Brussels.
Eustice, R. F. and Bruhn, C. M. 2006. Consumer acceptance and marketing of irradiated foods. In: *Comsumer Acceptance and Marketing of Irradiated Foods*, ed. C. H. Sommer, and X. Fan, 63–83. Chicago: Blackwell Publishing and IFT Press.
FAO and WHO. Assuring Food Safety and Quality: Guidelines for Strengthening National Food Control Systems. ISSN 0254-4725, FAO Food and Nutrition Paper 76, Food and Agriculture Organization of the United Nations and World Health Organization, Rome, p. 2–73 2003.
Farkas, J. 1988. *Irradiation of Dry Food Ingredients*. Boca Raton: CRC Press Inc.
Farkas, J. 1998. Irradiation as a method for decontaminating food -A review. *International Journal of Food Microbiology* 44: 189–204.
Fox, J. A. 2002. Influences on purchase of irradiated foods. *Food Technology* 56: 34–7.
Giroux, M. and M. Lacroix. 1998. Nutritional adequacy of irradiated meat—A review. *Food Research International* 31:257–64.
Glidewell, S. M., Deighton, N., Goodman, B. A., and Hillman, J. R. 1993. Detection of irradiated food: A review. *Journal of the Science of Food and Agriculture* 61: 281–300.
Grant, L. A. and D'Appolonia, B. L. 1991. Effect of low-level gamma radiation on water-soluble non-starchy polysaccharides isolated from hard red spring wheat flour and bran. *Cereal Chemistry* 68: 651–6.
Griffin, R. L. 2008. Role of irradiation as a phytosanytary measure. FAO/IAEA Regional training workshop on the application of international standards related to irradiation for sanitary and phytosanitary purposes, PNRI, 8–12 Dec.
Gunes, G. and Tekin, M. D. 2006. Consumer awareness and acceptance of irradiated foods: Results of a survey conducted on Turkish consumers. *LWT-Food Science and Technology* 39: 443–7.
Haine, H., Cerda, H., and Jones, L. 1995. Microgel electrophoresis of DNA to detect irradiation of foods. *Food Science and Technology Today* 9: 139–41.
Haire, D. L., Chen, G., Jansen, E. G., Fraser, L., and Lynch, J. A. 1997. Identification of irradiated foodstuffs: A review of the recent literature. *Food Research International* 30: 249–64.
Hajare, S. N., Dhokane, V. S., Shashidhar, R., Saroj, S., Sharma, A., and Bandekar, J. R. 2006. Radiation processing of minimally pineapple (Ananas comosus Merr.): Effect on nutritional and sensory quality. *Journal of Food Science* 71: 501–5.
Hall, C. W. and Trout, G. M. 1968. Objections to pasteurization. In: *Milk Pasteurization*, 5–8. Connecticut: The AVI publishing Company.
Hallman, G. J. 2011. Phytosanitary applications of irradiation. *Comprehensive reviews in Food Science and Food Safety* 10, 143–51.
Hallman, G. J. 2013. Control of stored product pests by ionizing radiation. *Journal of Stored Products Research* 52: 36–41.
Hashim, I. B., Resurreccion, A. V. A., and McWaiters, K. H. 1995. Descriptive sensory analysis of irradiated frozen or refrigerated chicken. *Journal of Food Science* 60: 664–6.
Hendrichs, J., Bloem, K., Hoch, G., Carpenter, J. E., Greany, P., and Robinson, A. S. 2009. Improving the cost-effectiveness, trade and safety of biological control for agricultural insect pests using nuclear techniques. *Biocontrol Science and Technology* 19: 3–22.
Henson, S. 1995. Demand-side constraints on the introduction of new food technologies: The case of food irradiation. *Food Policy* 20: 111–27.
Hocaoglu, A., Ahmet S. D., Tuncay, G., and Mehmet, D. 2012. Effects of gamma irradiation on chemical, microbial quality and shelf life of shrimp. *Radiation Physics and Chemistry* 81: 1923–9.

Horvatovich, P., Miesch, M., Hasselmann, C., and Marchioni, E. 2000. Supercritical fluid extraction of hydrocarbons and 2-alkylcyclobutanones for the detection of irradiated foodstuffs. *Journal of Chromatography* A 897: 259–68.

Houee-Levin, C. and Sicard-Roselli. 2001. Radiation chemistry of proteins. In: *Radiation Chemistry: Present Status and Future Trends*, ed. C. D. Jonash, and B. S. Rao, 553–82. Amsterdam: Elsevier Science B.V.

Husman, A. M. R., Bijkerk, P., Lodder, W., van den Berg, H., Pribil, W., Cabaj, A., Gehringer, P., Sommer, R., and Duizer, E. 2004. Calcivirus inactivation by nonionizing (253.7-nanometer-wavelength [UV]) and ionizing (gamma) radiation. *Applied Environmental Microbiology* 70: 5089–93.

Hwang, K. T., Yoo, J. H., Kim, C. K., Uhm, T. B., Kim, S. B., and Park, H. J. 2001. Hydrocarbons detected in irradiated and heat-treated eggs. *Food Research International* 34: 321–8.

IAEA. 1982. Training Manual on Food Irradiation Technology. 2nd ed., Joint FAO/IAEA Division of Isotope and Radiation of Atomic Energy for Food and Agricultural Development. Technical Report Series No. 114, IAEA, Vienna, Austria.

IAEA. 2002. Dosimetry for Food Irradiation. Joint FAO/IAEA Division of Isotope and Radiation of Atomic Energy for Food and Agricultural Development. Technical Reports Series No. 409, IAEA, Vienna.

IAEA website. 2013. http://nucleus.iaea.org/fitf/, Accessed on August 20, 2013.

ICGFI. 1994. Summary report on eleventh meeting of the international consultative group on food irradiation. Denpasar, Bali, Indonesia, 2–4 November.

ICGFI. 1999. Enhancing Food Safety Through Irradiation. International Consultative Group on Food Irradiation Policy Document, Vienna.

International Plant Protection Convention (IPPC) 2003. Guidelines for the use of irradiation as a phytosanitary measure. ISPM No. 18. FAO. Rome. ftp://ftp.fao.org/docrep/fao/006/y4835e/y4835e00.pdf. Accessed on July 01, 2014.

Jo, C., Kim, H. K., Kim, D. H., Lee, W. K., Ham, J. S., and Byun, M. W. 2007. Radiation sensitivity of selected pathogens in ice cream. *Food Control* 18: 859–65.

Jones, K., McPhee, S., Turner, A., Stuckey, T., and Betts, R. 1995. The direct epifluorescent filter technique (DEFT/aerobic) plate count (APC): A screening method for the detection of irradiated food. *Food Science and Technology Today* 9: 141–4.

Josephson, E. S. and Peterson, M. S. 1983. *Preservation of Food by Ionizing Radiation*. Boca Raton: CRC Press Inc.

Kanatt, S. R., Chander, R., and Sharma, A. 2006. Effect of radiation processing of lamb meat on its lipids. *Food Chemistry* 97: 80–6.

Kawamura, Y., Suzuki, N., Uchiyama, S., and Saito, Y. 1992. Germination test for identification of gamma-irradiated rice. *Radiation Physics and Chemistry* 39: 203–7.

Kawamura, K., Uchiyama, S., and Saito, Y. 1989. Improvement of the half embryo test for detection of gamma-irradiated grapefruit. *Journal of Food Science* 54: 1501–4.

Kawamura, Y., Sugita, T., Yamada, T., and Saito, Y. 1996. Half–embryo test for identification of irradiated citrus fruit: collaborative study. *Radiation Physics and Chemistry* 48: 665–8.

Kempner, E. S. 2001. Effects of high-energy electrons and gamma-rays directly on protein molecules. *Journal of Pharmaceutical Sciences* 90: 1637–46.

Khan, A. A., Khan, H. M., and Delincée, H. 2002. Identification of irradiated spices using the novel technique of DNA comet assay. *Journal Food Science* 67: 493–6.

Khan, A. A., Khan, H.M., and Delincée, H. 2005. DNA comet assay—A rapid screening method for detection of irradiated cereals and tree nuts. *Food Control* 16: 141–6.

Kim, B. K., Ahn, J. J., Shahbaz, H. M., Kim, C. T., and Kwon, J. H. 2013. Effect of drying treatment on physical identification characteristics of irradiated seasonings. *Food Analytical Methods* DOI: 10.1007/s12161-013-9623-7.

Kim, B. K., Akram, K., Kim, C. T., Kang, N. R., Lee, J. W., Ryang, J. H., and Kwon, J. H. 2012. Identification of low amount of irradiated spices (red pepper, garlic, ginger powder) with luminescence analysis. *Radiation Physics and Chemistry* 81: 1220–3.

Kim, K. S., Lee, J. M., and Hong C. H. 2004. Solid phase extraction (SPE) method for detection of irradiated meats. *Lebensmittel-Wissenschaft and Technologie* 37: 559–63.

Kim, M. J., Yook, H. S., and Byun M. W. 2000. Effects of gamma irradiation on microbial contamination and extraction yields of Korean medicinal herbs. *Radiation Physics and Chemistry* 57: 55–8.

Kilcast, D. 1994. Effect of irradiation on vitamins. *Food Chemistry* 49: 157–64.

Kitai, S. and Furuta, M. 2009. Change in thermoluminescence of irradiated paprika powder during storage under various temperature and humidity conditions. *Radiation Physics and Chemistry* 78:703–5.

Klinger, Y., Lapidot, M., and Ross, I. 1985. Feed racidication in Israel. An update. In: *Food Irradiation Processing*, 117–126. Vienna: IAEA.

Kuan, Y. H., Bhat, R., Patras, A., and Karim, A. A. 2013. Radiation processing of food proteins - A review on the recent developments. *Trends in Food Science and Technology* 30: 105–20.

Kuan, Y. H., Bhat, R., and Karim, A. A. 2011. Emulsifying and foaming properties of ultraviolet-irradiated egg white protein and sodium caseinate. *Journal of Agricultural and Food Chemistry* 59: 4111–8.

Kume, T. and Todoriki, S. 2013. Food irradiation in Asia, the European Union, and the United States: A status update. *Radioisotopes* 62: 291–9.

Kume, T., Furuta, M., Todoriki, S., Uenoyama, N., and Koboyashi, Y. 2009a. Status of food irradiation in the world. *Radiation Physics and Chemistry* 78: 222–6.

Kume, T., Furuta, M., Todoriki, S., Uenoyama, N., and Kobayashi, Y. 2009b. Quantity and economic scale of food irradiation in the world. *Radioisotopes* 58: 25–35.

Kwon, J. H. 1998. Application of irradiation technology to preserving and improving qualities of agricultural products. *Journal of Food Science and Nutrition* 3: 295–301.

Kwon, J. H. 2005. Effects of gamma irradiation and methyl bromide fumigation on the qualities of fresh chestnuts during storage. *Food Science and Biotechnology* 14: 181–4.

Kwon, J. H. 2010. *Safety and Understanding of Irradiated Food*. Seoul: Korea Food Safety Research Institute, ISBN 978-89-962714-2-0 94570.

Kwon, J. H., Byun M. W., and Cho, H. O. 1985. Effects of gamma irradiation dose and timing of treatment after harvest on the storeability of garlic bulbs. *Journal of Food Science* 50: 379–81.

Kwon, J. H., Choi, J. U., and Yoon, H. S. 1989. Sulfur-containing components of gamma- irradiated garlic bulbs. *Radiation Physics and Chemistry* 34: 969–72.

Kwon, J. H., Shahbaz, H. M., and Ahn, J.J. 2014. Advanced electron paramagnetic resonance spectroscopy for the identification of irradiated food. *American Laboratory* 46: 1–4.

Kwon, J. H., Yoon, S. H., Sohn, T. H., Byun, M. W., and Cho, H. O. 1984. Effect of gamma irradiation on the physiological characteristics of garlic bulbs during storage. *Korean Journal of Food Science and Technology* 16: 408–12.

Kyung, H. K., Ahn, J. J., Akram, K., and Kwon, J. H. 2012. Thermoluminescence analyses of irradiated dried sea foods using different methods of mineral separation. *Radiation Physics and Chemistry* 81: 1224–6.

Lacroix, M. and Lafortune, R. 2004. Combined effects of gamma irradiation and modified atmosphere packaging on bacterial resistance in grated carrots (Daucus carota). *Radiation Physics and Chemistry* 71: 77–80.

Lamuka, P. O., Sunki, G. R., Chawan, C. B., Rao, D. R., and Shackelford, L. A. 1992. Bacteriological quality of freshly processed broiler chickens as affected by carcass pretreatment and gamma irradiation. *Journal of Food Science* 57: 330–2.

Lee, J.W., Kim, J.H., Yoon, Y., Jo, C., and Byun, M. W. 2012. Potential applications of ionizing radiation. In: *Food Irradiation Research and Technology*, eds. X. Fan and C. H. Sommers. Hoboken: John Wiley & Sons, Inc. DOI:10.1002/9781118422557.ch21.

Lee, M. S., Lee, S. H., and Song, K. B. 2005. Effect of γ-irradiation on the physicochemical properties of soy protein isolate films. *Radiation Physics and Chemistry* 72: 35–40.

Lee, Y. S., Oh, S. H., Lee, J. W., Kim, J. H., Kim, D. S., and Byun, M. W. 2003. Effects of gamma irradiation on physicochemical and textural properties of starches. *Food Science and Biotechnology* 12: 508–12.

Li, A., Ha, Y., Wang, F., and Li, Y. 2010. Detection of hydrocarbons in irradiated chilled beef by HS-SPME–GC–MS and optimization of the method. *Journal of the American Oil Chemists' Society* 87: 731–6.

Liao, C. H. 2008. Growth of Salmonella on sprouting alfalfa seeds as affected by the inoculum size, native microbial load and Pseudomonas fluorescens 2–79. *Letters in Applied Microbiology* 46: 232–6.

Loaharanu, P. 1996. Irradiation as a cold pasteurization process of food. *Veterinary Parasitology* 94:71–82.

Loaharanu, P., Kava, R., and Choi, E. H. 2007. Irradiated Foods. 6th ed., American Council on Science and Health. http:/www.acsh.org.

Lund, B., Baird-Parker, A. C., and Gould, G. W. 1999. *The Microbiological Safety and Quality of Food*. New York: Springer Publishing.

Mallett, J. C., Beghian, L. E., Metcalf, T. G., and Kaylor, J. D. 1991. Potential of irradiation technology for improved shellfish sanitation. *J. Food Safety* 11: 231–45.

Marchioni, E. 2006. Detection of irradiated foods. In: *Food Irradiation Research and Technology*, eds. C. H. Sommers and X. Fan, pp. 85–103. Ames, Iowa: Blackwell Publishing.

Marchioni, E., Horvatovich, P., Charon, H., and Kuntz, F. 2005. Detection of irradiated ingredients included in low quantity in non–irradiated food matrix. 2. ESR analysis of mechanically recovered poultry meat and TL analysis of spices. *Journal of Agricultural and Food Chemistry* 53: 3774–8.

Marcos, R. R., de Oliveira, N. L., and del Mastro. 2007. Electron paramagnetic resonance study of some varieties of gamma-irradiated soybean. *Radiation Physics Chemistry* 76: 1459–62.

McKeever, S. W. S. 1985. *Thermoluminescence of Solids*. Cambridge: Cambridge University Press

McMurray, B. T., Brannigen, I. O., Hamilton, J. T. G., Boyd, D. R., and Stevenson, H. 1994. Detection of irradiated food using cyclobutanones. *Food Science and Technology Today* 8: 99–100.

McMurray, C. H., Stewart, E. M., Gray, R., and Pearce, J. 1996. *Detection Methods for Irradiated Foods—Current Status*. pp. 108–118. Cambridge, UK: Royal Society of Chemistry.

Micard, V., Belamri, R., Morel, M. H., and Guilbert, S. 2000. Properties of chemically and physically treated wheat gluten films. *Journal Agricultural and Food Chemistry* 48: 2948–53.

Morehouse, K. M. and Ku, Y. 1990. A gas–chromatographic method for the identification of gamma–irradiated frog legs. *Radiation Physics and Chemistry* 35: 337–41.

Mortimore, S. and Wallace, C. 1992. HACCP—A Practical Approach, London: Chapman and Hall.

Nawar, W. W. 1986. Volatiles from food irradiation. *Food Reviews International* 2: 45–78.

Nawar, W. W. and Balboni, J. J. 1970. Detection of irradiation treatments in foods. *Journal of the Association of Official and Analytical Chemists* 53: 726–9.

Nawar, W. W., Champagne, J. R., Dubravic, M. F., and LeTellier, P. R. 1969. Recovery and measurement of volatiles from lipids: Hydrocarbons in irradiated fats. *Journal of Agricultural and Food Chemistry* 17: 645–8.

Ndiaye, B., Horvatovich, P., Miesch, M., Hasselmann, C., and Marchioni, E. 1999. 2–Alkylcyclobutanones as markers for irradiated foodstuffs: III. Improvement of the field of application on the EN1785 method by using silver ion chromatography. *Journal of Chromatography A* 858: 109–15.

Neetoo, H. and Chen, H. 2011. Individual and combined application of dry heat with high hydrostatic pressure to inactivate Salmonella and *Escherichia coli* O157:H7 on alfalfa seeds. *Food Microbiology* 28: 119–27.

Oh, K. N., Lee, S. Y., Lee, H. J., Kim, K. E., and Yang, J. S. 2003. Screening of gamma irradiated spices in Korea by using a microbiological method (DEFT/APC). *Food Control* 14: 489–94.

Ostling, O. and Johanson, K. J. 1984. Microelectrophoretic study of radiation induced DNA damages in individual mammalian cells. *Biochemical and Biophysical Research Communications* 123: 291–8.

Pierson, M. D., and Corlett, D. A. 1992. HACCP—Principles and Applications. Chapman and Hall, New York.

Pietranera, M. S. A., Narvaiz, P., Horak, C., and Kairiyama, E. 2003. Irradiated Ice-creams for Immunosuppressed Patients. Radiation Physics and Chemistry 66: 357–65.

Preusser, F., Chithambo, M. L., Götte, T., Martini, M., Ramseyer, K., Sendezera, E. J., Susino, G. J., and Wintle, A. G. 2009. Quartz as a natural luminescence dosimeter. *Earth Science Reviews* 97: 84–214

Raffi, J. 1998. Identifying irradiated foods. *Trends in Analytical Chemistry* 17: 226–33.

Raffi, J. and Stocker, P. 1996. Electron paramagnetic resonance detection of irradiated foodstuffs. *Applied Magnetic Resonance* 10: 357–73.

Raffi, J., Yordanov, N. D., Chabane, S., Douifi, L., Gancheva, V., and Ivanova, S. 2000. Identification of irradiation treatment of aromatic herbs, spices and fruits by electron paramagnetic resonance and thermoluminescence. *Spectrochimica Acta A* 56: 409–16.

Resurreccion A. V. A., Galvez, F. E. F., Fletcher, S. M., and Misra, S. K. 1995. Consumer attitudes toward irradiated food: Results of a new study. *Journal of Food Protection* 58: 193–6.

Roberts, P.B. 2014. Food irradiation is safe: Half a century of studies. *Radiation Physics and Chemistry*. DOI: 10.1016/j.radphyschem.2014.05.016.

Ryser, E.T. 2009. Novel X-ray irradiation technology for the food industry. Paper presented at annual meeting of Korean Society of Food Science and Nutrition, Changwon, Nov. 4–6.

Sabularse, V. C., Liuzzo, J. A., Rao, R. M., and Grodner, R. M. 1991. Cooking Quality of Brown Rice as Influenced by Gamma Irradiation, Variety and Storage. *Journal of Food Science* 56: 96–8.

Salimov, R. A., Cherepkov, V. G., Kuksanov, N. K., and Kuznetzov, S. A., 2000. The use of electron accelerators for radiation disinfestation of grain. *Radiation Physics and Chemistry* 57: 625–7.

Sanderson, D. C. W., Carmichael, L. A., and Naylor, J. D. 1996. Recent advances in thermoluminescence and photostimulated luminescence detection methods for irradiated foods. In: *Detection Methods for Irradiated Foods: Current Status*, ed. C. H. McMurray, E. M. Stewart, R. Gray, J. Pearce, 124–38. Cambridge: The Royal Society of Chemistry.

Sanderson, D. C. W. 1991. Photostimulated luminescence (PSL): A new approach to identifying irradiated foods. In: Potential new methods of detection of irradiated food, J. Raffi, 159–67. Luxembourg: European Commission Report.

Scatter, S. L., Beardwood, K., and Wood, R. 1994. Limulus amoebocyte lysate test/gram negative bacteria count method for the detection of irradiated poultry: Results of two inter–laboratory studies. *Food Science and Technology Today* 8: 106–7.

Schulzki, G., Spiegelberg, A., Bögl, K. W., and Schreiber, G. A. 1995. Detection of radiation-induced hydrocarbons in camembert irradiated before and after the maturing process: Comparison of florisil column chromatography and on-line coupled liquid

chromatography–gas chromatography. *Journal of Agricultural and Food Chemistry* 43: 372–6.

Sokhey, A. S. and Hanna, M. A. 1993. Properties of irradiated starches. *Food Structure* 12: 397–410.

Song, B. S., Park J. G., Kim, J. H., Chio, J. I., Ahn, D. H., Chen, H., and Lee, J. W. 2012. Development of freeze-dried miyeokguk, Korean seaweed soup, as space food sterilized by irradiation. *Radiation Physics and Chemistry* 81: 1111–4.

Song, H. P., Kim, B., Choe, J. H., Jung, S., Kim, K. S., Kim, D. H., and Jo, C. 2009. Improvement of foaming ability of egg white product by irradiation and its application. *Radiation Physics and Chemistry* 78: 217–21.

Stevenson, M. H. and Stewart, E. M. 1995. Identification of irradiated food: the current status. *Radiation Physics and Chemistry* 46: 653–8.

Stevenson, M. H. 1992. Progress in the identification of irradiated food. *Trends in Food Science and Technology* 3: 257–62.

Stewart, E. M. 2001. Food irradiation chemistry. In: *Food irradiation: Principles and applications, ed. R. A. Molins*, 37–76. New York: John Wiley and Sons, Inc. Technology

Taipina, M. S., Lamardo L. C. A., Rodas M. A. B., and del Mastro, N. L. 2009. The effects of gamma irradiation on the vitamin E content and sensory qualities of pecan nuts (*Carya illinoensis*). *Ration Physics and Chemistry* 78: 611–3.

Theodoridis, G. and Manesiotis, P. 2002. Selective solid-phase extraction sorbent for caffeine made by molecular imprinting. *Journal of Chromatography A* 948: 163–9.

Thayer, D. W. 1995. Use of irradiation to kill enteric pathogens on meat and poultry. *Journal of Food Safety* 15: 181–12.

Thayer, D. W., Boyd, G., and Fett, W. F. 2003a. Gamma irradiation decontamination of alfalfa seeds naturally contaminated with Salmonella Mbandaka. *Journal of Food Science* 68: 1777–81.

Thayer, D. W., Rajkowski, K. T., Boyd, G., Cooke, P. H., and Soroka, D. S. 2003b. Inactivation of *Escherichia coli* O157:H7 and Salmonella by gamma irradiation of alfalfa seed intended for production of food sprouts. *Journal of Food Protection* 66:175–81.

Tsoulfanidis, N. 1995. *Measurement and Detection of Radiation*. 2nd edition. Washington: Taylor and Francis.

UNEP. 2000. The Montreal protocol on substances that deplete the ozone layer. United Nations Environment Programme. ISBN 92-807-1888-6.

Verbeek, F., Koppen, G., Schaeken, B., and Verschaeve, L. 2007. Automated detection of irradiated food with the comet assay. *Radiation Protection Dosimetry* 128: 421–6.

Villavicencio A. L. C. H., Mancini-Filho, J., Delincee, H., and Bognar, A. 2000. Effect of gamma irradiation on the thiamine, riboflavin and vitamin B6 content in two varieties of Brazilian beans. *Radiation Physics and Chemistry* 57: 299–303.

Waje, C. and Kwon, J. H. 2007. Improving the Food Safety of Seed Sprouts Through Irradiation Treatment. *Food Science and Biotechnology* 16: 171–6.

Waje, C., Kim, H. K., Kim, K. S., Todoriki, S., and Kwon, J.H. 2008. Physicochemical and microbiological qualities of steamed and irradiated ground black pepper (*Piper nigrum* L.). *Journal of Agricultural and Food Chemistry* 56: 4592–6.

Waje, C. K., Jun, S. Y., Lee, Y. K., Kim, B. N., Han, D. H., Jo, C., and Kwon, J. H. 2009. Microbial quality assessment and pathogen inactivation by electron beam and gamma irradiation of commercial seed sprouts. *Food Control* 20: 200–4.

Whitcomb, J. L. and Campiglia, A. D. 2001. Screening potential of solid-phase extraction and solid surface room temperature fluorimetry for polycyclic aromatic hydrocarbons in water samples. *Talanta* 55: 509–18.

WHO 1981. Wholesomeness of Irradiated Food, Report of Joint FAO/IAEA WHO Expert Committee, Technical Report Series 659, WHO, Geneva, 1981.

WHO. 1988. Food Irradiation—A technique for preserving and improving the safety of food. WHO/FAO, Geneva, Switzerland.

WHO. 1994. Safety and nutritional adequacy of irradiated food. World Health Organization, Geneva, Switzerland.

WHO. 1999. High-dose irradiation: Wholesomeness of food irradiated with doses above 10 kGy. Report of a joint FAO/IAEA/WHO study group. WHO Technical Report Series 890. World Health Organization, Geneva, Switzerland.

WHO 2003. Evaluation of certain veterinary drug residues in food (Sixtieth report of the Joint FAO/WHO Expert Committee on Food Additives). WHO Technical Report Series No. 918, 2003.

Yordanov, N. D., Aleksieva, K., Dimitrova, A., Georgieva, L., and Tzvetkova, E. 2006. Multifrequency EPR study on freeze-dried fruits before and after X-ray irradiation. *Radiation Physics and Chemistry* 75: 1069–74.

Yun, J., Li, X., Fan, X., Tang Y., Xiao, Y., and Wan S. 2012. Effect of gamma irradiation on microbial load, physicochemical and sensory characteristics of soybeans (Glycine max L. Merrill). *Radiation Physics and Chemistry* 81: 1198–202.

Yunoki, S., Sekiguchi, M., and Nakagawa, S. 2012. Photostimulated luminescence of corrugated fiberboard as an additional screening method for detecting radiated foods. *Radiation Measurements* 47: 561–4.

Yusof, N., Ramli, R. A. A., and Ali, F. 2007. Chemical, sensory and microbiological changes of gamma irradiated coconut cream powder. *Radiation Physics and Chemistry* 76: 1882–4.

Zegota, H. and Malolepszy, B. 2008. The decontamination of industrial casein and milk powder by irradiation. *Radiation Physics and Chemistry* 77: 1108–11.

14 Food Formulation

V. Giannou, Constantina Tzia, and Theodoros Varzakas

CONTENTS

14.1 Introduction 492
14.2 Types of Food Ingredients 493
14.2.1 Major Food Ingredients 493
14.2.1.1 Carbohydrates 493
14.2.1.2 Sweeteners 497
14.2.1.3 Proteins 498
14.2.1.4 Lipids 499
14.2.2 Minor Food Ingredients 501
14.2.2.1 Acidifiers 502
14.2.2.2 Anticaking Agents 502
14.2.2.3 Antimicrobial Agents 502
14.2.2.4 Antioxidants 502
14.2.2.5 Bulking Agents 503
14.2.2.6 Coloring Agents 503
14.2.2.7 Emulsifiers 504
14.2.2.8 Firming Agents 504
14.2.2.9 Flavor Enhancers 504
14.2.2.10 Flavorings 504
14.2.2.11 Glazing Agents 505
14.2.2.12 Humectants 505
14.2.2.13 Leavening Agents 505
14.2.2.14 Propellants 506
14.2.2.15 Stabilizers 506
14.2.2.16 Thickeners 506
14.2.2.17 Bioactive Compounds 507
14.2.2.18 Probiotics 508
14.2.2.19 Prebiotics 508
14.3 Food Applications 508
14.3.1 Pastry Products—Omega-3 Fatty Acids 508
14.3.1.1 Fillo Dough Products 512
14.3.1.2 Sponge Cake with Cocoa Filling Formulation 513
14.3.1.3 Tsoureki with Apricot Jam Formulation 513
14.3.2 Baked Products: Cereals and Polyphenols 514
14.3.2.1 Bake Rolls Formulation 515
14.3.2.2 Strudel with Apple-Cinnamon Formulation 516

14.3.2.3 Bake Bars Formulation 516
14.3.2.4 Vafla Dough with Hazelnut Filling Formulation 516
14.3.3 Micro and Nano-Emulsions 517
14.3.3.1 Low-Fat Meat Products 519
14.3.3.2 Prebiotic Fibers 519
14.3.3.3 Wax Oleogels 520
14.3.3.4 Snack Products 520
14.4 Conclusion 521
Further Reading 522

14.1 INTRODUCTION

Most processed food products are made by combining different raw materials in certain proportions. Food formulation describes the process of creating and designing such a food product to meet consumers' needs for superior sensory characteristics, high convenience and low price, and also satisfy their health, wellness, and safety concerns. From the manufacturer's point of view, it focuses on the identification of the structure and composition of food ingredients that provide the desired characteristics in the final product.

Food ingredients can be categorized into:

- Major food components (fats/lipids, proteins, carbohydrates, and water) and
- Minor food components (such as pigments, flavors, enzymes, and processing additives).

A food additive is any substance added to food, directly or indirectly affecting its characteristics. However, some food additives may also be inadvertently (incidentally) incorporated in foods during processing, packaging, or storage. It is important to note that the Food and Drug Administration (FDA) database contains a list of almost 3000 ingredients, which can be added in food products. All food additives are carefully governed by national and international legislation/regulations to ensure that foods are safe to eat and are accurately labeled.

Food additives are incorporated in a product in order to

- Improve or maintain its nutritional value (i.e., vitamins, minerals, or fiber are used to enhance the nutritional quality of a food).
- Maintain or improve safety and freshness (i.e., preservatives are used to prevent microbial spoilage and antioxidants to delay oxidative reactions).
- Improve taste, texture, and appearance (i.e., spices, colors, flavors, or sweeteners are added to enhance the taste and appearance of food, while emulsifiers, stabilizers, and thickeners to provide the adequate texture and consistency).

However, to reach a desired formulation, it is necessary to understand the role and function of each ingredient/additive and their effects on the physicochemical properties of the product as well as on its textural and sensorial qualities and shelf life.

14.2 TYPES OF FOOD INGREDIENTS

The most common types of food ingredients, their function, and examples of their use are presented in Table 14.1.

14.2.1 Major Food Ingredients

14.2.1.1 Carbohydrates

Most common organic compounds found in this category include sugars, starches, and fiber. Carbohydrates are categorized as simple and complex, according to their size. Simple carbohydrates are referred to as sugars and are among the most common food additives. Examples are sucrose, dextrose, fructose, and corn syrup. Complex carbohydrates are found in plants and seeds in the form of starch and fiber.

14.2.1.1.1 Starch

Starch consists of long chains of glucose and can be found in the form of amylose (straight chain polymer of glucose, 20–30% of starch structure) or amylopectin (highly branched polymer of glucose, 70–80% of starch structure). It accounts for 50–75% of the weight of cereal grain and 75% of the weight of potatoes. Commercial starch is usually produced from corn. However, sorghum, wheat, rice, arrowroot, tapioca, and potato can also be used. It can be used as a thickening agent due to its ability to form gels and as a texture enhancer. Modified starches are also available as food additives. They are prepared by the physical, enzymatic, or chemical treatment of native starch, in order to enhance its performance in different applications (i.e., increase stability against heat/cold, acid, and so on, decrease or increase viscosity, lengthen or shorten gelatinization time). Modified starches are used as thickening agents, stabilizers, or emulsifiers. Treatment of starch with alkali or acid yields degradation products, such as gums and dextrins.

Fibers refer to the indigestible complex carbohydrates found in plant cell walls and structures. Cellulose is the most common fiber, containing only glucose, while hemicelluloses and lignin are the other important types.

14.2.1.1.2 Fibers

Dietary fibers represent the heterogeneous mixture of residues that are derived from the outer coating or plant wall material of vegetables, grains, seeds, and fruits, which are indigestible by the enzymes present in the small intestine of humans.

They consist of a mixture of very different nonstarch complex carbohydrate and noncarbohydrate materials. The major classes of dietary fiber are cellulose, hemicelluloses, pectins, mucilages, gums, algal materials, and lignins. All the above except from lignins are polysaccharides. Fructo-oligo saccharides are also considered to be a form of fiber.

- Cellulose is a linear chain of glucose units.
- Hemicelluloses are highly branched structures found in plant cell walls. They are a diverse group with varying sugar compositions, including the

TABLE 14.1
Common Types of Food Ingredients

Ingredients Type	Function	Examples of Use	Names Found on Products Label
Preservatives	Prevent food spoilage from bacteria, molds, fungi, or yeast (antimicrobials); slow or prevent changes in color, flavor, or texture and delay rancidity (antioxidants); maintain freshness	Fruit sauces and jellies, beverages, baked goods, cured meats, oils and margarines, cereals, dressings, snack foods, fruits and vegetables	Ascorbic acid, citric acid, sodium benzoate, calcium propionate, sodium erythorbate, sodium nitrite, calcium sorbate, potassium sorbate, BHA, BHT, EDTA, tocopherols (vitamin E)
Sweeteners (Varzakas et al., 2012)	Add sweetness with or without the extra calories	Beverages, baked goods, confections, table-top sugar, substitutes, many processed foods	Sucrose (sugar), glucose, fructose, sorbitol, mannitol, corn syrup, high fructose corn syrup, saccharin, aspartame, sucralose, acesulfame potassium (acesulfame-K), neotame
Color additives	Offset color loss due to exposure to light, air, temperature extremes, moisture and storage conditions; correct natural variations in color; enhance colors that occur naturally; provide color to colorless and "fun" foods	Many processed foods, (candies, snack foods margarine, cheese, soft drinks, jams/jellies, gelatins, pudding and pie fillings)	FD&C Blue Nos. 1 and 2, FD&C Green No. 3, FD&C Red Nos. 3 and 40, FD&C Yellow No. 5 (tartrazine) and No. 6, Orange B, Citrus Red No. 2, annatto extract, beta-carotene, grape skin extract, cochineal extract or carmine, paprika oleoresin, caramel color, fruit and vegetable juices, saffron (Note: Exempt color additives are not required to be declared by name on labels but may be declared simply as colorings or color added)
Flavors and spices	Add specific flavors (natural and synthetic)	Pudding and pie fillings, gelatin dessert mixes, cake mixes, salad dressings, candies, soft drinks, ice cream, BBQ sauce	Natural flavoring, artificial flavor, and spices
Flavor enhancers	Enhance flavors already present in foods (without providing their own separate flavor)	Many processed foods	Monosodium glutamate (MSG), hydrolyzed soy protein, autolyzed yeast extract, disodium guanylate or inosinate

TABLE 14.1 (continued)
Common Types of Food Ingredients

Ingredients Type	Function	Examples of Use	Names Found on Products Label
Fat replacers	Provide expected texture and a creamy "mouth-feel" in reduced-fat foods	Baked goods, dressings, frozen desserts, confections, cake and dessert mixes, dairy products	Olestra, cellulose gel, carrageenan, polydextrose, modified food starch, microparticulated egg white protein, guar gum, xanthan gum, whey protein concentrate
Nutrients	Replace vitamins and minerals lost in processing (enrichment), add nutrients that may be lacking in the diet (fortification)	Flour, breads, cereals, rice, macaroni, margarine, salt, milk, fruit beverages, energy bars, instant breakfast drinks	Thiamine hydrochloride, riboflavin (Vitamin B_2), niacin, niacinamide, folate or folic acid, beta carotene, potassium iodide, iron or ferrous sulfate, alpha tocopherols, ascorbic acid, Vitamin D, amino acids (L-tryptophan, L-lysine, L-leucine, L-methionine)
Emulsifiers	Allow smooth mixing of ingredients, prevent separation Keep emulsified products stable, reduce stickiness, control crystallization, keep ingredients dispersed, and to help products dissolve more easily	Salad dressings, peanut butter, chocolate, margarine, frozen desserts	Soy lecithin, mono- and diglycerides, egg yolks, polysorbates, sorbitan monostearate
Stabilizers and thickeners, binders, texturizers	Produce uniform texture, improve "mouth-feel"	Frozen desserts, dairy products, cakes, pudding and gelatin mixes, dressings, jams and jellies, sauces	Gelatin, pectin, guar gum, carrageenan, xanthan gum, whey
Leavening agents	Promote rising of baked goods	Breads and other baked goods	Baking soda, monocalcium phosphate, calcium carbonate
Anti-caking agents	Keep powdered foods free-flowing, prevent moisture absorption	Salt, baking powder, confectioner's sugar	Calcium silicate, iron ammonium citrate, silicon dioxide
Humectants	Retain moisture	Shredded coconut, marshmallows, soft candies, confections	Glycerin, sorbitol

continued

TABLE 14.1 (continued)
Common Types of Food Ingredients

Ingredients Type	Function	Examples of Use	Names Found on Products Label
Yeast Nutrients	Promote growth of yeast	Breads and other baked goods	Calcium sulfate, ammonium phosphate
Dough strengtheners and conditioners	Produce more stable dough	Breads and other baked goods	Ammonium sulfate, azodicarbonamide, L-cysteine
Firming agents	Maintain crispness and firmness	Processed fruits and vegetables	Calcium chloride, calcium lactate
Enzyme preparations	Modify proteins, polysaccharides and fats	Cheese, dairy products, meat	Enzymes, lactase, papain, rennet, chymosin
Gases	Serve as propellant, aerate, or create carbonation	Oil cooking spray, whipped cream, carbonated beverages	Carbon dioxide, nitrous oxide

simple sugars mannose, glucose, galactose, xylose, arabinose, and an acid derived from glucose called glucuronic acid.

- Pectins contain an acidic sugar derived from galactose, galacturonic acid, in the primary chains, with side chains or branches containing less common sugars: arabinose, fucose, and xylose. They function as a glue that holds plant tissues together.
- Gums contain acidic sugars.
- Algal polysaccharides are products of edible seaweed.
- Lignins are the principal structural material of wood.

Fibers can be further categorized as insoluble or water soluble. Insoluble fiber includes cellulose and lignin. Cellulose is not digested, although colon bacteria may break it down by 40–80%. Lignin, on the contrary, passes through the digestive tract unchanged. This type of fiber swells in water, increases stool weight and stool frequency and helps prevent constipation, colonic inflammation, and hemorrhoids, by speeding up the movement of waste through the intestine. They are also believed to protect against heart diseases. Bran and oatmeal are the most common sources of insoluble fiber, deriving from the outer husk of kernels of wheat and other cereal grains. They can also be found in the skin of vegetables and fruits, whole grains (not white flour), high-fiber cereals, dried beans, broccoli, and bulgur wheat.

Soluble fibers contain noncellulose carbohydrates, including pectins, gums, algal polysaccharides and some types of hemicellulose. They have the ability to dissolve in water, swell, and become gelatinous. As they move through the digestive tract, they are fermented by bacteria and present several physiological effects. They lower

blood cholesterol and slow down the rate of stomach emptying, starch digestion, and glucose uptake, thus lowering the amount of insulin needed to process blood glucose after a meal. Soluble fibers can be found in fruits, cooked dried beans, chickpeas, barley, lentils, navy beans, vegetables such as squash and carrots, plus barley, oat, and rice bran. Guar gum, glucomannan, and pectins are common soluble fiber supplements.

Dietary fibers can help curb appetite creating the feeling of satiety, thus help control obesity. Fiber-rich foods also require longer chewing, which stimulates digestive juices and helps digestion. However, excessive fiber has been associated with bloating, gas, cramps, nausea, and diarrhea.

Carbohydrates are also differentiated into monosaccharides, dissacharides, oligosaccharides, and polysaccharides. Monosaccharides include simple sugars, such as glucose (the predominant carbohydrate of the body) and fructose, which are used as the building blocks of disaccharides and polysaccharides (i.e., cellulose and starch). They are usually colorless, water-soluble, and crystalline solids. Disaccharides contain two linked simple sugars. The most typical and widely used in food products member of the group is sucrose (table sugar) comprising a glucose and a fructose molecule. Oligosaccharides (i.e., maltodextrin) are the water-soluble fragments of complex carbohydrates, usually starch, and contain 3–10 glucose units. Finally, polysaccharides are long-chained polymers containing simple sugars linked together. Unlike sugars, complex carbohydrates do not taste sweet, and they are often insoluble in water.

Carbohydrates can also be classified according to their degree of processing. Refined carbohydrates, such as sugar and white flour, are highly purified materials, containing little, if any, of the nutrients found in the whole food from which the carbohydrate derived, supplying therefore mainly calories.

14.2.1.2 Sweeteners

14.2.1.2.1 Natural Sweeteners

Most natural sweeteners used in food processing are carbohydrate sugars or are produced from carbohydrates. Most important among these are the monosaccharides fructose and glucose and the disaccharides sucrose (table sugar). Table sugar is derived from sugarcane or beet roots through a purification process. Corn syrups are also commonly employed in food products. They are prepared from maize starch and contain different amounts of maltose and higher oligosaccharides, depending on their grade. They are used as texture softeners, volume and flavor enhancers, and prevent crystallization of sugar as well. High-fructose corn syrup (HFCS) is manufactured from corn syrup subjected to enzymatic processing, using the enzyme xylose isomerase, in order to convert some of its glucose into fructose and increase sweetness to the desired level. Due to its lower price compared to sugar, HFCS is extensively used in processed foods and beverages, such as bakery products, breakfast cereal, and soft drinks.

Sugar alcohols (or polyols) are a class of carbohydrates that are neither sugars nor alcohols. This group includes maltitol, sorbitol, mannitol, xylitol, erythritol, lactitol, and hydrolyzed starch hydrolysates (HSH). These popular sugar substitutes provide

the bulk and sweetness of sugar and corn syrup, but are incompletely absorbed in the intestine. Thus, they provide fewer calories and carbohydrates than sugar and result in a much slower and smaller rise in blood sugar and insulin. They are generally recognized as safe for diabetics to consume; therefore, products sweetened with these products may legally be labeled "sugar-free" in most countries. Sugar alcohols do not promote oral bacteria (xylitol in fact inhibits bacterial growth), thus do not cause tooth decay. For this reason, they are extensively used in chewing gums.

Natural sweeteners of noncarbohydrate origin are also incorporated in foods. Stevia is considered the most popular of these. It is derived from a herb (*Stevia rebaudiana*) of the sunflower family. Its leaves provide a variety of substances of sweet taste (about 300 times as sweet as sucrose or white table sugar), with no calories or carbohydrates. The two most abundant of these are stevioside and rebaudioside A, with the latter being considered to provide the better taste with no bitter aftertaste.

14.2.1.2.2 Artificial Sweeteners

They are commonly used in order to impart the desired sweetness to food products presenting however considerably smaller than sugar or no caloric load. Aspartame, saccharin, acesulfame-k, and sucralose are the most important members of this group showing numerous applications especially in soft drinks and chewing gums.

14.2.1.3 Proteins

Proteins are complex polymers containing a unique sequence of amino acids. When incorporated into the human body, they degrade and their structural units are used for the synthesis of new proteins, necessary for skin, blood, muscle, hair, bone, and nails, as well as of enzymes used as catalysts in the chemical reactions, which occur in the cells. As a food ingredient, proteins provide structure and function. They can increase gel strength, viscosity, or water-holding capacity and generate foams.

They are distinguished into vegetable and animal proteins, based on their origin. Vegetable proteins often contain less than the optimal amounts of certain essential amino acids such as lysine or methionine. Therefore, a combination of different vegetable sources is required to provide ample amounts of the essential amino acids. Exceptions to this rule are soybeans, dried beans, amaranth, and quinoa. Soy proteins are commonly used in several food applications such as prepared foods (soups, sauces), meat substitutes, diet foods, imitation milk products, and so on. Rice protein and wheat gluten are also incorporated in certain food systems.

Animal proteins are generally considered high-quality proteins as they contain sufficient amounts of all dietary essential amino acids. Meat, fish, poultry, eggs, and dairy products are good sources of animal proteins. However, these same sources provide excess cholesterol and saturated fat and lack fiber. However, meat is an exceptional source of zinc, iron, and vitamin B12, while dairy products contain calcium and many of them are fortified with vitamin D. Seafood is also an excellent source of protein, being at the same time usually low in fat. Fish such as salmon are little higher in fat, but they are rich in omega-3 fatty acids, as well. Common protein additives of animal origin are egg powders (white or yolk), and milk or whey powders, used mainly in confectionary and dairy products, respectively. Their advantage

over fresh goods is the lower price and the significantly extended shelf life. Finally, some proteins, such as meat myoglobin, provide color.

14.2.1.4 Lipids

Lipids are defined as water-insoluble organic substances found in animal and plant tissues. They include fats, oils, phospholipids, and waxes. Cholesterol, lecithin, and vitamins A, D, E, and β-carotene are some of the most prominent lipids. Lipids provide body, mouth feel, plasticity, moistness color, and flavor in food products. However, they are often sensitive toward rancidity, which mainly affects flavor and odor.

14.2.1.4.1 Fats

Fats are considered to be the most concentrated form of energy, supplying 9 kcal/g, which is more than twice as much as in carbohydrates or proteins. During digestion, they are broken down by the enzyme pancreatic lipase and released into the intestine. Fats may also serve the following functions: they carry flavors in foods and helps fat-rich foods to create a feeling of satiety by slowing the rate of stomach emptying.

Fats are classified as saturated or unsaturated, according to their fatty acid compositions. Saturated fats are found primarily in animal sources such as meat, egg yolks, yogurt, cheese, butter, and milk. This type of fat is often solid at room temperature. Examples are lard and hydrogenated vegetable oil (vegetable shortening). Excessive consumption of saturated fat has been linked to health problems such as high cholesterol and heart disease. If a fat contains less than one-third saturated fatty acids, it is considered unsaturated.

Unsaturated fats include monounsaturated and polyunsaturated fats, which are typically found in plant food sources and are usually liquid at room temperature.

14.2.1.4.2 Vegetable Oils

Vegetable oils are extracted from seeds, nuts, and fruits. They are mainly used to fry and sauté foods, in salad dressings, and as an ingredient in baking. They provide energy (9 kcal/g), vitamin E, and polyunsaturated fatty acids and contain no cholesterol as plants do not synthesize it. As mentioned earlier, vegetable oils can be classified into saturated, monounsaturated, and polyunsaturated oils.

- Saturated vegetable oils are sometimes called vegetable fats. These are predominantly solid at room temperature and tend to increase blood cholesterol levels, and are thus associated with higher risk of cardiovascular diseases. The most important members of this group are the tropical oils: palm kernel oil and coconut oil.
- Monounsaturated oils are rich in oleic acids and vitamin E. Olive oil is the predominant member of the group. Its advantage over other vegetable oils is that it lowers blood low-density lipoprotein (LDL), cholesterol (the less desirable form), without lowering the desirable high-density lipoprotein (HDL) cholesterol, thus considered to act protectively against cardiovascular disease. Canola oil, peanut oil, and some plant foods such as avocado also contain monounsaturated oils.

- Polyunsaturated oils contain high amounts of polyunsaturated fatty acids. Corn, cottonseed, safflower, sunflower, and soybean oil belong to this category. These lower LDL cholesterol levels, and HDL levels as well.

14.2.1.4.3 Shortenings

Vegetable shortening is produced from vegetable oil that has been solidified by a process called hydrogenation providing products with varying melting points and degrees of softness. Hydrogenation, adds variable amounts of hydrogen to polyunsaturated fatty acids, increasing their degree of saturation and consequently their hardness. Oil is thereinafter emulsified with emulsifying agents and chilled to solidify the oil and trap water. Additives such as salt, yellow coloring (β-carotene), vitamin A, preservatives, or butter flavoring may further be added. Vegetable shortenings are prepared from corn, cottonseed, olive, peanut, palm, safflower, sesame, or soybean oil and are also referred to as margarines. Butter (milk fat), lard (pork fat), and tallow (beef fat) are traditional shortenings of animal origin.

Butter is the saturated animal fat obtained from milk and cream that has been solidified by churning. It contains at least 80% milk fat, 16–18% water, and other ingredients such as casein and lactose and is available in salted or unsalted varieties. Its characteristic yellowish color is due to β-carotene, which is derived from the plants eaten by the animals. Spreadable butter is also available, containing additional water, thus less fat, fewer calories and less cholesterol than regular butter or margarine. Compared to vegetable shortenings, butter is believed to provide a richer and more flavorful mouthfeel without leaving a greasy feeling as it melts at body temperature.

Lard is made by pork fat that has been rendered (wet or dry process). Rendered lard produces an unpleasant smell when mixed with oxygen. To prevent this and improve its stability at room temperature, lard is often hydrogenated or treated with bleaching and deodorizing agents, emulsifiers and antioxidants, such as BHT. Lard provides a slightly nutty flavor and because of its richness, it creates very tender, flaky pastries, and pie crusts.

Common characteristics of all shortenings are that they remain solid at room temperature. Vegetable shortenings contain no cholesterol; however, they accommodate more trans-fatty acids than butter. Exceptions to this rule are cholesterol-lowering margarines which contain either sterol esters (from vegetable oils, soybean, and corn) or stanol esters (from wood pulp). When used in combination with a heart-healthy diet, these margarines can help lower low-density lipoprotein (LDL) cholesterol in some patients. "Diet" and salt-free products are available as well.

Apart from being used as a spread for baked goods, shortenings are mainly utilized to impart softness in bakery products (i.e., biscuits, bread, cookies) as well as to create flakiness in pastries and pie crusts. They further provide flavor, tenderness, and crispness to many foods. Their amount varies with the recipe. For example, bread and rolls usually contain 1–2% shortening; cakes 10–20%, and pastries up to 30%. In several recipes for baked goods, shortening is suggested to be creamed together with the sugar. This procedure traps air in the batter and creates a lighter finished product. Shortenings are additionally incorporated in whipped toppings, icings, and fillings. As most shortening have a high smoke point they can also be used for sautéing, frying, deep-frying, and stir-frying.

14.2.1.4.4 Fat Replacers/Substitutes

Fat substitutes are a variety of ingredients used to partially replace vegetable oil products or butter, and hence reduce the fat content of foods and the health considerations associated with high-fat diets. They are designed to impart similar functions (i.e., stabilize emulsions and foams and add viscosity, gloss and opacity to foods) and analogous physicochemical characteristics and mouthfeel as regular fat.

Fat replacers can be categorized into fat substitutes and fat mimetics. The former are also known as lipid- or fat-based replacers and are either chemically synthesized or derived from conventional fats/oils through enzymatic modification. These can be relatively stable at cooking or frying temperatures. Fat mimetics are carbohydrate- or protein-based substances, used to imitate the sensory and physical properties of fat. They are suitable for bakery products, but are not considered appropriate for frying and cooking as they have the tendency to bind excessive water and denature or caramelize at high temperatures. Protein-based fat replacers are produced by modifying protein, using egg white or whey from milk. However, the most common fat replacers available are carbohydrate based. These are the following:

- Microcrystalline cellulose. It is prepared from wood pulp and is noncaloric. It is used in dairy products, sauces, and frozen desserts.
- Dextrins and maltodextrins. They are fragments produced by partial hydrolysis of starch from corn, potato, oat, rice, wheat, or tapioca. They are used in salad dressings, baked goods, frostings and puddings, processed meat, frozen desserts, dairy products, margarine, spreads, and fillings.
- Modified food starch. These are prepared by acid or enzymatic hydrolysis, oxidation, dextrinization, crosslinking, or mono-substitution to achieve the desired functional and sensory properties. They are commonly used in high moisture foods, such as margarine spreads, salad dressings and sauces, baked goods, frostings and fillings, and in meat emulsions like sausages.
- Hydrocolloid gums. These include xantham, guar, locust bean, carrageenan and Arabic gum, and pectins. They are used in salad dressings, icings and glazes, desserts and ice cream, ground beef, baked goods, dairy products, and soups and sauces.
- Fruit-based fiber. They include fiber from apples, figs, and prunes and are mostly used in baked goods.

Fat substitutes are commonly found under brand names such as Simplesse, Olestra, or Oatrim. Finally, according to their digestibility, they are classified into digestible (partially or fully) fat substitutes (yielding up to 4 kcal/g) and nondigested fat substitutes (noncaloric).

14.2.2 Minor Food Ingredients

These are found or incorporated into the food systems in relatively small amounts and serve several functions. The most important of these are described.

14.2.2.1 Acidifiers

They are frequently incorporated into food systems, such as prepared foods and beverages, to increase the acidity (lower the pH) or impart an acid or tart taste. Thereby, their use may simultaneously inhibit microbial growth. Examples of common acidifiers are acetic, citric, adipic, L-tartaric or malic acid, glucono-δ-lactone, and sodium dihydrogen phosphate.

14.2.2.2 Anticaking Agents

They are substances added to powdered, granular, or crystalline food products to prevent lumping and agglomeration, thus permitting free-flowing, and facilitate their use. Typical products in which anticaking agents are incorporated are table salts, milk powders, egg mixes, confectionary mixes, coffee, sugar products, baking powder, and flours. Some anticaking agents are soluble in water while others are soluble in alcohols or other organic solvents. They function either by absorbing excess moisture or by coating particles and making them water repellent. Common substances used for this purpose are silicon dioxide (E551), calcium silicate (E552), sodium aluminosilicate (E554), potassium aluminum silicate (E555), aluminum silicate (E559), sodium ferrocyanide (E535), and potassium ferrocyanide (E536).

14.2.2.3 Antimicrobial Agents

The antimicrobials are substances used to extend the shelf life of food products by inhibiting spoilage caused by microorganisms and preventing growth of bacteria, molds, and yeasts. They are commonly listed between E200 and E290. Calcium propionate, sodium benzoate, benzoic, propionic and sorbic acid, sulfites, as well as salt and vinegar have been extensively used for this purpose on different products such as baked goods, salad dressings, shortenings, cheese, pickled foods, meat products or wines, and beverages. The mechanisms of action of food antimicrobials are complex and difficult to determine. In general, they are believed to interact with cell membranes, causing permeability changes or interference with uptake and transport, inactivation of essential enzymes, interference with genetic mechanisms or inhibition of protein synthesis.

14.2.2.4 Antioxidants

They are used to prevent lipid or vitamin oxidation and retard deterioration due to rancidity, discoloration, or off-flavors development caused by oxidation, thus prolonging shelf life. Antioxidants either react with oxygen to prevent oxidation or prevent the oxygen from reacting with the food by blocking the propagation phase of the autoxidation process. They can be natural substances, such as carotenoids and vitamins C and E, or synthetic chemicals, such as butylated hydroxyanisole (BHA), butylated hydroxytoluene (BHT), and propyl gallate (listed between E300-E326). Antioxidants are frequently incorporated in dry products, cheese, fruit and vegetable products, shortenings, and confectionary products (i.e., biscuits). Antibrowning agents may also be included in this category. They inhibit enzymatic browning of fresh-cut fruits and vegetables, thus control discoloration and prolong shelf life. Oxidative browning is usually caused by the enzyme polyphenol oxidase (PPO) which, in the presence of oxygen, converts phenolic compounds in fruits and vegetables into dark colored pigments.

14.2.2.5 Bulking Agents

Bulking agents or fillers are food additives used to increase the bulk of a food without significantly affecting its nutritional value. They are also appropriate for increasing the sense of satiety, especially in food products designed for weight reduction. Starch, dietary fibers, and gums are typically used for this purpose.

14.2.2.6 Coloring Agents

They are substances, dyes, or pigments used to improve the overall attractiveness of foods and drinks. A number of natural and synthetic colorants, in liquid, powder, gel, or paste form are available for use, listed between E100 and E180. Food colorants may serve several functions such as enhance or correct natural colors, cope with color loss or discoloration due to exposure to adverse processing and storage conditions, and provide attractive colors to colorless food products (i.e., candy).

14.2.2.6.1 Natural Food Colors

Natural colorings may be derived from plants, insects, and minerals. Plant colorings include substances mainly of the flavonoids, carotenoids, and chlorophyll group, as well as betalines and curcumin. More specifically, annatto, β-carotene, paprika, saffron, and turmeric range their colors from yellow to red, while caramel and roasted cottonseed flour create brown colors. Fruit and vegetable juices are also used to color foods. For example, grape extract can impart purple-red color, dehydrated beets contribute a dark red, while carrot oil and canthaxanthine may provide orange color in food products. Monascus pigments (an azaphilone mixture, which usually includes yellow, orange, and red) and algae are perhaps the most common sources of natural food colorants derived from microorganisms. Powdered algae, yellow corn oil, and tagetes (Aztec marigold) are added to chicken feed to yellow chicken skin and augment the color of egg yolk. Insect pigments are extracted from cochineal providing a group of pigments known as "quininoid pigments." The most popular member of this group is carmine (E120), representing a bright-red colored pigment obtained from the aluminum salt of carminic acid. Certain inorganic compounds are also approved as coloring agents. Ferrous gluconate develops a black color in ripe olives and titanium oxide can be used up to 1% in foods as a whitener. Sodium nitrite, though listed as an antimicrobial, also contributes pink color to processed meats such as hot dogs and ham. However, less than 10% of food coloring currently being used originates from natural products. The rest represents artificial dyes, synthesized from petroleum products.

14.2.2.6.2 Artificial Food Colors

The predominant dyes used in food products, such as candy, soft drinks, desserts such as ice cream, baked goods and sausages, are FD&C Blue No. 1 and No. 2, Green No. 3, Red No. 40, and Yellow No. 5 and No. 6, while Citrus Red No. 2 is mainly used to color orange skins. The FD&C designation implies that these dyes meet the standards of purity and are permitted for foods, drugs, and cosmetics. Compared to natural coloring agents, they present superior tinctorial strength, hue and stability, as well as higher availability and lower cost. However, synthetic colorants have long been accused to pose a greater potential health risk than any other class of food additive and have been associated with carcinogenicity in test animals.

14.2.2.7 Emulsifiers

They are added in certain food products in order to establish a uniform dispersion or stabilize an emulsion by increasing its kinetic stability. Emulsifiers typically consist of a lipophilic or hydrophobic part with good solubility in a nonaqueous phase, such as an oil or fat and a polar or hydrophilic part, soluble in water. Egg yolk, lecithin, mustard, carrageenan, sugar esters, sodium stearoyl lactylate (SSL) or mono- and diacylglycerides and their derivatives, such as DATEM (diacetyl tartaric (acid) ester of mMonoglyceride), are prevalent examples of food emulsifiers. They are used to retain bakery products from becoming stale, to stabilize fats in nondairy products, to suspend flavors and food coloring in processed foods, and to stabilize ice cream and mayonnaise.

14.2.2.8 Firming Agents

Fresh fruits and vegetables contain insoluble pectins around their fibrous tissues which keep them firm. During processing, their cell structure is degraded and pectins are converted to pectic acid, leading to a gradually softer texture. Firming agents are substances added prior to or during processing to maintain natural firmness and crispness of vegetables and fruits (i.e., peas, tomatoes, potatoes) when canned or pickled. They precipitate residual pectin, thus strengthen food structure and prevent its collapse. Aluminum (alum), calcium or magnesium sulfate, calcium lactate, and calcium or magnesium chloride are commonly used for this purpose.

14.2.2.9 Flavor Enhancers

They are used to increase the original taste/flavor of certain food products or mask undesirable features without imparting any other flavor. They are frequently found in soups, salad dressings, frozen dinners, dry blends, snack foods or used to intensify meat and spice flavorings in meats, condiments, pickles, candy, and baked goods. Monosodium glutamate (MSG), monoammodium glutamate, disodium guanylate, and disodium inosinate are common examples. Concerns have occasionally arisen about the toxicological effects of these substances in humans; however, these have not been clinically confirmed.

14.2.2.10 Flavorings

These are incorporated in order to impart a certain taste or aroma to foods, replace natural flavors lost during processing or imitate expensive natural flavors with less expensive ingredients. They are classified into natural and artificial flavorings.

Natural flavorings are derived from spices, herbs, fruit or fruit juices, vegetable or vegetable juices, plant material (i.e., barks, buds, roots or leaves), edible yeasts, meat, seafood, poultry, eggs, dairy products, or fermentation products thereof, whose significant function in food is flavoring rather than nutritional. These materials may be used as such (whole or ground/crushed) or processed to make a different flavor form such as essential oils (by distillation), oleoresins (by solvent extraction), or tinctures. Examples of natural flavors are allspice, bitter almond, anise, balm, basil, caraway, cardamom, cinnamon, celery seed, chervil, citron, cloves, coriander, cress, cumin, dill, fennel, fenugreek, ginger, lemon, licorice, marjoram, mint, mustard, nutmeg, oregano, paprika, parsley, rosemary, sage, savory, tarragon, thyme, turmeric, vanilla, and wintergreen.

Artificial flavorings include mixtures of synthetic compounds recognized as safe for use in foods and approved solvents (i.e., water, ethanol, propylene glycol, triethyl citrate, benzyl alcohol, and triacetin) or carriers (i.e., salt, maltodextrin, dextrose) as required to achieve the desired form, concentration, and result. Although they may also create new flavors, they are commonly used to imitate naturally existing flavors (i.e., artificial vanilla contains vanillin, the same compound as from vanilla beans). Their advantages over natural flavorings are that they can be more resistant to processing, cost less, be readily available, and more consistent in quality. One of the most important quality attributes of artificial flavorings, apart from their sensory outcome, is their purity. In fact, most of these products contain sufficient trace impurities, stemming either from the starting materials or processing conditions used in their manufacture, to display a spectrum of perceptible character notes. There are hundreds of flavoring compounds. Some of these are d-limonene for citrus flavor, menthol for mint flavor, 2-thienyl mercaptan for coffee-roasted flavors, nonanoic acid for coconut, cinnamaldehyde for cinnamon, and cola blends or hexyl hexanoate for strawberry.

14.2.2.11 Glazing Agents

These are natural or synthetic substances that impart a shiny, homogeneous, and appealing appearance or a protective coating against moisture loss/absorption when applied to the external surface of a food product. They may also increase palatability, preserve gloss, and inhibit food discoloration. Most natural glazing agents are derived from plants or insects. They include waxes (i.e., beeswax, carnauba, candelilla, and paraffin wax), chitosan-based films, petrolatum, stearic acid, and others. Glazing agents (also known as polishing agents) are commonly used to coat fruit and vegetable, chocolates and cocoa products, chewing gums, confectionary, savory snacks, and toppings.

14.2.2.12 Humectants

These are food additives with hydroscopic properties, which are utilized in food products in order to retain moisture and freshness, maintain a soft, palatable texture and inhibit crystallization. Polyols (i.e., glycerol, mannitol, sorbitol, or 1,2-propanediol) are examples thereof. Humectants are extensively used in confectionary products (i.e., candy) and powdered or dehydrated goods.

14.2.2.13 Leavening Agents

Leavening is the production or incorporation of gases into a baked product in order to increase volume and ovenspring and improve crumb texture and cell structure. Leavening agents used for this purpose are discriminated into yeasts and chemical leaveners.

14.2.2.13.1 Baker's Yeast

Strains of the yeast *Sacchromyces cerevisiae* are used to leaven bread, dinner rolls, and other similar bakery goods. They metabolize sugars added or produced in the dough, by the enzymatic hydrolysis of wheat starch, and generate carbon dioxide, which when trapped in the dough's network makes it rise. As yeast is a living

organism, it requires a specific temperature range for optimum performance. More specifically, the most favorable temperature for yeast to multiply is between 20°C and 27°C, while fermentation is more efficiently achieved between 27°C and 38°C. Yeast comes available both in fresh and dried form; the choice depending on the desired effect in the final product, the production process and the allowable cost.

14.2.2.13.2 Chemical Leavening Agents

Chemical leaveners are mixtures or compounds that release gases (usually CO_2) either when they react with an acid or a base, or through the application of moisture or heat. They are commonly used in cakes, biscuits, cookies, or quick breads. The most frequently used chemical leavening agents are baking soda (sodium bicarbonate) and baking powder. Sodium bicarbonate breaks down to carbon dioxide in the presence of acidic ingredients such as sour milk, fruit juices (i.e., orange or lemon), molasses, or cream of tartar. Baking powders typically contain three types of ingredients: sodium bicarbonate, an acidic chemical (i.e., cream of tartar or calcium acid phosphate), and an anticaking agent like cornstarch or calcium silicate to prevent caking. In the presence of water, the acidic ingredient reacts with the sodium bicarbonate to generate carbon dioxide bubbles. During baking, baking powder generates larger amounts of carbon dioxide compared to sodium bicarbonate alone. Nevertheless, products added with baking soda present a tender and lighter texture. Leavening agents are generally considered safe food additives. However, baking soda and baking powder add considerable sodium to breads, rolls, and crackers.

14.2.2.14 Propellants

Propellants provide the necessary pressure to force a liquid/fluid food out of a pressurized container and expel it in the form of cream or paste (i.e., cream cheese, ketchup), foam (whipping cream), spray, or mist. The most commonly used propellants include nitrogen (E941), nitrous oxide (E942), and carbon dioxide (E290). Due to its low solubility in water, fat and oil, N_2 is preferably used when foam formation is not desired (i.e., in ketchup). The opposite stands for N_2O and CO_2 which are highly soluble in water.

14.2.2.15 Stabilizers

These substances are used to maintain a uniform dispersion of two or more components. Although they are not classified as emulsifiers, they assist in stabilizing food emulsions and foams. They are also incorporated in food system in order to provide a firmer and more stable texture profile and prevent the evaporation of volatile flavor components. Stabilizers are used both in dry and liquid products. They include several natural gums, such as carrageenan, xanthan or locust bean gum, as well as natural and modified starches. Typical products in which they are commonly applied are jams, milk and yogurt products, ice cream, bakery and confectionary products, infant formulas, salad dressings, soups, and shortenings.

14.2.2.16 Thickeners

Unlike stabilizers, which produce more stable suspensions, thickeners are added to provide more viscous solution, thus increase the viscosity of a mixture, without

modifying any other properties. Therefore, they increase the consistency of food products, prevent ingredient from separating, and impart "body." They are found in soft drinks, salad dressings, sauces and gravies, ice cream, yogurt, whipped cream, puddings, frozen desserts, cheese, soups, and baby food. Many thickeners are naturally occurring polysaccharides (i.e., agar, carrageenan, pectin, and alginates). Their action relies on water absorption by starch granules, which during heating generates swelling and causes fluid thickening. Chemically modified starches are also used for this purpose.

14.2.2.17 Bioactive Compounds

Certain food compounds (bioactive) can have beneficial effects on human health or wellness or prevent chronic diseases and hence develop effective functional foods. An integrated approach is required taking into account aspects from the whole food production chain—from farm to fork, that is, from primary production of raw materials with appropriate levels of the bioactive compounds to the effects of these compounds on consumer health as well as consumer behavior issues.

Bioactive ingredients may refer to the application of nutraceuticals or bioactive ingredients in foods like, for example, prebiotics, probiotics, flavonoids, phytosterols, phytostanols, bioactive peptides, and bioactive carbohydrates. To develop safe and effective functional foods, pre-market modeling and postmarketing surveillance are required due to nutritional requirements based on the total dietary intake that may include several foods and nutraceuticals (food supplements, herbs, and herb medicines) with interacting active ingredients. There is need to have a reliable system for evaluating health claims and safety of new functional foods. This needs to be harmonized in EU countries.

Moreover, an in-depth understanding of consumer needs and purchasing behavior with respect to diet and health is required along with more intense identification of health-promoting bioactive compounds.

Optimization of the intake and upper safe limit values of functional bioactive components needs to be determined.

Nutraceuticals are natural, bioactive chemical compounds that are characterized by health-promoting, disease-preventing, or medicinal properties.

Omega-3 acids are essential polyunsaturated fatty acids naturally occurring in the diet. The three main omega-3s are alpha-linolenic acid (ALA), which may have beneficial effects against certain cancers; eicosapentaenoic acid (EPA), which is the precursor of all activities in immune defense system and power tool for heart protection; and docosahexaenoic acid (DHA), which helps build infants' brain tissue.

Phytochemicals include phenolic compounds, essential fatty acids, flavonoids, sterols and stanols, and phytoestrogens.

Encapsulation is a method used in the pharmaceutical and food industries to protect and control the release of aromatic compounds. Recently, nutraceuticals have been encapsulated with a beneficial effect on health. Encapsulation can help protect these ingredients from oxidation reactions and deterioration as well as the increase of their solubility in water. It is associated with nanotechnology due to the interactions at molecular level. Selected bibliography is described in more detail in another chapter, although some references have been quoted here.

14.2.2.18 Probiotics

Probiotics are defined as live microorganisms which when administered in adequate amounts confer a health benefit on the host. Lactic acid bacteria (LAB) and bifidobacteria are the most common types of microbes used as probiotics, but certain yeasts and bacilli may also be used. They are considered nonpathogenic, nonputrefactive, nontoxigenic, saccharolytic organisms, and appear to cause no deleterious activity in the intestinal tract. They are supposed to reach the large intestine and contribute to the formation of an optimal intestinal flora. They also limit the growth of disease-causing bacteria and other harmful organisms in the intestinal tract that can cause digestive problems such as diarrhea, constipation, and flatulence. Probiotics are commonly consumed as part of fermented foods inoculated with special, active and live cultures, such as in yogurt or other fermented milk products (i.e., kefir). Other products considered as a good vehicle for probiotics are: pickles, soy milk, olives in brine, and dark chocolate.

14.2.2.19 Prebiotics

Prebiotics are nutrients or dietary supplements that help maintain a balance among the bacteria naturally found in the gastrointestinal tract. More specifically, they do not provide an exogenous source of live bacteria, but selectively stimulate the proliferation and/or activity of desirable bacterial populations (even up to 100-fold) already resident in the intestinal tract of the host by providing more of the nutrients that they feed on. Most prebiotics identified so far, are nondigestible, fermentable carbohydrates. They are naturally found in several foods, such as Jerusalem artichokes, onions, honey, blueberries, and leeks. Most important substances with prebiotic function are trans-galactooligosaccharide, inulin, fructooligosaccharides, lactulose, and mannan oligosaccharides (MOS).

It is found that when prebiotics and probiotics are received together they act in a complementary and synergistic manner. For this, foods containing both probiotic cultures and prebiotic ingredients are often termed as synbiotics.

14.3 FOOD APPLICATIONS

14.3.1 Pastry Products—Omega-3 Fatty Acids

Pastry products comprise a big category of food products. They are produced as frozen and their main raw material is wheat flour. Wheat flour is the main ingredient of bakery, biscuit, and confectionery products. Wheat flour can form the dough, which is elastic, under appropriate conditions. Soft wheat (*Triticum vulgare*) is used in the production of bakery flour and covers more than 90% of world production. Flour must be purchased from approved suppliers (Varzakas, 2011). Tables 14.2 through 14.16 show different formulations and more specifically ham and cheese pie, pumpkin pie, chicken pie, ham and cheese croissant, chocolate-cocoa croissant, sausage pie, custard filled pastry, cheese pie pastry, potato ograden, peinirli, soufflé with noodles, spinach pie, cheese pie baked in the oven, vegetable pie and milk pie formulation, respectively.

TABLE 14.2
Ham and Cheese Pie Formulation

Product name	Ham and cheese pie/deep frozen product
Raw materials	Dough: wheat flour, olive oil, salt, water Filling: ham, hard cheese, and Edam cheese
Packaging	1st: aluminum or paper, 2nd: sachet polypropylene, 3rd: carton, 4th: carton box

TABLE 14.3
Pumpkin Pie Formulation

Product name	Pumpkin pie/deep frozen product
Raw materials	Dough: wheat flour, olive oil, salt, water Filling: pumpkin, sugar, semolina, cinnamon
Packaging	1st: aluminum or paper, 2nd: sachet P.P, 3rd: carton, 4th: carton box

TABLE 14.4
Chicken Pie Formulation

Product Name	Chicken pie
Raw materials	Dough: wheat flour, olive oil, salt, water Filling: chicken (fillet, chest, leg), onion, parsley, crumb, Gouda cheese, pepper vegetable, mustard, salt, pepper
Packaging	1st: aluminum or paper, 2nd: sachet P.P, 3rd: carton, 4th: carton box

TABLE 14.5
Ham and Cheese Croissant Formulation

Product name	Ham cheese croissant
Raw materials	Dough: flour, salt, yeast, eggs, margarine Filling: ham, gouda cheese
Packaging	1st: aluminum or paper, 2nd: sachet P.P, 3rd: carton, 4th: carton box

TABLE 14.6
Chocolate-Cocoa Croissant Formulation

Product name	Chocolate-cocoa croissant
Raw materials	Dough: wheat flour, margarine, sugar, salt, yeast, eggs, Stabilizer: mono and diglycerides of fatty acids, vanillin, Preservative: calcium propionate 0.2%. Filling: cocoa (sugar, hydrogenated vegetable oils, low fat cocoa powder, skimmed milk powder, alcohol, Emulsifier: lactic acid esters of mono and diglycerides of fatty acids, Gelling agent: sodium alginate, vanillin, Preservative: potassium sorbate 0.1%)
Packaging	1st: aluminum or paper, 2nd: sachet P.P, 3rd: carton, 4th: carton box

TABLE 14.7
Sausage Pie Formulation

Product name	Sausage pie
Raw materials	Dough: flour, salt, yeast, eggs, margarine Filling: traditional sausage
Packaging	1st: aluminum or paper, 2nd: sachet P.P, 3rd: carton, 4th: carton box

TABLE 14.8
Custard Filled Pastry Formulation

Product name	Custard filled pastry
Raw materials	Dough: wheat flour, olive oil, salt, water Filling: fresh milk, semolina, sugar, vanilla
Packaging	1st: aluminum or paper, 2nd: sachet P.P, 3rd: carton, 4th: carton box

TABLE 14.9
Cheese Pie Pastry Formulation

Product name	Cheese pie pastry
Raw materials	Dough: wheat flour, olive oil, salt, water Filling: cheese (barrel feta), cream cheese, egg, pepper
Packaging	1st: aluminum or paper, 2nd: sachet P.P, 3rd: carton, 4th: carton box

TABLE 14.10
Potato Ograden Formulation

Product name	Potato ograden
Raw materials	Potato Filling: ham, bacon, Gouda cheese, Mozzarella, Edam cheeses
Packaging	1st: aluminum or paper, 2nd: sachet P.P, 3rd: carton, 4th: carton box

TABLE 14.11
Peinirli Formulation

Product name	Peinirli
Raw materials	Dough: flour, salt, yeast, eggs, butter, sugar, water Filling: tomato sauce, ham, bacon, Gouda, Mozzarella, Edam
Packaging	1st: aluminum or paper, 2nd: sachet P.P, 3rd: carton, 4th: carton box

TABLE 14.12
Soufflé with Noodles Formulation

Product name	Soufflé with traditional noodles
Raw material	Dough: traditional noodles Filling: ham, bacon, cheese Gouda, Mozzarella, Edam
Packaging	1st: aluminum or paper, 2nd: sachet P.P, 3rd: carton, 4th: carton box

TABLE 14.13
Spinach Pie Formulation

Product name	Spinach pie
Raw materials	Dough: wheat flour, olive oil, salt, water Filling: fresh spinach, onion, dill, cheese feta, salt, oil
Packaging	1st: aluminum or paper, 2nd: sachet P.P, 3rd: carton, 4th: carton box

TABLE 14.14
Cheese Pie Baked in the Oven Formulation

Product name	Cheese pie
Raw material	Dough: flour, salt, yeast, eggs, margarine Filling: cheese feta, cream feta, skim-milk feta, cheese gouda
Packaging	1st: aluminum or paper, 2nd: sachet P.P, 3rd: carton, 4th: carton box

TABLE 14.15
Vegetable Pie Formulation

Product name	Vegetable pie
Raw materials	Dough: wheat flour, olive oil, salt, water Filling: wild herbs, leek, dill, cheese feta, salt, oil
Packaging	1st: aluminum or paper, 2nd: sachet P.P, 3rd: carton, 4th: carton box

TABLE 14.16
Milk Pie Formulation

Product name	Milk pie
Raw material	Dough: wheat flour, olive oil, salt, water Filling: milk, wheat flour, margarine, sugar, egg, vanilla
Packaging	1st: aluminum or paper, 2nd: sachet P.P, 3rd: carton, 4th: carton box

14.3.1.1 Fillo Dough Products

Varzakas et al. (2011) reported on the use of functional fillo dough products with the incorporation of high omega-3 fatty acids and phytosterol esters.

Two formulas were prepared for experimentation.

Production of Functional Apollo Fillo

A. Formula for Omega –3 Fillo Dough

Flour	100 kg
Water	16.0 L
Omega-3 oil	5.0 kg
Salt	3.0 >>
Vegetable oil	0.5 >>
Citric acid	0.1 >>

Sorbate	0.1 >>
Sodium propionate	0.3 >>

B. Formulation for Plant Sterol Fillo Dough

Flour	100 kg
Water	16 L
Sterol oil	3.8 kg
Vegetable oil	0.5 >>
Salt	3.0 >>
Sodium Propionate	0.3 >>
Citric acid	0.1 >>
Sorbate	0.1

Note: A: High-Omega 3 flax seed oil 12 g per 1000 g dough (Polar Foods) and/or (Omevital 30% MP Gold contained 88 mg EPA?DHA omega-3).
B: For sterols, Vegapure 95 FF (Cognis Nutrition and Health Dept.)
Production of fillo dough incorporating omega-3 fatty acids
Fillo dough was prepared by mixing flour, water, salt, additives with a solution of omega-3 or sterol oil emulsion. The dough was mixed thoroughly and then dried using electric heaters. It was then cut, freeze dried, and finely ground and stored at the freezer at −18°C prior to analysis.

14.3.1.2 Sponge Cake with Cocoa Filling Formulation

Sponge cake formulation is presented in Table 14.17. The main ingredients are sugar, wheat flour, vegetable oil, and cocoa filling.

14.3.1.3 Tsoureki with Apricot Jam Formulation

Tsoureki is a Greek product made of wheat flour, sugar, margarine and butter as well as the required filling, in our case apricot jam as described in Table 14.18.

TABLE 14.17
Sponge Cake with Cocoa Filling Formulation

Product name	Sponge cake
Raw materials	Sugar, wheat flour, vegetable oil, whole fresh egg, yoghurt, skimmed milk powder, dextrose, Raising agents: trisodium diphosphate and sodium hydrogen carbonate, salt, flavors, Preservative: potassium sorbate 0.1%. Cocoa filling (sugar, hydrogenated vegetable oils, defatted cocoa powder, skimmed milk powder, butter, egg yolk powder, alcohol, Emulsifier: lactic acid esters of mono and diglycerides of fatty acids, Gelling agent: sodium alginate, vanillin, Preservative: potassium sorbate 0.1%).
Packaging	Laminated P.P film

TABLE 14.18
Tsoureki with Apricot Jam Formulation

Product name	Tsoureki
Raw materials	Wheat flour, sugar, margarine, butter, eggs, skimmed milk powder, corn syrup, natural yeast, Stabilizers: mono and diglycerides of fatty acids and sorbitol, flavors, Preservative: calcium propionate 0.2%, machlepi, mastic oil. Apricot jam (corn syrup, apricots, sugar, flavors, Gelling agent: pectin, Acidifier: citric acid, Coloring: E160A, Preservative: potassium sorbate 0.1%).
Packaging	Laminated P.P film

14.3.2 Baked Products: Cereals and Polyphenols

Baked cereal products are among the most consumed foods in the western world. Today, producers in the food industry are strongly concerned about the formulation issues of such products, as they need to innovate while meeting the requirements of global quality. Healthy and sustainable products are targeted nowadays.

However, there is criticism at using partially hydrogenated fats, which favor a smoother texture and a better stability toward oxidation, but nevertheless induce higher contents of trans fatty acids. Bakery products also largely use palm oil, one of the world's most versatile raw materials but which is questioned for the low sustainability of its culture, despite its high technological performance (Wicke et al., 2008).

However, when designing new formulas for baked products, the question that needs to be raised is the impact of these new ingredients on the chemical transformations occurring during the production chain.

Actually, many complex phenomena occur in dough during preparation and baking of cereal products, leading to textural, physicochemical, and organoleptic changes such as volume expansion, starch gelatinization, protein denaturation, fat melting, browning, and formation of flavor compounds (Plutowska and Wardencki, 2007; Purlis, 2010).

Other phenomena include Maillard reaction (MR), caramelization (CR), and lipid oxidation. The Maillard reaction occurs between the carbonyl groups of reducing sugars and the $-NH_2$ functions of amino acids, peptides, and proteins. Caramelization depends on direct degradation of sugars. Lipid oxidation is a radical chain reaction, which can be decomposed into three phases (initiation with formation of free radicals, propagation, and finally termination with formation of nonradical products) (Kiokias et al., 2008).

Concerning bakery products, several studies have been conducted in order to gain an understanding of the effects of both formulation and process on the generation of volatile compounds from MR and CR. Pozo-Bayon et al. (2006) studied the effects of egg substitutes on the aroma profile of sponge cakes and Rega et al. (2009) investigated the generation of volatile compounds during the baking operation of sponge cakes.

Maire et al. (2013) investigated the effect of ingredients on the reactions occurring during the making of sponge cake and leading to the generation of volatile compounds related to flavor quality. To obtain systems sensitive to lipid oxidation (LO), a formulation design was applied varying the composition of fatty matter and eggs.

Oxidation of polyunsaturated fatty acids (PUFA) and formation of related volatile compounds were followed at the different steps of cake-making. Optimized dynamic solid phase micro extraction was applied to selectively extract either volatile or semi-volatile compounds directly from the baking vapors.

They showed for the first time that in the case of alveolar baked products, lipid oxidation occurs very early during the step of dough preparation and to a minor extent during the baking process. The generation of lipid oxidation compounds depends on PUFA content and on the presence of endogenous antioxidants in the raw matter. Egg yolk seemed to play a double role on reactivity: protecting unsaturated lipids from oxidation and being necessary to generate a broad class of compounds of the Maillard reaction during baking and linked to the typical flavor of sponge cake.

Diets containing phytochemicals such as the polyphenolics can deliver health benefits including the potential to reduce risk of cardiovascular disease and certain types of cancer in humans as reviewed by Awika and Rooney (2004). Different sorghum varieties vary widely in their type and concentration of polyphenolic compounds (Dlamini et al., 2007).

As sorghum products are gluten free, they lack the elastic gluten network, which is vital for expanded texture development in staple food such as breads, and hence in these foods the use of sorghum can face the sensory problem of being dense and having an undesirable texture (Taylor and Emmambux, 2010; Taylor et al., 2006). A process that can induce a desirable expanded, crunchy texture in gluten-free foods is high-temperature high-pressure extrusion (HTHPE) cooking. HTHPE is a highly controllable and efficient single-unit food manufacturing process (Huber, 2000). The potential of extrusion cooking to be used for the manufacture of ready-to-eat products with more desirable nutritional characteristics than those currently on the market has been recently reviewed (Brennan et al., 2013). Maize flour is widely used for the manufacture of expanded snack-like products using HTHPE.

High-temperature high-pressure extrusion of sorghum–maize composite flour, potential for healthy food manufacture, was investigated by Licata et al. (2013) by factorial experimental design to determine the effect of level of sorghum in dry mix (15–60%); final barrel zone temperature (120–150°C); total moisture in barrel (21.4–25.8%); total input rate (2.3–6.8 kg h^{-1}); and screw speed (250–450 rpm) on extrudate slowly digestible starch (SDS), phenolic content, antioxidant capacity, protein digestibility, density, and expansion ratio. Extrudate SDS increased with increasing sorghum level and decreased as the barrel temperature increased. Total phenolic content and antioxidant capacity were positively associated with sorghum level.

Protein digestibility was associated negatively with sorghum level and positively with barrel temperature. Extrudate density was associated positively with total moisture and negatively with barrel temperature and input rate. Sorghum in dry mix, final barrel zone temperature, and total moisture in barrel were the three most significant independent variables influencing extrudate-dependant variables.

14.3.2.1 Bake Rolls Formulation

Bake rolls is crunchy bread crisps or bagel chips produced from wheat flour, vegetable oil, salt, sugar, and yeast in its plain form (Table 14.19). Different flavors can be added such as oregano, garlic, onion, and others.

TABLE 14.19
Bake Rolls Formulation

Product name	Bake rolls (bagel chips) with salt seasoning
Raw materials	Wheat flour, vegetable oil, salt, sugar, yeast
Packaging	Laminated P.P film consisting of paper, OPP, LDPE, adhesive, and inks

14.3.2.2 Strudel with Apple-Cinnamon Formulation

Strudel is a puff pastry product derived from wheat flour. Flour is produced from wheat kernels with the aid of the milling process. Milling aims at separating the wheat endosperm from the bran coating and embryo or germ and consequently comminuting the endosperm to a fine powder.

Strudel manufacturing starts with mixing of the raw materials in the dough preparation. One of the raw materials as mentioned before is predough or mother dough. This predough has been prepared in small twin arm mixers and then placed in a conditioned place at constant temperature of 18°C for proofing. Predough is mixed with other raw materials such as flour and water in a double spiral mixer until the formation of the final dough.

The ready formed dough is taken to a double arm elevator tilter through which it is lifted to through the dough into the reception dough hopper, if required. Dough is then cut into big pieces through a double automatic dough extruder and taken to an automatic lamination line. In this line, dough becomes sheet and is divided into two compartments. These two sheets are placed one on top of the other in a sandwich form with a margarine layer between them. The sandwich is then refined through rotating cylinders and taken to a conveyor belt. Margarine sheet is added between the dough sheets followed by formation of puff pastry products and the final dough sheets are cut and placed into trays (Varzakas and Arvanitoyannis, 2007; Tsarouhas et al., 2009).

Refrigeration of dough block then takes place where the already cut dough sheets are placed in the fridge for a certain period of time and temperature. Dough sheets are then transferred to the second lamination. Puff pastry products are formed, dough sheets are cut and each piece is formed in the appropriate shape. Addition of fillings with the appropriate fillings then follows such as apple-cinnamon described in Table 14.20.

14.3.2.3 Bake Bars Formulation

Bake bars is a twisted baked dough product with main ingredients of wheat flour, margarine, yeast, and salt as shown in Table 14.21.

14.3.2.4 Vafla Dough with Hazelnut Filling Formulation

Vafla is a dough product consisting of sugar, wheat flour, vegetable oil, whey powder, hazelnut paste as shown in Table 14.22.

TABLE 14.20
Strudel with Apple-Cinnamon Formulation

Product name	Strudel with apple and cinnamon filling
Raw materials	Dough: wheat flour, margarine, sugar, eggs, butter, stabilizer: mono and diglycerides of fatty acids, corn syrup, skimmed milk powder, yeast, salt, flavours, vanillin, Preservative: calcium propionate 0.2%. APPLE AND CINNAMON: corn syrup, chopped apples, sugar, Gelling agent: Pectin, Acidifier: Citric acid, flavor, cinnamon, Preservative: potassium sorbate 0.1%.
Packaging	Laminated P.P film

TABLE 14.21
Bake Bars Formulation

Product name	Bake bars (bagel chips) with salt seasoning
Raw materials	Wheat flour, margarine, yeast, salt, dextrose
Packaging	Laminated P.P film

TABLE 14.22
Vafla Dough with Hazelnut Filling Formulation

Product name	Vafla dough with hazelnut filling
Raw materials	Sugar, wheat flour, vegetable oil, whey powder, hazelnut paste, full fat milk, cocoa powder, lecithin, salt, aromatic substances.
Packaging	Laminated P.P film

14.3.3 Micro and Nano-Emulsions

Recently, there has been great interest in utilizing micro and nano-emulsions to encapsulate bioactive components for applications in food and beverage products (McClements and Rao, 2011). Oil-in-water nano-emulsions consist of small lipid droplets ($r < 100$ nm) dispersed within an aqueous continuous phase. Nano-emulsions are thermodynamically unstable systems that tend to break down over time (Qian et al., 2012a, 2012b). Nano-emulsions containing β-carotene have been studied by several authors. Qian et al. (2012a) showed that β-carotene can be effectively encapsulated within food-grade nano-emulsions stabilized by globular proteins or nonionic surfactants using a high pressure microfluidizer.

The application of β-carotene as natural colorant in food and nutraceutical products requires an appropriate formulation in order to protect the active compound

from degradation and overcome the low bioavailability due to a low solubility in aqueous media. De Paz et al. (2014) presented a study of the formulation of β-carotene using four different modified n-octenyl succinate (OSA) starches as carrier materials by precipitation from a pressurized ethyl acetatein–water emulsion. The best results, with encapsulation efficiencies of 70–80% and particle sizes in the sub-micrometer range, were achieved using an OSA-starch refined from waxy maize at concentrations of at least 100 g L^{-1}. Moreover, experiments using ethanol instead of ethyl acetate as organic solvent have been carried out in order to assess the influence of the emulsification, solvent displacement, and antisolvent precipitation processes on product characteristics. Equivalent particle sizes were obtained in experiments with ethanol, but with encapsulation efficiencies below 40%, indicating that the formation of an emulsion template is essential in order to achieve a high encapsulation efficiency, while particle sizes are determined by antisolvent precipitation processes.

Recently, niosomes have been used as nutraceutical vehicles of functional components, useful in the prevention of many diseases caused by oxidative stress, with the aim to control their delivery into the body and to increase the nutritional quality of food dairy products with which these products can be enriched. Tavano et al. (2014) developed novel niosomal formulations containing nutritional supplements such as gallic acid, ascorbic acid, curcumin, and quercetin as single agents and in combination, to evaluate the effect of the active molecules co-encapsulation on the physicochemical properties of the carriers, on their antioxidant properties and capability of releasing the encapsulated materials. Results suggest that the co-encapsulations of gallic acid/curcumin and ascorbic acid/quercetin mix influence their physicochemical properties and their entrapment efficiencies with respect to the formulations containing the single antioxidant; also, the antioxidants releases appeared to improve and their combinations resulted in a promoted ability of reducing free radicals, due to a synergic antioxidant action.

The following encapsulation and delivery techniques have been reported in literature for the stabilization and delivery of citral and other lemon oil derivatives in food, cosmetics, and pharmaceutical industries, most of them being based on the soft colloidal systems. Spray drying, oil-in-water emulsions, multilayer emulsions, nanoemulsions, molecular complexes, and self-assembly delivery systems.

Citral, one of the most important natural flavoring compound having intense lemon aroma and flavor, is widely used as an additive in foods, beverages, and cosmetics with high consumer acceptance. Citral is chemically unstable and degrades over time in aqueous solutions due to acid catalyzed and oxidative reactions leading to loss of desirable flavor and formation of off-flavors. Therefore, incorporation of citral into foods and beverages is a major challenge for the food industry because their chemical deterioration needs to be inhibited to minimize loss of product quality. The task to find the appropriate delivery system is most challenging for food industry. Maswal and Dar (2014) reviewed the encapsulation and delivery techniques of citral mostly based on colloidal systems. Moreover, the remaining technical challenges of such delivery systems like insignificant stabilization of citral, use of nonbiocompatible constituents, instability to the environmental stress, and difficulty of their preparation are discussed for prospective development of such formulations.

14.3.3.1 Low-Fat Meat Products

Manufacture of low-fat sausages is usually achieved by two basic principles: the use of lean meats (which increases cost) and/or reduction of fat and caloric content by adding water ingredients that introduce less or no calories.

In emulsified meat products, diminishing fat without increasing water content results in a harder product (Hand et al., 1987), while fat replacement with water increases exudative and cooking losses (Su et al., 2008) and also affects texture and juiciness of the product (Cierach et al., 2009). However, Ordóñez et al. (2001) indicated that low-fat (10%) frankfurters with a texture profile similar to standard ones could be manufactured.

In order to reduce these problems different strategies have been applied such as addition of proteins (soy proteins, whey protein concentrate, gluten, sodium caseinate), gums (xanthan, locust bean gum, carrageenans, microcellulose, pectins, konjac), and/or sodium polyphosphate in different combinations (Candogan and Kolsarici, 2003; Pietrasik, 2003; Lurueña-Martínez et al., 2004; Hsu and Sun, 2006; Ayadi et al., 2009; Muchenje et al., 2009; Youssef and Barbut, 2010, 2011; Brewer, 2012; Jiménez-Colmenero et al., 2012).

Marchetti et al. (2014) used response surface methodology to analyze the effect of milk proteins and 2:1 κ:ι-carrageenans on cooking loss (CL), weight lost by centrifugation (WLC), and texture attributes of low-fat meat sausages with pre-emulsified fish oil. A central-composite design was used to develop models for the objective responses. Changes in carrageenans affected the responses more than milk protein levels. Convenience functions were calculated for CL, WLC, hardness, and springiness of the product. Responses were optimized simultaneously minimizing CL and WLC; ranges for hardness and springiness corresponded to commercial products (20 g of pork fat/100 g). The optimum corresponded to 0.593 g of carrageenans/100 g and 0.320 g of milk proteins and its total lipid content was 6.3 g/100 g. This formulation was prepared and evaluated showing a good agreement between predicted and experimental responses. These additives could produce low-fat meat sausages with pre-emulsified fish oil with good nutritional quality and similar characteristics than traditional ones.

14.3.3.2 Prebiotic Fibers

Oligosaccharide-based soluble fibers have widely gained acceptance as effective prebiotics (Molis et al., 1996). Several studies have investigated the incorporation of insoluble bran fibers with dairy proteins in conventional steam extrusion to improve the nutrient density of expanded products (Walsh and Wood, 2010; Onwulata et al., 2011).

Prebiotic soluble fiber (fructooligosaccharides)-incorporated whey protein crisps were produced by low-shear supercritical fluid extrusion (SCFX), which utilizes supercritical CO_2 as an expansion agent instead of steam as reported by Paraman et al. (2013). Protein crisps with desirable qualities were obtained with a formulation containing 8% prebiotic fiber and 60% whey protein concentrate (WPC-80), which gave the final product with a protein content of 49.6% (w/w). A maximum of 70% WPC-80 and 8% prebiotic fiber could be incorporated to produce expanded protein crisps; however, increasing WPC-80 from 50% to 70% decreased the end-product

expansion ratio from 3.1 to 1.2 and increased the product hardness and piece density from 1.3 to 2.8 kN and 0.63 to 0.75 g mL^{-1}, respectively. Addition of 8% prebiotic fiber did not affect the textural qualities of final products. The process produced an expanded protein matrix with unique internal microstructure of uniformly distributed closed cells. Amino acid analysis indicated that 90% of the total lysine and 92% of the total essential amino acids were retained after SCFX processing and oven-drying, indicating the preservation of protein nutritional quality during the process.

Supercritical fluid extrusion (SCFX) is a modified low-shear process utilizing supercritical CO_2 (SC-CO_2) instead of steam as a blowing agent. The SCFX process produces highly expanded low-density product temperatures below 100°C. With minimal processing loss, shear- and heat-sensitive compounds can be effectively incorporated to produce next-generation healthy snacks (Cho and Rizvi, 2010) and texturized protein ingredients for functional applications (Manoi and Rizvi, 2008).

14.3.3.3 Wax Oleogels

Zulim-Botega et al. (2013a) examined the potential to use rice bran wax (RBW) oleogels to replace solid fat in ice cream. The oleogels were made from 90% high-oleic sunflower oil (HOSO) and 10% RBW. They showed that after emulsification into an ice cream mix, the oleogel droplets gelled at a temperature lower than 70°C. A blend of mono- and di-glycerides and polysorbate 80 was able to partially displace adsorbed proteins from the oleogel droplets during aging and the fat emulsion partially aggregated during whipping and freezing in a batch freezer.

Zulim-Botega et al. (2013b) investigated the influence of emulsifiers, waxes, fat concentration, and processing conditions on the application of wax oleogel to replace solid fat content and create optimal fat structure in ice cream. Ice creams with 10% or 15% fat were formulated with rice bran wax (RBW), candelilla wax (CDW), or carnauba wax (CBW) oleogels, containing 10% wax and 90% high-oleic sunflower oil. The ice creams were produced using batch or continuous freezing processes. Transmission electron microscopy (TEM) and cryo-scanning electron microscopy were used to evaluate the microstructure of ice cream and the ultrastructure of oleogel droplets in ice cream mixes. Among the wax oleogels, RBW oleogel had the ability to form and sustain structure in 15% fat ice creams when glycerol monooleate (GMO) was used as the emulsifier. TEM images revealed that the high degree of fat structuring observed in GMO samples was associated with the RBW crystal morphology within the fat droplet, which was characterized by the growth of crystals at the outer edge of the droplet. Continuous freezing improved fat structuring compared to batch freezing.

RBW oleogels established better structure compared to CDW or CBW oleogels. These results demonstrate that RBW oleogel has the potential to develop fat structure in ice cream in the presence of GMO and sufficiently high concentrations of oleogel.

14.3.3.4 Snack Products

14.3.3.4.1 Corn Curls

In Table 14.23 corn curls formulation is described as reported by Varzakas and Arvanitoyannis (2006). The formula is based on corn grits, potato flour (emulsifier:

TABLE 14.23
Corn Curls Formulation

Product name	Corn curls with cheese seasoning
Raw materials	Corn grits, vegetable oils, cheese powders, rice flour, potato flour (emulsifier: mono and diglycerides of fatty acids [E471], stabilizer [E450] and preservative [E223]), seasonings, salt, flavor: monosodium glutamate, Coloring: Norbixin (E160b), additives: potassium hydroxide (E525), propylene glycol.
Packaging	Laminated P.P film

TABLE 14.24
Potato Chips Plain Formulation

Product name	Potato chips plain
Raw material	Potato (~60%), vegetable oil (~36.5%) Flavor: salt (~2%)
Packaging	Laminated P.P film

mono and diglycerides of fatty acids [E471], stabilizer [E450], and preservative [E223]), rice flour, seasoning, salt, and vegetable oils, (flavorings: monosodium glutamate, coloring: Norbixin [E 160b]).

14.3.3.4.2 Potato Chips Manufacturing

As reported by Arvanitoyannis and Varzakas (2007) potato chips are manufactured after potatoes have been peeled, sliced, and fried in vegetable oils and then glazed with different seasonings. A plain potato chips formulation is shown in Table 14.24.

14.4 CONCLUSION

Designing and developing new food products and evolving the existing ones according to modern market trends and consumers' requirements has always been a challenge for food engineers. New product design in particular, relies on the identification of all design, process, product and market parameters, which when properly combined will provide a successful result.

However, in order to impart the desired characteristics to the final product, it is necessary to thoroughly understand the functions and properties of different food ingredients and additives. These have long been used to preserve, flavor, thicken, stabilize, and color foods. Their use, however, and especially their origin have been a matter of discussion for decades. Modern trends lean toward more natural, less-processed ingredients with functional properties and health-promoting claims. New techniques and approaches (i.e., use of biotechnology) are also being investigated and applied in order to allow the production of more sophisticated additives.

FURTHER READING

Akoh C.C. 1998. Fat replacers. *Food Technology*, 52 (3): 47–53.

Arvanitoyannis I., Varzakas T. 2007. Application of failure mode and effect analysis (FMEA), cause and effect analysis and Pareto diagram in conjunction with HACCP to a potato chips manufacturing plant. *International Journal of Food Science and Technology*, 42: 1424–1442.

Awika J.M., Rooney L.W. 2004. Sorghum phytochemicals and their potential impact on human health. *Phytochemistry*, 65: 1199–1221.

Ayadi M.A., Kechaou A., Makni I., Attia H. 2009. Influence of carrageenan addition on turkey meat sausages properties. *Journal of Food Engineering*, 93: 278–283.

Beckley J.H., Foley M.M., Topp, E.J., Huang J.C., Prinyawiwatkul, W. 2007. *Accelerating New Food Product Design and Development*. Iowa: Blackwell Publishing and the Institute of Food Technologists.

Belitz H.-D., Grosch W., Schieberle P. 2009. *Food Chemistry* (4th Ed.). Berlin-Heidelberg: Springer-Verlag.

Bell L.N. 2001. Stability testing of nutraceuticals and functional foods. In: *Handbook of Nutraceuticals and Functional Foods*, R.E.C. Wildman (Ed.). New York: CRC Press, pp. 501–516.

Bergonzi M.C., Bilia A.R., Di Bari L., Mazzi G., Vincieri F.F. 2007. Studies on the ineractions between some flavonols and cyclodextrins. *Bioorg. Med. Chem. Lett.*, 17: 5744–5748.

Branen A.L., Davidson P.M., Salminen S., Thorngate J.H. III. 2002. *Food Additives* (2nd Ed.). New York: Marcel Dekker, Inc.

Brennan M.A., Derbyshire E., Tiwari B.K., Brennan C.S. 2013. Ready-to-eat snack products: The role of extrusion technology in developing consumer acceptable and nutritious snacks. *International Journal of Food Science and Technology*, 48: 893–902.

Brenner K. 1983. The essence of spray dried flavors: The state of the art. *Perfum. Flavor.*, 8: 40.

Brewer M.S. 2012. Reducing the fat content in ground beef without sacrificing quality: A review. *Meat Science*, 91: 385–395.

Buffo R., Reineccius G.A. 2000. Optimization of gum acacia/modified starch/maltodextrin blends for the spray drying of flavors. *Perfum. Flavor.*, 25: 45–54.

Candogan K., Kolsarici N. 2003. The effects of carrageenan and pectin on some quality characteristics of low-fat beef frankfurters. *Meat Science*, 64: 199–206.

Chattopadhyaya S., Singhal R.S., Kulkarni P.R. 1988. Oxidised starch as gum Arabic substitute for encapsulation of flavours. *Carbohydr. Polym.*, 37: 143–144.

Cho K.Y., Rizvi S.S.H. 2010. New generation of healthy snack food by supercritical fluid extrusion. *Journal of Food Processing and Preservation*, 34: 192–218.

Cierach M., Modzelewska-Kapitula M., Szaciło K. 2009. The influence of carrageenan on the properties of low-fat frankfurters. *Meat Science*, 82: 295–299.

Connors K.A. 1997. The stability of cyclodextrin complexes in solution. *Chem. Rev.*, 97: 1325–1357.

Coultate T.P. 2002. *Food—The Chemistry of its Components* (4th Ed.). Cambridge: The Royal Society of Chemistry.

Damodaran S., Parkin K., Fennema O.R. 2008. *Fennema's Food Chemistry* (4th Ed.). Boca Raton, FL: Taylor and Francis Group, LLC.

Davidson P.M., Sofos J.N., Branen A.L. 2005. *Antimicrobials in Food* (3rd Ed.). Boca Raton, FL: Taylor and Francis Group, LLC.

de Paz E., Martín A., Bartolomé A., Largo M., Cocero M.J. 2014. Development of water-soluble b-carotene formulations by high temperature, high-pressure emulsification and antisolvent precipitation. *Food Hydrocolloids*, 37: 14–24.

Dlamini N.R., Taylor J.R.N., Rooney L.W. 2007. The effect of sorghum type and processing on the antioxidant properties of African sorghum-based foods. *Food Chemistry*, 105: 1412–1419.

Feng Y., Shao Y., Chen F. 2012. Monascus pigments. *Applied Microbiology and Biotechnology*, 96: 1421–1440.

Gibbs B.F., Kermasha S., Alli I., Mulligan C.N. 1999. Encapsulation in the food industry: A review. *Int. J. Food Sci. Nutr.*, 50: 213–224.

Gordon D.T. 1999. Defining dietary fiber—A progress report. *Cereal Foods World*, 44 (5): 336.

Gouin S. 2004. Microencapsulation: Industrial appraisal of existing technologies and trends. *Trends Food Sci. Tech.*, 15: 330–347.

Graves R.E. 1972. Uses for microencapsulation in food additives. *Cereal Sci. Today*, 17: 107.

Hand L.W., Hollingsworth C.A., Calkins C.R., Mandigo R.W. 1987. Effects of preblending, reduced fat and salt levels on frankfurter characteristics. *Journal of Food Science*, 52: 1149–1151.

Hedges A.R. 1998. Industrial applications of cyclodextrines. *Chem. Rev.*, 98: 2035–2044.

Heinzelmann K., Franke K., Jensen B., Haahr A.M. 2000. Protection of fish oil from oxidation by microencapsulation using freeze-drying techniques. *Eur. J. Lipid Sci. Tech.*, 102: 114–121.

Hsu S.Y., Sun L.-Y. 2006. Comparisons on 10 non-meat protein fat substitutes for low-fat Kung-wans. *Journal of Food Engineering*, 74: 47–53.

Huber G.R. 2000. Twin-screw extruders. In: *Extruders in Food Applications*, M.N. Riaz (Ed.). Boca Raton: CRC Press, pp. 81–114.

Hui Y.H. 2006. *Bakery Products Science and Technology*. Iowa: Blackwell Publishing.

IFIC, FDA 2010. Food Ingredients and Colors. International Food Information Council (IFIC) Foundation—US Food and Drug Administration (FDA). http://www.fda.gov/downloads/Food/FoodIngredientsPackaging/ucm094249.pdf

Iyengar R., McEvily A.J. 1992. Anti-browning agents: Alternatives to the use of sulfites in foods. *Trends in Food Science and Technology*, 31: 60–64.

Jiménez-Colmenero F., Cofrades S., Herrero A.M., Fernández-Martín F., Rodríguez-Salas L., Ruiz-Capillas C. 2012. Konjac gel fat analogue for use in meat products: Comparison with pork fats. *Food Hydrocolloid*, 26: 63–72.

Kant A., Linforth R.S.T., Hort J., Taylor A.J. 2004. Effect of β-cyclodextrin on aroma release and flavour perception. *J. Agr. Food Chem.*, 52: 2028–2035.

Kimoto T., Koya S., Hino K., Yamamoto Y., Nomura Y. 2000. Renal carcinogenesis induced by ferric nitrilotriacetate in mice and protection from it by Brazilian propolis and artepillin C. *Pathol. Int.*, 50: 679–689.

Kiokias S., Varzakas T., Oreopoulou V. 2008. *In vitro* activity of vitamins, flavonoids, and natural phenolic antioxidants against the oxidative deterioration of oil-based systems. *Crit. Rev. Food Sci. and Nutr.*, 48: 78–93.

Lee Y.K., Salminen S. 2009. *Handbook of Probiotics and Prebiotics* (2nd Ed.) New Jersey: John Wiley and Sons, Inc.

Licata R., Chu J., Wang S., Coorey R., James A., Zhao Y., Johnson S. 2013. Determination of formulation and processing factors affecting slowly digestible starch, protein digestibility and antioxidant capacity of extruded sorghum–maize composite flour. *International Journal of Food Science and Technology*, doi: 10.1111/ijfs.12444.

Liong M.-T. 2011. *Probiotics—Biology, Genetics and Health Aspects.* Berlin-Heidelberg: Springer-Verlag.

Loftsson T., Brewster M.E. 1996. Pharmaceutical applications of cyclodextrins drug solubilization and stabilization. *J. Pharm. Sci.*, 85: 1017–1025.

Loftsson T., Masson M. 2001. Cyclodextrins in topical drug formulations: Theory and practice. *Int. J. Pharm.*, 225: 15–30.

Lurueña-Martínez M.A., Vivar-Quintana A.M., Revilla I. 2004. Effect of locust bean/xanthan gum addition and replacement of pork fat with olive oil on the quality characteristics of low-fat frankfurters. *Meat Science*, 68: 383–389.

Maire M., Rega B., Cuvelier M.-E., Soto P., Giampaoli P. 2013. Lipid oxidation in baked products: Impact of formula and process on the generation of volatile compounds. *Food Chemistry*, 141: 3510–3518.

Manoi K., Rizvi S.S.H. 2008. Rheological characterizations of texturized whey protein concentrate-based powders produced by reactive supercritical fluid extrusion. *Food Research International*, 41: 786–796.

Marchetti L., Andrés S.C., Califano A.N. 2014. Low-fat meat sausages with fish oil: Optimization of milk proteins and carrageenan contents using response surface methodology. *Meat Science*, 96: 1297–1303.

Maswal M., Dar A.A. 2014. Formulation challenges in encapsulation and delivery of citral for improved food quality. *Food Hydrocolloids*, 37: 182–195.

Matz S.A. 1991. *Bakery Technology and Engineering*. New York: Springer.

McClements D.J., Rao J. 2011. Food-grade nanoemulsions: Formulation, fabrication, properties, performance, biological fate, and potential toxicity. *Critical Reviews in Food Science and Nutrition*, 51: 285–330.

Molis C., Flourie B., Ouarne F. et al. 1996. Digestion, excretion, and energy value of fructooligosaccharides in healthy humans. *The American Journal of Clinical Nutrition*, 64: 324–328.

Mollet H., Grubenrnann A. 2001. *Formulation Technology*. Weinheim: Wiley-VCH Verlag GmbH.

Mourtzinos I., Kalogeropoulos N., Papadakis S.E., Konstantinou K., Karathanos V.T. 2008. Encapsulation of nutraceutical monoterpenes in β-cyclodextrin and modified starch. *J. Food Sci.*, 73 (1): 89–94.

Moustafa A., Stauffer C. 1997. *Bakery Fats*. Brussels: American Soybean Association.

Msagati T.A.M. 2013. *The Chemistry of Food Additives and Preservatives*. Iowa: John Wiley and Sons, Ltd.

Muchenje V., Dzama K., Chimonyo M., Strydom P.E., Hugo A., Raats J.G. 2009. Some biochemical aspects pertaining to beef eating quality and consumer health: A review. *Food Chemistry*, 112: 279–289.

Norton J.E., Fryer P.J., Norton I.T. 2013. *Formulation Engineering of Foods*. West Sussex: John Wiley and Sons, Ltd.

Onwulata C.I., Tunick M.H., Qi P.X. 2011. Extrusion texturized dairy proteins: Processing and application. *Advances in Food and Nutrition Research*, 62: 173.

Ordóñez M., Rovira J., Jaime I. 2001. The relationship between the composition and texture of conventional and low-fat frankfurters. *International Journal of Food Science and Technology*, 36: 749–758.

Orsia O., Ricardo S., Funaria M., Sílvia R.C., Bankova V. 2005. Effects of Brazilian and Bulgarian propolis on bactericidal activity of macrophages against *Salmonella typhimurium*. *Int. Immunopharm.*, 5: 359–368.

Pandey R.M., Upadhyay S.K. 2012. Food Additive. In: *Food Additive*, Y. El-Samragy (Ed.). Rijeka: InTech. ISBN: 978-953-51-0067-6, DOI: 10.5772/34455. Available from: http://www.intechopen.com/books/food-additive/food-additive

Paraman I., Supriyadi S., Wagner M.E., Rizvi S.S.H. 2013. Prebiotic fibre-incorporated whey protein crisps processed by supercritical fluid extrusion. *International Journal of Food Science and Technology*, 48: 2193–2199.

Pietrasik Z. 2003. Binding and textural properties of beef gels processed with κ-carrageenan, egg albumin and microbial transglutaminase. *Meat Science*, 63: 317–324.

Plutowska B., Wardencki W. 2007. Aromagrams—Aromatic profiles in the appreciation of food quality. *Food Chemistry*, 101: 845–872.

Pozo-Bayon M.A., Guichard E., Cayot N. 2006. Feasibility and application of solvent assisted flavour evaporation and standard addition method to quantify the aroma compounds in flavoured baked matrices. *Food Chemistry*, 99: 416–423.

Preedy V.R., Ross Watson R., Patel V.B. 2011. *Flour and Breads and their Fortification in Health and Disease Prevention*. London: Elsevier, Inc.

Purlis E. 2010. Browning development in bakery products—A review. *Journal of Food Engineering*, 99: 239–249.

Qi Z.H., Xu A. 1999. Starch based ingredients for flow encapsulation. *Cereal Food World*, 44: 460–465.

Qian C., Decker E.A., Xiao H., McClements D.J. 2012a. Physical and chemical stability of β-carotene-enriched nanoemulsions: Influence of pH, ionic strength, temperature, and emulsifier type. *Food Chemistry*, 132: 1221–1229.

Qian C., Decker E.A., Xiao H., McClements D.J. 2012b. Nanoemulsion delivery systems: Influence of carrier oil on β-carotene bioaccessibility. *Food Chemistry*, 135: 1440–1447.

Rega B., Guerard A., Delarue J., Maire M., Giampaoli P. 2009. On-line dynamic HS-SPME for monitoring endogenous aroma compounds released during the baking of a model cake. *Food Chemistry*, 112:9–17.

Reineccius G. 2006. *Flavor Chemistry and Technology* (2nd Ed.). Boca Raton, FL: Taylor and Francis Group, LLC.

Reineccius G.A. 1988. Spray drying of food flavours. In: *Flavour Encapsulation*, G.A. Reineccius, S.J. Risch (Eds.). Washington: ACS, pp. 55–66.

Reineccius G.A. 1995. Controlled release techniques in the food industry. In: *Encapsulation and Controlled Release of Food Ingredients*, S.J. Risch, G.A. Reineccius (Eds.). New York: ACS, pp. 2–7.

Risch S. 1995. Encapsulation: Overview of uses and techniques. In: *Encapsulation and Controlled Release of Food Ingredients*, S.J. Risch, G.A. Reineccius (Eds.). New York: ACS, pp. 2–7.

Ronzio R. 2003. *The Encyclopedia of Nutrition and Good Health* (2nd Ed.). New York: Robert Ronzio.

Saenger W. 1980. Cyclodextrin inclusion compounds in research and industry. *Angew. Chem. Int. Ed. Engl.*, 19: 344–362.

Schneeman B.O. 2000. Relationship of food, nutrition and health (Ch. 1). In: *Essentials of Functional Foods*, M.K. Schmidl, T.P. Labuza (Eds.). Gaithersburg: Aspen Publishers, Inc., pp. 3–7.

Schrooyen P.M., van der Meer R., De Kruif C.G. 2001. Microencapsulation: Its application in nutrition. *Pro. Nutr. Soc.*, 60: 475–479.

Schultz T.H. 1956. Incorporation of natural fruit flavors into fruit juice powders. Locking of citrus oils in sucrose and dextrose. *Food Tech.*, 10: 57–60.

Soottitantawata A., Takayama K., Okamura K., Muranaka D., Yoshiia H., Furuta T., Ohkawara M., Linko P. 2005. Microencapsulation of l-menthol by spray drying and its release characteristics. *Innov. Food Sci. Emerg. Technol.*, 6: 163–170.

Sparks R.E., Jacobs I.C. 1999. Selection of coating and microencapsulation processes. *Control. Release Delivery Syst. Pestic.*, 12: 23–29.

Stella V.J., Rao V.M., Zannou E.A., Zia V. 1999. Mechanisms of drug release from cyclodextrin complexes. *Adv. Drug Deliver. Rev.*, 36: 3–16.

Su Y.K., Bowers J.A., Zayas J.F. 2008. Physical characteristics and microstructure of reduced-fat frankfurters as affected by salt and emulsified fats stabilized with nonmeat proteins. *Journal of Food Science*, 65: 123–128.

Sungsoo Cho S., Dreher M.L. 2001. *Handbook of Dietary Fiber*. New York: Marcel Dekker, Inc.

Szejtli J. 1998. Introduction and general overview of cyclodextrin chemistry. *Chem. Rev.*, 98: 1743–1753.

Szente L., Szejtli J. 2004. Cyclodextrins as food ingredients. *Trends Food Sci. Tech.*, 15: 137–142.

Tavano L., Muzzalupo R., Picci N., de Cindio B. 2014. Co-encapsulation of antioxidants into niosomal carriers: Gastrointestinal release studies for nutraceutical applications. *Colloids and Surfaces B: Biointerfaces*, 114: 82–88.

Taylor J.R.N., Emmambux M.N. 2010. Developments in our understanding of sorghum polysaccharides and their health benefits. *Journal of Cereal Chemistry*, 87: 263–271.

Taylor J.R.N., Schober T.J., Bean S.R. 2006. Novel food and non-food uses for sorghum and millets. *Journal of Cereal Science*, 44: 252–271.

Tsarouhas P.H., Arvanitoyannis I.S., Varzakas T.H. 2009. Reliability and maintainability analysis of cheese (feta) production line in a Greek medium size company: A case study. *Journal of Food Engineering*, 94: 233–240.

Tsarouhas P.H., Varzakas T.H., Arvanitoyannis I.S. 2009. Reliability and maintainability analysis of Strudel production line with experimental data; A case study. *Journal of Food Engineering*, 91: 250–259.

Varzakas T., Arvanitoyannis I.S. 2006. Application of failure mode and effect analysis (FMEA), cause and effect analysis and Pareto diagram in conjunction with HACCP to a corn curl manufacturing plant. *Critical Reviews of Food Science and Nutrition*, 47 (4): 363–387.

Varzakas T., Arvanitoyannis I.S. 2007. Application of failure mode and effect analysis (FMEA), cause and effect analysis and Pareto diagram in conjunction with HACCP to a Strudel manufacturing plant. *International Journal of Food Science and Technology*, 42: 1156–1176.

Varzakas T., Labropoulos A., Anestis S. 2011. Addressing new functional fillo products through nutrition and healthy ingredients: Hi omega-3 fatty acids and phytosterol esters. *Proceedings of the 11th International Congress on Engineering and Food*, 22–25 May, organized by NTUA, Athens, Greece. pp. 2147–2148.

Varzakas T.H. 2011. Application of ISO22000, failure mode and effect analysis (FMEA) cause and effect diagrams and Pareto in conjunction with HACCP and risk assessment for processing of pastry products. *Critical Reviews in Food Science and Nutrition*, 51 (8): 762–782.

Varzakas, T., Labropoulos, A., and Anestis, S. 2012. *Sweeteners: Nutritional Aspects, Applications and Production Technology*. Boca Raton FL: CRC Press, Taylor and Francis Group.

Versic R.J. 1988. Flavor encapsulation, an overview (Ch. 1). *ACS Symposium Flavor Encapsulation, Series 370*. Washington, DC: ACS, pp. 5.

Walsh M.K., Wood A.M. 2010. Properties of extrusion-expanded whey protein products containing fiber. *International Journal of Food Properties*, 13: 702–712.

Walton N.J., Mayer M.J., Narbad A. 2003. Vanillin. *Phytochemistry*, 63: 505–515.

Webb G.P. 2006. *Dietary Supplements and Functional Foods*. Oxford: Blackwell Publishing, Ltd., Ch. 5, pp. 109–111, Ch. 8, pp. 165–166.

Wicke B., Dornburg V., Junginger M., Faaij A. 2008. Different oil palm production systems for energy purposes and their greenhouse gas implications. *Biomass and Bioenergy*, 32: 1322–1337.

Wildman R.E.C. 2001. *Handbook of Nutraceuticals and Fuctional Foods*. New York: CRC press.

Wrolstad R.E., Acree T.E., Decker E.A., Penner M.H., Reid D.S., Schwartz S.J., Shoemaker C.F., Smith D., Sporns P. 2000. *Handbook of Food Analytical Chemistry—Water, Proteins, Enzymes, Lipids, and Carbohydrates*. New Jersey: John Wiley and Sons, Inc.

Youssef M.K., Barbut S. 2010. Effects of caseinate, whey and milk proteins on emulsified beef meat batters prepared with different protein levels. *Journal of Muscle Foods*, 21: 785–800.

Youssef M.K., Barbut S. 2011. Fat reduction in comminuted meat products-effects of beef fat, regular and pre-emulsified canola oil. *Meat Science*, 87(4): 356–60.

Zeller B.L., Saleeb F.Z., Ludescher R.D. 1999. Trends in development of porous carbohydrate food ingredients for use in flavor encapsulation. *Trends Food Sci. Tech.*, 9: 389–394.

Zulim Botega D.C., Marangoni A.G., Smith A.K., Goff H.D. 2013a. The potential application of rice bran wax oleogel to replace solid fat and enhance unsaturated fat content in ice cream. *Journal of Food Science*, 78 (9): 1334–1339.

Zulim Botega D.C., Marangoni A.G., Smith A.K., Goff H.D. 2013b. Development of formulations and processes to incorporate wax oleogels in ice cream. *Journal of Food Science*, 78 (12): 1845–1851.

15 Reaction Kinetics

Petros S. Taoukis, Theofania N. Tsironi, and Maria C. Giannakourou

CONTENTS

15.1 Introduction 529
15.2 Kinetics of Food Reactions 531
15.2.1 Basic Principles 531
15.2.2 Determining the Order of Reaction 533
15.2.2.1 Differential Methods 533
15.2.2.2 Integral Methods 534
15.2.2.3 Method of Half Lives 534
15.2.3 Effect of Environmental Factors 535
15.2.3.1 Temperature 535
15.2.3.2 Effect of Other Environmental Factors 541
15.3 Reaction Kinetics in Shelf-Life Prediction 545
15.3.1 Accelerated Shelf-Life Testing 545
15.3.2 Temperature Dependence of Main Shelf-Life Indices 548
15.3.3 Shelf-Life Prediction and Management of the Food Chain 548
15.4 Application of Food Kinetics in Shelf-Life Prediction: Examples of Shelf-Life Modeling of Food Products 550
15.5 Application of TTI as Shelf-Life Predictors during Distribution 559
References 561

15.1 INTRODUCTION

Advances in new, cost-efficient, environmental friendly and versatile methods of food processing and preservation have been presented and implemented over the past years to meet the continually increasing consumer demands for quality foods with particular focus on their nutritional and functional aspects. The quality of processed foods is not a simple property; it depends not only on the initial integrity of the raw materials but also on the changes occurring during processing and subsequent storage that may result in potential losses and decreased bioavailability. Therefore, quality is an attribute of food, on which understandably a lot of consideration is focused. *Food quality* can be defined as the assemblage of properties that differentiate individual units and influence the degree of acceptability of the food by the consumer or user (Kramer and Twigg 1968). Owing to the nature of foods as physicochemically and biologically active systems, food quality is a dynamic state continuously moving to reduced levels (with the

notable exception of the cases of maturation and aging). Therefore, for each particular food, there is a finite length of time after production within which it will retain a required level of quality organoleptically and safetywise, under stated conditions of storage. This period of time can be generally defined as the *shelf life* of the food product. There is no established, uniformly applicable definition of shelf life. The definition of shelf life and the criteria for the determination of the end of shelf life are dependent on specific commodities and on the definition's intended use (i.e., for regulatory vs. marketing purposes). Food-related authorities have proposed various definitions that can serve as guidelines. The International Institute of Refrigeration (IIR) recommendations for frozen food (IIR 1972) introduce two different definitions. *High quality life* (HQL) is the time from freezing of the product for a just noticeable sensory difference to develop (70–80% correct answers in a triangular sensory test). Another type of shelf-life definition that can be extended to other types of food products is the *practical storage life* (PSL). PSL is the period of proper (frozen) storage after processing (freezing) of an initially high-quality product during which the sensory quality remains suitable for consumption or for the process intended. PSL is usually in the order of two to three times longer than HQL. *Time of minimum durability*, introduced by the EEC directive on food labeling, is defined as the time during which the foodstuff retains its specific properties when properly stored is different in principle from the aforementioned ones, in that it relates to properties of the product itself and not to considerations of its use. It is a working definition for the food scientist satisfying the often made fundamental assumption that the highest quality product is the freshly processed (or harvested) one. However, since characteristic properties are overlaid, a decision has to be made at what level the change in a certain characteristic or the development of an undesirable one can be detected by the consumer. For example, if having a specific flavor means the absence of off-flavors, it has to be decided at what intensity levels these flavors are detectable by the consumer. Thus, this definition is closely related to the HQL definition. Chemical, microbiological, and physical tests are being used widely in the study of food quality. Characteristics used by the consumer for evaluation of a product, such as flavor, color, and textural properties can be measured instrumentally or chemically. The study of the chemical and biological reactions and physical changes that occur in the food during and after processing allow the recognition of the ones that are most important to its safety, integrity, and overall quality. Physicochemical or microbiological parameters can be used to quantitatively assess quality. The values of these parameters can be correlated to sensory results for the same food and a limit that corresponds to the lowest acceptable sensory quality can be set. However, caution should be drawn to the fact that correlation of values of individual chemical parameters to sensory data is often not straightforward because overall organoleptic quality is a composite of a number of changing factors (Trant et al., 1981). The relative contribution of each factor to the overall quality may vary at different levels of quality or at different storage conditions. Food kinetics is based on the thorough study of the rates at which physicochemical reactions proceed. The area of kinetics in food systems has received a great deal of attention in past years, primarily due to efforts to

optimize or at least maximize the quality of food products during processing and storage (Villota and Hawkes 2007). Moreover, a good understanding of reaction kinetics can provide a systematic approach on how to redesign the formulation of food products to better preserve the desirable sensory, nutritional, and functional components system and minimize the evolution of undesirable products. For example, chemical changes as a result of enzymatic action, oxidative reactions, and nonenzymatic browning can lead to quality deterioration. The use of chemical kinetics, the study of the rates, and mechanisms that are involved in the reactions of interest, and the mathematical relationships that best describe the influence of temperature on the reaction rate constants have been used to model changes in food quality. In parallel, significant published work regarding mathematical modeling has focused on microbiological safety and spoilage in a variety of food matrices.

15.2 KINETICS OF FOOD REACTIONS

15.2.1 Basic Principles

The established methodology consists of first identifying the chemical and biological reactions that influence the quality and the safety of the food. Through a careful study of the food components and the process, the reactions judged to have the most critical impact on the deterioration rate, can be established. On the basis of this analysis and without underestimating the underlying complexity of food systems, the change of food quality can be represented by the loss of one or more quantifiable quality indices, symbolized by A. (e.g., a nutrient or characteristic flavor) or by the formation of an undesirable product B (e.g., an off flavor or discoloration). The rate of change of A and B can, in general, be represented by Equation 15.1:

$$\begin{aligned} r_A &= -\frac{d[A]}{dt} = k \cdot [A]^n \\ r_B &= \frac{d[B]}{dt} = k' \cdot [B]^{n'} \end{aligned} \tag{15.1}$$

The quality factors $[A]$ and $[B]$ are usually quantifiable chemical, physical, microbiological, or sensory parameters, selected so as to representatively describe the quality deterioration of the particular food system. The constants k and k' are the apparent reaction rate constants and n and n' are the apparent orders of the respective reactions. The use of the term "apparent" indicates that Equation 15.1 does not necessarily describe the mechanism of the measured phenomenon. A general equation describing the loss of the quality factor A in a food system may be expressed as

$$f_q(A) = k(C_i, E_j) \cdot t \tag{15.2}$$

TABLE 15.1
Quality Function-Based Deterioration of Quality Index A

Apparent Reaction Order	Quality Function f_q (A_t)
0	$A_o - A_t$
1	$\ln(A_o/A_t)$
2	$1/A_o - 1/A_t$
n (n ≠ 1)	$\frac{1}{n-1}\left(A_t^{1-n} - A_o^{1-n}\right)$

where f_q can be defined as the quality function of the food and k, the apparent reaction rate constant, is a function of composition factors C_i, such as concentration of reactive compounds, inorganic catalysts, enzymes, reaction inhibitors, pH, water activity, as well as microbial populations, and of environmental factors, E_j, such as temperature, relative humidity, total pressure, and partial pressure of different gases, light, and mechanical stresses.

In experimental kinetic studies, it is impossible to measure the reaction rate itself. Instead, the concentration of A or B is measured (directly or indirectly) as a function of time. If these concentrations are plotted against time and smooth curves are fitted either graphically or using a statistical fitting method (e.g., polynomial regression), the reaction rates may be obtained by graphical or numerical differentiation of the curves. Regardless of the value of n in Equation 15.1, Equation 15.2 can be expressed in the form:

$$\mathrm{Q(A)} = k \cdot t \tag{15.3}$$

where the expression Q(A) is defined as the quality function of the food.

The form of the quality function of the food for an apparent zero, 1st, 2nd, and nth order reaction can be derived from Equation 15.3 and is shown in Table 15.1.

The overwhelming majority of the food reactions that have been studied are characterized as pseudo-zero or pseudo-first order (Labuza 1984). Characteristic examples are listed in Table 15.2.

TABLE 15.2
Important Quality Loss Reactions that Follow Zero or First-Order Kinetics

Zero order	☐ Overall Quality of Frozen Foods
	☐ Nonenzymatic browning
First order	☐ Vitamin loss
	☐ Microbial death/growth
	☐ Oxidative color loss
	☐ Texture loss in heat processing

Having established the apparent order of the quality determining reaction statistical analysis of the parameter k, the rate constant is required, to obtain an estimate of the error in the determination of k (Labuza and Kamman 1983). If least-square methods by linear regression are used to estimate the parameters, their 95% confidence limits can be calculated using the Student's t distribution. A list of standardized residuals and a residual plot is a useful statistical tool that allows evaluation of how well the chosen equation can model the data and also permit the recognition of extreme or outlier values that may be the result of experimental errors or other extraneous effects and should be excluded from the calculations (Arabshashi and Lund 1985). The standardized residuals should be randomly distributed around zero and usually within −2 and +2. Any data that generate standard residuals outside this range are possible outliers.

15.2.2 Determining the Order of Reaction

To reliably decide the appropriate apparent order and quality function, the experimental design should provide for enough measurements of concentration change of the quality index. If the reaction is not carried far enough (<50% conversion) both zero and first order might not differ from a goodness-of-fit point of view. However, if the end of shelf life is within less than 20% conversion, for practical purposes either model is sufficient.

Practically, once the parameter A that should describe a food system degradation is selected, it is necessary to proceed to a suitable experimental design, so as to produce data of the change of A over time (Giannakourou and Taoukis 2007). Analysis of this information to estimate the most appropriate reaction order can be accomplished by differential or other methods (Karel and Lund 2003; Lund 1983; Margerison 1969).

15.2.2.1 Differential Methods

The equation of unknown order used to describe the system change has the following form:

$$\frac{dA}{dt} = rate(r) = -k \cdot [A]^n \tag{15.4}$$

- $[A]$ is plotted versus time, and a smooth curve is drawn as shown in Figure 15.1a
- The slope is $d[A]/dt$ and can be determined at various points in time by:
  - Drawing tangent to curve
  - PSL taking $d[A]$ for each dt (need lots of data points)
- $\ln dA/dt$ is plotted versus $\ln A$ as in Figure 15.1b

$$\ln \frac{d[A]}{dt} = \ln k + n \cdot \ln[A] \tag{15.5}$$

where the slope is the order of the reaction n, estimated from algebraic substitution.

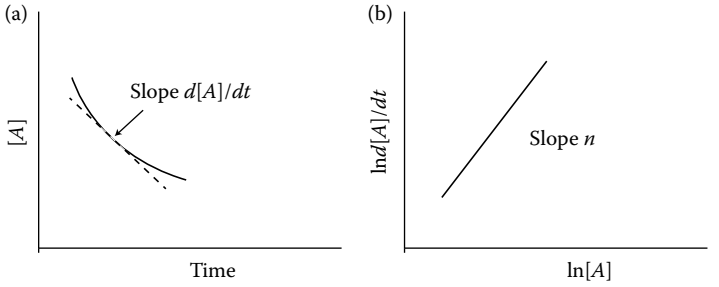


FIGURE 15.1 (a) Plot of concentration [*A*] versus time and (b) plot of ln(*d*[*A*]/*dt*) versus ln[*A*] to determine the slope *n*.

15.2.2.2 Integral Methods

This is a trial-and-error process where a reaction functional form is assumed:

$$\frac{d[A]}{dt} = -k \cdot F[A] \Rightarrow \int_{A_i}^{A_f} \frac{d[A]}{F[A]} = \int_0^t -k\, dt = -k \cdot t \tag{15.6}$$

and the term of $\int_{A_i}^{A_f} (d[A]/F[A])$ is calculated from the data measurements available.

If the plot or the regression of this term versus time yields a linear function passing through the origin (0,0) with slope $-k$ then the hypothesis was correct; otherwise, a new assumption is made and the procedure is repeated.

15.2.2.3 Method of Half Lives

The half-life ($t_{1/2}$) is the time required for the parameter A to lose half of its initial concentration. Table 15.3 summarizes the mathematical form of $t_{1/2}$ for the different reaction rate orders.

TABLE 15.3
Forms of Half-Life for the Different Reaction Orders

Order of Reaction	$t_{1/2}$ (half-life)
First (1)	$\frac{k}{0.693}$
Second (2)	$\frac{1}{k \cdot A_o}$
n^{th} order (n)	$\frac{1}{k \cdot [n-1]} \frac{2^{n-1}-1}{A_o^{n-1}}$

Alternatively, life can be also determined for any decided fractional decrease. If f is the decimal fraction of (A/A_o) and $n = 1$, then

$$\ln\frac{A}{A_o} = -k \cdot t \Rightarrow \ln\frac{fA_o}{A_o} = \ln[f] = -k \cdot t \Rightarrow k = -\frac{\ln[f]}{t_f} \tag{15.7}$$

where t_f fraction life in time units. A well-known example of this methodology refers to the decrease by 1 log cycle of microorganisms in microbial death. In that case, $f = 0.1$, t_f is called D value and Equation 15.7 becomes

$$k = -\frac{\ln 0.1}{D} \Rightarrow D = \frac{2.3}{k} \tag{15.8}$$

15.2.3 Effect of Environmental Factors

15.2.3.1 Temperature

Kinetic equations for shelf-life estimation are specific to the food studied and the environmental conditions used. Among the environmental factors considered (temperature, relative humidity, total pressure, and partial pressure of different gases, light, and mechanical stresses), the one being invariably emphasized and introduced in the shelf-life model is temperature (Taoukis and Giannakourou 2004). It strongly affects post-processing reaction rates and during subsequent handling, distribution and storage cannot be controlled a priori by means such as food packaging and depends on the imposed environmental (storage) conditions.

The prevailing effect of temperature on the rate of food-related reaction rates has long been the subject of research and a significant number of kinetic studies of important indices, of physical, chemical, microbiological, or sensory deterioration of foods have been published. The most prevalent and widely used model is the Arrhenius relation, derived from thermodynamic laws as well as statistical mechanics principles:

$$k = k_A \cdot \exp\left(\frac{-E_A}{RT}\right) \tag{15.9}$$

with k_A representing the Arrhenius equation constant and E_A, in Joules or calories per mole, is defined as the activation energy, that is, the excess energy barrier that quality parameter A needs to overcome to proceed to degradation products. R is the universal gas constant (1.9872 cal/mol K or 8.3144 J/mol K). To estimate the temperature effect on the reaction rate of a specific quality deterioration mode, values of k are estimated at different temperatures, in the range of interest, and lnk is plotted versus the term of $1/T$ in a semilog graph. A straight line is obtained with a slope of $-E_A/R$ from which the activation energy is calculated.

It should be noted that the Arrhenius equation implies that k_A is the theoretical value of the reaction rate at 0 K. Alternatively, the use of a reference temperature,

T_{ref}, is recommended, corresponding to a representative value in the temperature range of the process/storage of study. Equation 15.9 is then mathematically transformed as follows (Equation 15.10):

$$k = k_{ref} \exp\left[\frac{-E_A}{R}\left(\frac{1}{T} - \frac{1}{T_{ref}}\right)\right] \tag{15.10}$$

where k_{ref} is the rate constant at the reference temperature T_{ref}. The value of E_A is, in that case, calculated from the linear regression of lnk versus $(1/T - 1/T_{ref})$. Values of T_{ref} usually employed are 255 K for frozen, 277 K for chilled, and 295 K for ambient temperature stored food products. Besides giving the constant a practical physical meaning, the above transformation of the Arrhenius equation provides enhanced stability during numerical parameter estimation and integration.

When only three points in the Arrhenius plot are used for the determination of E_A, the 95% confidence limits of the Arrhenius parameters, as estimated with statistical tools, are usually wide. If narrower limits are required, experiments must include more temperatures in the range of interest. According to the optimum scheme of Lenz and Lund (1980), an optimum number of 5 or 6 isothermal experiments are adequate to obtain a satisfactory accuracy.

Alternatively to isothermal kinetic analysis, the study at a single nonisothermal temperature profile is proposed, where temperature varies with time, following a predetermined function of $T(t)$. In that case, Equation 15.3 is modified as follows, assuming a first-order reaction (Equation 15.11):

$$A = A_o \cdot \exp\left[-k_A \cdot \int_0^t \exp\left(-\frac{E_A}{R} \cdot \frac{1}{T(t)}\right) dt\right] \tag{15.11}$$

where the integral is calculated by numerical techniques. This approach requires a very strict temperature control and is very sensitive to experimental error in concentration measurements. In a comparative study, the isothermal method at three different constant temperatures gave better results for the estimation of the Arrhenius parameters than the nonisothermal approach with a linearly increasing temperature at the same range and for equal number of data points (Yoshioka et al. 1987). The non-uniform temperature within the samples, as well as the difficulty in recognizing a deviation from an Arrhenius behavior should also be considered when applying the non-isothermal technique.

Numerous shelf-life models based on the Arrhenius equation have been published to describe either the temperature dependence of quality loss (Buedo et al. 2001; Giannakourou and Taoukis 2002; Hertog et al. 1997; Tsironi et al. 2011; Tsironi and Taoukis 2014) or the combined effect of temperature with other environmental factors (Koutsoumanis et al. 2000; Seyhan et al. 2002; Zimmermann et al. 2013). Although the Arrhenius equation is commonly used to describe temperature dependence of the reaction rate in most food systems, deviations may occur as reported by several authors including Labuza and Riboh (1982) and Taoukis et al. (1997). In fact, a large number

of factors may contribute to deviations. Phase changes are often involved. Fats may change to the liquid state contributing to the mobilization of organic reactants or vice versa (Templeman et al. 1977). In frozen foods, the effect of phase change of the water of the food is very pronounced in the immediate subfreezing temperature range. The Arrhenius plot would, therefore, show an abrupt change in this range and a single Arrhenius line should not be used in case the freezing point is crossed within the temperature range studied. Other phase change phenomena are also important. Carbohydrates in the amorphous state may crystallize at lower temperatures, creating more free water for other reactions but reducing the amount of available sugars for reaction (Kim et al. 1981). A characteristic case is the phenomenon of staling of bread (Zobel 1973). Retrogradation of the amylopectin and a redistribution of moisture between starch and gluten have been implicated in staling.

Glass transition is related to dramatic changes of food mechanical properties and molecular mobility (Roos 2013) and may occur in carbohydrate-containing foods, when storage conditions are suddenly modified, such as during rapid cooling or solvent removal. Examples of the formation of metastable glasses that deteriorate following a kinetic pattern that deviates from the Arrhenius law, include frozen carbohydrate-containing solutions or food products (Biliaderis et al. 1999; Blond and Simatos 1991; Carrington et al. 1996; Champion et al. 2000; Furuki 2002), spraydried milk (Bushill et al. 1965), whey powder, and dehydrated vegetables (Buera and Karel 1993), osmotically dehydrofrozen fruits and vegetables (Chiralt et al. 2001; Torreggiani et al. 1999), and so on.

In the systems that are subject to glass transition, due to drastic acceleration of the diffusion-controlled reactions above T_g, the dependence of the rate of a food reaction on temperature cannot be described by a single Arrhenius equation. In the rubbery state above T_g, the activation energy is not constant, but is rather a function of temperature. This behavior has been often described by an alternative equation, the Williams–Landel–Ferry (WLF) expression (Equation 15.12) that empirically models the temperature dependence of mechanical and dielectric relaxations in the range $T_g < T < T_g + 100$:

$$\log \frac{k_{ref}}{k} = \frac{C_1 \cdot (T - T_{ref})}{C_2 + (T - T_{ref})} \tag{15.12}$$

where k_{ref} is the rate constant at the reference temperature T_{ref} ($T_{ref} > T_g$) and C_1, C_2 are system-dependent coefficients. Williams et al. (1955), assuming $T_{ref} = T_g$ and applying WLF equation for data available for various polymers, estimated mean values of the coefficients $C_1 = -17.44$ and $C_2 = 51.6$. However, the uniform application of these constants is often problematic (Buera and Karel 1993; Peleg 1992; Terefe and Hendrickx 2002) and the calculation of system-specific values, whenever possible, should be preferred, using Equation 15.12 with $T_{ref} = T_g$ and rearranging the mathematical expression to the following form (Equation 15.13):

$$\left[\log \frac{k_g}{k}\right]^{-1} = \frac{-C_2}{C_1 \cdot (T - T_g)} - \frac{1}{C_1} \tag{15.13}$$

such that a plot of

$$\left[\log\frac{k_g}{k}\right]^{-1} \text{ vs. } \frac{1}{T - T_g} \tag{15.14}$$

gives a straight line with a slope equal to $-C_2/C_1$ and an intercept of $-1/C_1$, if the WLF model is successfully applied. Nelson (1993) suggested the determination of WLF coefficients when applying the WLF equation to describe ascorbic acid degradation in maltodextrin-based systems of various moisture levels. These coefficients were found to depend not only on the type of the matrix in question, but also on the water content. In the same study, it was observed in several cases that in the rubbery zone of the matrices, the Arrhenius equation described more adequately than the WLF model the temperature dependence of the loss of ascorbic acid. Terefe and Hendrickx (2002) studied the kinetics of the pectin methylesterase catalyzed de-esterification of pectin in frozen food model in a wide temperature range (–24–20°C) and observed that a single Arrhenius plot could not describe the temperature dependence in the whole range. The same observation was made by Terefe et al. (2002) for the alkaline phosphatase catalyzed hydrolysis of disodium *p*-nitrophenyl phosphate in the range from –28°C to 20°C; the Arrhenius plot was curved as the temperature approached $T_{g'}$, in the rubbery state of the matrix, due to the extra temperature dependence which is not accounted for in the Arrhenius model. The shift in the slope of an Arrhenius plot observed in the aforementioned enzymatic reactions may indicate a change in the activation energy or a change in the controlling mechanism. Owing to mechanical and mobility properties between glassy and rubbery systems, a break in the Arrhenius plot at or near the glass transition temperature of the system may be expected. However, from data of Lim and Reid (1991), the Arrhenius plot for an enzyme hydrolysis reaction within a partially frozen maltodextrin DE 25 above the estimated T_g' of the system was quite linear and the expected curvature was not observed. In order for this deviation from the Arrhenius linearity to be obvious, study over a broader temperature range is required; however, this is not possible for frozen systems since these matrices melt at slightly higher temperatures, and they are transformed to liquids above 0°C.

At this point, it should be stressed out that in some cases, measuring the glass transition temperature may not be adequate for explaining the break in an Arrhenius plot (Giannakourou and Taoukis 2003c; Manzocco et al. 1999; Terefe and Hendrickx 2002) and other changes should be taken into consideration.

The study of the temperature dependence of microbial growth has been an area of increased activity. The described kinetic principles are applied to compile the necessary data for modeling growth behavior, in the multidisciplinary field of predictive microbiology (Buchanan 1993; McClure et al. 1994; McMeekin et al. 1993, 2008; McMeekin 2007). In the field of predictive microbiology, several temperature dependence equations have been proposed for describing the k(T) function, where k is the exponential growth rate of the microorganism in question. Most prominently used in the suboptimal temperature range are the Arrhenius and the Belehradek equation

(McMeekin et al. 1993). The Belehradek equation (Belehradek, 1930) has the following generalized form (Equation 15.15):

$$k = a \cdot (T - T_0)^d \tag{15.15}$$

where a and d are parameters to be fitted and t_0 is regarded as the "biological zero," that is a temperature at and below which no growth is possible. To avoid this assumption, Ratkowsky et al. (1983) changed T_o to T_{min} and proposed the square root model (Equation 15.16):

$$\sqrt{k} = b \cdot (T - T_{min}) \tag{15.16}$$

$$\sqrt{k} = b \cdot (T - T_{min})\left\{1 - \exp\left[c \cdot (T - T_{max})\right]\right\} \tag{15.16a}$$

where k is the growth rate, b is the slope of the regression line of $\sqrt{k}$ versus T, and T_{min} is the hypothetical growth temperature where the regression line cuts the T-axis at $\sqrt{k} = 0$.

T_{min} is usually 2–3°C lower than the temperature at which growth is actually observed and has been described as notional or conceptual temperature. Equation 15.11 was later extended to the form of Equation 15.16a to cover the entire biokinetic temperature range (Ratkowsky et al. 1983). The terms T_{min} and T_{max} can be used to classify microbes in a more objective manner as psychrophiles, mesophiles, or thermophiles (McDonald and Sun 1999). However, it should be stressed that since it is very difficult to obtain accurate data at extremely low growth rates, it should be pointed out that T_{min} and T_{max} may differ from the true temperature limits. Despite this problem, Equations 15.16 and 15.16a have been successfully applied to many data sets in the predictive microbiology literature.

Eyring's equation was applied in the pharmaceuticals sector (Kirkwood 1977) and it has the following mathematical expression (Equation 15.17):

$$\ln k = \ln\left(\frac{k_B}{h}\right) + \frac{S}{R} - \frac{H}{RT} + \ln T \tag{15.17}$$

where H is the heat of activation, h is the Planck constant, k_B is the Boltzmann constant, and S is the entropy. The significance of this equation lies in the fact that it relates the effect of temperature on the reaction rate constant to the fundamental terms of enthalpy and entropy changes and, consequently, one could estimate the enthalpy/entropy compensation in food reactions (Labuza 1980). If, for instance, the enthalpy of activation has a high value, this would lead to a quite slow reaction rate at moderate temperatures; this could, however, be compensated by an increase in activation entropy such that the reaction can still proceed at a measurable rate (Van Boekel 2000).

Temperature dependence has been traditionally expressed in the food industry and the food science and biochemistry literature as Q_{10} (Taoukis 2003). Q_{10} is defined as the ratio of the reaction rate constants at temperatures differing by 10°C

or the change of shelf life θ_s when the food is stored at a temperature higher by 10°C (Equation 15.18):

$$Q_{10} = \frac{k_{(T+10)}}{k_{(T)}} = \frac{\theta_s(T)}{\theta_s \cdot (T + 10)} \tag{15.18}$$

The Q_{10} approach in essence introduces a temperature dependence equation in the form of Equation 15.19:

$$k(T) = k_o \cdot e^{bT} \Rightarrow \ln k = \ln k_o + b \cdot T \tag{15.19}$$

which implies that if $\ln k$ is plotted versus temperature (instead of $1/T$ of the Arrhenius equation), a straight line is obtained. Alternatively, shelf life (t_s) can be plotted versus temperature, following Equation 15.20:

$$t_s(T) = t_{so} \cdot e^{-bT} \Rightarrow \ln t_s = \ln t_{so} - b \cdot T \tag{15.20}$$

where the resulting plots are often called shelf-life plots, where b is the slope of the shelf-life plot and t_{so} is the intercept. The *shelf-life plots* are true straight lines only for narrow temperature ranges of 10–20°C (Labuza 1984). Within this interval, Q_{10} and b are functions of temperature, correlated to the activation energy of the food quality deterioration reaction, following Equation 15.21

$$\ln Q_{10} = 10b = \frac{E_A}{R} \frac{10}{T \cdot (T + 10)} \tag{15.21}$$

Shown in Table 15.4 are the dependence of Q_{10} on temperature and E_A and important types of food reactions that fall in the respective range of values of Q_{10} and E_A.

Another term used for temperature dependence of microbial inactivation kinetics in canning and sometimes of food quality loss (Hayakawa 1973) is the z-value. The value of z is the temperature change that causes a tenfold change in the reaction rate constant. As in the case of Q_{10}, z depends on the reference temperature and is related to b and E_A by Equation 15.22:

$$z = \frac{\ln 10}{b} = \frac{(\ln 10) \cdot R \cdot T^2}{E_A} \tag{15.22}$$

TABLE 15.4
Q_{10} Dependence on E_A and Temperature

E_A (kJ/mol)	Q_{10} (at 5°C)	Q_{10} (at 20°C)	Q_{10} (at 40°C)	Typical Food Reactions
42	1.87	1.76	1.64	Diffusion controlled, enzymic, hydrolytic
85	3.51	3.10	2.70	Lipid oxidation, nutrient loss
125	6.58	5.47	4.45	Nonenzymic browning

15.2.3.2 Effect of Other Environmental Factors

Moisture content and water activity (a_w) are two among the most important E_j factors besides temperature that affect the rate of food deterioration reactions. Water activity describes the degree of boundness of the water contained in the food and its availability to act as a solvent and participate in chemical reactions (Labuza 1975).

Critical levels of a_w can be recognized above which undesirable deterioration of food occurs. Controlling a_w is the basis for preservation of dry and intermediate moisture foods (IMF). Minimum a_w values for growth can be defined for different microbial species. For example, the most tolerant pathogenic bacterium is *Staphylococcus aureus*, which can grow down to an a_w of 0.85–0.86. This is often used as the critical level of pathogenicity in foods. Beuchat (1981) gives minimum a_w values for a number of commonly encountered microorganisms of public health significance.

Textural quality is also greatly affected by moisture content and water activity. Dry, crisp foods (e.g. potato chips, crackers) become texturally unacceptable upon gaining moisture above the 0.35–0.5 a_w range (Katz and Labuza 1981). IMF like dried fruits and bakery goods, upon losing moisture below an a_w of 0.5–0.7, become unacceptably hard (Kochhar and Rossel 1982). Recrystallization phenomena of dry amorphous sugars caused by reaching an a_w of 0.35–0.4 affect texture and quality loss reaction rates, as already mentioned.

Besides the specific critical a_w limits, water activity has a pronounced effect on chemical reactions. This effect plays a very important role in the preservation of IMF and dry foods. Generally, the ability of water to act as a solvent, reaction medium, and as a reactant itself increases with increasing a_w. As a result, many deteriorative reactions increase exponentially in rate with increasing a_w above the value corresponding to the monolayer moisture. This can be represented schematically in a global food stability map (Figure 15.2).

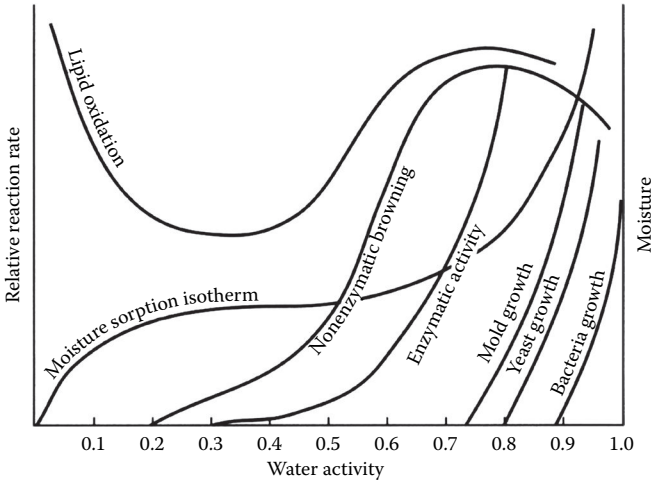


FIGURE 15.2 Indicative food stability map, showing the effect of a_w and moisture content on the rates of important deterioration reactions. (Adapted from Labuza, T. P. 1980. *Food Technology* 34(2):67.)

The critical a_w limits for microbial growth and the relative rates of reactions important to food preservation such as lipid oxidation and non-enzymatic browning can be seen in Figure 15.2. The underlying reasons for this behavior have been the subject of several studies (Taoukis and Richardson 2007). Most reactions have minimal rates up to the monolayer value. Lipid oxidation shows the peculiarity of a minimum at the monolayer (m_o) with increased rates below and above it (Labuza 1975; Quast et al. 1972).

The proposed theories that attempt to explain the effect of a_w on food deterioration reaction as well as ways to systematically approach and model this effect are discussed by Labuza (1980). The moisture content and water activity can influence the kinetic parameters (k_A, E_A), the concentrations of the reactants, and in some cases even the apparent reaction order, n. Most relevant studies have modeled either k_A as a function of a_w (Labuza 1980) related to the change of mobility of reactants due to a_w dependent changes of viscosity, or E_A as a function of a_w (Mizrahi et al. 1970a,b; Tazi et al. 2009; Vaikousi et al. 2008). The inverse relationship of E_A with a_w (increase in a_w decreases E_A and vice versa) could be theoretically explained by the proposed phenomenon of enthalpy–entropy compensation. The applicability of this theory and data that support it have been discussed by Labuza (1980).

Additionally, moisture content and a_w directly affect the glass transition temperature of the system. With increasing a_w, T_g decreases. As was discussed in the previous section, transverse of T_g and change into the rubbery state, has pronounced effects, not only in texture and viscosity dependent phenomena but also in reaction rates and their temperature dependence. It has been proposed for dehydrated systems that a critical moisture content/a_w alternative to the monolayer value of the BET theory, is the value at which the dehydrated system has a T_g of 25°C (Roos 1993). Consideration of these critical values contribute to explain textural changes occurring at distinct a_w and ambient temperatures (e.g., loss of crispness of snack foods above 0.3–0.5 or unacceptable hardness of IMF foods below 0.7–0.5) but their practical significance in a_w-dependent chemical reactions is not straightforward and cannot be viewed in isolation. Nelson and Labuza (1994) reviewed cases where the fundamental assumption that reaction rates within the ruberry state were dramatically higher than in the "stable" glassy state was not verified. In complex systems, matrix porosity, molecular size, and phenomena such as collapse and crystallization occurring in the rubbery state, result in more complicated behavior. Both water activity and glass transition theory contribute to explain the relationship between moisture content and deteriorative reaction rates. It should be stressed though, that in contrast to the well-established moisture isotherm determination, that is, the moisture–a_w relation, accurate determination of T_g as a function of moisture in a real food system is a difficult task and an area where much more work is needed. Furthermore, caution should be exercised when extrapolating state-of-the-art knowledge to matters of safety. Water activity, used as mentioned above as an index of microbial stability, is a well-established and practical tool in the context of hurdle technology. Additional criteria related to T_g should be considered only after careful challenge and sufficient experimental evidence (Chirife and Buera 1994).

Mathematical models that incorporate the effect of a_w as an additional parameter can be used for shelf-life predictions of moisture-sensitive foods (Cardoso and Labuza 1983; Mizrahi et al. 1970a; Risbo 2003). Such predictions can be applied to

packaged foods in conjunction with moisture transfer models developed based on the properties of the food and the packaging materials (Taoukis et al. 1988). Also accelerated shelf-life test (ASLT) methods have been used to predict shelf life at normal conditions based on data collected at high temperature and high humidity conditions (Mizrahi et al. 1970b).

Deterioration of a dehydrated low calorie dessert mix studied by Taoukis and Skiadi (1998) as a function of temperature, T, and water activity, a_w, is presented below as example. Kinetic studies of the reaction, characteristic for the quality degradation of this food, namely aspartame degradation were conducted. Apparent reaction rates, k, and the quality function of the food based on the above index, were determined at several temperature and a_w conditions. The dependence of k on these parameters was modeled as a function, $k = f(T,a_w)$, based on the Arrhenius relation.

The decomposition of aspartame as a function of temperature can be represented as an apparent first-order reaction by the equation:

$$\ln[\text{APM/APMo}] = -kt \tag{15.23}$$

Plot of ln[APM/APMo] as a function of time was a straight line as it was calculated with least-squares method, with slope, k (d^{-1}) and confidence level 95%. Table 15.5 summarizes rate constants and half-life for all conditions employed (T, a_w).

As can be seen in the Arrhenius plot (Figure 15.3), activation energy can be considered practically constant at the different water activities (parallel lines with $R^2 > 0.98$), while the Arrhenius constant k_A varies significantly for the different water activities. k_A can be given as a function of a_w by the equation $k_A = k_o \exp(b \cdot a_w)$, which gave a very good regression to the experimental data ($R^2 = 0.98$). The kinetic model can be expressed by the following equation:

$$\ln[\text{APM/APM}_\text{O}] = -k_o \exp\left(b \cdot a_w - \frac{E_A}{RT}\right) t \tag{15.24}$$

Constants k_o, b, and E_A were calculated by multiple linear regression of lnk versus $1/T$ and a_w, for all the data:

$$k_o = 7.73 \times 10^6\,\text{d}^{-1} \quad b = 2.24643 \quad \text{and} \quad E_A = 56.7\ \text{kJ/mol} \quad (R^2 = 0.976).$$

TABLE 15.5
Rate Constants and Half Life for Aspartame Degradation

	$a_w = 0.318$		$a_w = 0.492$		$a_w = 0.748$	
T (°C)	k	$t_{1/2}$ (days)	k	$t_{1/2}$ (days)	k	$t_{1/2}$ (days)
30	–0.00292	237	–0.00383	181	–0.00722	96
34	–0.00393	176	–0.00455	152	–0.01082	64
40	–0.00594	117	–0.00736	94	–0.01497	46
45	–0.00816	85	–0.01016	68	–0.02053	34

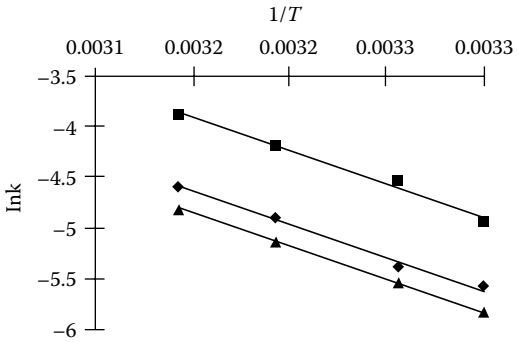


FIGURE 15.3 Arrhenius plot for aspartame degradation at a_w ▲ 0.318, ◆ 0.492, and ■ 0.748.

The pH of the food system is another determining factor. The effect of pH on different microbial, enzymatic, and protein reactions has been studied in model biochemical or food systems. Enzymatic and microbial activity exhibits an optimum pH range and limits above and below which activity ceases, much like the response to temperature. The functionality and solubility of proteins depend strongly on pH, with the solubility usually being at a minimum near the isoelectric point (Cheftel et al. 1985), having a direct effect on their behavior in reactions.

Examples of important acid–base catalyzed reactions are non-enzymatic browning and aspartame decomposition. Nonenzymatic browning of proteins shows a minimum near pH = 3–4 and high rates in the near neutral–alkaline range (Feeney et al. 1975; Feeney and Whitaker 1982). Aspartame degradation is reported at a minimum at pH = 4.5 (Holmer 1984), although the buffering capacity of the system and the specific ions present have significant effect (Tsoumbeli and Labuza 1991). Jalbout and Shipar (2007) proposed mechanisms of glyoxal and glycine in the advanced stage of non-enzymatic browning reaction and reported the basic condition as the most favorable for the production of pyrazines, followed by the isoelectric point of glycine (pH ≈ 6) and neutral conditions.

Few studies consider the interaction between pH and other factors, for example temperature. Such studies (Bell and Labuza 1994a,b; Weissman et al. 1993) show the significance of these interactions and the need for such information for the design and optimization of real systems. Significant progress in elucidating and modeling the combined effect to microbial growth of factors such as T, pH, a_w, or salt concentration has been achieved in the field of predictive microbiology (Coroller et al. 2012; Messens et al. 2003; Neumeyer et al. 1997; Panagou et al. 2010; Pin et al. 2011; Ross and McMeekin 1994; Rosso et al. 1995; Valero et al. 2009).

Gas composition also affects certain quality loss reactions. Oxygen affects both the rate and apparent order of oxidative reactions, based on its presence in limiting or excess amounts (Labuza 1971). Exclusion or limitation of O_2 by nitrogen flushing or vacuum packaging reduces redox potential and slows down undesirable reactions. Furthermore, the presence and relative amount of other gases, especially carbon dioxide, and second ethylene and CO, strongly affects biological and microbial reactions in fresh meat, fruit, and vegetables. The mode of action of CO_2 is partly connected

to surface acidification (Parkin and Brown 1982) but additional mechanisms, not clearly established, are in action. Quantitative modeling of the combined effect on microbial growth of temperature is an area of current research (Willocx et al. 1993). Different systems require different O_2–CO_2–N_2 ratios to achieve maximum shelf-life extension. Often excess CO_2 can be detrimental. Alternatively, hypobaric storage, whereby total pressure is reduced, has been studied. Comprehensive reviews of controlled and modified atmosphere packaging (CAP/MAP) technology are given by Kader (1986), Labuza and Breene (1989), and Sivertsvik and Jeksrud (2002).

Another important environmental aspect, recently assuming high investigating priority, is pressure. Traditionally, processing of foods has involved thermal treatments with the specific goal of making foods microbiologically safe. With greater concerns over the nutritional benefits of foods as well as qualitative aspects such as texture and color, investigation into advanced food-processing techniques has resulted in the emergence of various new technologies within the food industry. One area of recent interest is the use of ultra-high-pressure processing of foods, also referred to as high hydrostatic pressure and high-pressure processing. According to the Le Chatelier principle, any reaction, conformational change, or phase change that is accompanied by a decrease in volume will be favored at high pressure, while reactions involving an increase in volume will be inhibited.

Mathematical modeling of the effect of a specific technology during processing of foods on the quality and safety factors is a prerequisite for its optimal application. However, the extension of predictive modeling to food processing and design is a great challenge. The complexity of these models ranges from the simple (e.g., empirical kinetics) to the highly complex (e.g., fluid dynamics coupled with heat transfer and reactions) (Trystram 2012). For HHP processing, the effect of temperature and pressure on the rate constants of food deteriorative indices can be expressed through the Arrhenius and the Eyring equations, respectively (Johnson and Eyring 1970). The effect of both pressure and temperature on the remaining concentration of a quality or safety index may be expressed by more complex equation (Gogou et al. 2010; Katsaros et al. 2009; Valdramidis et al. 2007, 2012).

Key effects sought from high pressure technology include (Knorr 1993) (a) inactivation of microorganisms; (b) modification of biopolymers (protein denaturation, enzyme inactivation, or activation, degradation); (c) increased product functionality (e.g., density, freezing temperatures, texture); and (d) quality retention (e.g., color, flavor due to the fact that only nonvalent bonds are affected by pressure). Kinetic studies of changes occurring during high pressure processing and their effects on shelf life of the foods have been recently published and further research is necessary for this technology to be globally applied.

15.3 REACTION KINETICS IN SHELF-LIFE PREDICTION

15.3.1 Accelerated Shelf-Life Testing

When deciding about important aspects of a food product introduction to the market competition, knowledge of its shelf life and, in particular, the dependence of quality loss on temperature conditions is essential (Fu and Labuza 1993). The

criterion for the end of shelf life varies depending on the special characteristics of the product in question, and on consumer sensitivity. For most processed perishable or semiperishable foods, assuming that the essential requirement for product safety is met, their shelf life is based mostly on sensory and microbiological quality (Fu and Labuza 1993). For products with an extended shelf life, as in the case of most frozen foods, slow chemical reactions are the main deterioration pathways, which are frequently not readily recognizable by consumers. In addition, temperature fluctuations may occur in distribution and retail holding for frozen storage. If the objective is to get a rapid estimation of the expected shelf life of the product, then an ASLT can be used in the range of interest. Taking into account the limitations or possible deviations from the Arrhenius law, the ASLT involves the use of the Arrhenius equation at higher testing temperatures in a thorough shelf-life study and extrapolation of the kinetic results to normal, nonabusive storage conditions. This procedure is used to substantially reduce the experimental time, through the acceleration of the quality deterioration reactions.

Designing a shelf-life test is a synthetic approach that requires sufficient understanding of all food-related disciplines, namely food engineering food chemistry, food microbiology, analytical chemistry, physical chemistry, polymer science, and food regulations. The following steps outline the ASLT procedure:

1. Evaluate the microbiological safety factors for the proposed food product and process. The use of the hazard analysis critical control point principles is a good approach to be followed from the design stage. If major potential problems exist at this stage (i.e., CCPs exist that are difficult to control), the formula or process should be changed.
2. Determine from a thorough analysis of the food constituents, the process and the intended storage conditions, which biological and physicochemical reactions will significantly affect shelf life and hence can be used as quality loss indices. A good knowledge of the system, previous experience, and a thorough literature search are the tools to fulfill this step. If, from this analysis, it seems likely, without actual testing, that required shelf life is not likely to be achieved because of serious quality loss potential, product design improvement must be considered.
3. Select the package to be used for the shelf-life test. Frozen, chilled, and canned foods can be packaged in the actual product packaging. Dry products should be stored in sealed glass containers or impermeable pouches at the product's specified moisture and a_w.
4. Define the test's storage temperatures. Storage temperatures are chosen based on the type of shelf-life testing. Elevated temperatures are used in accelerated shelf-life testing to obtain data for prediction of shelf life at lower temperature or for prediction of shelf life under variable time–temperature distributions.
5. From the desired shelf life at the expected storage and handling temperatures, and based on available information on the most likely Q_{10}, calculate duration of testing at each selected temperature. If no information is

available on the expected Q_{10} value, minimum three testing temperatures should be used.

6. Decide the type and frequency of tests to be conducted at each temperature. A useful formula to determine the minimum frequency of testing at all temperatures based on the testing protocol at the highest temperature:

$$f_2 = f_1 \cdot Q_{10}^{\Delta T/10} \tag{15.25}$$

where f_1 is the time between tests (e.g., days, weeks) at highest test temperature T_1; f_2 is the time between tests at any lower temperature T_2; and T is the difference in degrees Celsius between T_1 and T_2. Usually, more frequent testing is recommended, especially if the Q_{10} is not accurately known. Use of too long intervals may result in an inaccurate determination of shelf life and invalidate the experiment. At each storage condition, at least six data points are required to minimize statistical errors; otherwise, the statistical confidence in the obtained shelf-life value is significantly reduced.

7. Plot the data as it is collected to determine the reaction order and to decide whether test frequency should be altered. It is a common practice for the data not to be analyzed until the experiment is over and then it is recognized that changes in the testing protocol, affected early on, would have added significantly to the reliability of the results.
8. From each test storage condition, determine reaction order and rate, make the appropriate Arrhenius plot, and predict the shelf life at the desired actual storage condition. Product can also be stored at the final condition, to determine its shelf life and test the validity of the prediction. However, in industry this is uncommon because of time and cost constraints. It is a much more effective and realistic practice to test the obtained predictive shelf-life model by conducting an additional test at a controlled variable temperature.

With an effective use of ASLT, an experiment that normally takes a year, can be completed in about a month, if the testing temperature is raised by 20°C. The duration of the shelf-life determination by ASLT depends on the E_A of the quality deterioration phenomena as shown in Table 15.6.

TABLE 15.6
Time to Complete an ASLT Test for a Low Moisture Food Product of 2 Years Targeted Shelf Life at Ambient Storage Depending on the Temperature Sensitivity (E_A) of the Shelf Life Determining Reaction

	ASLT Storage Temperature	
E_A (kJ/mol)	Testing Time at 40°C	Testing Time at 45°C
45	224 d	171 d
85	78 d	47 d
125	28 d	13 d

15.3.2 Temperature Dependence of Main Shelf-Life Indices

The first step to develop a reliable and accurate shelf-life model is to carefully select the most appropriate index that reflects the quality deterioration of the food of interest. For the description of quality loss, chemical, microbiological, and physical parameters are kinetically studied and the appropriate measuring techniques are applied. Based on relevant literature and the observations obtained by preliminary, accelerated tests, chemical and biological reactions, and physical changes are carefully evaluated to distinguish the factors that are most significant to product safety, integrity, and overall quality (Labuza 1984). Kinetic data relevant to shelf life exist in the current literature for most food products. A lot of these data are not fully exploitable as it is not a result of a systematic kinetic approach that would allow modeling and prediction for other conditions and similar systems.

Microbiological spoilage, lipid oxidation, nonenzymatic browning, and vitamin loss are among the most significant quality deteriorating factors that signal the end of food shelf life. Moreover, in a lot of recent work, more complicated models have been developed to integrate the effect of more than one parameter. For example, more complex models have been presented to describe microbial growth in fish products (Koutsoumanis et al. 2000; Tsironi and Taoukis 2014), in poultry meat (Bruckner et al. 2013), or in vegetable-based food products (Dekker et al. 2013; Manios et al. 2014). Mejlholm et al. (2010) proposed a model describing the effect of several variables (i.e., temperature, a_w, pH, phenol concentration, nitrites, and CO_2) on the growth of *Listeria monocytogenes* in processed and ready-to-eat meat and seafood. The application of high pressure (as a "cold pasteurization" method) has been also extensively kinetically studied recently in a variety of products (Katsaros et al. 2009a; Valdramidis et al. 2007; Zimmermann et al. 2013).

As far as nonenzymatic browning causing quality loss, numerous kinetic studies have been also recently published (Baeza et al. 2007; Damasceno et al. 2008; Purlis 2010; Quevedo et al. 2011; Valdramidis et al. 2010). Vaikousi et al. (2009) evaluated a kinetic model describing the observed browning responses of honey under dynamic heating conditions, to examine the applicability of the developed model over fluctuating temperature–time protocols.

When nutritional issues are selected as the dominating quality loss factor, vitamin C decrease is usually the shelf-life criterion used (Giannakourou and Taoukis 2003b; Polydera et al. 2003; Roig et al. 1999; Zheng and Hongfei 2011). Derossi et al. (2010) performed a kinetic study of ascorbic acid changes and shelf-life estimation of strawberry juice stored under nonisothermal conditions using a Weibullian-logistic model. B6 vitamin degradation was kinetically studied in beef muscle during cooking by Kondjoyan et al. (2013).

15.3.3 Shelf-Life Prediction and Management of the Food Chain

The main target of a thorough kinetic study, in a wide range of temperatures, of the behavior of dominating quality indices of a food, is a validated, mathematical shelf-life model. The application of this model would then allow for a reliable prediction of the quality loss of the product in question at time–temperature conditions that differ

from the experimental ones. This necessity of full knowledge of the effect of temperature on the loss of quality parameters, is the different time–temperature history of each product during its actual distribution in the postprocessing chain, to the consumer end. Previous and recent surveys in the retail and the consumer stocking level confirm the detrimental temperature abuse for chilled, as well as for frozen foods (Giannakourou and Taoukis 2003a; FRISBEE project database). Food products are, therefore, probably expected to be exposed to a variable temperature environment, that not infrequently includes stages of abusive storage or handling conditions.

To perform a kinetic analysis, the most common method is the classic successive two-step ordinary linear least-squares fit. The first step is the regression of the quality function (Table 15.1; i.e., A_o for zero-order, or ln (A_t/A_o) for a first-order reaction) versus time, at each temperature, to estimate the rate constant k, and the initial concentration A_o. The estimation of A_o avoids bias in the determination, and provides an additional criterion of the adequacy of the model to describe the experimental data. *A* significant discrepancy between the estimated and experimental A_o suggests that a problem exists. The problem may be due to an inadequate kinetic model, large experimental error, insufficient number of data, and so on. The second step is regression of ln(k) versus $[1/T - 1/T_{ref}]$ to obtain the estimate of k_{ref} and E_A/R (Equation 15.10).

In a general form, the value of the quality function at time t is calculated by the following integral Equation 15.26, where $T(t)$ describes the change of temperature as a function of time:

$$f_q(A) = \int k[T(t)]\, dt \tag{15.26}$$

To represent the integrated effect of the temperature variability on product quality degradation, the term of the effective temperature, T_{eff}, can be introduced. T_{eff} is defined as the constant temperature that results in the same quality value as the variable temperature distribution over the same time period. This approach that equals the overall effect of a nonisothermal handling with a single, constant value simplifies Equation 15.26 to the following expression (Equation 15.27):

$$f_q(A) = \int_0^{t_{tot}} k(T(t))\, dt = k_{eff} t_{tot} \tag{15.27}$$

where k_{eff} is the value of the rate of the quality loss reaction at the effective temperature. If the $T(t)$ function can be described by a step sequence, or, equivalently, can be discretized in small time increments t_i of constant temperature T_i (with $\Sigma t_i = t_{tot}$), then Equation 15.20 can be expressed by Equation 15.28, assuming the applicability of Arrhenius equation:

$$k_{ref} \sum_i \left(\exp\left[-\frac{E_A}{R} \left(\frac{1}{T_i} - \frac{1}{T_{ref}} \right) \right] t_i \right) = k_{eff} t_{tot} \tag{15.28}$$

From Equation 15.28, the value of k_{eff} can be estimated, and subsequently, from the Arrhenius model, the effective temperature T_{eff} can be calculated.

To calculate the fraction of shelf life consumed at the end of each stage, f_{con}, the time/temperature/tolerance (TTT) approach (Fu and Labuza 1993; Van Arsdel et al. 1969) can be used. According to this methodology, the f_{con} is estimated as the sum of the times at each constant temperature segment t_i, divided by the shelf life at that, particular temperature θ_i (Equation 15.29):

$$f_{con} = \sum \frac{t_i}{\theta_i} \tag{15.29}$$

where index i represents the different time–temperature steps within the particular stage of study. The remaining shelf life of products can be calculated at a reference temperature, representative of their storage conditions, after each stage as $(1 - \Sigma f_{con})\theta$, where θ is the shelf life at that reference temperature.

15.4 APPLICATION OF FOOD KINETICS IN SHELF-LIFE PREDICTION: EXAMPLES OF SHELF-LIFE MODELING OF FOOD PRODUCTS

EXAMPLE 1: VITAMIN C LOSS IN FROZEN GREEN PEAS

When trying to apply food kinetics in shelf-life prediction, in most practical cases a three-step methodology, already described in the section of accelerated shelf-life testing, is used due to its simplicity and convenience. In the first case study presented, the quality loss of frozen green peas (Giannakourou and Taoukis 2003b) was assessed. More specifically, the successive stages of study involved the following:

First Stage: Kinetic Analysis of the Main Quality Indices of Frozen Green Peas

In this stage, the main quality indices of frozen green peas were studied under different, isothermal conditions, continuously monitored and registered, through data loggers. Color, texture, and vitamin C loss were chosen as the most appropriate quality attributes, describing in an adequate way frozen green peas quality profile. In this case study, vitamin C loss will be presented in detail, aiming at producing a kinetic model that mathematically describes this degradation in the whole range of frozen storage. The average retention of ascorbic acid is expressed relatively to an initial, average value of day 0 of the experiment, where C_{vit} represents the concentration of ascorbic acid in 100 g of raw material. The first step of a kinetic study is to assess the order of the reaction (vitamin C loss). Therefore, measurements of vitamin C were carried out at appropriate time intervals, at five constant temperatures. Analysis of this information versus time showed that in all cases, vitamin C loss could be adequately described by an apparent first-order reaction (Equation 15.30):

$$C_{vit} = C_{vit0}e^{-k_{vit}t} \quad \text{or} \quad \ln\frac{C_{vit}}{C_{vit0}} = -k_{vit}t \tag{15.30}$$

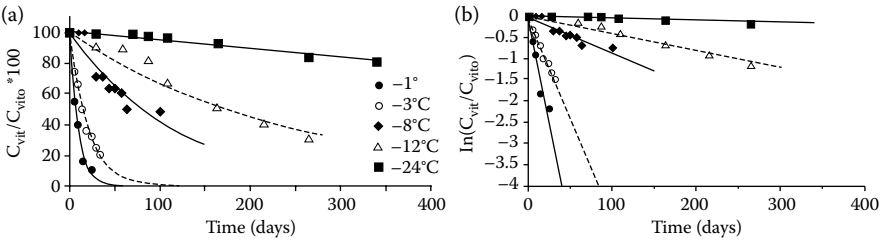


FIGURE 15.4 Vitamin C loss of frozen green peas during its storage at five temperatures (a) in C_{vit}/C_{vit0} versus t axis and (b) in $\ln(C_{vit}/C_{vit0})$ versus t axis.

where C_{vit} and C_{vit0} are the concentrations of L-ascorbic acid at time t and zero, respectively, and k_{vit} is the apparent reaction rate of vitamin C loss, estimated by the slope of the linearized plot of $\ln(C_{vit}/C_{vit0})$ versus t. In Figure 15.4a and b, vitamin C loss is shown in different axis, so as to demonstrate the choice of apparent first order.

Second Stage: Temperature Dependence of the Reaction

After determining the most important and representative quality indices for the specific product and deciding the reaction order of the quality loss reaction, the temperature dependence of the reaction is assessed. Initially, the Arrhenius kinetics was applied using the slopes calculated for all temperatures of Figure 15.4b and Equation 15.10 (Figure 15.5).

Indeed, Arrhenius kinetics expressed adequately the temperature dependence of vitamin C loss, and the estimated activation energies E_A are shown in Table 15.7. In the same table, for practical reasons, Q_{10} value has been also calculated.

Apart from the previous analysis, an alternative approach of modeling the temperature dependence of the deterioration reaction was also applied, namely the WLF equation (Equation 15.12). WLF model ($T_g' \cong -25°C$ and $T_{ref} = -20°C$), shown in Figure 15.6 for green peas, gives an adequate fit ($R^2 = 0.957$) but the estimated coefficient values ($C_1 = -3.5$ and $C_2 = 35.4$) were out of the range referenced in the literature as WLF values in the rubbery state (Roos 1995; Slade and Levine 1991).

These results do not support any preference at the WLF model over the Arrhenius in the temperature range tested for the specific tissue studied. The Arrhenius approach was deemed adequate to represent temperature dependence

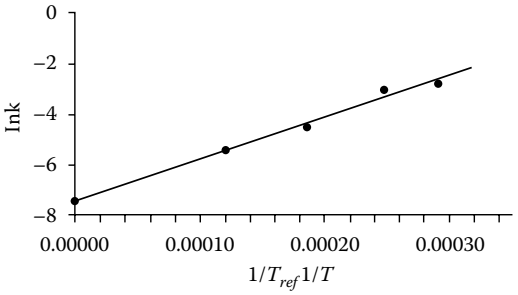


FIGURE 15.5 Arrhenius plot of the temperature dependence of the rates of vitamin C loss of frozen green peas ($T_{ref} = -20°C$).

TABLE 15.7
Arrhenius Parameters and Statistics, Q_{10} Values and Shelf Life at Four Temperatures in the Frozen Storage Range for Frozen Green Peas

Kinetic Parameters for Vitamin C Loss in Frozen Green Peas	
E_A (kJ/mol)	97.9 ± 9.6[a]
k_{ref} (1/d)	0.00213
R^2	0.958
Q_{10} (in the range –15 to –5°C)	5.5
Shelf Life (days)[b]	
Temperature	
–5°C	24
–10°C	56
–15°C	132
–20°C	325

[a] 95% confidence intervals based on the statistical variation of the kinetic parameters of the Arrhenius model (regression analysis).
[b] Shelf life is based on 50% vitamin C loss.

of ascorbic acid degradation within the rubbery state of frozen vegetable matrices, such as green peas.

Third Stage: Kinetic Model Validation under Nonisothermal Conditions

In this stage, the mathematical models developed under isothermal conditions should be tested and verified under dynamic storage conditions, to be able to expand their applicability at realistic, nonisothermal time–temperature conditions. The established kinetic model of vitamin C loss was validated at dynamic storage conditions in programmable freezer-incubators. To demonstrate the integrated effect of the temperature variability on product quality, the term of the effective temperature T_{eff} is introduced. T_{eff}, which is defined as the constant temperature that results in the same quality value as the variable temperature distribution over the same time period, is based on the Arrhenius model and integrates in a single

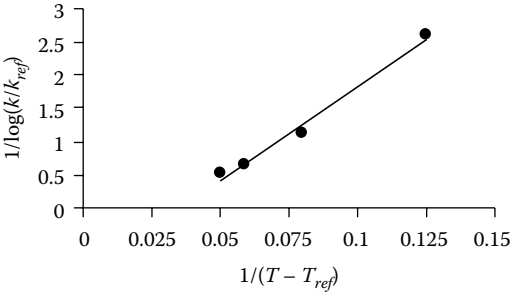


FIGURE 15.6 WLF plot of the temperature dependence of the rates of vitamin C loss of frozen green peas (T_{ref} = –20°C).

value the effect of the variable temperature profile. In this case, the validation experiment involved storage of green peas in an incubator programmed so as to have a $T_{eff} \approx -4.4$°C (Figure 15.7).

Predicted rate of loss, k_{eff}, $k_{pred} = 0.0268 \pm 0.0038$ (1/d) is in good agreement with the experimentally estimated ones, k_{exp}, $k_{exp} = 0.0252$ (1/d) ($R^2 = 0.947$), so that the established kinetic model is deemed adequate to predict vitamin C loss under variable temperature conditions. Based on the validated kinetic model, the shelf life of green peas at different temperatures in the frozen range, based on nutritional criteria is reported in Table 15.7.

As it will be clearly illustrated in the following example, the importance of the model's validation under dynamic conditions is to reliably expand its use in real time–temperature conditions of the chill chain, that may deviate significantly from the ideal or even the expected ones (Giannakourou and Taoukis 2003a, 2007).

EXAMPLE 2: QUALITY DETERIORATION OF FROZEN FISH PRODUCTS

To demonstrate the usefulness of the TTT approach in assessing the effect of temperature conditions during transport and storage on food quality, an example in the real distribution chain of frozen foods is considered. This case study is based on experimental data on the quality loss of blueshark slices (*Prionace glauca*) generated recently within IQ-Freshlabel European Project. The objective of IQ-Freshlabel (www.iq-freshlabel.eu) is the development and testing of intelligent labels for chilled and frozen food products and the promotion of the influence of smart labels application on waste reduction, food quality, and safety in the European supply chains. Methodology is developed for the selection of the optimum time–temperature integrators (TTI) design of specific frozen fish products, and their application is validated in cold chain simulating trials (Giannoglou et al. 2013).

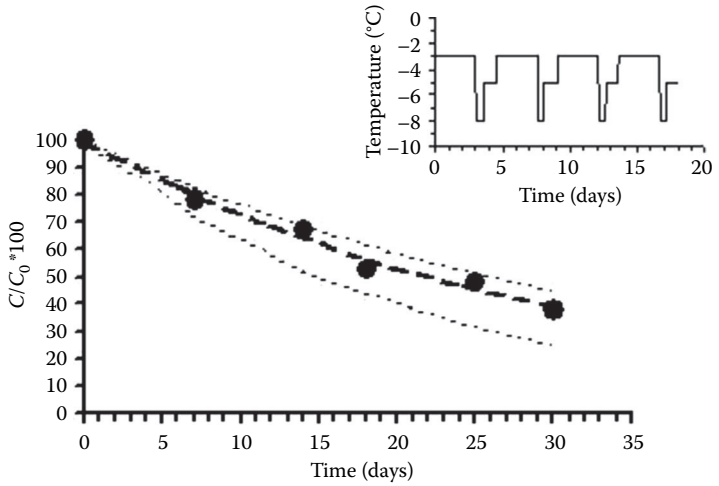


FIGURE 15.7 Comparison of experimental (closed circles) and predicted results of vitamin C loss of frozen green peas for exposure at the shown variable temperature profile. The solid line represents the exponential fit of the quality measurements and dotted lines depict the upper and lower 95% confidence range of quality predicted for T_{eff}.

In this study, the quality loss of frozen blueshark slices was assessed and the methodology used also included three main steps, as previously described in the previous example. The parameters chosen for frozen blueshark slices were 2-thiobarbituric acid reactive substances (TBARS), total volatile basic nitrogen (TVB-N), and sensory scoring, which were measured in the temperature range between –5°C and –12°C (accelerated shelf-life test). An independent experiment at –15°C was also implemented for the validation of the developed mathematical models. TVB-N increased following first-order kinetics. TBARs increased and sensory scoring (overall impression) decreased with time following zero-order kinetics. The rates of TVB-N, TBARs, and sensory scoring changes of frozen blueshark slices, as calculated by the fittings in Figure 15.8a–c, are presented in Table 15.8.

Based on the values selected at the end of shelf life of the aforementioned indices and the temperature dependence of their rate constants expressed by the Arrhenius kinetics, the following equations for shelf-life calculation can be used, respectively:

$$\frac{\ln C_{TVB-N,l}}{C_{TVB-N,o}} = k_{ref,TVB-N} \cdot \exp\left[\frac{-E_{a(TVB-N)}}{R}\left(\frac{1}{T} - \frac{1}{T_{ref}}\right)\right] \cdot t_{SL} \tag{15.31}$$

$$C_{TBARs,l} - C_{TBARs,o} = k_{ref,TBARs} \cdot \exp\left[\frac{-E_{a(TBARs)}}{R}\left(\frac{1}{T} - \frac{1}{T_{ref}}\right)\right] \cdot t_{SL} \tag{15.32}$$

$$s_l - s_o = k_{ref,s} \cdot \exp\left[\frac{-E_{a(s)}}{R}\left(\frac{1}{T} - \frac{1}{T_{ref}}\right)\right] \cdot t_{SL} \tag{15.33}$$

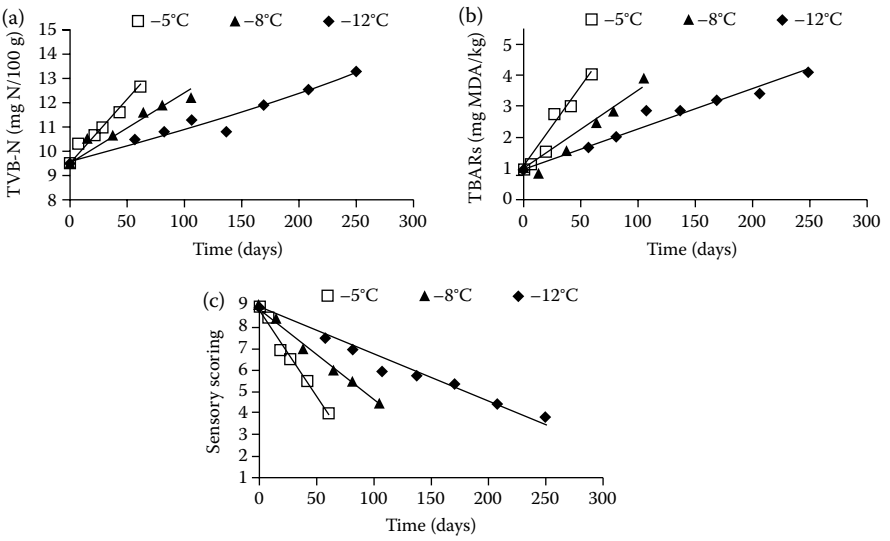


FIGURE 15.8 Quality deterioration of frozen blueshark slices during isothermal storage at –5°C, –8°C, and –12°C (a) TVB-N, (b) TBARs, and (c) sensory scoring (overall impression).

TABLE 15.8
Rates of TVB-N, TBARs, and Sensory Scoring Changes of Frozen Blueshark Slices Stored Isothermally at –5°C, –8°C, and –12°C and Statistics of Curve Fittings

	TVB-N		
Temperature	k **(days^{-1})**	R^2	**Equation**
–5°C	0.0048	0.959	$\frac{C_{TVB-N}}{C_{TVB-N_o}} = \exp(k_{TVB-N} \cdot t)$
–8°C	0.0026	0.886	
–12°C	0.0013	0.939	
	TBARs		
Temperature	k **(days^{-1})**	R^2	**Equation**
–5°C	0.0511	0.952	$C_{TBARs} = C_{TBARs_o} + k_{TBARs} \cdot t$
–8°C	0.0250	0.939	
–12°C	0.0129	0.959	
	Sensory Scoring		
Temperature	k **(days^{-1})**	R^2	**Equation**
–5°C	– 0.0850	0.993	$s_{ov.impr.} = s_{ov.impr._o} + k_{ov.impres.} \cdot t$
–8°C	– 0.0444	0.989	
–12°C	– 0.0218	0.926	

where t_{SL} is the shelf life (days) of frozen blueshark slices, $C_{TVB\text{-}N,l}$, $C_{TBARS,l}$, and s_l are the limits for TVB-N, TBARs, and overall impression, respectively, $C_{TVB\text{-}N,o}$, $C_{TBARS,o}$, and s_o are the initial TVB-N, TBARs, and overall impression, respectively, k_{ref} is the rate constant of change of each quality index at $T_{ref} = -15$°C, E_A is the activation energy of the respective quality index and R is the universal gas constant.

After determining the most important and representative quality indices for the specific product and deciding the reaction order of the quality loss reaction, the temperature dependence of the reaction is assessed based on the Arrhenius kinetics and Equations 15.31 through 15.33 (Figure 15.8a–c and Figure 15.9a–c) (Giannoglou et al. 2013). The parameters of the developed models for each quality index are presented in Table 15.9.

The equations developed allow for the estimation of shelf life of frozen blueshark slices if the storage temperature is known. To validate the mathematical models, an independent long-lasting experiment is carried out at –15°C and the experimentally determined quality deterioration rates are compared with the predictions of the developed mathematical models (Table 15.10):

$$\%RE = [(k_{\exp} - k_{pred})/k_{\exp}] \times 100 \tag{15.34}$$

The results of the previous kinetic analysis will be verified in this stage, under dynamic storage conditions, to be able to expand their applicability at realistic, nonisothermal time–temperature conditions. The importance of this "expanded" use is underlined by the diversity of time–temperature handling of a product during its actual distribution in the postprocessing chain, to the consumer end (Giannakourou and Taoukis 2007) as confirmed by recent data, retrieved by the

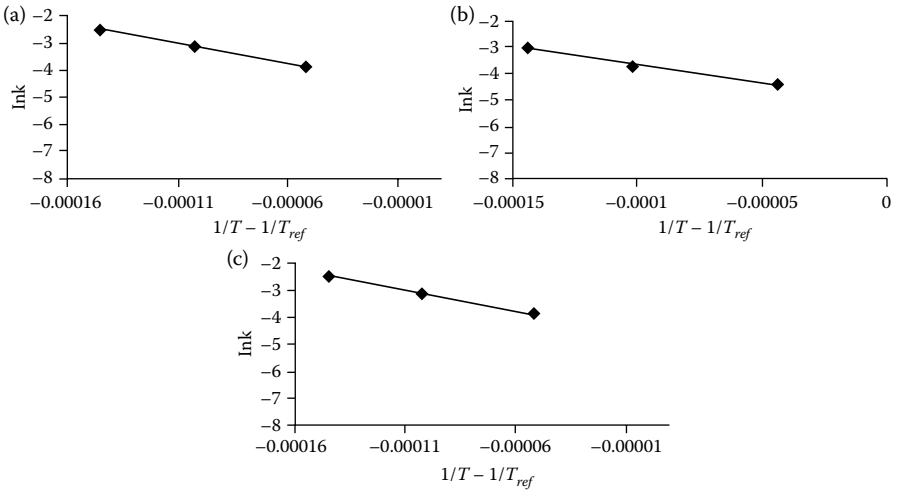


FIGURE 15.9 Arrhenius plots of (a) TVB-N, (b) TBARs, and (c) sensory scoring change rates for the temperature range –5°C to –12°C.

user-friendly database of the FRISBEE project (Food Refrigeration Innovations for Safety, Consumers' Benefit, Environmental Impact and Energy Optimisation Along the Cold Chain in Europe, FP7, Food, Agriculture and Fisheries, and Biotechnology). Based on this set of data, carried out at almost 320 retail display points for frozen foods in different countries, it was shown that in almost 36% of retail storage the temperature was higher than –18°C, with 8% exceeding the –14°C. As far as home freezing cabinets are concerned, from the same database (including almost 200 households), it was found that in more than 30% of cases, operating temperatures were inappropriate for frozen foods storage (Figure 15.10a and b).

On the basis of these observations, products may be exposed to very different temperature conditions that could also include stages of abusive storage or handling conditions.

To fully understand the need to take into account the real time–temperature history of the product, and not assume a common scenario, the methodology previously described for kinetic analysis will be used, for the case study of frozen blueshark. Using Equation 15.29 and the kinetic results of Table 15.9, the fraction of shelf life consumed at the end of each stage, f_{con}, can be calculated. To illustrate the importance of assessing the effect of the real temperature conditions during transport and storage on food quality, a realistic scenario of 200 days distribution will be studied, based on FRISBEE database. It includes an initial stage of 40 days storage in the packing plant, followed by transportation and storage in a distribution center for 40 days. Subsequently, frozen blueshark slices are kept at the retail display for 60 days, before being purchased by the final consumers that store them in their domestic freezer for 60 days before cooking and consumption. At the end of the assumed cycle, that is, the time of consumption, the remaining shelf life of frozen blueshark slices (at –15°C) according to TVB-N value and sensory acceptability will be estimated.

The nominal remaining shelf life at –15°C, which does not consider the time–temperature history of the products, would be more than 100 days.

TABLE 15.9
Selected Parameters and Values of the Developed Arrhenius-Type Shelf-Life Models for Frozen Blueshark Slices (T_{ref} = –15°C, R = 8.314 J/mol K)

TVB-N		TBARs		Overall Impression	
$C_{TVB\text{-}N,o}$ (mg/100 g)	9.6	$C_{TBAR's,o}$ (mgMDA/100 g)	0.98	$S_{,o}$	9
$C_{TVB\text{-}N,l}$ (mg/100 g)	12	$C_{TBARs,l}$ (mgMDA/100 g)	3.5	$S_{,l}$	5
$k_{ref,\ TVB\text{-}N}$ (d^{-1}):	0.00072 ± 0.00001	$k_{ref,\ TBARs}$ (d^{-1}):	0.0068 ± 0.0002	$k_{ref,S}$ (d^{-1}):	0.0101 ± 0.0010
$E_{a,\ TVB\text{-}N}$ (kJ/mol)	108.1 ± 6.7	$E_{a,\ TBARs}$ (kJ/mol)	113.4 ± 5.3	$E_{a,S}$ (kJ/mol)	121.9 ± 2.4
R^2	0.997	R^2	0.988	R^2	0.999

TABLE 15.10
Quality Deterioration Rates of Frozen Blueshark Slices Stored at –15°C Calculated by the Arrhenius-type Model (k_{pred}) and Determined Experimentally (k_{exp}) and Relative Errors (RE)

TVB-N		TBARs		Overall Impression	
k_{pred} (d^{-1})	k_{exp} (d^{-1})	k_{pred} (d^{-1})	k_{exp} (d^{-1})	k_{pred} (d^{-1})	k_{exp} (d^{-1})
0.00072	0.00064	0.0068	0.0069	0.0101	0.0117
RE = –12.5%		RE = –1.4%		RE = 13.7%	

Therefore, applying the main principles of TTT approach, the shelf life of frozen blueshark slices was estimated—and subsequently the value of f_{con}—at the end of each stage, taking as main quality criterion either TVB-N value or sensory scoring, two indices which were shown to give similar results. To demonstrate the significance of the real temperature conditions, two alternative distribution scenarios were assumed, both retrieved from FRISBEE database, based on data input of the real frozen chain. The first scenario, scenario (a) (Figure 15.11a) was a milder one, with very low temperatures at the first two stages of the chain (warehouse and distribution center). In Figure 15.11b, f_{con} is plotted at the end of each stage, showing that the end of the cycle, the frozen product is still of more than acceptable quality, since f_{con} is only 0.5, meaning that it still has almost 200 days of remaining shelf life if isothermally handled at –15°C (more than its nominal remaining shelf life). It should be also pointed out that both quality criteria tested (TVB-N and sensory scoring) give the same estimation of the fraction of shelf life consumed.

Alternatively, applying a more abusive scenario (scenario (b)) (Figure 15.12a), remaining shelf life is estimated at the end of each stage (estimated at an isothermal handling at –15°C). In this case, at the end of its lifecycle, frozen blueshark slices have less than 50 days (45 days) of remaining shelf life, if isothermally handled at –15°C, much less than expected—based on the "use by" date-remaining shelf life.

On the basis of the aforementioned observations, the significance of monitoring the real time–temperature history of the product throughout its distribution is illustrated, to reliably estimate its quality status, at any point of its lifecycle. If the temperature conditions of the products could be continuously monitored, for example, by inexpensive time–temperature integrators, reliable estimation of the

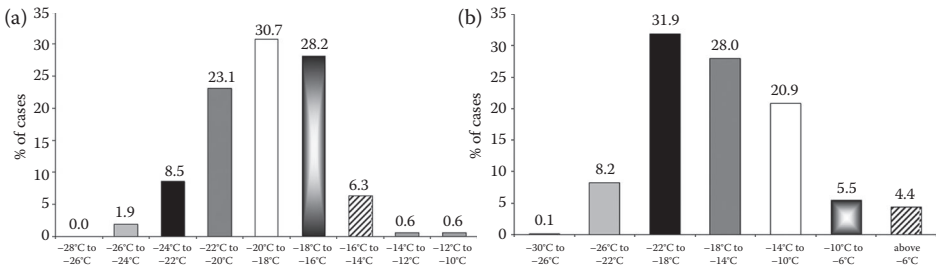


FIGURE 15.10 Temperature distribution in (a) retail display and (b) domestic freezers. (From database of FRISBEE project 2013.)

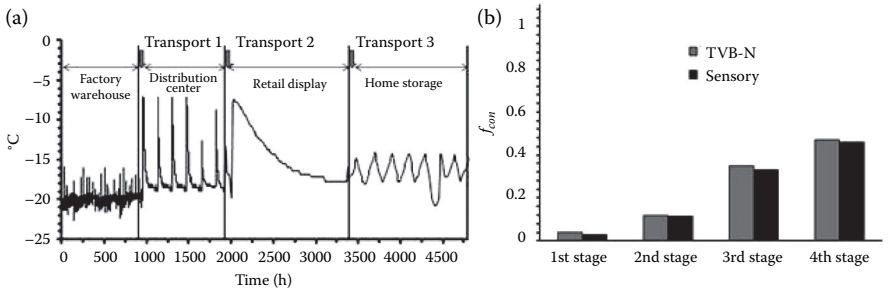


FIGURE 15.11 (a) Indicative temperature distribution (scenario (a)) (From database of FRISBEE project 2013) of frozen blueshark slices and (b) fraction of total shelf life consumed at the end of each stage.

quality status and the remaining shelf life of the products could be performed based on the presented modeling of the quality indices. This could allow better management and optimization of the cold chain from manufacture to consumption.

15.5 APPLICATION OF TTI AS SHELF-LIFE PREDICTORS DURING DISTRIBUTION

Smart or intelligent packaging allows monitoring of the shelf life in the dynamic conditions of the food chain. TTI are smart labels that show an easily measurable, time–temperature-dependent change that cumulatively reflects the time–temperature history of the food product (Taoukis and Labuza 2003). Prerequisite for application of TTI is the systematic kinetic modeling of the temperature dependence of shelf life of the target food products. Similar kinetic study is needed for the TTI response. On the basis of reliable models of the shelf life and the kinetics, both the products and the TTI response, the effect of temperature can be monitored, and quantitatively translated to food quality, from production to the point of consumption. The selection and use of the optimum TTI for a particular product could lead to realistic control of the cold chain (Tsironi et al. 2011) while reliable estimation of the quality status and the

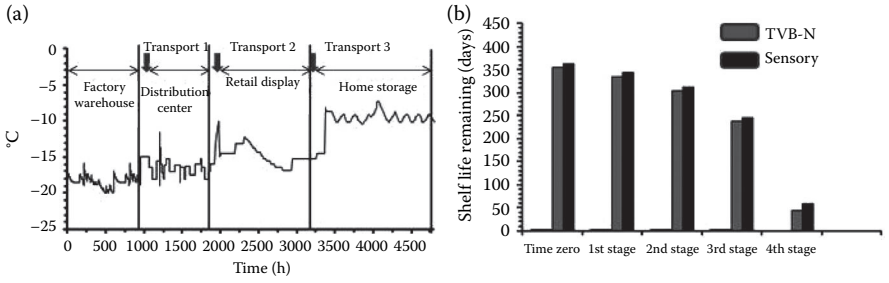


FIGURE 15.12 (a) Indicative temperature distribution (scenario (b)) (From database of FRISBEE project 2013) of frozen blueshark slices and (b) remaining shelf life at the end of each stage, estimated at –15°C.

remaining shelf life could be performed, allowing better management and optimization from production to the point of consumption (Giannakourou et al. 2001; Tsironi et al. 2008).

The basic principles of TTI modeling and application for quality monitoring are detailed (Taoukis and Labuza 1989a, b). Combining Equations 15.25 and 15.26, loss of shelf life of a food (based on the deterioration of the selected index, C) can be expressed (Taoukis et al. 2012):

$$f_q(C) = k_{C_{ref}} \exp\left(-\frac{\mathrm{E_A}}{\mathrm{R}}\left(\frac{1}{T} - \frac{1}{T_{ref}}\right)\right) t \tag{15.35}$$

where E_A is the activation energy of the reaction that controls quality loss. Similar to Equation 15.35, a response function $F(X)$ can be defined for TTI such that $\mathrm{F(X)} = k_I t$, with k_I an Arrhenius function of T.

The value of the functions, $f_q(C)_t$ at time t, after exposure at a known variable temperature exposure, $T(t)$, can be found by Equation 15.27, when the term of the effective temperature T_{eff} is introduced. For a TTI exposed to the same temperature fluctuations, $T(t)$, as the food product, and corresponding to an effective temperature T_{eff}, the response function can be similarly expressed as

$$F(X) = k_{I_{ref}} \int_0^t \exp\left(-\frac{E_{A_I}}{R}\left(\frac{1}{T} - \frac{1}{T_{ref}}\right)\right) dt = k_{I_{ref}} \exp\left(-\frac{E_{A_I}}{R}\left(\frac{1}{T_{eff}} - \frac{1}{T_{ref}}\right)\right) t \tag{15.36}$$

where $k_{I_{ref}}$ and E_{A_I} are the Arrhenius parameters of the TTI.

Thus, the basic elements for a TTI-based food quality monitoring scheme are (a) a well-established kinetic model to describe quality loss of the food; (b) the response function of the TTI; and (c) the temperature dependence of both food quality loss and TTI response rate, expressed by the respective values of the activation energies. The essence in TTI implementation algorithm lies in the calculation of the T_{eff} of the exposure (Equation 15.36), based on the TTI response reading (Figure 15.12), that is, assumed to describe the integrated effect of temperature history on food quality loss. This assumption requires that food quality degradation and TTI response rate are similarly affected by temperature, that is, the activation energies of the two phenomena do not differ by more than 25 kJ/mol. Under these conditions the application scheme would reliably provide the extent of the quality deterioration of the food and a prediction of the remaining shelf life at any assumed average storage temperature (Taoukis et al. 2012).

According to previous studies (Giannakourou and Taoukis 2002, 2003a; Giannakourou et al. 2005; Tsironi et al. 2009, 2011), it was well established that at any point of distribution, if the appropriate TTI was selected based on the aforementioned criteria (illustrated in Figure 15.13), TTI response could be correlated to the quality level and provide a reliable indication of the product's remaining shelf life.

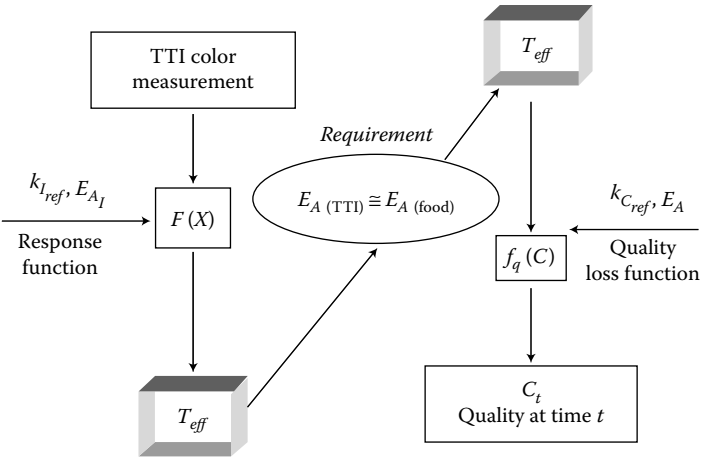


FIGURE 15.13 Application scheme of TTI as quality monitors and tools for predicting food remaining shelf life. All kinetic data necessary as input for food quality loss and TTI response are also shown (From Taoukis, P. S., Giannakourou, M.C., and Tsironi, T.N. 2012. In *Handbook of Frozen Food Processing and Packaging*, ed. D.W. Sun, 2nd edn., Chapter 13, Boca Raton: CRC Press, Taylor & Francis, pp. 273–299.)

Furthermore, based on TTI prediction, an optimized management system for frozen product distribution management and stock rotation, least shelf life first out was developed, as an alternative to the conventional "first in first out policy" (Giannakourou and Taoukis 2002, 2003a, Tsironi et al. 2009). The application of least shelf life first out, which promotes products based on TTI's indication instead of a random rotation system, reduces rejected products and improves quality distribution at consumer levels.

TTI can be consequently considered as useful decision-support tools for the optimization of the current inventory management system, to improve consumer's acceptability. With continuous improvement, this stock-rotation policy could encompass information about the initial quality variability of raw material, process parameters, and so on, additionally to the temperature variability (Koutsoumanis et al. 2002; Giannakourou et al. 2001).

Overall, the cornerstone of any quality management system is reliable and validated kinetic models based on the principles described in this chapter and outlined in the presented examples.

REFERENCES

Arabshashi, A., and Lund, D. B. 1985.Considerations in calculating kinetic parameters from experimental data. *Journal of Food Process Engineering* 7:239–251.

Baeza, R., Milenicki, D., Zamora, M. C., and Chirife, J. 2007. Effect of environmental daily temperature fluctuations over one year storage on the prediction of non-enzymatic browning in reduced-moisture foods stored at "ambient" temperature. *Food Control*. 18:1532–1537.

Belehradek, J. 1930. Temperature coefficients in biology. *Biological Reviews* 5(1):30–58.

Bell, L. N., and Labuza, T. P. 1994b. Influence of the low-moisture state on pH and its implications for reaction kinetics. *Journal of Food Engineering* 22:291–312.

Bell, L. N., and Labuza, T. P. 1994a. Aspartame stability in commercially sterilized flavored dairy beverages. *Journal of Dairy Science* 77:34–38.

Beuchat, L. R.1981. Microbial stability as affected by water activity. *Cereal Foods World* 26:345–349.

Biliaderis, C. G., Swan, R. S., and Arvanitoyannis, I. 1999. Physicochemical properties of commercial starch hydrolyzates in the frozen state. *Food Chemistry* 64:537–546.

Blond, G., and Simatos, D. 1991. Glass transition of the amorphous phase in frozen aqueous systems. *Thermochimica Acta* 175:239–247.

Bruckner, S., Albrecht, A., Petersen, B., and Kreyenschmidt, J. 2013.A predictive shelf life model as a tool for the improvement of quality management in pork and poultry chains. *Food Control* 29:451–460.

Buchanan, R. L. 1993. Predictive food microbiology. *Trends Food Science and Technology* 4:6–11.

Buedo, A. P., Elustondo, M. P., and Urbicain, M. J. 2001. Non-enzymatic browning of peach juice concentrate during storage. *Innovative Food Science & Emerging Technologies* 1:255–260.

Buera, P. and Karel, M. 1993. Application of the WLF equation to describe the combined effects of moisture, temperature and physical changes on non-enzymatic browning rates in food systems. *Journal of Food Processing and Preservation* 17:31–47.

Bushill, J. H., Wright, W. B., Fuller, C. H. F., and Bell, A. V. 1965. The crystallization of lactose with particular reference to its occurrence in milk powders. *Journal of the Science of Food and Agriculture* 16:622.

Cardoso, G., and Labuza, T. P. 1983. Effect of temperature and humidity on moisture transport for pasta packaging material. *British Journal of Food Technology* 18:587.

Carrington, A. K., Goff, H. D., and Stanley, D. W. 1996. Structure and stability of the glassy state in rapidly and slowly cooled carbohydrate solutions. *Food Research International* 29(2):207–213.

Champion, D., Blond, G., Le Meste, M., and Simatos, D. 2000. Reaction rate modeling in cryoconcentrated solutions: Alkaline phosphatase catalyzed DNPP hydrolysis. *Journal of Agricultural and Food Chemistry* 48:4942–4947.

Cheftel, J. C., Cuq, J., and Lorient, D. 1985. Aminoacids, peptides and proteins. In: *Food Chemistry*, ed. O. R. Fennema, New York: Marcel Dekker.

Chiralt, A., Martinez-Navarette, N., Martinez-Monzo, J., Talens, P., Moraga, G., Ayala, A., and Fito, P. 2001. Changes in mechanical properties throughout osmotic processes. Cryoprotectant effect. *Journal of Food Engineering*. 49:129–135.

Chirife, J., and Buera, P. 1994. Water activity, glass transition and microbial stability in concentrated/semimoist food systems. *Journal of Food Science* 59:921–927.

Coroller, L., Kan-King-Yu, D., Leguerinel, I., Mafart, P., and Membre, J. M. 2012. Modelling growth, growth/no growth interface and non thermal inactivation areas of *Listeria* in foods. *International Journal of Food Microbiology*. 152:139–152.

Damasceno, L. F., Fernandes, F. N., Magalhãesa, M. A., and Brito, E. S. 2008. Non-enzymatic browning in clarified cashew apple juice during thermal treatment: Kinetics and process control. *Food Chemistry* 106(1):172–179.

Dekker, M., Dekkers, E., Jasper, A., Baár, C., and Verkerk, R. 2013. Predictive modelling of vegetable firmness after thermal pre-treatments and steaming. *Innovative Food Science & Emerging Technologies* (In press, doi: 10.1016/j.ifset.2013.10.015).

Derossi, A., De Pilli, T., and Fiore, A. G. 2010. Vitamin C kinetic degradation of strawberry juice stored under non-isothermal conditions. *LWT—Food Science and Technology* 43(4):590–595.

Feeney, R. E., and Whitaker, J. R. 1982. The Maillard reaction and its preservation. In *Food Protein Deterioration, Mechanisms and Functionality*, ed. J. P. Cerry. Washington, DC: ACS Symposium series ACS, pp. 201–229.

Feeney, R. E., Blackenhorn, G., and Dixon, H. B. F.1975. Carbohydrate-amine reactions in protein chemistry. *Advances Protein Chemistry* 29:135–203.

Fu, B., and Labuza, T. P. 1993. Shelf-life prediction: Theory and application. *Food Control* 4:125–133.

Furuki, T. 2002. Effect of molecular structure on thermodynamic properties of carbohydrates. A calorimetric study of aqueous di- and oligosaccharides at subzero temperatures. *Carbohydrate Research* 337:441–450.

Giannakourou, M. C., Koutsoumanis, K., Nychas, G. J. E., and Taoukis, P. S. 2001. Development and assessment of an intelligent shelf life decision system for quality optimization of the food chill chain. *Journal of Food Protection* 64(7):1051–1057.

Giannakourou, M. C., and Taoukis, P. S. 2002. Systematic application of Time Temperature Integrators as tools for control of frozen vegetable quality. *Journal of Food Science* 67(6):2221–2228.

Giannakourou, M. C., and Taoukis, P. S. 2003a. Application of a TTI-based distribution management system for quality optimisation of frozen vegetables at the consumer end. *Journal of Food Science* 68(1):201–209.

Giannakourou, M. C. and Taoukis, P. S. 2003b. Kinetic modelling of Vitamin C loss in frozen green vegetables under variable storage conditions. *Food Chemistry* 83(1):33–41.

Giannakourou, M. C., and Taoukis, P. S. 2003c. Stability of dehydrofrozen green peas pretreated with non conventional osmotic agents. *Journal of Food Science* 68(6):2002–2010.

Giannakourou, M. C., and Taoukis, P. S. 2007. Reaction kinetics. In *Handbook of Food and Bioprocess Modelling Techniques*, eds. S. S. Sablani, M. S. Rahman, A. K. Datta, and A. S. Mujumdar, Chapter 7, pp. 235–263. New York: CRC Press, Taylor & Francis Group.

Giannakourou, M. C., Koutsoumanis, K., Dermesonlouoglou, E., and Taoukis, P. S. 2001. Applicability of the intelligent shelf life decision system for control of nutritional quality of frozen vegetables. *ISHS Acta Horticulture* 566:275–280.

Giannakourou, M. C., Koutsoumanis, K., Nychas, G. J. E., and Taoukis, P. S. 2005. Field evaluation of the application of time temperature integrators for monitoring fish quality in the chill chain. *International Journal of Food Microbiology* 102(3):323–336.

Giannoglou, M., Platakou, E., Tsironi, T., and Taoukis, P. 2013. Monitoring and optimization of the chain of chilled and frozen food products with TTI smart labels. *2nd IIR International Conference on Sustainability and the Cold Chain*. Paris, April 2–4, pp. 60.

Gogou, E., Katapodis, P., Christakopoulos, P., and Taoukis, P. S. 2010. Effect of water activity on the thermal stability of *Thermomyces lanuginosus* xylanases for process time–temperature integration. *Journal of Food Engineering* 100(4):649–655.

Hayakawa, K. 1973. New procedure for calculating parametric values for evaluating cooling treatments applied to fresh foods. *Canadian Institute of Food Science and Technology Journal* 6(3):197.

Hertog, M. L. A. T. M., Tijskens, L. M. M., and Hak, P. S. 1997. The effects of temperature and senescence on the accumulation of reducing sugars during storage of potato (*Solanum tuberosum* L.) tubers: A mathematical model. *Postharvest Biology and Technology* 10:67–79.

Holmer, B. 1984. Properties and stability of aspartame. *Food Technology* 38:50–55.

International Institute of Refrigeration. 1972. *Recommendations for the Processing and Handling of Frozen Foods*. 2nd edn. Paris: International Institute of Refrigeration.

Jalbout, A. F., and Shipar, M. A. H. 2007. Formation of pyrazines in hydroxyacetaldehyde and glycine nonenzymatic browning Maillard reaction: A computational study. *Food Chemistry* 103(4):1208–1216.

Johnson, F. H., and Eyring, H. 1970. The kinetic basis of pressure effects in biology and chemistry. In *High Pressure Effects on Cellular Processes*, ed. A. M. Zimmerman, pp. 1–44. New York: Academic Press.

Kader, A. A. 1986. Biochemical and physiological basis for effects of controlled and modified atmospheres on fruits and vegetables. *Food Technology* 40(5):99.

Karel, M., and Lund, D. B. (eds) 2003. Reaction kinetics. In *Physical Principles of Food Preservation*. New York: Marcel Dekker, Inc.

Katsaros, G. I., Katapodis, P., and Taoukis, P. S. 2009. Modeling the effect of temperature and high hydrostatic pressure on the proteolytic activity of kiwi fruit juice. *Journal of Food Engineering* 94(1):40–45.

Katsaros, G. I., Giannoglou, M., and Taoukis, P. S. 2009a. Kinetic study of the combined effect of high hydrostatic pressure and temperature on the activity of *Lactobacillus delbrueckii* ssp. *bulgaricus* aminopeptidases. *Journal of Food Science*. 74(5): E219–225.

Katz, E. E., and Labuza, T. P. 1981. Effect of water activity on the sensory crispness and mechanical deformation of snack food products. *Journal of Food Science* 46:403.

Kim, M. N., Saltmarch, M., and Labuza, T. P. 1981. Nonenzymatic browning of hygroscopic whey powders in open vs. sealed pouches. Fresh and extended shelf life refrigerated foods. *Journal of Food Processing and Preservation* 5:49.

Kirkwood, T. B. L. 1977. Predicting the stability of biological standards and products. *Biometrics* 33:736.

Knorr, D. 1993. Effects of high-hydrostatic-pressure processes on food safety and quality. *Food Technology* 47(6):155–161.

Kochhar, S. P., and Rossel, J. B. 1982. A vegetable oiling agent for dried fruits. *Journal of Food Technology* 17:661.

Kondjoyan, A., Kohler, A., Realini, C. E., Portanguen, S., Kowalski, R., Clerjon, S., Gatellier, P., Chevolleau, S., Bonny, J. M., and Debrauwer, L. 2013. Towards models for the prediction of beef meat quality during cooking. *Meat Science* 97(3):323–331.

Koutsoumanis, K. P., Taoukis, P. S., Drosinos, E. H., and Nychas, G. J. E. 2000. Applicability of an Arrhenius model for the combined effect of temperature and CO_2 packaging on the spoilage microflora of fish. *Applied and Environmental Microbiology* 66(8):3528–3534.

Koutsoumanis, K., Giannakourou, M. C., Taoukis, P. S., and Nychas, G. J. E. 2002. Application of shelf life decision system (SLDS) to marine cultured fish quality. *International Journal of Food Microbiology* 73:375–382.

Kramer, A., and Twigg, B. 1968. Measure of frozen food quality and quality changes. In *The Freezing Preservation of Foods*. 4th edn., Vol. 2, ed. D. K. Tressler. Westport, CT: AVI Pub. Co.

Labuza, T. P. 1975. Oxidative changes in foods at low and intermediate moisture levels. In *Water Relations of Foods*, ed. R. Duckworth, p. 455. New York: Academic Press.

Labuza, T. P. 1984. Application of chemical kinetics to deterioration of foods. *Journal of Chemical Education* 61:348–358.

Labuza, T. P. 1971. Kinetics of lipid oxidation of foods. *C.R.C. Rev. Food Technology* 2:355.

Labuza, T. P. 1980. Temperature/enthalpy/entropy compensation in food reactions. *Food Technology* 34(2):67.

Labuza, T. P., and Riboh, D. 1982. Theory and applications of Arrhenius kinetics to the prediction of nutrient losses in food. *Food Technology* 36:66–74.

Labuza, T. P., and Breene, W. M. 1989. Applications of "active packaging" for improvement of shelf life and nutritional quality of fresh and extended shelf life refrigerated foods. *Journal of Food Processing and Preservation* 13:1–69.

Labuza, T. P., and Kamman, J. 1983. Reaction kinetics and accelerated tests simulation as a function of temperature. In *Applications of Computers in Food Research*, ed. I. Saguy, Chapter 4. New York: Marcel Dekker.

Lenz, M. K., and Lund, D. B. 1980. Experimental procedures for determining destruction kinetics of food components. *Food Technology* 34(2):51.

Lim, M. H., and Reid, D. S. 1991. Studies of reaction kinetics in relation to the Tg′ of polymers in frozen food model systems. In *Water Relationships in Foods*. eds H. Levine, and L. Slade. pp. 103–122. New York: Plenum Press.

Lund, D. B. 1983. Considerations in modeling food processes. *Food Technology* 37(1):92.

Manios, S. G., Lambert, R. J. W., and Skandamis, P. N. 2014. A generic model for spoilage of acidic emulsified foods: Combining physicochemical data, diversity and levels of specific spoilage organisms. *International Journal of Food Microbiology* 170:1–11.

Manzocco, L., Nicoli, M. C., Anese, M., Pitotti, A., and Maltini, E. 1999. Polyphenoloxidase and peroxidase activity in partially frozen systems with different physical properties. *Food Research International* 31(5):363–370.

Margerison, D. 1969. The treatment of experimental data. In *The Practice of Kinetics, Vol I Comprehensive Chemical Kinetics*, eds C. H. Banford, and C. F. H. Tipper. New York: Elsevier.

McClure, P. J., Blackburn, M. B., Cole, P. S., Curtis, P. S., Jones, J. E., Legan, J. D., Ogden, I. D. et al. 1994. Modeling the growth, survival and death of microorganisms in foods: The UK Foodmodel approach. *International Journal of Food Microbiology* 23:265–275.

McDonald, K., and Sun, D.-W. 1999. Review: Predictive food microbiology for the meat industry. *International Journal of Food Microbiology* 52:1–27.

McMeekin, T. A., Olley, J. N., Ross, T., and Ratkowsky, D. A. 1993. *Predictive Microbiology: Theory and Application,* pp. 87–115. New York: John Wiley and Sons Inc.

McMeekin, T., Bowman, J., McQuestin, O., Mellefont, L., Ross, T., and Tamplin, M. 2008. The future of predictive microbiology: Strategic research, innovative applications and great expectations. *International Journal of Food Microbiology* 128:2–9.

McMeekin, T.A. 2007. Predictive microbiology: Quantitative science delivering quantifiable benefits to the meat industry and other food industries. *Meat Science* 77:17–27.

Mejlholm, O., Gunvig, A., Borggaard, C., Blom-Hanssen, J., Mellefont, L., Ross, T., Leroi, F., Else, T., Visser, D., and Dalgaard, P. 2010. Predicting growth rates and growth boundary of *Listeria monocytogenes*—An international validation study with focus on processed and ready-to-eat meat and seafood. *International Journal of Food Microbiology* 141:137–150.

Messens, W., Verluyten, J., Leroy, F., and De Vuyst, L. 2003. Modelling growth and bacteriocin production by *Lactobacillus curvatus* LTH 1174 in response to temperature and pH values used for European sausage fermentation processes. *International Journal of Food Microbiology* 81(1):41–52.

Mizrahi, S., Labuza, T. P., and Karel, M. 1970a. Computer aided predictions of food storage stability. *Journal of Food Science* 35:799–803.

Mizrahi, S., Labuza, T. P., and Karel, M. 1970b. Feasibility of accelerated tests for browning in dehydrated cabbage. *Journal of Food Science* 35:804–807.

Nelson, K. A. 1993. Reaction kinetics of food stability: Comparison of glass transition and classical models for temperature and moisture dependence. PhD thesis. University of Minnesota.

Nelson, K., and Labuza, T. P. 1994. Water activity and food polymer science: Implications of state on Arrhenius and WLF models in predicting shelf life. *Journal of Food Engineering* 22:271–290.

Neumeyer, K., Ross, T., and McMeekin, T. A. 1997. Development of a predictive model to describe the effects of temperature and water activity on the growth of spoilage *Pseudomonads*. *International Journal of Food Microbiology* 38:45–54.

Panagou, E.Z., Chelonas, S., Chatzipavlidis, I., and Nychas, G. J. E. 2010. Modelling the effect of temperature and water activity on the growth rate and growth/no growth interface of *Byssochlamys fulva* and *Byssochlamys nivea*. *Food Microbiology*. 27:618–627.

Parkin, K. L., and Brown, W. D. 1982. Preservation of seafood with modified atmospheres. In: *Chemistry and Biochemistry of Marine Food Products*, pp. 453–465. Ed. E. Martin, Westport, CT: AVI.

Peleg, M. 1992. On the use of WLF model in polymers and foods. *Critical Reviews in Food Science and Nutrition* 32:59–66.

Pin, C., Avendaño-Perez, G., Cosciani-Cunico, E., Gómez, N., Gounadaki, A., Nychas, G. J., Skandamis, P., and Barker, G. 2011. Modelling *Salmonella* concentration throughout the pork supply chain by considering growth and survival in fluctuating conditions of temperature, pH and a_w. *International Journal of Food Microbiology* 145(1):96–102.

Polydera, A. C., Stoforos, N. G., and Taoukis, P. S. 2003. Comparative shelf life study and vitamin C loss kinetics in pasteurised and high pressure processed reconstituted orange juice. *Journal of Food Engineering* 60(1):21–29.

Purlis, E. 2010. Browning development in bakery products—A review. *Journal of Food Engineering* 99:239–249.

Quast, D. G., Karel, M., and Rand, W. 1972. Development of a mathematical model for oxidation of potato chips as a function of oxygen pressure, extent of oxidation and equilibrium relative humidity. *Journal of Food Science* 37:679.

Quevedo, R., Ronceros, B., Garcia, K., Lopez, P., and Pedreschi, F. 2011. Enzymatic browning in sliced and puréed avocado: A fractal kinetic study. *Journal of Food Engineering* 105:210–215.

Ratkowsky, D. A., Lowry, R. K., McMeekin, T. A., Stokes, A. N., and Chandler, R. E. 1983. Model for bacterial culture growth rate throughout the entire biokinetic temperature range. *Journal of Bacteriology* 154:1222–1226.

Risbo, J. 2003. The dynamics of moisture migration in packaged multi-component food systems I: Shelf life predictions for a cereal–raisin system. *Journal of Food Engineering* 58(3):239–246.

Roig, M. G., Bello, J. F., Rivera, Z. S., and Kennedy, J. F. 1999. Studies on the occurrence of non-enzymatic browning during storage of citrus juice. *Food Research International* 32(9):609–619.

Roos, Y. H. 1993. Water activity and physical state effects on amorphous food stability. *Journal of Food Processing and Preservation* 16:433–452.

Roos, Y. H. 2013. Relaxations, glass transition and engineering properties of food solids. In: *Edvances in Food Process Engineering Research and Applications*, eds. S. Yanniotis, P. Taoukis, N. G. Stoforos, and V. T. Karathanos, Chapter 4, pp. 79–90. New York: Springer.

Roos, Y. H. 1995. Glass transition-related physicochemical changes in foods. *Food Technology* 10, 97–102.

Ross, T., and McMeekin, T. A. 1994. Predictive microbiology. *International Journal of Food Microbiology* 23:242–264.

Rosso, L., Lobry, J. R., Bajard, S., and Flandrois, J. P. 1995. Convenient model to describe the combined effects of temperature and pH on microbial growth. *Applied and Environmental Microbiology* 61:610–616.

Seyhan, F., Tijskens, L. M. M., and Evranuz, O. 2002. Modelling temperature and pH dependence of lipase and peroxidase activity in Turkish hazelnuts. *Journal of Food Engineering* 52:387–395.

Sivertsvik, M., and Jeksrud, W. K. 2002. Review: A review of modified atmosphere packaging of fish and fishery products—Significance of microbial growth, activities and safety. *International Journal of Food Science and Technology* 37:107–127.

Slade, L., and Levine, H. 1991. Beyond water activity: Recent advances based on an alternative approach to the assessment of food quality and safety. *Food Science and Nutrition* 30(2,3):115–357.

Taoukis, P. S. 2003. Q_{10}. In: *Encyclopedia of Agricultural, Food and Biological Engineering*. ed. D. Heldman, New York:Marcel Dekker, Inc.

Taoukis, P. S., Giannakourou, M. C., and Tsironi, T. N. 2012. Monitoring and control of the cold chain. In *Handbook of Frozen Food Processing and Packaging*. eds D. W. Sun, 2nd edn., Chapter 13, pp. 273–299, Boca Raton: CRC Press, Taylor & Francis.

Taoukis, P. S., El Meskine, A., and Labuza, T. P. 1988. Moisture transfer and shelf life of packagedfoods. In *Food and Packaging Interactions*, eds. J. H. Hotchkiss, ACS Symposium Series No. 365, Washington D.C.: ACS, pp. 243–261.

Taoukis, P. S., Labuza, T. P., and Saguy, I. S. 1997. Kinetics of food deterioration and shelf life prediction. In *Handbook of Food Engineering Practice*. eds K. J. Valentas, E. Rotstein and R. P Singh. New York: CRC Press.

Taoukis, P. S., and Skiadi, O. 1998. Shelf life prediction modelling of packaged dehydrated foods for dynamic temperature and relative humidity storage conditions. In *Food Quality Modelling*, pp.31–39. eds B. M. Nicolai and J. De Baerdemaeker, Office for Official Publications of the European Commission. Luxembourg: ECSC-EC-EAEC, (COST 915- COPERNICUS CIPA- CT94–0120)

Taoukis, P., and Labuza, T. P. 2003. Time temperature indicators. In *Novel Food Packaging Techniques*. ed. R. Ahvenainen, Woodhead Publ., Cambridge, UK.

Taoukis, P. S., and Giannakourou, M. C. 2004. Temperature and food stability: Analysis and control. In *Understanding and Measuring the Shelf-Life of Food*, ed. R. Steele, Chapter 3, pp. 42–68, Cambridge, UK: Woodhead Publishing Ltd.

Taoukis, P. S., and Labuza, T. P. 1989a. Applicability of time-temperature indicators as shelf life monitors of food products. *Journal of Food Science* 54(4):783–789.

Taoukis, P. S., and Labuza, T. P. 1989b. Reliability of time-temperature indicators as food quality monitors under nonisothermal conditions. *Journal of Food Science* 54(4):789–792.

Taoukis, P. S., and Richardson, M. 2007. Principles of intermediate-moisture foods and related technology. In *Water Activity in Foods: Fundamentals and Applications.* eds. G. V. Barbosa-Cánovas, A. J. Fontana Jr., S. J. Schmidt, and T. P. Labuza, Ames, Iowa, USA: ISUP, Inc. Blackwell Publishing.

Tazi, S., Plantevin, F., Di Falco, C., Puigserver, A., and Ajandouz, H. 2009. Effects of light, temperature and water activity on the kinetics of lipoxidation in almond-based products. *Food Chemistry* 115(3):958–964.

Templeman, G., Sholl, J. J., and Labuza, T. P. 1977. Evaluation of several NMR techniques for solids in fat determination in commercial fats. *Journal of Food Science* 42:432.

Terefe, N. S., and Hendrickx, M. E. 2002. Kinetics of the pectin methylesterase catalyzed de-esterification of pectin in frozen food model systems. *Biotechnology Progress* 18:221–228.

Terefe, N. S., Mokwena, K. K., Van Loey, A., and Hendrickx, M. E. 2002. Kinetics of the alkaline phosphatase catalyzed hydrolysis of disodium p-nitrophenyl phospate in frozen model systems. *Biotechnology Progress* 18:1249–1256.

Torreggiani, D., Forni, E., Guercilena, I., Maestrelli, A., Bertolo, G., Archer, G. P., Kennedy, C. J. et al. 1999. Modification of glass transition temperature through carbohydrates additions: Effect upon colour and anthocyanin pigment stability in frozen strawberry juices. *Food Research International* 32:441–446.

Trant, A. S., Pangborn, R. M., and Little, A. C. 1981. Potential fallacy of correlating hedonic responses with physical and chemical measurements. *Journal of Food Science* 41:583.

Trystram, G. 2012. Modelling of food and food processes. *Journal of Food Engineering* 110:269–277.

Tsironi, T., Stamatiou, A., Giannoglou, M., Velliou, E., and Taoukis, P. S. 2011. Predictive modelling and selection of Time Temperature Integrators for monitoring the shelf

life of modified atmosphere packed gilthead seabream fillets. *LWT-Food Science and Technology* 44:1156–1163.

Tsironi, T. N., and Taoukis, P. S. 2014. Effect of processing parameters on water activity and shelf life of osmotically dehydrated fish filets. *Journal of Food Engineering* 123:188–192.

Tsironi, T., Dermesonlouoglou, E., Giannakourou, M., and Taoukis, P. 2009. Shelf life modelling of frozen shrimp at variable temperature conditions. *LWT- Food Science and Technology* 42, 664–671.

Tsironi, T., Gogou, E., Velliou, E., and Taoukis, P. S. 2008. Application and validation of the TTI based chill chain management system SMAS on shelf life optimization of vacuum packed chilled tuna slices. *International Journal of Food Microbiology* 128(1):108–115.

Tsoumbeli, M. N., and Labuza, T. P. 1991. Accelerated kinetic study of aspartame degradation in the neutral pH range. *Journal of Food Science* 56:1671–1675.

Vaikousi, H., Koutsoumanis, K., and Biliaderis, C. G. 2008. Kinetic modelling of non-enzymatic browning of apple juice concentrates differing in water activity under isothermal and dynamic heating conditions. *Food Chemistry* 107(2):785–796.

Vaikousi, H., Koutsoumanis, K., and Billiaderis, C. G. 2009. Kinetic modelling of non-enzymatic browning in honey and diluted honey systems subjected to isothermal and dynamic heating protocols. *Journal of Food Engineering* 95(4):541–550.

Valdramidis, V. P., Geeraerd, A. H., Poschet, F., Ly-Nguyen, B., Van Opstal, I., Van Loey, A. M., Michiels, C. W., Hendrickx, M. E., and Van Impe, J. F. 2007. Model based process design of the combined high pressure and mild heat treatment ensuring safety and quality of a carrot simulant system. *Journal of Food Engineering* 78(3):1010–1021.

Valdramidis, V. P., Taoukis, P. S., Stoforos, N. G., and Van Impe, J. F. M. 2012. Modeling the kinetics of microbial and quality attributes of fluid food during novel thermal and non-thermal processes. In *Novel Thermal and Non-Thermal Technologies for Fluid Foods*, ed. P. J. Cullen, Brijesh, K. Tiwari and Vasilis P. Valdramidis, Chapter 14, pp. 433–471. San Diego: Academic Press.

Valdramidis, V. P., Cullen, P. J., Tiwari, B. K., and O' Donnell, C. P. 2010. Quantitative modelling approaches for ascorbic acid degradation and non-enzymatic browning of orange juice during ultrasound processing. *Journal of Food Engineering* 96:449–454.

Valero, A., Pérez-Rodríguez, F., Carrasco, E., Fuentes-Alventosa, J. M., García-Gimeno, R. M., and Zurera, G. 2009. Modelling the growth boundaries of *Staphylococcus aureus*: Effect of temperature, pH and water activity. *International Journal of Food Microbiology* 133(1–2):186–194.

Van Arsdel, W. B., Coply, M. J., and Olson, R. L. 1969. *Quality and Stability of Frozen Foods*. New York: Wiley-Interscience.

Van Boekel, M. A. J. S. 2000. Kinetic modeling. In *Food Process Modeling*. eds L. M. M. Tijskens, M. L. A. T. M. Hertog, and B. M. Nicolaï, pp. 35–59. New York: CRC Press.

Villota, R., and Hawkes, J. G. 2007. Reaction kinetics in food systems. In *Handbook of Food Engineering*, 2nd edn, pp. 125–287. eds D. R. Heldman and D. B. Lund. New York: CRC Press.

Weissman, I., Ramon, O., Kopelman, I. J., and Mizrahi, S. 1993. A kinetic model for accelerated tests of Maillard browning in a liquid model system. *Journal of Food Processing and Preservation* 17:455–470.

Williams, M. L., Landel, R. F., and Ferry, J. D. 1955. The temperature dependence of relaxation mechanisms in amorphous polymers and other glass-forming liquids. *Journal of the American Chemical Society* 77:3701–3707.

Willocx, F., Mercier, M., Hendrickx, M., and Tobback, P. 1993. Modelling the influence of temperature and carbon dioxide upon the growth of *Pseudomonas fluorescens*. *Food Microbiology* 10:159–173.

Yoshioka, S., Aso, Y., and Uchiyama, M. 1987. Statistical evaluation of nonisothermal prediction of drug stability. *Journal of Pharmaceutical Sciences* 76(10):794–798.

Zheng, H., and Hongfei, L. 2011. Effect of microwave pretreatment on the kinetics of ascorbic acid degradation and peroxidase inactivation in different parts of green asparagus (*Asparagus officinalis* L.) during water blanching. *Food Chemistry*. 128:1087–1093.

Zimmermann, M., Schaffner, D. W., and Aragao, G. M. F. 2013. Modeling the inactivation kinetics of *Bacillus coagulans* spores in tomato pulp from the combined effect of high pressure and moderate temperature. *LWT-Food Science and Technology* 53:107–112.

Zobel, H. F. 1973. A review of bread staling. *Baker's Dig*. 47(5):52.

Food and Culinary Science

FOOD ENGINEERING HANDBOOK

FOOD ENGINEERING FUNDAMENTALS

Food Engineering Handbook: Food Engineering Fundamentals provides a stimulating and up-to-date review of food engineering phenomena. Combining theory with a practical, hands-on approach, this book covers the key aspects of food engineering, from mass and heat transfer to steam and boilers, heat exchangers, diffusion, and absorption. A complement to *Food Engineering Handbook: Food Process Engineering*, this text:

- Explains the interactions between different food constituents that might lead to changes in food properties
- Describes the characterization of the heating behavior of foods, their heat transfer, heat exchangers, and the equipment used in each food engineering method
- Discusses rheology, fluid flow, evaporation, and distillation and includes illustrative case studies of food behaviors

Presenting cutting-edge information, **Food Engineering Handbook: Food Engineering Fundamentals** is an essential reference on the fundamental concepts associated with food engineering today.

K24306

CRC Press
Taylor & Francis Group
an **informa** business
www.crcpress.com

6000 Broken Sound Parkway, NW
Suite 300, Boca Raton, FL 33487
711 Third Avenue
New York, NY 10017
2 Park Square, Milton Park
Abingdon, Oxon OX14 4RN, UK

ISBN: 978-1-4822-6169-1
90000
9 781482 261691